Giuliano Mariani • Gianpiero Manca • Federica Orsini
Sergi Vidal-Sicart • Renato A. Valdés Olmos
Editors

Atlas of Lymphoscintigraphy and Sentinel Node Mapping

A Pictorial Case-Based Approach

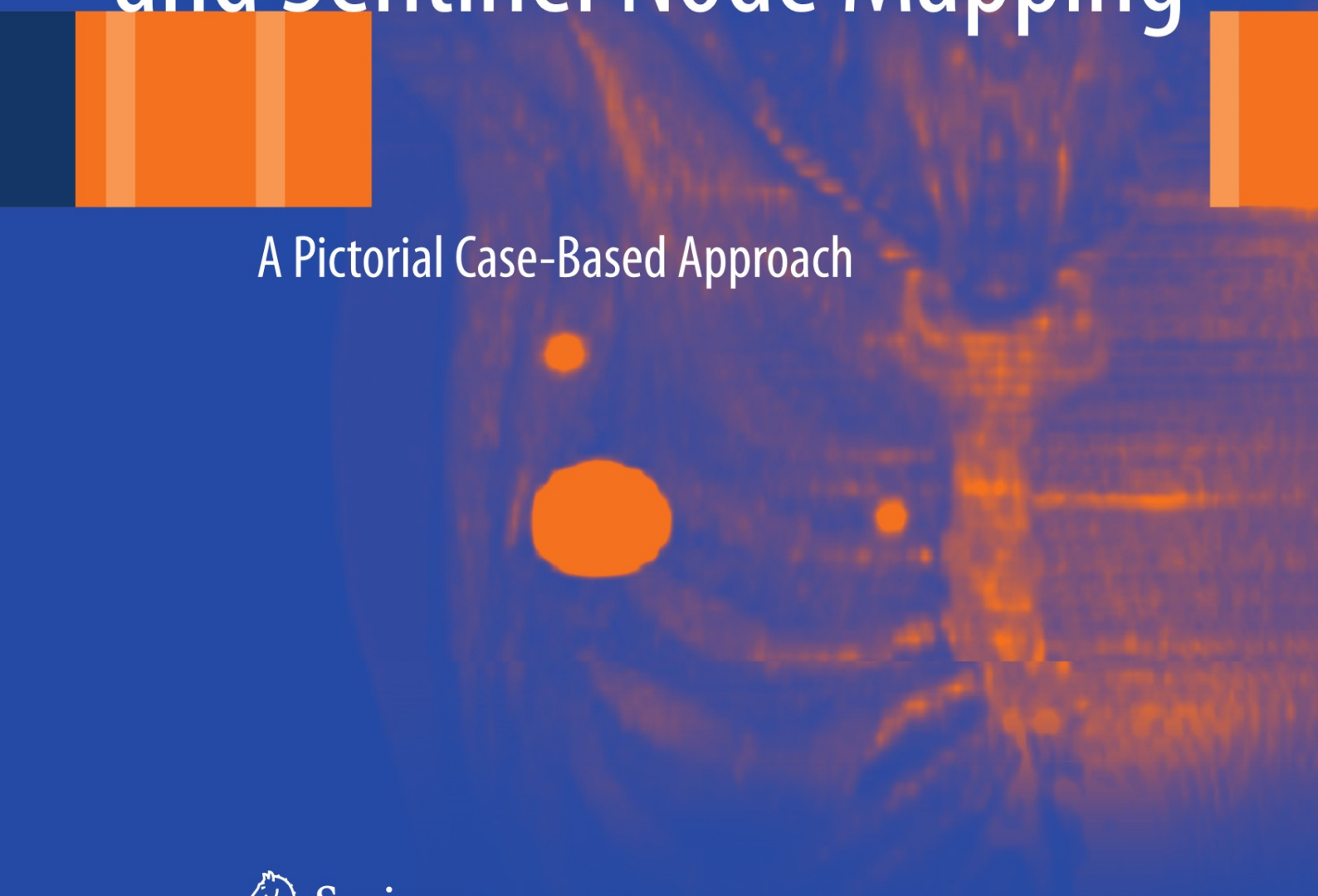

Springer

Atlas of Lymphoscintigraphy and Sentinel Node Mapping

Giuliano Mariani • Gianpiero Manca
Federica Orsini • Sergi Vidal-Sicart
Renato A. Valdés Olmos
Editors

Atlas of Lymphoscintigraphy and Sentinel Node Mapping

A Pictorial Case-Based Approach

Forewords by Peter J. Ell and Giovanni Lucignani

Springer

Editors
Giuliano Mariani
Regional Center of Nuclear Medicine
University of Pisa Medical School
Pisa, Italy

Gianpiero Manca
Regional Center of Nuclear Medicine
University of Pisa Medical School
Pisa, Italy

Federica Orsini
Regional Center of Nuclear Medicine
University of Pisa Medical School
Pisa, Italy

Sergi Vidal-Sicart
Nuclear Medicine, Hospital Clínic
Barcelona, Barcelona, Spain

Renato A. Valdés Olmos
Nuclear Medicine, Division of Diagnostic
Oncology, Netherlands Cancer Institute
– Antoni van Leeuwenhoek Hospital,
Amsterdam, the Netherlands

ISBN 978-88-470-2765-7 ISBN 978-88-470-2766-4 (eBook)
DOI 10.1007/978-88-470-2766-4
Springer Milan Dordrecht Heidelberg London New York

Library of Congress Control Number: 2012948629

7 6 5 4 3 2 1 2012 2013 2014
Cover design: Ikona S.r.l., Milan, Italy
Typesetting: Grafiche Porpora S.r.l., Segrate (MI), Italy

Springer-Verlag Italia S.r.l. – Via Decembrio 28 – I-20137 Milan
Springer is a part of Springer Science+Business Media (www.springer.com)

Foreword

The expertise available in centers from Amsterdam, Pisa, Barcelona and Rome has contributed to this timely production entitled *Atlas of Lymphoscintigraphy and Sentinel Node Mapping*. The volume, ably led by Giuliano Mariani, is beautifully produced (as we are now used to with Springer publications) and profusely illustrated, with interesting and thought-provoking case material. The book consists of 16 chapters; the first five are dedicated to lymphoscintigraphy, and the remaining eleven discuss in significant detail the concept, technologies and areas of clinical utility of the sentinel lymph node biopsy approach (SLNB). A clear separation is hence made by the authors, which is to be recommended as too much confusion still remains in some quarters between SLNB, four-nodal sampling, guided nodal biopsy and other variations.

A good textbook/atlas is enjoyable to read and thought provoking, offers answers and stimulates questions, and is kept for second and third readings. On all these accounts, this production falls into this category.

Lymphoscintigraphy, namely image mapping of lymph node basins and flow, represents one of the oldest applications of the radioactive tracer method. As early as 1953, Sherman and Ter-Pogossian described the nodal uptake of radiolabeled gold, following interstitial administration (*Cancer* 6:238). It represents a most elegant approach to learning the physiology of the lymphatic system, its plasticity, surprisingly varied pathways and response to pathogenic aggression. It is therefore appropriate that the authors begin by describing the anatomy and physiology of the lymphatic circulation. They underline that even today we continue to modify our views on the intricate pathways of lymph flow, throwing new light, inter alia, on the posterior lymphatic network of the breast (denied by Sappey and Rouvière). Mention is made of axillary reverse mapping, an interesting topic that is not frequently addressed. Since Figure 1.1 refers to the additional removal of three internal mammary nodes, it is relevant to note that Chapter 9 clarifies the current role of internal mammary dissection (see below).

As the authors clearly state, “despite the experience acquired over so many decades, protocols for performing lymphoscintigraphy are not yet standardized, and remarkable differences between centers still persist”. This point is underlined in the subsequent chapters dedicated to lymph node mapping. There is a good discussion concerning the variables in this process, from particle size, to specific activity of the labeling methodology (this aspect could be discussed further) and the depth and site of tracer administration. Tracer administration is very nicely documented in Chapter 4, where illustration of deep versus superficial tracer routes leads to rather different pathways being demonstrated – excellent images document this (Figure 4.6 and others). This aspect is discussed in detail for lymphatic mapping of the arms and legs. Similar discussion that has pervaded the initial development of SLNB in breast cancer is reflected in the variety of clinical cases illustrated in Chapter 9, with widely different modalities of radiocolloid injection.

Lymphedema and its differential diagnosis is elegantly described and discussed in Chapter 5. The various technologies of cutaneous ultrasonography, Doppler ultrasound, computed tomography (CT) and magnetic resonance and lymphoscintigraphy are discussed and amply illustrated and commented on, with seven figures. The indications for this technique are outlined: differential diagnosis of edema to distinguish venous from lymphatic etiology;

assessment of pathways of lymphatic drainage; quantitation of lymph flow; identification of patients at high risk of developing lymphedema following axillary lymph node dissection; and evaluation of the efficacy of therapeutic interventions. Twenty-one well-illustrated clinical cases are shown, with presentation of the clinical history and discussion of findings.

An excellent chapter (Chapter 6) gives an overview of the concept of the sentinel lymph node in oncology. Helpful diagrams help the reader to understand this concept, and less appropriate definitions of what constitutes a sentinel node are given prominence. There has been much confusion in the literature, and this chapter will help to clarify ongoing misunderstandings. There follows a chapter on preoperative imaging, intraoperative gamma probe guidance and imaging, and multimodality imaging. The authors show multiple examples of their practice, with single photon emission computed tomography (SPECT)/CT playing an interesting role to further aid precise localization. The use of transmission sources to delineate body contours during planar imaging is recommended. The use of portable imaging probes and novel tracking devices are also discussed and illustrated. A comprehensive and excellent discussion is offered in a chapter dedicated to SPECT/CT in the context of SLNB detection (Chapter 8). High-quality images are presented, which aid the reader to appreciate the advantages of three-dimensional (3D) imaging. Readers should recognize, however, that while SPECT/CT may represent a valuable adjunct to conventional planar imaging, SLNB has achieved its high reputation because of its simplicity and accuracy (especially in cancers of the breast and melanoma). The additional burden of imaging complexity is best reserved for other applications of SLNB (head and neck, chest, gastrointestinal (GI) tract and gynecological applications, etc.), where the added value of a 3D approach is relevant.

The next eight chapters are dedicated to a discussion of specific cancer types and SLNB: these concern the breast, cutaneous melanoma, head and neck cancer, non-small-cell lung cancer, and cancers of the GI tract, the female reproductive system, the male reproductive system and the kidney and bladder. While the first two applications in breast carcinoma and cutaneous melanoma have now seen SLNB firmly incorporated in the preoperative management of these patients, and indeed it has become best practice, the other applications represent work in progress and await further evidence gathering.

Chapter 9, dedicated to SLNB in breast carcinoma, is extensively cross-referenced, again with high-quality clinical examples and figures and 13 case presentations, including an extensive discussion concerning the management of these patients in the light of what has been learned with SLNB. In this area, divergent views and practice between centers of excellence have been documented, in relation to the depth of tracer administration (from intratumoral injection to superficial administration, various particle sizes of colloids, for and against internal mammary dissection), with significant divergent practice seen amongst centers of excellence in Australia, USA and Europe. This chapter is essential reading, with a second reading and reflection being highly recommended. The latest Z0011 trial is also discussed. It is relevant to note that, despite all the variations encountered worldwide, the benefits of the SLNB method seem overwhelming, whatever the approach taken. Formal training programs have now become established and are readily available.

As the authors state in Chapter 10, dedicated to SLNB in melanoma, lymphatic drainage is highly variable in this cancer, thus making lymphoscintigraphy mandatory. It is in this context that mapping nodes, and the flow and drainage patterns of lymph, has truly brought to the fore the elegance and clinical relevance of lymphoscintigraphy. The authors clearly describe the main indications and contraindications of this method, and discuss in detail the approach that needs to be taken. Well-documented cases allow the reader to understand the best use of this method; common and rarer variants are presented, pitfalls are discussed, and eight detailed clinical cases illustrated and discussed. This is a further excellent contribution.

There is a well-illustrated chapter on the role of SLNB in head and neck cancers and further chapters pointing to future developments with SLNB in the other pathologies in the lung, GI tract, male and female reproductive systems, and kidney and bladder.

As already stated, this text and atlas is a must for all those interested in early cancer

staging, oncologists, radiotherapists, nuclear medicine and imaging doctors, and scientists. This publication fills a gap and is hence timely! The authors are to be commended for their significant effort and commitment.

October 2012

Peter J. Ell FMedSci DR HC
Professor Emeritus UCL
Fellow Academy of Medical Sciences
London, UK

Foreword

The publication of this Atlas is an important achievement for the "Radioguided Surgery" Study Group of the Italian Association of Nuclear Medicine (AIMN), not least because it will allow the group's expertise to be shared with colleagues worldwide. It is also a tangible reflection of the high level of professionalism and cooperation that exists within the group.

The fact that it is published by Springer will certainly help the AIMN in its pursuit of a key aim: to promote the efficient dissemination of scientific data and advances in the field of nuclear medicine that have relevance to other disciplines. In this regard, this Atlas follows in the footsteps of other publications produced within the context of the Italian nuclear medicine community.

As current president of the AIMN, I am therefore delighted by the completion of this volume, which will undoubtedly strengthen our knowledge of diagnostic nuclear medicine.

October 2012

Giovanni Lucignani
President of the Italian Association
of Nuclear Medicine (AIMN)

Preface

Lymphoscintigraphy is a nuclear-medicine imaging procedure that provides information on the functional status of the lymphatic system. This technique was originally introduced into clinical practice for identification of the causes of peripheral edema (for example, as a result of impaired lymphatic versus impaired venous flow), or for characterization of patients with lymph effusions. More recent and widespread applications of lymphoscintigraphy form the basis for radioguided biopsy of the sentinel lymph node in patients with solid epithelial cancers.

The concept of sentinel lymph node biopsy in oncologic surgery is related to the fact that any solid tumor drains in an orderly fashion via the lymphatic system, from the lower to the upper levels. Therefore, the sentinel node, namely the first lymph node encountered by lymph draining from the tumor site, is most likely to be the first one to be affected by metastasis, while a negative sentinel lymph node makes it highly unlikely that other lymph nodes along the same lymphatic pathway will be affected.

Sentinel lymph node biopsy and lymphatic mapping were initially developed in patients with cancer of the penis, and further refined in patients with melanoma, under the assumption that examination of the first regional lymph node that drains the lesion would predict the status of the remainder of the nodes in that region. It was further assumed that if no tumor cells are observed in the sentinel lymph node, the morbidity associated with extensive lymph node dissection could be avoided. This assumption has been confirmed in widespread clinical trials, carried out mostly in patients with breast cancer or melanoma, but also in patients with cancer of the penis or vulva. As a result, sentinel lymph node evaluation has become an integral component of treatment planning in patients with these tumors, particularly for staging and prognostic purposes.

The introductory chapters of this atlas-book present basic concepts about the anatomy, physiology, and pathophysiology of lymphatic circulation (Chapters 1 and 2), as well as some methodological aspects of lymphoscintigraphy, including radiopharmaceuticals and instrumentation (Chapter 3). In the subsequent clinical chapters, leading world experts present the state of the art of lymphoscintigraphy for characterizing different clinical conditions involving impaired lymphatic circulation, as well as the most advanced and successful techniques for sentinel lymph node mapping and radioguided sentinel lymph node biopsy.

After presenting the correct methodological approach to performing lymphoscintigraphy for evaluating patients with edema of the extremities (Chapter 4), the first clinical section of the book concerns the nononcologic applications of lymphoscintigraphy, such as those designed to assess the obstructive and/or dysfunctional disease of the lymphatic system causing lymphedema or intracavitary lymph effusions (Chapter 5).

Chapter 6 introduces the concept of sentinel lymph node biopsy in surgical oncology, while Chapter 7 provides the essential tools for correct interpretation of both planar and tomographic lymphoscintigraphy, including the latest single photon emission computed tomography/computed tomography (SPECT/CT) fusion imaging modalities. The final chapters emphasize the clinical impact of radioguided sentinel lymph node biopsy, presented within the framework of a multidisciplinary approach to performing such procedure in specific malignancies, i.e., breast cancer (Chapter 9), cutaneous melanoma (Chapter 10), head

and neck cancers (Chapter 11), lung cancer (Chapter 12), gastrointestinal cancers (Chapter 13), cancers of the female and male reproductive system (Chapters 14 and 15, respectively), and, finally, kidney and bladder cancers (Chapter 16).

Each chapter on the clinical applications of lymphoscintigraphy in different anatomic regions or disease conditions includes an introductory section concerning the pathophysiology of the specific disease; the clinical relevance and impact of lymphoscintigraphy in such conditions is then demonstrated by a collection of richly illustrated teaching cases describing the lymphoscintigraphic patterns most commonly observed, as well as anatomic variants and technical pitfalls of the procedure.

No other books published to date have addressed the issues of lymphoscintigraphy with the same approach as that of this book, namely "case-based learning". In our view, this book therefore represents an ideal learning tool, especially for residents in nuclear medicine and for specialists in nuclear medicine who are entering the field, as well as a useful integration aid for residents in surgery (especially oncologic surgery) and for surgeons entering the field.

Although this book was initially conceived as an initiative of the Study Group on "Radioguided Surgery" of the Italian Association of Nuclear Medicine (AIMN), its scope has then expanded to encompass the contribution of international experts as well, thus reflecting the worldwide trend for increasing applications of lymphoscintigraphy.

Individual chapters are written by specialists, who have also provided images and clinical cases for the clinical chapters. In addition to these experts, many other colleagues from Italy (mostly within the Study Group on "Radioguided Surgery" of the AIMN) and abroad have provided a number of interesting clinical cases. We are therefore deeply indebted and grateful to all these people for their collaborative effort and for their invaluable contributions to this publication. In particular, three of the residents in nuclear medicine at the University of Pisa (Dr Manuel Tredici, Dr Valerio Duce, and Dr Sara Mazzarri) deserve special acknowledgements for their hard work and supportive collaboration.

We also wish to thank the team at Springer for making it possible to publish this book in such timely fashion.

October 2012 The Editors

Contents

1 The Anatomy and Physiology of Lymphatic Circulation 1
Pieter J. Tanis and Omgo E. Nieweg

1.1 Introduction 1
1.2 The Physiology of Lymph Flow 1
1.3 Anatomy of the Lymphatic System 2
1.4 Lymphatic Visualization Techniques 3
References 4

2 The Pathophysiology of Lymphatic Circulation in Different Disease Conditions 7
Rossella Di Stefano, Paola Anna Erba, and Giovanni D'Errico

2.1 Introduction 7
2.2 Lymphatic Circulation and Lipid Absorption 9
2.3 Pathophysiology of Lymph Drainage Failure 9
2.4 Edema 9
2.5 Lymphedema 10
2.6 Lymphatic Malignancies 13
2.7 Acute Lymphangitis 13
2.8 Lymphatic Circulation in Obesity and Cardiovascular Disease 13
2.9 Intracavitary Lymphedema 14
References 14

3 Methodological Aspects of Lymphoscintigraphy: Radiopharmaceuticals and Instrumentation 17
Paola Anna Erba, Giuseppina Bisogni, Alberto Del Guerra, and Giuliano Mariani

3.1 Radiopharmaceuticals 17
3.2 Instrumentation 20
References 23

4 Methodological Aspects of Lymphoscintigraphy: Bicompartmental Versus Monocompartmental Radiocolloid Administration 27
Paola Anna Erba, Martina Sollini, Giovanni D'Errico, and Giuliano Mariani

4.1 Introduction 27
4.2 Methodology 27
4.3 Imaging 31
4.4 Qualitative Visual Interpretation 31

4.5 Lymphoscintigraphy with Stress Test 32
4.6 Quantitative Lymphoscintigraphy 32
References 36

5 Lymphoscintigraphy for the Differential Diagnosis of Peripheral Edema and Intracavitary Lymph Effusion 39
Paola Anna Erba, Martina Sollini, and Roberto Boni

5.1 Introduction 39
5.2 Differential Diagnosis 40
5.3 Diagnostic Characterization 40
5.4 Management of Lymphedema 43
5.5 Lymphoscintigraphy in the Management of Lymphedema 44
Clinical Cases
Case 5.1 - Upper Limb Monocompartmental Lymphoscintigraphy in Stage III Primary Lymphedema of the Upper Left Arm Without Lymphadenomegaly 48
Case 5.2 - Upper Limb Monocompartmental Lymphoscintigraphy in Non-Pitting Edema of the Upper Left Limb in Patient with Rheumatoid Arthritis 49
Case 5.3 - Axillary Reverse Mapping Lymphoscintigraphy in Breast Cancer Patient with Positive Sentinel Lymph Node Before Lymphadenectomy 50
Case 5.4 - Axillary Reverse Mapping Lymphoscintigraphy in Breast Cancer Patient with Infiltrative Lobular Carcinoma and Positive Sentinel Lymph Node Before Lymphadenectomy 51
Case 5.5 - Lower Limb Monocompartmental Lymphoscintigraphy in Patient with Bilateral Swelling and Non-Pitting Edema of the Lower Limbs 52
Case 5.6 - Lower Limb Bicompartmental Lymphoscintigraphy in Patient with Edema of the Left Lower Limb 53
Case 5.7 - Lower Limb Monocompartmental Lymphoscintigraphy in Patient with Bilateral Lower Limb Lymphedema 55
Case 5.8 - Lower Limb Monocompartmental Lymphoscintigraphy in Patient Previously Submitted to Left Saphenectomy 57
Case 5.9 - Lower Limb Monocompartmental Lymphoscintigraphy in Patient with History of Lymphadenectomy of the Groin Basin for Melanoma 58
Case 5.10 - Post-Exercise Lower Limb Monocompartmental Lymphoscintigraphy in Patient with Bilateral Leg Edema 59
Case 5.11 - Lower Limb Monocompartmental Lymphoscintigraphy at Rest and Post-Exercise with Semiquantitative Evaluation of the Tracer Appearance Time in Patient with Lymphedema of the Left Lower Limb Post Left Groin Lymphadenectomy 60
Case 5.12 - Lower Limb Monocompartmental Lymphoscintigraphy at Rest and Post-Exercise with Semiquantitative Evaluation of the Tracer Appearance Time in Patient with Right Lower Limb Primary Lymphedema, Clinical Stage 3 According to Foeldi 62
Case 5.13 - Lower Limb Monocompartmental Lymphoscintigraphy at Rest and Post-Exercise with Semiquantitative Evaluation of the Tracer Appearance Time in Patient with Post-Lymph Nodal Dissection Lymphedema of the Lower Limbs 64

Case 5.14 - Post-Exercise Lower Limb Monocompartmental Lymphoscintigraphy in Patient with Acute Edema of the Left Lower Limb and Painful Left Inguinal Lymphadenomegaly 66
Case 5.15 - Lower Limb Monocompartmental Lymphoscintigraphy at Rest and Post-Exercise with Semiquantitative Evaluation of the Tracer Appearance Time in Patient with Secondary Lymphedema of the Right Lower Limb 68
Case 5.16 - Lower Limb Monocompartmental Lymphoscintigraphy in Patient with Secondary Bilateral Non-Pitting Edema of the Lower Extremities, More Evident on the Left, and Left Ureteral Obstruction Due to Lymphocele 70
Case 5.17 - Lower Limb Bicompartimental Lymphoscintigraphy in Patient with Post-Traumatic Edema of the Left Leg Associated with Disability Grade 3 According to Ricci Scale, at Baseline and After 5 Years of Multiple Surgeries and Cycles of Therapy. 73
Case 5.18 - Upper and Lower Limb Bicompartmental Lymphoscintigraphy in Patient with Bilateral Feet and Ankle Edema, More Prevalent in Left Side 76
Case 5.19 - Upper and Lower Limb Bicompartmental Lymphoscintigraphy in Patient with Right Pelvic Para-Vesical and Inguinal Swelling . . 78
Case 5.20 - Lower Limb Bicompartmental Lymphoscintigraphy in Patient with Edema of the Scrotum 82
Case 5.21 - Lower Limb Monocompartmental Lymphoscintigraphy in Patient with Post-Surgical Chylopericardium (Ductus Arteriosus), Treated with Thoracentesis 84
References 85

6 The Sentinel Lymph Node Concept in Oncologic Surgery 87
Omgo E. Nieweg

6.1 History 87
6.2 Concept and Definition 88
6.3 Concluding Remarks 92
References 92

7 General Concepts on Radioguided Sentinel Lymph Node Biopsy: Preoperative Imaging, Intraoperative Gamma-Probe Guidance, Intraoperative Imaging, and Multimodality Imaging 95
Federica Orsini, Federica Guidoccio, Sergi Vidal-Sicart, Renato A. Valdés Olmos, and Giuliano Mariani

7.1 Introduction 95
7.2 Preoperative Imaging. 96
7.3 Intraoperative Gamma-probe Guidance 100
7.4 Intraoperative and Multimodality Imaging 102
References 109

8 SPECT/CT Image Generation and Criteria for Sentinel Node Mapping 111
Renato A. Valdés Olmos and Sergi Vidal-Sicart

8.1 Introduction 111
8.2 The Clinical Problem 111
8.3 Image Generation with SPECT/CT 112
8.4 General Indications and Contraindications for SPECT/CT 113
8.5 Comprehensive Interpretation of Preoperative Imaging of Sentinel Lymph Nodes 114
8.6 SPECT/CT as a Roadmap for Intraoperative Detection of Sentinel Lymph Nodes 118
References 119

9 Preoperative and Intraoperative Lymphatic Mapping for Radioguided Sentinel Node Biopsy in Breast Cancer 121
Gianpiero Manca, Manuel Tredici, Valerio Duce, Sara Mazzarri, Federica Orsini, Serena Chiacchio, Armando E. Giuliano, and Giuliano Mariani

9.1 Introduction 121
9.2 The Clinical Problem 122
9.3 Lymphatic Drainage of the Breast 123
9.4 Lymphoscintigraphy 124
9.5 Contribution of SPECT/CT 128
9.6 Intraoperative Detection 131
9.7 Internal Mammary Chain 132
9.8 Accuracy of Radioguided Sentinel Lymph Node Biopsy 133
9.9 Long-term Outcome of Sentinel Lymph Node Biopsy 135
9.10 Indications and Contraindications for Sentinel Lymph Node Biopsy 136
9.11 Controversial Indications 136
9.12 Certification for Sentinel Lymph Node Biopsy in Patients with Breast Cancer 137

Clinical Cases

Case 9.1 - Sentinel Node Mapping in Breast Cancer: Drainage to Axillary Nodes After Periareolar Injection (Planar Imaging) 138
Case 9.2 - Sentinel Node Mapping in Breast Cancer: Drainage to Multiple Axillary Nodes After Intradermal Injection (Planar Imaging) 139
Case 9.3 - Sentinel Node Mapping in Breast Cancer: Drainage to Single Axillary Node After Intra-Peritumoral Injection (Planar Imaging) . . 140
Case 9.4 - Sentinel Node Mapping in Breast Cancer: Drainage to Axillary Nodes After Intradermal Injection (Planar and SPECT/CT Imaging) 141
Case 9.5 - Sentinel Node Mapping in Breast Cancer: Drainage to Axillary Nodes After Subareolar Injection (Planar and SPECT/CT Imaging) 144
Case 9.6 - Sentinel Node Mapping in Breast Cancer: Failure of Lymphatic Drainage (Due to Metastatic Axillary Nodes) After Intratumoral and Subdermal Injection (Planar and SPECT/CT Imaging) 146
Case 9.7 - Sentinel Node Mapping in Breast Cancer: Failure of Lymphatic Drainage After Intratumoral and Subdermal Injection; Subsequent Visualization of Axillary Nodes After Periareolar Injection (Planar Imaging) 148

Case 9.8 - Sentinel Node Mapping in Breast Cancer: Prior Axillary Lymph Node Dissection with Controlateral Axillary Migration After Subdermal Injection (Planar Imaging) 149
Case 9.9 - Sentinel Node Mapping in Breast Cancer: Drainage to a Single Node of the Inner Mammary Chain After Peritumoral Injection (Planar Imaging) 150
Case 9.10 - Sentinel Node Mapping in Breast Cancer: Drainage to Multiple Axillary and Inner Mammary Chain Nodes After Subareolar Injection (Planar and SPECT/CT Imaging) 151
Case 9.11 - Sentinel Node Mapping in Breast Cancer: Drainage to Multiple Axillary and Inner Mammary Chain Nodes After Subareolar Injection (Planar and SPECT/CT Imaging) 155
Case 9.12 - Sentinel Node Mapping in Breast Cancer: Drainage to Multiple Intramammary and Axillary Nodes After Subareolar and Intradermal Injection (Planar and SPECT/CT Imaging) 159
Case 9.13 - Sentinel Node Mapping in Breast Cancer: Drainage to Multiple Intramammary and Axillary Nodes After Subareolar and Intradermal Injection (Planar and SPECT/CT Imaging) 161
References 164

10 Preoperative and Intraoperative Lymphatic Mapping for Radioguided Sentinel Node Biopsy in Cutaneous Melanoma 169
Sergi Vidal-Sicart and Renato A. Valdés Olmos

10.1 Introduction 169
10.2 The Clinical Problem 169
10.3 Lymphatic Drainage of the Skin and Nodal Groups 170
10.4 Indications and Contraindications for Sentinel Lymph Node Biopsy 170
10.5 Radiocolloid Injection 171
10.6 Preoperative Imaging of Sentinel Lymph Nodes 172
10.7 Contribution of SPECT/CT 173
10.8 Intraoperative Imaging 174
10.9 Common and Rare Variants 175
10.10 Technical Pitfalls in Lymphatic Mapping 178
Clinical Cases
Case 10.1 - Sentinel Node Mapping in Melanoma of the Head and Neck: Drainage to “in Transit” Nodes in the Occipital Region (Planar Imaging) 181
Case 10.2 - Sentinel Node Mapping in Melanoma of the Abdomen: Drainage to Axillary and Parasternal Nodes (Planar Imaging) 182
Case 10.3 - Sentinel Node Mapping in Melanoma of the Back: Drainage to “in Transit” Paravertebral Nodes (Planar Imaging) 183
Case 10.4 - Sentinel Node Mapping in Melanoma of the Back: Bilateral Drainage to Left “in Transit” Subscapular and Left Axillary Nodes (Planar Imaging) 184
Case 10.5 - Sentinel Node Mapping in Melanoma of the Head and Neck: Drainage to Ipsilateral Cervical Nodes (Planar and SPECT/CT Imaging) 185
Case 10.6 - Sentinel Node Mapping in Melanoma of the Right Scapular Region: Drainage to Ipsilateral Cervical Nodes (Planar and SPECT/CT Imaging) 189

Case 10.7 - Sentinel Node Mapping in Melanoma of the Back: Drainage to Bilateral Supraclavicular Nodes and Ipsilateral Cervical and Axillary Nodes (Planar and SPECT/CT Imaging) 191
Case 10.8 - Sentinel Node Mapping in Melanoma of the Back: Drainage to Groin Nodes (Planar and SPECT/CT Imaging) 195
References 198

11 Preoperative and Intraoperative Lymphatic Mapping for Radioguided Sentinel Node Biopsy in Head and Neck Cancers 199
Renato A. Valdés Olmos, W. Martin C. Klop, and Oscar R. Brouwer

11.1 Introduction 199
11.2 The Clinical Problem 199
11.3 Indications and Contraindications for Sentinel Lymph Node Biopsy 199
11.4 Radiocolloid and Modalities of Injection 199
11.5 Preoperative Imaging of Sentinel Lymph Nodes 201
11.6 Lymphatic Drainage and Lymph Node Groups of the Neck 201
11.7 Intraoperative Detection of Sentinel Lymph Nodes 202
11.8 Contribution of SPECT/CT 204
11.9 Intraoperative Imaging 204
11.10 Common and Rare Variants 204
11.11 Technical Pitfalls 206
11.12 Accuracy of Radioguided Sentinel Lymph Node Biopsy 208
Clinical Cases
Case 11.1 - Sentinel Node Mapping in Carcinoma of the Hard Palate: Drainage to Bilateral Submandibolar Nodes After Submucosal Peritumoral Injection (Planar Imaging) 209
Case 11.2 - Sentinel Node Mapping in Oral Cavity Carcinoma: Drainage to Ipsilateral Submandibolar Nodes After Submucosal Peritumoral Injection (Planar Imaging) 211
Case 11.3 - Sentinel Node Mapping in Carcinoma of the Tongue: Drainage to Bilateral Cervical Nodes After Submucosal Peritumoral Injection (Planar Imaging) 213
Case 11.4 - Sentinel Node Mapping in Carcinoma of the Tongue: Drainage to Ipsilateral Cervical Nodes After Submucosal Peritumoral Injection (Planar Imaging) 215
Case 11.5 - Sentinel Node Mapping in Thyroid Carcinoma: Drainage to Ipsilateral Cervical Node After Intratumoral Injection (Planar and SPECT/CT Imaging) 216
Case 11.6 - Sentinel Node Mapping in Thyroid Carcinoma: Drainage to Bilateral Cervical Nodes After Intratumoral Injection (SPECT/CT Imaging) 217
Case 11.7 - Sentinel Node Mapping in Thyroid Carcinoma: Drainage to Multiple Ipsilateral Cervical Nodes After Intratumoral Injection (Planar and SPECT/CT Imaging) 219
Case 11.8 - Sentinel Node Mapping in Carcinoma of the Tongue: Drainage to Ipsilateral Cervical Nodes After Intratumoral Injection (Planar and SPECT/CT Imaging) 221
References 223

12 Preoperative and Intraoperative Lymphatic Mapping for Radioguided Sentinel Node Biopsy in Non-Small-Cell Lung Cancer 225
Giuseppe Boni, Franca M. A. Melfi, Gianpiero Manca, Federico Davini, and Giuliano Mariani

12.1 Introduction 225
12.2 The Clinical Problem 225
12.3 Indications for Sentinel Lymph Node Biopsy 226
12.4 Sentinel Lymph Node Biopsy Techniques in Non-Small-Cell Lung Cancer 226
12.5 Preoperative Imaging of Sentinel Lymph Nodes 227
12.6 Intraoperative Detection of Sentinel Lymph Nodes 227
12.7 Accuracy and Perspectives of Radioguided Sentinel Lymph Node Biopsy 227
References 228

13 Preoperative and Intraoperative Lymphatic Mapping for Radioguided Sentinel Node Biopsy in Cancers of the Gastrointestinal Tract 231
Carmen Balagué and José Luis Pallarés

13.1 Introduction 231
13.2 Sentinel Lymph Node Mapping in Esophagogastric Cancer 231
13.3 Sentinel Lymph Node Mapping in Colon Cancer 234
Clinical Cases
Case 13.1 - Sentinel Node Mapping in Rectal Cancer: Drainage to Hemorrhoidal Nodes After Submucosal Peritumoral Injection (Planar Imaging) 240
Case 13.2 - Sentinel Node Mapping in Cancer of Ascending Colon: Drainage to Lumbo-Aortic Nodes After Submucosal Peritumoral Injection (SPECT/CT Imaging) 241
Case 13.3 - Sentinel Node Mapping in Rectal Cancer: Drainage to Lumbo-Aortic Nodes After Submucosal Peritumoral Injection (Planar, SPECT/CT and Intraoperative Imaging) 242
Case 13.4 - Sentinel Node Mapping in Cancer of Ascending Colon: “Ex Vivo” Technique with Peritumoral Blue Dye and Radiocolloid Injection . . 245
References 247

14 Preoperative and Intraoperative Lymphatic Mapping for Radioguided Sentinel Node Biopsy in Cancers of the Female Reproductive System 249
Pilar Paredes and Sergi Vidal-Sicart

14.1 Introduction 249
14.2 The Clinical Problem 249
14.3 Lymphatic Drainage of Gynecological Tumors 250
14.4 Indications and Contraindications for Sentinel Lymph Node Biopsy 251
14.5 Modalities of Radiocolloid Injection 251
14.6 Preoperative Sentinel Lymph Node Imaging 253
14.7 Contribution of SPECT/CT 254
14.8 Intraoperative Detection of Sentinel Lymph Nodes 256
14.9 Intraoperative Imaging 256
14.10 Common and Rare Variants (with Possible Misinterpretation) 257
14.11 Technical Pitfalls in Lymphatic Mapping 259

Clinical Cases
Case 14.1 - Sentinel Node Mapping in Vulvar Carcinoma: Drainage to Bilateral Inguinal and Iliac Nodes After Intradermical Injection (Planar Imaging) 261
Case 14.2 - Sentinel Node Mapping in Endometrial Carcinoma: Drainage to One-Sided Lumbo-Aortic Nodes After Submucosal Peritumoral Injection (Planar Imaging) 262
Case 14.3 - Sentinel Node Mapping in Endometrial Carcinoma: Drainage to One-Sided Lumbo-Aortic Nodes After Intratumoral Injection (Planar and SPECT/CT Imaging) 264
Case 14.4 - Sentinel Node Mapping in Cervical Carcinoma: Drainage to Bilateral Iliac Nodes After Submucosal Peritumoral Injection (Planar and SPECT/CT Imaging) 266
References 268

15 Preoperative and Intraoperative Lymphatic Mapping for Radioguided Sentinel Node Biopsy in Cancers of the Male Reproductive System 269
Oscar R. Brouwer, Willem Meinhardt, Simon Horenblas, and Renato A. Valdés Olmos

15.1 Introduction 269
15.2 The Clinical Problem 269
15.3 Indications and Contraindications for Sentinel Lymph Node Biopsy 270
15.4 Radiocolloid and Modalities of Injection 270
15.5 Preoperative Imaging of Sentinel Lymph Nodes 272
15.6 Lymphatic Drainage 273
15.7 Intraoperative Detection of Sentinel Lymph Nodes 273
15.8 Contribution of SPECT/CT 273
15.9 Intraoperative Imaging 275
15.10 Common and Rare Variants 276
15.11 Technical Pitfalls 276
15.12 Accuracy of Radioguided Sentinel Lymph Node Biopsy 279
Clinical Cases
Case 15.1 - Sentinel Node Mapping in Prostate Carcinoma: Drainage to Bilateral Iliac Nodes After Peritumoral Injection (Planar Image) . . 280
Case 15.2 - Sentinel Node Mapping in Penile Carcinoma: Drainage to Bilateral Groin Nodes After Peritumoral Injection (Planar Image) 281
Case 15.3 - Sentinel Node Mapping in Testicle Cancer: Drainage to Lumbo-Aortic Nodes After Intratumoral Injection (Planar and SPECT/CT Imaging) 282
References 283

16 Preoperative and Intraoperative Lymphatic Mapping for Radioguided Sentinel Node Biopsy in Kidney and Bladder Cancers 285
Axel Bex, Oscar R. Brouwer, and Renato A. Valdés Olmos

16.1 Introduction 285
16.2 The Clinical Problem 285
16.3 Lymphatic Drainage and Nodal Groups in Renal Cancer 286
16.4 Lymphatic Drainage and Nodal Groups in Bladder Cancer 287
16.5 Radiocolloid Administration in Renal and Bladder Cancer 287

16.6 Preoperative Imaging of Sentinel Lymph Nodes in Renal and Bladder Cancer 288
16.7 Intraoperative Detection of Sentinel Lymph Nodes in Renal and Bladder Cancer 289
16.8 Contribution of SPECT/CT 290
16.9 Intraoperative Imaging 290
16.10 Accuracy of Radioguided Sentinel Lymph Node Biopsy in Renal Cancer 290
Clinical Cases
Case 16.1 - Sentinel Node Mapping in Renal Cancer: Drainage to Two Lumbo-Aortic Nodes After Intratumoral Injection (SPECT/CT Imaging) 291
Case 16.2 - Sentinel Node Mapping in Bladder Cancer: Drainage to Iliac Node After Peritumoral Injection (Planar and SPECT/CT Imaging) 292
References 293

Contributors

Filippo Antonica Center of Nuclear Medicine, University of Bari Medical School, Bari, Italy

Carmen Balagué General and Digestive Surgery, Hospital de la Santa Creu I Sant Pau, Barcelona, Spain

Roberto Bartoletti Oncologic Rehabilitation, IDI IRCCS, Rome, Italy

Axel Bex Urology, Division of Surgical Oncology, Netherlands Cancer Institute – Antoni van Leeuwenhoek Hospital, Amsterdam, the Netherlands

Giuseppina Bisogni Department of Physics "E. Fermi", University of Pisa, IFNR Section, Pisa, Italy

Pierluigi Bonatti Surgery, Santo Spirito Hospital, Rome, Italy

Giuseppe Boni Regional Center of Nuclear Medicine, University of Pisa Medical School, Pisa, Italy

Roberto Boni Regional Center of Nuclear Medicine, University of Pisa Medical School, Pisa, Italy

Oscar R. Brouwer Nuclear Medicine, Division of Diagnostic Oncology, Netherlands Cancer Institute – Antoni van Leeuwenhoek Hospital, Amsterdam, the Netherlands

Paolo Carcoforo Nuclear Medicine Unit, Diagnostic of Imaging and Laboratory Medicine Department, S. Anna University-Hospital of Ferrara, Ferrara, Italy

Serena Chiacchio Regional Center of Nuclear Medicine, University of Pisa Medical School, Pisa, Italy

Corrado Cittanti Nuclear Medicine Unit, Diagnostic Imaging and Laboratory Medicine Department, S. Anna University-Hospital of Ferrara, Ferrara, Italy

Federico Davini Nuclear Medicine, Department of Oncology Transplant and new Technology in Medicine University of Pisa Medical School, Pisa, Italy

Valerio Duce Regional Center of Nuclear Medicine, University of Pisa Medical School, Pisa, Italy

Joan Duch Hospital de la Santa Creu I Sant Pau, Barcelona, Spain

Valentina de Cristofaro Nuclear Medicine Unit, Diagnostic Imaging and Laboratory Medicine Department, S. Anna University-Hospital of Ferrara, Ferrara, Italy

Giovanni D'Errico Department of Nuclear Medicine, Medical Research, Rome, Italy

Alberto Del Guerra Department of Physics "E. Fermi", University of Pisa, Pisa, Italy

Rossella Di Stefano Cardiac Thoracic and Vascular Department, University of Pisa, Pisa, Italy

Paola Anna Erba Regional Center of Nuclear Medicine, University of Pisa Medical School, Pisa, Italy

Luciano Feggi Nuclear Medicine Unit, Diagnostic Imaging and Laboratory Medicine Department, S. Anna University-Hospital of Ferrara, Ferrara, Italy

Armando E. Giuliano Surgical Oncology, Samuel Oschin Comprehensive Cancer Institute, Cedars-Sinai Medical Center, Los Angeles, California, USA

Federica Guidoccio Regional Center of Nuclear Medicine, University of Pisa Medical School, Pisa, Italy

Simon Horenblas Urology, Netherlands Cancer Institute – Antoni van Leeuwenhoek Hospital, Amsterdam, the Netherlands

W. Martin C. Klop Head and Neck Oncology, Netherlands Cancer Institute – Antoni van Leeuwenhoek Hospital, Amsterdam, the Netherlands

Luisa Locantore Regional Center of Nuclear Medicine, University of Pisa Medical School, Pisa, Italy

Gianpiero Manca Regional Center of Nuclear Medicine, University of Pisa Medical School, Pisa, Italy

Lucio Mango Nuclear Medicine, S. Camillo Forlanini Hospital, Rome, Italy

Giuliano Mariani Regional Center of Nuclear Medicine, University of Pisa Medical School, Pisa, Italy

Sara Mazzarri Regional Center of Nuclear Medicine, University of Pisa Medical School, Pisa, Italy

Willem Meinhardt Urology, Netherlands Cancer Institute – Antoni van Leeuwenhoek Hospital, Amsterdam, the Netherlands

Franca M. A. Melfi Nuclear Medicine, Department of Oncology Transplant and new Technology in Medicine University of Pisa Medical School, Pisa, Italy

Omgo E. Nieweg Skin and Melanoma Center and Department of Surgery, Netherlands Cancer Institute - Antoni van Leeuwenhoek Hospital, Amsterdam, the Netherlands

Federica Orsini Regional Center of Nuclear Medicine, University of Pisa Medical School, Pisa, Italy

Marco Pagan Nuclear Medicine, Cristo Re Hospital, Rome, Italy

José Luis Pallarés General and Digestive Surgery, Hospital de la Santa Creu I Sant Pau, Barcelona, Spain

Stefano Panareo Nuclear Medicine Unit, Diagnostic Imaging and Laboratory Medicine Department, S. Anna University-Hospital of Ferrara, Ferrara, Italy

Pílar Paredes Nuclear Medicine, Hospital Clínic Barcelona, Barcelona, Spain

Chiara Peterle Nuclear Medicine Unit, Diagnostic Imaging and Laboratory Medicine Department, S. Anna University-Hospital of Ferrara, Ferrara, Italy

Siavash Rahimi Hystology, San Carlo IDI IRCCS Hospital, Rome, Italy

Ilaria Rambaldi Nuclear Medicine Unit, Diagnostic Imaging and Laboratory Medicine Department, S. Anna University-Hospital of Ferrara, Ferrara, Italy

Maria Antonia Renna Center of Nuclear Medicine, University of Bari Medical School, Bari, Italy

Virginia Rossetti Nuclear Medicine Unit, Diagnostic Imaging and Laboratory Medicine Department, S. Anna University-Hospital of Ferrara, Ferrara, Italy

Giuseppe Rubini Center of Nuclear Medicine, University of Bari Medical School, Bari, Italy

Ivan Santi Nuclear Medicine Unit, Diagnostic Imaging and Laboratory Medicine Department, S. Anna University-Hospital of Ferrara, Ferrara, Italy

Dalila Serafini Surgery, Santo Spirito Hospital, Rome, Italy

Martina Sollini Regional Center of Nuclear Medicine, University of Pisa Medical School, Pisa, Italy

Pieter J. Tanis Surgery, Academic Medical Center, Amsterdam, the Netherlands

Girolamo Tartaglione Nuclear Medicine, Cristo Re Hospital, Rome, Italy

Manuel Tredici Regional Center of Nuclear Medicine, University of Pisa Medical School, Pisa, Italy

Renato A. Valdés Olmos Nuclear Medicine, Division of Diagnostic Oncology, Netherlands Cancer Institute – Antoni van Leeuwenhoek Hospital, Amsterdam, the Netherlands

Guido Ventroni Nuclear Medicine, S. Camillo Forlanini Hospital, Rome, Italy

Sergi Vidal-Sicart Nuclear Medicine, Hospital Clínic Barcelona, Barcelona, Spain

Maurizio Giovanni Vigili ENT, San Carlo IDI IRCCS Hospital, Rome, Italy

The Anatomy and Physiology of Lymphatic Circulation

1

Pieter J. Tanis and Omgo E. Nieweg

1.1 Introduction

The lymphatic system, a complex network of ducts and nodes diffused throughout the human body, exhibits considerable variation that is comparable to other anatomical structures such as the arterial or venous system. Excess of interstitial fluid is returned to the blood circulation via the lymphatic system. In contrast to the blood circulation, lymph flow is unidirectional, away from the different tissues. Lymph is similar to blood plasma and contains immune cells as part of the defense against microorganisms. Furthermore, lymphatic capillaries in the intestinal villi absorb the fats and fat-soluble vitamins that give the lymph its milky appearance in this part of the lymphatic system.

In the last few centuries, the lymphatic system has become an important field of interest in oncology. The lymphatic system functions in two opposing ways in cancer: defense against circulating tumor cells, but on the other hand a route for metastasis and a site of tumor growth if the defense mechanism fails. The significant impact of lymphatic dissemination on the staging, treatment, and outcome of solid cancers has stimulated investigations aimed at gaining more insight into several aspects of the lymphatic system.

The aim of this chapter is not to provide a complete overview of lymphatic anatomy and physiology, but rather to point out some topics that are relevant for clinicians involved in lymphatic mapping of cancer and to outline recent developments and subjects for further research.

1.2 The Physiology of Lymph Flow

Lymph flow starts with absorption of interstitial fluid through the inter-endothelial junctions of the lymphatic capillaries, which function like valves [1]. Small particles up to 25 nm in size may enter the openings at this level, whereas larger particles are transported through the lymphatic endothelium by pinocytosis. Lymphatic capillaries are kept open by collagen filaments attached to the surrounding connective tissue. The osmotic pressure gradient is important for filling lymphatic capillaries. Since the capillaries have no valves, the lymph fluid may flow either way.

The next lymphatic structures are the collecting lymphatic vessels. In these vessels, numerous bicuspid semilunar valves positioned every 2–3 mm prevent backflow of lymph [2]. There is active propulsion of lymph by longitudinal and circular layers of smooth muscle, which contract 10–15 times per minute. Lymphatic peristalsis is regulated by several delicate mechanisms [3, 4]. Because of the presence of valves, intermittent external pressure is another mechanism for unidirectional flow.

Subsequently, lymph flows from the lymphatic collecting vessels into the marginal sinus of the lymph nodes. From this subcapsular sinus, lymph subsequently drains into medullary sinuses between the germinal centres, where it comes into contact with numerous phagocytic cells. The so filtered lymph is collected at the lymph node hilum into the efferent lymphatic vessel. Different types of relationships exist between lymph vessels and lymph nodes, in which the germinal centres may be bypassed [5, 6]. A few large lymphatic trunks eventually transport the daily production of 2–4 L of lymph from the whole body into the venous circulation at the junction of the internal jugular and subclavian veins [7].

P. J. Tanis (✉)
Surgery
Academic Medical Center
Amsterdam, the Netherlands
e-mail: p.j.tanis@amc.uva.nl

G. Mariani et al. (eds.), *Atlas of Lymphoscintigraphy and Sentinel Node Mapping*,
DOI 10.1007/978-88-470-2766-4_1

1.3 Anatomy of the Lymphatic System

The lymphatic systems of the different tissues and organs are quite similar, although some specific features exist. Lymphatic capillaries are abundant in the skin, but also in other covering structures such as the periosteum of bone and joint capsules. Furthermore, rich lymphatic plexuses are found beneath the mesothelium of the pleural, peritoneal, and pericardial cavities, and beneath the mucosa of the digestive, respiratory, and genitourinary tracts. Most solid organs like the liver, spleen, adrenal gland, kidney, prostate, testis, uterus, and ovary have a superficial or subserous lymphatic plexus [8]. In contrast, deep lymphatics within the parenchyma have only been clearly demonstrated in the adrenal gland, kidney, and ovary. Lymphatic capillaries are probably absent in the central nervous system, striated muscles, eyeball, and inner ear. The collecting lymphatic vessels are present in nearly all vascularized tissues and are often situated in close relationship to the blood vessels. The interested reader is referred to one of the classical textbooks for an extensive description of the lymphatic systems in the human body [8, 9]. For the purpose of this chapter, the two most extensively studied lymphatic systems in the era of sentinel lymph node biopsy (SLNB) will be described in more detail, namely the breast and the skin.

1.3.1 Lymphatics of the Breast

First of all, it should be realized that study of the lymphatic drainage of the breast is still ongoing, though it started as long ago as the end of the 18th century [10]. Current research is mainly focused on unravelling the network of extensively communicating small lymphatic vessels from both the overlying skin and parenchyma of the different regions of the mammary gland. These vessels join into several collecting ducts that are connected to specific lymph nodes within each separate lymph node basin. This broad anatomical concept originates from the numerous lymphatic drainage patterns that have been observed during lymphatic mapping of breast cancer in the last two decades. These clinical observations do not match with more simplified concepts from the past. The most well known of these latter descriptions originates from Sappey. He assumed a centripetal lymph flow from the mammary ducts to a common subareolar plexus. From this lymphatic plexus, a medial and a lateral collecting vessel were assumed to pass to the axilla. This system was suggested to have multiple anastomoses with a superficial system consisting of dermal lymphatics from the upper anterolateral chest wall, which also drain to the axilla. Sappey and others, like Rouvière, denied the so-called posterior lymphatic network of the breast [11]. This posterior network, which was originally described at the end of the 18th century, mainly drains

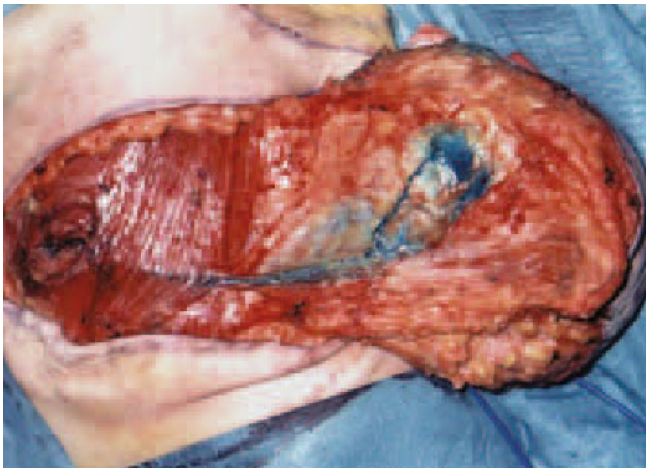

Fig. 1.1 A blue-stained lymphatic running from a tumor in the upper outer quadrant of the left breast along the posterior surface of the breast, through the pectoral muscle to the third intercostal space. This lymphatic was seen during mastectomy after removal of two axillary SLNs and of three internal mammary chain lymph nodes

to the internal mammary chain and to interpectoral (Rotter) lymph nodes [6]. Collecting lymphatic vessels at the posterior aspect of the breast draining to these lymphatic basins may be encountered in blue-dye mapping during mastectomy (Fig. 1.1).

Several other nodal basins draining the breast have subsequently been described: supraclavicular lymph nodes, intercostal nodes, the contralateral internal mammary chain, intramammary nodes, paramammary (Gerota) nodes at the level of the inframammary fold (Fig. 1.2), and even the contralateral axilla in nonphysiological circumstances [12–16]. Furthermore, the axilla, the main lymphatic basin draining the breast, has been subdivided into external mammary lymph nodes, scapular nodes, central nodes, axillary vein nodes, and subclavicular nodes [9, 17]. Drainage patterns from each region of the breast have been quantified using lymphoscintigraphic data [18, 19]. The anatomical relation between the lymphatic drainage of the breast and of the arm at the level of the axilla has been increasingly studied in recent years [20]. A clinical application of combined lymphatic mapping of the arm and breast is axillary reverse mapping [21]. The objective of this approach is to identify and subsequently spare lymphatic ducts and nodes that are essential for lymph drainage of the upper extremity during breast SLNB, in order to prevent lymphedema. Initial results have shown that specific regions of the breast and arm may have a common sentinel lymph node (SLN).

1.3.2 Lymphatics of the Skin

The skin has a very rich lymphatic network, which is connected to the main lymphatic basins in the groin, axilla, and

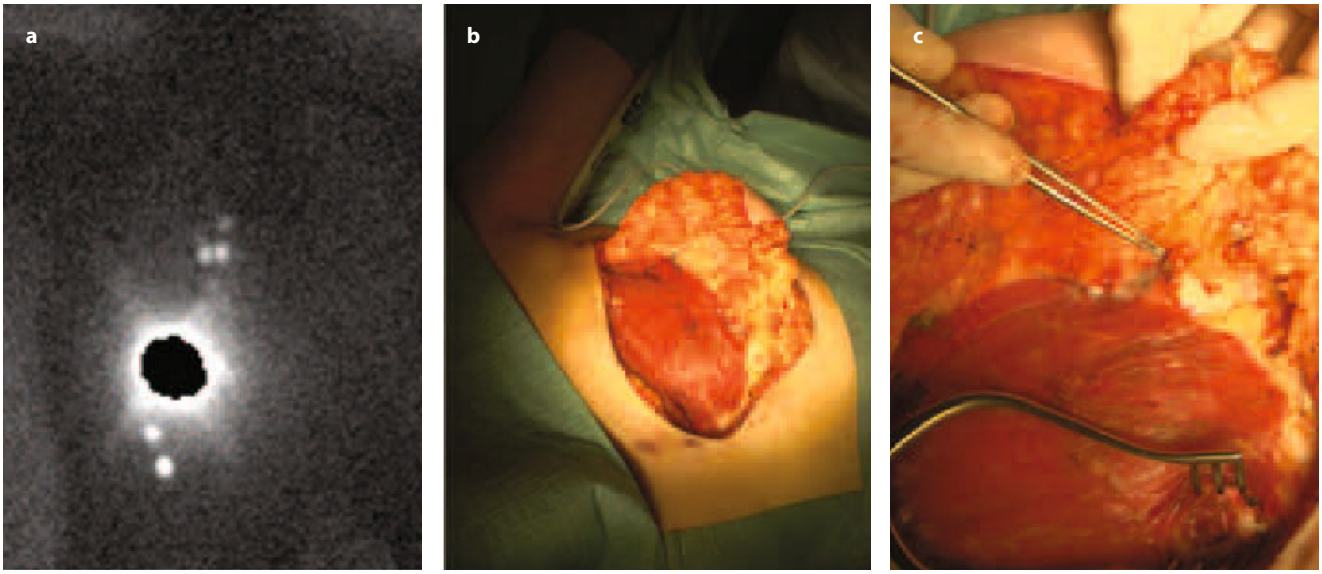

Fig. 1.2 Paramammary lymph node. **a** Lymphoscintigraphy using technetium-99 (^{99m}Tc)-nanocolloid with direct drainage to paramammary lymph nodes at the level of the inframammary fold. **b** (overview), **c** (detail), Intraoperative identification of a paramammary lymph node with a tiny blue afferent lymphatic duct during mastectomy indicated by the tweezers; an internal mammary chain SLN was also retrieved

neck, but also to several less well-known lymph node locations. The SLN concept has contributed substantially to current knowledge of lymphatic drainage of the skin. Clinical application of lymphatic mapping using blue dye started in the late 1980s in patients with melanoma, and is now one of the most frequent indications for SLNB besides breast cancer. Prediction of lymphatic drainage from the truncal skin has for a long time been defined according to Sappey's lines (midline and transverse at the umbilicus). Recently, analysis of more than 5,000 lymphoscintigrams from the Melanoma Institute of Australia has shown that drainage often crosses these lines, which therefore have a much greater zone of ambiguity than postulated by Sappey [22]. Several unexpected drainage routes have in fact been visualized to lymph nodes in the epitrochlear fossa, popliteal fossa, triangular intermuscular space, bicipital sulcus, and subcutaneously in the flank or adjacent to the areola [23]. Studying lymphatic drainage in a canine torso, Suami and colleagues found perforating lymph vessels originating from the skin, which penetrated the abdominal wall and directly drained into para-aortic lymph nodes [24].

Similar to subdivision of the axillary basin, the groin has been subdivided into different zones [25]. The groin lymph nodes receive lymph from the leg, the trunk, and the external genitals. Lymphatic drainage patterns to the groin with corresponding first- and second-tier lymph nodes differ depending on the specific area of the skin [26, 27]. Collecting lymphatic vessels from the limb may also bypass the groin to para-iliac lymph nodes in the pelvis. Miura and colleagues defined the great and small saphenous lymphatic vessels and a third deep lymphatic drainage ascending along the main three arteries of the lower leg with direct drainage to the inferior iliac nodes [28].

Drainage from the upper part of the trunk and upper limb is rather complex, given the potential connections to lymphatic basins in the neck besides the axilla [29]. The neck has been traditionally subdivided into different nodal levels, to enable selective neck dissection for cancers from different skin areas. This relatively rough anatomical classification has been refined in the SLN era. Lymphatic mapping has revealed an almost inexhaustible variation from the skin of the head and neck to the numerous neighboring lymph nodes. Lymphatic drainage patterns may be even discordant over time in the head and neck, as demonstrated by serial repeat lymphoscintigraphy [30, 31]. These observations are probably related to physiological changes, technical shortcomings, or the close anatomical relationships in the head and neck region.

1.4 Lymphatic Visualization Techniques

The techniques that are used to visualize the lymphatic system, as well as the physiological conditions in which the studies are performed, have significant implications for the information that is gained. Anatomists often use cadavers, while surgeons and nuclear medicine physicians examine the lymphatic system under the physiological conditions of a living human. Differences in physiologic conditions or age may have contributed to conflicting anatomical theories, for example by studying the lymphatic anatomy of the mammary gland in pregnant women or fetuses [32, 33].

Nevertheless, the most important determinants for unravelling the anatomy of the lymphatic system are the type of tracer and injection site. Anatomists have used materials like air, oil, milk, Indian ink, and mercury with subsequent macroscopic visualization of the relatively large lymphatic vessels. This approach has several methodological limitations related to the dilution of the tracer, accuracy of tissue dissection, and size restrictions of macroscopic identification.

Lymphangiographic studies using direct tracer administration into the lymphatic vessel are intrinsically different from techniques based on interstitial tracer injection into the tissues of interest, with subsequent tracer uptake into the lymphatic capillaries. The latter approach is considered to mirror more closely the actual clinical conditions, as it reflects the normal physiological mechanisms of lymph formation at the site of interest.

The introduction of radiopharmaceuticals for lymphatic mapping has constituted an important step forward in refinement of the lymphatic anatomy, by obviating the need for macroscopic visualization. By using colloidal gold-198 (^{198}Au) particles of about 5 nm in size, pioneers like Hultborn, Turner-Warwick, and Vendrell-Torné were able to determine dominant and minor lymphatic drainage routes from different regions of the breast [34–36]. Suami et al recently published anatomical cadaver studies based on techniques combining both types of approach [37]. Very small lymph vessels were microscopically cannulated and injected with a radio-opaque contrast medium in both antegrade and retrograde directions. After completion of all injections, radiographs were made of the whole specimen and parallel slices, followed by computerized image processing. Three-dimensional images of the arrangement of lymphatic ducts could even be obtained by using high-resolution computed tomographic lymphangiography [38].

Besides dyes and radiocolloids, fluorescent tracers in the near-infrared spectrum are increasingly being used for lymphatic mapping. Parungo and colleagues used quantum dots and the dye HSA800 to study lymphatic drainage from the peritoneal cavity in rats [39]. These authors were able to identify primary drainage to the celiac, superior mesenteric, and periportal lymph nodes, with rerouting directly to intrathoracic nodes via chest wall lymphatics after bowel resection. Using the same technique, they also demonstrated that the highest mediastinal lymph nodes of station I are the first-echelon nodes of the pleural space in rats and pigs [40]. By using two different quantum dots, two separate lymphatic drainage pathways can be simultaneously visualized in a two-color image, as demonstrated by a Japanese group [41]. Such technique enables further exploration of overlapping lymphatic drainage patterns. Indocyanine green (ICG) fluorescence lymphography is increasingly being used in routine clinical practice of SLNB, but is also a promising method to increase our knowledge of physiology of the lymphatic system [42].

References

1. Schmid-Schonbein GW (1990) Microlymphatics and lymph flow. Physiol Rev 70:987–1028
2. Foster RS Jr (1996) General anatomy of the lymphatic system. Surg Oncol Clin N Am 5:1–13
3. Aukland K, Reed RK (1993) Interstitial-lymphatic mechanisms in the control of extracellular fluid volume. Physiol Rev 73:1–78
4. Olszewski WL, Engeset A (1979) Lymphatic contractions. N Engl J Med 300:316
5. Ludwig J (1962) Ueber Kurschlusswege der Lymphbahnen und ihre Beziehungen zur lymphogen Krebsmetastasierung. Pathol Microbiol 25:329–334
6. Tanis PJ, Nieweg OE, Valdes Olmos RA et al (2001) Anatomy and physiology of lymphatic drainage of the breast from the perspective of sentinel node biopsy. J Am Coll Surg 192:399–409
7. Browse NL, Stewart G (1985) Lymphoedema: pathophysiology and classification. J Cardiovasc Surg 26:91–106
8. Gray H (1918) The lymphatic system. In: Gray H (ed) Anatomy of the human body. Lea & Febiger, Philadelphia. www.bartleby.com/107/. Accessed 7 June 2012
9. Haagensen CD (1972) Lymphatics of the breast. In: Haagensen CD, Feind KR, Herter FP et al (eds) The lymphatics in cancer. WB Saunders Company, Philadelphia, pp 300–387
10. Blumgart EI, Uren RF, Nielsen PM et al (2011) Lymphatic drainage and tumour prevalence in the breast: a statistical analysis of symmetry, gender and node field independence. J Anat 218:652–659
11. Tanis PJ, van Rijk MC, Nieweg OE (2005) The posterior lymphatic network of the breast rediscovered. J Surg Oncol 91:195–198
12. Barranger E, Montravers F, Kerrou K et al (2004) Contralateral axillary sentinel lymph node drainage in breast cancer: a case report. J Surg Oncol 86:167–169
13. Caplan I (1975) Revision anatomique du système lymphatique de la glande mammaire (a propos de 200 cas). Bull Assoc Anat 59:121–137
14. Perre CI, Hoefnagel CA, Kroon BB et al (1996) Altered lymphatic drainage after lymphadenectomy or radiotherapy of the axilla in patients with breast cancer. Br J Surg 83:1258
15. Tanis PJ, Nieweg OE, Valdes Olmos RA et al (2002) Impact of non-axillary sentinel node biopsy on staging and treatment of breast cancer patients. Br J Cancer 87:705–710
16. van der Ploeg IM, Oldenburg HS, Rutgers EJ et al (2010) Lymphatic drainage patterns from the treated breast. Ann Surg Oncol 17:1069–1075
17. Spratt JS (1979) Anatomy of the breast. Major Probl Clin Surg 5:1–13
18. Blumgart EI, Uren RF, Nielsen PM et al (2011) Predicting lymphatic drainage patterns and primary tumour location in patients with breast cancer. Breast Cancer Res Treat 130:699–705
19. Estourgie SH, Nieweg OE, Valdes Olmos RA et al (2004) Lymphatic drainage patterns from the breast. Ann Surg 239:232–237
20. Pavlista D, Eliska O (2012) Relationship between the lymphatic drainage of the breast and the upper extremity: a postmortem study. Ann Surg Oncol 24 April, epub ahead of print
21. Noguchi M (2010) Axillary reverse mapping for breast cancer. Breast Cancer Res Treat 119:529–535
22. Reynolds HM, Dunbar PR, Uren RF et al (2007) Three-dimensional visualisation of lymphatic drainage patterns in patients with cutaneous melanoma. Lancet Oncol 8:806–812
23. Roozendaal GK, de Vries JD, van Poll D et al (2001) Sentinel nodes outside lymph node basins in patients with melanoma. Br J Surg 88:305–308
24. Suami H, O'Neill JK, Pan WR et al (2008) Perforating lymph vessels in the canine torso: direct lymph pathway from skin to the deep lymphatics. Plast Reconstr Surg 121:31–36

25. Daseler EH, Anson BJ, Reimann AF (1948) Radical excision of the inguinal and iliac lymph glands; a study based upon 450 anatomical dissections and upon supportive clinical observations. Surg Gynecol Obstet 87:679–694
26. Leijte JA, Valdes Olmos RA, Nieweg OE et al (2008) Anatomical mapping of lymphatic drainage in penile carcinoma with SPECT-CT: implications for the extent of inguinal lymph node dissection. Eur Urol 54:885–890
27. van der Ploeg IM, Kroon BB, Valdes Olmos RA et al (2009) Evaluation of lymphatic drainage patterns to the groin and implications for the extent of groin dissection in melanoma patients. Ann Surg Oncol 16:2994–2999
28. Miura H, Ono S, Nagahata M et al (2010) Lymphoscintigraphy for sentinel lymph node mapping in Japanese patients with malignant skin neoplasms of the lower extremities: comparison with previously investigated Japanese lymphatic anatomy. Ann Nucl Med 24:601–608
29. Veenstra HJ, Klop WM, Speijers MJ et al (2012) Lymphatic drainage patterns from melanomas on the shoulder or upper trunk to cervical lymph nodes and implications for the extent of neck dissection. Ann Surg Oncol 11 May, epub ahead of print
30. Kapteijn BA, Nieweg OE, Valdes Olmos RA et al (1996) Reproducibility of lymphoscintigraphy for lymphatic mapping in cutaneous melanoma. J Nucl Med 37:972–975
31. Willis AI, Ridge JA (2007) Discordant lymphatic drainage patterns revealed by serial lymphoscintigraphy in cutaneous head and neck malignancies. Head Neck 29:979–985
32. Pan WR, Suami H, Taylor GI (2008) Senile changes in human lymph nodes. Lymphat Res Biol 6:77–83
33. Suami H, Pan WR, Taylor GI (2009) Historical review of breast lymphatic studies. Clin Anat 22:531–536
34. Hultborn A, Hulten L, Roos B et al (1971) Topography of lymph drainage from mammary gland and hand to axillary lymph nodes. Acta Radiol Ther Phys Biol 10:65–72
35. Turner-Warwick RT (1959) The lymphatics of the breast. Br J Surg 46:574–582
36. Vendrell-Torné E, Setoain-Quinquer J, Domenech-Torne FM (1972) Study of normal mammary lymphatic drainage using radioactive isotopes. J Nucl Med 13:801–805
37. Suami H, Pan WR, Mann GB et al (2008) The lymphatic anatomy of the breast and its implications for sentinel lymph node biopsy: a human cadaver study. Ann Surg Oncol 15:863–871
38. Pan WR, Rozen WM, Stella DL et al (2009) A three-dimensional analysis of the lymphatics of a bilateral breast specimen: a human cadaveric study. Clin Breast Cancer 9:86–91
39. Parungo CP, Soybel DI, Colson YL et al (2007) Lymphatic drainage of the peritoneal space: a pattern dependent on bowel lymphatics. Ann Surg Oncol 14:286–298
40. Parungo CP, Colson YL, Kim SW et al (2005) Sentinel lymph node mapping of the pleural space. Chest 127:1799–1804
41. Hama Y, Koyama Y, Urano Y et al (2007) Simultaneous two-color spectral fluorescence lymphangiography with near infrared quantum dots to map two lymphatic flows from the breast and the upper extremity. Breast Cancer Res Treat 103:23–28
42. Unno N, Nishiyama M, Suzuki M et al (2010) A novel method of measuring human lymphatic pumping using indocyanine green fluorescence lymphography. J Vasc Surg 52:946–952

The Pathophysiology of Lymphatic Circulation in Different Disease Conditions

2

Rossella Di Stefano, Paola Anna Erba, and Giovanni D'Errico

2.1 Introduction

The lymphatic circulation should be considered as part of the peripheral cardiovascular system, as it interlinks closely with blood circulation both at its origins (the interstitial space) and at its final drainage point (the thoracic duct). To a large extent, the anatomy of lymphatic channels parallels that of the veins, and the two systems show many similarities in structure and function.

The lymphatic circulation includes the lymph, the lymphatic vessels, the lymph nodes (stations along the drainage route where fluid and cell exchanges between blood and lymph occur), and other lymphoid tissue, particularly the spleen and bone marrow. Through its own specialized cell, the lymphocyte, a close relationship exists between the peripheral lymphatic system, blood circulation (Fig. 2.1), spleen, and liver. Therefore, while lymph drainage has a predominant "plumbing" role, the lymphatic circulation also has important immunological roles. Fig. 2.2 schematically presents the distribution of the lymphatic system, as represented by the main lymphatic channels and lymph node stations throughout the body.

At the distal capillaries, the systemic circulation loses about 2–4 L of fluid and about 100 g of protein daily into the interstitium. The normal physiology of lymphatics deals with draining these materials, which cannot return to the bloodstream directly, from the tissue spaces. Colloids, several types of cells (extravasated red cells, macrophages, lymphocytes, tumor cells, etc.), bacteria, and other microorganisms are channeled through the lymphatics, presumably as a protective mechanism to prevent noxious agents from directly entering the bloodstream. This is the reason why cellulitis and erysipelas can be recurrent problems with lymphedema. Similarly, inorganic materials such as carbon and silica are removed by the lymphatics, as witnessed by the black-stained pulmonary lymph nodes in coal miners.

Fig. 2.3 schematically presents the structure of the initial lymphatic circulation. The lymphatic vascular network consists of smaller blind-ended capillaries and larger collecting lymphatic vessels. The lymphatic capillaries are composed of a single layer of overlapping endothelial cells and lack a continuous basement membrane and pericytes (i.e., the smooth muscle-like contractile cells that wrap around the outer surface of blood vessels). Therefore, the lymphatic capillaries are highly permeable to interstitial fluid and macromolecules, so that, when the surrounding interstitial pressure changes, these vessels either expand and fill with lymph or contract and push lymph along [1]. These lymphatic capillaries first drain into precollecting lymphatic vessels, which will eventually merge into larger secondary collecting lymphatic vessels covered by smooth muscle cells, which provide contractile activity to assist lymph flow, and possess a continuous basement membrane. Tissue fluid collected in the larger collecting lymphatics drains into the thoracic duct and is then returned to the blood circulation through lymphatic–venous connections at the junction of the jugular and subclavian veins.

Under normal circumstances, water acts predominantly as a solvent or vehicle for the colloids, cells, and other materials that can be drained only via the lymph route. Nevertheless, lymphatics also serve as an "overflow pipe" to drain excess interstitial fluid. This role of the lymphatic circulation as a "safety valve" against fluid overload incriminates the lymphatic system somehow in every form of edema.

R. Di Stefano (✉)
Cardiac Thoracic and Vascular Department
University of Pisa, Pisa, Italy
e-mail: r.distefano@ao-pisa.toscana.it

G. Mariani et al. (eds.), *Atlas of Lymphoscintigraphy and Sentinel Node Mapping*,
DOI 10.1007/978-88-470-2766-4_2

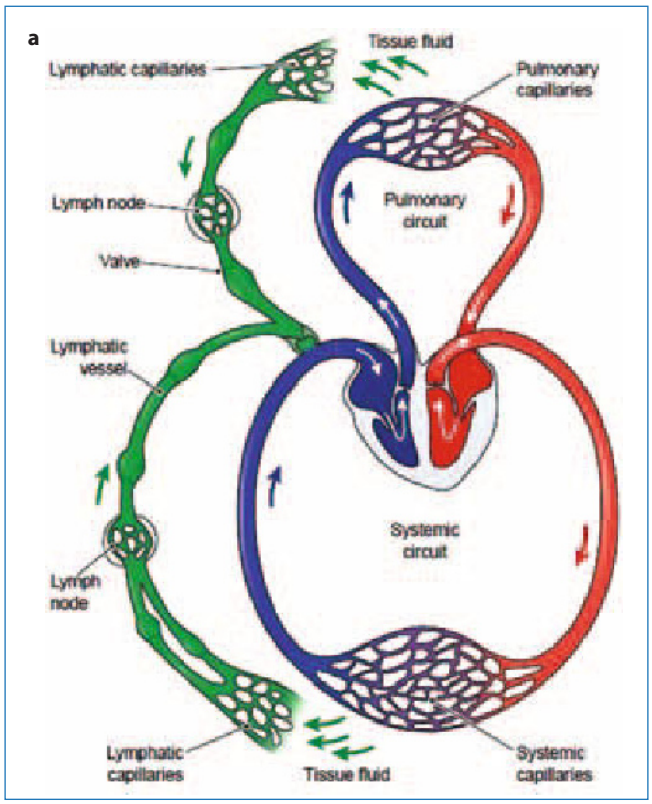

Fig. 2.1 **a** Schematic representation of the vascular circulation (arterial system, *red*; venous system, *blue*) and of lymphatic circulation (*green*), and their interrelationship. A net of lymphatic capillaries drains tissue fluid and macromolecules from tissues through major lymphatic vessels and lymph nodes. The major thoracic duct receives lymph originating throughout the whole body, but not from the right arm, right portion of the thorax, and neck and head, where lymph is directly collected by the right lymphatic duct. Therefore, the lymph is driven into the venous system through the left subclavian and the right subclavian veins, respectively; from http://encyclopedia.lubopitko-bg.com/Lymphatic_Circulation.html, with permission. **b** Magnified schematization of the connections between vascular and lymphatic circulation at the site of peripheral arteriovenous anastomosis; adapted from http://www.medars.it/galleries/lymphnodes_4.htm

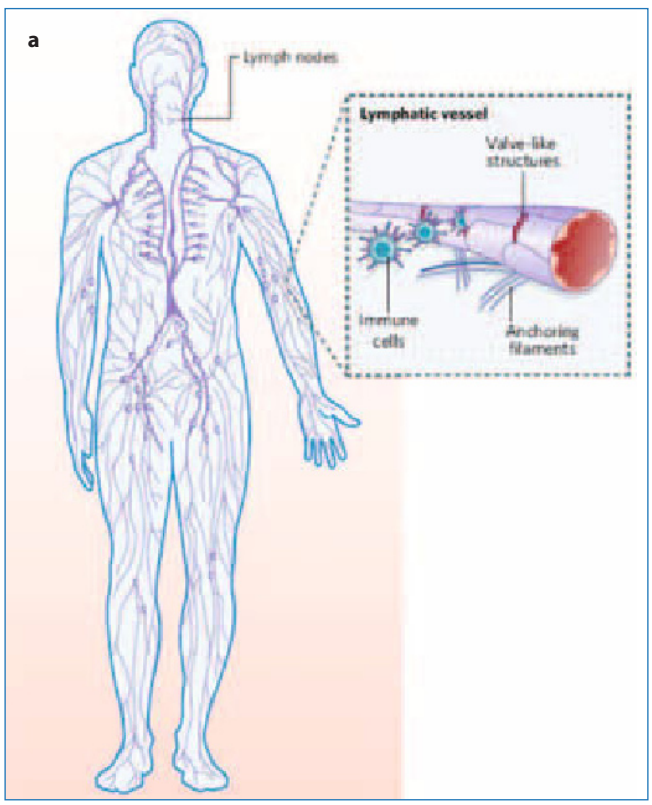

Fig. 2.2 Schematic representation of the lymphatic system throughout the body. **a** General overview, regardless of sex; the insert shows the vessels of the lymphatic system, which present valve-like structures that let immune cells pass in and out; adapted from [1]. **b** Overview of lymphatic circulation in women, showing the especially rich system draining the mammary gland, mostly merging to the periareolar plexus of Sappey, then draining to axillary lymph nodes; reproduced from http://www.photo-dictionary.com/phrase/7712/lymphatic-system.html

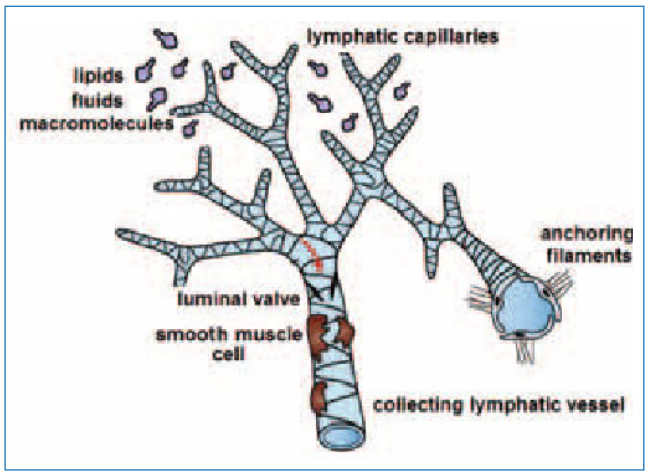

Fig. 2.3 Schematic representation of the initial lymphatic vascular network. The lymphatic capillaries are composed of a single layer of overlapping endothelial cells and lack a continuous basement membrane. Collecting lymphatic vessels have smooth muscle cells, a basement membrane, and luminal valves that prevent backflow of lymph. The unique structure of capillary lymphatic vessels accounts for the uptake of interstitial fluid, macromolecules, cells, and lipids that filtrate continuously from the blood capillary network; adapted from [2]

2.2 Lymphatic Circulation and Lipid Absorption

Lymphatic circulation is essential for the absorption of lipids from the intestine. The major products of lipid digestion (fatty acids and 2-monoglycerides) enter the enterocyte by simple diffusion and/or via a specific fatty acid transporter protein in the membrane. Once inside the enterocyte, fatty acids and monoglyceride are transported into the endoplasmic reticulum, where they are used to synthesize triglycerides. Beginning in the endoplasmic reticulum and continuing in the Golgi apparatus, triglycerides are packaged with cholesterol, lipoproteins, and other lipids, into particles called chylomicrons. Transport of lipids into the circulation is different from what occurs with sugars and amino acids. In fact, instead of being absorbed directly into capillary blood, chylomicrons are transported first into the lymphatic vessels that penetrate each intestinal villus.

Chylomicron-rich lymph then drains into the lymphatic system, which rapidly flows into the blood. Blood-borne chylomicrons are rapidly disassembled and their constitutent lipids utilized throughout the body. When large numbers of chylomicrons are being absorbed, lymph draining from the small intestine has a milky appearance, such that the mesenteric lymphatics are easy to see (first described by Aselli in the 17th century as venae alba et lacteae or "white veins").

These intestinal lymphatics offer a specialized absorption pathway through which dietary lipids, fat-soluble vitamins, lipophilic xenobiotics, and lipophilic drugs can gain access to the systemic circulation. Compounds absorbed by the intestinal lymphatics drain via the cisterna chyli and the thoracic duct, thus entering the systemic circulation at the junction of the left internal jugular vein with the left subclavian vein, thereby avoiding potential first-pass metabolism. Consequently, drug transport via the intestinal lymphatics may confer delivery advantages in terms of increased bioavailability and the possibility of directing delivery to the lymphatic system.

2.3 Pathophysiology of Lymph Drainage Failure

The physiology of lymphatic circulation requires three intimately interconnected steps: (1) transport of fluid and other materials (prelymph) across the interstitial space and into the initial lymphatics; (2) movement of lymph through the network of noncontractile initial lymphatics; and (3) active pumping of lymph through a series of contractile collecting trunks. Lower-limb drainage is relatively slow at rest with the legs supine; the most potent stimulus to lymph flow is weight bearing, and in particular activation of the calf muscle pumps during walking. This is likely due to a sudden increase in lymphatic preload, with a consequent increase in intrinsic pumping, rather than passive squeezing of lymphatics by the muscles (as happens with the veins) generating lymph drainage in the legs.

2.4 Edema

Edema is an excess of interstitial fluid. The volume of interstitial fluid must increase by over 100% before edema becomes clinically detectable. Edema develops when the rate of capillary filtration rate exceeds that of lymphatic drainage for a sufficient period, a condition that results from an imbalance between capillary filtration and lymph drainage:

$$dv/dt = F_v - F_l$$

where dv/dt is the rate of swelling, F_v is the net capillary filtration rate, and F_l is lymph flow.

Therefore, it follows that the pathogenesis of any edema involves either a high filtration rate or a low lymph flow, or a combination of the two. Elevation of capillary pressure is usually secondary to chronic elevation of venous pressure caused by heart failure, fluid overload, or deep vein thrombosis. Reduced plasma colloid osmotic pressure (e.g., hypoproteinemia) raises the net filtration rate and lymph flow; changes in capillary permeability (e.g., inflammation) increase the escape of protein into the interstitium, and water follows osmotically. Impairment of lymph drainage results

Table 2.1 Mechanisms and causes of lymph drainage failure

Mechanism	Causes
Reduction of lymph-conducting pathways	Aplasia–hypoplasia of the whole vessel Acquired obliteration of the lymphatic lumen
Poorly functioning pathways	Failure of pump contractility
Obstructed pathways	Scar from lymphadenectomy, radiation therapy, or infection
Incompetent lymphatics with reflux	Megalymphatics Lymphatic hyperplasia

in the predominant accumulation of protein and water in the interstitial space, since lymph is the sole route for returning escaped protein to the plasma.

Most edemas arise from increased capillary filtration overwhelming lymph drainage; therefore, any edema incriminates the lymphatic system through its failure to keep up with demand. Edema is initially soft and pitting, then hard, non-pitting, and accompanied by skin thickening. Impairment of the local immune response leads to recurrent skin infections, further insult to the tissue, and worsening of edema. Chronic limb enlargement causes functional impairment, disfiguration of the limb, and severe psychological damage.

2.5 Lymphedema

Lymphedema is an edema arising principally from a failure of lymph drainage, which can be caused by a number of factors (Table 2.1, Fig. 2.4).

First, there may be an intrinsic abnormality of the lymph-conducting pathways. Such conditions are referred to as primary lymphedema, which means that no other identifiable causes can be found. Primary lymphedema occurs because of imperfect development of the lymphatic vascular system in utero. It can be familial (as with Milroy's disease and Meige's syndrome), or genetic, such as that associated with Turner's and Noonan's syndromes or the congenital vascular syndrome Klippel–Trénaunay, where malformed lymphatics coexist with an aberrant venous system. Sporadic cases of primary lymphedema are more frequent than the familial or genetic-associated forms. Distal hyplopasia of the lymphatics of the leg is the most common cause of primary lymphedema of the lower limbs.

The identification of mutant genes in hereditary human lymphedemas has defined some crucial pathways during lymphovascular development. For example, one of the most common primary lymphedemas, lymphedema–distichiasis syndrome (LD), is an autosomal dominant disorder with variable expression. It is caused by mutations in the *RBFOX2* (*FOXC2*) gene, which codes for FOXC2, a transcription factor involved in development of the lymphatic and vascular system [4]. LD is characterized by late childhood or pubertal onset lymphedema of the limbs, and by distichiasis

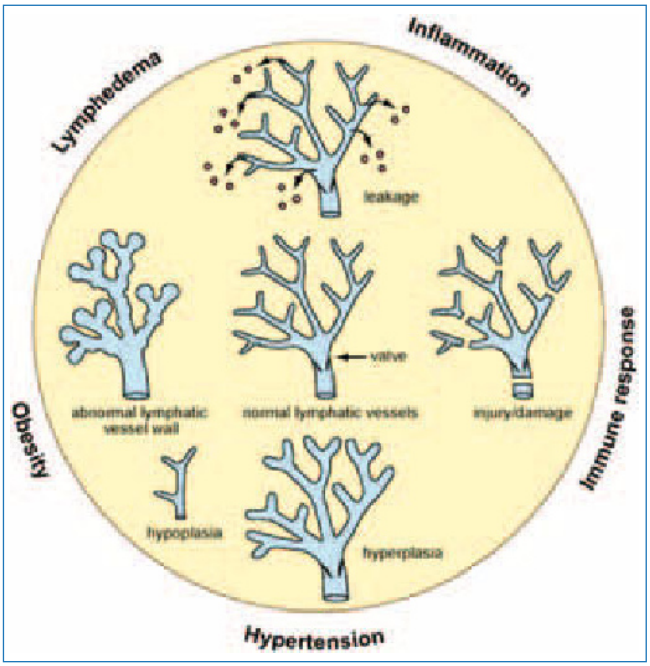

Fig. 2.4 Different types of alterations in the lymphatic vascular network can lead to a variety of pathological conditions or can impact the inflammatory or immune responses. Hypoplastic, hyperplastic, mispatterned, or damaged (e.g., mechanical) lymphatics can result in different types of primary or secondary lymphedema. Leaky lymphatics can also promote obesity; adapted from [2]

(double row of eyelashes). While the latter is the most common expression of LD, venous insufficiency occurs in half of patients. Other associations have been reported, including congenital heart disease, ptosis, cleft lip/palate, and spinal extradural cysts.

Another example of genetic primary lymphedema is provided by Milroy's disease, which is characterized by early-onset congenital lymphedema. In this syndrome, heterozygous missense mutations in the *FLT4* (*VEGFR3*) gene inactivate the kinase activity of VEGFR3.

The currently known mutations of genes involved in lymphatic development associated with primary lymphedema are *GJC2*, *RBFOX2* (*FOXC2*), *CCBE1*, *FLT4* (*VEGFR3*), *PTPN14*, *GATA2*, and *SOX18* [5].

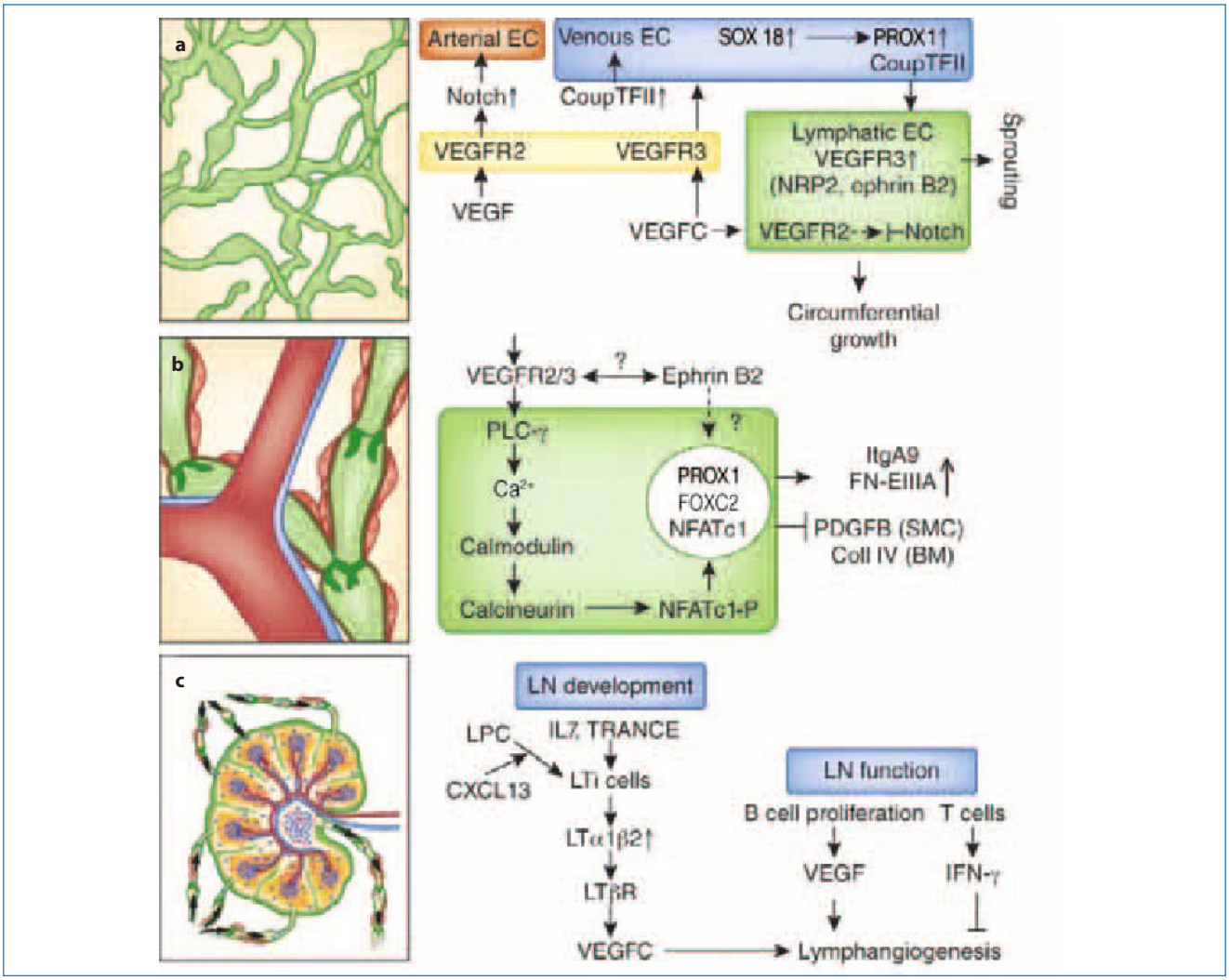

Fig. 2.5 The main molecular mechanisms involved in the development and growth of the lymphatic system. **a** Lymphatic capillaries derive from venous endothelial cells. After arteriovenous differentiation controlled by Notch and COUPTFII (NR2F2) transcription factors, SOX18 activates PROX1, which interacts with COUPTFII (NR2F2) and induces lymphatic endothelial differentiation [6, 7], involving enhanced expression of VEGFR3 (FLT4). VEGFC then induces the sprouting of the lymphatic endothelial cells to generate new vessels [8]. VEGFC and VEGF can also increase the size of lymphatic vessels by stimulating circumferential growth. **b** Formation of lymphatic valves requires a calcium-induced signal via phospholipase C-γ and calmodulin to calcineurin, which dephosphorylates the NFATc1 transcription factor, which enters the nucleus and induces valve-specific genes in a complex with FOXC2 (Petrova T., University of Lausanne, personal communication cited in [5]) [9]. VEGFR2 (KDR), VEGFR3 (FLT4) and ephrin-B2 (EFNB2) are upstream regulators of the pathways necessary for valve development [10]. PDGFB and collagen IV production is inhibited simultaneously. **c** In developing lymph nodes, lymphangiogenesis is first induced when IL7 and TRANCE (TNFSF11) stimulate LTi cells that develop from lymphatic precursor cells under the influence of the chemokine CXCL13 [11]. The LTi cells produce LTa1b2, which activates VEGFC expression via the LTβ receptor in stromal organizer cells [12]. In adult lymph nodes, B-cell proliferation stimulates VEGF-mediated lymphangiogenesis [13], whereas T-cell-derived cytokines restrict lymphangiogenesis by producing interferon-γ [14]. *COUPTFII*, chicken of albumin upstream promoter transcription factor II; *CXCL13*, chemokine (cys x cys motif) ligand 13; *EC*, endothelial cell; *FOXC2*, forkhead box protein C2; *IL7*, interleukin-7; *ItgA9*, integrin a9; *LN*, lymph node; *LPC*, lymphatic precursor cell; *LTα1β2*, eterotrimeric lymphotoxin (α1β2); *LTβR*, LTβ receptor; *NFATc1*, nuclear factor of activated T-cells, cytoplasmic, calcineurin-dependent 1; *Notch*, neurogenic locus notch homolog protein; *NRP2*, neuropilin 2; *PDGFB*, platelet-derived growth factor; *PLC-γ*, phospholipase C-γ; *PROX1*, prospero-related homeodomain transcript factor; *SOX18*, sex determining region Y Box 18; *TRANCE*, tumor necrosis factor (ligand) superfamily, member 11; *VEGF*, vascular endothelial growth factor; *VEGFR*, vascular endothelial growth factor receptor; adapted from [5], with permission

Lymphoangiogenesis requires adequate expression of the C isoform of the vascular endothelial growth factor (VEGF), which binds to its receptors (VEGFR2 and VEGFR3) under the control of the master regulator of lymphoangiogenesis, the transcription factor PROX1 [6]. Fig. 2.5 presents the main molecular mechanisms involved in the development and growth of the lymphatic system.

Although genetic molecular investigation contributes

Table 2.2 Genes identified in different lymphedema syndromes [5]

Gene	Disease name	Clinical manifestation
FLT4 (VEGFR-3)	Hereditary lymphedema IA (AD)	Congenital lymphedema
GJC2	Hereditary lymphedema IC (AD)	Lymphedema of the extremities, onset at < 15 years of age
RBFOX2 (FOXC2)	Lymphedema–distichiasis syndome	Lymphedema of mainly lower limbs, double row of eyelashes, varicose veins
CCBE1	Hennekam lymphangiectasia–lymphedema syndrome (AR)	Lymphedema of the extremities, intestinal lymphangiectasias, mental retardation
SOX18	Hypotrichosis–lymphedema–teleangiectasia syndrome (AD)	Lymphedema, alopecia, teleangiectasia
PTPN14	Lymphedema–choanal atresia syndrome (AR)	Lymphedema of lower limbs in children, lack of nasal airways
GATA2	Emberger's syndrome (AD)	Lymphedema of lower extremities and genitalia, immune dysfunction, cutaneous warts, deafness

AD, autosomal dominant; *AR*, autosomal recessive.

to provide proper genetic counseling for parents of an affected child with congenital lymphedema, it cannot explain those forms presenting later in life (lymphedema tarda). In these cases, the latent period before swelling manifests clinically suggests that a failure of growth or regeneration following damage or injury might be the real cause underlying edema, rather an abnormal development of the lymphatics since birth. Table 2.2 lists the genes identified in the various lymphedema syndromes [5].

Concerning secondary lymphedemas, obliterative processes consequent to lymphangiothrombosis or lymphangitis might occur in the same way as for veins, since lymph can clot in the same way as blood; unfortunately, there is no clinical investigation for ascertaining the presence of lymph thrombosis. Damage to the lymph-conducting pathways may occur secondary to any number of causes originating primarily outside the lymphatic system. Secondary lymphedema is more common than primary lymphedema, as it can result from a wide variety of causes, such as post-thrombotic syndrome, surgical or radiation therapy, trauma, and parasitic infections.

In chronic venous insufficiency, as in post-thrombotic syndrome, most of the interstitial fluid is unable to return to the heart by way of the obstructed veins. As a result, the volume of fluid transported by the lower-extremity lymphatics increases, in order to compensate for the venous occlusion. This safety-valve function of the lymph vessels continues until the lymphatic valvular mechanism becomes insufficient; then reflux occurs, swelling of the limb increases, and ulcers develop.

Lymphedema frequently coexists with lipedema, a condition affecting only women. Lipedema is a bilateral, symmetrical swelling of the lower extremities extending from the pelvic brim to the ankles. Histologically, its hallmark is a gross increase in the subcutaneous fat layer, only limited to the areas mentioned above (pelvic brim to ankles). The patient may be normal in weight, or even thin in the upper half of the body, but grossly obese from the pelvic brim down. In lipedema, the lymph vessels are coiled, the prelymphatic canals and initial lymph vessels are abnormal, the velocity of lymph transport is reduced, and lymphedema involves both lower extremities (including the feet).

Upper arm lymphedema is to be expected after axillary lymph node dissection for breast cancer surgery, and/or radiation therapy. The incidence of breast-cancer-related lymphedema ranges from 6% to 70%; however, it may be a common underreported morbidity, considering the relation between lymphatic drainage of the upper extremity and of the breast in the caudal part of the axilla [15]. Lymphedema is generally localized to the arm on the side of the breast surgery, and patients with a high peripheral blood vascular filtration rate seem to be predisposed to this complication [16, 17]. A clear relationship between the number of lymph nodes removed and the risk of lymphedema has not been definitely established, and clinical trials are focusing on the reduction of axillary lymph node dissections even in the presence of a positive sentinel lymph node [18].

The most common cancers in which treatment gives rise to lower-limb lymphedema are melanoma, sarcoma, and pelvic tumors (including of the cervix, uterus, and prostate); it is noteworthy that pelvic cancers and infiltrating sarcomas can present with lymphedema.

Trauma of the lymphatic channels (either from elective surgery or by accident) has to be extensive in order to induce lymphedema. Indeed, the experimental reproduction of lymphedema is extremely difficult, due to the highly efficient regenerative potential of lymphatics. It is probably the failure of lymphatics to regenerate and reanastomose satisfactorily through scarred or irradiated tissue that is responsible for lymphedema secondary to cancer treatment.

Parasitic lymphedema is the most common cause of lymphedema worldwide. It is caused by the microfilariae of *Wuchereria bancrofti* and *Brugia malayi*, which can be transmitted to humans by different mosquito species. When

these microfilariae reach the lymph vessels, they develop into adult worms; the resulting inflammation and fibrosis cause progressively increasing lymphatic obstruction. Elephantiasis is the result of repeated infections, developing over many years.

2.6 Lymphatic Malignancies

Solid tumors can originate in the lymphatic tissues. Lymphangiosarcoma, a malignant tumor of unknown molecular pathogenesis, causes primary or secondary lymphedema. Lymphangioleiomyomatosis is a tumor characterized by the infiltration of abnormal smooth-muscle-like cells through the pulmonary interstitium, perivascular spaces, and lymphatics of young female individuals, and it leads to lymphatic disruption and eventual respiratory failure. Kaposi's sarcoma is an angiogenic tumor of lymphatic endothelial cells. Most of these tumors are investigated for their responsiveness to VEGFR3-blocking antibody, IMC-3C5, which recently entered phase I clinical trials.

The lymphatic vessels also provide a route for tumor cells to metastasize, and the lymph node microenviroment may select tumor cells with increased metastatic potential.

2.7 Acute Lymphangitis

Lymphatic vessels, together with lymph nodes, evolved as a host defense system with the purpose of preventing or limiting noxious agents entering the systemic circulation. To this end, the inflammatory response may be profound and an overt lymphangitis and/or lymphadenitis can arise. Lymphangitis is constituted by inflammation of the lymphatic collectors, and is clinically evident as a red streak up the limb corresponding to the inflamed vessels. Edema is often an accompanying feature. Infection is generally limited to the lymph nodes, and lymphadenitis may give rise to painful swelling in the groin or axilla (depending on the site of infection).

Lymphangitis may occur without any demonstrable inflammation, or can be recurrent. When lymphatic insufficiency exists and the local system fails in its host defense duty, recurrent infection can occur, presenting clinically as recurrent cellulitis/erysipela.

Erysipela is a skin infection that is usually caused by β-hemolytic group A streptococci. After having had erysipela in an extremity, a significant percentage of patients develop persistent swelling or suffer from recurrent erysipelas. The persistent swelling after erysipelas is then most likely caused by secondary lymphedema. However, a recent study [19] proved that patients presenting with a first episode of erysipela often have signs at lymphoscintigraphy of pre-existing lymphatic impairment in the other, clinically non affected, leg. This means that subclinical lymphatic dysfunction of both legs may be an important predisposing factor. Therefore, treatment of erysipelas should focus not only on the infection, but also on the lymphological aspects; in this regard, long-term treatment for lymphedema is essential in order to prevent recurrence of erysipelas and aggravation of the pre-existing lymphatic impairment.

Based on the clinical experience that lymphangitis or cellulitis are not always followed by the development of lymphedema, it can be speculated that lymphedema is the result of vulnerable lymphatics with pre-existing lymphatic insufficiency, although proving which came first – the cellulitis or the lymphatic insufficiency – is difficult.

2.8 Lymphatic Circulation in Obesity and Cardiovascular Disease

Some abnormality in the pathophysiologic regulation of lymphatic circulation might be involved in the pathogenesis of obesity, atherosclerosis, and cardiovascular diseases. The link between lymphatic function and adipose biology has recently been recognized [20]. Lymph nodes and collecting lymphatic vessels are usually embedded in visceral or subcutaneous fat, thus suggesting some relationship between the lymphatic vessels and adipose metabolism. Additionally, ectopic growth of adipose tissue is observed in edematous regions of patients suffering from chronic lymphedema. In rats, chronic inflammation of the peripheral lymph nodes increases the number of adipocytes surrounding the nodes. Moreover, perinodal adipose tissue undergoes dynamic changes in response to low-level inflammation, as occurs in insulin resistance, type 2 diabetes, and cardiovascular disease. Increased deposition of subcutaneous fat in edematous regions has been described in lymphedema-carrying Chy-mice with heterozygous inactivating mutation in *Flt4* (*VEGFR3*), thus supporting the hypothesis that the lymph is adipogenic. Indeed, mice with heterozygous *Prox1*-inactivating mutation were found to have leaky lymphatic vessels and to develop obesity and inflammation resembling late-onset obesity in humans. *Prox1* heterozygous mice constitute the first in-vivo model of lymphatic-mediated obesity, where the leading cause of the obese phenotype is abnormal lymph leakage due to disruption in lymphatic vascular integrity, particularly of the mesenteric lymphatic vessels; leakage of lymph exerts a potent adipogenic stimulus, although the exact factor responsible for such stimulus is currently still unknown.

The lymphatic vessels have also a role in atherosclerotic plaques, where they are present in the adventitia of arteries adjacent to small blood vessels, the vasa vasorum, which are expanded in atherosclerotic plaques [21]. Mice lacking

apolipoprotein E develop not only atherosclerotic plaques, but also dysfunctional lymphatic vessels [22]. It is speculated that the lymphatic circulation could provide a protective pathway for lipid and inflammatory cell efflux from the arterial wall, thus contrasting the development of atherosclerotic plaques. However, it is still to be proven whether improved lymphatic circulation might improve myocardial function, particularly in the infarcted or dilated heart, where wall tension is grossly elevated.

2.9 Intracavitary Lymphedema

Chyle is a "milky lymph," which flows from the lacteals of the gut through the cisterna chyli and then through the thoracic duct. Chylous ascites is the accumulation of milky chyle in the peritoneal cavity. Chylous ascites has been reported after surgical procedures such as abdominal aortic aneurysm repair, radical gastrectomy, duodenectomy, nephrectomy, and Wilms' tumor resection. Neoplastic infiltration of the abdominal lymphatic and lymphnodal structures, as well as traumas (abdominal trauma, often iatrogenic, as in lymphadenectomy in the surgical treatment of renal carcinoma), lymphatic dysplasia, intraperitoneal lymphatic fistula within the framework of congenital defects of the lymphatic system, rupture of the lymphatic cyst, as well as any infectious and inflammatory process in lymph nodes, account for other causes of chylous ascites.

Abdominal distension is the most common symptom. Ascitic fluid with triglyceride levels greater than 110 mg/dL is diagnostic of chylous ascites. The gross appearance of the ascitic fluid correlates poorly with absolute triglyceride levels, because turbidity also reflects the size of the chylomicrons. A high total leukocyte count with marked lymphocytic predominance is also present. The total protein content usually varies from 1.4 g/dL to 6.4 g/dL, with a mean of 3.7 g/dl.

Chylothorax is a form of lipid pleural effusion characterized by the presence of chyle in the pleural space, which can be the result of obstruction or disruption of the thoracic duct, or one of its major tributaries. A triglyceride concentration above 110 mg/dL is virtually diagnostic, but the presence of chylomicrons confirms the diagnosis. However, chylothorax defined by these criteria represents a heterogeneous group of clinical entities. The presence of chylomicrons or triglyceride levels above 110 mg/dL in a pleural effusion should be considered evidence of chyle leakage of indeterminate clinical significance. In the case of an acute or chronic chylothorax due to possible injury of the thoracic duct, this evaluation is crucial, as surgical ligation of the thoracic duct is often considered. In contrast, a cholesterol-rich effusion is typically the result of longstanding pleurisy with elevated cholesterol levels in the pleural space; most cases of cholesterol pleural effusions are attributed to tuberculous or rheumatoid pleurisy. It is critical to distinguish between a chylothorax and a cholesterol effusion. A chylothorax develops after injury or obstruction of the thoracic duct, leading to leakage of chyle into the pleural space, and is characterized by an increased triglyceride concentration and by the presence of chylomicrons. In contrast, a cholesterol effusion is a longstanding effusion associated with an elevated cholesterol concentration (usually greater than 250 mg/dL) and with a thick pleural rind; this condition represents a form of lung entrapment.

The accumulation of chyle in the pericardial space, or chylopericardium, is a condition that occurs most frequently after trauma, or cardiac or thoracic surgery, or in association with tumors, tuberculosis, or lymphangiomatosis. When its precise cause cannot be identified, it is called primary or idiopathic chylopericardium, a quite rare clinical condition. The etiology can be primary or the result of various clinical situations, particularly trauma (thoracic duct lesions), neoplasms (primary such as lymphangioma or through invasion of the lymphatic system by other neoplasms), and filaria infection. Primary forms are the result of malformation of the intestinal lymph circulation and its relationship with the systemic circulation, resulting in megalymphatics that develop fistulas following even minimal trauma, and that can be located at atypical sites in the body.

References

1. Brown P (2005) Lymphatic system: unlocking the drains. Nature 436:456–458
2. Wang Y, Oliver G (2010) Current views on the function of the lymphatic vasculature in health and disease. Genes Dev 24:2115–2126
3. Leak LV, Burke JF.(1966) Fine structure of the lymphatic capillary and the adjoining connective tissue area. Am J Anat 118:785–809
4. Sutkowska E, Gil J, Stembalska A, Hill-Bator A et al (2012) Novel mutation in the FOXC2 gene in three generations of a family with lymphoedema-distichiasis syndrome. Gene 498:96–99
5. Alitalo K (2011) The lymphatic vasculature in disease. Nat Med 17:1371–1380
6. Wigle JT, Oliver G (1999) Prox 1 function is required for the development of the murine lymphatic system. Cell 98:769–778
7. Srinivasan RS, Geng X, Yang Y et al (2010) The nuclear hormone receptor Coup-TFII is required for the initiation and early maintenance of Prox1 expression in lymphatic endothelial cells. Genes Dev 24:696–707
8. Karkkainen, MJ, Haiko P, Sainio K et al (2004) Vascular endothelial growth factor C is required for sprouting of the first lymphatic vessels from embryonic veins. Nat Immunol 5:74–80
9. Norrmén, C, Ivanov KI, Cheng J et al (2009) FOXC2 controls formation and maturation of lymphatic collecting vessels through cooperation with NFATc1. J Cell Biol 185:439–457
10. Bazigou, E, Lyons OT, Smith A (2011) Genes regulating lymphangiogenesis control venous valve formation and maintenance in mice. J Clin Invest 121:2984–2992
11. van de Pavert, SA, Mebius RE (2010) New insights into the development of lymphoid tissues. Nat Rev Immunol 10:664–674
12. Vondenhoff M.F, Greuter M, Goverse G et al. (2009) LTbetaR signaling induces cytokine expression and up-regulates lymphangiogenic factors in lymph node anlagen. J Immunol 182:5439–5445

13. Angeli V, Ginhoux F, Llogrà J et al. (2006) B cell–driven lymphangiogenesis in inflamed lymph nodes enhances dendritic cell mobilization. Immunity 24:203–215
14. Kataru, R.P, Kim H, Jang C et al (2011) T lymphocytes negatively regulate lymph node lymphatic vessel formation. Immunity 34:96–102
15. Pavlista D, Eliska O (2012) Relationship between the lymphatic drainage of the breast and the upper extremity: a postmortem study. Ann Surg Oncol 24 April, epub ahead of print
16. Stanton AW, Modi S, Mellor RH et al (2009) Recent advances in breast cancer-related lymphedema of the arm: lymphatic pump failure and predisposing factors. Lymphat Res Biol 7:29–45
17. McLaughlin SA (2012) Lymphedema: separating fact from fiction. Oncology 26:242–249
18. Wjcinski S, Nuengsrl S, Hillemanns P et al (2012) Axillary dissection in primary breast cancer: variations of the surgical technique and influence on morbidity. Cancer Manag Res 4:121–127
19. Damstra RJ, Van Steensel MAM, Boomsma JHB et al (2008) Erysipelas as a sign of subclinical primary lymphoedema: a prospective quantitative scintigraphic study of 40 patients with unilateral erysipelas of the leg. Br J Dermatol 158:1210–1215
20. Harvey NL (2008) The link between lymphatic function and adipose biology. Ann NY Acad Sci 1131:82–88
21. Nakano T, Nakashima Y, Yonemitsu Y et al (2005) Angiogenesis and lymphangiogenesis and expression of lymphangiogenic factors in the atherosclerotic intima of human coronary arteries. Hum Pathol 36:330–340
22. Lim HY, Rutkowski JM, Helft J et al (2009) Hypercholesterolemic mice exhibit lymphatic vessel dysfunction and degeneration. Am J Pathol 175:1328–1337

Methodological Aspects of Lymphoscintigraphy: Radiopharmaceuticals and Instrumentation

3

Paola Anna Erba, Giuseppina Bisogni, Alberto Del Guerra, and Giuliano Mariani

3.1 Radiopharmaceuticals

3.1.1 Introduction

Deposition of radioactive colloids in regional lymph nodes was first observed by Walker after subcutaneous injection of colloidal gold-198 (^{198}Au) [1]. Since a significant fraction of the activity remained at the injection site after subcutaneous administration of colloidal ^{198}Au (a radionuclide with a significant component of beta decay), the radiation burden at the injection site limited the activity that could be safely administered. This led to a search for agents with more favorable physical characteristics.

^{198}Au was soon replaced by particulate materials labeled with technetium-99m (^{99m}Tc, half-life = 6 hours, 140 keV gamma radiation, availability through a generator), the most widely employed radionuclide in routine diagnostic procedures. The agents developed for this purpose include ^{99m}Tc–sulfur colloids, ^{99m}Tc–nano and microaggregated albumin, and ^{99m}Tc–antimony sulfide [2–14]. Unfortunately, neither ^{99m}Tc–antimony sulfide nor ^{99m}Tc–human serum albumin are currently available in the United States. ^{99m}Tc–albumin nanocolloid (Nanocoll) and ^{99m}Tc–rhenium sulfide colloids are used in Europe [15–18]. Filtered ^{99m}Tc–sulfur colloid (to limit particle size to <100 nm) is one of the most commonly employed radiopharmaceuticals for lymphoscintigraphy in the United States. In addition, other radiocolloids such as ^{99m}Tc–stannous phytate [4], denatured ^{99m}Tc–collagen colloid, and ^{99m}Tc–stannous fluoride, can be used. ^{99m}Tc–labeled dextran 70, a sucrose polymer of high molecular weight, is another radiopharmaceutical option that can be used for sentinel lymph node (SLN) detection [19]; although it is not a true colloid, this compound behaves in a similar fashion as radiocolloids following interstitial injection. Table 3.1 lists the main features of radiopharmaceuticals that have been employed for lymphoscintigraphy, while Figs. 3.1 and 3.2 show the considerable variability in particle size among different preparations.

Generally, the labeling procedure consists of adsorption of ^{99m}Tc on the particle's surface at nonspecific sites. The quantity of colloid, and hence the available adsorption surface, must be in large excess. In other cases, the labeling procedure is carried out as a process of coprecipitation of ^{99m}Tc.

Many factors influence the transport of molecules from the interstitium to the lymphatic vessels. Since solutes have to interact and cross over with components of the extracellular matrix to enter the lymphatic circulation, the composition of the extracellular matrix and the properties of the solute have a significant influence on their ability to move through the interstitium into the lymphatics [29]. The most important properties of molecules in this regard are weight, size, shape, and charge [30–32].

Although molecules are transported by both convection and diffusion, their size has a major impact on which mechanism dominates [33, 34]. Small molecules are primarily transported by diffusion, which is a slow process over longer distances. The slower transport of the largest molecules is explained by mechanical interaction with the components of the extracellular matrix, which slows down movements of the molecules.

The uptake and retention of radiocolloids in lymph nodes depends greatly on the fact that they undergo phagocytosis once they have entered the lymphatic circulation and have been transported to the lymph nodes. The lymph node is a highly complex structure that contains lymphocytes, plasma cells, and macrophages, in a collagen sheath. One fraction of the colloid remains inside the lymph node, where phagocytosis by macrophages occurs. The remaining portion, espe-

P. A. Erba (✉)
Regional Center of Nuclear Medicine, University of Pisa Medical School
Pisa, Italy
e-mail: p.erba@med.unipi.it

G. Mariani et al. (eds.), *Atlas of Lymphoscintigraphy and Sentinel Node Mapping*,
DOI 10.1007/978-88-470-2766-4_3

Radiocolloid	Particle size, nm	References
^{198}Au-colloid	5; 9–15	[5, 20]
^{99m}Tc–rhenium colloid (TCK-1)	10–40; 50–500	[2, 21]
^{99m}Tc–rhenium colloid (TCK-17)	50–200; 45; 3–15	[2, 22]
^{99m}Tc–antimony sulfur colloid	2–15; 40	[2, 23]
^{99m}Tc–sulfur colloid	100–1000	[24]
Filtered ^{99m}Tc–sulfur colloid	38 (mean)	[25]
^{99m}Tc–stannous sulfur colloid	20–60	[26]
^{99m}Tc–albumin nanocolloid (Nanocoll)	<80	[27]
^{99m}Tc–microaggregated albumin (Microlite)	10	[2]

Table 3.1 Colloidal radiotracers and their particle size; modified from [6] with permission

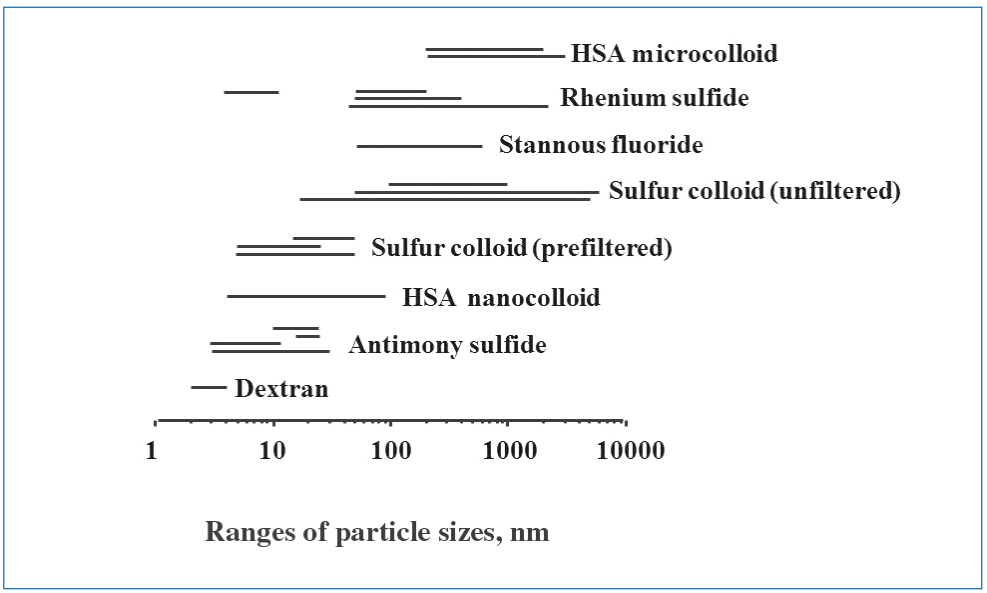

Fig. 3.1 Schematic representation of the ranges of particle sizes in nm in the main radiopharmaceuticals employed for lymphoscintigraphy. *HSA*, human serum albumin

cially the smaller-size fraction, proceeds through the efferent lymph vessels toward the next lymph node(s).

Colloids enter and exit the lymphatic circulation at different speed, depending on their sizes. Their migration through the lymphatic system is also inversely related to particle size. Particles smaller than a few nanometers usually leak into the blood capillaries, whereas larger particles (up to about 100 nm) can enter the lymphatic capillaries and be transported to lymph nodes, where phagocytosis takes place [35]. Very small particles (<30 nm) migrate rapidly, with a small proportion remaining in the first lymph node encountered, therefore resulting in the visualization of additional nodes along the same lymphatic path. Larger particles (>100 nm) are trapped in the interstitial compartment for a relatively long period of time [14]. The fraction of tracer that is phagocytized locally or in lymph nodes increases with increasing size [36]. The smaller the molecule, the less convection influences its transport. Convection of dextrans of similar form, shape, and charge has been found to be significantly faster at a molecular weight of 71 kDa than for lighter (3 kDa and 40 kDa) and heavier (2 MDa) dextrans [37]. Albumin is convected three times more slowly than dextran of similar weight (71 kDa), thus suggesting that both the shape and the uneven distribution of charges in the albumin molecule have a relevant impact on its ability to move through the extracellular matrix.

Thus, molecules of similar size can vary in their transport properties. In particular, negatively charged dextrans convect faster than neutrally charged dextran of similar size and shape, demonstrating that negatively charged molecules move more easily through the extracellular matrix. This feature is explained by the fixed negative charge of the glucosaminoglycans in the extracellular matrix. The repelling forces between the negatively charged molecules and the negatively charged extracellular matrix components are likely to reduce mechanical interaction, and thus lower the resistance against convection.

Differences in the surface characteristics of colloids may account for differences in lymph nodes uptake [32]. Early studies with liposomes have shown that specific surface

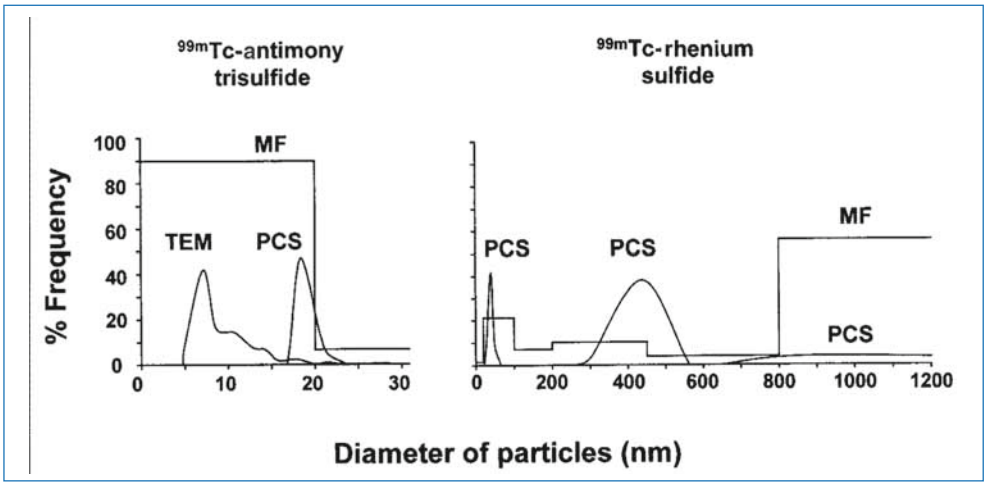

Fig. 3.2 Comparison of transmission electron microscopy (*TEM*), photon correlation spectroscopy (*PCS*), and membrane filtration (*MF*) to characterize size distribution of ^{99m}Tc–antimony trisulfide colloid, ^{99m}Tc–rhenium sulfide colloid. Adapted from [28], with permission

properties (such as charge, hydrophobicity, and the presence of targeting ligands) can influence both the rate of particle drainage from a subcutaneous injection site and the distribution within the lymphatic system. In rats, for instance, small, negatively charged liposomes localize in lymph nodes more effectively than positively charged vesicles when administered subcutaneously into the dorsal surface of the footpad [38].

These considerations are the main determinants for the selection of suitable molecules, both for peripheral lymphoscintigraphy and lymphoscintigraphic assessment of SLNs. In fact, when quantification in peripheral lymphoscintigraphy is performed by assessing tracer retention in local lymph nodes, the radiopharmaceutical should be characterized by high retention in the lymph nodes, i.e., have a molecular size that promotes phagocytosis. Conversely, if depot washout techniques are used, smaller tracers that mimic in-vivo transport of plasma proteins in the lymphatics (with faster interstitial and lymphatic transport and less local retention) are needed to produce faster and more reliable clearance data [39].

In the case of sentinel lymph node biopsy (SLNB), the use of small particle size may cause problems to the surgeon in distinguishing between the true SLN(s) and other radioactive sites. The use of large particles reduces considerably the number of lymph nodes detected. It has been estimated that for a colloid size between 20 nm and 1000 nm, an average of 1.3 lymph nodes are detected; whereas, particles smaller than 80 nm are able to show an average of 1.7 lymph nodes [40–45]. However, the trend of larger molecules to remain at the injection site, and their failure to enter the lymphatic system, may result in delayed or even no visualization of lymph nodes [46]. Therefore, the optimal colloidal size for lymphoscintigraphy is believed to be at least 80 nm and ideally around 200 nm [47].

There are significant advantages of using filtered ^{99m}Tc–sulfur colloid, including its low cost, excellent safety profile, and demonstrated clinical value. Nevertheless, this agent has several disadvantages, including minimal absorption from the injection site (typically <5% is absorbed), especially following subcutaneous administration; whereas intradermal administration is associated with faster absorption and visualization of the cutaneous lymphatics, often within 1 minute after radiocolloid injection. Even in the absence of beta radiation, the conversion electrons from ^{99m}Tc result in a radiation dose of 1–5 rads/injection site (depending on the volume of the injectate and activity administered).

The slow transit into the lymphatic system requires prolonged imaging times. Furthermore, the unpredictable nature of the absorption and transit can make it very difficult to reliably calculate tracer-disappearance rates. ^{99m}Tc–sulfur colloid also requires an acidic pH to retain its stability, which often causes the patient to experience burning pain at the injection site [39]. The large particle size of ^{99m}Tc–sulfur colloid (30–1000 nm) [25] contributes to the minimal absorption and slow transit. An attempt to circumvent these difficulties led to the evaluation of filtered sulfur colloid for lymphoscintigraphy [25]. Utilization of a 0.1 μm filter yielded sulfur colloid with a stable particle size of <50 nm. The properties of this filtered colloid are similar to those of antimony trisulfide colloid.

Albumin nanocolloid (Nanocoll) has a reproducible colloid size distribution (95% of the particles are <80 nm) and ease of labeling. Its rapid clearance from the injection site makes it suitable for quantitative studies, and injections are reportedly painless. Thus, ^{99m}Tc–albumin nanocolloid may be more suitable for quantitative studies than ^{99m}Tc–sulfur colloid.

3.1.2 Injected Volume and Activity

The effects of varying concentrations of particles and the influence of injected volume and activity parameters on the

outcome of lymphoscintigraphy are still unclear. Bourgeois has investigated the effect of variable amount (0.02 mg versus 0.2 mg) and volume (0.2 mL versus 1.0 mL) of ^{99m}Tc–human serum albumin nanocolloids injected subcutaneously in the foot on lymph node uptake after 1 hour, during peripheral lymphoscintigraphy. He found that inguinal activity was highest using the highest quantity in the lowest volume [48].

Improvement in the SLN identification rate, from 83% to 94%, has been demonstrated with a 50% increase of injected activity [49]. Regarding volume of the injectate, because of the nonphysiologic increase in interstitial pressure, the administration of a large volume of injectate may lead to drainage in both homoregional non-SLNs and in additional drainage regions [50].

3.1.3 Factors Affecting Radiocolloid Uptake

Mechanical massage over the radiocolloid injection site enhances the uptake and weakens the inverse correlation between particle size and speed of lymphatic drainage. Besides the influence of particle surface properties on radiocolloid uptake [32], an increase in venous pressure decreases the concentration of macromolecules and leukocytes in the lymph [51]. Particle uptake by the lymphatic system is also temperature dependent. In this regard, protein transport across canine lymphatic endothelium is enhanced with increasing temperature [52]. In addition to temperature, the pH of lymph or interstitial fluid may also alter lymph or particle uptake/transport. The colloid osmotic pressure of body fluids increases as pH increases (2.1 mmHg per pH unit) [53]. Whether pH differences in interstitial or lymphatic fluid affect particle uptake in vivo, however, remains to be investigated.

Studies on prenodal collecting lymphatics of the lower extremities have shown that exercise also increases lymph flow [54, 55]. The type and intensity of the exercise have an important effect on lymphatic function, and therefore on the outcome of a lymphoscintigraphic examination (see Chapter 4 for specific stress protocols).

3.2 Instrumentation

3.2.1 Introduction

The identification of the SLN is based on the associated use of blue dye and/or lymphoscintigraphy [56]. To increase the performance of the SLN procedure over conventional imaging with large-field-of-view gamma cameras, intraoperative portable gamma cameras have recently been developed to obtain preoperative imaging of the SLN. The following sections present a review of the available intraoperative probes and portable imaging devices, their working principles, and clinical implementation.

3.2.2 Intraoperative Probes

The working principle of intraoperative probes for detection of the SLN (also called gamma probes) is conversion of the 140 keV photons emitted by ^{99m}Tc into electrons, by photoelectric effect or Compton scattering, and the production of a signal processed by custom readout electronics [49].

The intraoperative probes for SLN detection can be divided into two categories: the first includes probes based on scintillation detectors (both crystal and plastic types) and the second group is formed by semiconductor-based probes [58–70]. The typical configuration for intraoperative probes, for both scintillators and semiconductors, is shown in Fig. 3.3.

The most significant parameters defining the performances of gamma probes consist of: (1) overall sensitivity (efficiency); (2) spatial resolution (radial and lateral); (3) energy resolution; and (4) signal-to-noise ratio.

Sensitivity is the detected count rate per unit of activity, and it is determined at the tip of the probe. Radial resolution is the width of the measurement cone where the radiation is detected at a defined distance. With a wider cone, the background signal may overcome the target source. With a narrower cone, the background will be reduced and detection of the target source will be more accurate. Lateral spatial resolution is the capability to accurately localize the position of a target source and to separate two adjacent sources. Energy resolution is the capacity of the gamma-detection system to discriminate between radiations of different energy. This property is essential to distinguish between two simultaneously administered radionuclides that have different energies and to discriminate scattered from primary photons. The last property relates to the ability of the probe to discriminate the signal from the target with respect to the noise represented by the background radiation within the surrounding tissue.

The scintillator absorbs the radiation and emits a number of visible photons proportional to the energy absorbed. The visible light is measured by a photon detector, usually a photomultiplier (PMT). The crystals used in scintillator detector probes include thallium-activated sodium iodide (NaI[Tl]), thallium-activated cesium iodide (CsI[Tl]), cerium-activated lutetium ortosilicate (LSO[Ce]), bismuth germanate (BGO), and cerium-doped gadolinium orthosilicate (GSO[Ce]).

The high penetration power of gamma rays means that background events could come from parts of the patient outside the target volume of interest. Although a fraction of these events is attenuated within the patient body, in order to further reduce the background the gamma probes are equipped with a shield (material such as lead, tungsten, gold or plati-

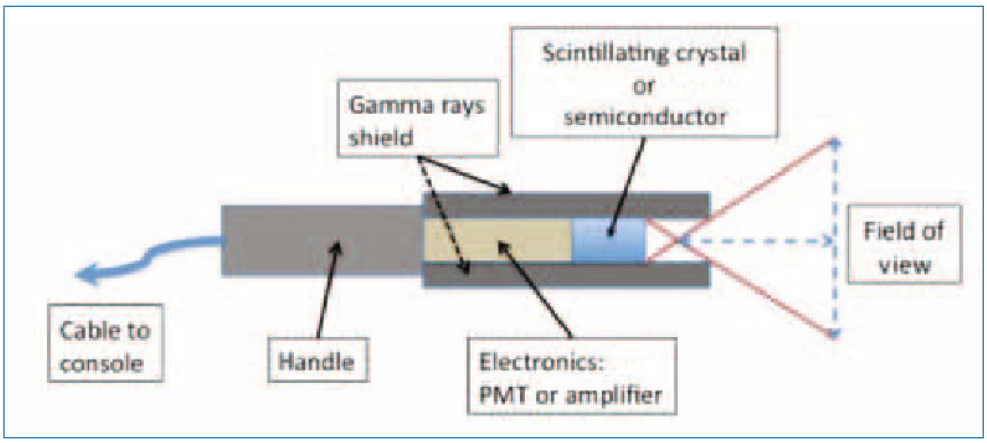

Fig. 3.3 General design of an intraoperative gamma probe

num) and collimators (designed with different length and aperture for different fields of view) that prevent attenuated radiation from nontarget locations (i.e., scattered radiation) from accessing the detector head and thus producing spurious counts. Side and back shielding can be important when there is a localized radiation source (the injection site of the ^{99m}Tc-labeled agent for radioguided biopsy of the SLN) in close proximity with the target (the SLN). Collimation of the detector head results in better spatial resolution and higher signal-to-noise ratio as compared to radiation emitted from surrounding tissues. However, when collimation is too pronounced, it reduces the sensitivity of the probes, by decreasing the detection aperture and lengthening the distance to the actual source position. Furthermore, a thicker shielding or a longer collimator is needed when detecting higher-energy gamma radiation, but this increases the overall weight and size of the gamma probe.

The final elements in the system are the electronics and the readout. Since the scintillator detector provides a signal that is proportional to the deposited energy, it is possible to perform spectroscopy and to set the sensitive energy range of the probe to select the desired gamma energy and eliminate part of the scattered radiation. The count rate of the probe is then fed to a rate meter, which also drives an audio output. An increase in loudness or frequency indicates to the surgeon proximity of the probe to the target tissue.

Semiconductors are a valid alternative to scintillators as detector material for the intraoperative probes. When radiation is absorbed in a solid-state detector, ionization occurs by promoting electrons out of the valence band to the conduction band where electrons can flow in the crystal lattice. When the electron moves to the conduction band, a positive charge (hole) in the lattice is created, which is free to move in the valence band. If an electric field is applied across the sensitive volume of the detector, the excess of charge (both electrons and holes) is collected by the opposite electrodes, providing a signal that is proportional to the energy released in the detector. Crystalline materials that are used in such detectors are cadmium telluride (CdTe), cadmium zinc telluride (CdZnTe), and mercuric iodide (HgI_2).

Scintillation-type detection systems present both advantages and disavantages, with respect to semiconductor-based systems. On one hand, scintillator-based detectors have a higher sensitivity (because of the higher density and atomic number, they are better suited for medium to high gamma-energy detection), but a poorer energy resolution and scatter rejection, due to the indirect mechanism of the radiation detection (the primary gamma converts in the scintillator, then the light should be conveyed to the PMT and the signal finally converted from optical to electrical). Furthermore, scintillation-type detectors tend to have a much bulkier probe head profile and weight. On the other hand, semiconductor-based probes are direct detectors (the energy released in the material by radiation is directly converted into a charge signal) and thus they have a higher energy-resolution and scatter-rejection capability. Likewise, semiconductor-based probes tend to have a much more compact probe head design; they can be manufactured in small size and can have a very thin entrance window that allows low-energy beta and gamma rays to be counted.

Many commercial intraoperative gamma probes are available; an example of a gamma probe with its console is presented in Fig. 3.4 [71].

Several factors determine the choice of a particular intraoperative probe. From the point of view of the surgeon, many desirable design features of detection probe systems are important [57, 69]. Gamma probes for radioguided biopsy of the sentinel node require high spatial resolution to allow for a more precise localization of small lymph node candidates.

Other features such as the shape, weight, and ergonomic design of an intraoperative probe are critical. The audible signal and digital display of the detector control unit are also important for providing critical output information to the surgeon, enabling quick and accurate localization of the ra-

Fig. 3.4 Gamma probe Neo2000 from Neoprobe (Devicor Medical Products, Inc., Cincinnati, OH). The gamma probe (in the foreground) is shown with a removable collimator. Display of the control unit shows the count rate over 20-sec intervals, represented both with a numerical readout (at the center in the top of the monitor) and with an analog-like signal (vertical scale at the left of the monitor)

dionuclide without distraction from the overall activity in the surgical field. Flexibility and adaptability of the system are also relevant to different clinical issues; important features include removable side shielding, interchangeable collimators, interchangeable detector probes, and user-adjustable energy windows for different radionuclides. Finally, the recent development of hand-held self-contained gamma-detection probes based on wireless technology eliminates the need for cables that normally connect the probe to the control unit [72, 73].

3.2.3 Portable Gamma Cameras

As long as nonimaging intraoperative probes are still the standard equipment for detection of the radiolabeled tissue in the operating room, they cannot provide further details on source configuration. The exact localization of a source can only be performed if the tip is in direct contact with the tissue after dissection.

In this regard, intraoperative real-time imaging with portable gamma cameras provides an overview of all radioactive hot spots in the whole surgical field [64, 74]. For instance, its position can be adjusted to also show sentinel nodes near the injection area, which can easily be overlooked by using the nonimaging probe. Differentiation between a SLN and an upper-tier node is determined by the number of counts simultaneously recorded with the cameras, and it can be related to the preoperative scintigraphic images. The gamma camera can also be used in conjunction with the gamma probes.

Imaging devices must meet several requirements to be employed in intraoperative practice. Among them are a portable and stable design, no delay between image acquisition and display (real-time imaging), and the possibility for continuous monitoring, spatial orientation on screen, and real-time quantification and display of the counts recorded. Finally, they should also have an adequate spatial resolution, sensitivity, and field of view.

Examples of such cameras are shown in Fig. 3.5. While the first devices were quite heavy and bulky hand-held devices, new-generation portable gamma cameras are lighter and/or equipped with stable support systems.

Among the instruments available on the market, we mention only a few that implement these requirements with different approaches in the radiation detector. One of the most used devices is the Sentinella S102 (from GEM Imaging, Valencia) [75], which is equipped with a CsI(Na) continuous scintillating crystal readout by position-sensitive PMTs and different collimators (pinhole collimators, 2.5 mm and 4 mm in diameter, and divergent) (Fig. 3.5a). The pinhole collimator enables visualization of the whole surgical field, depending on the distance between the camera and the source. The field of view is 4×4 cm at 3 cm from the source, and 20×20 cm at 15 cm from the source. This device has been integrated in a mobile and ergonomic support that is easily adjustable. The imaging head is located on one arm that allows positioning on the specific area. Another approach is based on the use of cadmium zinc telluride (CdZnTe) as a radiation detector. For instance, in the Anzai eZ-SCOPE handheld gamma camera [76], the detector is manufactured with a single tile of CdZnTe, patterned in an array of 16×16 pixels at a pitch of 2 mm. The head is equipped with a series of interchangeable parallel-hole collimators to achieve different performances in terms of spatial resolution and/or sensitivity. The field of view is 3.2×3.2 cm and the weight is 800 g (Fig. 3.5b).

A further development of the intraoperative gamma camera, is the LumaGEM from Gamma Medica Ideas [77]. Like the previous one, it is still based on CdZnTe pixel technology and was originally developed for gamma imaging of the breast. The field of view is 13×13 cm and the intrinsic spatial resolution is 2 mm. This camera is also equipped with an exchangeable parallel-hole collimator and is integrated in a workstand articulated arm.

In the long run, the PMT-based systems will be replaced by cameras consisting of scintillators coupled to solid-state photodetectors. In these systems, the photodetector will be an array of photodiodes (more likely silicon photomultipliers, the so-called SiPMs) coupled to a slab or a matrix of crystals designed to be coupled one to one to the photosensors [78]. In such a way, the thickness of the detector (com-

Fig. 3.5 **a** Latest-generation portable gamma camera with improved ergometric details and adequate support system for intraoperative use. **b** Portable gamma camera weighing less than 1 kg but without a support system

prehending crystal, photodiodes, and electronics) coupled to a shallow collimator could be less than 5 cm, so that it would be compact enough to be brought into an operating room as an intraoperative imaging probe.

References

1. Walker LA (1950) Localization of radioactive colloids in lymph nodes. J Lab Clin Med 36:440–449
2. Sherman AI, Ter-Pogossian M (1953) Lymph-node concentration of radioactive colloidal gold following interstitial injection. Cancer 6:1238–1240
3. Segal AW, Gregoriadis G, Black CD (1975) Liposomes as vehicles for the local release of drugs. Clin Sci Mol Med 49:99–106
4. Ikeda I, Inoue O, Kurata K (1976) New preparation method for 99mTc-phytate. J Nucl Med 17:389–393
5. Strand SE, Persson BR (1979) Quantitative lymphoscintigraphy I: Basic concepts for optimal uptake of radiocolloids in the parasternal lymph nodes of rabbits. J Nucl Med 20:1038–1046
6. Bergqvist L, Strand SE, Persson BR (1983) Particle sizing and biokinetics of interstitial lymphoscintigraphic agents. Semin Nucl Med 13:9–19
7. Turner JH (1983) Post-traumatic avascular necrosis of the femoral head predicted by preoperative technetium-99m antimony-colloid scan. An experimental and clinical study. J Bone Joint Surg Am 65:786–796
8. Patel HM, Boodle KM, Vaughan-Jones R (1984) Assessment of the potential uses of liposomes for lymphoscintigraphy and lymphatic drug delivery. Failure of 99m-technetium marker to represent intact liposomes in lymph nodes. Biochim Biophys Acta 801:76–86
9. Patel HM, Russell NJ (1988) Liposomes: from membrane model to therapeutic applications. Biochem Soc Trans 6:909–910
10. Strand SE, Bergqvist L (1989) Radiolabeled colloids and macromolecules in the lymphatic system. Crit Rev Ther Drug Carrier Syst 6:211–238
11. Allen TM, Hansen CB, Guo LS (1993) Subcutaneous administration of liposomes: a comparison with the intravenous and intraperitoneal routes of injection. Biochim Biophys Acta 25:9–16
12. Moghimi SM, Davis SS (1994) Innovations in avoiding particle clearance from blood by Kupffer cells: cause for reflection. Crit Rev Ther Drug Carrier Syst 11:31–59
13. Ikomi F, Hanna GK, Schmid-Schönbein GW (1995) Mechanism of colloidal particle uptake into the lymphatic system: basic study with percutaneous lymphography. Radiology 196:107–113
14. Moghimi SM, Rajabi-Siahboomi R (1996) Advanced colloid-based systems for efficient delivery of drugs and diagnostic agents to the lymphatic tissues. Prog Biophys Mol Biol 65:221–249
15. Pecking A, Firmin F, Rain JD et al (1980) [Lymphoedema of the upper limb following surgery or radiotherapy. Investigation by indirect radioactive lymphography.] Nouv Presse Med 9:3349–3351
16. Bräutigam P, Vanscheidt W, Földi E et al (1993) The importance of the subfascial lymphatics in the diagnosis of lower limb edema: investigations with semiquantitative lymphoscintigraphy. Angiology 44:464–470

17. Mostbeck A, Partsch H (1999) Isotope lymphography – possibilities and limits in evaluation of lymph transport. Wien Med Wochenschr 149:87–91
18. Partsch H (2003) Practical aspects of indirect lymphography and lymphoscintigraphy. Lymphat Res Biol 1:71–74
19. Henze E, Schelbert HR, Collins JD et al (1982) Lymphoscintigraphy with Tc-99m-labeled dextran. J Nucl Med 23:923–929
20. Kazem I, Antoniades J, Brady LW et al (1968) Clinical evaluation of lymph node scanning utilizing colloidal gold 198. Radiology 90:905–911
21. Nagai K, Ito Y, Otsuka N et al (1980) [Clinical usefullness on accumulation of 99mTc-rhenium colloid in lymph nodes.] Radioisotopes 29:549–551
22. Nagai K, Ito Y, Otsuka N, Muranaka A (1982) Deposition of small 99mTc-labelled colloids in bone marrow and lymph nodes. Eur J Nucl Med 7:66–70
23. Warbick A, Ege GN, Henkelman RM, et al (1977) An evaluation of radiocolloid sizing techniques. J Nucl Med 18:827–834
24. Davis MA, Jones AG, Trindade H (1974) A rapid and accurate method for sizing radiocolloids. J Nucl Med 15:923–928
25. Hung JC, Wiseman GA, Wahner HW et al (1995) Filtered technetium-99m-sulfur colloid evaluated for lymphoscintigraphy. J Nucl Med 36:1895–1901
26. Kleinhans E, Baumeister RG, Hahn D et al (1985) Evaluation of transport kinetics in lymphoscintigraphy: follow-up study in patients with transplanted lymphatic vessels. Eur J Nucl Med 10:349–352
27. Gommans GM, Gommans E, van der Zant FM et al (2009) 99mTc Nanocoll: a radiopharmaceutical for sentinel node localisation in breast cancer--in vitro and in vivo results. Appl Radiat Isot 67:1550–1558
28. Tsopelas C (2001) Particle size analysis of ^{99m}Tc-labeled and unlabeled antimony trisulfide and rhenium sulfide colloids intended for lymphoscintigraphic application. J Nucl Med 42:460–466
29. Swartz MA (2001) The physiology of the lymphatic system. Adv Drug Deliv Rev 50:3–20
30. Atkins HL, Hauser W, Richards P (1970) Visualization of mediastinal lymph nodes after intraperitoneal administration of 99m Tc-sulfur colloid. Nucl Med (Stuttg) 9:275–278
31. Frier M, Griffiths P, Ramsey A (1981) The physical and chemical characteristics of sulphur colloids. Eur J Nucl Med 6:255–260
32. Ikomi F, Hanna GK, Schmid-Schönbein GW (1999) Size- and surface-dependent uptake of colloid particles into the lymphatic system. Lymphology 32:90–102
33. Aukland K, Reed RK (1993) Interstitial-lymphatic mechanisms in the control of extracellular fluid volume. Physiol Rev 73:1–78
34. Swartz MA, Fleury ME (2007) Interstitial flow and its effects in soft tissues. Annu Rev Biomed Eng 9:229–256
35. Mariani G, Moresco L, Viale G et al (2001) Radioguided sentinel lymph node biopsy in breast cancer surgery. J Nucl Med 42:1198–1215
36. Weiss M, Gildehaus FJ, Brinkbäumer K et al (2005) [Lymph kinetics with technetium-99m labeled radiopharmaceuticals. Animal studies.] Nuklearmedizin 44:156–165
37. Reddy ST, Berk DA, Jain RK et al (2006) A sensitive in vivo model for quantifying interstitial convective transport of injected macromolecules and nanoparticles. J Appl Physiol 101:1162–1169
38. Mangat S, Patel HM (1985) Lymph node localization of non-specific antibody-coated liposomes. Life Sci 36:1917–1925
39. Szuba A, Shin WS, Strauss HW et al (2003) The third circulation: radionuclide lymphoscintigraphy in the evaluation of lymphedema. J Nucl Med 44:43–57
40. Paganelli G, De Cicco C, Cremonesi M et al (1998) Optimized sentinel node scintigraphy in breast cancer. Q J Nucl Med 42:49–53
41. De Cicco C, Cremonesi M, Luini A et al (1998) Lymphoscintigraphy and radioguided biopsy of the sentinel axillary node in breast cancer. J Nucl Med 39:2080–2084
42. Wilhelm AJ, Mijnhout GS, Franssen EJ (1999) Radiopharmaceuticals in sentinel lymph-node detection – an overview. Eur J Nucl Med 26:S36–42
43. Noguchi M (2002) Sentinel lymph node biopsy and breast cancer. Br J Surg 89:21–34
44. Trifirò G, Viale G, Gentilini O et al (2004) Sentinel node detection in pre-operative axillary staging. Eur J Nucl Med Mol Imaging 31:S46–55
45. Leidenius MH, Leppanen EA, Krogerus LA et al (2004) The impact of radiopharmaceutical particle size on the visualization and identification of sentinel nodes in breast cancer. Nucl Med Commun 25:233–238
46. Nieweg OE, Jansen L, Valdes Olmos RA et al (1999) Lymphatic mapping and sentinel lymph node biopsy in breast cancer. Eur J Nucl Med 26:S11–16
47. Chinol M, Paganelli G (1999) Current status of commercial colloidal preparations for sentinel lymph node detection. Eur J Nucl Med 26:560
48. Bourgeois P (2007) Scintigraphic investigations of the lymphatic system: the influence of injected volume and quantity of labeled colloidal tracer. J Nucl Med 48:693–695
49. Valdés-Olmos RA, Jansen L, Hoefnagel CA et al (2000) Evaluation of mammary lymphoscintigraphy by a single intratumoral injection for sentinel node identification. J Nucl Med 41:1500–1506
50. Werner JA, Dünne AA, Ramaswamy A et al (2002) Number and location of radiolabeled, intraoperatively identified sentinel nodes in 48 head and neck cancer patients with clinically staged N0 and N1 neck. Eur Arch Otorhinolaryngol 259:91–96
51. Ikomi F, Hunt J, Hanna G et al (1996) Interstitial fluid, plasma protein, colloid, and leukocyte uptake into initial lymphatics. J Appl Physiol 81:2060–2067
52. O'Morchoe CC, Jones WR 3rd, Jarosz HM et al (1984) Temperature dependence of protein transport across lymphatic endothelium in vitro. J Cell Biol 98:629–40
53. Lund T, Wiig H, Reed RK, Aukland K (1987) A 'new' mechanism for oedema generation: strongly negative interstitial fluid pressure causes rapid fluid flow into thermally injured skin. Acta Physiol Scand 129:433–435
54. Engeset A, Sokolowski J, Olszewski WL (1977) Variation in output of leukocytes and erythrocytes in human peripheral lymph during rest and activity. Lymphology 10:198–203
55. Olszewski W, Engeset A, Jaeger PM et al (1977) Flow and composition of leg lymph in normal men during venous stasis, muscular activity and local hyperthermia. Acta Physiol Scand 99:149–155
56. Mathelin C, Piqueras I, Guyonnet JL (2006) [Development of technologies for sentinel lymph node biopsy in case of breast cancer.] Gynecol Obstet Fertil 34:521–525
57. Povoski SP, Neff RL, Mojzisik CM et al (2009) A comprehensive overview of radioguided surgery using gamma detection probe technology. World J Surg Oncol 7:11
58. Woolfenden JM, Barber HB (1989) Radiation detector probes for tumor localization using tumor-seeking radioactive tracers. AJR Am J Roentgenol 153:35–39
59. Barber HB, Barrett HH, Hickernell TS et al (1991) Comparison of NaI(Tl), CdTe, and HgI2 surgical probes: physical characterization. Med Phys 8:373–381
60. Kwo DP, Barber HB, Barrett HH et al (1991) Comparison of NaI(T1), CdTe, and HgI2 surgical probes: effect of scatter compensation on probe performance. Med Phys 8:382–389
61. Thurston MO (1994) Development of the gamma-detecting probe for radioimmunoguided surgery. In Martin EW (ed) Radioimmunoguided surgery (RIGS) in the detection and treatment of colorectal cancer. R.G. Landes Company, Austin, Texas, pp 41–65
62. Tiourina T, Arends B, Huysmans D et al (1998) Evaluation of surgical gamma probes for radio-guided sentinel node localisation. Eur J Nucl Med 25:1224–1231

63. Schneebaum S, Even-Sapir E, Cohen M et al (1999) Clinical applications of gamma-detection probes-radio-guided surgery. Eur J Nucl Med 6:S26-S35
64. Hoffman EJ, Tornai MP, Janecek M et al (1999) Intra-operative probes and imaging probes. Eur J Nucl Med 26:913–35
65. Zanzonico P, Heller S (2000) The intra-operative gamma probe: basic principles and choices available. Semin Nucl Med 30:33–48
66. Ricard M (2001) Intra-operative detection of radiolabeled compounds using a hand held gamma probe. Nucl Instrum Meth Phys Res A 458:26–33
67. Zanzonico P (2002) The intra-operative gamma probe: design, operation, and safety. In Cody HS (ed) Sentinel lymph node biopsy. Informa Health Care, London, pp 45–68
68. Wengenmair H, Kopp J (2005) Gamma probes for sentinel lymph node localization: quality criteria, minimal requirements and quality of commercially available systems. http://www.sln-kompetenzzentrum.de/gammaprobes.pdf. Accessed 31 May 2012
69. Mariani G, Vaiano A, Nibale O et al (2005) Is the "ideal" gamma-probe for intra-operative radio-guided surgery conceivable? J Nucl Med 46:388–390
70. Moffat FL Jr (2007) Targeting gold at the end of the rainbow: surgical gamma probes in the 21st century. J Surg Oncol 96:286–289
71. Sarikaya I, Sarikaya A, Reba RC (2008) Gamma probes and their use in tumor detection in colorectal cancer. Int Semin Surg Oncol 5:25
72. Navigator GPS Tyco healthcare. http://www.rmdmedical.com/navigator.html. Accessed 31 May 2012
73. SenoRx. Gamma Finder. http://www.senorx.com/products/SNDetection/GammaFinder.asp. Accessed 19 June 2012
74. Bluetooth® Gamma Detection Probe, Neoprobe Corporation http://www.neoprobe.com/PDF/Model%201100%20and%201101%20Bluetooth%20Manual_English.pdf. Accessed 31 May 2012
75. Sentinella s-102. http://www.gem-imaging.com/. Accessed 31 May 2012
76. Anzai eZ-scope. http://www.nuclemed.be. Accessed 31 May 2012
77. Luma GEM. http://www.gm-ideas.com/. Accessed 31 May 2012
78. Heckathorne E, Tiefer L, Daghighian F, Dahlbom M (2008) Evaluation of arrays of silicon photomultipliers for beta imaging. In: Nuclear Science Symposium Conference Record, 2008. NSS '08. IEEE, pp 1626 – 1631

4 Methodological Aspects of Lymphoscintigraphy: Bicompartmental Versus Monocompartmental Radiocolloid Administration

Paola Anna Erba, Martina Sollini, Giovanni D'Errico, and Giuliano Mariani

4.1 Introduction

Interstitial injection of radiolabeled compounds with sequential scanning imaging has been used since the 1950s to investigate the lymphatic system. This minimally invasive procedure, which simply requires intradermal or subcutaneous injection of a radiocolloid, has largely replaced the more invasive and technically difficult technique of lymphangiography [1].

Despite the experience acquired over so many decades, protocols for performing lymphoscintigraphy are not yet standardized, and remarkable differences between centers still persist. The main differences include important issues such as the type and site of injection, the use of dynamic and/or static acquisitions, and even the sequence of scintigraphic acquisitions. An additional crucial issue for performing lymphoscintigraphy is choice of radiopharmaceutical, as discussed in detail in Chapter 3 of this book.

4.2 Methodology

Lymphoscintigraphy is based on the interstitial injection of a suitable radiopharmaceutical, a radiolabeled colloid where the size of the constituent particles is predefined within a certain range, so that they are too large to be removed by entering the venous side of the blood capillaries, yet too small to be retained indefinitely at the injection site (as occurs for radiolabeled macroaggregates of human albumin); particles with such properties are in the range of 5–10 nm up to about 1,000–2,000 nm. After having been deposited in the extracellular fluid, these particles enter into the initial lymphatics by both direct passage through the interendothelial openings and vesicular transport through the endothelial cells [2, 3].

The interstitial route of administration is adequate for exploring lymphatic circulation because of some intrinsic features of lymphatic anatomy, and the fact that lymphatic vessels originate in the connective interstitium near the blood vessels. The initial lymphatics are closely interconnected in a hexagonal pattern, through a set of precollectors, with deeper lymphatics in the dermis, where lymph fluid is transported in a centripetal fashion through collecting ducts and then to lymph nodes [3–5]. Therefore, exploration of the functional integrity of the lymphatic system begins with the demonstration of normal transport of extracellular fluid, followed by evaluation of lymph flow along the lymphatic collectors until it reaches the main thoracic lymph duct.

Fluid transport into the initial lymphatics occurs against a pressure gradient [3], since the interstitial fluid pressure in the skin and subcutaneous tissue is slightly negative (–0.15 – 0.44 mmHg), [6, 7], whereas the pressure in the lymphatic capillaries of the skin is positive [8, 9]. The mechanisms allowing transport of particles against such a pressure gradient include the presence of a suction force (generated through contraction of the collecting lymphatics), coupled with the episodic increases in interstitial fluid pressure created during tissue movements [10]; active transendothelial transport [4] and phagocytosis followed by migration of macrophages into the lymphatic vessels also play a role [11]. Lymph flow progression in the collectors depends predominantly on lymphatic contraction [12].

The site of radiocolloid injection has a strong influence on the final results of lymphoscintigraphy. In fact, both the subcutaneous and the intradermal routes of injection are utilized in routine studies of superficial lymphatic circulation of the extremities. There is an ongoing debate as to which injection technique is best. Subcutaneous injection, recommended by many investigators [1, 13–15], has the advantage of negligible clearance of the radiocolloid through the blood

P. A. Erba (✉)
Regional Center of Nuclear Medicine, University of Pisa Medical School
Pisa, Italy
e-mail: p.erba@med.unipi.it

G. Mariani et al. (eds.), *Atlas of Lymphoscintigraphy and Sentinel Node Mapping*,
DOI 10.1007/978-88-470-2766-4_4

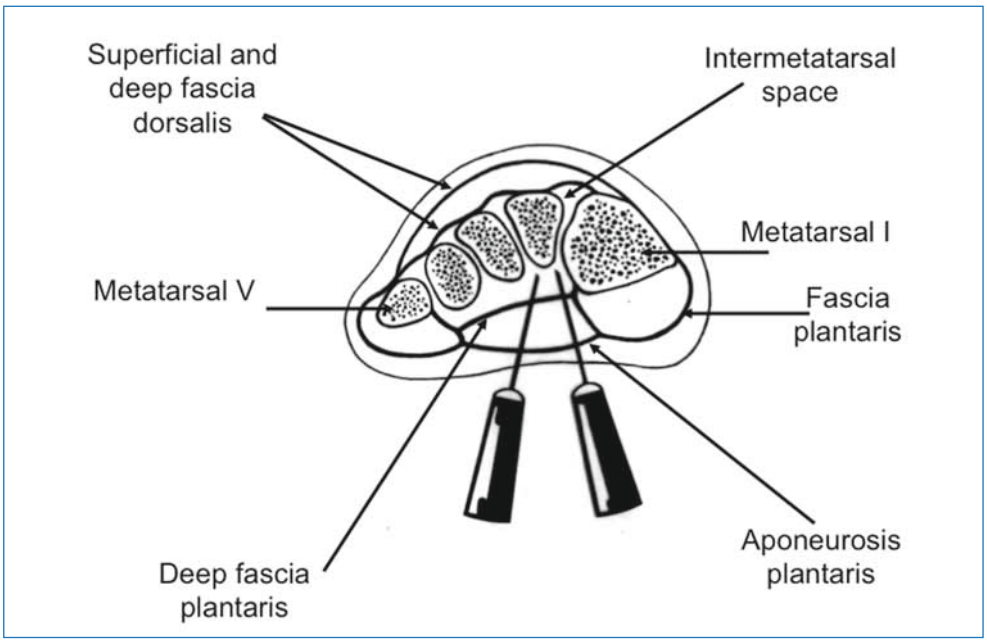

Fig. 4.1 Schematic representation of the modality of radiocolloid injection for evaluating the deep lymphatic circulation of the lower extremities. Two aliquots are injected respectively in the first and second intermetatarsal spaces, which are identified by palpating the soles of both feet immediately proximal to the distal heads of the metatarsal bones

vessels [1]. According to Mostbeck and Partsch, who compared subcutaneous and intramuscular injections of ^{99m}Tc-albumin nanocolloid, subcutaneous injection produced more reliable results, since, using quantitative parameters, it enables the user to distinguish patients with lymphedema from healthy volunteers [16]. Nevertheless, the intradermal injection route is still preferred by other authors [17–23].

However, it has been pointed out that the optimal route of injection may vary depending on the radiopharmaceutical employed, with subcutaneous injection being optimal for the colloidal agents [16, 24]. Intradermal administration of noncolloidal agents is associated with very rapid lymphatic transport, thus facilitating rapid evaluation and better quantification of lymphatic flow [21], although a non-negligible fraction of the radiopharmaceutical is removed from the injection site by way of the blood capillaries. Other colloidal or noncolloidal agents administered intradermally may not be as diagnostically reliable as ^{99m}Tc-HSA. However, comparison of intradermal and subcutaneous injections with ^{99m}Tc-HSA reveals better tracer kinetics after intradermal injection, and slow or no transport after subcutaneous injections [18].

Contrary to the superficial (or epifascial) routes of administration mentioned above (which result in visualization of the superficial lymphatic circulation), subfascial radiocolloid injection is utilized for exploring the deep lymphatic system of the extremities. This is normally achieved simply by injecting the radiocolloid intramuscularly.

When both epifascial and subfascial injections are performed sequentially, the procedure is called two-compartment lymphoscintigraphy. This approach is preferable for differentiating the possibly different mechanisms of extremity edema [24–26]. In fact, evaluating both the deep and the superficial circulation enhances the diagnostic accuracy of lymphoscintigraphy, as in this way it is possible to identify abnormalities of either the deep and/or superficial lymphatic circulation.

In both phases of two-compartment lymphoscintigraphy, the radiocolloid is injected using a 25G, 15 mm long needle, and administering a small volume of the radiocolloid suspension (0.2–0.3 mL) containing an activity of about 11–18 MBq. The procedure adopted in our center is described next.

For the deep lymphatic circulation of the lower extremities, we inject two aliquots of radiocolloid (7 MBq each) in 0.1 mL in the first and second intermetatarsal space (identified by palpating the soles of both feet immediately proximal to the distal heads of the metatarsal bones, Fig. 4.1) on each side, inserting the needle by about 12–13 mm, to reach the intermetatarsal muscles below the deep fascia plantaris (Fig. 4.2). For the deep lymphatic circulation of the upper extremities, the radiocolloid (similar volume and activity as for the lower extremities) is injected in the second and third intermetacarpal space (identified by palpating the palms of both hands and the fossa in the intermetacarpal space immediately proximal to the distal heads of the metacarpal bones, Fig. 4.3) on each side, inserting the needle by about 10–12 mm to reach the intermetacarpal muscles below the deep fascia palmaris (Fig. 4.4).

For superficial lymphoscintigraphy, we prepare syringes in a similar manner as for deep lymphoscintigraphy, but with slightly higher radioactivity content (about 15–18 MBq). We inject two aliquots on the dorsum of each foot or each hand

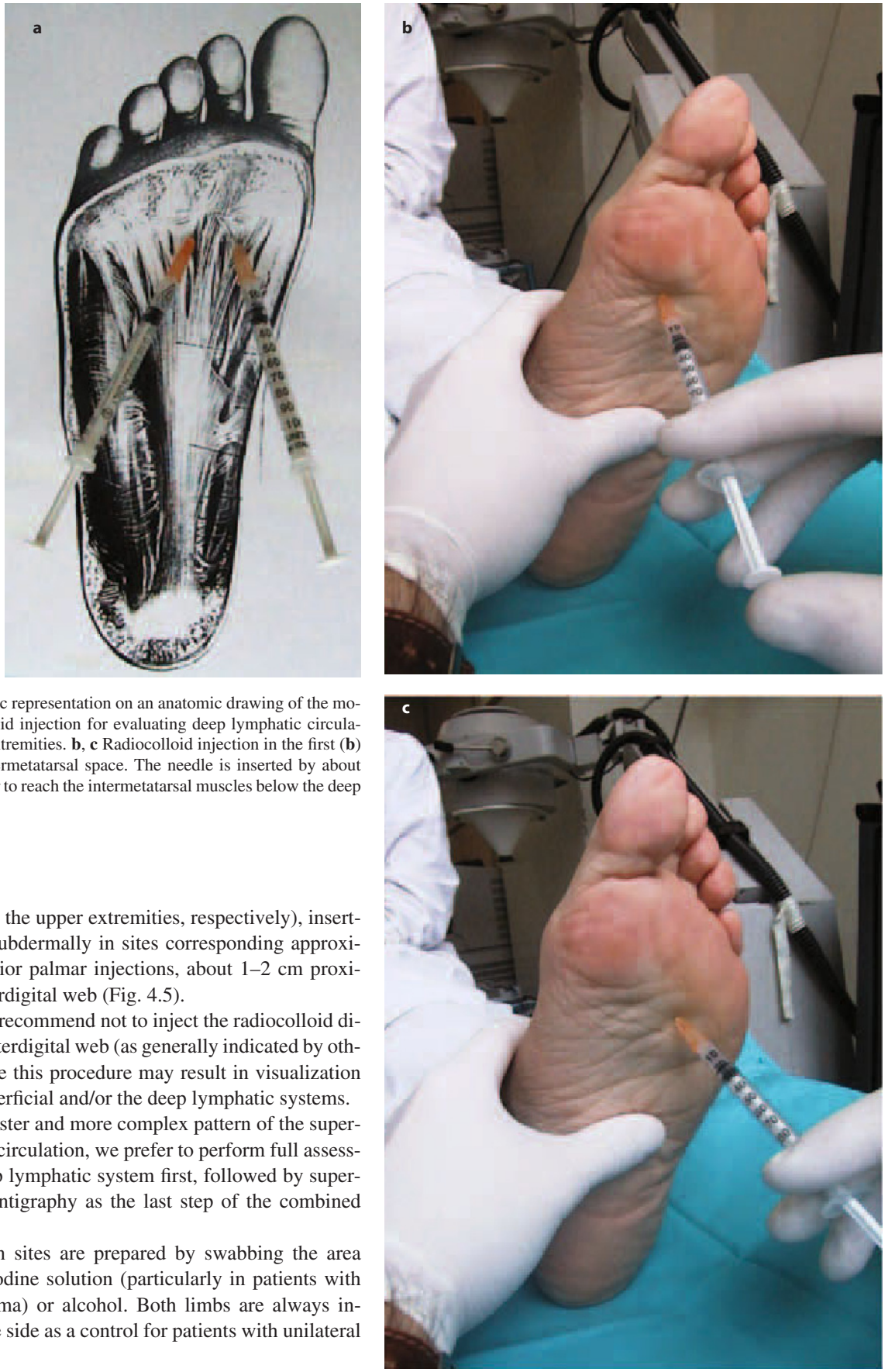

Fig. 4.2 **a** Schematic representation on an anatomic drawing of the modality of radiocolloid injection for evaluating deep lymphatic circulation of the lower extremities. **b**, **c** Radiocolloid injection in the first (**b**) and second (**c**) intermetatarsal space. The needle is inserted by about 12–13 mm, in order to reach the intermetatarsal muscles below the deep fascia plantaris

(for the lower or the upper extremities, respectively), inserting the needle subdermally in sites corresponding approximately to the prior palmar injections, about 1–2 cm proximally to the interdigital web (Fig. 4.5).

We strongly recommend not to inject the radiocolloid directly into the interdigital web (as generally indicated by other authors), since this procedure may result in visualization of either the superficial and/or the deep lymphatic systems.

Due to the faster and more complex pattern of the superficial lymphatic circulation, we prefer to perform full assessment of the deep lymphatic system first, followed by superficial lymphoscintigraphy as the last step of the combined procedure.

The injection sites are prepared by swabbing the area with either an iodine solution (particularly in patients with frank lymphedema) or alcohol. Both limbs are always injected, using one side as a control for patients with unilateral lymphedema.

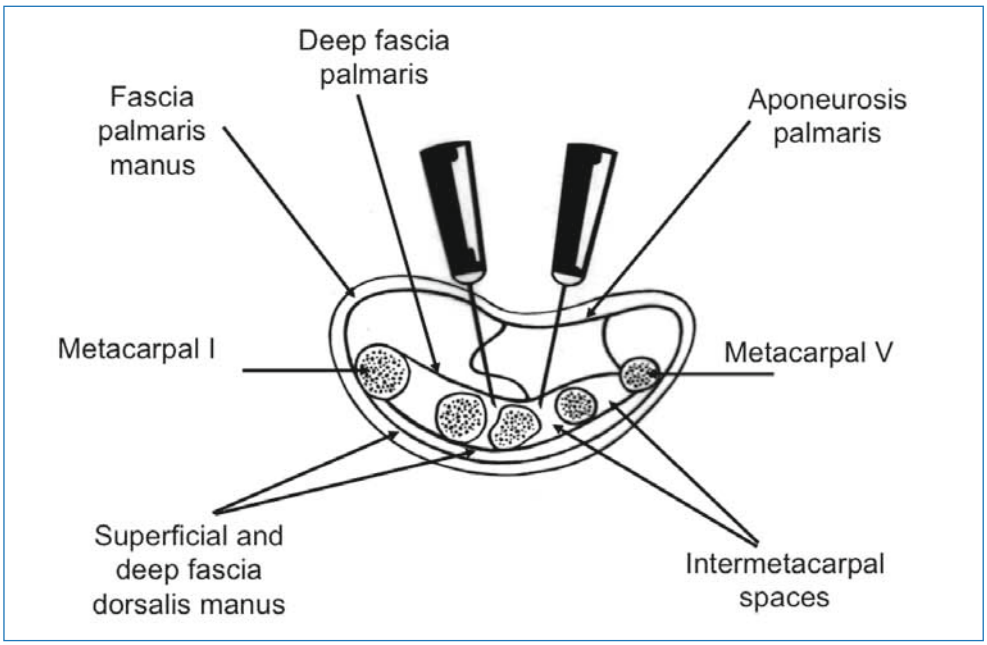

Fig. 4.3 Schematic representation of the modality of radiocolloid injection for evaluating the deep lymphatic circulation of the upper extremities. Two aliquots are injected respectively in the second and third intermetacarpal space, which are identified by palpating the palms of both hands immediately proximal to the distal heads of the metacarpal bones

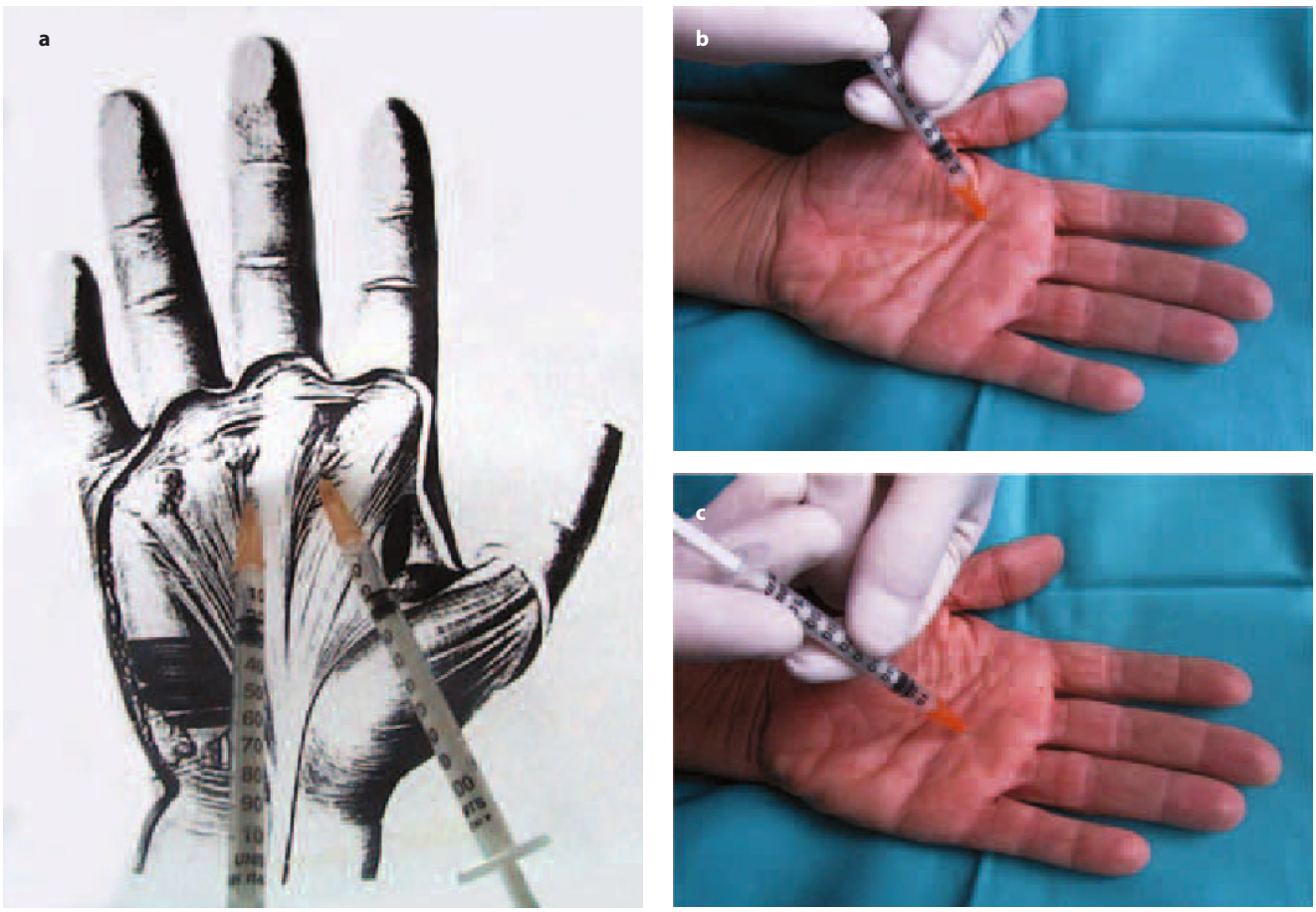

Fig. 4.4 Evaluation of the deep lymphatic circulation. **a** Schematic representation on an anatomic drawing of the modality of radiocolloid injection for evaluating deep lymphatic circulation of the upper extremities. **b**, **c** Radiocolloid injection in the second (**b**) and third (**c**) intermetacarpal space. The needle is inserted by about 10–12 mm, in order to reach the intermetacarpal muscles below the deep fascia palmaris

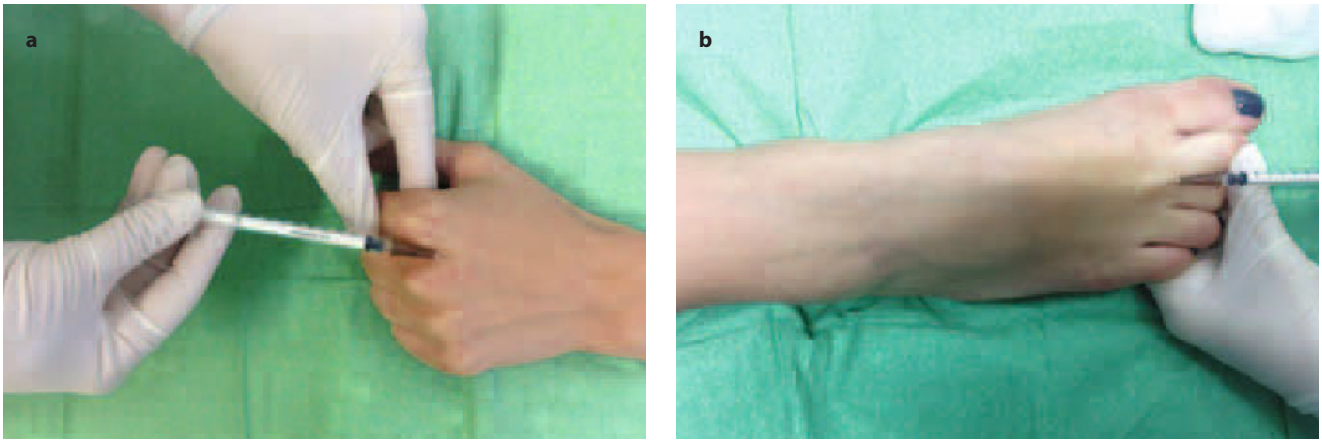

Fig. 4.5 Superficial lymphoscintigraphy. The two aliquots are injected on the dorsum of each hand (**a**) or foot (**b**), inserting the needle subdermally in sites corresponding approximately to the previous palmar injections, about 1–2 cm proximal to the interdigital web

4.3 Imaging

Images should be recorded with a dual-detector gamma camera, using high-resolution parallel-hole collimators, in both the spot-view and whole-body mode. Images should be recorded with a 20% window centered on the 140 keV photopeak of ^{99m}Tc. Spot views can be acquired from the feet to the pelvis (for the lower limbs) and from the hands to the axilla (including the chest, for the upper limbs) for about 3–5 minutes, starting from the most distal to the most proximal portion of the limbs. Final spot views of the abdomen should also be acquired, to confirm passage of the radiocolloid to the systemic blood circulation within a physiological time window (as demonstrated by visualization of the liver and spleen), repeating the acquisitions until 4–6 hours after administration in case of delayed radiocolloid drainage. After acquiring the spot images, a whole-body scan can be useful, from the distal feet to the abdomen for the lower limbs, and from the hands to the chest and upper abdomen for the upper limbs, using a scan speed of 12 cm/minute.

Dynamic imaging is necessary if quantitation of lymphatic flow is planned (see below). Single photon emission computed tomography (SPECT) or SPECT/CT (imaging) are not generally required, but may be acquired if needed.

For intracavitary lymph effusions, dual-phase lymphoscintigrapy is generally performed. Subcutaneous injection in the interdigital space of both feet is preferred, since the superficial circulation of the lower limbs accounts for the majority of lymph transport. During preparation for the exam, before radiocolloid injection, any external drainage line should be closed, whenever present. The gamma camera is generally positioned over the site of the effusion, and dynamic images are acquired from the time of radiocolloid injection until there is evidence of radioactivity accumulation at the effusion site. Usually images are acquired for up to 8 hours with sequential time points approximately every 30 minutes. During the second phase, a delayed image is acquired, consisting of acquisition of the region of interest in the same conditions as in the first phase, but with the drainage open. Although part of the radiopharmaceutical may be too large and can be trapped in the inguinal lymph nodes, the remaining part is sufficient to reach the thoracic duct to demonstrate a possible lymphatic leak. Static images followed by SPECT and SPECT/CT acquisitions may complete the set of images, depending on the site of the intracavitary effusion.

Sintigraphic acquisitions should be displayed with the intensity maximized, to depict the small fraction of radiocolloid that migrates from the injection site to the more proximal lymphatic stations.

4.4 Qualitative Visual Interpretation

Qualitative lymphoscintigraphy is, in many cases, sufficient to establish a definite diagnosis [27]. However, there is still a lack of consensus on the criteria to be used for visual interpretation of limphoscintigraphy, and expertise plays a critical role for diagnosis, particularly in the case of borderline conditions [28].

Typical examples of normal two-compartment lymphoscintigraphy are shown in Figs. 4.6 and 4.7. Abnormal findings include asymmetric visualization of lymphatic channels and collateral lymphatic channels, interrupted lymphatic vessels and lymph collection, asymmetric or absent visualization of regional lymph nodes, and the presence of "dermal flow" and/or "dermal back flow" [24–26].

For intracavitary lymph effusion, differences in radioactivity accumulated in all the images at the site of interest should be evaluated in order to define: (a) the normal pattern, when no significant differences in distribution of radiocol-

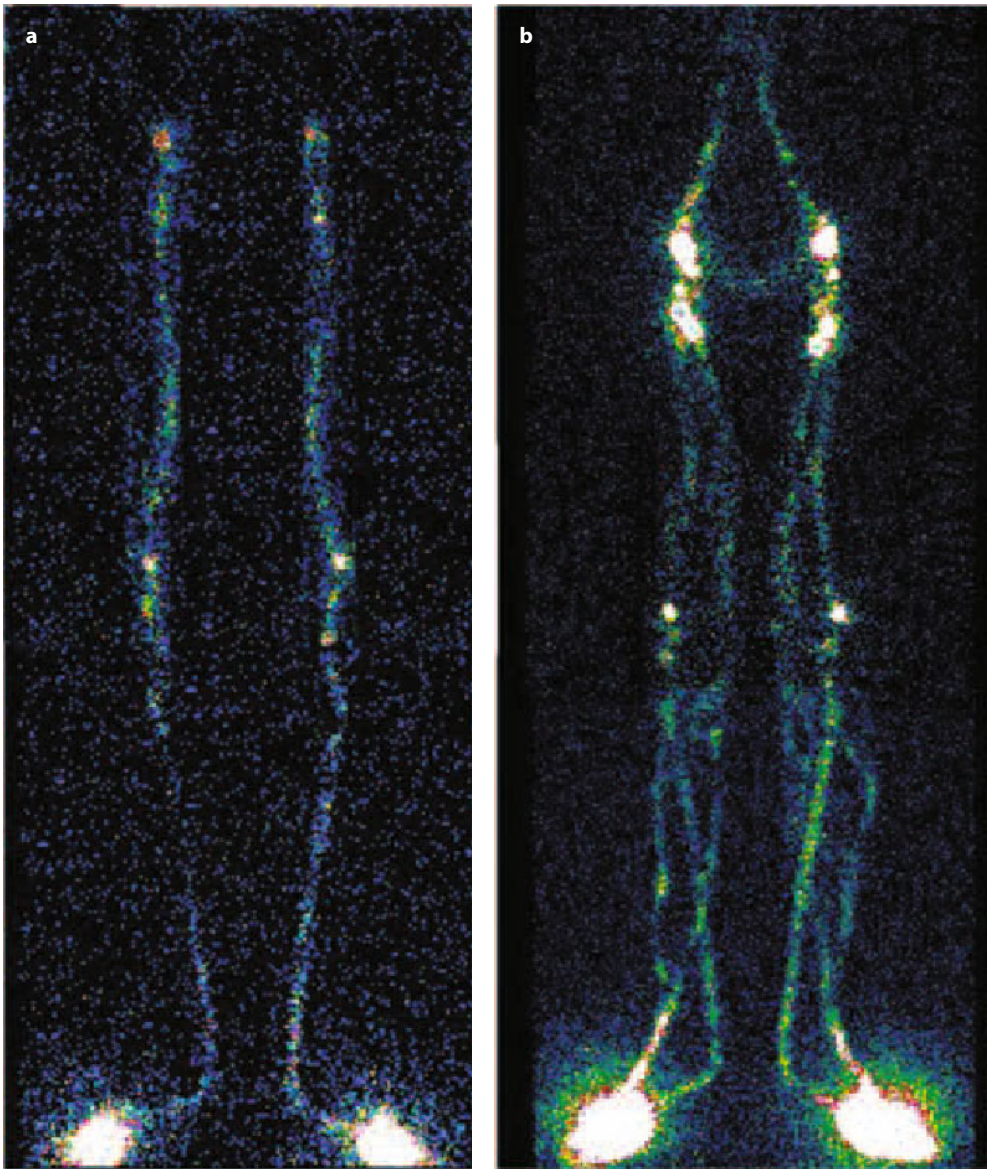

Fig. 4.6 Typical example of a normal pattern of two-compartment lymphoscintigraphy in the lower limbs. **a** Step one of lymphoscintigraphy, obtained after deep injection as described in the text: symmetric migration of the radiocolloid along the vessels of the deep lymphatic circulation, with visualization of both the popliteal and inguinal lymph nodes. **b** Step two of lymphoscintigraphy, obtained after subsequent radiocolloid injection in the subdermal space, as described in the text; in addition to the deep lymphatic vessels (still visualized by prior deep radiocolloid injection), the superficial lymphatic circulation is now visualized. The image therefore represents the sum of the two lymphatic systems, deep and superficial. From the superficial injection site, a single lymphatic vessel originates on both sides, immediately dividing into two collaterals, one pointing symmetrically along the medial portion of the legs and thighs until the groin and the other pointing laterally; both vessels merge at the groin into the inguinal lymph nodes and continue in the main pelvic and abdominal lymphatic system

loids in all images are detected up to the 24th hour; (b) a positive test, in the presence of focal accumulation of radiocolloid that increases throughout the acquisitions until the end of the first phase; (c) disappearance in the last acquisition at 24 hours.

4.5 Lymphoscintigraphy with Stress Test

Lymphoscintigraphy can be performed by applying an intervention designed to augment lymphatic flow – such as changes in temperature, physical exertion, or administration of a pharmacologic agent. Although stress lymphoscintigraphy is recommended by most authors for its enhanced sensitivity and for its utility in the quantification of lymphatic flow [24, 29], this approach is not universally employed [13, 15]. In the lower extremities, stress maneuvers include walking [30], standing [20], limb massage [21, 31], standardized treadmill exercise [23], and bicycle exercise [25]. In the upper extremities, the use of either repetitive squeezing of a rubber ball, a handgrip exercise device [32], or massage [21] has been proposed. Massage, exercise, and standing each enhance radiocolloid absorption from the injection site [20, 31, 33]. Table 4.1 lists the different stress tests used by different authors.

4.6 Quantitative Lymphoscintigraphy

Quantitation of lymphatic flow through lymphoscintigraphy has been proposed by many authors to enhance sensitivity of the technique in the diagnosis of lymphatic impairment [1]. According to the procedures employed, different quantitative parameters can be derived.

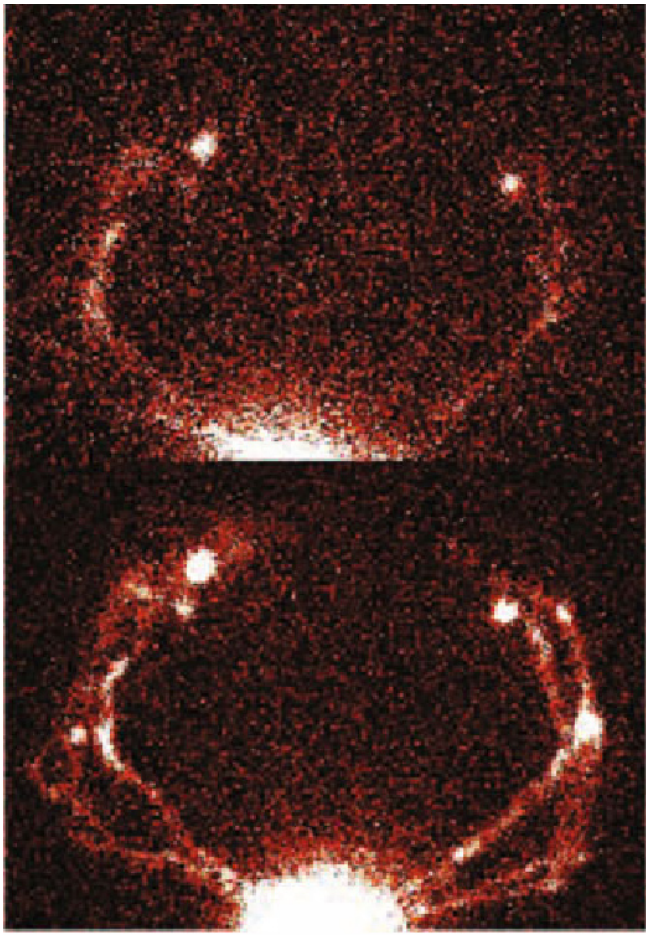

Fig. 4.7 Typical example of a normal pattern of two-compartment lymphoscintigraphy of the upper extremities (the two hands are joined together in the lower part of the imaging field). *Upper panel*: during step one of lymphoscintigraphy, obtained after deep injection as described in the text, the radiocolloid migrates symmetrically along the vessels of the deep lymphatic circulation, with visualization of the axillary lymph nodes. *Lower panel*: during step two of lymphoscintigraphy, obtained after subequent radiocolloid injection in the subdermal space, as described in the text, in addition to the deep lymphatic vessels (still visualized by prior deep radiocolloid injection), the superficial lymphatic circulation is now visualized. The image therefore represents the sum of the two lymphatic systems, deep and superficial. From the superficial injection site, a single vessel originates, immediately dividing into collateral lymphatic channels, which point along the lateral aspect of the arms up to the epitrochlear lymph nodes, and further on up to the axillary lymph nodes

4.6.1 Transport Index

The transport index (TI) [32] is an overall parameter of transport kinetics ranging from 0 (normal) to 45 (pathological), designed by combining visual assessment of five criteria: spatial and temporal distribution of the radiocolloid, time of lymph node visualization, and graded visualization of lymph nodes and lymphatic vessels. In a healthy extremity, the TI should be <10. Following treatment, changes in this parameter are significantly correlated with volume changes of the extremities.

4.6.2 Transport Time

Transit time (TT) is the time it takes for the radiocolloid to reach the inguinal lymph nodes, and has originally been proposed for use only in lower-limb lymphoscintigraphy. When using large-size particle radiopharmaceutical such as ^{99m}Tc-human immunoglobulin, imaging up to 3 hours is necessary, since this agent is drained slowly from the injection site to the lymph nodes. When using filtered ^{99m}Tc–sulfur colloids or ^{99m}Tc-nanocolloids, shorter acquisition times are adequate, with better-quality images allowing easier interpretation [57, 58]. Although this parameter correlates with the severity of lymphatic dysfunction, a certain variability in TT estimation has been reported, suggesting that the information provided by the TT index should be employed in association with visual interpretation of the images for improved diagnostic accuracy [34].

4.6.3 Tracer Appearance Time

The tracer appearance time (TAT) is calculated as the time it takes for the radiocolloid to drain from the injection site to locoregional lymph nodes (normal value <10 minutes when using ^{99m}Tc-nanocolliod and intradermal injection at the first interdigital space) [58].

4.6.4 Transport Capacity

Transport capacity (TC) assesses the clearance of injected radioactivity, calculated as the ratio between the amount of activity transported from the depots to the groin lymph nodes in the first 2 hours after injection, and the injected activity; the normal reference limit is 15%. This parameter offers an objective measure of lymphatic function, capable of detecting reduced lymphatic drainage in the early stages, even before the appearance of clinical manifestations, or of qualitative changes in the lymphoscintigraphic pattern [1, 24, 25, 31, 35, 36, 59–62].

4.6.5 Removal Rate Constant

The removal rate constant (RRC) represents local lymph flow per unit distribution volume of the flow marker; it is reduced by about 25% in the presence of lymphatic dysfunction involving a local impairment of lymphatic drainage [23, 37, 63].

Table 4.1 Quantitative lymphoscintigraphy and stress tests in lymphedema: main clinical experience

Radiotracer	Route	ROIs	Imaging	
^{99m}Tc-nanocolloid	sc	IS	10×6 seconds, 120×60 seconds dynamic + static	
^{99m}Tc–antimony trisulfide colloids	sc	LN	Dynamic	
^{99m}Tc-HSA	id + sc	IS, LN	0–45 minutes dynamic, 0, 45, 90 minutes static	
^{99m}Tc-nanocolloid	sc, im	LN	15 minutes	
^{99m}Tc-nanocolloid	sc	LN	2 hours	
^{99m}Tc-HSA	sc	IS	10 minutes	
^{99m}Tc-nanocolloid	sc	IS	0, 20 minutes, 2 hours static	
^{99m}Tc-HSA	sc	LN	Static + dynamic + static	
^{99m}Tc–antimony trisulfide colloids	sc	Unknown	Unknown	
^{99m}Tc-HIG	sc	IS and LN	Dynamic + static up to 5.8 hours	
^{99m}Tc-HIG	id	LN, IS	0–2 hours dynamic + static	
^{111}In/^{99m}Tc-HSA/HIgG	sc		3 hours	
^{99m}Tc-nanocolloid	sc	LN, liver	45, 150 minutes half-body images	
^{99m}Tc–rhenium sulphide	sc	IS	0–40 minutes	
^{99m}Tc-HIG	id	IS	1 minutes; 5×1 hour	
^{99m}Tc-HSA	im	IS	4 hours	
^{99m}Tc–antimony colloids	sc	IS	1 hour	
^{99m}Tc–antimony colloids	sc	IS and LN	65 minutes	
^{99m}Tc-nanocolloid	sc	IS, LN	0–30 minutes, dynamic; 35 minutes + 3 hours, static	
^{99m}Tc-nanocolloid	id	IS, LN		
^{99m}Tc–antimony colloids	sc		20–40 minutes, 1 hour, 2 hours	
^{99m}Tc-HSA	id	LN	0–30 minutes	
^{99m}Tc-HIG, ^{99m}Tc-nanocolloid	sc, id	IS	Dynamic intervals 10–171 minutes	
^{99m}Tc-nanocolloid	sc	Unknown	0–100 min dynamic + static	
^{99m}Tc-nanocolloid	sc, id	IS, LN	0–100 minutes dynamic	
^{99m}Tc-nanocolloid	sc	IS	Static	
^{99m}Tc-HSA	sc	IS	0–25 minutes dynamic	

sc, subcutaneous injection; *id*, intradermal injection; *im*, intramuscular injection; *IS*, injection site; *LN*, lymph-node; *ID*, injected dose; *HSA*, human serum albumin; *HIG*, human immunoglobulin; *HIgG*, human immunoglobulin G; *ROI*, region of interest.

	Stress	Parameter	Author
	1. Passive electric foot ergometer at 30 cycles/minute for 2 hours 2. Climb 150 steps	LN uptake % ID after both sessions of exercise	Weissleder et al., 1988 [1]
	None	Modified transport index	Cambria et al., 1993 [14]
	Walk	Clearance rate, LN uptake (time–activity curve)	Nawaz et al., 1990 [19]
	15 minutes walking on a horizontal treadmill 3.2 km/hour	LN uptake % ID depth correction	Mostbeck and Partsch, 1999 [23]; Partsch, 1995 [24]
	Bicycle 25 W	Lymph vessels uptake	Bräutigam et al., 1993 [25]
	3 hours walking	Clearance rate	Kataoka et al., 1991 [30]
	Flexed and straightened feet 20 movements/minute for 20 minutes	Transit time	Dabrowski et al., 2008 [34]
	Standardized treadmill walk (20 times) + walk at the brisk pace for 60 minutes	LN uptake at 2 hours	Damstra et al., 2008 [35]
	None	LN uptake	Gloviczki et al., 1989 [36]
	Squeezing a ball in the hands simultaneously, together with flexion at the elbow and pronation of the forearm (20 cycles/minute)	Removal rate constant	Stanton et al., 2001 [37]
	None	Lymphatic transit time	Modi et al., 2007 [38]
	30 fist clenchings	Clearance rate	Pain et al., 2002 [39]
	None	Liver to lymph node ratio	Stamp and Peters, 2012 [40]
	None	Colloid clearance	Pecking, 1995 [41]; Pecking et al., 1997 [42]
	None	Clearance rate	Svensson et al., 1999 [43]
	100 submaximal contractions in 10 minutes	Clearance rate	Havas et al., 1997 [44]
	Bouts of arm cranking for 5 minutes at 0.6 W/kg or 75 contractions in 2.5 minutes at 50% maximum voluntary contraction	Clearance rate	Lane et al., 2005 [45]
	12 repeated sets of arm cranking for 2.5 minutes at 0.6 W/kg or 12 repeated sets of arm cranking for 2.5 minutes at 0.3 W/kg	Clearance rate	Lane et al., 2006 [46]
	Phase I no movement; phase II feet/toes movements for 5 minutes; phase III 1 hour walking	Extraction % ID and LN uptake (time–activity curve with correction for decay and background)	Bourgeois et al., 1997 [47]
	Walk 3 hours	ROI analysis	Ketterings and Zeddeman, 1997 [48]
	Normal walking 20 minutes	Clearance rate; LN uptake % ID	Proby et al., 1990 [49]
	Standing 15 minutes	LN uptake (time–activity curve)	Suga et al., 2001 [50]
	None	Depot disappearance rate constant	O'Mahony et al., 2004, 2006 [51, 52]
	Tip-toeing exercise in unison for 5 minutes; walk for 30 minutes	Extraction % ID and LN uptake (time–activity curve)	Bourgeois, 2007 [53]
	None	LN % ID	Bourgeois et al., 2009 [54]
	1. Massage + limb elevation	Tracer appearance time	Tartaglione et al., 2010 [55]
	2. Walk/exercise 2 minutes		
	Ergometric bicycle 75 W × 10 minutes	Wash rate constant	Jensen et al., 2012 [56]

4.6.6 Depot Activity Transported to Inguinal Lymph Nodes

This modified method is employed in a few protocols to estimate the depot clearance rate; by using attenuation correction, it takes into account the individual variation in tissue depth, in order to improve quantitation of lymph node activity and to make this parameter more reliable [1, 24, 25, 38].

4.6.7 Uptake Index of the Left Inguinal to the Right Inguinal Lymph Nodes

The uptake index of the left inguinal (UIL) to the right inguinal lymph nodes (UIR) provides the radioactivity ratio for inguinal nodes calculated in the whole-body images acquired at 2 hours post-injection, and requires measurement of radioactivity at the injection site immediately after the administration, to calculate the percentage of the radiocolloid administered into the left/right foot (WpL/WpR). Therefore, UIL/UIR is calculated as the percentage of count rate in the lymph nodes of the left/right inguinal region divided by the count rate over the total body ´ WpL/WpR [34]. The UIL/UIR ratio is also used to identify lymphatic dysfunction; however, some variability in UIL/UIR determination has been reported, thus suggesting that this quantitative parameter should also be employed in association with visual interpretation of the images for improved diagnostic accuracy.

4.6.8 Washout Rate Constant and Depot Half-Life

The washout rate constant (k) and depot half-life ($T_{½} = \ln 2/k$) are parameters of lymphatic function that are calculated by linear regression analysis of the time–activity curve derived from images obtained over 20–25 minutes, starting 40 minutes after the injection of 10 MBq of ^{99m}Tc-HSA (30 minutes of rest + 10 minutes of ergometer cycle at 75 W). The depot half-life is prolonged in the case of lymphatic dysfunction (4.6 hours versus 2.7 hours in normal controls when using ^{99m}Tc-nanocolloid); clearance of ^{99m}Tc-HSA is generally faster [23]. However, these parameters are influenced by the radiopharmaceutical injection technique, and consequently are somewhat unreliable to assess lymphatic dysfunction [28, 38, 39, 64–70].

4.6.9 Liver to Nodal Ratio

The liver-to-nodal ratio (L/N ratio) is calculated based on regions of interest (ROIs) drawn respectively around the right lobe of the liver and around the ilio-inguinal lymph nodes bilaterally in the anterior-view images acquired at 45 minutes and 150 minutes; counts within the ROIs are corrected for background (ROIs on the same horizontal levels as the liver and lateral to the right edge of the ilio-inguinal nodes, respectively). Normal values are 1.8×10^{-6} per pixel (range $1.3–5.5 \times 10^{-6}$ per pixel) at 45 minutes, and 2.5×10^{-6} per pixel (range $1.5–5.0 \times 10^{-6}$ per pixel) at 150 minutes. The 150-minute L/N ratio is most frequently found to be abnormal in patients with lymphatic dysfunction, and correlates well with the severity of lymphoscintigraphic abnormalities [40].

In patients with intracavitary lymph effusion, quantitative evaluation is performed assessing the ratio values (K) between the mean activity/per pixel detected (in all the sequential acquisitions) on ROIs integrated on the focal zone (suspected pathological area – “ROIp”) and the mean activity/per pixel measured on a “nontarget area” (considered a healthy area – “ROIh”) located, as a rule, contralaterally. Accordingly, K is calculated as the ratio ROIp/ROIh. Therefore, a lymphoscintigraphy is defined as normal when stable K values are obtained throughout all of the images. On the other hand, increasing K values at sequential imaging times are consistent with the presence of intracavitary lymph effusion.

It should be noted that clearance values from the injection site may not, on their own, allow, discrimination of lymphedema from normal lymphatic function, as qualitative evaluation is invariably required [24].

References

1. Weissleder H, Weissleder R (1988) Lymphedema: evaluation of qualitative and quantitative lymphoscintigraphy in 238 patients. Radiology 167:729–735
2. Cornford ME, Oldendorf WH (1993) Terminal endothelial cells of lymph capillaries as active transport structures involved in the formation of lymph in rat skin. Lymphology 26:67–78
3. Szuba A, Rockson SG (1997) Lymphedema: anatomy, physiology and pathogenesis. Vasc Med 2:321–326
4. Ikomi F, Schmid-Schönbein GW (1995) Lymph transport in the skin. Clin Dermatol 13:419–427
5. Lubach D, Lüdemann W, Berens von Rautenfeld D (1996) Recent findings on the angioarchitecture of the lymph vessel system of human skin. Br J Dermatol 135:733–737
6. Adair TH, Vance GA, Montani JP et al (1991) Effect of skin concavity on subcutaneous tissue fluid pressure. Am J Physiol Heart Circ Physiol 261:H349–353
7. Aukland K, Reed RK (1993) Interstitial-lymphatic mechanisms in the control of extracellular fluid volume. Physiol Rev 73:1–78
8. Spiegel M, Vesti B, Shore A et al (1991) [Pressure measurement in lymph capillaries of the human skin.] Vasa Suppl 33:278
9. Spiegel M, Vesti B, Shore A et al (1992) Pressure of lymphatic capillaries in human skin. Am J Physiol Heart Circ Physiol 262:H1208–1210
10. Reddy NP, Patel K (1995) A mathematical model of flow through the terminal lymphatics. Med Eng Phys 17:134–140
11. Ikomi F, Hunt J, Hanna G et al (1996) Interstitial fluid, plasma pro-

tein, colloid, and leukocyte uptake into initial lymphatics. J Appl Physiol 81:2060–2067
12. Olszewski WL, Jamal S, Manokaran G et al (1997) Bacteriologic studies of skin, tissue fluid, lymph, and lymph nodes in patients with filarial lymphedema. Am J Trop Med Hyg 57:7–15
13. Pecking AP (1999) Possibilities and restriction of isotopic lymphography for the assessment of therapeutic effects in lymphedema. Wien Med Wochenschr 149:105–106
14. Cambria RA, Gloviczki P, Naessens JM et al (1993) Noninvasive evaluation of the lymphatic system with lymphoscintigraphy: a prospective, semiquantitative analysis in 386 extremities. J Vasc Surg 18:773–782
15. Mortimer PS (1995) Evaluation of lymphatic function: abnormal lymph drainage in venous disease. Int Angiol 14:32–35
16. Mostbeck A, Partsch H (1999) [Isotope lymphography – possibilities and limits in evaluation of lymph transport.] Wien Med Wochenschr 149:87–91
17. Ohtake E, Matsui K (1986) Lymphoscintigraphy in patients with lymphedema. A new approach using intradermal injections of technetium-99m human serum albumin. Clin Nucl Med 11:474–478
18. McNeill GC, Witte MH, Witte CL et al (1989) Whole-body lymphangioscintigraphy: preferred method for initial assessment of the peripheral lymphatic system. Radiology 172:495–502
19. Nawaz MK, Hamad MM, Abdel-Dayem HM et al (1990) Tc-99m human serum albumin lymphoscintigraphy in lymphedema of the lower extremities. Clin Nucl Med 15:794–799
20. Nawaz MK, Hamad MM, Abdel-Dayem HM et al (1992) Lymphoscintigraphy in lymphedema of the lower limbs using ^{99m}Tc HSA. Angiology 43:147–154
21. Suga K, Uchisako H, Nakanishi T et al (1991) Lymphoscintigraphic assessment of leg oedema following arterial reconstruction using a load produced by standing. Nucl Med Commun 12:907–917
22. Williams WH, Witte CL, Witte MH et al (2000) Radionuclide lymphangioscintigraphy in the evaluation of peripheral lymphedema. Clin Nucl Med 25:451–464
23. Miranda F Jr, Perez MC, Castiglioni M et al (2001) Effect of sequential intermittent pneumatic compression on both leg lymphedema volume and on lymph transport as semi-quantitatively evaluated by lymphoscintigraphy. Lymphology 4:135–141
24. Partsch H (1995) Assessment of abnormal lymph drainage for the diagnosis of lymphedema by isotopic lymphangiography and by indirect lymphography. Clin Dermatol 13:445–450
25. Bräutigam P, Vanscheidt W, Földi E et al (1993) The importance of the subfascial lymphatics in the diagnosis of lower limb edema: investigations with semiquantitative lymphoscintigraphy. Angiology 44:464–470
26. Bräutigam P, Földi E, Schaiper I et al (1998) Analysis of lymphatic drainage in various forms of leg edema using two compartment lymphoscintigraphy. Lymphology 31:43–55
27. Partsch H (2003) Practical aspects of indirect lymphography and lymphoscintigraphy. Lymphat Res Biol 1:71–74
28. Jensen MR, Simonsen L, Karlsmark T et al (2010) Lymphoedema of the lower extremities--background, pathophysiology and diagnostic considerations. Clin Physiol Funct Imaging 30:389–398
29. Ogawa Y, Hayashi K (1999) [99mTc-DTPA-HSA lymphoscintigraphy in lymphedema of the lower extremities: diagnostic significance of dynamic study and muscular exercise.] Kaku Igaku 36:31–36
30. Kataoka M, Kawamura M, Hamada K et al (1991) Quantitative lymphoscintigraphy using 99Tcm human serum albumin in patients with previously treated uterine cancer. Br J Radiol 64:1119–1121
31. Rijke AM, Croft BY, Johnson RA et al (1990) Lymphoscintigraphy and lymphedema of the lower extremities. J Nucl Med 31:990–998
32. Kleinhans E, Baumeister RG, Hahn D et al (1985) Evaluation of transport kinetics in lymphoscintigraphy: follow-up study in patients with transplanted lymphatic vessels. Eur J Nucl Med 10:349–352
33. Ikomi F, Hanna GK, Schmid-Schönbein GW (1995) Mechanism of colloidal particle uptake into the lymphatic system: basic study with percutaneous lymphography. Radiology 196:107–113
34. Dabrowski J, Merkert R, Kuśmierek J (2008) Optimized lymphoscintigraphy and diagnostics of lymphatic oedema of the lower extremities. Nucl Med Rev Cent East Eur 11:26–29
35. Damstra RJ, van Steensel MA, Boomsma JH et al (2008) Erysipelas as a sign of subclinical primary lymphoedema: a prospective quantitative scintigraphic study of 40 patients with unilateral erysipelas of the leg. Br J Dermatol 158:1210–1215
36. Gloviczki P, Calcagno D, Schirger A et al (1989) Noninvasive evaluation of the swollen extremity: experiences with 190 lymphoscintigraphic examinations. J Vasc Surg 9:683–690
37. Stanton AW, Svensson WE, Mellor RH et al (2001) Differences in lymph drainage between swollen and non-swollen regions in arms with breast-cancer-related lymphoedema. Clin Sci (Lond) 101:131–40
38. Modi S, Stanton AW, Svensson WE et al (2007) Human lymphatic pumping measured in healthy and lymphoedematous arms by lymphatic congestion lymphoscintigraphy. J Physiol 15:271–285
39. Pain SJ, Nicholas RS, Barber RW et al (2002) Quantification of lymphatic function for investigation of lymphedema: depot clearance and rate of appearance of soluble macromolecules in blood. J Nucl Med 43:318–324
40. Stamp GF, Peters AM (2012) Peripheral lymphovenous communication in lymphoedema. Nucl Med Commun 33:701–707
41. Pecking AP (1995) Evaluation by lymphoscintigraphy of the effect of a micronized flavonoid (Daflon 500 mg) in the treatment of upper limb lymphedema. Int Angiol 14:39–43
42. Pecking AP, Fevrier B, Wargon C et al (1997) Efficacy of Daflon 500 mg in the treatment of lymphedema (secondary to conventional therapy of breast cancer). Angiology 48:93–98
43. Svensson W, Glass DM, Bradley D et al (1999) Measurement of lymphatic function with technetium-99m-labelled polyclonal immunoglobulin. Eur J Nucl Med 26:504–510
44. Havas E, Parviainen T, Vuorela J et al (1997) Lymph flow dynamics in exercising human skeletal muscle as detected by scintography. J Physiol 504:233–239
45. Lane K, Worsley D, McKenzie D (2005) Lymphoscintigraphy to evaluate the effects of upper body dynamic exercise and handgrip exercise on radiopharmaceutical clearance from hands of healthy females. Lymphat Res Biol 3:16–24
46. Lane K, Dolan L, Worsley D et al (2006) Lymphoscintigraphy to evaluate the effect of high versus low intensity upper body dynamic exercise on lymphatic function in healthy females. Lymphat Res Biol 4:159–165
47. Bourgeois P, Munck, D, Becker C et al (1997) A three phase lymphoscintigraphic investigation protocol for the evaluation of lower limbedemas. Eur J Lymphol Rel Probl 21:10–21
48. Ketterings C, Zeddeman S (1997) Use of the C-scan in evaluation of peripheral lymphedema. Lymphology 30:49–62
49. Proby CM, Gane JN, Joseph AE et al (1990) Investigation of the swollen limb with isotope lymphography. Br J Dermatol 123:29–37
50. Suga K, Kume N, Matsunaga N et al (2001) Assessment of leg oedema by dynamic lymphoscintigraphy with intradermal injection of technetium-99m human serum albumin and load produced by standing. Eur J Nucl Med 28:294–303
51. O'Mahony S, Rose SL, Chilvers AJ et al (2004) Finding an optimal method for imaging lymphatic vessels of the upper limb. Eur J Nucl Med Mol Imaging 31:555–63
52. O'Mahony S, Solanki CK, Barber RW et al (2006) Imaging of lymphatic vessels in breast cancer-related lymphedema: intradermal versus subcutaneous injection of ^{99m}Tc-immunoglobulin. Am J Roentgenol 186:1349–1355

53. Bourgeois P (2007) Scintigraphic investigations of the lymphatic system: the influence of injected volume and quantity of labeled colloidal tracer. J Nucl Med 48:693–695
54. Bourgeois P, Leduc O, Belgrado JP et al (2009) Scintigraphic investigations of the superficial lymphatic system: quantitative differences between intradermal and subcutaneous injection. Nucl Med Commun 30:270–274
55. Tartaglione G, Pagan M, Morese R et al (2010) Intradermal lymphoscintigraphy at rest and after exercise: a new technique for the functional assessment of the lymphatic system in patients with lymphoedema. Nucl Med Commun 31:547–551
56. Jensen MR, Simonsen L, Karlsmark T et al (2012) The washout rate of a subcutaneous ^{99m}Tc-HSA depot in lower extremity lymphoedema. Clin Physiol Funct Imaging 32:126–132
57. Hung JC, Wiseman GA, Wahner HW et al (1995) Filtered technetium-99m-sulfur colloid evaluated for lymphoscintigraphy. J Nucl Med 36:1895–1901
58. Tartaglione G, Rubello D (2010) The evolving methodology to perform limb lymphoscintigraphy: from rest to exercise acquisition protocol. Microvasc Res 80:540–4
59. Burnand KG, McGuinness CL, Lagattolla NR et al (2002) Value of isotope lymphography in the diagnosis of lymphoedema of the leg. Br J Surg 89:74–78
60. Brorson H, Svensson H, Norrgren K et al (1998) Liposuction reduces arm lymphedema without significantly altering the already impaired lymph transport. Lymphology 31:156–172
61. Carena M, Campini R, Zelaschi G et al (1988) Quantitative lymphoscintigraphy. Eur J Nucl Med 14:88–92
62. Bourgeois P, Dargent JL, Larsimont D et al (2009) Lymphoscintigraphy in angiomyomatous hamartomas and primary lower limb lymphedema. Clin Nucl Med 34:405–409
63. Noer I, Lassen NA (1979) Evidence of active transport (filtration?) of plasma proteins across the capillary walls in muscle and subcutis. Acta Physiol Scand Suppl 463:105–110
64. Stanton AW, Modi S, Bennett Britton TM et al (2009) Lymphatic drainage in the muscle and subcutis of the arm after breast cancer treatment. Breast Cancer Res Treat 117:549–557
65. Stanton AW, Modi S, Mellor RH et al (2006) A quantitative lymphoscintigraphic evaluation of lymphatic function in the swollen hands of women with lymphoedema following breast cancer treatment. Clin Sci (Lond) 11:553–561
66. Pain SJ, Barber RW, Ballinger JR et al (2004) Tissue-to-blood transport of radiolabelled immunoglobulin injected into the web spaces of the hands of normal subjects and patients with breast cancer-related lymphoedema. J Vasc Res 41:183–192
67. Pain SJ, Barber RW, Ballinger JR et al (2003) Side-to-side symmetry of radioprotein transfer from tissue space to systemic vasculature following subcutaneous injection in normal subjects and patients with breast cancer. Eur J Nucl Med Mol Imaging 30:657–61
68. Pain SJ, Barber RW, Ballinger JR et al (2004) Local vascular access of radioprotein injected subcutaneously in healthy subjects and patients with breast cancer-related lymphedema. J Nucl Med 45:789–796
69. Modi S, Stanton AW, Mellor RH et al (2005) Regional distribution of epifascial swelling and epifascial lymph drainage rate constants in breast cancer-related lymphedema. Lymphat Res Biol 3:3–15
70. Gothard L, Stanton A, MacLaren J et al (2004) Non-randomised phase II trial of hyperbaric oxygen therapy in patients with chronic arm lymphoedema and tissue fibrosis after radiotherapy for early breast cancer. Radiother Oncol 70:217–224

5 Lymphoscintigraphy for the Differential Diagnosis of Peripheral Edema and Intracavitary Lymph Effusion

Paola Anna Erba, Martina Sollini, and Roberto Boni

5.1 Introduction

Patients with lower-extremity lymphedema initially present with unilateral painless swelling that starts on the dorsal aspect of the foot, but eventually progresses to involve the proximal portion of the limb. The edema is initially a pitting edema, but over time the subcutaneous tissue becomes fibrotic, resulting in nonpitting brawny edema. The edema can then spread circumferentially if treatment is not initiated, involving the skin, which becomes hyperkeratotic, hyperpigmented, and papillomatous or verrucous, with increased skin turgor. The Kaposi–Stemmer sign, in which the examiner is unable to pinch a fold of skin at the base of the second toe on the dorsal aspect of the foot, indicates clinical lymphedema [1–3]. Ultimately, the skin is at risk for ulcerating and subsequent infection. Swelling associated with lymphedema results in a sensation of heaviness, discomfort, and impaired mobility of the limb. Angiosarcoma may develop in chronic lymphedematous limbs (Stewart–Treves syndrome), but is most commonly seen in the upper extremity following mastectomy with axillary lymph node dissection [4]. This condition is often referred to as lymphangiosarcoma, which is actually a misnomer, since the tumor is not derived from lymphatic vessels, but is rather derived from vascular endothelial cells within a condition of chronic lymphedema.

The International Society of Lymphology has established a staging system for defining the severity of this disease [5]. It is thus possible to identify the progression of the condition and the potential for successful treatment and improvement. This staging system, which applies only to the limbs (arms and legs), is based on the degree of swelling and the condition of the skin and tissues. The current version of the ISL lymphedema staging system consists of four levels, graded from 0 to III.

- *Stage O lymphedema*: *latent or preclinical stage* – at this stage, the patient is at risk of developing lymphedema; however, no swelling or other visible evidence of impaired lymph drainage is present. Stage 0 can be present for months, or years, before more serious signs appear. If specialized treatment is started at this stage, it may be possible to prevent the development of further stages of lymphedema.
- *Stage I lymphedema* is an early accumulation of fluid that is relatively high in protein content. There is visible swelling with protein-rich lymph. The swelling can be temporarily reduced by elevation of the limb; however, it soon reappears when the limb is returned to a normal position. The swollen tissues are soft, and pitting edema is present. Treatment should initiate as early as these clinical signs are detected, since waiting for the swelling to increase, or for an infection to develop, only makes the condition more difficult to treat. Prompt treatment of this stage can often control the condition and may prevent it from becoming more severe.
- *Stage II lymphedema* is a further increase in swelling accompanied by concomitant tissue changes. Elevation of the limb will not reduce the swelling, and tissues become increasingly firm, due to fibrosis. Pressure against the limb produces only a slight pitting, or no pitting at all. The tissue changes at this stage increase the risks of even greater swelling, fibrosis, infections, and skin problems. Stage II lymphedema can usually be improved with intense treatment.
- *Stage III lymphedema,* also known as *lymphostatic elephantiasis*, is a condition in which the tissue becomes extremely swollen and thickened, due to blockage of lymph flow and build up of fluid in tissues. The tissues become increasingly fibrotic. Pressure does not produce any pitting. Normal elasticity is lost, and the skin hangs in folds

P. A. Erba (✉)
Regional Center of Nuclear Medicine, University of Pisa Medical School
Pisa, Italy
e-mail: p.erba@med.unipi.it

G. Mariani et al. (eds.), *Atlas of Lymphoscintigraphy and Sentinel Node Mapping*,
DOI 10.1007/978-88-470-2766-4_5 © Springer-Verlag Italia 2013

and may change color. *Papillomas* and *hyperkeratosis* can develop. Changes in skin texture are disfiguring and can limit mobility. Infections become more common because of increased risk of ulcerations of the skin. These infections include fungal infections and open wounds that form within the skin folds. With intense therapy, stage III lymphedema can be improved and potentially be prevented from becoming even worse; however, it is rarely reversed to an earlier stage.

A new classification of limb lymphedema was proposed in 2009, inspired by the **C**linical, **E**tiologic, **A**natomic, and **P**athophysiologic (CEAP) classification for chronic venous insufficiency of the lower limbs. It adopts the acronym CEAP by adding the letter **L** (**L**ymphatic) to underline the aspect "lymphedema". This clinical classification is subdivided into five classes, depending on the presence of clinical signs such as the extent of lymphedema, the presence of lymphangitis and/or leg ulcers, and the loss of functionality of the limb. The etiological aspect considers two types of alterations of the lymphatic system: congenital and acquired. The anatomic classification aims at identifying the anatomical structures involved. Pathophysiological conditions are subdivided into five groups: agenesia or hypoplasia, hyperplasia, reflux, overload, and obstruction. The CEAP-L classification was created to categorize patients with definite and objective marks, to generate clinical reports with a common and clear vocabulary, to stage the disease, to evaluate treatment, and to obtain epidemiological and statistical data [6].

5.2 Differential Diagnosis

Lymphedema should be considered whenever an edematous extremity without pain or inflammation is observed. Chronic venous insufficiency can be difficult to differentiate from early lymphedema, because both have pitting edema, and the skin changes typical of late-stage lymphedema are not yet present. Nevertheless, chronic venous insufficiency is often bilateral, rather than unilateral as is generally the case for lymphedema. Lymphoscintigraphy may be necessary to distinguish the two conditions, although such discrimination cannot always be made, since chronic venous insufficiency can actually lead to secondary lymphedema. Similarly, deep vein thrombosis can cause a postphlebitic syndrome, which can result in lipodermatosclerosis and chronic swelling of the limb [2, 3] In nonfilarial regions of tropical Africa, Central America, and the Indian subcontinent, there is a condition that clinically presents in a similar fashion as filariasis, called podoconiosis, or nonfilarial elephantiasis.

Exclusion of general medical causes of lower-extremity swelling should be a priority. These causes include, but are not limited to, renal failure, protein-losing nephropathy, hypoalbuminemia, congestive heart failure, pulmonary hypertension, drug-induced edema, obesity, and pregnancy [7]. Other conditions to consider in differential diagnosis include lipedema (also known as lipomatosis of the leg), "armchair legs" (a descriptive term that results from sitting in a chair all day and night with one's legs in a dependent position), and postoperative swelling.

5.3 Diagnostic Characterization

Objective measurement of limb swelling can be problematic. On the other hand, assessing differences in extremity size and quantitative discrepancies between the unaffected and the affected limbs is critical, particularly in the early phases of lymphedema. Estimation of differences in limb volume has been used as an indirect measure of changes in lymph fluid volume over time or with treatment, and is typically done through circumferential measurements, or through immersion techniques based on measurement of volume displacement [8]. However, these methods are time consuming and somewhat operator dependent. Moreover, since these techniques measure only the overall volume of the limbs, possible differences in volume caused by left–right dominance, muscle atrophy, fibrous tissue deposition, or weight gain may incorrectly be attributed to fluid accumulation [9].

Bioimpedance spectroscopy (BIS) is a noninvasive procedure where an electrical current is passed through a body segment, and impedance to current flow is subsequently measured. This technique, which attempts to directly measure lymph fluid volume [10], is based on the principle that tissues such as fat and bone act as insulators, while electrolytic fluids conduct electricity; these features would make it possible to assess properties unique to lymphatic fluid, through measurement of the flow of current. BIS measures lymphedema, based on the fact that low-frequency currents selectively pass through extracellular fluid compartments, whereas high-frequency currents pass through both the intracellular and the extracellular fluids (the latter being selectively expanded in lymphedema) [11]. BIS analyzes both lymph fluid impedance and total fluid impedance [12], and impedance to current flow has been found to inversely correlate with fluid accumulation; therefore, reduced impedance values in an extremity indicate the presence of lymphedema.

A variety of other techniques have been described to measure limb edema, but most of them have not been validated or are too complex or expensive for routine use [13, 14]. A practical difficulty in the clinical setting, even with validated techniques, is that extravascular fluid volume undergoes cyclic changes over days or weeks, and limb volume also has a pronounced circadian variation.

High-resolution cutaneous ultrasonography may be used to identify lymphedema, based on the presence of increased

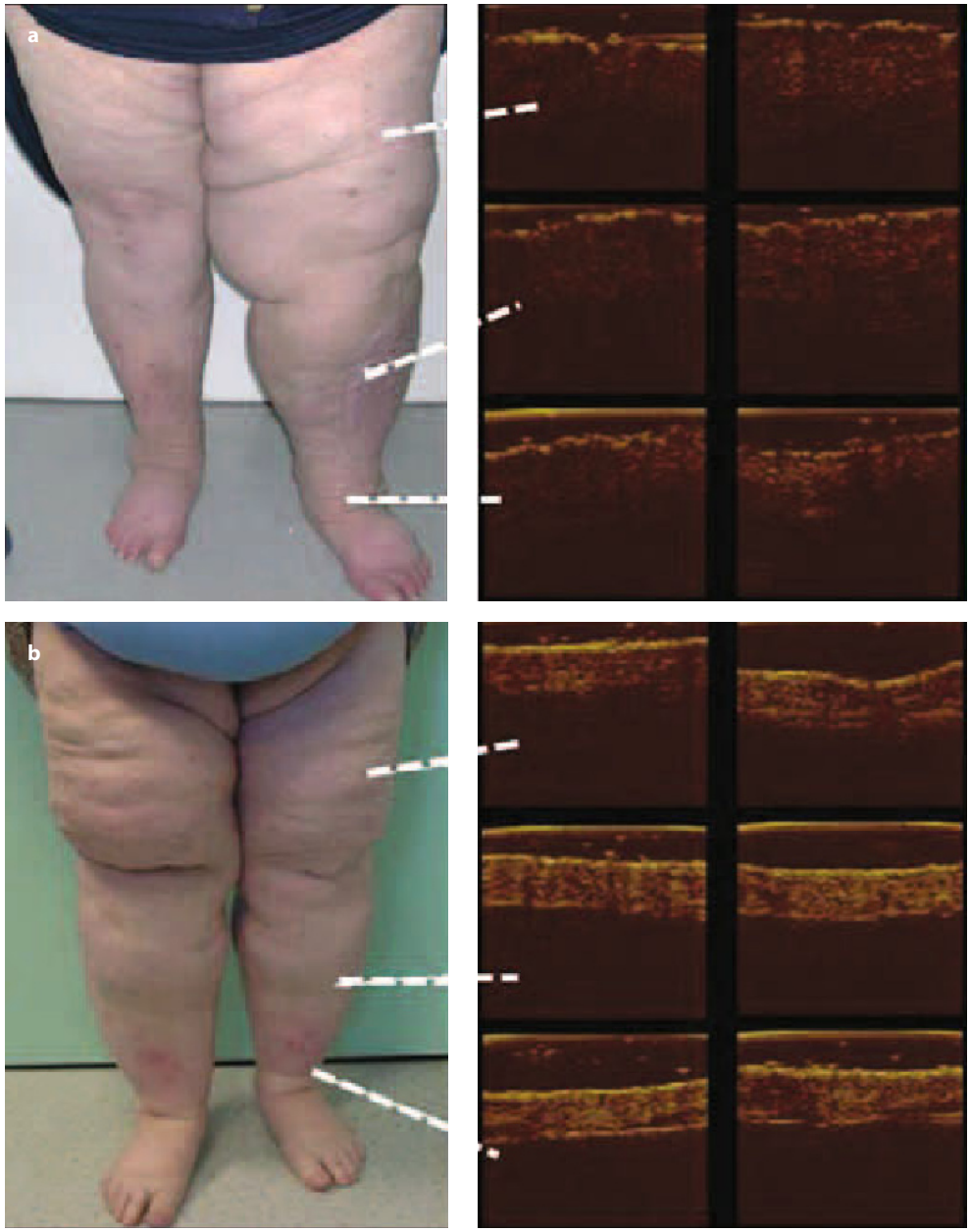

Fig. 5.1 Clinical appearance (*left panels*) and ultrasound pattern (*right panels*) in patients with lymphoedema (**a**) or lipedema (**b**). Increased volume of both lower limbs with predominant enlargement of the left is evident in the patient with lymphedema; the corresponding ultrasound examination indicates decreased echogenicity and increased thickness of the dermis. In the patient with lipedema, increased lower limb volume is similarly evident, but with more pronounced symmetry; the corresponding ultrasound examination identifies normal echogenicity and thickness of the dermis, therefore confirming the diagnosis of lipedema versus lymphedema; from [18], with permission

dermal thickness and decreased echogenicity as compared with lipedema and venous insufficiency [15]. In fact, in lymphedema a loss of echogenicity of the skin and a global and homogeneous dermal hypoechogenicity are observed, in contrast to the elective superficial dermis localization of edema described in venous insufficiency [16, 17]. These findings are caused by the accumulation of protein-rich exudative interstitial fluid in the skin and subcutaneous tissue; this fluid remains trapped at the production site because of its high protein content, whereas transudate edema caused by venous insufficiency is more mobile and accumulates in the superficial dermis. However, in order to analyze dermal changes for identifying and quantifying dermal edema, the ultrasound device should operate at 20 MHz [18]. Fig. 5.1 shows the clinical and ultrasound appearance for patients with lymphedema and with lipedema, respectively.

Whenever the clinical diagnosis of lymphedema is controversial, it can be either confirmed or ruled out with lymphoscintigraphy, which is considered the method of choice to evaluate the lymphatic pathways and their drainage pattern [19]. Direct lymphangiography using an iodine oil contrast agent capable of visualizing the lymphatics [20] is no longer routinely performed, because it can lead to life-threatening complications and is difficult to perform [21]. Fig. 5.2 shows an example of direct lymphangiography.

X-ray computed tomography (CT) scanning or magnetic

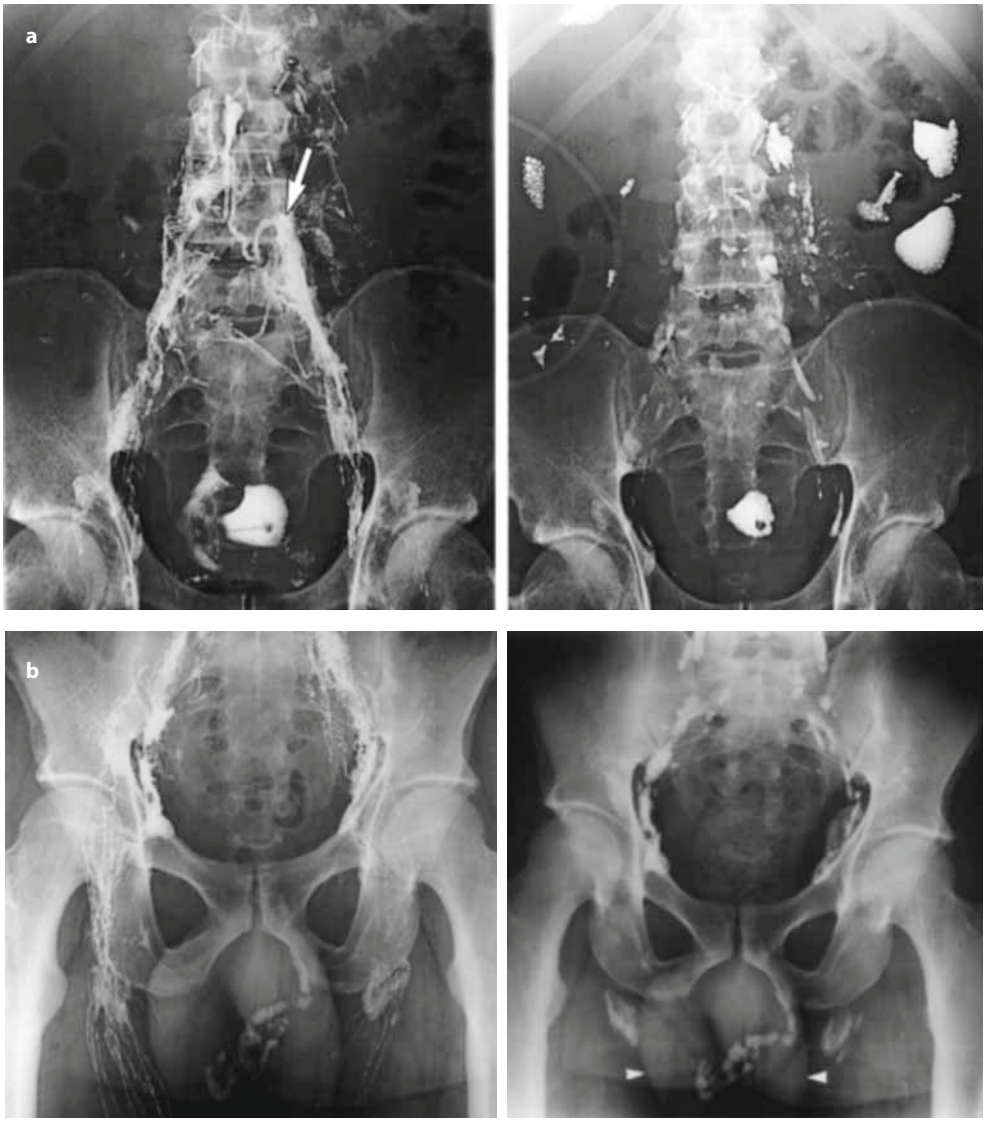

Fig. 5.2 **a** Iodine oil lymphogram in a patient with chylous ascites, affected by AIDS-related peritoneal tuberculosis. Images obtained during the filling phase (*left panel*) show peritoneal extravasation of the contrast material. The site of leakage is seen immediately to the left of L4 (*arrow*). Images obtained during the storage phase (*right panel*) show extensive leakage in the form of oily droplets within the peritoneal cavity. **b** External genitalia lymphedema of parasitic origin: images obtained during the filling phase (*left panel*) show filling of the scrotum by left-sided lymphatic reflux; images obtained during the lymph node phase at 24 hours (*right panel*) show accumulation of contrast material in the scrotum (*arrowheads*). The lymph nodes are normal. **c** Edema of the left leg caused by aplasia of the lymphatic vessels. The lymphogram obtained immediately after administration of the contrast agent shows no lymphatic vessels, and perivascular extravasation. Lymphatic drainage of the contrast material occurs mainly along the venous vessel sheaths; from [22], with permission

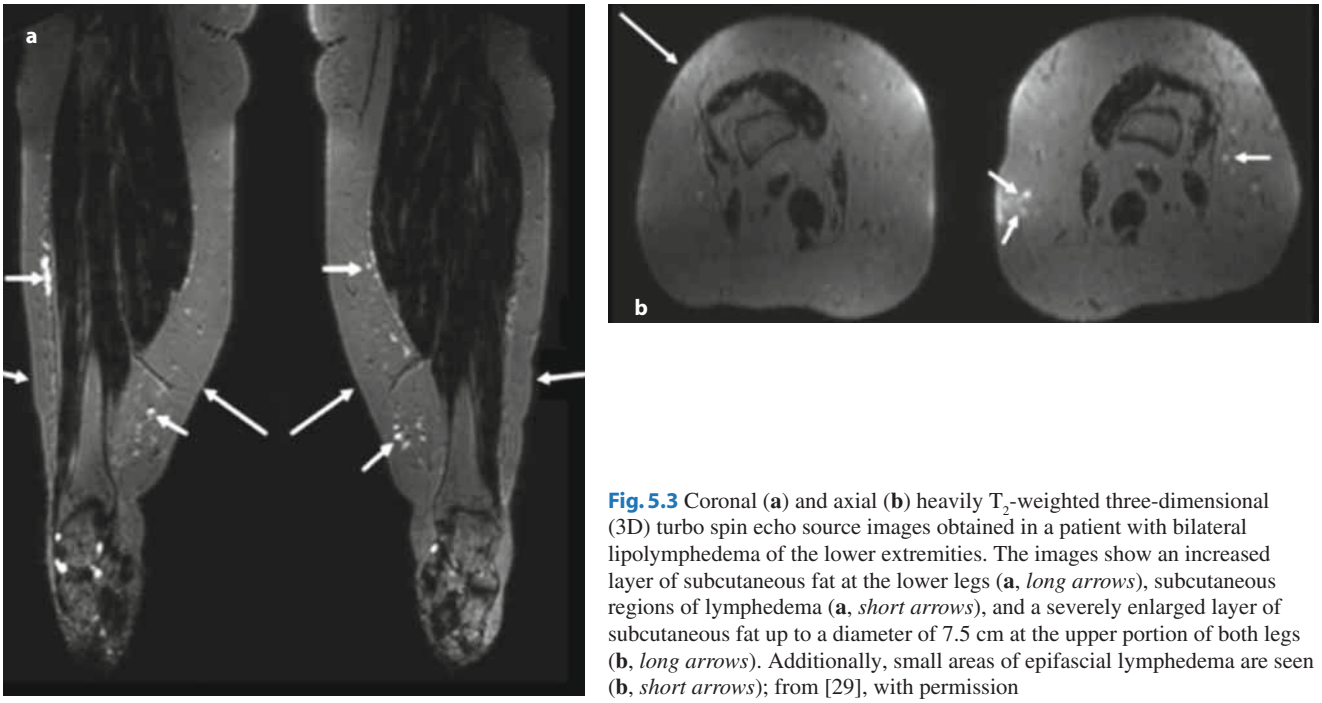

Fig. 5.3 Coronal (**a**) and axial (**b**) heavily T_2-weighted three-dimensional (3D) turbo spin echo source images obtained in a patient with bilateral lipolymphedema of the lower extremities. The images show an increased layer of subcutaneous fat at the lower legs (**a**, *long arrows*), subcutaneous regions of lymphedema (**a**, *short arrows*), and a severely enlarged layer of subcutaneous fat up to a diameter of 7.5 cm at the upper portion of both legs (**b**, *long arrows*). Additionally, small areas of epifascial lymphedema are seen (**b**, *short arrows*); from [29], with permission

resonance imaging (MRI) of the lower extremity can also detect a "honeycomb" pattern of the subcutaneous tissue that is not characteristic of other types of edema. CT and MRI have been used to describe the morphologic changes due to the subcutaneous lipomatous hypertrophy [23–26]. High-resolution magnetic resonance lymphangiography (MRL) with interstitial intracutaneous injection of an extracellular paramagnetic contrast agent has recently been proposed for identifying abnormal lymphatic pathways [27–29]. This technique, which has proved to be technically feasible in patients with primary or secondary lymphedema [30–32], visualizes the lymphatic vessels in a limb with lymph flow disturbances, but not the lymphatic vessels of a healthy limb. This is probably due to the faster lymph flow speed in the healthy limb. Therefore, disorders of lymph circulation should be suspected when contrast-enhanced lymphatic vessels are visualized with this test. Migration of the contrast agent by the draining lymphatic system to regional lymph nodes also allows real-time inspection of the transport function of the lymphatic system and of the lymph nodes, within a reasonable length of time. Furthermore, the specificity of absorption and transport of the contrast agent by the lymphatic system permits visualization of detailed morphologic changes of the lymphatic vessels and of the regional lymph nodes. Finally, quantitative assessment of abnormal lymph flow kinetics may be achieved by tracing the flow within the lymphatic vessels and comparing dynamic nodal enhancement and time–signal intensity curves between edematous and contralateral limbs. Figs. 5.3 to 5.5 depict different MRL patterns in patients with lymphedema. However, it should be noted that MRL is still in an experimental validation phase, since the extravascular intracutaneous injection of contrast agents is an off-label use of such compounds. Side effects such as moderate necrosis, hemorrhage, and edema have been described. Furthermore, incorrect interstitial injection of the contrast agent may lead to severe venous contamination.

A venous Doppler ultrasound examination is often needed to assess for deep venous thrombosis or venous disease, which can be associated with lymphedema. In fact, 20–30% of patients with advanced chronic venous disease have associated lymphatic dysfunction, presumably due to secondary damage from overload, or from recurrent cellulitis [33].

If filariasis is suspected, a blood smear can be performed (collected at night) looking for the presence of microfilariae. Antigen testing by immunochromatographic card test (Binax) or enzyme-linked immunosorbent assay (TropBio) is more sensitive than microfilariae detection, irrespective of the time of day blood is drawn [34].

In addition to a thorough clinical history and physical examination, other diagnostic tests to rule out alternative causes of lower-extremity edema may include a complete metabolic profile, serum albumin, and urinalysis to screen for renal failure, hypoalbuminemia, and/or protein-losing enteropathy.

5.4 Management of Lymphedema

Limb lymphedema is associated with significant morbidity in terms of the functional, cosmetic, and emotional conse-

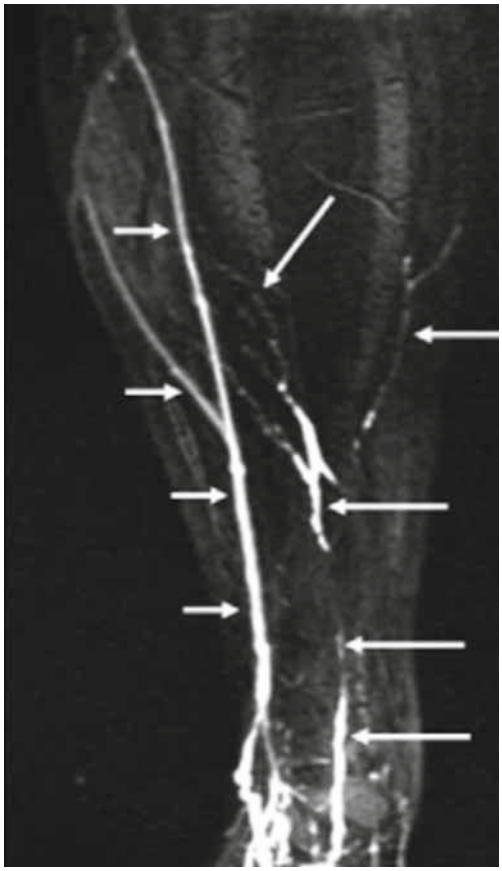

Fig. 5.4 Frontal 3D spoiled gradient-echo MRL maximum intensity projection image obtained 45 minutes after gadoteridol injection in a patient with bilateral lipedema, showing clearly enlarged lymphatic vessels with a typical bead-like appearance up to a diameter of 2 mm at the level of the right lower leg (*large arrows*), indicating a subclinical status of lipolymphedema. High uptake of contrast material is evident in the lymphatic vessels at the right lower leg as well as in a vein (*small arrows*); from [29], with permission

quences of this chronic and potentially disabling condition. Treatment efforts aim at minimizing the associated swelling, at restoring cosmesis and functionality of the limb, and at preventing potential complications associated with lymphedema (such as cellulitis and lymphangitis). Treatments are lengthy and expensive, and involve a multidisciplinary approach that can include rehabilitative lymphedema therapy (elevation, exercise, compression devices, manual lymph drainage), skin care, and surgery [35, 36].

Drug therapies have so far been disappointing in the management of lymphedema. Although family physicians often prescribe diuretic drugs, this therapy is actually not beneficial in lymphedema. Coumarin, a benzopyrone, has been reported to have some favorable effect on lymphedema, probably due to its mechanism of action that reduces vascular permeability, and thus capillary filtration. Additionally, coumarin is thought to activate macrophage activity, which increases protein degradation, thus resulting in a reduction in fibrotic tissue. However, the clinical trials reported so far are generally of poor quality, long-term results of treatment of lymphedema with these agents are not available, and some reports of hepatotoxicity cause serious concern [37].

5.5 Lymphoscintigraphy in the Management of Lymphedema

Qualitative and quantitative lymphoscintigraphy has been widely used for assessing the efficacy of treatments for lymphedema, including microsurgery [38–41], manual lymphatic massage [42–47], pneumatic compression [48–50], hyperthermia [51], and pharmacologic therapies [52, 53]. In women undergoing therapy for post-mastectomy lymphedema, the degree of impairment of lymphatic function prior to the treatment, as assessed by lymphoscintigraphy, correlates inversely with the outcome of manual lymphatic therapy [54]. Similarly, in patients with clinical stage I unilateral extremity lymphedema, lymphoscintigraphy can predict the long-term response to multi-approach physical therapy. In this regard, the visualization of a main lymphatic vessel without collateral lymphatic vessels has been reported to be the best predictor for a favorable response [55], as also was persisting lymph node visualization 4 hours after radiocolloid administration [56]. Lymphatic regeneration following both free-tissue [57] and lymphatic-vessel transplantation [58] has also been assessed with lymphoscintigraphy. Additionally, lymphoscintigraphic classification of patients with secondary lymphedema correlates closely with the clinical stage scale and with findings at intraoperative examination during lymphaticovenous anastomosis [59]. In unilateral lymphedema, lymphoscintigraphic abnormalities of the contralateral limb may also be demonstrated in about 32% of patients [60].

Lymphoscintigraphy may also be used to predict the risk of developing lymphedema. In fact, in patients undergoing surgery for breast cancer, abnormalities of lymphatic drainage in postsurgical lymphoscintigraphy increase the risk of developing arm lymphedema [61, 62]. Similarly, functional lymphatic changes detected by lymphoscintigraphy after external beam radiation therapy can predict the development of arm lymphedema. Recently, lymphoscintigraphy including SPECT/CT of the axillary region has been employed to evaluate the impact of including, as target volumes in the radiation treatment plan, lymph nodes involved in arm drainage that could affect lymphedema [63]. This study demonstrated that radiation doses to these lymph nodes can vary between zero and the full prescribed dose, therefore possibly affecting the development of lymphedema.

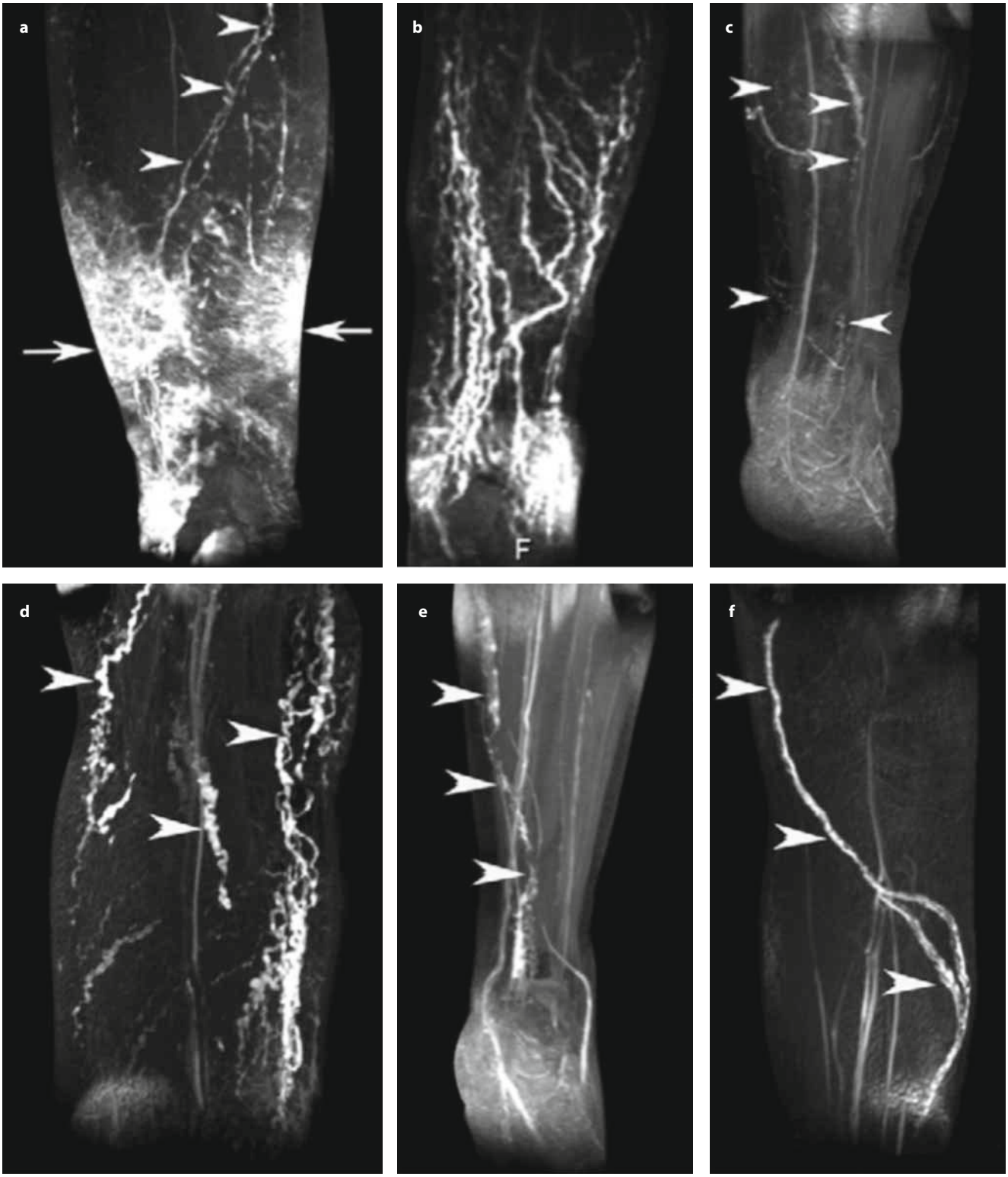

Fig. 5.5 3D contrast MRLs displaying various patterns of lymphatic drainage. **a** Increased skin lymphatic and dermal back flow in the medial and lateral region of the lower leg (*arrows*), and dilated collectors in the upper part of the leg (*arrowheads*). **b** Radially arranged dilated vessels in the lower leg of a patient with primary lymphedema. **c** Enhanced lymphatic vessels (*arrowheads*) distributed as a slender network over the lower extremity. **d** Bunches of extremely dilated and significantly enhanced lymphatic vessels (*arrowheads*) located in the medial and lateral portion of the thigh. **e** Single enhanced and dilated lymphatic vessel in a patient with primary lymphedema (*arrowheads*) with irregular outline in the leg. **f** Intensely enhanced dilated lymph vessel (*arrowheads*) with clear outline in the thigh; from [30], with permission

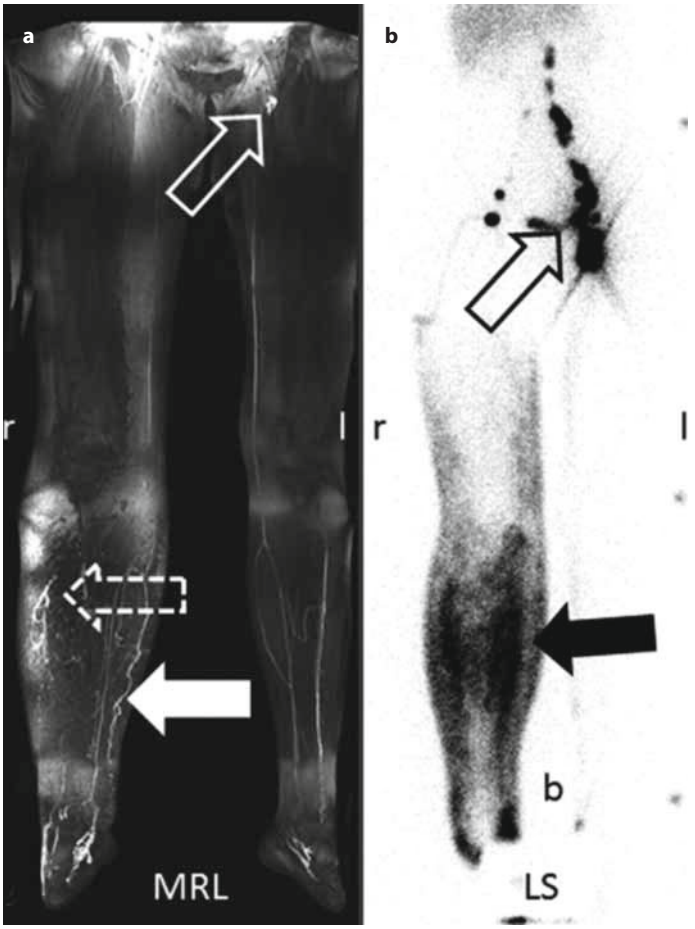

Fig. 5.6 Patient with stage II lymphedema of the right leg. **a** MRL image obtained with a 3.0 T system after intracutaneous injection of gadopentetate dimeglumine and mepivacaine in the first three interdigital spaces of the forefoot. **b** Late phase (2 hours) lymphoscintigraphic images. In the right leg, diffuse lymphatic drainage (*dashed arrow*) and lymphangiectasia (*solid white arrow*) were detectable. MRL shows an early enhancing lymph node in the left groin (*open arrow*) and no contralateral iliac lymph node enhancement, thus suggesting delayed drainage in this leg. Lymphoscintigraphy clearly depicts a diffuse drainage pattern (*solid black arrow*) and diminished right-sided inguinal lymph nodes. The radiocolloid was almost completely drained from the left leg at the time of acquisition, so that lymph vessels on this side were no longer visible. From [31], with permission

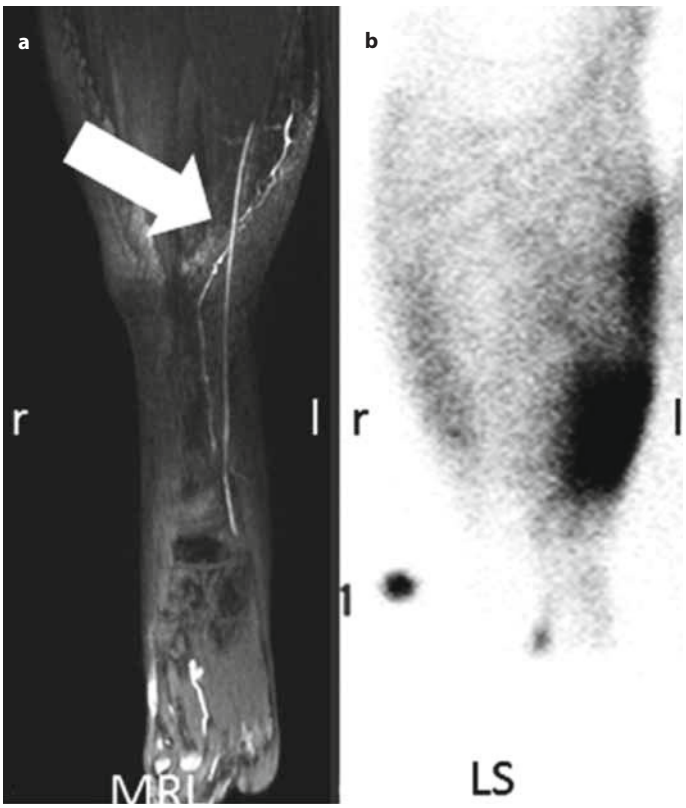

Fig. 5.7 Patient with stage II lymphedema of the left leg. **a** MRL image obtained with a 3.0 T magnetic resonance system after injection of gadopentetate dimeglumine and mepivacaine in the first three interdigital spaces of the forefoot. **b** Late-phase (2 hours) lymphoscintigraphic images. Lymphoscintigraphy shows that the pretibial lymph vessel is masked by the localized dermal backflow, whereas the lymph vessel is clearly visible in the MRL image (**a**, *large white arrow*). The marker position is indicated by "1". From [31], with permission

The lack of visualization of inguinal lymph nodes also predicted late postoperative leg edema in patients with tibial fractures treated surgically [31].

The first correlations between the lymphoscintigraphic pattern as evaluated with technetium-99m (^{99m}Tc)- nanocolloid (injected subcutaneously at the interdigital web) and MRL findings (3 T system, gadopentetate dimeglumine and mepivacaine injected intracutaneously in the first three interdigital spaces of the forefoot) demonstrated clear concordance between the results of the two techniques, with lymphoscintigraphy visualizing better the inguinal lymph nodes, and MRL depicting the lymph vessels and morphology of lymph vessel abnormalities) [22]. Figs. 5.6 and 5.7 represent two examples of comparison between the two techniques in the same patient.

The indications for lymphoscintigraphy can schematically be summarized as follows:

- differential diagnosis of edema to distinguish venous from lymphatic etiology
- assessment of pathways of lymphatic drainage
- quantitation of lymph flow
- identification of patients at high risk of developing lymphedema following axillary lymph node dissection
- evaluation of the efficacy of therapeutic interventions for lymphedema.

Clinical Cases

Case 5.1
Upper Limb Monocompartmental Lymphoscintigraphy in Stage III Primary Lymphedema of the Upper Left Arm Without Lymphadenomegaly

Luciano Feggi, Chiara Peterle, Corrado Cittanti, Valentina de Cristofaro, Stefano Panareo, Ilaria Rambaldi, Virginia Rossetti, and Ivan Santi

Background Clinical Case

A 45-year-old woman presented with spontaneous onset of mild non-pitting swelling in the upper left arm, in absence of vascular lesions (stage III primary lymphedema with no lymphadenomegaly).

Anatomic location of edema: left upper limb.

Lymphoscintigraphy

Lymphoscintigraphy was performed following administration of two aliquots of 2 mL containing 111 MBq ^{99m}Tc-albumin nanocolloid. Radiopharmaceutical injections were performed superficially into both hands (injection in 1st, 2nd, 3rd and 4th interdigital space in each hand). A dual-detector SPECT gamma camera (E-cam Siemens Medical Solutions, Hoffman Estates, IL) equipped with low-energy high-resolution (LEHR) collimators was used to obtain planar images. Planar images were acquired 5 min (early images) and 4 h (late images) after injection in anterior view (256×256 matrix, zoom factor 1.00, acquisition time 200 s for each view).

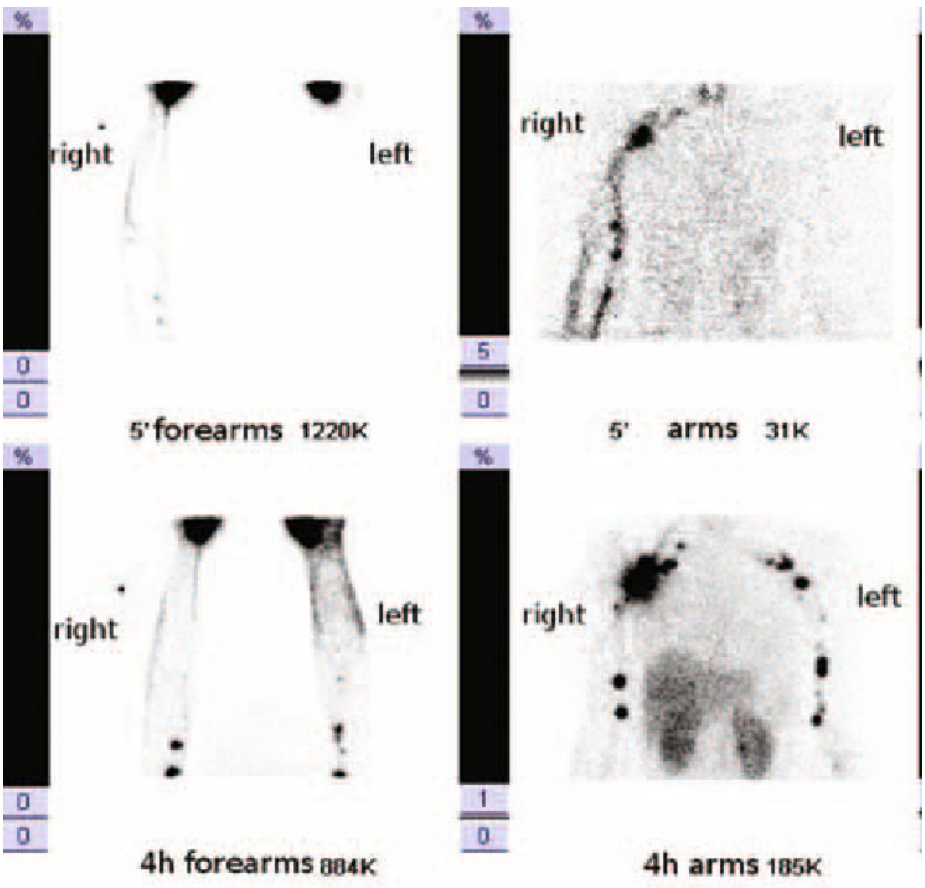

Fig. 1 Delayed drainage at the left upper limb in the early acquisitions and "dermal flow" in the 4 h acquisitions. A similar pattern is observed for lymph node uptake in the spot acquisitions over the thorax-upper abdomen: no lymph node uptake in the left axilla in the early acquisitions, however with some uptake in the delayed acquisitions (the left side lymph nodes remaining always less evident that the contralateral lymph nodes). Based on the results of lymphoscintigraphy, the patient underwent combined therapy for lymphedema (pneumatic compression, wrapping of forearm and massages)

Case 5.2
Upper Limb Monocompartmental Lymphoscintigraphy in Non-Pitting Edema of the Upper Left Limb in Patient with Rheumatoid Arthritis

Luciano Feggi, Chiara Peterle, Corrado Cittanti, Valentina de Cristofaro, Stefano Panareo, Ilaria Rambaldi, Virginia Rossetti, and Ivan Santi

Background Clinical Case

A 40-year-old woman with history of rheumatoid arthritis and mild non-pitting edema in left upper limb (left hand and forearm) for 6 months.

Anatomic location of edema: left upper limb.

Lymphoscintigraphy

Lymphoscintigraphy was performed following administration of two aliquots of 2 mL containing 74 MBq ^{99m}Tc-albumin nanocolloid. Radiopharmaceutical injections were performed superficially and bilaterally (injection in 1st, 2nd, 3rd, and 4th interdigital space in each hand). A dual-detector SPECT gamma camera (E-cam Siemens Medical Solutions, Hoffman Estates, IL) was used to obtain planar images. Time of acquisition after injection: 5 min after injections (early images): (a) hands and forearms (laid upon collimator); (b) arms and thorax; 4 h after injection (late images): (a) hands and forearms (laid upon collimator); (b) arms and thorax (256×256 matrix, zoom factor 1.00, acquisition time 200 s for each view).

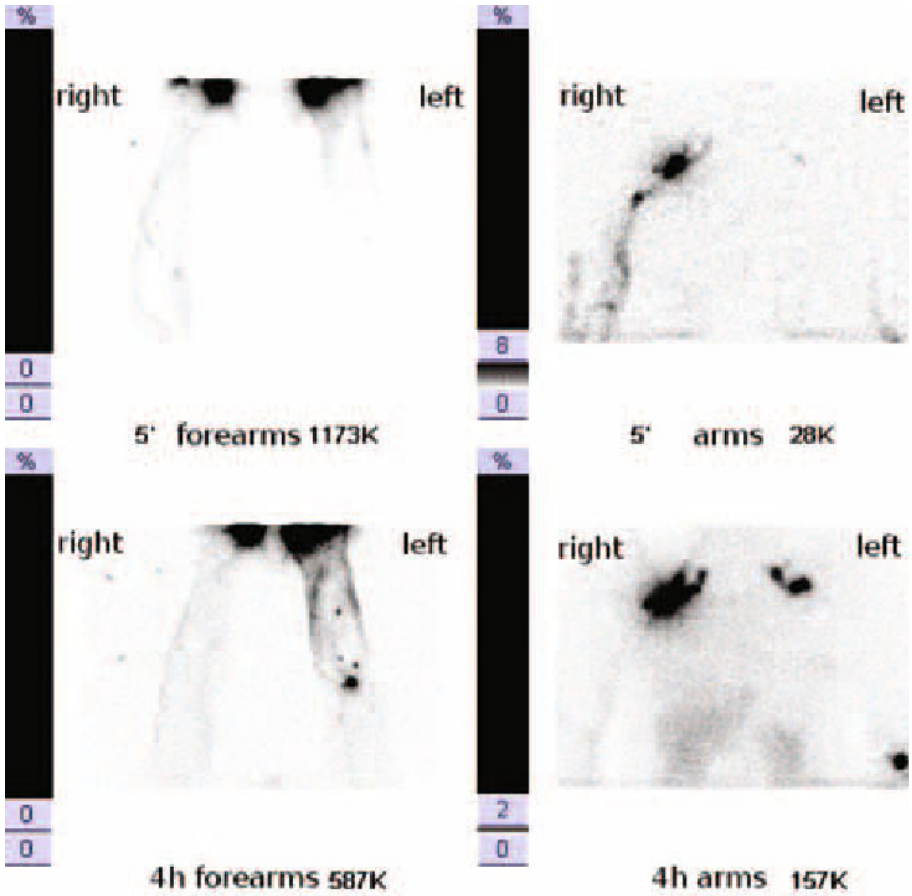

Fig. 1 Delayed drainage at left upper limb in the early acquisitions and "dermal flow" in the 4 h acquisitions. The pattern of lymphatic drainage is not totally normal also in the right arm, where no uptake in epitroclear lymph nodes can be observed. No lymph node uptake in the left axilla at early imaging, with some uptake in the delayed acquisitions (but still much less intense than in the right axilla). Based on the results of lymphoscintigraphy, the patient underwent combined therapy for lymphedema (pneumatic compression, wrapping of forearm and massages)

Case 5.3
Axillary Reverse Mapping Lymphoscintigraphy in Breast Cancer Patient with Positive Sentinel Lymph Node Before Lymphadenectomy

Luciano Feggi, Chiara Peterle, Corrado Cittanti, Valentina de Cristofaro, Stefano Panareo, Ilaria Rambaldi, Virginia Rossetti, Ivan Santi, and Paolo Carcoforo

Background Clinical Case

A 66-year-old woman underwent surgery for a left breast cancer finding positive sentinel lymph node. Axillary dissection is necessary in patients with positive sentinel lymph nodes in breast cancer; in axillary basin lymph nodes may drain from either breast or arm; still, a lymph node which drains from both breast and arm is very rarely found, so the surgeon can spare a few nodes to preserve lymphatic arm drainage. The ARM technique (axillary reverse mapping) allows to mark lymph nodes which drains from both hand and arm, so the surgeon can distinguish radioactive nodes (arm drainage) from "cold" ones (breast drainage) and remove only the breast-related ones.

Anatomic location of edema: no edema.

Lymphoscintigraphy

Lymphoscintigraphy was performed following administration of two aliquots of 0.4 mL containing 74 MBq ^{99m}Tc-albumin nanocolloid. Radiopharmaceutical injections were performed superficially and bilaterally (injection in 1st, 2nd, 3rd, and 4th interdigital space in each hand). A dual-detector SPECT gamma camera (E-cam Siemens Medical Solutions, Hoffman Estates, IL) equipped with low-energy high-resolution (LEHR) collimators was used to obtain planar images. Time of acquisition after injection: (a) hands and forearms, 5 min after injection (laid upon collimator); (b) arms, 10 min after injection (anterior planar view); (c) axillary regions and thorax, 15 min after injection (anterior planar scan using cobalt wire as a landmark); (d) 2nd acquisition only on axillary regions and thorax (anterior planar scan using cobalt wire as a landmark). Before late image of axillary regions and thorax, a radioguided occult lesion localization (ROLL) (after 2nd nanocolloid intratumoral injection with ultrasound guidance) was performed to allow the surgeon to remove the breast primary tumor and left axillary nodes in one single time.

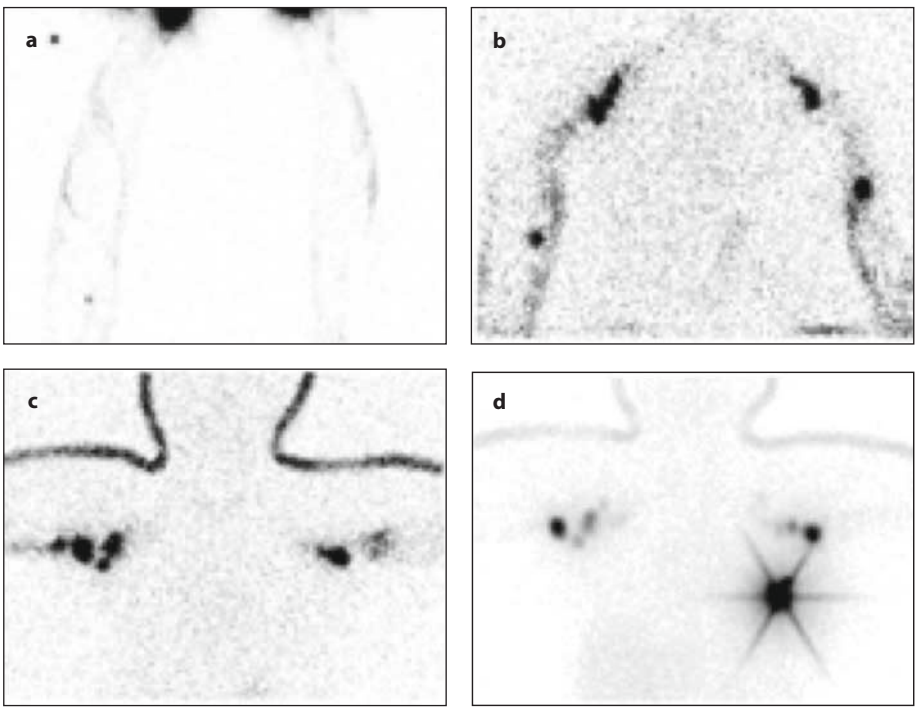

Fig. 1 Early acquisitions (**a**, **b** and **c**): normal lymphatic drainage in both upper limbs (mild delay in left upper limb early drainage; a month earlier, the patient underwent sentinel lymph node removal in the left axillary basin). In *panel* **d** (late acquisition) the axillary reverse mapping lymphoscintigraphy (ARM) is displayed, while the hottest focus in the left breast corresponds to intratumoral injection of ^{99m}Tc-albumin macroaggregates for ROLL. The lymph nodes that drain the upper limb, that accumulate the radiocolloid, will be spared during axillary dissection, thus decreasing the risk of secondary lymphedema possibly caused by axillary dissection

Case 5.4
Axillary Reverse Mapping Lymphoscintigraphy in Breast Cancer Patient with Infiltrative Lobular Carcinoma and Positive Sentinel Lymph Node Before Lymphadenectomy

Luciano Feggi, Chiara Peterle, Corrado Cittanti, Valentina de Cristofaro, Stefano Panareo, Ilaria Rambaldi, Virginia Rossetti, Ivan Santi, and Paolo Carcoforo

Background Clinical Case

A 49-year-old woman with left breast cancer (infiltrative lobular carcinoma with positive sentinel lymph node); we performed an ARM lymphoscintigraphy (axillary reverse mapping lymphoscintigraphy), before the surgeon performed axillary dissection to spare lymph nodes that drain from hand and arm.

Anatomic location of edema: no edema.

Lymphoscintigraphy

Lymphoscintigraphy was performed following administration of two aliquots of 0.4 mL containing 74 MBq ^{99m}Tc-albumin nanocolloid. Radiopharmaceutical injections were performed superficially and bilaterally (injection in 1st, 2nd, 3rd, and 4th interdigital space in each hand). A dual-detector SPECT gamma camera (E-cam Siemens Medical Solutions, Hoffman Estates, IL) equipped with low-energy high-resolution (LEHR) collimators was used to obtain planar images. Planar images were acquired in anterior view (256×256 matrix, zoom factor 1.00, acquisition time 200 s for each view). Time of acquisition after injection: (a) hands and forearms, 5 min after injection (laid upon collimator); (b) arms, 10 min after injection (anterior planar scan); (c) axillary regions and thorax, 15 min after injection (anterior planar scan using cobalt wire as a landmark); (d) 2nd acquisition only (late image) on axillary regions and thorax (anterior planar scan using cobalt wire as a landmark).

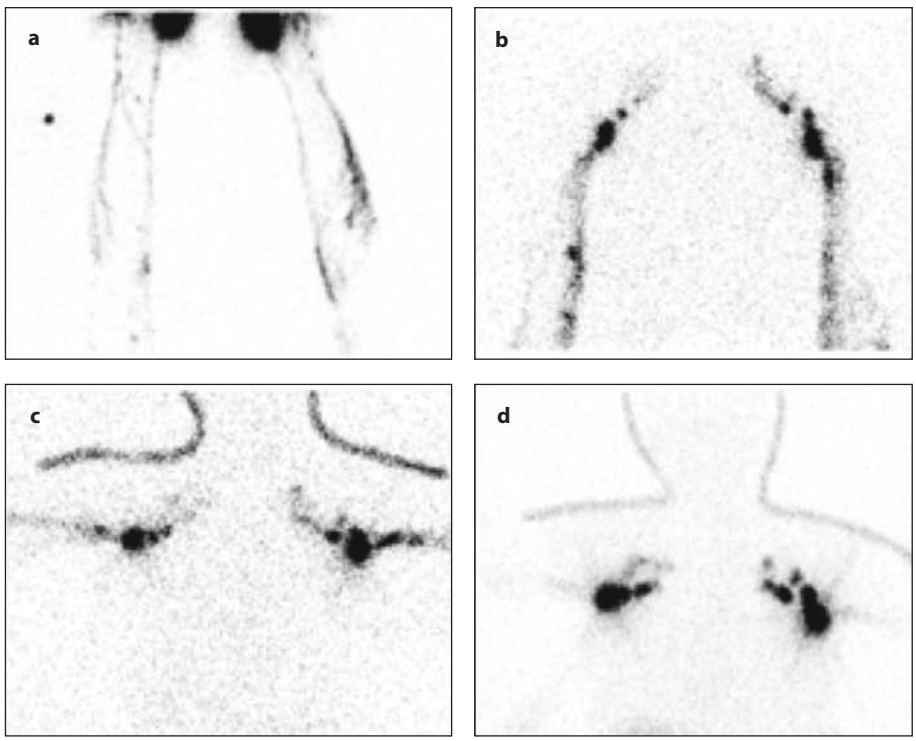

Fig. 1 Early images (**a**, **b** and **c**) show normal lymphatic drainage in both upper limbs (mild delay in left upper limb early drainage; one month earlier, the patient underwent sentinel lymph node removal in the left axillary basin). *Panel* **d** is the late scan of axilla and thorax. The lymph nodes that drain the upper limb, that accumulate the radiocolloid, will be spared during axillary dissection, thus decreasing the severity of secondary lymphedema possibly caused by axillary dissection

Case 5.5
Lower Limb Monocompartmental Lymphoscintigraphy in Patient with Bilateral Swelling and Non-Pitting Edema of the Lower Limbs

Luciano Feggi, Chiara Peterle, Corrado Cittanti, Valentina de Cristofaro, Stefano Panareo, Ilaria Rambaldi, Virginia Rossetti, and Ivan Santi

Background Clinical Case

A 62-year-old man with spontaneous onset of bilateral swelling and non-pitting edema in the lower limbs lasting since one year.

Anatomic location of edema: lower limbs.

Lymphoscintigraphy

Lymphoscintigraphy was performed following administration of two aliquots of 2 mL containing 111 MBq ^{99m}Tc-albumin nanocolloid. Radiopharmaceutical injections were performed superficially and bilaterally (injection in 1st, 2nd, and 4th interdigital space and in the outer retromalleolar space in each foot). A dual-detector SPECT gamma camera (E-cam Siemens Medical Solutions, Hoffman Estates, IL) equipped with low-energy high-resolution (LEHR) collimators was used to obtain planar images. Planar images were acquired 10 min after radiopharmaceutical administration and walking exercise and 4 h respectively after injection (256×256 matrix, zoom factor 1.00, acquisition time 200 s for each view) in anterior planar scan from feet to abdominal region.

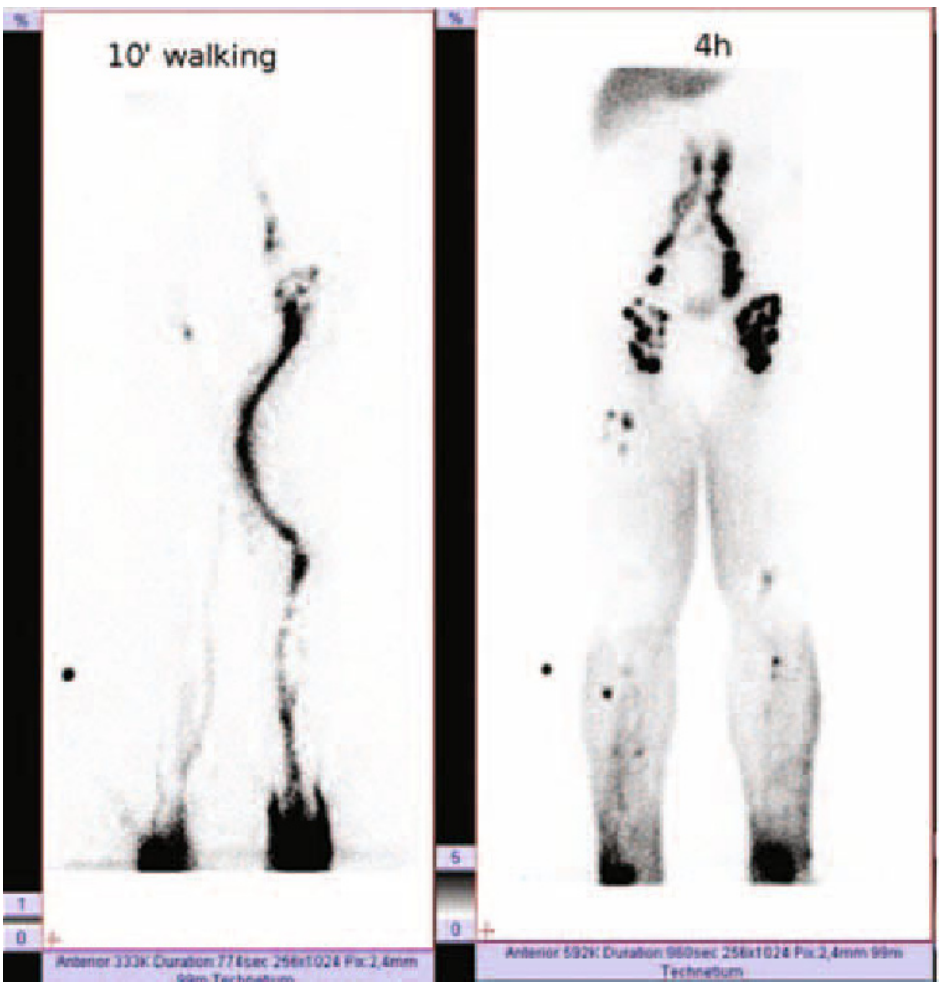

Fig. 1 Bilateral abnormal patterns of lymphatic drainage, as indicated by markedly delayed flow on the right side and midly delayed flow on the left side in the early acquisition. The delayed acquisition shows the presence of bilateral "dermal back flow" with asymmetrical lymph node uptake (including an alteranate pattern from the popliteal to the inguinal and to the lumbo-aortic lymph nodes). Based on the results of lymphoscintigraphy, the patient underwent combined therapy for lymphedema (pneumatic compression, wrapping of forearm and massages)

Case 5.6
Lower Limb Bicompartmental Lymphoscintigraphy in Patient with Edema of the Left Lower Limb

Paola Anna Erba and Luisa Locantore

Background Clinical Case

A 47-year-old women with edema of the left lower limb. Normal Doppler-ultrasound. No family history of lymphedema.

Anatomic location of edema: lower left limb.

Lymphoscintigraphy

For the deep lymphatic circulation (DLC): two aliquots of ^{99m}Tc-nanocolloid, 7 MBq each of injection in 0.1 mL in the first and second intermetatarsal space, identified by palpating the soles of both feet immediately proximal to the distal heads of the metatarsal bones on each side, inserting the needle by about 12–13 mm to reach the intermetatarsal muscles below the deep fascia plantaris. *For the superficial lymphatic circulation (SLC)*: three aliquots of about 10 MBq in 0.1 mL on the dorsum of either each foot, inserting the needle subdermally in sites corresponding approximately to the prior palmar injections, about 1–2 cm proximally to the interdigital web. Spot and whole-body images were obtained from the distal feet up to the abdomen.

Spot images: 180 s/view, matrix 128×128, zoom 1.33
Whole-body images: matrix 128×1024, zoom 1, speed: 12 cm/min

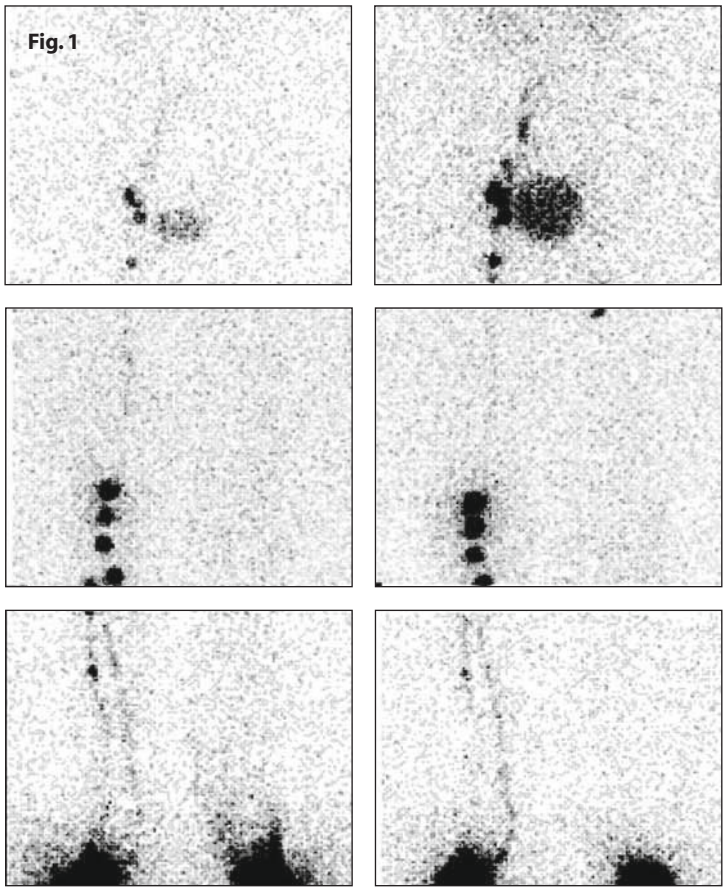

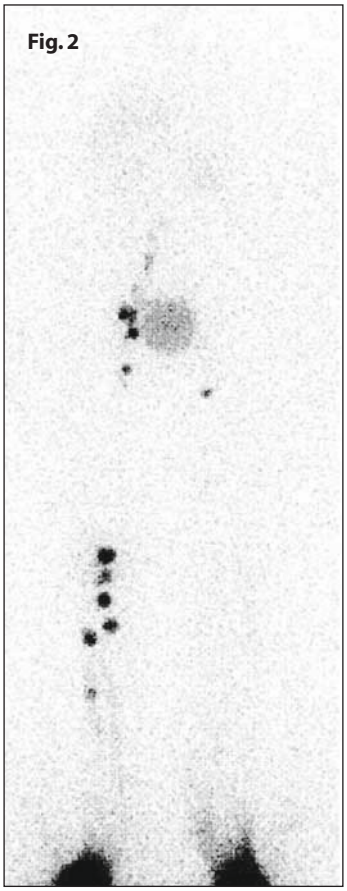

Figs. 1 and 2 Clear impairment of left lower lymph flow is evident in both the spot images (*Fig. 1*) and the whole-body image (*Fig. 2*), with minimal "dermal flow" at the distal medial portion of the left leg after radiocolloid injection for evaluating the DLC. No uptake can be seen in the left popliteal lymph nodes, while a single inguinal lymph node is detected after radiocolloid injection for the SLC. In addition, the DLC and SLC are simultaneously visualized at the right lower limb after radiocolloid injection for evaluating the DLC, indicating communication between the deep and the superficial lymphatic circulations. Multiple popliteal lymph nodes are detected on the right side, with normal pattern of the inguinal lymph nodes. Lumbo-aortic lymph nodes are faintly visualized, similarly as liver uptake

Case 5.7
Lower Limb Monocompartmental Lymphoscintigraphy in Patient with Bilateral Lower Limb Lymphedema

Giuseppe Rubini and Filippo Antonica

Background Clinical Case

A 32-year-old man with bilateral lower limb lymphedema. Clinicians suspected congenital dysplasia of the lower limb lymphatic vessels. Legs appeared edematous, size increased and the patient complained about fatigue and continuous pain even during sleep-time. His daily actions were very limited.

Anatomic location of edema: lower limbs.

Lymphoscintigraphy

Lymphoscintigraphy was performed following injections of two aliquots containing ^{99m}Tc-albumin nanocolloid, 37 MBq each of injection in 0.1 mL in the first and second intermetatarsal space. A dual-detector SPECT gamma camera (Millennium GE Healthcare, Milwaukee, WI) equipped with low-energy high-resolution (LEHR) collimators was used to obtain whole-body images after radiopharmaceutical injection. Whole-body planar images were acquired in anteroposterior projection, with a 256×1024 matrix and zoom factor 1.00 (speed: 12 cm/min) from the distal feet up to the abdomen.

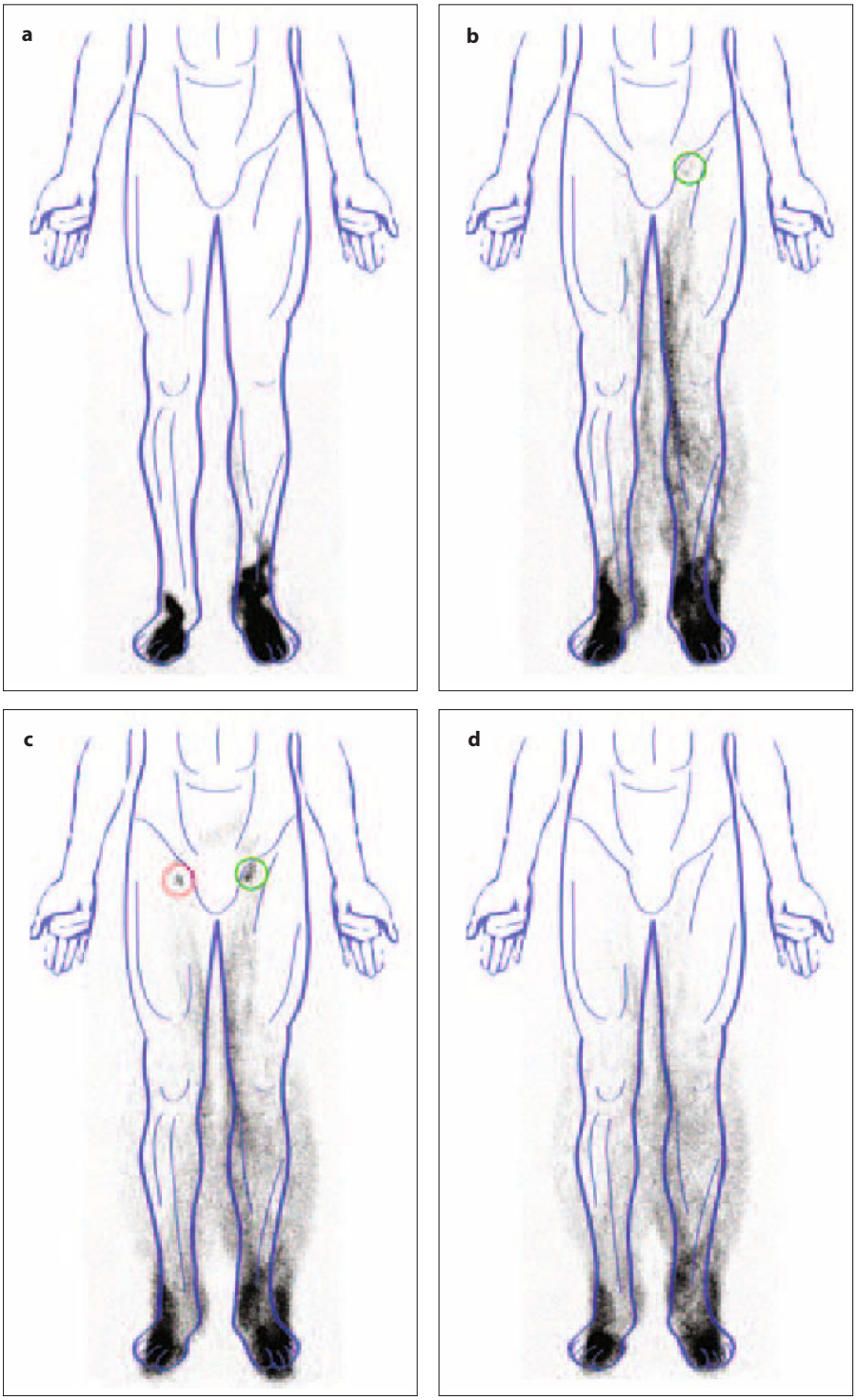

Fig. 1 Schematic representation of whole-body images in anterior view at 5-10, 30, 60, and 90 min (**a–d**, respectively) after radiocolloid injection and walking to stimulate lymphatic circulation. Radiocolloid drainage is delayed in both lower limbs, especially on the right side (no visualization of the groin lymph nodes in early scans). In later acquisitions, the right groin lymph nodes appear (*red circle*), delayed with respect to the right groin (*green circles*)

Case 5.8
Lower Limb Monocompartmental Lymphoscintigraphy in Patient Previously Submitted to Left Saphenectomy

Giuseppe Rubini and Filippo Antonica

Background Clinical Case

A 68-year-old woman previously submitted to saphenectomy of the left limb.
Left limb appeared cold, size increased, and patient reported size increasing especially in the last year. Echo-color doppler revealed decreased blood flow and tissue edema.

Anatomic location of edema: lower limbs.

Lymphoscintigraphy

Lymphoscintigraphy was performed following injections of two 0.1 mL aliquots containing 36 MBq ^{99m}Tc-albumin nanocolloid, in the first and second intermetatarsal space. A dual-detector SPECT gamma camera (Millennium GE Healthcare, Milwaukee, WI) equipped with low-energy high-resolution (LEHR) collimators was used to obtain whole-body images after radiopharmaceutical injection. Whole-body planar images were acquired in anteroposterior projection, with a 256 × 1024 matrix and zoom factor 1.00 (speed:12 cm/min) from the distal feet up to the abdomen.

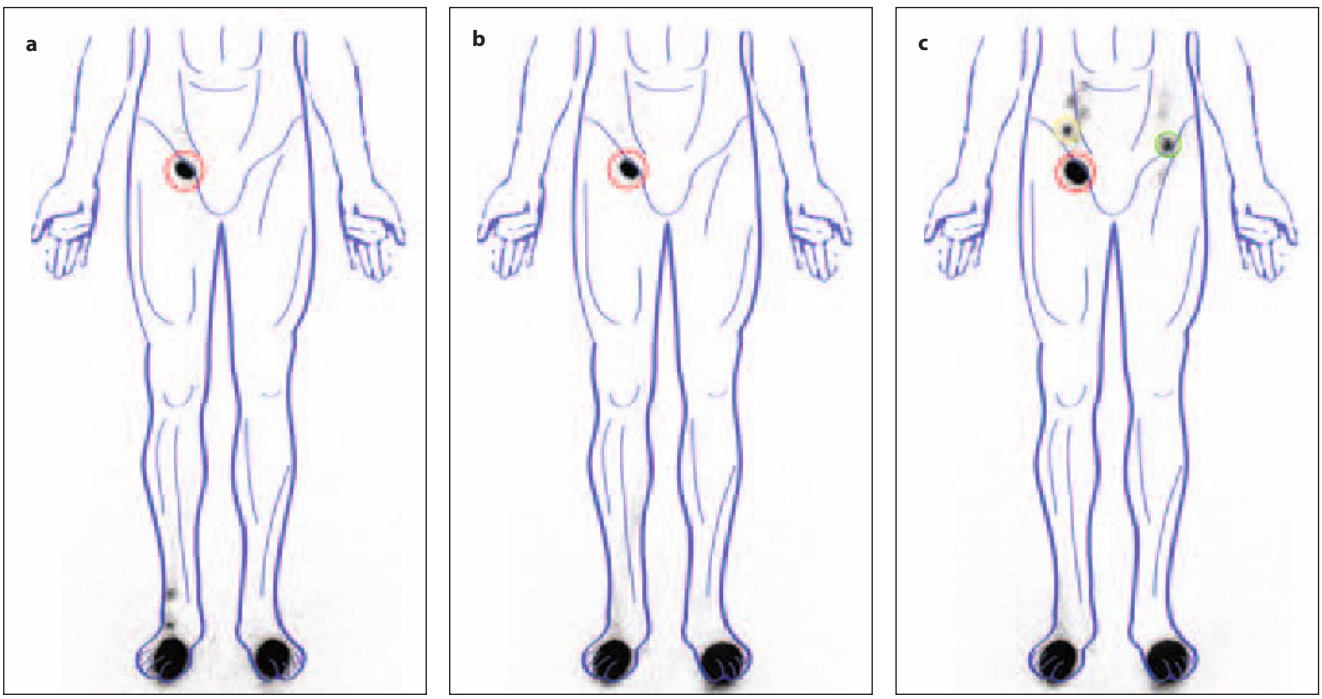

Fig. 1 Schematic representation of whole body images in anterior view at 5-10, 30, and 60 min (**a–c** respectively) after radiocolloid injection. Radiocolloid drainage is delayed in the left lower limb (no visualization of the groin lymph nodes in the early scans). In later acquisitions, the left groin lymph nodes appear (*green circle*). Radiocolloid drainage is normal in the right lower limb (*red* and *yellow circles*). These scintigraphic findings suggest secondary impairment of lymphatic drainage in the left lower limb

Case 5.9
Lower Limb Monocompartmental Lymphoscintigraphy in Patient with History of Lymphadenectomy of the Groin Basin for Melanoma

Giuseppe Rubini and Filippo Antonica

Background Clinical Case

Patient with history of cutaneous melanoma of the right foot already surgically removed and submitted to lymphadenectomy of the groin basin due to groin sentinel lymph node positivity for metastasis. The surgeon also removed pelvic lymph nodes to guarantee surgical radicality. Physical examination did not reveal any lymphadenopathy or lymphedema.

Anatomic location of edema: lower limbs.

Lymphoscintigraphy

Lymphoscintigraphy was performed following injections of two 0.1 mL aliquots containing 36 MBq ^{99m}Tc-albumin nanocolloid, in the first and second intermetatarsal space. A dual-detector SPECT gamma camera (Millennium GE Healthcare, Milwaukee, WI) equipped with low-energy high-resolution (LEHR) collimators was used to obtain whole-body images after radiopharmaceutical injection. Whole-body planar images were acquired in anteroposterior projection, with a 256×1024 matrix and zoom factor 1.00 (speed:12 cm/min) from the distal feet up to the abdomen.

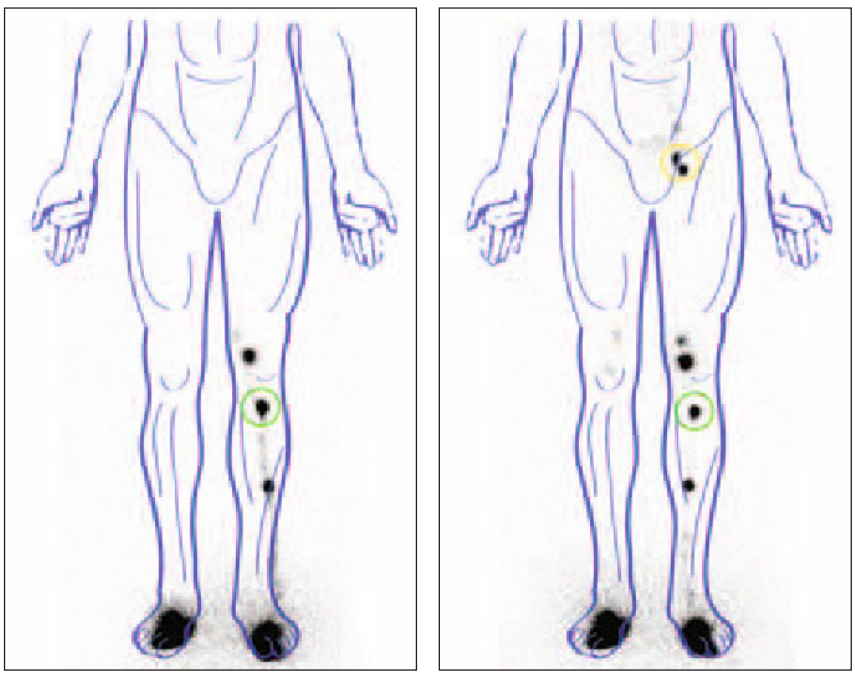

Fig. 1 Schematic representations of whole body scans in anterior view, 5-10 min (*left panel*) and 30 min (*right panel*) after radiocolloid injection. Lymphatic drainage is delayed in the right lower limb (no visualization of the groin lymph nodes). Drainage is normal in the left lower limb, with normal visualization of the popliteal (*green circle*) and inguinal (*yellow circle*) lymph nodes

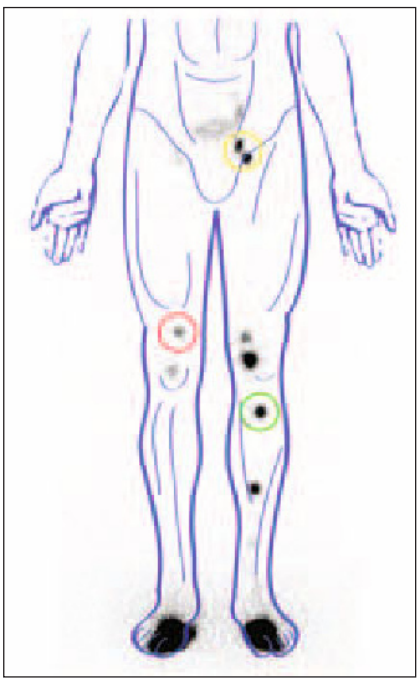

Fig. 2 Schematic representation of whole body scans in anterior view 90 min after radiocolloid injection. In this delayed scan, the right popliteal lymph nodes appear (*red circle*), with faint visualization of the right groin lymph nodes. Radiocolloid drainage is normal in the left lower limb, with normal visualization of the popliteal (*green circle*) and inguinal (*yellow circle*) lymph nodes. These scintigraphic findings suggest secondary impairment of the lymphatic circulation in the right lower limb

Case 5.10
Post-Exercise Lower Limb Monocompartmental Lymphoscintigraphy in Patient with Bilateral Leg Edema

Luciano Feggi, Chiara Peterle, Corrado Cittanti, Valentina de Cristofaro, Stefano Panareo, Ilaria Rambaldi, Virginia Rossetti, and Ivan Santi

Background Clinical Case

A 50-year-old woman with previous hysterectomy due to uterine fibromatosis and multiple removals of lipomas of the legs underwent investigation, because of mild edema of the legs, more noticeable in the right one; ultrasound, performed before lymphoscintigraphy, showed saphenous–femoral vein junction incontinence with ectasia. Lymphadenomegaly was found in the right inguinal region.

Anatomic location of edema: lower limbs (more evident in right one).

Lymphoscintigraphy

Lymphoscintigraphy was performed following administration of two doses of 2 mL containing 111 MBq ^{99m}Tc-albumin nanocolloid. Radiopharmaceutical injections were performed superficially and bilaterally (injection in 1st, 2nd, and 4th interdigital space and in the outer retromalleolar space in each foot). A dual-detector SPECT gamma camera (E-cam Siemens Medical Solutions, Hoffman Estates, IL) equipped with low-energy high-resolution (LEHR) collimators was used to obtain planar images. Planar images were acquired 10 min (after radiopharmaceutical administration and walking exercise) and 4 h respectively after injection (256×256 matrix, zoom factor 1.00, acquisition time 200 s for each view) in anterior planar scans from feet to abdominal region.

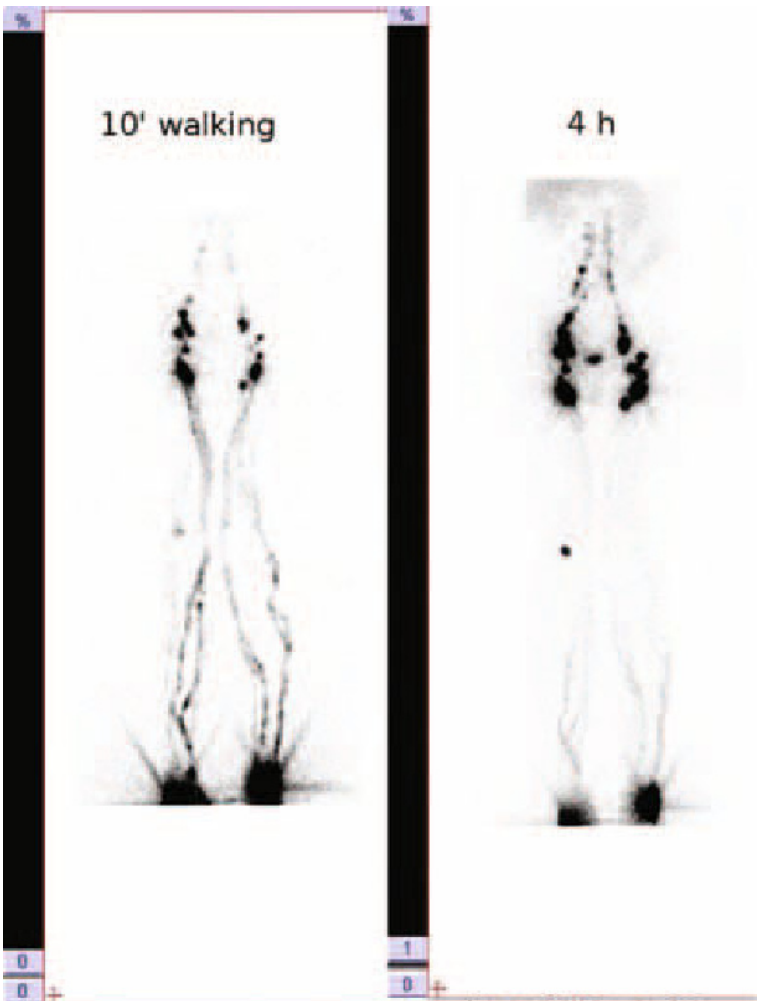

Fig. 1 Near-normal visualization of bilateral lymphatic trunks and inguinal lymphatic basins both in the early and in the delayed (4 h) acquisitions. A single popliteal lymph node is visualized, only in the right lower limb (mild abnormality)

Case 5.11
Lower Limb Monocompartmental Lymphoscintigraphy at Rest and Post-Exercise with Semiquantitative Evaluation of the Tracer Appearance Time in Patient with Lymphedema of the Left Lower Limb Post Left Groin Lymphadenectomy

Girolamo Tartaglione, Roberto Bartoletti, and Marco Pagan

Background Clinical Case

A 45-year-old woman, with lymphedema of the left lower limb and history of cutaneous melanoma of the gluteus (pN1M0) and left groin lymph nodal dissection.

Anatomic location of edema: lower limb.

Lymphoscintigraphy

All tight clothes and elastics were removed before tracer injection. Two aliquots of 0.3 mL containing 50 MBq ^{99m}Tc-albumin-nanocolloid were injected intradermally at the first interdigital area, on the top of the feet. Gentle massage was performed after injection in the area. Two scans were acquired starting immediately after injection (the first on the legs and the second on the thighs) following these parameters: planar static scan, pre-set time 5 min, matrix 128×128, 140 Kev ± 10%, anterior and posterior views. A dual head gamma camera (GE-Infinia) equipped with low-energy general purpose (LEGP) collimators was used to provide increased sensitivity. If delayed or absent lymphatic drainage was perceived, then the patient was invited to perform 2 min of continuous isotonic exercise (walking). A post-exercise static scan was acquired (128×128, 5 min) until the regional lymph nodes were visualized. The Tracer Appearance Time (TAT, normal value less than 10 min) and lymph drainage patterns after exercise (see timeline) were evaluated.

Figs. 1 and 2 The scan at rest shows near-normal visualization of the main lymphatic vessels of the lower limbs, a normal TAT, with a time-dependent increase accumulation of the radiocolloid in the left groin region. After exercise, radioactivity accumulation increases even further in the left groin region (lymphatic leakage?). In this case exercise revealed a local failure of lymphatic drainage, which was helpful to develop a combined treatment approach

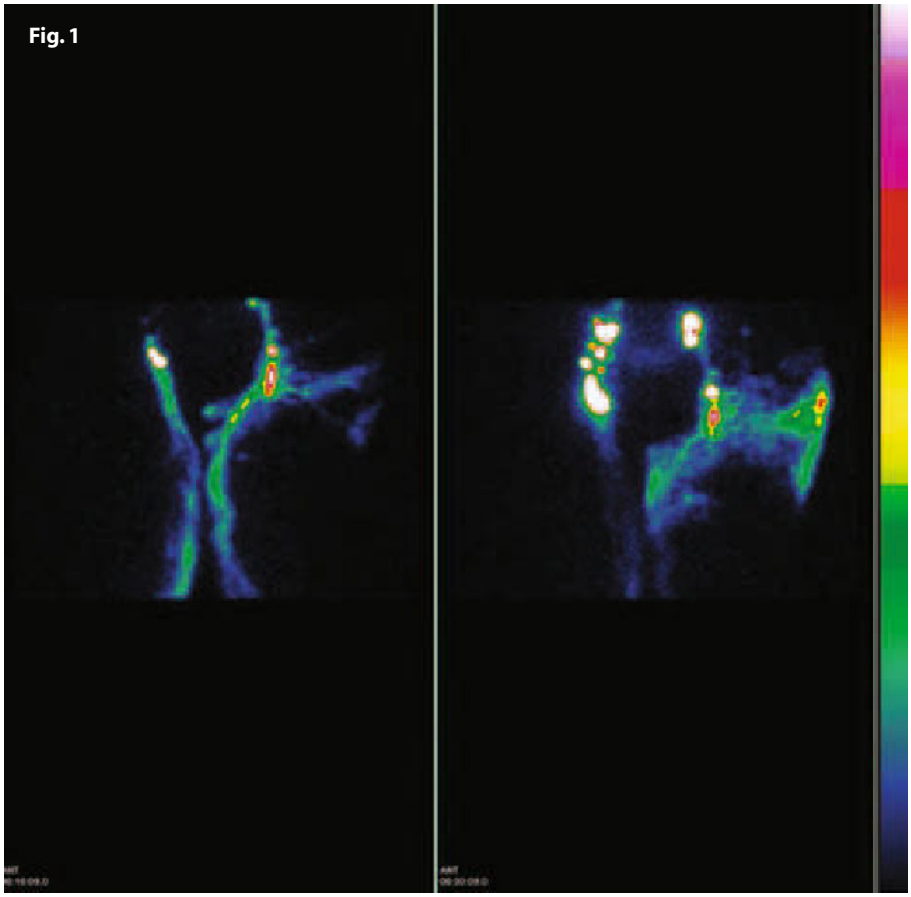

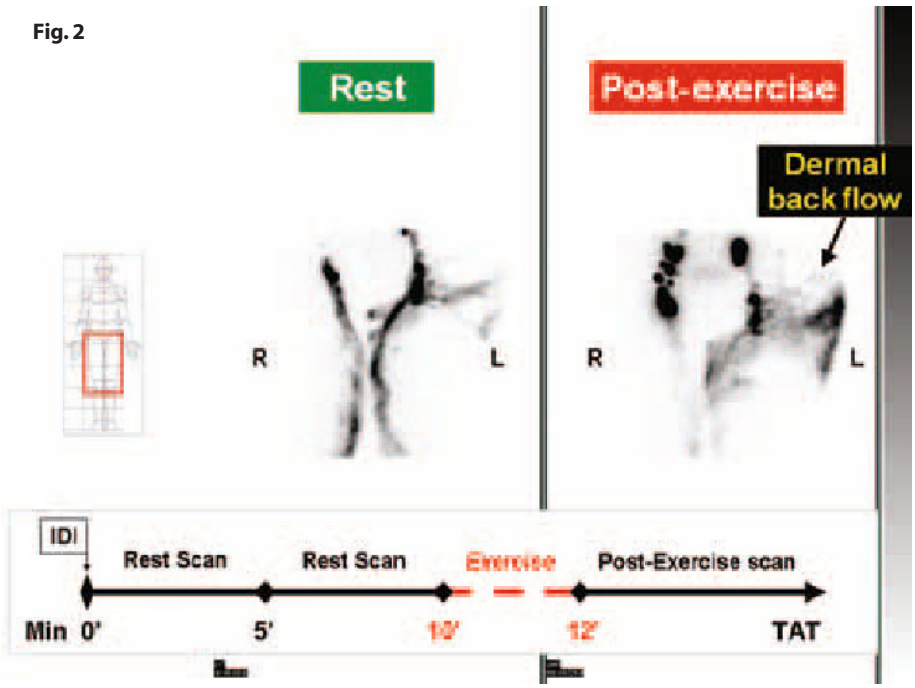

Case 5.12
Lower Limb Monocompartmental Lymphoscintigraphy at Rest and Post-Exercise with Semiquantitative Evaluation of the Tracer Appearance Time in Patient with Right Lower Limb Primary Lymphedema, Clinical Stage 3 According to Foeldi

Girolamo Tartaglione, Roberto Bartoletti, and Marco Pagan

Background Clinical Case

A 54-year-old woman, affected by a right lower limb primary lymphoedema of clinical stage 3 according to Foeldi. The tissue at this stage is hard (fibrotic) and edema is non-pitting. The swelling is almost irreversible and the limb is very large and swollen.

Anatomic location of edema: right lower limb.

Lymphoscintigraphy

All tight clothes and elastics were removed before tracer injection. Two aliquots of 0.3 mL containing 50 MBq ^{99m}Tc-albumin-nanocolloid were injected intradermally at the first interdigital area, on the top of the feet. Gentle massage was performed after injection in the area. Two scans were acquired starting immediately after injection (the first on the legs and the second on the thighs) following these parameters: planar static scan, pre-set time 5 min, matrix 128×128, 140 Kev ± 10%, anterior and posterior views. A dual head gamma camera (GE-Infinia) equipped with low-energy general purpose (LEGP) collimators was used to provide increased sensitivity. If delayed or absent lymphatic drainage was perceived, then the patient was invited to perform 2 min of continuous isotonic exercise (walking). A post-exercise static scan was acquired (128×128, 5 min) until the regional lymph nodes were visualized. The Tracer Appearence Time (TAT, normal value less than 10 min) and lymph drainage patterns after exercise (see timeline) were evaluated.

Figs. 1 and 2 The scan at rest shows severely delayed lymphatic drainage on the right side, with visualization of a rich collateral circulation along the small saphena; no detectable lymph flow on the left side. After exercise, intense dermal back-flow appears on the right side, while a normal lymph drainage can be observed on the left side. Dermal back-flow is usuallly observed in case of severe obstruction of the main lymph pathway; when the pressure gradient increases over a certain threshold, it causes incompetence of the lymphatic vessel's valves, which causes inversion of lymph flow towards the dermis. In this patient, compression bandage therapy was ineffective, whereas a standard program of combined physical therapy yielded moderate clinical improvement

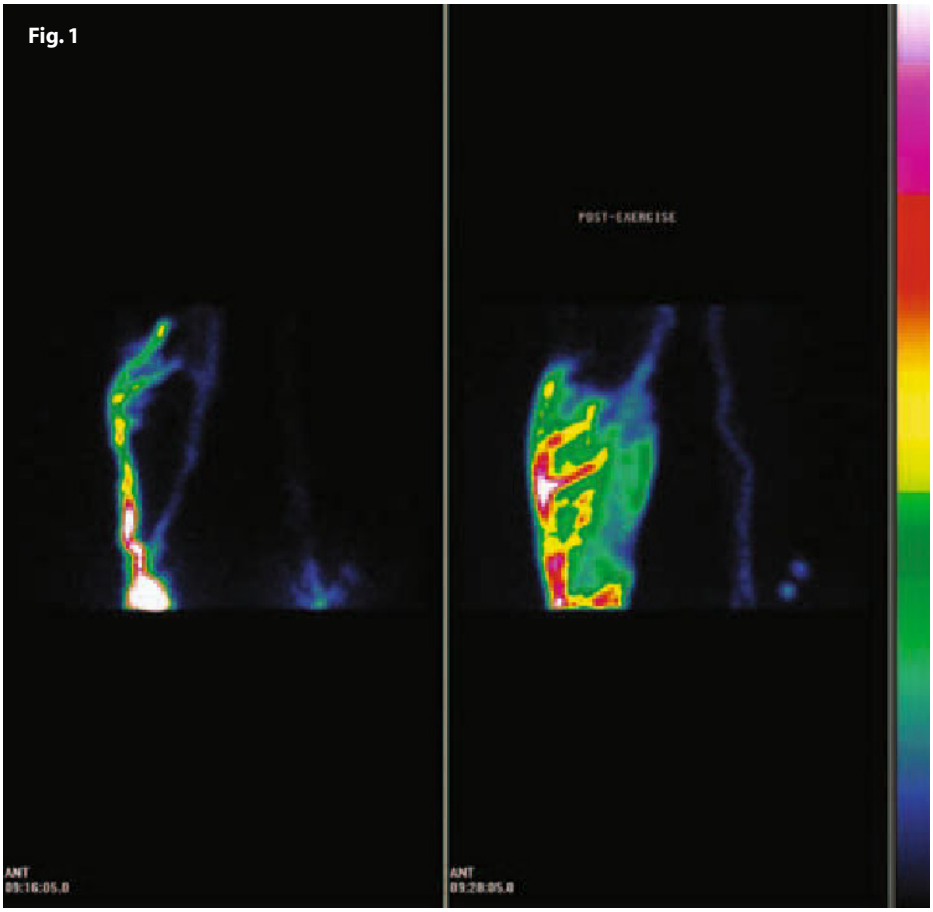

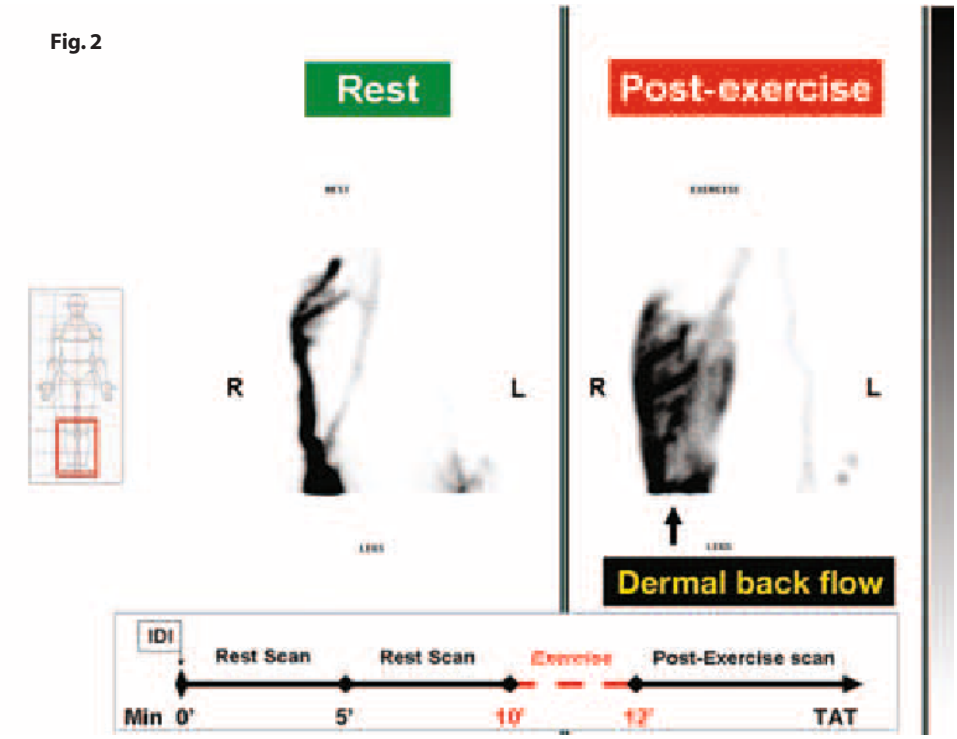

Case 5.13
Lower Limb Monocompartmental Lymphoscintigraphy at Rest and Post-Exercise with Semiquantitative Evaluation of the Tracer Appearance Time in Patient with Post-Lymph Nodal Dissection Lymphedema of the Lower Limbs

Girolamo Tartaglione, Roberto Bartoletti, and Marco Pagan

Background Clinical Case

A 46-year-old man, affected by lymphedema of the lower limbs (clinical stage 2 according to Foeldi) secondary to bilateral groin lymph nodal dissection for cutaneous melanoma (7 years previously). The patient was treated in several centers with combined physical therapy programs, including a personalized program of exercise.

Anatomic location of edema: lower limbs.

Lymphoscintigraphy

All tight clothes and elastics were removed before tracer injection. Two aliquots of 0.3 mL containing 50 MBq ^{99m}Tc-albumin-nanocolloid, were injected intradermally at the first interdigital area, on the top of the feet. Gentle massage was performed after injection in the area. Two scans were acquired starting immediately after injection (the first on the legs and the second on the thighs) following these parameters: planar static scan, pre-set time 5 min, matrix 128×128, 140 Kev ± 10%, anterior and posterior views. A dual head gamma camera (GE-Infinia) equipped with low-energy general purpose (LEGP) collimators was used to provide increased sensitivity. If delayed or absent lymphatic drainage was perceived, then the patient was invited to perform 2 min of continuous isotonic exercise (walking). A post-exercise static scan was acquired (128×128, 5 min) until the regional lymph nodes were visualized. The Tracer Appearance Time (TAT, normal value less than 10 min) and lymph drainage patterns after exercise were evaluated.

Figs. 1 and 2 The rest scan shows delayed lymph drainage in the left leg, with normal lymph drainage in the right leg. Exercise accelerated lymph drainage in the left leg. A second lymph drainage pathway was observed in the right leg, with unusual uptake of a popliteal lymph node.
The scan demonstrates a shunt between the superficial and deep lymphatic system, as a compensatory mechanism in lymphedema of the right lower limb

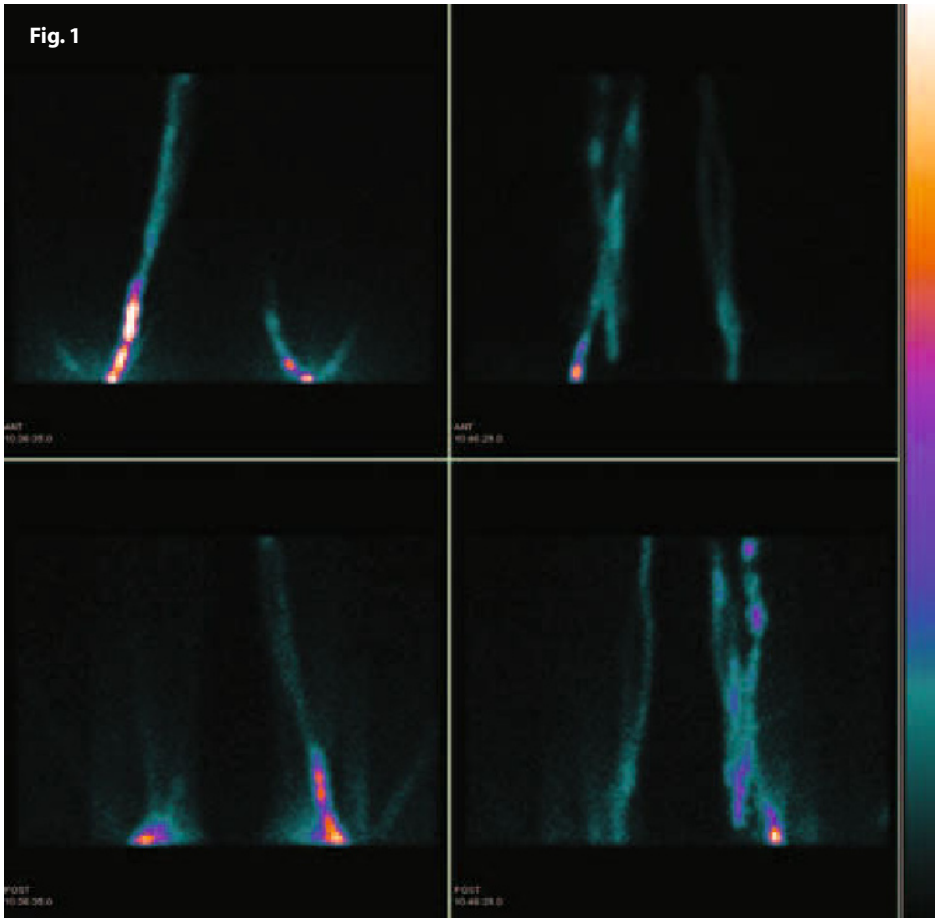

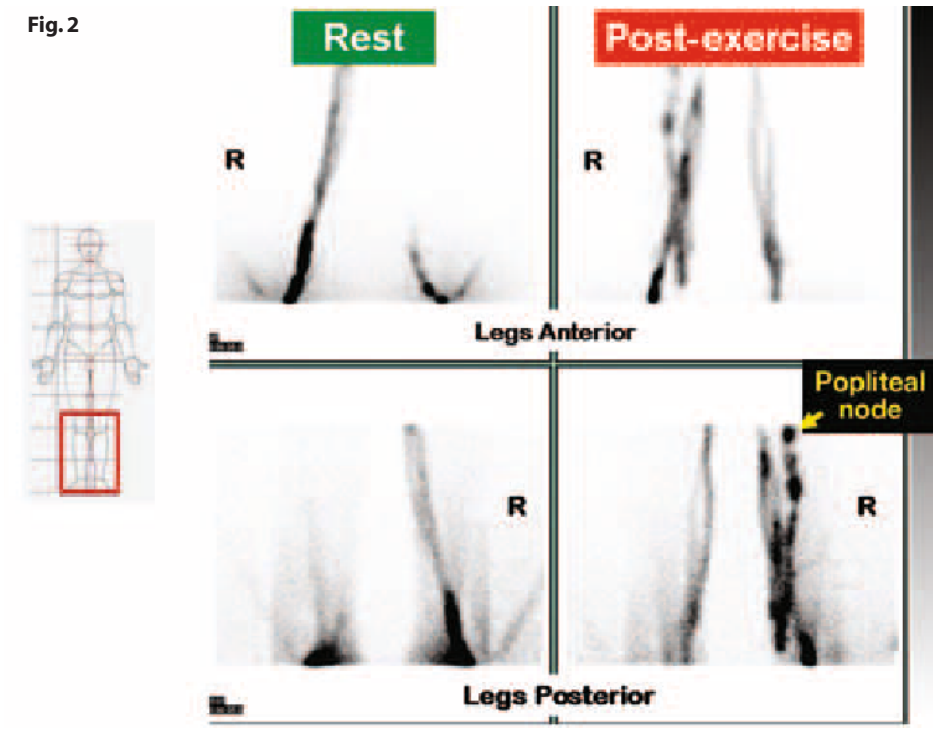

Case 5.14
Post-Exercise Lower Limb Monocompartmental Lymphoscintigraphy in Patient with Acute Edema of the Left Lower Limb and Painful Left Inguinal Lymphadenomegaly

Luciano Feggi, Chiara Peterle, Corrado Cittanti, Valentina de Cristofaro, Stefano Panareo, Ilaria Rambaldi, Virginia Rossetti, Ivan Santi, and Paolo Carcoforo

Background Clinical Case

A 77-year-old woman with pain and swelling of the left lower limb; ultrasound detected left inguinal lymphoadenomegaly; after surgical removal, histological diagnosis was metastasis of neuroendocrine carcinoma (poorly differentiated), consistent with Merkel cell carcinoma metastasis (T2N1Mx). Her clinical presentation included edema of the left lower limb and pain; there was a left inguinal scar after surgical removal.

Anatomic location of edema: left lower limb.

Lymphoscintigraphy

Lymphoscintigraphy was performed following administration of two aliquots of 2 mL containing 111 MBq ^{99m}Tc-albumin nanocolloid. Radiopharmaceutical injections were performed superficially and bilaterally (injection in 1st, 2nd, and 4th interdigital space and in the outer retromalleolar space in each foot). A dual-detector SPECT gamma camera (E-cam Siemens Medical Solutions, Hoffman Estates, IL) equipped with low-energy high-resolution (LEHR) collimators was used to obtain planar images. Planar images were acquired 5 min and 4 h respectively after injection (256×256 matrix, zoom factor 1.00, acquisition time 200 s for each view) in anterior planar views of the feet and legs, thighs, and inguinal regions.

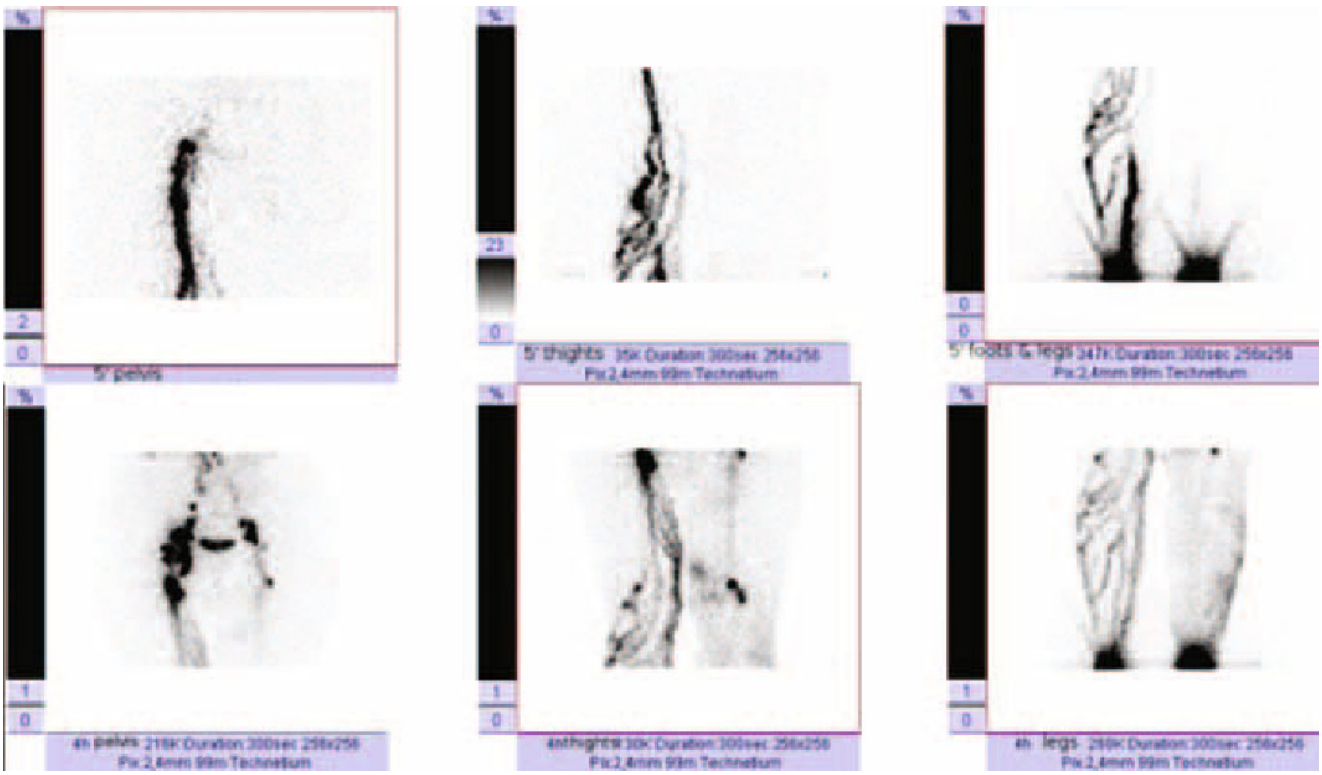

Fig. 1 Delayed lymphatic drainage of the left lower limb, with abnormal lymphatic function both in the early acquisition (only the right main lymphatic channel being visualized) and in the 4 h image (mild "dermal flow" in left leg). In the inguinal regions, asymmetrical radiocolloid uptake is observed in the lymph nodes (fewer nodes in left inguinal region). This pattern suggested involvement of the left inguinal lymph nodes causing abnormal drainage in the left lower limb. The patient therefore underwent further examinations, including a [^{18}F]FDG PET/CT scan that visualized a primary tumor in the skin covering the left knee

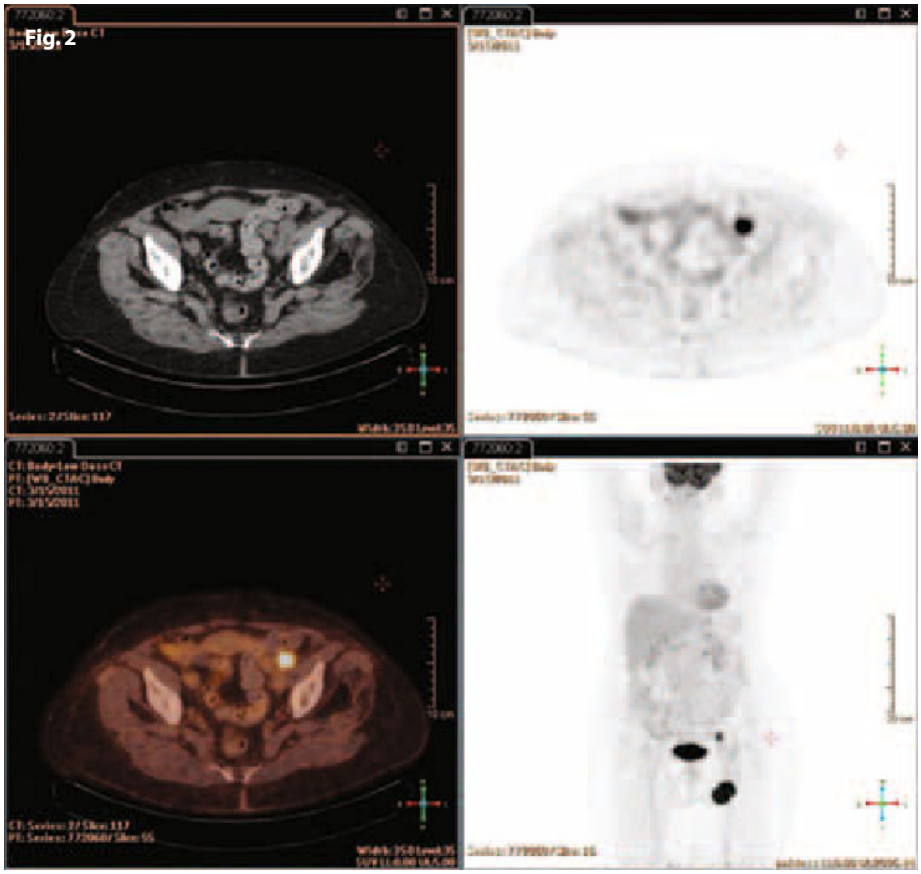

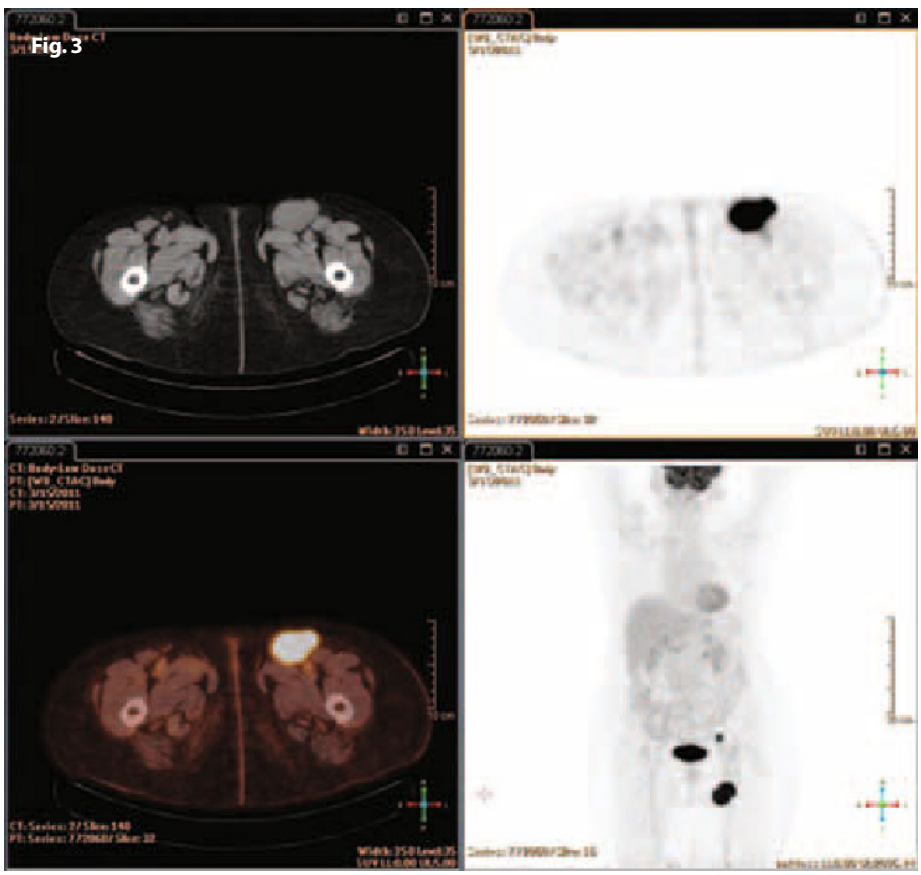

Figs. 2 and 3 [^{18}F]FDG PET/CT scan visualizing metastatic nodes in the left inguinal basin causing the abnormal lymphatic drainage in the left extremity

Case 5.15
Lower Limb Monocompartmental Lymphoscintigraphy at Rest and Post-Exercise with Semiquantitative Evaluation of the Tracer Appearance Time in Patient with Secondary Lymphedema of the Right Lower Limb

Girolamo Tartaglione, Roberto Bartoletti, and Marco Pagan

Background Clinical Case

A 71-year-old woman was submitted to surgical removal of primary melanoma of the right leg and sentinel lymph node biopsy of the popliteal lymph node (pN0). About 3 months after surgery she developed a lymphedema of right lower limb.

Anatomic location of edema: right lower limb.

Lymphoscintigraphy

All tight clothes and elastics were removed before tracer injection. Aliquots of 0.3 mL containing 50 MBq ^{99m}Tc-albumin-nanocolloid were injected intradermally at the first interdigital area, on the top of the feet. Gentle massage was performed after injection in the area. Two scans were acquired starting immediately after injection (the first on the legs and the second on the thighs) following these parameters: planar static scan, pre-set time 5 min, matrix 128×128, 140 Kev ± 10%, anterior and posterior views. A dual head gamma camera (GE-Infinia) equipped with low-energy general purpose (LEGP) collimators was used to provide increased sensitivity. If delayed or absent lymphatic drainage was perceived, then the patient was invited to perform 2 min of continuous isotonic exercise (walking). A post-exercise static scan was acquired (128×128, 5 min) until the regional lymph nodes were visualized. The Tracer Appearance Time (TAT, normal value less than 10 min) and lymph drainage patterns after exercise were evaluated.

Figs. 1 and 2 The scans at rest visualize three superficial collateral lymph channels of the right limb with normal visualization of lymph nodes in the right groin (TAT <10 min), and delayed lymph drainage of the left leg. Isotonic exercise accelerated lymph drainage toward the left groin's lymph nodes (TAT = 16 min), with a collateral lymph pathway and an area of radiocolloid collection in the middle third of the left leg. This test revealed a pre-existing lymphatic disease of the lower limbs. A personalized program of combined physical therapy was based on the findings of lymphoscintigraphy

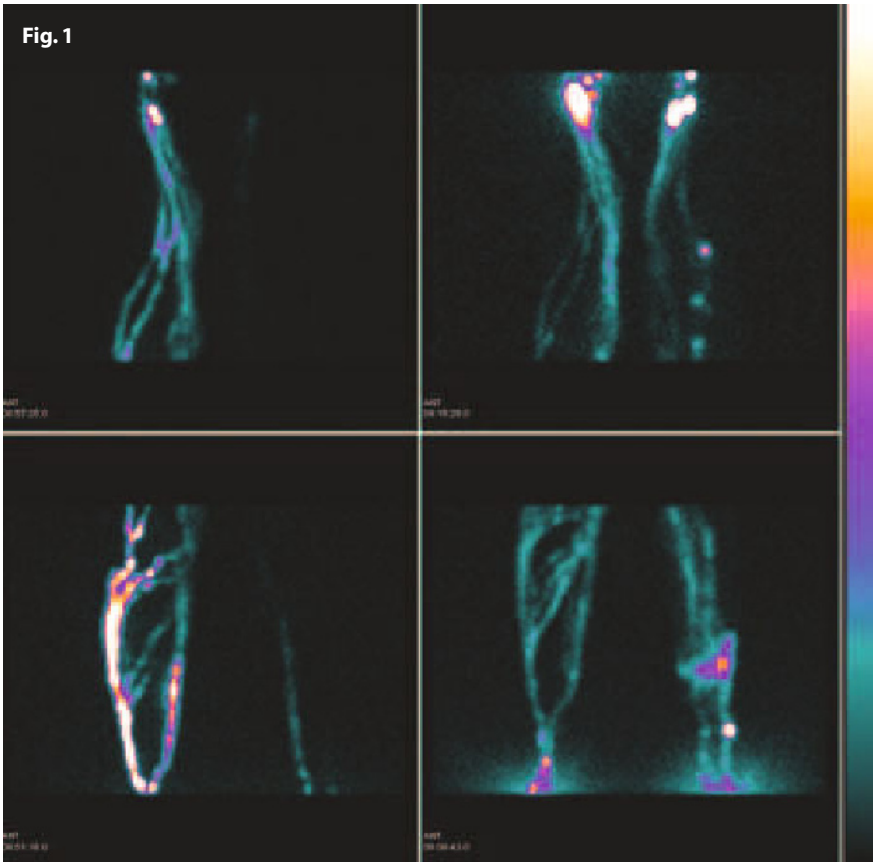

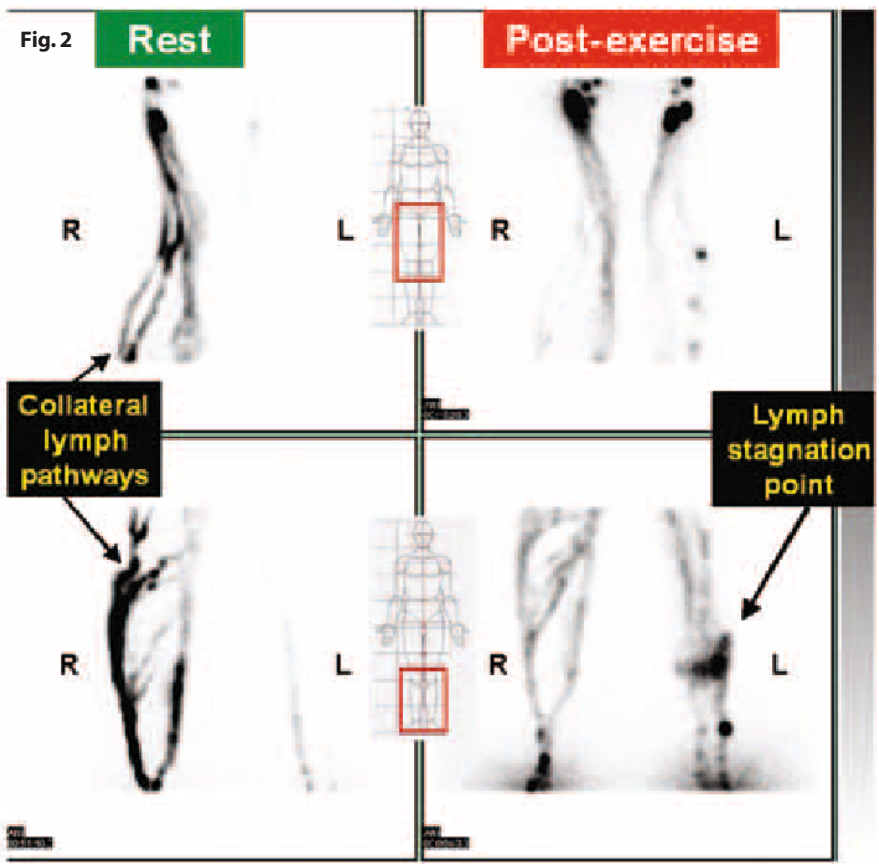

Case 5.16
Lower Limb Monocompartmental Lymphoscintigraphy in Patient with Secondary Bilateral Non-Pitting Edema of the Lower Extremities, More Evident on the Left, and Left Ureteral Obstruction Due to Lymphocele

Luciano Feggi, Chiara Peterle, Corrado Cittanti, Valentina de Cristofaro, Stefano Panareo, Ilaria Rambaldi, Virginia Rossetti, Ivan Santi, and Paolo Carcoforo

Background Clinical Case

A 47-year-old woman with melanoma of the left leg and metastasis of the inguinal homolateral lymph nodes underwent surgery (removal of melanoma and left inguinal and iliac lymphoadenectomy). After 7 years, during follow-up, CT detected a large pelvic mass, which remained undiagnosed (lymphocele? ovarian cyst?). Two years later, the patient suffered from left ureteral obstruction by compression of a pelvic mass on the third tract of the ureter. Patient reported bilateral swelling in the lower limbs, more evident on the left. Therefore her clinical presentation includes bilateral non-pitting edema of the lower extremities, more evident on the left, and left ureteral obstruction, which needs nephrostomy.

Anatomic location of edema: lower limbs (more evident in left one).

Lymphoscintigraphy

Lymphoscintigraphy was performed following administration of two aliquots of 2 mL containing 111 MBq ^{99m}Tc-albumin nanocolloid. Radiopharmaceutical injections were performed superficially and bilaterally (injection in 1st, 2nd, and 4th interdigital space and in the outer retromalleolar space in each foot). A dual-detector SPECT gamma camera (E-cam Siemens Medical Solutions, Hoffman Estates, IL) equipped with low-energy high-resolution (LEHR) collimators was used to obtain planar images. Planar images were acquired 5 min, 1 h, 4 h and 24 h respectively after injection in an anterior view (256×256 matrix, zoom factor 1.00, acquisition time 200 s for each view). SPECT/CT was acquired 24 h after radiopharmaceutical administration (60 s for each frame, CT slice thickness: 1 mm, tube current of 30 mA, tube voltage of 13 kV).

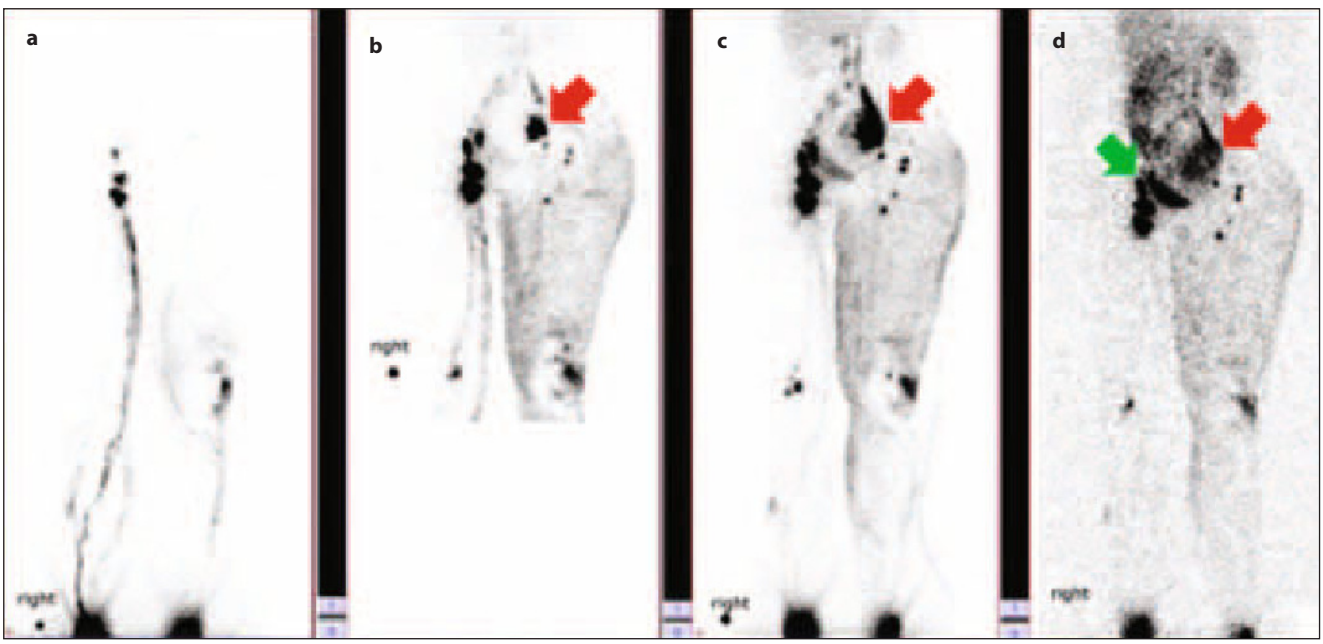

Fig. 1 "Whole body" images exteneding from the feet to the lower abdomen. From left to right: **a** 5 min after radiocolloid injection, normal drainage is noted in the right limb (visualization of a main lymphatic channel and inguinal lymph nodes), whereas in the left limb lymphatic drainage is delayed (the radiocolloid almost stops at the knee). **b** 1 h after injection, acquisition from knees to abdomen: normal drainage in right limb with "dermal flow/back flow" in the left thigh, without visualization of the inferior inguinal lymph nodes (prior lymphoadenectomy). Bilateral iliac nodes and an area of tracer uptake only on the left (*red arrow*) are visualized. **c** Planar scan (feet to abdomen) at 4 h: normal lymphatic drainage on the right limb; popliteal lymph nodes are visualized bilaterally (mostly on the left side), with "dermal flow/back flow" in the thigh; faint radiocolloid uptake in the left inguinal region; in this scan, the pelvic area of radiocolloid accumulation on the left (*red arrow*) appears more evident and larger; there is slight visualization of the bladder and the reticuloendothelial system. **d** 24 h scan: the radiocolloid has cleared almost completely from the right lower limb; radioactivity accumulation in the left pelvic area (*red arrow*) has expanded to a larger area. Radioactivity accumulation in the bladder is more evident (*green arrow*), whereas the other sites of uptake remain almost identical. SPECT/CT was performed in order to better characterize this pattern of distribution of the radiocolloid

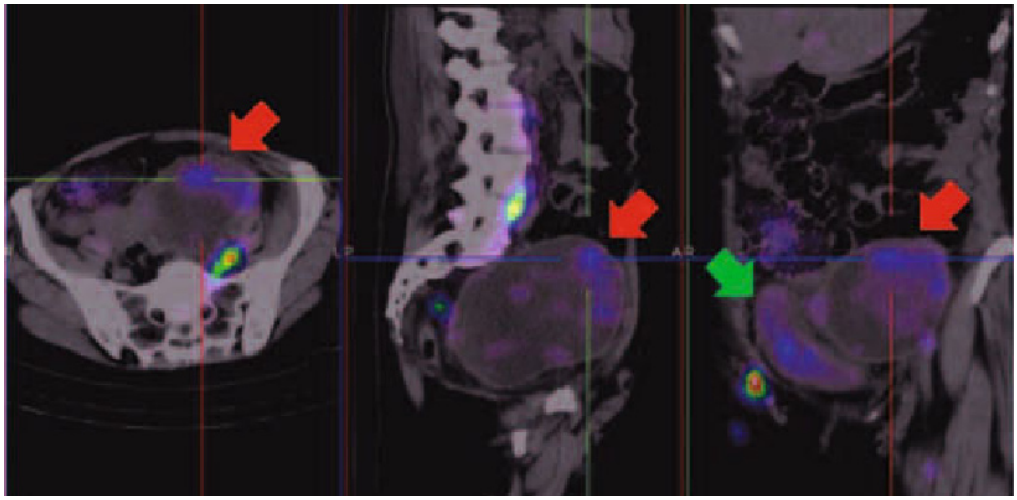

Fig. 2 Multiplanar reconstruction (MPR) fusion SPECT/CT (24 h after injection): a large pelvic mass is seen on the left (*red arrow*), near to the bladder (*green arrow*), with retention of a very low amount of radioactivity

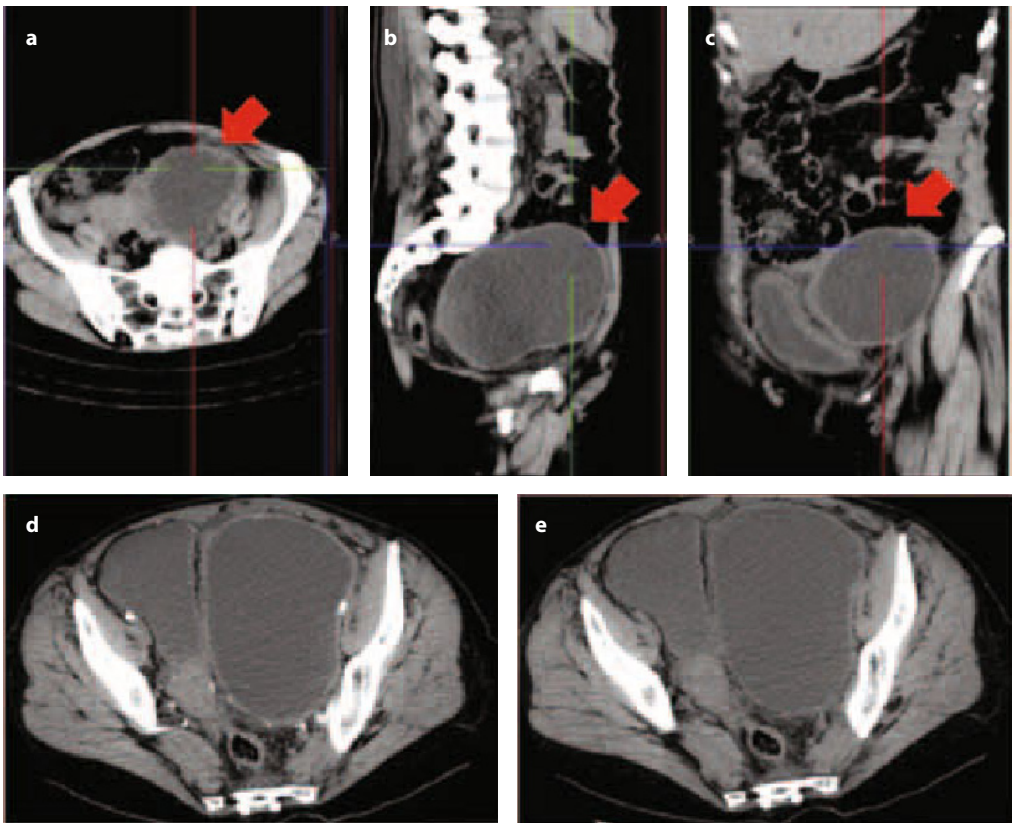

Fig. 3 MPR SPECT/CT acquisition (CT only). In the CT component of the acquisition, the content of the pelvic mass (*red arrow*) has radiodensity Hounsfield Unit values typical of a fluid (**a, b** and **c**). In a diagnostic CT the pelvic mass does not show contrast enhancement: **d** contrast-enhanced transiaxail section; **e** corresponding no-contrast CT section

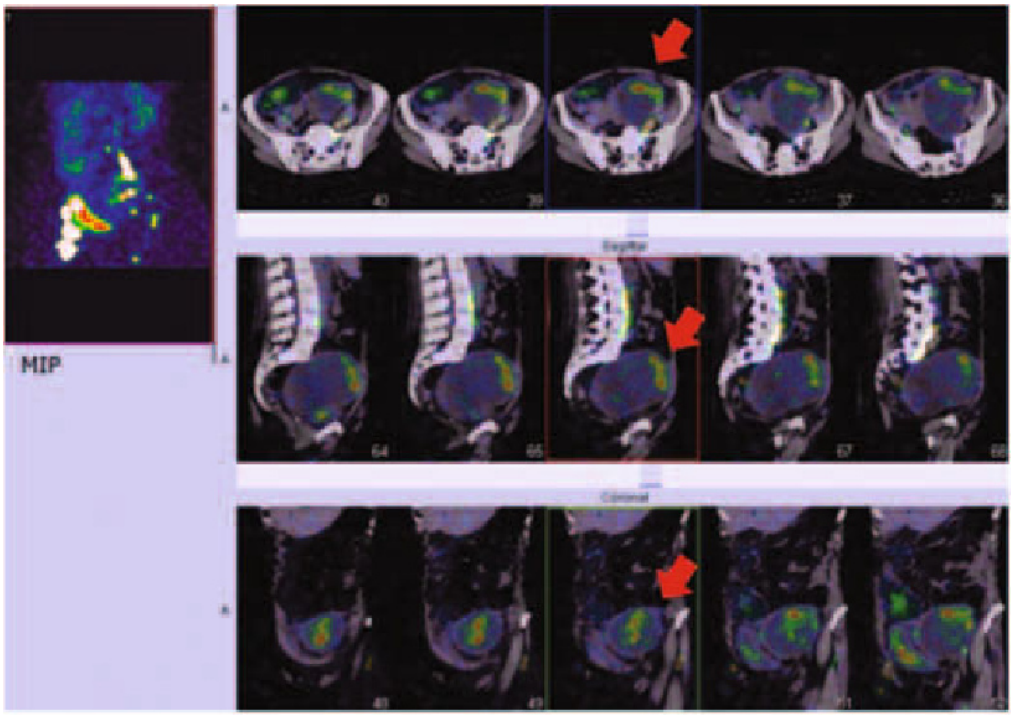

Fig. 4 MPR SPECT/CT fusion images. Lymphoscintigraphy confirmed the suspicion that the pelvic mass was a lymphocele. Therefore, the patient underwent surgery, which restored a normal left nephro-ureteral function

Case 5.17
Lower Limb Bicompartimental Lymphoscintigraphy in Patient with Post-Traumatic Edema of the Left Leg Associated with Disability Grade 3 According to Ricci Scale, at Baseline and After 5 Years of Multiple Surgeries and Cycles of Therapy

Paola Anna Erba and Luisa Locantore

Background Clinical Case

A 36-year-old man with post-traumatic edema of the left leg. After crush injury, the patient had multiple surgical procedures for the presence of tissue necrosis and cheloids, with cutaneous graft. Before the accident, the patient had had a left leg saphenectomy performed. There is stage V lymphedema of the lower left limb with cutaneous retraction of the proximal and medial portion of the leg, hyperkeratosis, lymphatic vesicles, eczema, and ulcerations. A disability grade 3 according to Ricci scale was present.

Anatomic location of edema: lower left limb.

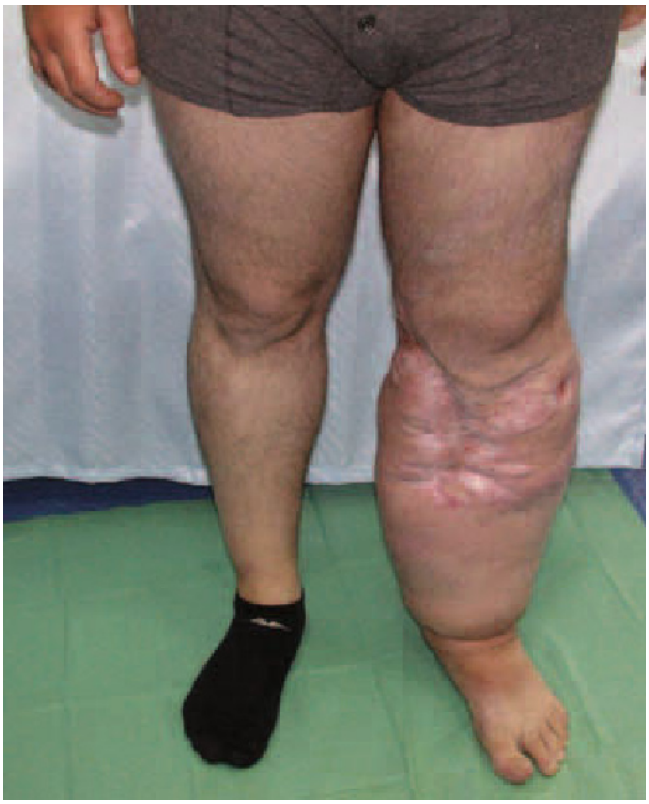

Fig. 1 The patient's legs at baseline scan

Lymphoscintigraphy

Lower Limbs

For the deep lymphatic circulation (DLC): two aliquots of ^{99m}Tc-nanocolloid, 7 MBq each of injection in 0.1 mL in the first and second intermetatarsal space, identified by palpating the soles of both feet immediately proximal to the distal heads of the metatarsal bones on each side, inserting the needle by about 12–13 mm to reach the intermetatarsal muscles below the deep fascia plantaris.

For the superficial lymphatic circulation (SLC): three aliquots of about 10 MBq in 0.1 mL on the dorsum of each foot, inserting the needle subdermally in sites corresponding approximately to the prior palmar injections, about 1–2 cm proximally to the interdigital web. Spot and whole-body images were obtained from the distal feet up to the abdomen.

Spot images: 180 s/view, matrix 128×128, zoom 1.33
Whole-body images: matrix 256×1024, zoom 1, speed: 12 cm/min

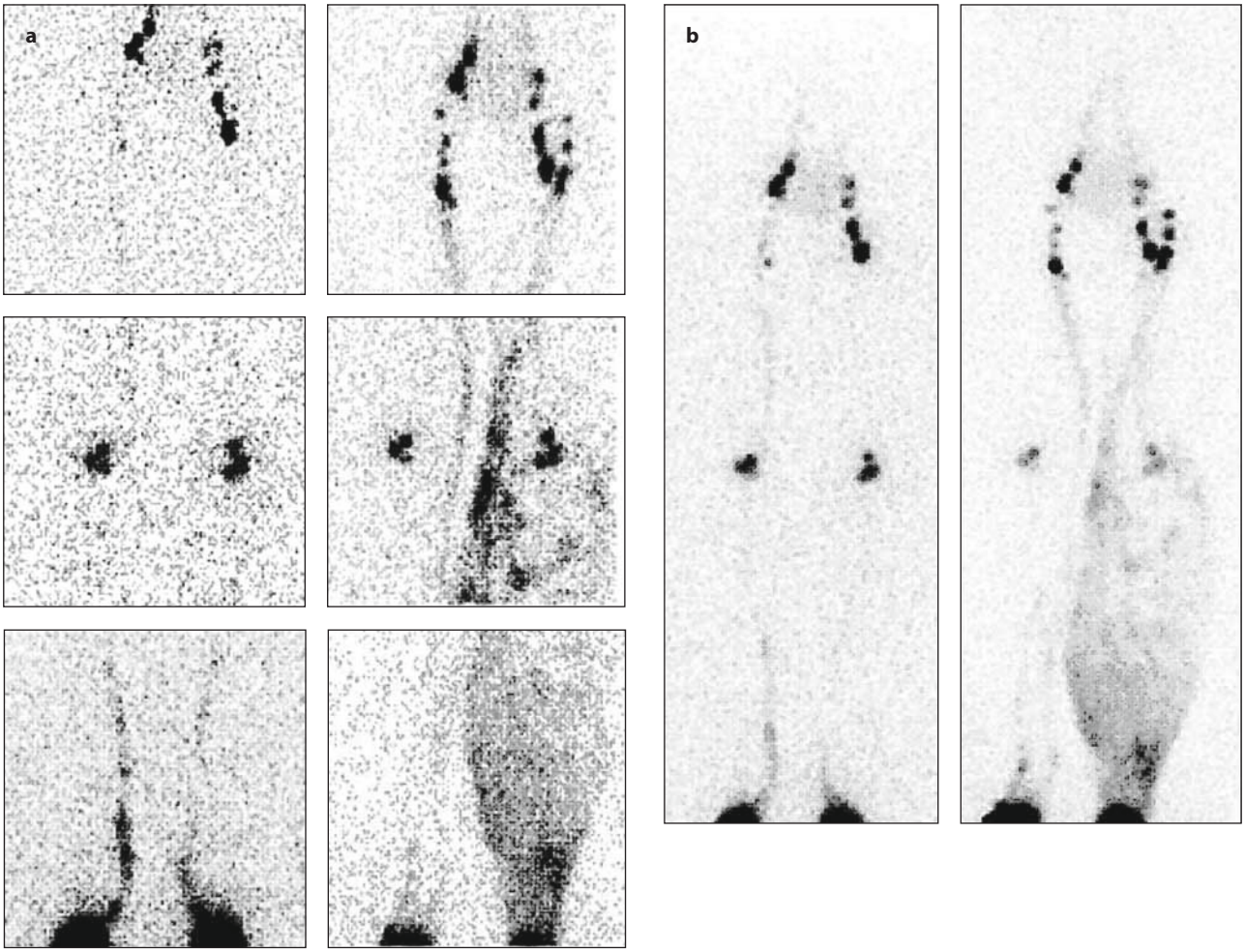

Fig. 2 Baseline lymphoscintigraphy. The spot images (**a**, *right*) and the whole-body image (**b**, *right*) show a normal deep lymphatic circulation with a relatively delayed right distal flow; normal popliteal and inguinal lymph nodes are detected with only faint visualization of the inferior right inguinal lymph nodes. After radiocolloid injection for assessing the superficial lymphatic circulation, a normal right lymph flow was depicted. Conversely, "dermal flow" and "dermal back flow" up to mid-thigh are present at the left limb, with preservation of the main lymphatic vessel. New lymph nodes appear in the inguinal region. No radiocolloid progression through the lumbo-aortic lymph nodes is detected and liver uptake of the radiocolloid is not observed

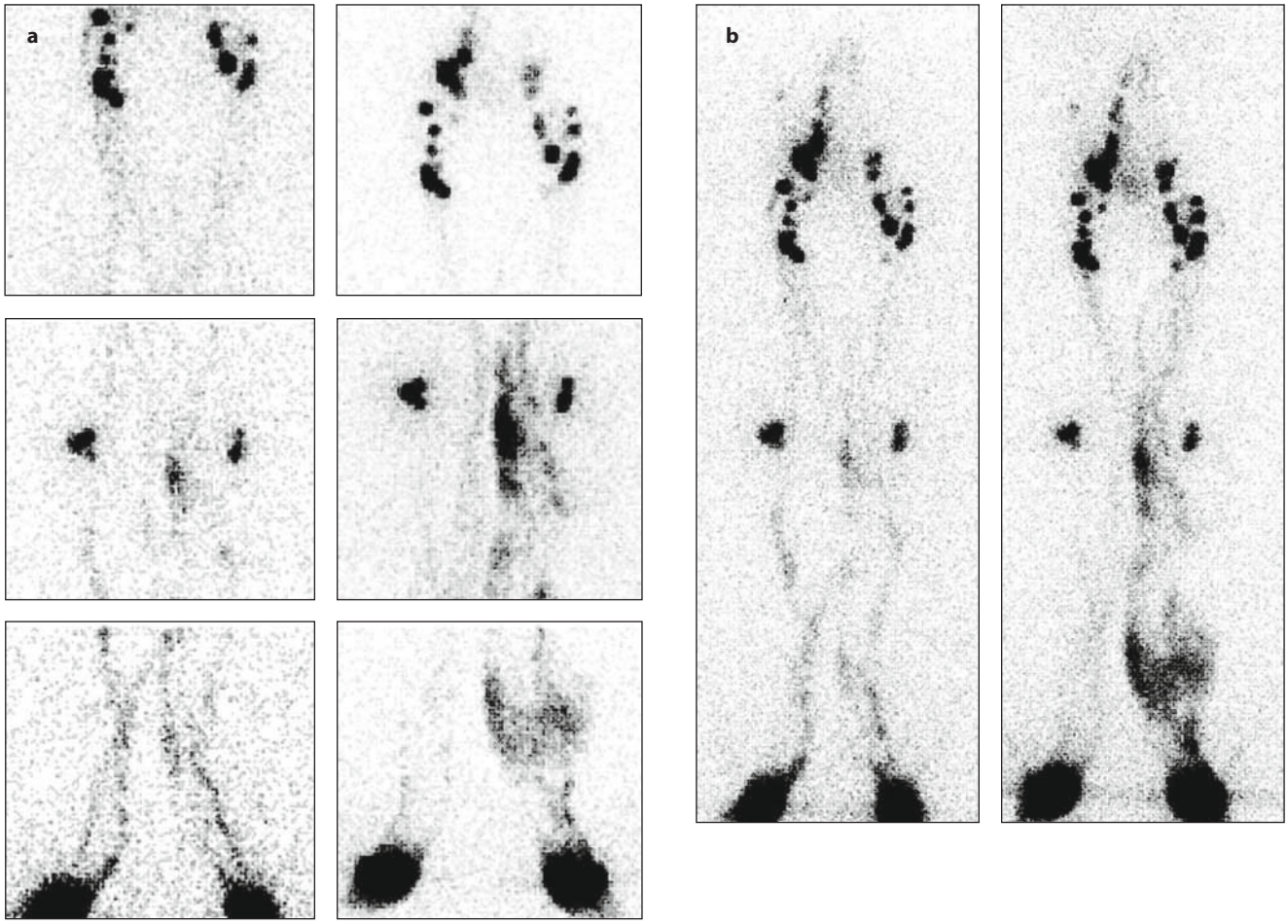

Fig. 3 Follow-up lymphoscintigraphy performed after 5 years of subsequent surgical procedures and multiple cycles of therapy. Spot images (anterior view, **a** *left column* DLC, *right column* DLC and SLC) and whole-body images (**b**, *left column* DLC, *right column* DLC and SLC) demonstrated a significant reduction of the left limb "dermal flow" and "dermal back flow" with enhanced lymphatic flow through both the deep and the superficial lymphatic circulation. However, collateral lymphatic channels are still visualized after injection for evaluation of the SLC, with enhanced uptake at the site of popliteal lymph nodes; furthermore, increased radiocolloid accumulation along the soft tissue of the lower part of the leg is still present. the pattern of lymphatic drainage for the right leg remains normal. Based on these findings, a new, less aggressive treatment plan was designed, to maintain these favourable results

Case 5.18
Upper and Lower Limb Bicompartmental Lymphoscintigraphy in Patient with Bilateral Feet and Ankle Edema, More Prevalent in Left Side

Paola Anna Erba and Luisa Locantore

Background Clinical Case

A 62-year-old woman with bilateral edema mainly at the distal part of the leg and the feet, worsening in the last 10 months. Doppler-ultrasound negative. Ultrasound of the soft tissue showing an increased thickening of the derma, which is hypoechogenic, representing an interstitial edema.

Anatomic location of edema: bilateral feet and ankles, major at the left side.

Lymphoscintigraphy

Upper Limbs

For the deep lymphatic circulation (DLC): two aliquots of ^{99m}Tc-nanocolloid, 7 MBq each of injection in 0.1 mL in the first and second intermetacarpal space, identified by palpating the palms of both hands immediately proximal to the distal heads of the metacarpal bones on each side, inserting the needle by about 12–13 mm to reach the intermetacarpal muscles below the deep fascia. *For the superficial lymphatic circulation (SLC)*: three aliquots of about 10 MBq in 0.1 mL on the dorsum of each hand, inserting the needle subdermally in sites corresponding approximately to the prior palmar injections, about 1–2 cm proximally to the interdigital web. Spot and whole-body images of both arms, thorax and upper abdomen.

Lower Limbs

For the DLC: two aliquots of ^{99m}Tc-nanocolloid, 7 MBq each of injection in 0.1 mL in the first and second intermetatarsal space, identified by palpating the soles of both feet immediately proximal to the distal heads of the metatarsal bones on each side, inserting the needle by about 12–13 mm to reach the intermetatarsal muscles below the deep fascia plantaris. *For the SLC*: three aliquots of about 10 MBq in 0.1 mL on the dorsum of each foot, inserting the needle subdermally in sites corresponding approximately to the prior palmar injections, about 1–2 cm proximally to the interdigital web. Spot and whole-body images were obtained from the distal feet up to the abdomen.

Spot images: 180 s/view, matrix 128×128, zoom 1.33
Whole-body images: matrix 256×1024, zoom 1, speed: 12 cm/min

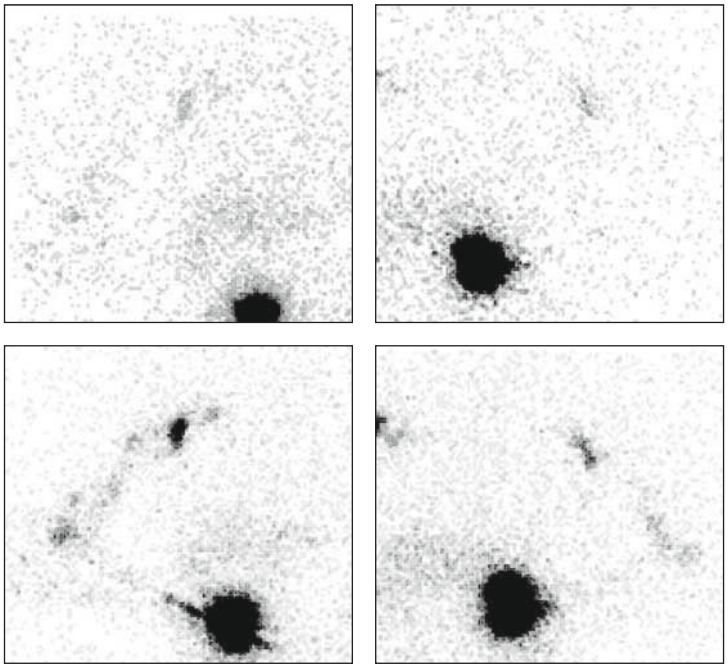

Fig. 1 Lymphoscintigraphy of upper limbs, spot images (*upper panel*: DLC; *lower panel*: SLC). A normal deep and superficial lymphatic circulation of the left upper limb is present with mild delay of the superficial circulation. Faint uptake is present at epitrochlear lymph nodes, while axillary lymph nodes are bilaterally visualized, despite being low in number

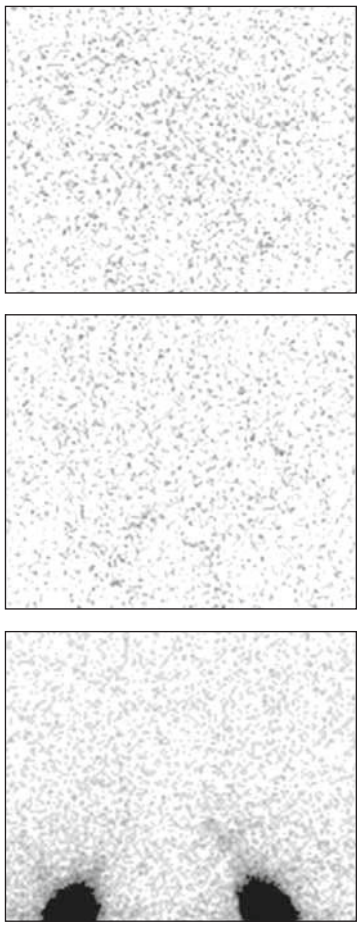

Fig. 2 Spot images of lymphoscintigraphy of the lower limbs of the DLC from the distal feet to the inguinal region of the lower limbs. No radiocolloid migration from the injection sites

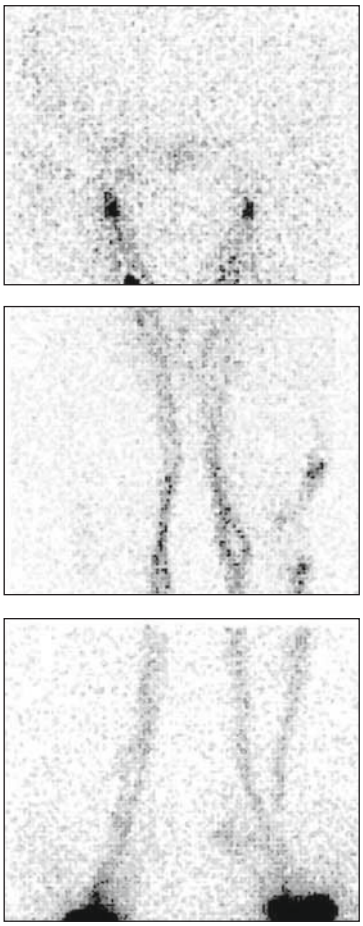

Fig. 3 Spot images of lymphoscintigraphy of the lower limbs of the DLC and SLC from the distal feet to the inguinal region. Images show a normal SLC at the right lower limb, while at the left limb collateral channels are visualized, with sites of uptake representing lymphatic collection along the exteranl margin thigh. No popliteal lymph nodes can be detected, while only few lymph nodes are detected at the inguinal region

This is a typical example of lower limb lymphedema due to an impairment of the DLC with conserved function of the SLC; however, signs of overload of the SLC are also present at the left lower limb. Arm circulation is normal.

Case 5.19
Upper and Lower Limb Bicompartmental Lymphoscintigraphy in Patient with Right Pelvic Para-Vesical and Inguinal Swelling

Paola Anna Erba and Luisa Locantore

Background Clinical Case

A 33-year-old man with right pelvic (alongside the bladder) and right inguinal swelling. CT finding of multiple cystic lesions suspected for cystic lymphoangiomatosis, localized in the retroperitoneal space, at the splenic lodge, in the bone (ribs, vertebral bodies, and pelvic bones of maximum 23 mm) and in the pelvis (about 10 cm). Negative [^{18}F]FDG-PET/CT findings.

Anatomic location of edema: right inguinal.

Lymphoscintigraphy

Upper Limbs

For the deep lymphatic circulation (DLC): two aliquots of ^{99m}Tc-nanocolloid, 7 MBq each of injection in 0.1 mL in the first and second intermetacarpal space, identified by palpating the palms of both hands immediately proximal to the distal heads of the metacarpal bones on each side, inserting the needle by about 12–13 mm to reach the intermetacarpal muscles below the deep fascia.

For the superficial lymphatic circulation (SLC): three aliquots of about 10 MBq in 0.1 mL on the dorsum of each hand, inserting the needle subdermally in sites corresponding approximately to the prior palmar injections, about 1–2 cm proximally to the interdigital web. Spot and whole-body images of both arms, thorax and upper abdomen.

Lower Limbs

For the DLC: two aliquots of ^{99m}Tc-nanocolloid, 7 MBq each of injection in 0.1 mL in the first and second intermetatarsal space, identified by palpating the soles of both feet immediately proximal to the distal heads of the metatarsal bones on each side, inserting the needle by about 12–13 mm to reach the intermetatarsal muscles below the deep fascia plantaris.
For the SLC: three aliquots of about 10 MBq in 0.1 mL on the dorsum of each foot, inserting the needle subdermally in sites corresponding approximately to the prior palmar injections, about 1–2 cm proximally to the interdigital web. Spot and whole-body images were obtained from the distal feet up to the abdomen.

Spot images: 180 s/view, matrix 128×128, zoom 1.33
Whole-body images: matrix 256×1024, zoom 1, speed: 12 cm/min

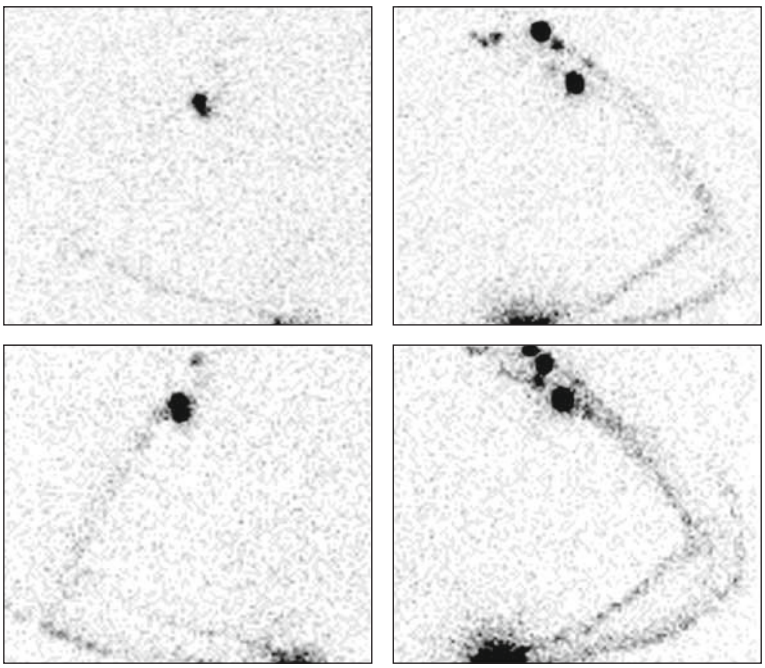

Fig. 1 Lymphoscintigraphy of the upper limbs, spot images. *Upper panels*: DLC. *Lower panels*: DLC and SLC

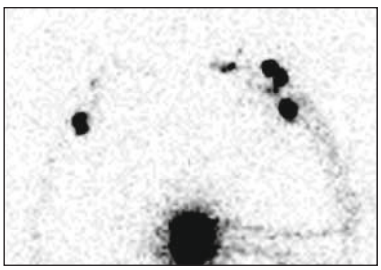

Fig. 2 Anterior view of the thoracic and upper abdominal regions, showing a normal deep and superficial lymphatic circulation of the right upper limb; for the left upper limb simultaneous visualization of DLC and SCL was observed immediately after the first injection (for DLC). No epitrochlear lymph nodes were detected and also the right axillary lymph nodes were faintly visualized (mainly first level nodes). The left axillary nodes were normal. At the end of this phase of the scan radiocolloids had not yet localized in the liver

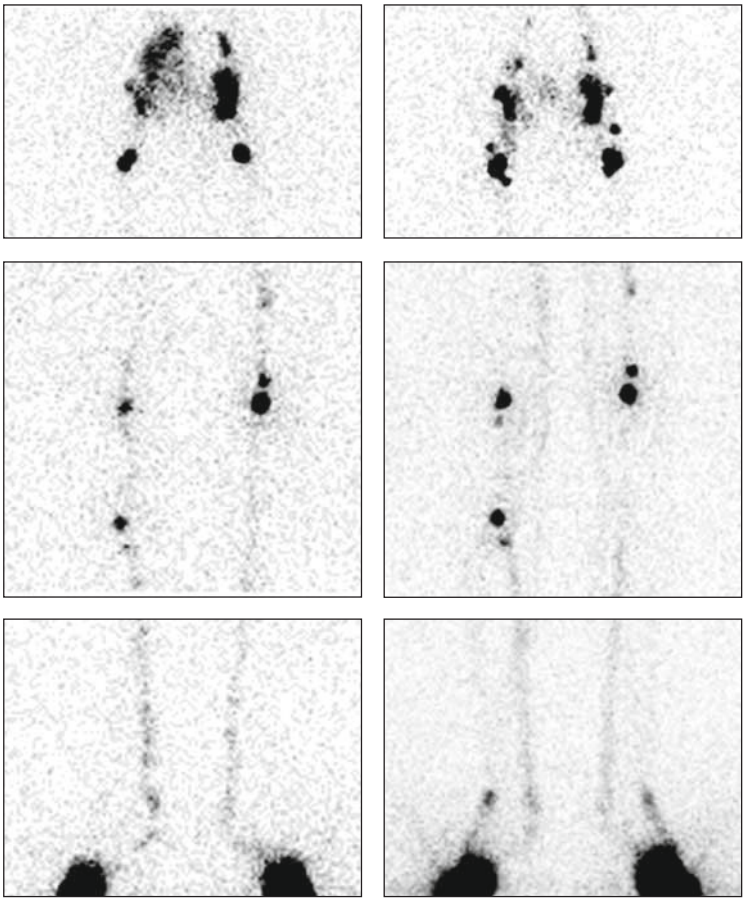

Fig. 3 Spot images of lower limbs during lymphoscintigraphy from the distal feet to the inguinal region. *Left column*: DLC. *Right column*: SLC

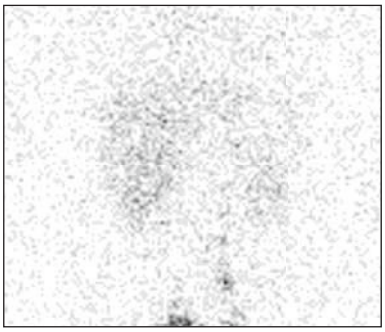

Fig. 4 Spot images of the abdomen, anterior view

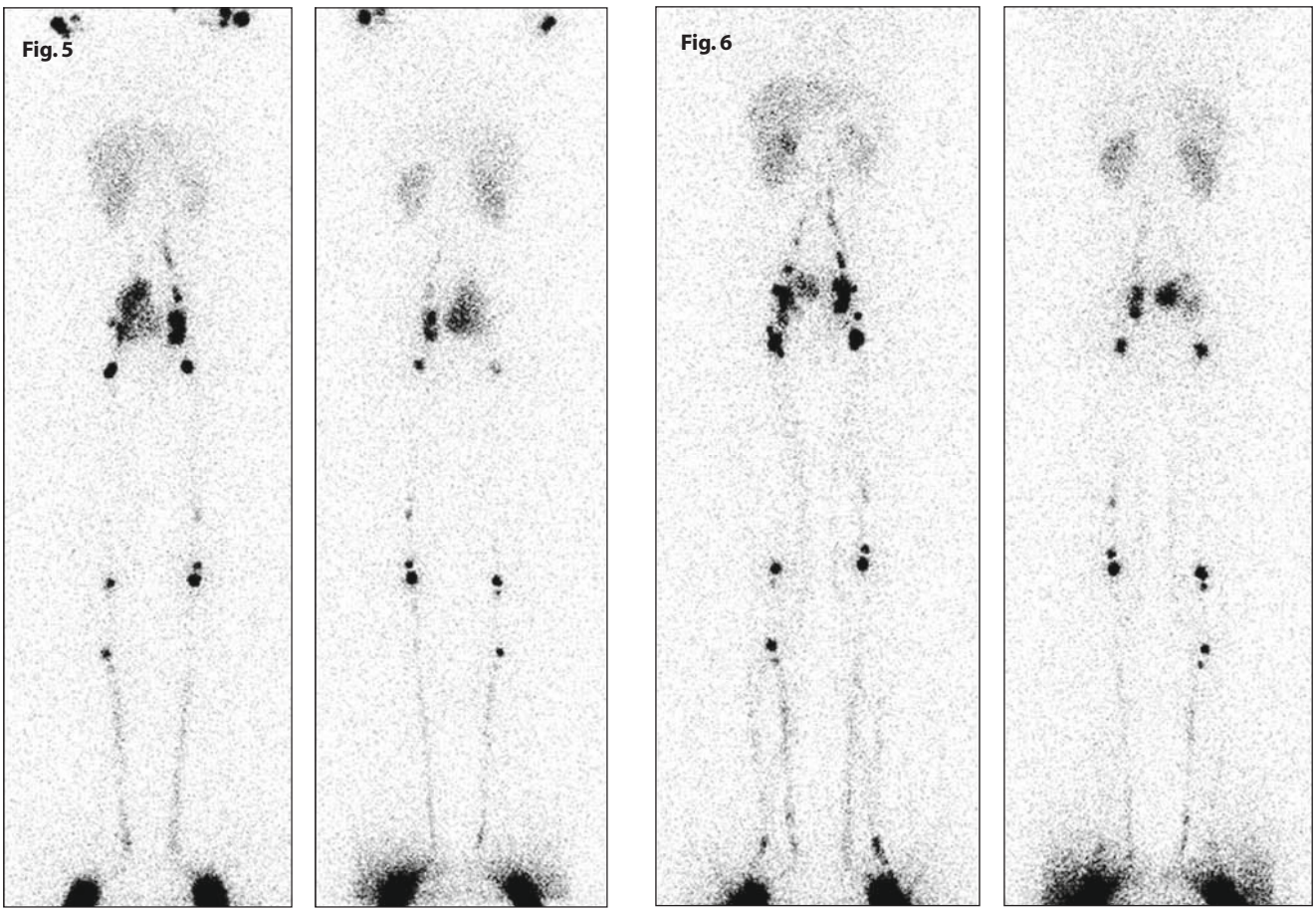

Fig. 5 Whole body images (*left column*, anterior view; *right column*, posterior view) after radiocolloid injection for the assessment of DLC, and **Fig. 6** with both DLC and SLC

Normal bilateral lymph flow was depicted, with only mild delay for the right SLC in the medial and distal part of the leg. Interestingly, two sites of radiopharmaceutical accumulation are evident. The first is at the pelvis localized near the bladder, at the right side, and which is receiving the lymph from the deep lymphatic system. The second is in the upper abdominal area, at the level of the upper right kidney portion which is supplied by the SLC. Normal lymph node images were seen for the popliteal lymph nodes bilaterally and for the left inguinal node. Progression through the lombo-aortic lymph nodes is present, as well as faint liver uptake of the radiocolloids.

The exam demonstrated the lymphatic nature of both the pelvic and the abdominal collections, therefore confirming the clinical diagnosis of cystic lymphoangiomatosis.

Case 5.20
Lower Limb Bicompartmental Lymphoscintigraphy in Patient with Edema of the Scrotum

Paola Anna Erba and Luisa Locantore

Background Clinical Case

A 72-year-old man with edema of the scrotum but no edema of upper or lower extremities. Previous surgery for left inguinal hernia.

Anatomic location of edema: scrotum.

Lymphoscintigraphy

For the deep lymphatic circulation (DLC): two aliquots of ^{99m}Tc-nanocolloid, 7 MBq each of injection in 0.1 mL into the first and second intermetatarsal space, identified by palpating the soles of both feet immediately proximal to the distal heads of the metatarsal bones on each side, inserting the needle by about 12–13 mm to reach the intermetatarsal muscles below the deep fascia plantaris.

For the superficial lymphatic circulation (SLC): three aliquots of about 10 MBq in 0.1 mL on the dorsum of each foot, inserting the needle subdermally in sites corresponding approximately to the prior palmar injections, about 1–2 cm proximally to the interdigital web. Spot and whole-body images were obtained from the distal feet up to the abdomen.

Spot images: 180 s/view, matrix 128×128, zoom 1.33
Whole-body images: matrix 256×1024, zoom 1, speed: 12 cm/min

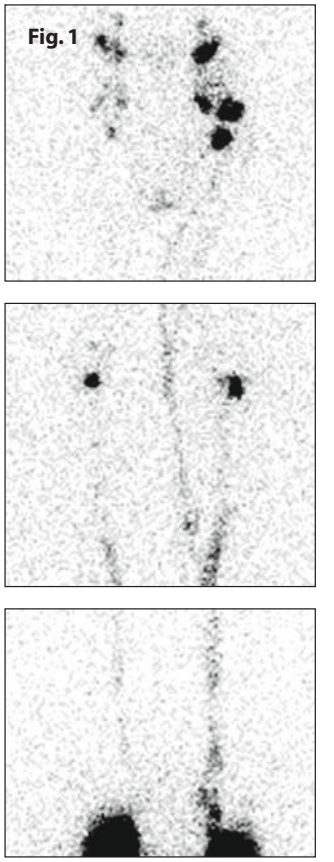

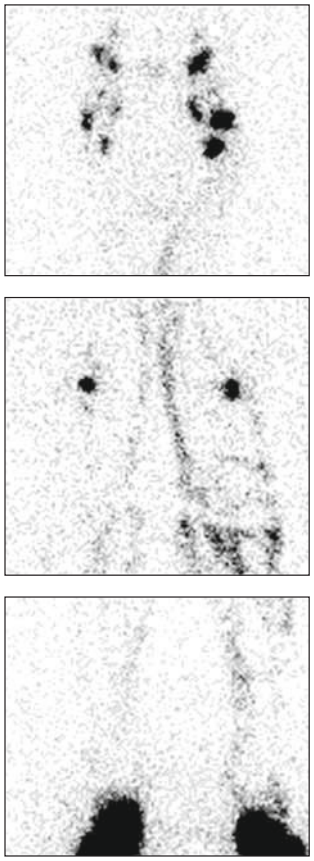

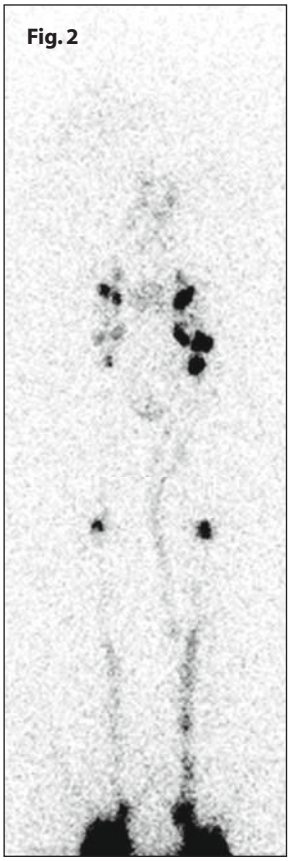

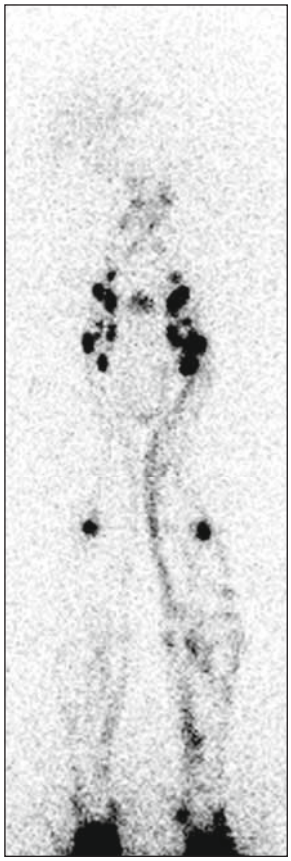

Figs. 1 and 2 Lymphoscintigraphy, spot images (*Fig. 1*) and whole body images (*Fig. 2*) of the lower limbs (*left column*, DLC; *right column* DLC and SLC). Normal deep lymphatic circulation of the right lower limbs with a relatively slow right distal flow; normal popliteal and inguinal nodes are detected, with only faint visualization of the inferior right inguinal lymph nodes. At the left lower limb, concomitant DLC and SLC are visible, both delayed as compared to the right DLC and SLC. In additiona, radiocolloid accumulation is also clearly depicted, localized medially at the left proximal thigh, which is consistent with the edema of the scrotum. Normal popliteal and inguinal nodes are detected also on the left side

After injections for assessment of the SLC, a normal right lymph flow was depicted, with only mild delay in the medial and distal part of the leg. Conversely, at the left limb, multiple collateral vessels are evident with lymph collection at the proximal left leg; preservation of the main lymphatic vessel is present. New images of the lymph nodes appear at the inguinal region. The lymph collection at the left scrotum persists, without increasing significantly the uptake of the radiocolloid. Progression through the lombo-aortic lymph nodes is present, as well as faint liver uptake of the radiocolloids.

The exam demonstrated the lymphatic origin of the edema of the scrotum, which is alimented by both the deep and the superficial lymphatic circulation and is evident after injection at the intermetatarsal space. Therefore, the same technique of injection was used for the subsequent injection of the blue dye during surgery performed to detect the site of lymphatic leakage. After the injection, which was performed after the preparation of the main operative field, a passive movement of the patient's leg was performed to allow the blue dye to reach the site of leak. As soon as the operative field became blue, indicating blue dye extravasation, the surgeon searched for the site of leakage, then performed the suture.

Case 5.21
Lower Limb Monocompartmental Lymphoscintigraphy in Patient with Post-Surgical Chylopericardium (Ductus Arteriosus), Treated with Thoracentesis

Paola Anna Erba and Luisa Locantore

Background Clinical Case

Girl, aged 1 year, with post-surgical chylopericardium (ductus arteriosus), treated with thoracentesis.

Anatomic location of edema: pericardium.

Lymphoscintigraphy

Lower Limbs

For the superficial lymphatic circulation (SLC): three aliquots of about 10 MBq in 0.1 mL on the dorsum of either each foot, inserting the needle subdermally, about 1–2 cm proximally to the interdigital web. Spot and whole-body images were obtained from the distal feet up to the the abdomen.

Spot images: 180 s/view, matrix 128×128, zoom 1.33
Whole-body images: matrix 256×1024, zoom 1, speed: 12 cm/min

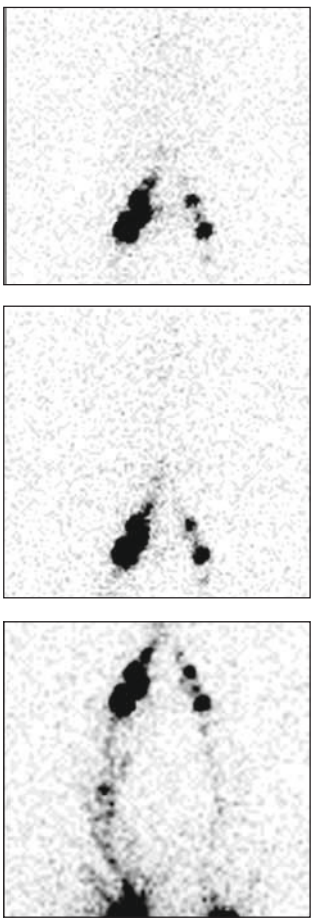

Fig. 1 Early spot lymphoscintigraphic acquisitions (SLC) of the lower limbs from the distal feet to the liver, acquired immediately after subdermal radiocolloid administration. A normal lymphatic drainage pattern is present at the left side. At the right side, there are indirect signs of overloaded drainage with delayed radiocolloid migration along dilated lymphatic vessels and delayed appearance of dermal back flow at the leg. Popliteal and inguinal lymph nodes are detected (mainly at right side). At this time, no radiocolloid accumulation is detectable in the thorax

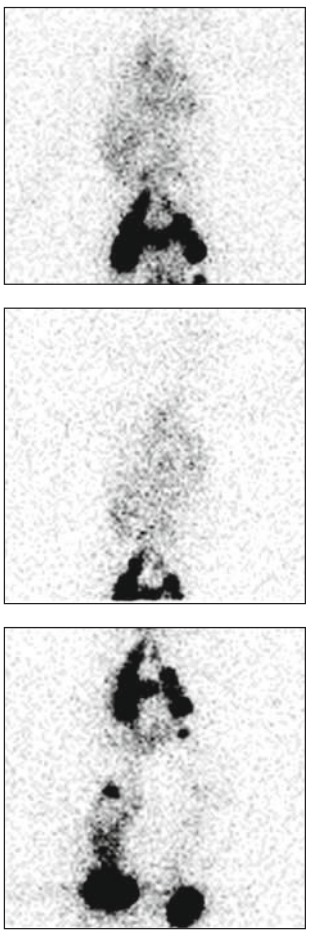

Fig. 2 Delayed spot lymphoscintigrahic acquisitions (SLC) of the lower limbs from the distal feet to the liver acquired 2 h after radiocolloid injection. A clear pattern of dermal back flow at the leg is observed, with persisting uptake in lymph nodes. Physiological visualization of the liver. In these images, faint radiocolloid accumulation can be detected in the thorax, localized in the mediastinal space and cardiac region, demonstrating the persistence of chylopericardium. A sample of pleuropericardial fluid was withdrawn from a mediastinal catheter; gamma-counting of this sample confirmed radiocolloid localization, further confirming the lymphatic origin of the effusion

References

1. Mortimer PS (1995) Managing lymphedema. Clin Dermatol 13: 499–505
2. Ely JW, Osheroff JA, Chambliss ML et al (2006) Approach to leg edema of unclear etiology. J Am Board Fam Med 19:148–160
3. Tiwari A, ChengK, Button M et al (2003) Differential diagnosis, investigation, and current treatment of lower limb lymphedema. Arch Surg 138:152–156
4. Durr HR, Pellengahr C, Nerlich A et al (2000) Angiosarcoma associated with chronic lymphedema (Stewart-Treves syndrome) of the leg: MR imaging. Skeletal Radiol 29:413–416
5. The International Society of Lymphology (2009) The diagnosis and treatment of peripheral lymphedema. 2009 Consensus Document of the International Society of Lymphology. Lymphology 42:51–60
6. Gasbarro V, Michelini S, Antignani PL et al (2009) The CEAP-L classification for lymphedemas of the limbs: the Italian experience. Int Angiol 28:315–324
7. Mortimer PS (2000) ABC of arterial and venous disease: swollen lower limb-2: lymphoedema. BMJ 320:1527–1529
8. Kaulesar Sukul DM, den Hoed PT et al (1993) Direct and indirect methods for the quantification of leg volume: comparison between water displacement volumetry, the disk model method and the frustum sign model method, using the correlation coefficient and the limits of agreement. J Biomed Eng 15:477–480
9. Mikes DM, Cha BA, Dym CL et al (1999) Bioelectrical impedance analysis revisited. Lymphology 32:157–165
10. Cornish BH, Bunce IH, Ward LC et al 1996 Bioelectrical impedance for monitoring the efficacy of lymphoedema treatment programmes. Breast Cancer Res Treat 38:169–176
11. Cornish BH, Chapman M, Thomas BJ et al (2000) Early diagnosis of lymphedema in postsurgery breast cancer patients. Ann N Y Acad Sci 904:571–575
12. Cha K, Chertow GM, Gonzalez J et al (1995) Multifrequency bioelectrical impedance estimates the distribution of body water. J Appl Physiol 79:1316–1319
13. Cavezzi A, Schingale F, Elio C (2010) Limb volume measurement: from the past methods to optoelectronic technologies, bioimpedance analysis and laser based devices. Int Angiol 29:392–394
14. Mayrovitz HN, Sims N, Macdonald J (2000) Assessment of limb volume by manual and automated methods in patients with limb edema or lymphedema. Adv Skin Wound Care 13:272–276
15. Mellor RH, Bush NL, Stanton AW et al (2004) Dual-frequency ultrasound examination of skin and subcutis thickness in breast cancer-related lymphedema. Breast J 10:496–503
16. Gniadecka M (1996) Localization of dermal edema in lipodermatosclerosis, lymphedema, and cardiac insufficiency. J Am Acad Dermatol 35:37–41
17. Hu D, Phan TT, Cherry GW et al (1998) Dermal oedema assessed by high frequency ultrasound in venous leg ulcers. Br J Dermatol 138:815–820
18. Naouri M, Samimi M, Atlan M et al (2010) High-resolution cutaneous ultrasonography to differenatiate lipoedema from lymphedema. Br J Dermatol 163:296–301
19. Cambria RA, Gloviczki P, Naessens JM (1993) Noninvasive evaluation of the lymphatic system with lymphoscintigraphy: a prospective, semiquantitative analysis in 386 extremities. J Vasc Surg18:773–778
20. Hreshchyshyn MM, Sheehan FR (1960) Proc Amer Ass Cancer Res 3:121
21. Jackson RJ (1966) Complications of lymphography. Br Med J 14:1203–1205
22. Guermazi A, Brice P, Hennequin C et al (2003) Lymphography: an old technique retains its usefulness. Radiographics 23:1541–1558
23. Aström KG, Abdsaleh S, Brenning GC et al (2001) MR imaging of primary, secondary, and mixed forms of lymphedema. Acta Radiol 42:409–416
24. Hadjis NS, Carr DH, Banks L et al (1995) The role of CT in the diagnosis of primary lymphedema of the lower limb. AJR Am J Roentgenol 144:361–364.
25. Monnin-Delhom ED, Gallix BP, Achard C et al (2002) High resolution unenhanced computed tomography in patients with swollen legs. Lymphology 35:121–128
26. Lohrmann C, Földi E, Bartholomä JP et al (2006) MR imaging of the lymphatic system: distribution and contrast enhancement of gadodiamide after intradermal injection. Lymphology 39:156–163
27. Lohrmann C, Foeldi E, Speck O et al (2006) High-resolution MR lymphangiography in patients with primary and secondary lymphedema. AJR Am J Roentgenol 187:556–561
28. Lohrmann C, Kautz O, Speck O et al (2006) Chronic lymphedema: detected with high-resolution magnetic resonance lymphangiography. J Comput Assist Tomogr 30:688
29. Lohrmann C, Foeldi E, Langer M (2009) MR imaging of the lymphatic system in patients with lipedema and lipo-lymphedema. Microvasc Res 77:335–339
30. Liu NF, Lu Q, Jiang ZH et al (2009) Anatomic and functional evaluation of the lymphatics and lymph nodes in diagnosis of lymphatic circulation disorders with contrast magnetic resonance lymphangiography. J Vasc Surg 49:980–987
31. Notohamiprodjo M, Weiss M, Baumeister RG et al (2012) MR Lymphangiography at 3.0 T: correlation with lymphoscintigraphy. Radiology 20 April, epub ahead of print
32. Bull RH, Gane JN, Evans JE et al (1993) Abnormal lymph drainage in patients with chronic venous leg ulcers. J Am Acad Dermatol 28:585–590
33. Weil GJ, Ramzy RMR (2007) Diagnostic tools for filariasis elimination programs. Trends Parasitol 23:78–82
34. Brennan MJ, Miller LT, American Cancer Society Lymphedema Workshop (1998) Workgroup III: Overview of treatment options and review of the current role and use of compression garments, intermittent pumps, and exercise in the management of lymphedema. Cancer 83:2821–2827
35. Vignes S (2002) Role of surgery in the treatment of lymphedema. Rev Med Interne 23:426–430
36. Andrejak M, Gersberg M, Sgro C et al (1998) French pharmacovigilance survey evaluating the hepatic toxicity of Coumarin. Pharmacoepidemiol Drug Saf 7:S45–S50
37. Campisi C (1999) Lymphoedema: modern diagnostic and therapeutic aspects. Int Angiol 18:14–24
38. Ho LC, Lai MF, Yeates M, Fernandez V (1988) Microlymphatic bypass in obstructive lymphoedema.Br J Plast Surg 41:475–484
39. Campisi C, Davini D, Bellini C et al (2006) Lymphatic microsurgery for the treatment of lymphedema. Microsurgery 26:65–69
40. Gloviczki P, Fisher J, Hollier LH et al. (1988) Microsurgical lymphovenous anastomosis for treatment of lymphedema: a critical review. J Vasc Surg 7:647–652
41. François A, Richaud C, Bouchet JY et al (1989) Does medical treatment of lymphedema act by increasing lymph flow? Vasa 18:281–286
42. Proby CM, Gane JN, Joseph AE et al (1190) Investigation of the swollen limb with isotope lymphography. Br J Dermatol 123:29–37
43. Hwang JH, Kwon JY, Lee KW et al (1999) Changes in lymphatic function after complex physical therapy for lymphedema. Lymphology 32:15–21
44. Kim DI, Huh S, Hwang JH et al (1999) Venous dynamics in leg lymphedema. Lymphology 32:11–14
45. Kafejian-Haddad AP, Perez JM et al (2006) Lymphscintigraphic evaluation of manual lymphatic drainage for lower extremity lymphedema. Lymphology 39:41–48

46. Chang L, Cheng MF, Chang HH et al (2011) The role of lymphoscintigraphy in diagnosis and monitor the response of physiotherapeutic technique in congenital lymphedema. Clin Nucl Med 36:11–12
47. Partsch H, Stöberl C, Wruhs M et al (1989) Indirect lymphography with iotrolan. Fortschr Geb Rontgenstrahlen Nuklearmed Erganzungsbd 128:178–181
48. Baulieu F, Baulieu JL, Vaillant L et al (1989) Factorial analysis in radionuclide lymphography: assessment of the effects of sequential pneumatic compression. Lymphology 2:178–185
49. Olszewski WL, Cwikla J, Zaleska M et al (2011) Pathways of lymph and tissue fluid flow during intermittent pneumatic massage of lower limbs with obstructive lymphedema. Lymphology 44:54–64
50. Liu NF, Olszewski W (1993) The influence of local hyperthermia on lymphedema and lymphedematous skin of the human leg. Lymphology 26:28–37
51. Pecking AP, Février B, Wargon C et al (1997) Efficacy of Daflon 500 mg in the treatment of lymphedema (secondary to conventional therapy of breast cancer). Angiology 48:93–98
52. Moore TA, Reynolds JC, Kenney RT et al (1996) Diethylcarbamazine-induced reversal of early lymphatic dysfunction in a patient with bancroftian filariasis: assessment with use of lymphoscintigraphy. Clin Infect Dis 23:1007–1011
53. Szuba A, Cooke JP, Yousuf S et al (2000) Decongestive lymphatic therapy for patients with cancer-related or primary lymphedema. Am J Med 109:296–300
54. Hwang JH, Choi JY, Lee JY et al (2007) Lymphscintigraphy predicts response to complex physical therapy in patients with early stage extremity lymphedema. Lymphology 40:172–176
55. Gironet N, Baulieu F, Giraudeau B et al (2004) Lymphedema of the limb: predictors of efficacy of combined physical therapy. Ann Dermatol Venereol 131:775–779
56. Slavin SA, Upton J, Kaplan WD et al (1997) An investigation of lymphatic function following free-tissue transfer. Plast Reconstr Surg. 99:730–741; discussion 742–743
57. Weiss M, Baumeister RG, Hahn K (2003) Planning and monitoring of autologous lymph vessel transplantation by means of nuclear medicine lymphoscintigraphy. Handchir Mikrochir Plast Chir 35:210–215
58. Mikami T, Hosono M, Yabuki Y et al (2011) Classification of lymphoscintigraphy and relevance to surgical indication for lymphaticovenous anastomosis in upper limb lymphedema. Lymphology 44:155–167
59. Burnand KM, Glass DM, Mortimer PS et al (2012) Lymphatic dysfunction in the apparently clinically normal contralateral limbs of patients with unilateral lower limb swelling. Clin Nucl Med 37:9–13
60. Bourgeois P, Frühling J, Henry J (1983) Postoperative axillary lymphoscintigraphy in the management of breast cancer. Int J Radiat Oncol Biol Phys 9:29–32
61. Frühling JG, Bourgeois P (1983) Axillary lymphoscintigraphy: current status in the treatment of breast cancer. Crit Rev Oncol Hematol 1:1–20
62. Das IJ, Cheville AL, Scheuermann J et al (2011) Use of lymphoscintigraphy in radiation treatment of primary breast cancer in the context of lymphedema risk reduction. Radiother Oncol 100:293–298
63. Baulieu F, Itti R, Taieb W et al (1985) Lymphoscintigraphy. A predictive test of post-traumatic lymphedema of the lower limbs. Rev Chir Orthop Reparatrice Appar Mot 71:327–332

The Sentinel Lymph Node Concept in Oncologic Surgery

6

Omgo E. Nieweg

6.1 History

For many years, regional lymph node dissection routinely accompanied the surgical procedure for various solid cancers, even if the nodes appeared clinically normal. This practice was based on the observations by the German pathologist Rudolf L.K. Virchow (1821–1902) that lymph nodes filter particulate matter from lymph fluid and that cancer metastasizes via lymph ducts to the lymph nodes [1]. These important findings inspired the American surgeon William S. Halsted to develop the mastectomy with *en bloc* axillary lymph node dissection for breast cancer at the end of the 19th century [2]. Halsted's hypothesis entails that cancer generally metastasizes first to a regional lymph node. This node acts as a filter that temporarily prevents further spread of cancer cells. This barrier creates a window of opportunity for radical local–regional surgery to cure the patient. In the 1980s, work carried out by Dr Bernard Fisher and others appeared to refute the Halsted hypothesis [3, 4]. Their assertion implied that cancer does not spread in an orderly fashion. The Fisher hypothesis indicates rather that lymph nodes and distant sites tend to become involved simultaneously and that lymph nodes are ineffective as barriers to further dissemination. As a result, lymph node metastasis was presumed to indicate that the disease had spread to various sites and that curative surgery was no longer an option.

Nevertheless, some surgeons held on to the Halstedian view and developed the concept further. Squamous cell carcinoma of the penis tends to metastasize to lymph nodes but not to distant sites until a late stage. In 1977, the Paraguayan surgeon Ramon Cabañas suggested that penile cancer initially drains to a particular lymph node that is always at the same location in the groin, and called this node the "sentinel" node [5]. The node was defined by its constant anatomic position. For penile cancer this assumption appears plausible, because the primary cancer is always found in the exact same location, on the glans. However, the hypothesis that lymph drainage rigorously follows a pattern to a lymph node that is always in the exact same location did not hold. Urologists found that results from biopsy of this sentinel node were not sufficiently reliable to make the removal procedure routine clinical practice [6, 7].

Donald L. Morton, a surgeon at the John Wayne Cancer Center in Santa Monica, and his pathologist Alistair J. Cochran from the University of California Los Angeles, took the sentinel lymph node (SLN) procedure a major step forward in the late 1980s, by proposing the innovative concept of "lymphatic mapping with sentinel lymph node biopsy" (SLNB) for melanoma [8]. They suggested that a melanoma can drain to any node in a particular lymph node field (or basin), depending on the location of the primary lesion and with certain individual variability. They developed a technique to identify and remove this lymph node. Lymphoscintigraphy identifies the basin to which the tumor drains and indicates the number of SLNs. Single photon emission computed tomography/computed tomography (SPECT/CT) now visualizes the exact anatomic location. Delicate dissection of the afferent lymph ducts after administration of a blue dye at the lesion site guides the surgeon to the sentinel node (Fig. 6.1). Radioactivity of the node is gauged with a gamma-ray detection probe and confirms that it is the correct lymph node. The pathologist obtains multiple sections from the node and can use sensitive immunohistochemistry staining techniques to detect even minute deposits of malignant cells.

It has been demonstrated that the hypothesis of Morton and Cochran is correct and that lymphatic dissemination generally occurs in a sequential fashion [9, 10]. The SLN is indeed the first node to be involved and its tumor status reflects the status of the entire lymph node field.

O. E. Nieweg (✉)
Skin and Melanoma Centre and Department of Surgery
Netherlands Cancer Institute – Antoni van Leeuwenhoek Hospital
Amsterdam, the Netherlands
E-mail: o.nieweg@nki.nl

G. Mariani et al. (eds.), *Atlas of Lymphoscintigraphy and Sentinel Node Mapping*,
DOI 10.1007/978-88-470-2766-4_6

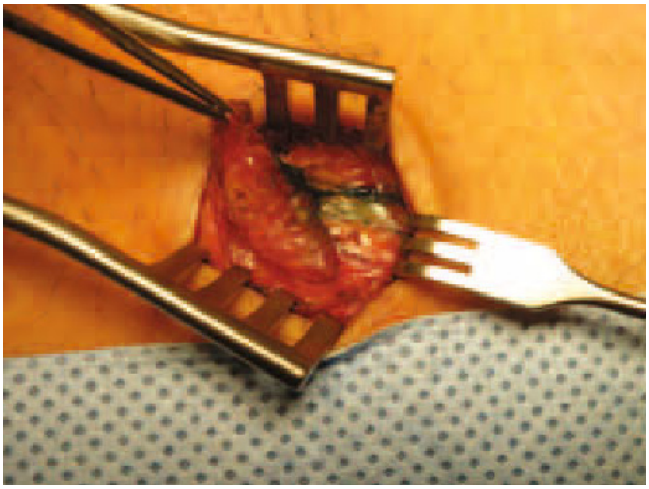

Fig. 6.1 Blue lymph channel beginning to stain a sentinel lymph node

6.2 Concept and Definition

The concept of lymphatic mapping is based on the notion that lymph fluid from a primary cancer drains to a particular regional lymph node (Fig. 6.2). This is the SLN (first-tier node, first-echelon lymph node). From this node, lymph fluid passes through efferent lymph vessels to other nodes. When tumor cells spread, they will first lodge in the SLN. This is the node at greatest risk of harboring tumor cells. Other nodes may subsequently become involved, in a stepwise fashion. The essential element of the concept is the afferent vessel that collects lymph from the tumor and delivers it to the node that acts as the first filter.

Morton et al. used the definition "a sentinel node is the initial lymph node upon which the primary tumour drains" [8]. The word "initial" is liable to misinterpretation. For instance, multiple lymph vessels may link the tumor to multiple nodes that may not necessarily show up simultaneously on the images (see below). To avoid confusion, the definition was slightly modified to "a sentinel node is any lymph node on the direct drainage pathway from the primary tumour." This definition reflects the physiology of lymph drainage and the stepwise dissemination of cancer through the lymphatic system. This is the definition most experts adhere to.

Later, this definition was challenged [11–15]. Some investigators have come up with their own definitions (Table 6.1) [16–19]. This is understandable, since specialists from different fields are involved and each is addressing the concept from their own background and perspective.

Lymphoscintigrams may be difficult to interpret, as they tend to depict multiple nodes and do not always clearly indicate the order of lymph drainage. Also, the surgical procedure is not always easy. SLNB requires a considerable ability to think in a three-dimensional fashion. The surgeon needs to translate the one-dimensional probe readings and the two-dimensional scintigrams into a three-dimensional image in his mind. Also, the blue lymphatic vessel that guides the surgeon to the sentinel node is very fragile. It requires considerable experience and finesse to dissect this delicate structure in a small, confined space, through a small incision, in a lymph node basin that may be deep. For these reasons, some surgeons have sought easier criteria to determine which node(s) to remove in the situation that lymphoscintigraphy depicts multiple nodes.

Some investigators define the sentinel node as the lymph node closest to the primary lesion [20]. It is often true that the node closest to the tumor is indeed (the) one into which the lymph vessel from the tumor drains, but this is not always the case (Fig. 6.3). Therefore, this anatomy-based definition does not take into account the physiology of lymph drainage.

Other investigators define the sentinel node as the first lymph node that becomes visible on the lymphoscintigraphic images. It is inevitable that the first node that is depicted lies on a direct drainage pathway from the cancer and must be classified as a sentinel node. However, this definition does not acknowledge the fact that more than one lymph node can be on a direct drainage pathway and that there may be reasons that prevent all the nodes involved becoming visible simultaneously. For instance, there may be two lymph vessels originating in the tumor that drain into different lymph nodes (Fig. 6.4). Sometimes, a single lymph duct splits up in two channels going to separate nodes (Fig. 6.5). Tumor cells may follow either route and both lymph nodes are at direct risk of being involved. Because the speed of lymph flow may be quite different in the two channels, lymphoscintigraphy may visualize one node before the other. This does not imply that the other node needs not be removed. All nodes in direct drainage contact with the primary tumor are directly at risk of harboring tumor cells. All these first-tier nodes should be harvested and examined by the pathologist. Therefore, the definition of the SLN being the first node to be visualized is too narrow; too few nodes are designated as sentinel nodes and metastases may be overlooked.

When lymphoscintigraphy shows multiple lymph nodes, some people consider only the one that is most clearly visualized on the scintigrams or the one that yields the highest probe reading as the sentinel node [19]. This definition of the "hottest" lymph node being the sentinel node has several drawbacks. Again, lymph fluid can drain directly to multiple nodes and one can collect more of the radiocolloid than another (Fig. 6.6). The size of the lymph node also determines the amount of radioactivity that can be accumulated. Its location is also relevant: a superficial lymph node lies a short distance from the gamma camera or the gamma-ray detection probe and will yield more counts than a node that contains three times as much of the tracer but lies at twice the distance. Some of the radiocolloid may pass through the

Table 6.1 Less appropriate definitions of a sentinel node

• Lymph node closest to the primary lesion
• First lymph node depicted on the lymphoscintigraphy images
• Lymph node with the highest count rate
• Any radioactive lymph node
• Lymph node with a count rate that is a certain factor higher than the background or compared to nonsentinel nodes
• Lymph node with a count rate that exceeds a certain fraction of the hottest node
• Blue lymph node

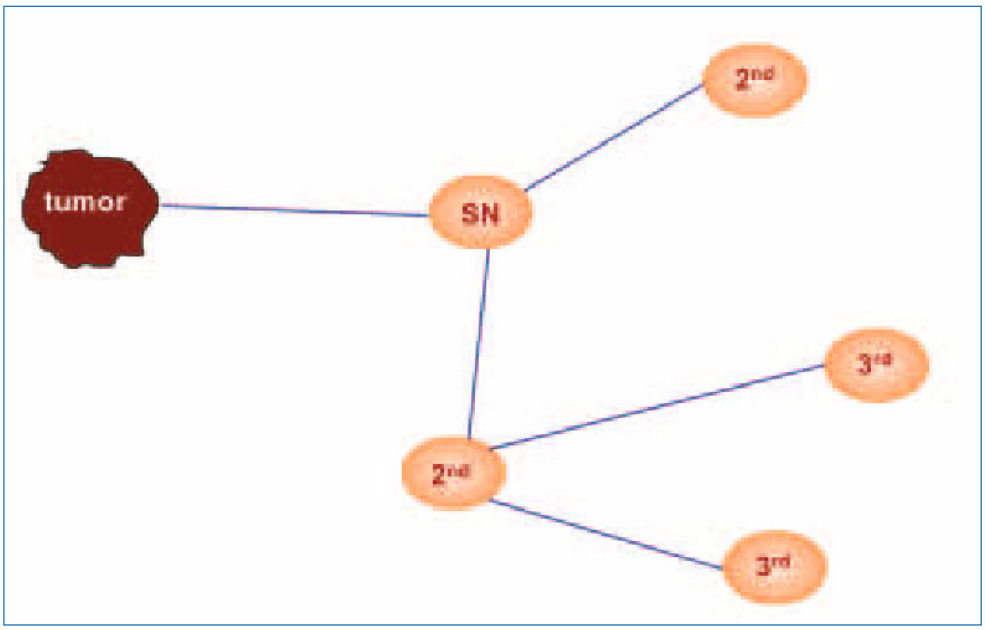

Fig. 6.2 The concept of lymphatic mapping is based on the notion that lymph fluid from a primary cancer drains to a particular regional lymph node. *SN* = sentinel node, 2^{nd} = second-tier lymph node, 3^{rd} = third-tier lymph node

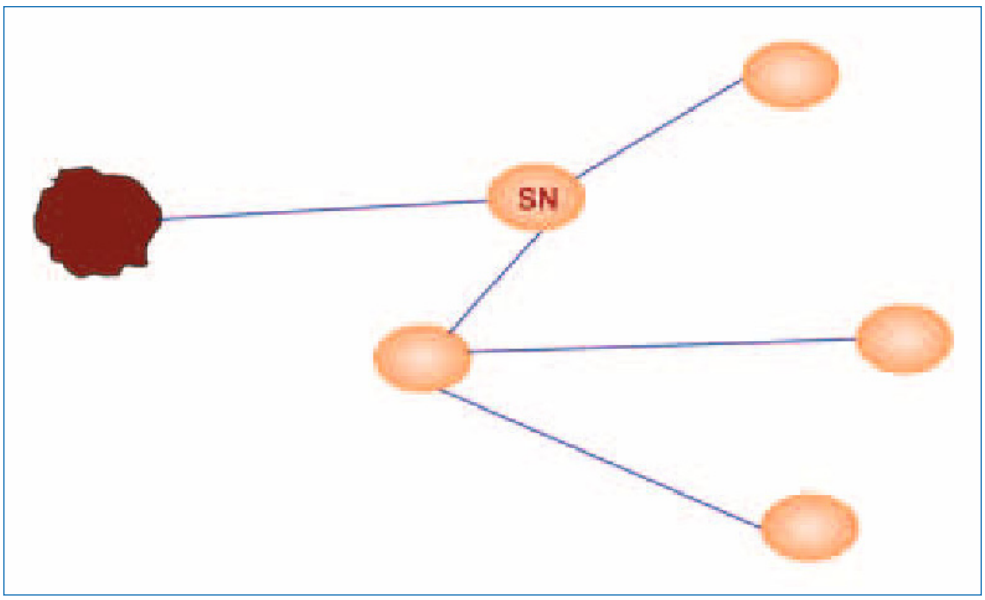

Fig. 6.3 Alternative definition. The lymph node closest to the cancer is not necessarily directly at risk of receiving tumor cells. *SN* = sentinel node

first lymph node and move on to subsequent nodes. A large second-echelon lymph node – or one with more active macrophages – may accumulate more radiocolloid than a small first-echelon node (Fig. 6.7).

The amount of radiocolloid that is accumulated by a lymph node depends not only on its position in the drainage order, but also on the number of lymphatic channels that enter the node and on parameters such as the speed of lymph

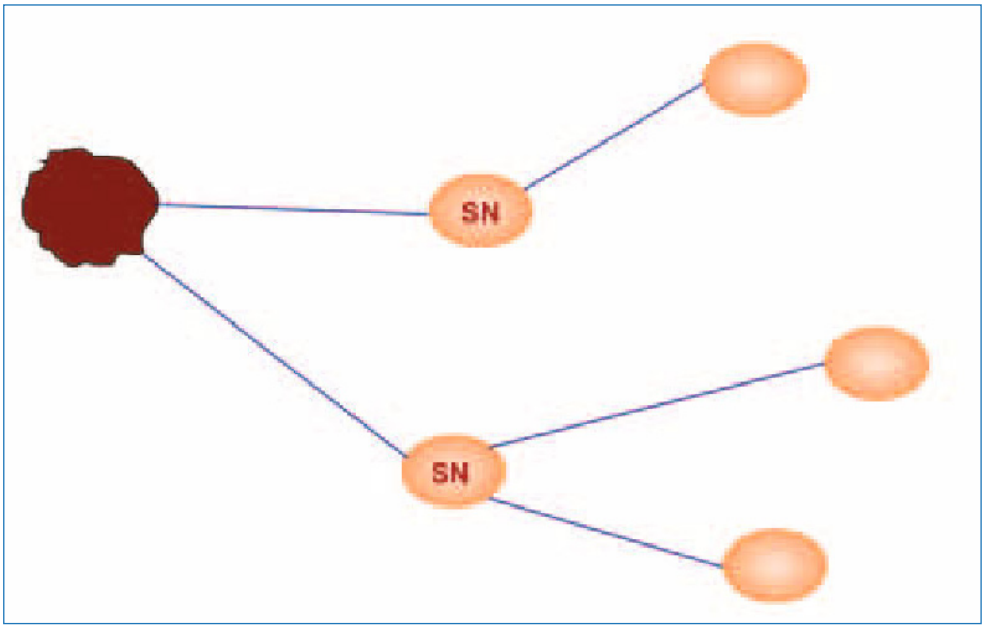

Fig. 6.4 Two lymph vessels originating in the tumor draining upon separate lymph nodes. *SN* = sentinel node

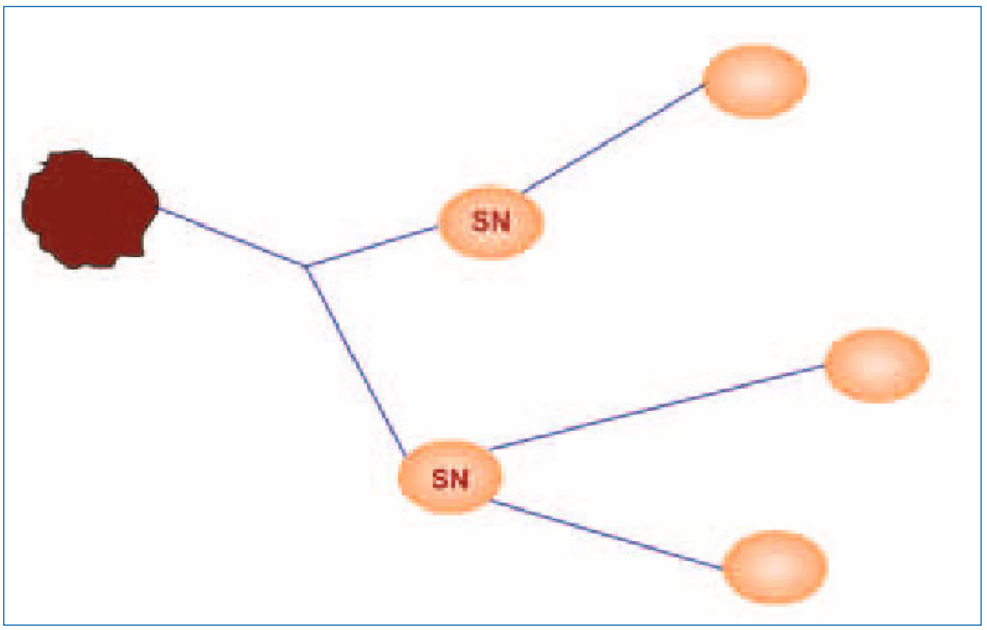

Fig. 6.5 Lymph duct dividing into two channels leading to separate lymph nodes. *SN* = sentinel node

flow. Yet another reason for a node to receive a sparse lymph supply is that the flow to that particular node is hampered by metastatic disease obstructing its ingress (Fig. 6.8) [21]. Therefore, there are a number of reasons not to classify a lymph node as a sentinel node based on its superior brightness on the scintigram or on the highest probe reading.

Some surgeons rely on their probe to find the SLN without preoperative imaging or use of a blue dye. They tend to assume that any radioactive node identified with the gamma-ray detection probe is a SLN, and they define a sentinel node as such. This point of view does not acknowledge the possibility that some of the radiocolloid may pass through the first-tier lymph node and lodge in secondary nodes that are not directly at risk of harboring metastatic disease. This definition is too liberal and too many lymph nodes are removed as a result. One report indicated that up to 37 SLNs could be removed from a single basin [22].

Another definition is based on the sentinel node-to-background count ratio. This definition also has shortcomings. Various factors determine the accumulation of the radiopharmaceutical in a lymph node, like the size of the colloid particles and their surface features, the size of the lymph

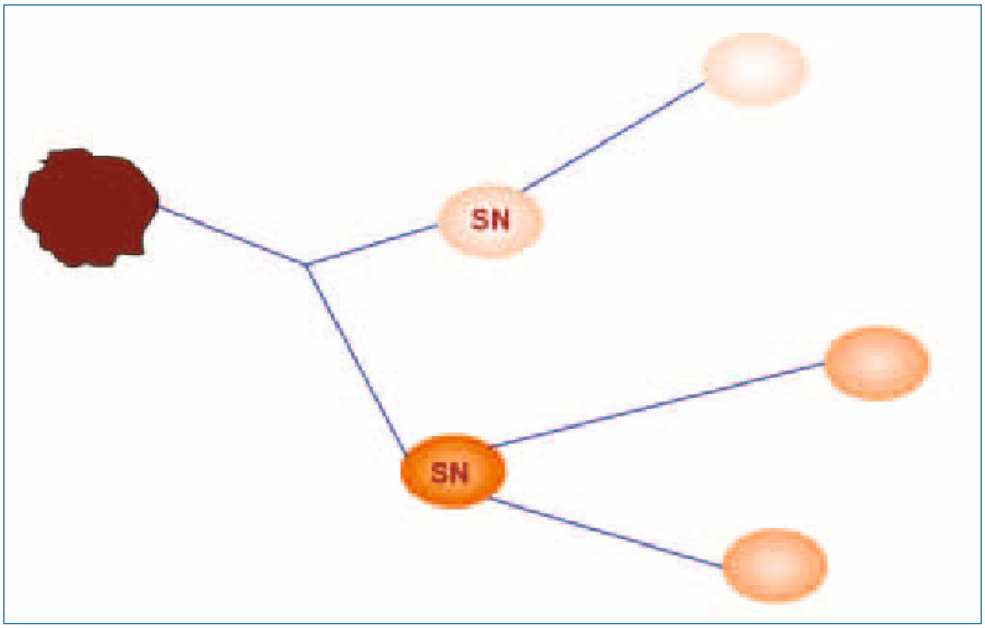

Fig. 6.6 Lymph fluid can drain directly to multiple nodes and one may accumulate more radiocolloid than another. *SN* = sentinel node

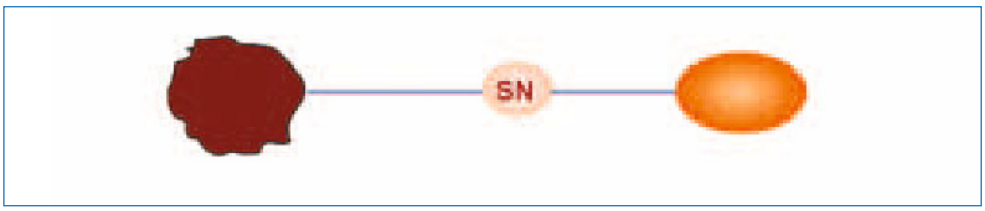

Fig. 6.7 A large second-echelon lymph node – or one with more active macrophages – may accumulate more of the radicolloid than a small first-echelon lymph node. *SN* = sentinel node

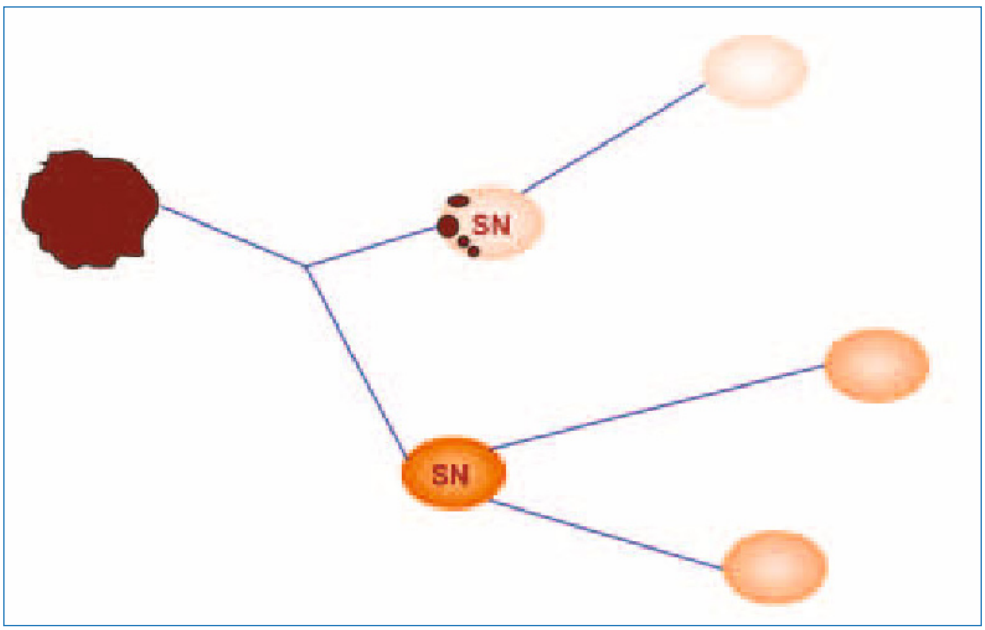

Fig. 6.8 Lymph flow to sentinel node hampered by metastatic disease. *SN* = sentinel node

node, the activity of its macrophages, and the speed of lymph flow. The speed of lymph flow fluctuates and depends on factors like physical exercise, time of day, medication, massaging of the injection site, and hydration state of the patient. As a result, radiocolloid uptake in a node to which the cancer drains is highly variable. In breast cancer patients, the 95% uptake range varies between 0.001% and 2.5% of the injected activity, and in melanoma patients it is between 0.06% and 3.6% [23]. Different surgeons use different backgrounds to calculate the count ratio. Some surgeons obtain

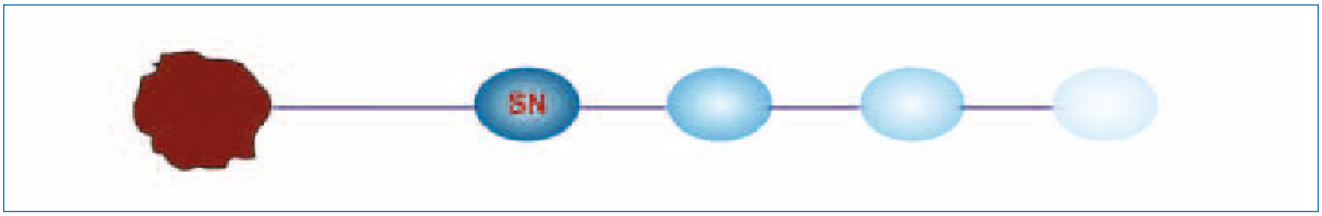

Fig. 6.9 Blue dye is not retained in the sentinel lymph node. It flows through downstream and stains a string of subsequent lymph nodes. *SN* = sentinel node

the background reading in the lymph node basin; others use a location elsewhere in the body or outside the body.

The sentinel-node-to-non-sentinel-node ratio is another parameter used to determine whether a lymph node is a sentinel node. This approach implies that one has to find a non-SLN first and then examine the other nodes with the probe to determine whether the designated count rate is reached. The node-to-hottest-node ratio is yet another criterion. The approaches exploiting aspects of the radiocolloid accumulation cannot be used in 15% to 30% of the lymph nodes on a direct drainage pathway from a primary breast cancer that are not radioactive at all [24, 25]. One is left with the conclusion that the definition of a SLN cannot reliably be based on factors that can be measured with the gamma-ray detection probe alone.

Some surgeons consider every lymph node that is stained blue to be a sentinel node. Unlike the radiocolloid, the blue dye is not retained in a node by the macrophages. It just flows through and moves on to the next node downstream. There will rapidly be a string of blue nodes of which only the first one is directly at risk of containing tumor cells (Fig. 6.9).

All these alternative definitions have their flaws. The definition that a SLN is any lymph node that receives afferent lymphatic drainage directly from a primary tumor best reflects the route that the tumor cells travel and the concept of stepwise spread of cancer through the lymphatic system. However, this definition requires a meticulous technique of lymphoscintigraphy, conscientious interpretation of the images, and precise dissection of the lymphatic ducts [26, 27]. Even then, one occasionally encounters a confusing situation with multiple hot and blue nodes without a demonstrable lymph vessel that points out the SLN. These are the reasons why surgeons opt for seemingly clear-cut definitions that are based on the anatomy or on the tools they use in their quest. These alternative definitions may be correct most of the time, but they are not based on the physiology of lymph drainage, or on the biology of the disease [12]. Thus, the SLN is not always the node closest to the tumor. The SLN is not just the node that is depicted first on the images, neither is it necessarily the most radioactive node, or a radioactive node *per se*, nor is it always a node that is more or less radioactive than another node or in comparison with some other tissue. Not every SLN is blue, and not every blue node is a sentinel node. It is best to pursue the nodes on a direct lymphatic pathway from the tumor. In the occasional situation in which it is unclear whether a certain lymph node is a sentinel node, the surgeon should proceed and remove such a node.

6.3 Concluding Remarks

Lymphatic mapping requires a concerted effort from the nuclear medicine physician, surgeon, and pathologist. Lymphoscintigraphy visualizes the nodes receiving lymph fluid from the lesion site and has taught us that tumors can drain to lymph nodes in locations that we were previously not aware of. The procedure enables more accurate staging because the surgeon identifies the lymph nodes at the greatest risk of harboring metastatic disease. The morbidity of the procedure is limited. The pathologist is inclined to obtain multiple sections and use sensitive immunohistochemistry staining techniques in addition to the standard hematoxylin and eosin staining. Lymphatic mapping provides better information on the prognosis. The procedure allows patients with lymph node metastasis to be treated in an early phase. This improves the chance of survival in patients with nodal involvement from penile cancer or melanoma [28, 29]. Many patients with breast cancer or vulvar cancer are spared an unnecessary lymph node dissection and more patients are identified who may benefit from adjuvant systemic therapy. After description of its success in patients with these diseases, lymphatic mapping was quickly explored in other cancer types, as described in the subsequent chapters. It can be concluded that lymphatic mapping with SLNB is one of the most interesting and important developments in clinical oncology in recent years and fits perfectly with the current trend for more conservative surgery in cancer patients.

References

1. Tanis PJ, Nieweg OE, Valdés Olmos RA et al (2001) History of sentinel node and validation of the technique. Breast Cancer Res 3:109–112
2. Halsted WS (1894) The results of operations for the cure of cancer of the breast performed at the Johns Hopkins Hospital from June 1889 to January 1894. Johns Hopkins Hosp Bull 4:297–323

3. No authors listed (1980) Cancer research campaign (King's/Cambridge) trial for early breast cancer. A detailed update at the tenth year. Cancer Research Campaign Working Party. Lancet 2(8185):55–60
4. Fisher B, Redmond C, Fisher ER et al (1985) Ten-year results of a randomized clinical trial comparing radical mastectomy and total mastectomy with or without radiation. N Engl J Med 312:674–681
5. Cabañas RM (1977) An approach for the treatment of penile cancer. Cancer 39:456–466
6. Bouchot O, Bouvier S, Bochereau G, Jeddi M (1993) [Cancer of the penis: the value of systematic biopsy of the superficial inguinal lymph nodes in clinical N0 stage patients.] Prog Urol 3:228–233
7. Pettaway CA, Pisters LL, Dinney CPN et al (1995) Sentinel lymph node dissection for penile carcinoma: M.D. Anderson Cancer Center experience. J Urol 154:1999–2003
8. Morton DL, Wen D-R, Wong JH et al (1992) Technical details of intraoperative lymphatic mapping for early stage melanoma. Arch Surg 127:392–399
9. Reintgen D, Cruse CW, Wells K et al (1994) The orderly progression of melanoma nodal metastases. Ann Surg 220:759–767
10. Kapteijn BA, Nieweg OE, Peterse JL et al (1998) Identification and biopsy of the sentinel lymph node in breast cancer. Eur J Surg Oncol 24:427–430
11. Morton DL, Bostick PJ (1999) Will the true sentinel node please stand? Ann Surg Oncol 6:12–14
12. Balch CM, Ross MI (1999) Sentinel lymphadenectomy for melanoma – is it a substitute for elective lymphadenectomy? Ann Surg Oncol 6:416–417
13. Thompson JF, Uren RF (2000) What is a 'sentinel' lymph node? Eur J Surg Oncol 26:103–104
14. Nieweg OE, Tanis PJ, Kroon BBR (2001) The definition of a sentinel node. Ann Surg Oncol 9:538–541
15. Coit DG (2001) The "true" sentinel lymph node: in search of an operational definition of a biological phenomenon. Ann Surg Oncol 8:187–189
16. Veronesi U, Paganelli G, Galimberti V et al (1997) Sentinel-node biopsy to avoid axillary dissection in breast cancer with clinically negative lymph-nodes. Lancet 349:1864–1867
17. De Cicco C, Sideri M, Bartolomei M et al (1997) Sentinel node detection by lymphoscintigraphy and gamma detecting probe in patients with vulvar cancer. J Nucl Med 38:33P [abstract].
18. Gershenwald JE, Tseng CH, Thompson W et al (1998) Improved sentinel lymph node localization in patients with primary melanoma with the use of radiolabeled colloid. Surgery 124:203–210
19. Boxen I, McCready D, Ballinger JR (1999) Sentinel node detection and definition may depend on the imaging agent and timing. Clin Nucl Med 24:390–394
20. Taylor AT, Murray D, Herda S et al (1996) Dynamic lymphoscintigraphy to identify the sentinel and satellite nodes. Clin Nucl Med 21:755–758
21. Leijte JAP, Van der Ploeg IMC, Valdés Olmos RA et al (2009) Visualization of tumor-blockage and rerouting of lymphatic drainage in penile cancer patients using SPECT/CT. J Nucl Med 50:364–367
22. Liu LC, Parrett BM, Jenkins T et al (2011) Selective sentinel lymph node dissection for melanoma: importance of harvesting nodes with lower radioactive counts without the need for blue dye. Ann Surg Oncol 18:2919–2924
23. Jansen L (2000) Sentinel node biopsy: evolving from melanoma to breast cancer. [Thesis] University of Amsterdam, Amsterdam
24. Cox CE, Pendas S, Cox JM et al (1998) Guidelines for sentinel node biopsy and lymphatic mapping of patients with breast cancer. Ann Surg 227:645–651
25. De Vries J, Doting MHE, Jansen L et al (1999). Sentinel node localisation in breast cancer in two institutions. Eur J Nucl Med 26(Suppl):S67
26. Rutgers EJT, Jansen L, Nieweg OE et al (1998) Technique of sentinel node biopsy in breast cancer. Eur J Surg Oncol 24:316–319
27. Nieweg OE, Jansen L, Kroon BBR (1998) Technique of lymphatic mapping and sentinel node biopsy for melanoma. Eur J Surg Oncol 24:520–524
28. Kroon BK, Horenblas S, Lont AP et al (2005) Patients with penile carcinoma benefit from immediate resection of clinically occult lymph node metastases. J Urol 173:816–819
29. Morton DL, Thompson JF, Essner R et al (2006) Immediate versus delayed lymphadectomy in the management of primary melanoma. N Engl J Med 355:1307–1317

7 General Concepts on Radioguided Sentinel Lymph Node Biopsy: Preoperative Imaging, Intraoperative Gamma-Probe Guidance, Intraoperative Imaging, and Multimodality Imaging

Federica Orsini, Federica Guidoccio, Sergi Vidal-Sicart, Renato A. Valdés Olmos, and Giuliano Mariani

7.1 Introduction

Lymphoscintigraphy is an essential component for radioguided sentinel lymph node biopsy (SLNB), which is now routinely employed in clinical practice for treating patients with breast cancer [1] or melanoma [2]. SLNB is used to assess the tumoral involvement of lymph nodes not only for staging (parameter N of the TNM [tumor, node, metastases] system) and prognostic stratification, but also for therapeutic purposes [3]. This procedure is part of the so-called "radioguided surgery," a whole spectrum of nuclear medicine applications based on the combination of preoperative imaging, intraoperative detection, and postoperative techniques, involving close collaboration between at least three different specialties (nuclear medicine, surgery, pathology, and sometimes radiology and health physics as well) [4].

Originally introduced in the early 1990s, the sentinel lymph node (SLN) procedure optimizes the detection of occult lymph node metastases in patients without clinical evidence of local–regional involvement. The histopathology of the sentinel nodes(s) identified by the procedure, and resected, can distinguish macrometastases (>2 mm in size), micrometastases (between 0.2 mm and 2 mm), and submicrometastases (<0.2 mm), as specified in the 7th edition of the American Joint Committee on Cancer (AJCC) cancer staging manual [5]. This is possible because the pathologist is now able to focus on much fewer lymph nodes than those normally retrieved during conventional radical lymphadenectomy of a certain basin, so a more detailed histopathologic examination of the sentinel node(s) can be carried out, using more histologic sections (to encompass virtually the entire lymph node) and more sensitive techniques (immunohistochemistry in addition to hematoxylin and eosin staining, and even molecular analysis) [5].

Radioguided surgical procedures are generally less invasive and/or less aggressive than traditional surgical approaches. In the case of radioguided biopsy of the SLN, instead of a total lymphadenectomy (for example of the homolateral axilla in breast cancer), patients undergo surgical removal of only one (or a few) lymph node(s), thus reducing both immediate and long-term postsurgical complications, such as lymphedema, motor/sensory nerve damage, and functional impairment of the shoulder/arm. This novel surgical strategy is based on the hypothesis that lymphatic drainage to a regional lymph node basin follows an orderly, predictable pattern, and on the function of lymph nodes on a direct drainage pathway as effective filters for tumor cells. Consequently, all lymph nodes with direct drainage from the primary tumor are considered as sentinel nodes.

At present, SNLB is routinely performed in patients with breast cancer or melanoma, but this application is continuously expanding to other epithelial solid cancers. In fact, the presence or absence of metastasis in the SLN(s) has a significant impact on the therapeutic strategy for breast cancers and melanomas. In patients with early cancer, if the SLN does not contain metastasis, the surgical approach should aim to remove the primary tumor and avoid unnecessary regional node dissection. In fact, it is extremely unlikely that nonsentinel lymph nodes contain metastasis when the sentinel node is free from tumor cells; thus, extensive lymph node dissection is unnecessary in this circumstance. On the other hand, patients whose SLN contains metastasis usually require dissection of regional lymph nodes [6].

Imaging is made possible by interstitial administration at the tumor site of radiolabeled colloid particles that drain from the injection site through the lymphatic system, then selectively accumulate by phagocytosis into the macrophages of the SLNs, with consequent prolonged retention. Colloid

F. Orsini (✉)
Regional Center of Nuclear Medicine,
University of Pisa Medical School, Pisa, Italy
e-mail: federicaors@gmail.com

G. Mariani et al. (eds.), *Atlas of Lymphoscintigraphy and Sentinel Node Mapping*,
DOI 10.1007/978-88-470-2766-4_7 © Springer-Verlag Italia 2013

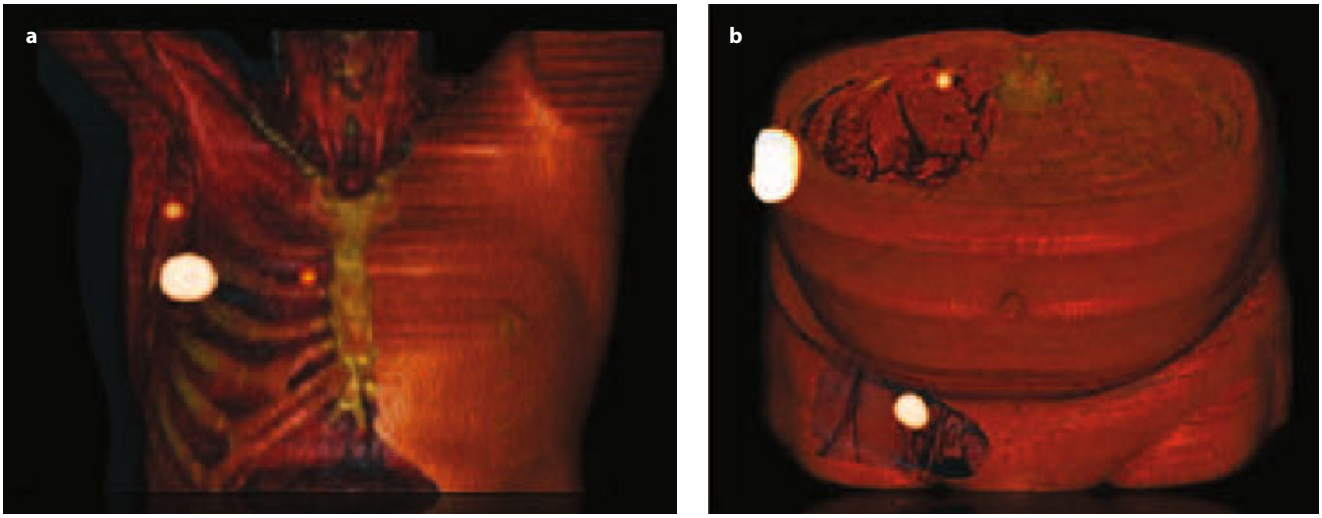

Fig. 7.1 Example of post-processing elaboration of SPECT/CT images. In both cases layers of the tegument have been focally "removed/canceled" asymmetrically between the two sides of the body so to show the underlying anatomy. **a** Lymphoscintigraphy for SLN mapping in a patient with breast cancer, clearly showing migration of ^{99m}Tc nanocolloid both to an axillary SLN and to an internal mammary chain sentinel node. **b** Lymphoscintigraphy for SLN mapping in a patient with melanoma at the right flank, clearly showing migration of ^{99m}Tc nanocolloid both to a sentinel lymph node in the right groin and to a sentinel node in the retroperitoneal area of the abdomen

particles labelled with technetium-99m (^{99m}Tc) are currently used for this purpose. The general term "colloid" indicates a class of macromolecules of micellar size varying in size between about 5 nm and 1000 nm (0.005–1 μm), with similar physicochemical and biological patterns. The speed of lymphatic drainage from the site of interstitial injection, and the amount retained in the SLN, depend mainly on the size of the radiocolloid used, which may be either an inorganic substance (gold-198 [^{198}Au] colloid, ^{99m}Tc–antimony sulfur, ^{99m}Tc–sulfur colloid, ^{99m}Tc–stannous fluoride, ^{99m}Tc–rhenium sulfur), or derived from biological substances (nano- or microcolloidal human serum albumin). Small-sized radiocolloids (smaller than about 100 nm) migrate quite quickly from the injection site through the lymphatic system, but they are not efficiently retained in the sentinel node. On the other hand, larger-sized radiocolloids are retained more efficiently in the SLN, but their migration from the interstitial administration site is slower.

^{99m}Tc–albumin-nanocolloid (which has a quite narrow range of particle size, with over 90% of the particles being smaller than 80 nm) is commercially available and most widely employed in Europe, while ^{99m}Tc-sulfur colloid (with a wide range of particle size between about 20 nm and 400 nm) is widely employed in the USA [7].

Lymphoscintigraphy, a mandatory preoperative step of the entire SLNB procedure, is normally performed with conventional gamma cameras. When the gamma camera is combined with a computed tomography (CT) component to constitute a hybrid SPECT/CT tomograph, the fused images obtained are highly useful, especially in the case of complex anatomical regions and/or unusual lymphatic drainage patterns (Fig. 7.1). In fact, they provide the surgeon with a morphologic and functional roadmap (CT component and SPECT component, respectively) for planning the procedure with minimal surgical access and operating time. For immediate decision-making during surgery, intraoperative exploration of the surgical field is performed with the widely validated procedure based on the so-called hand-held "gamma probe." While this instrumentation produces a numerical readout and an acoustic signal that is proportional to radioactivity accumulation, as a guide in the surgical field, the recently developed portable gamma cameras enable real-time scintigraphic imaging of the surgical field. All these instruments allow selective identification of the SLN(s) to be removed by the surgeon and analyzed by the pathologist. This interaction between technologies and medical disciplines permits continuous refinement of the methodology and improves the outcome of radioguided surgical procedures.

7.2 Preoperative Imaging

Lymphoscintigraphy is generally performed in the afternoon of the day preceding surgery if the operation is scheduled in the early morning, or on the same day 4–6 hours prior to surgery, depending on the logistics of the institution. For same-day procedures, a smaller activity of radiocolloid is generally administered (at least 15–20 MBq) compared to the two-day procedure (at least 37–74 MBq).

The gamma camera energy selection peak is centered on the 140 keV of ^{99m}Tc (with a window of ±10%), and the use of high-resolution collimator(s) and of a 256 × 256 acquisi-

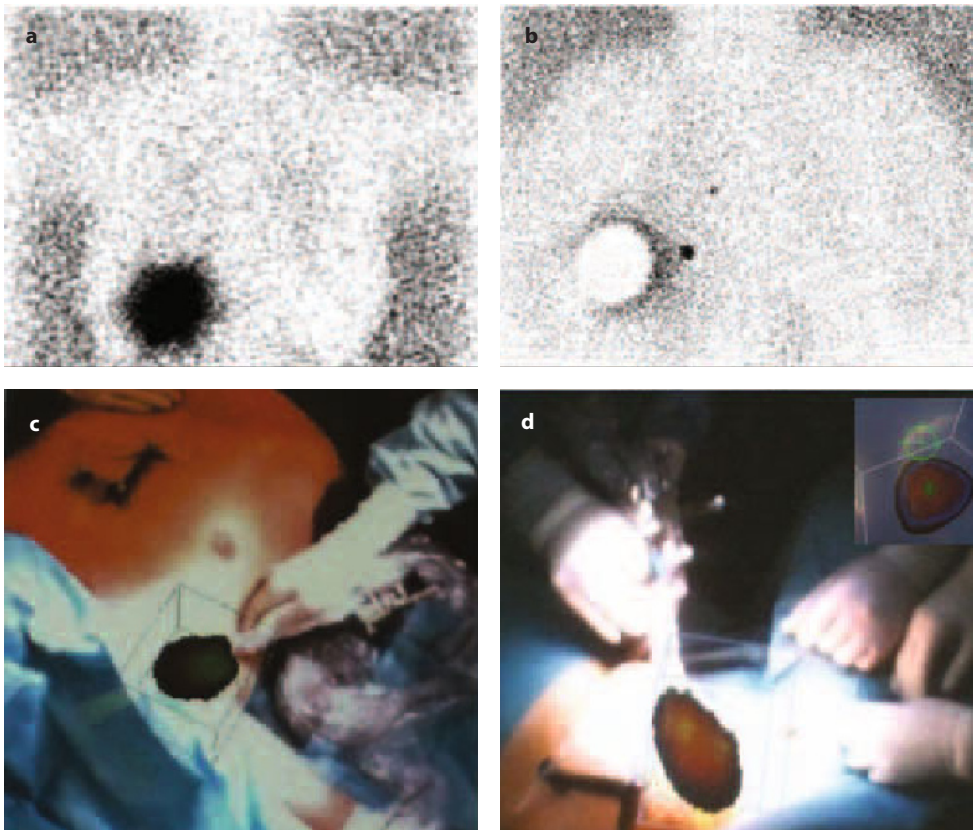

Fig. 7.2 *Upper panels* show planar scintigraphy (with flood phantom for body contour, see further below) obtained in a breast cancer patient about 2 hours after injecting ^{99m}Tc-nanocolloidal albumin intratumorally (**a**). Besides intense radioactivity remaining at the injection site, this image shows no migration of the radiocolloid to axillary SLNs. The *right image* (**b**) was taken 16 hours later, using a lead plate to cover the injection site. A hot spot is depicted in the close vicinity of injection, corresponding to an internal mammary chain SLN. The *lower panels* show overlay of the freehand SPECT 3D image on the intraoperative video image of the same patient, for easier anatomical correlation. **c** Scanning of the axilla without visualization of the lymph nodes. **d** Intraoperative visualization of the sentinel node in the right internal mammary chain (insert in the *upper right square*)

tion matrix is preferred; a pinhole collimator may occasionally be used to improve spatial resolution.

While dynamic acquisition is needed especially when rapid lymphatic drainage is anticipated (melanoma, head and neck, penile, testicular, and vulvar cancer), it can nevertheless also provide relevant information for identifying the actual SLN(s) (versus higher-echelon nodes) in other malignancies, particularly breast cancer. Concerning breast cancer in particular, the patient is positioned supine with her arms raised above the head, and the collimator is placed as close as possible to the axillary region. Anterior, anterior-oblique, and lateral images are acquired. A cobalt-57 (^{57}Co) flood source can be positioned between the patient's body and the collimator, in order to obtain some reference anatomic landmarks in the scintigraphic image (Figs. 7.2 and 7.3). Alternatively, the body contour can be identified by moving a ^{57}Co point source along the patient's body during scintigraphic acquisition (Fig. 7.4).

Besides identifying the SLNs, lymphoscintigraphy is also useful to identify an unusual lymph draining basin, as well as an internal mammary chain or even intramammary, interpectoral, or infraclavicular lymph nodes [8] (Fig. 7.5), or additional sentinel nodes in areas of deep lymphatic drainage such as the pelvis, abdomen or mediastinum. SPECT/CT imaging could be particularly important in these cases. The use of SPECT/CT acquisitions can be directly oriented to the anatomical localization of sentinel nodes, thus obviating the problem of identifying anatomic landmarks as a reference for topographic location of the SLN(s) [9–11].

An additional useful application of SPECT/CT is in cases where the SLN is not visualized on planar imaging. In this situation, only SPECT/CT imaging can allow sentinel node identification; in fact, due to the correction for tissue attenuation, SPECT/CT is usually more sensitive than planar images and may particularly be useful in obese patients (Fig. 7.6). Moreover, SPECT/CT may be necessary for the localization of sentinel nodes in areas with complex anatomy and a high number of lymph nodes (such as the head and neck).

However, SPECT/CT does not replace planar lymphoscintigraphy, but should rather be considered as a complementary imaging modality. In fact, contrary to SPECT/CT, planar lymphoscintigraphy allows the cutaneous projection of the SLN to be marked with a dermographic pen, in order to help the surgeon localize the site for the best surgical access. In current protocols, SPECT/CT is performed following delayed planar imaging (mostly 2–4 hours after radiocolloid administration). This sequence of acquisitions is helpful to clarify the role of both modalities. Planar dynamic acquisitions allow better visualization of the routes of lymphatic drainage. Dynamic acquisition usually consists of sets of a few minutes each (generally 1–5 minutes) or sequen-

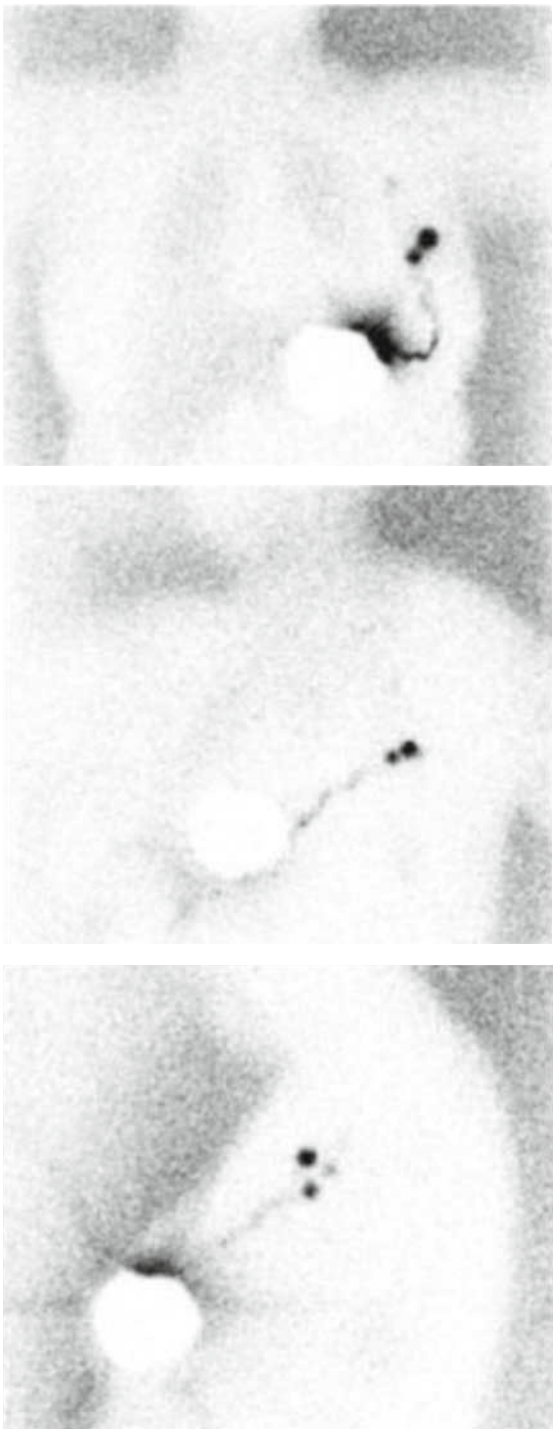

Fig. 7.3 Planar lymphoscintigraphy of a patient with breast cancer obtained between 20 minutes and 30 minutes after injecting about 111 MBq of ^{99m}Tc-nanocolloidal albumin peri-areolarly in a patient with cancer of the left breast. The *upper image* shows an anterior projection, the *central image* an oblique view and the *lower image* a lateral projection. Images were taken using a lead circle to cover the injection site. All images were acquired using a single-head gamma camera and a high-resolution, low-energy collimator (acquisition time 2 minutes). The ^{99m}Tc flood phantom placed opposite the gamma camera head produces the body contour delineation. While two axillary SLNs are visualized in the anterior and oblique projection, three nodes are visualized in the lateral projection

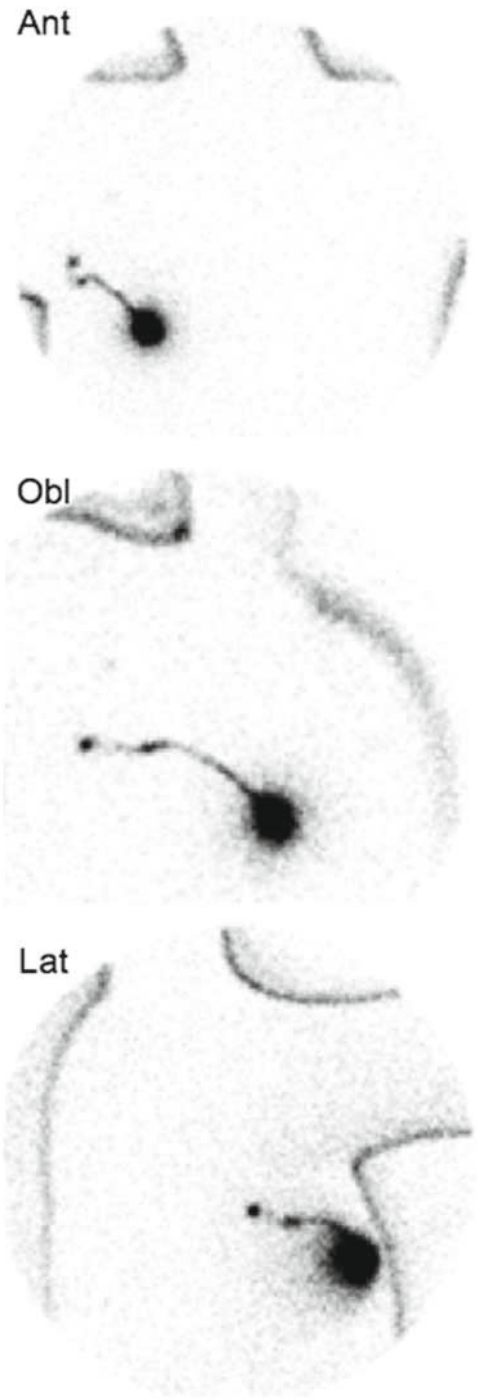

Fig. 7.4 Body contour delineation obtained by moving a ^{57}Co point source along body of the patient during acquisition of the planar scintigraphic images. In this patient with cancer of the right breast, ^{99m}Tc-nanocolloidal albumin was injected peri-areolarly. Images acquired in the anterior projection (*Ant*, upper panel), right anterior oblique projection (*Obl*, central panel), and right lateral view (*Lat*, lower panel) visualize migration of the radiocolloid through a lymphatic channel to a single SLN in the axilla

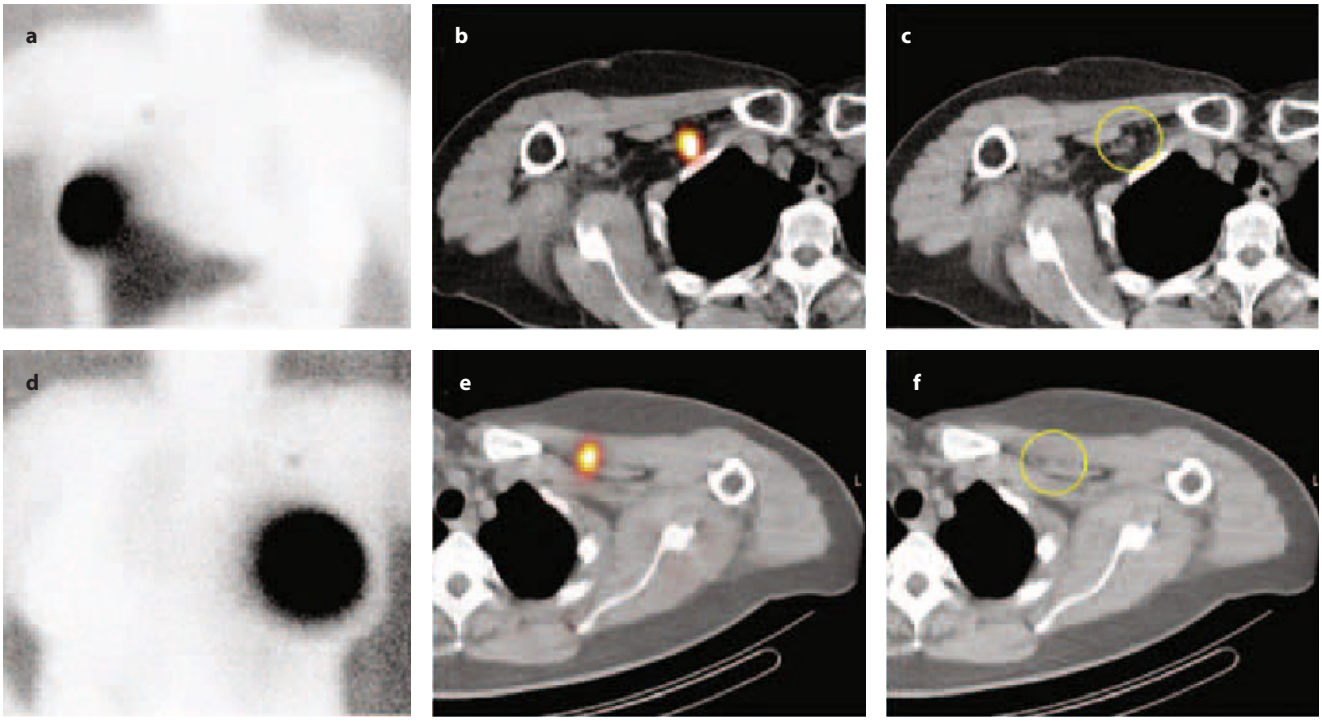

Fig. 7.5 Added value of SPECT/CT imaging in two different patients in whom planar scintigraphy shows focal uptake in the retroclavicular area; the patients had cancer located in the right breast (**a**) and in the left breast (**d**), respectively. **b**, **e** Fused axial SPECT/CT sections, showing the location of the two SLNs between the pectoral muscles. These sentinel nodes correspond to two single lymph nodes in the CT images (**c**, **f**, *yellow circle*), respectively

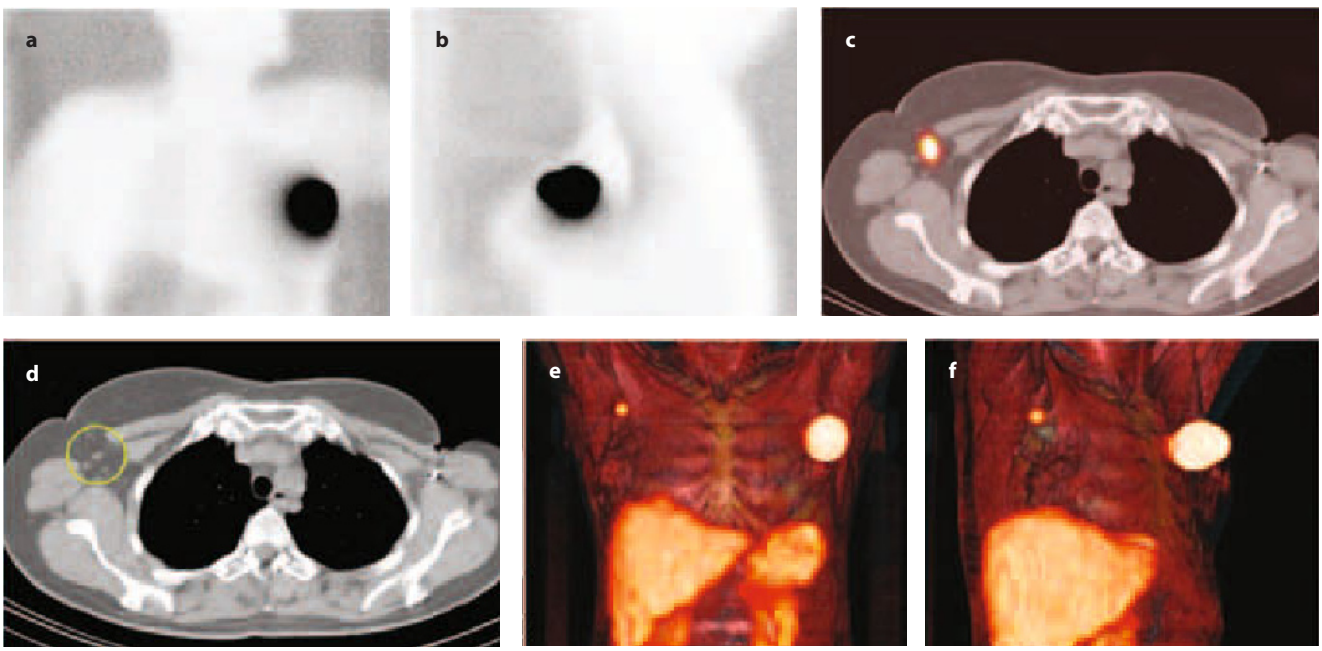

Fig. 7.6 Example of lymphatic drainage to the contralateral axilla in a patient with breast cancer. Anterior (**a**) and left lateral (**b**) planar images show no drainage from the site of intratumoral radiocolloid injection in the left breast (body contour obtained with a flood source placed beneath the patient's body). By contrast, on the fused axial SPECT/CT image, a SLN is clearly visualized at the border of the right pectoral muscle (**c**), corresponding to a single lymph node on the CT image (**d**, *yellow circle*). This SLN is displayed using 3D volume rendering for a better anatomical recognition in the anterior (**e**) and right anterior-oblique views (**f**)

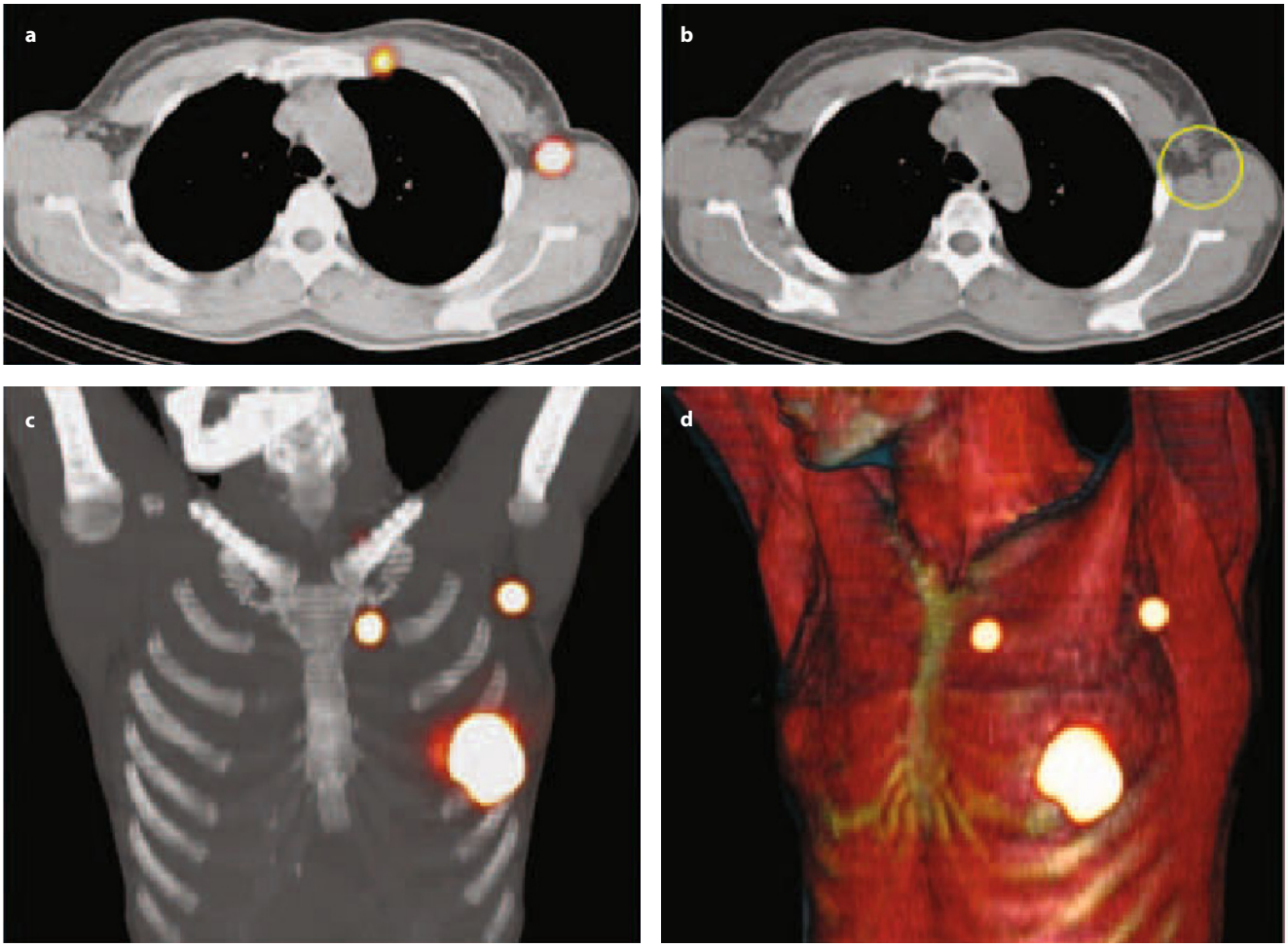

Fig. 7.7 Patient with breast cancer. **a** Fused axial SPECT/CT section obtained during lymphoscintigraphy, showing two SLNs, respectively in the left internal mammary chain and in the left axilla. **b** The *yellow circle* corresponds to a small lymph node seen on axial CT. **c** Fused coronal SPECT/CT displayed as a maximum intensity projection, showing a SLN in the left axilla and an internal mammary chain sentinel node in the second left intercostal space. **d** SPECT/CT with volume rendering for 3D display, showing the two SLNs, respectively in the left internal mammary chain and in the left axilla, with their anatomic localizations with reference to muscles and bones

tial sets of static images in the preset count mode (generally 300,000–500,000 counts) acquired starting immediately after radiocolloid injection until there is clear scintigraphic visualization of the lymphatic routes and SLN(s).

Multiplanar reconstruction (MPR) enables two-dimensional display of fusion images in relation to CT and SPECT, with the use of cross-reference lines allowing navigation between axial, coronal, and sagittal views. At the same time, this tool enables correlation of the radioactive sentinel nodes seen on fused SPECT/CT with the lymph nodes seen on CT (Fig. 7.7a, b). This information may be helpful during the intraoperative procedure, as well as for assessing the completeness of excision using portable gamma cameras or probes.

Fused SPECT/CT images may also be displayed using maximum intensity projection (MIP). This tool enables three-dimensional (3D) display, and improves anatomical localization of SLNs by adding various slices (Fig. 7.7c).

When using volume rendering for 3D display, different colors are assigned to anatomical structures such as muscle, bone, and skin. This facilitates better identification of anatomical reference points and incorporates an additional dimension in the recognition of SLNs (Fig. 7.7d).

7.3 Intraoperative Gamma-probe Guidance

The so-called gamma probe is used to count radioactivity in the surgical field intraoperatively, without producing any

scintigraphic image but yielding both a numerical readout and an audible signal that is proportional to the counting rate.

The detector is usually of limited size, basically a long narrow cylinder with a diameter of 12–18 mm, sometimes slightly angled in order to allow easier handling within the surgical field. The gamma probe can be utilized in the surgical field because it is made of a material that can be sterilized (usually metal), or it can simply be covered with a sterilized wrapping (such as those used for intraoperative ultrasound probes). Through the digital readout and acoustic signal, the gamma probe enables the surgeon to precisely localize areas of maximum radioactivity accumulation, thus guiding identification and removal of the target tissue [12–15].

The commercially available gamma probes can be divided into crystal scintillation and semiconductor probes. Further technical features of the probe vary, depending upon whether the radiopharmaceuticals are labeled with ^{99m}Tc or other radionuclides, including positron-emitting radiopharmaceuticals [16–18].

The probe is connected to a small control unit, equipped with a portable laptop or tablet, usually with a flexible cable that may also be covered with sterilized wrapping; nevertheless, bluetooth-like connections have now become available, permitting easy use of the entire instrument in the operating room. The energy window for detection/counting is usually around 140 Kev (for ^{99m}Tc-labeled radiopharmaceuticals), but can vary depending on the radionuclide employed. At the same time, the unit usually emits an audible signal, the pitch/tone of which varies proportionally to the counting rates. The acoustic signal helps the surgeon to explore the surgical field without looking at the control unit display.

The sensitivity (counting rate per unit of radioactivity), energy resolution (ability to detect "true" counts arising in the target versus secondary scattered radiation), spatial resolution (ability to identify very close radioactive sources as distinct from each other), and linearity of counting (relates to the dead time) are the most important parameters of the probe in detecting radiation. Therefore, the main important tasks of a probe include sufficient sensitivity (to identify a weakly active sentinel node when attenuated by, typically, up to 5 cm of soft tissue) and energy and spatial resolution (to discriminate the activity of a certain energy within the SLN from that originating from other sites).

More recently, with the development of positron emission tomography (PET) techniques, intraoperative probes specifically designed to detect the high-energy gamma rays originating from the annihilation process have become commercially available, thus enabling radioguidance for PET radiopharmaceuticals [19, 20].

Nevertheless, major advances in the whole process of SLN mapping, in both the preoperative and the intraoperative phases, have been made possible by the use of SPECT/CT and/or intraoperative imaging probes. In fact, hybrid imaging with SPECT/CT supplies the surgeon with anatomotopographic information that guides resection through the optimal surgical access according to the principle of least invasive surgery [21, 22].

As exemplified in Fig. 7.8, this approach is especially useful when planning surgery in complex anatomical regions such as the head and neck or the pelvis [23–29].

Just before starting surgery, and with the patient already positioned on the operating table, the gamma probe is initially utilized to scan the sentinel lymph nodal basin(s) and/or any other region where radiocolloid accumulation has been visualized, in order to confirm correct identification of the SLN(s). Using the images and skin markings as guides, the probe (placed over the regions of highest counts) can be used to select the optimum location for incision. After incision, the probe is then introduced through the surgical field to explore the expected localization of the sentinel nodes, which are usually easily identified by acoustic signal on the basis of high target/background count rates. After removing the lymph nodes, the operative field is explored again with the probe, assessing residual radioactivity to confirm removal of the hot node(s). If necessary, the search must continue for possible further radioactive lymph nodes. The SLN and any other nodes so identified are then sent for complete histopathologic analysis.

Counts are recorded per unit time with the probe in the operative field, over the node, before excision (in vivo) and after excision (ex vivo). A background tissue count is also recorded with the probe pointing away from the injection site, nodal activity, or other physiologic accumulations (i.e., liver) [30].

In breast cancer, once the learning phase of SLNB has been completed, the success rate of lymphoscintigraphy and intraoperative gamma-probe counting in identifying SLN(s) is higher than 96–97% in experienced centers. This value is greater than that commonly experienced using blue dye alone (75–80%), while combining radioguidance with the blue dye leads to a 98–99% success rate in SLN identification [31]. Blue dye can be injected around the primary tumor or scar (in a similar way to how the radiocolloid was injected) 10–20 minutes prior to the operation. Administration should be performed after the patient is anaesthetized, to avoid a painful injection. Within 5–15 minutes, the SLN is colored. Currently, the most commonly used dyes are patent blue V, isosulfan blue, and methylene blue. The additional value of dyes may be observed in cases with macrometastasis in the SLN. In fact, such SLN involvement may inhibit radiocolloid accumulation, if tumor cells have replaced most of the normal lymph node tissue [32]. In these cases a new first draining node is seen (Fig. 7.9) [33]. A notable disadvantage of using blue dyes instead of radiotracers is that blue dyes are not helpful if extra-axillary nodes (internal mammary or supraclavicular) are to be evaluated [34, 35].

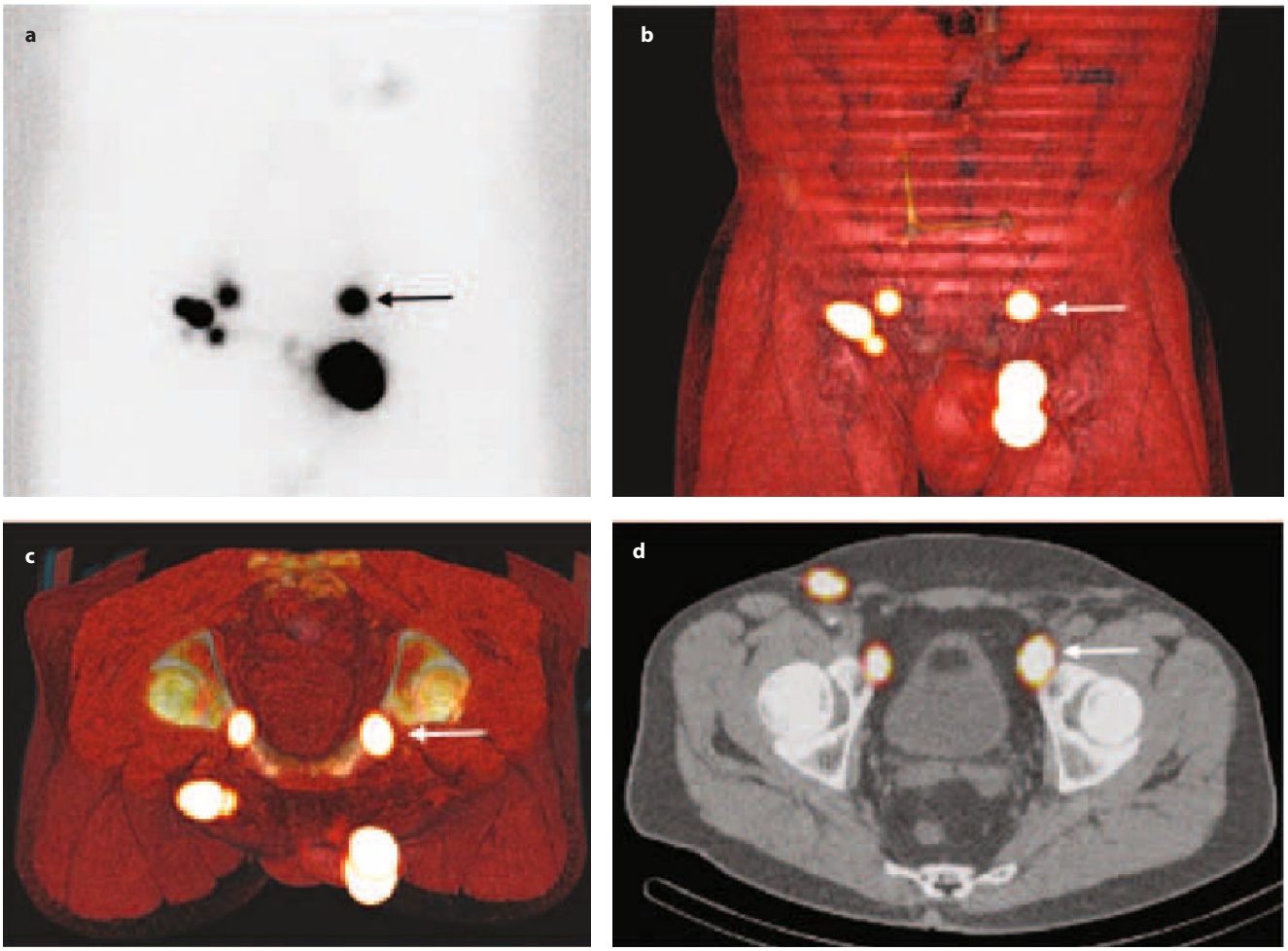

Fig. 7.8 Lymphoscintigraphy in a patient with penile cancer, where the different panels correspond to different modalities of representation and the arrow indicates the same SLN on the left side, correctly assigned to a specific topographic location on the basis of tridimensional imaging. **a** Planar anterior image showing lymphatic drainage to both sides, seemingly to groin lymph nodes (single SLN on the left, *arrow*). **b** SPECT/CT with volume rendering for 3D display in the anterior view (again to seemingly groin SLNs; the *arrow* points to the same SLN indicated in panel **a**). **c** SPECT/CT with volume rendering for 3D display in a cranial view (the bottom side corresponds to the anterior side of the body) showing bilateral external iliac SLNs (the *arrow* indicates the SLN now correctly classified as external iliac SLN). **d** Fused axial SPECT/CT section showing anatomic location of three of the lymph nodes (two on the right and one on the left) at different depths in the pelvis (the *arrow* indicates the left external iliac SLN)

7.4 Intraoperative and Multimodality Imaging

Currently, the trend of surgery is towards adopting minimally invasive approaches for a growing spectrum of procedures. This includes oncological surgery, as it implies much faster post-surgical recovery of patients. For optimally planning and performing these approaches, the most crucial issue is accurate preoperative characterization of the surgical procedure, which is achieved through diagnostic imaging. In this regard, maximum benefit for the success of minimally invasive surgery derives from integration of anatomical (e.g., CT) and metabolic/functional imaging, the latter being typically provided by nuclear medicine procedures. These features contribute to a better characterization of the lesion to be removed, and in many cases enable subsequent intraoperative guidance through the use of devices particularly designed for this use [36, 37].

During the last decade, intraoperative imaging probes have become commercially available for clinical practice, and the use of such hand-held portable gamma cameras is now increasing. By providing real-time imaging with a global overview of all radioactive hot spots in the whole surgical field [38], intraoperative imaging with portable gamma cameras can be used during either open surgery or laparoscopic procedures; the information so gained can be combined with data obtained with conventional or laparoscopic gamma-probe counting [39, 40].

There are several recent reports on the use of portable

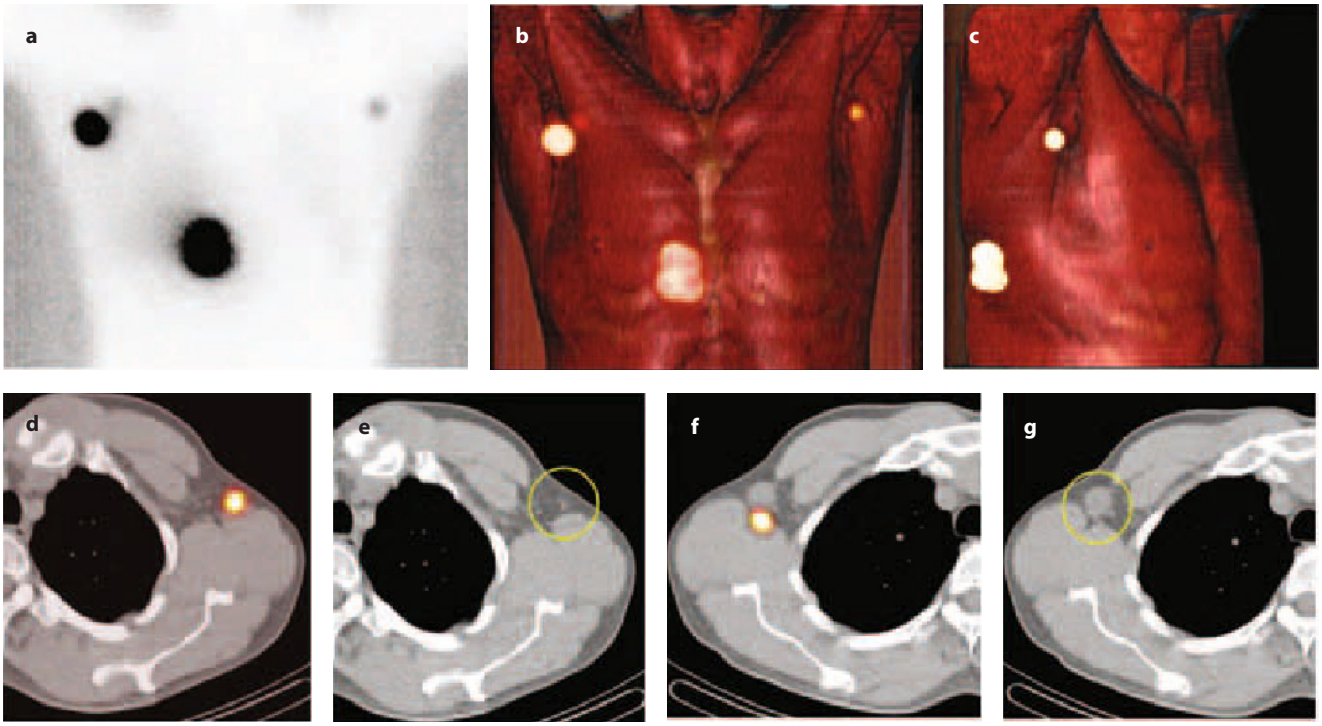

Fig. 7.9 Patient with melanoma located in the back of the right torso. **a** Planar anterior view showing lymphatic drainage to both axillae, as better demonstrated by SPECT/CT with volume rendering for 3D display, respectively in the anterior and in the right oblique view (**b** and **c**). **d–g** Fused axial SPECT/CT section at two different levels, showing the location of radioactive lymph nodes, in the left axilla (**d**) and right axilla (**f**). The corresponding CT sections show that the hot lymph node in the left axilla corresponds to a normal-sized node (*yellow circle* in **e**), while in the right axilla the hot lymph node (of approximately normal size) is located posterior to a grossly enlarged, most likely metastatic, lymph node not visualized by lymphscintigraphy (*yellow circle* in **g**)

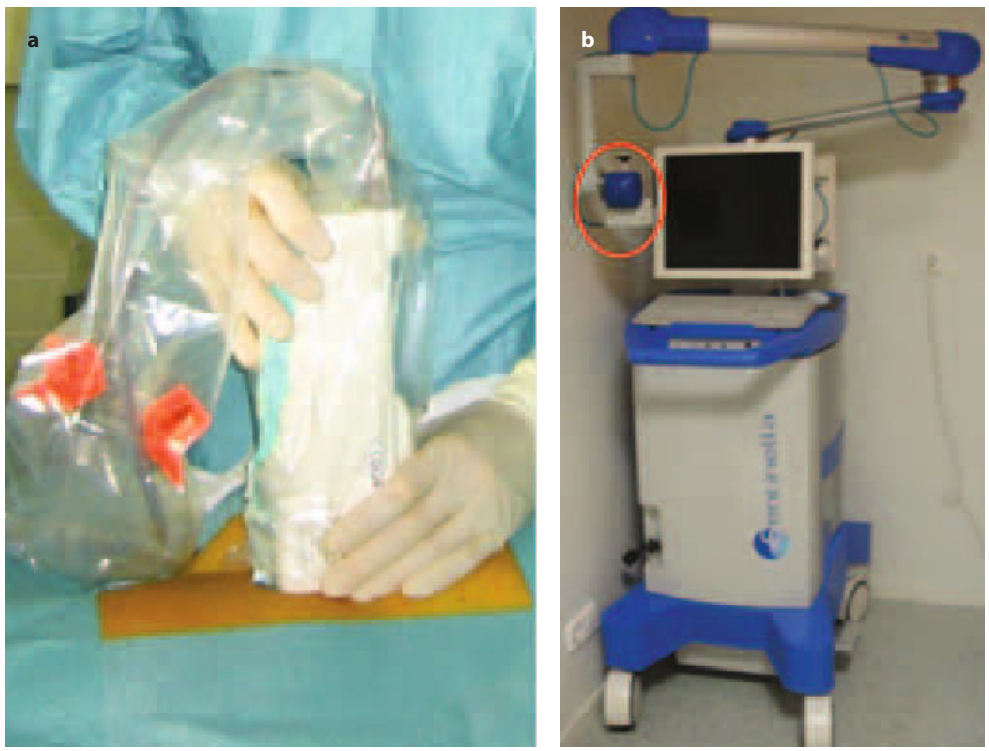

Fig. 7.10 Examples of portable gamma cameras. **a** light-weight portable gamma camera (less than 1 kg), without support system. **b** latest-generation portable gamma camera with improved ergonometry and adequate and stable support system for intraoperative use; this unit incorporates a laser pointer to center the image and adjust the scanning procedure

gamma cameras in clinical and experimental settings. These devices play a remarkable role in the incorporation of imaging during surgery and can be combined with the information obtained preoperatively by lymphoscintigraphy or SPECT/CT. Using the anatomic landmarks of SPECT/CT, the portable device can be oriented to surgical targets in the operating room [41]. There is no delay between image acquisition and display (real-time imaging), with the possibility of continuous monitoring and spatial orientation on the screen. Real-time quantification of the count rates recorded should also be displayed.

The development of such cameras is shown in Fig. 7.10. While the first devices were heavy hand-held devices, the new generation of such equipment includes portable gamma cameras that are lighter, or equipped with stable support systems.

Among the products commercially available, one of the most used devices is equipped with a CsI(Na) (cesium iodide doped with sodium) continuous scintillating crystal and different collimators (pinhole collimators, 2.5 mm and 4 mm in diameter, and divergent). The pinhole collimator can enable visualization of the whole surgical field (depending on the distance between the camera and the source). The field of view varies between 4 × 4 cm at 3 cm from the source and 20 × 20 cm at 15 cm from the source. This device has been integrated in a mobile and an ergonomic support that is easily adjustable. The imaging head is located on one arm that allows optimal positioning on the specific area to be explored.

Another approach is based on the use of cadmium zinc telluride (CdZnTe) as the radiation detector. For instance, the detector is made of a single tile of CdZnTe, patterned in an array of 16 × 16 pixels at a pitch of 2 mm. The head is equipped with a series of interchangeable parallel-hole collimators to achieve different performances in terms of spatial resolution and/or sensitivity. The field of view is 3.2 × 3.2 cm and the weight is 800 g [42].

A further development is represented by an intraoperative gamma camera that is still based on the CdZnTe pixel technology, and has originally been developed for breast imaging. The field of view is 13 × 13 cm and the intrinsic spatial resolution is 2 mm. This camera is also equipped with interchangeable parallel-hole collimators and is integrated in a workstand articulated arm.

However, since nonimaging probes are still the standard equipment for detection of radiolabeled tissue in the operating room, the role of intraoperative imaging is generally limited, at least so far, to constituting an additional aid to the surgeon for identification of the SLN. Some authors have tried to assess the added value of portable gamma cameras in clinical practice. Their usefulness in patients with breast cancer is being established in the following conditions: (a) when no conventional gamma camera is available; (b) in particular cases with difficult drainage or extra-axillary drainage (intrammamary and internal mammary chain nodes) [43]; (c) in cases of only faint lymph nodal radiocolloid uptake; (d) when the SLN is located very close to the injection site; or (e) in cases of significant photon emission and scatter from the injection site. In fact, the position of the portable gamma camera can be changed and adjusted in such a manner as to acquire special-angle views, so that sentinel nodes near the injection area can also be shown.

Moreover, some studies have reported detection of SLNs that had been missed when only the gamma probe was used. In fact, using an intraoperative imaging device implies the possibility of monitoring the lymphatic basin before and after removal of the hot nodes, in order to verify the completeness of lymph node excision [44] (Fig. 7.11). After excision of each lymph node, a new image is acquired and compared with the image acquired before excision (Fig. 7.12). If focal radioactivity remains at the same location, it is concluded that another possible SLN is still in place. Thus, the use of a portable gamma camera in addition to the gamma probe appears valuable in providing certainty about whether the sentinel nodes have been adequately removed (Fig. 7.13). Removing extra nodes that probably receive direct lymph drainage from the tumor should be weighed up against the fact that the surgical time is prolonged. However, even if additional time is needed, this extra time may be sufficiently useful in the context of sentinel node procedures that are likely to be difficult, since the use of the gamma camera might reduce the possibility of missing a malignant sentinel node [45, 46].

Discrimination between the true SLN and a second-tier radioactive node is based on the radioactive counts simultaneously recorded with the portable, small-field-of-view cameras, and can be related to the preoperative scintigraphic images. Although the majority of these cases can be solved with the presurgical information provided by SPECT/CT, real-time images acquired with a portable gamma camera enhance the reliability of using the gamma probe, by adding a clear image of surgical fields [47], and could represent an alternative to hybrid imaging.

In the operating room, the gamma camera can be placed above the previously marked sentinel node locations using some external point sources (such as barium-133 [^{133}Ba], gadolinium-153 [^{153}Gd] or iodine-125 [^{125}I]); alternatively, in some gamma cameras a laser pointer is fitted to the device. In those devices where a laser pointer is included (Sentinella; Oncovision), it is displayed as a red cross over the patient's skin. The position of this red cross is visible on the equipment's computer screen.

During surgery, an initial 30–60-second image is acquired with the gamma camera, to assess the surgical field and validate sentinel node uptake. This time can be longer when the lymph nodes are depicted as areas with faint focal uptake. After incision, if there is any difficulty in finding

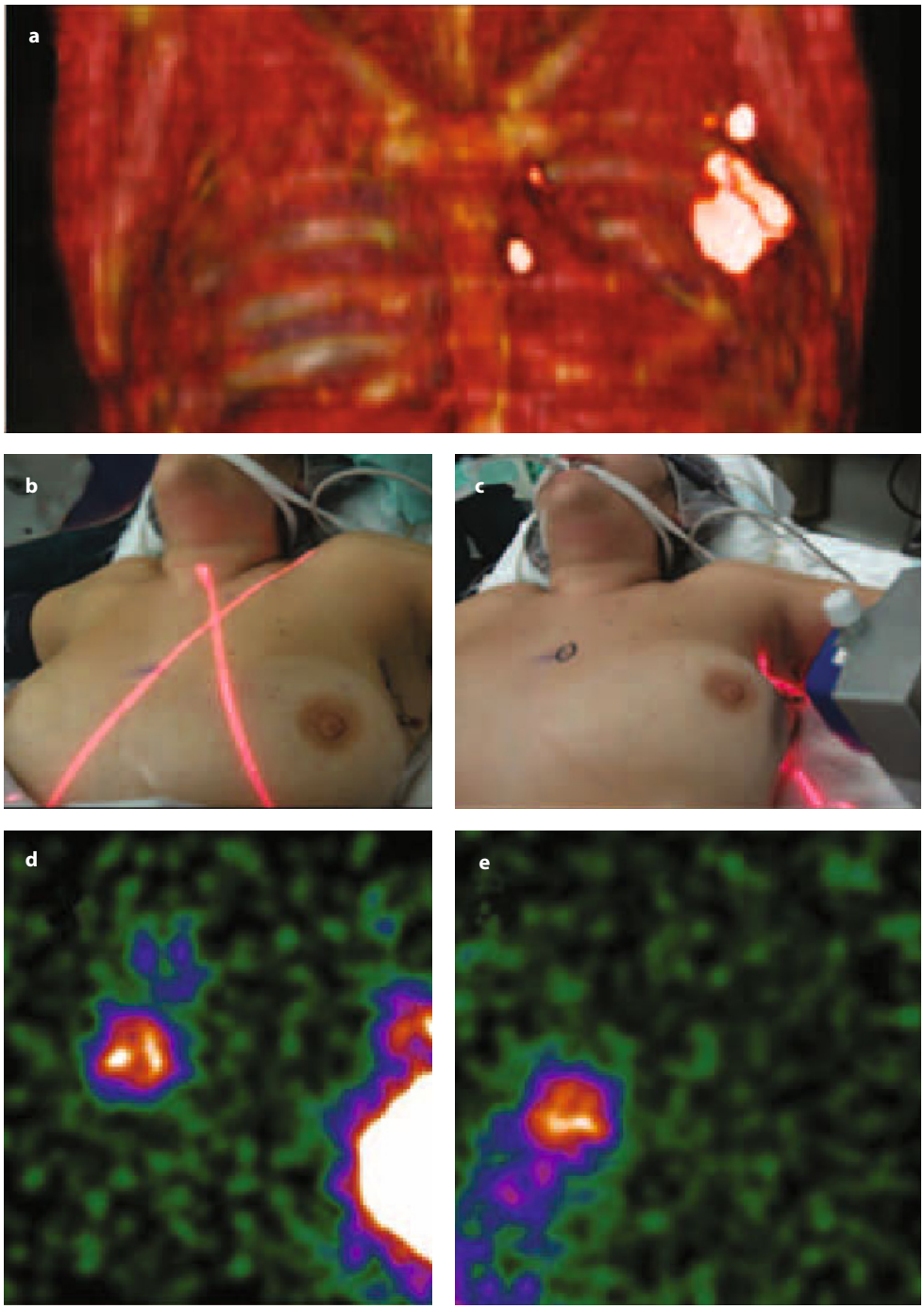

Fig. 7.11 Preoperative images in a 42-year old patient with a T1 cancer in her left breast. **a** 3D reconstruction image after processing SPECT/CT data. **b** A scintigraphic anterior view is acquired by placing the portable gamma camera in previously marked points on the skin (inner mammary chain, see laser cross-pointers). **c** The portable gamma camera can be placed in different positions to better depict the lymph nodes; in this picture it is tilted in an oblique view. **d** Visualization of an inner mammary chain lymph node, with partial vision of the injection site (image corresponding to position of the gamma camera as in **b**). **e** Visualization of an axillary lymph node depicted with the gamma camera positioned as in **c**

the precise location of the sentinel node using the gamma probe, another 30–120-second image, depending on the level of lymph node uptake, is acquired using the portable gamma camera.

The use of the external point sources facilitates SLN localization, as these sources can be depicted separately on the screen of the portable gamma camera, thus functioning as a pointer in the search for the nodes. The matching of two signals (^{99m}Tc signal and ^{153}Gd, ^{133}Ba, or ^{125}I pointer signals) indicates the correct location of the sentinel nodes. This location is then checked using the gamma probe. After sentinel node retrieval, another set of images is acquired to ascertain the absence of the previously visualized sentinel nodes, or to ascertain the presence of remaining nodes (additional sentinel nodes or second-tier nodes [Fig. 7.14]).

Thanks to novel technological possibilities, combining a spatial localization system and two tracking targets to be fixed on a conventional hand-held gamma probe results in

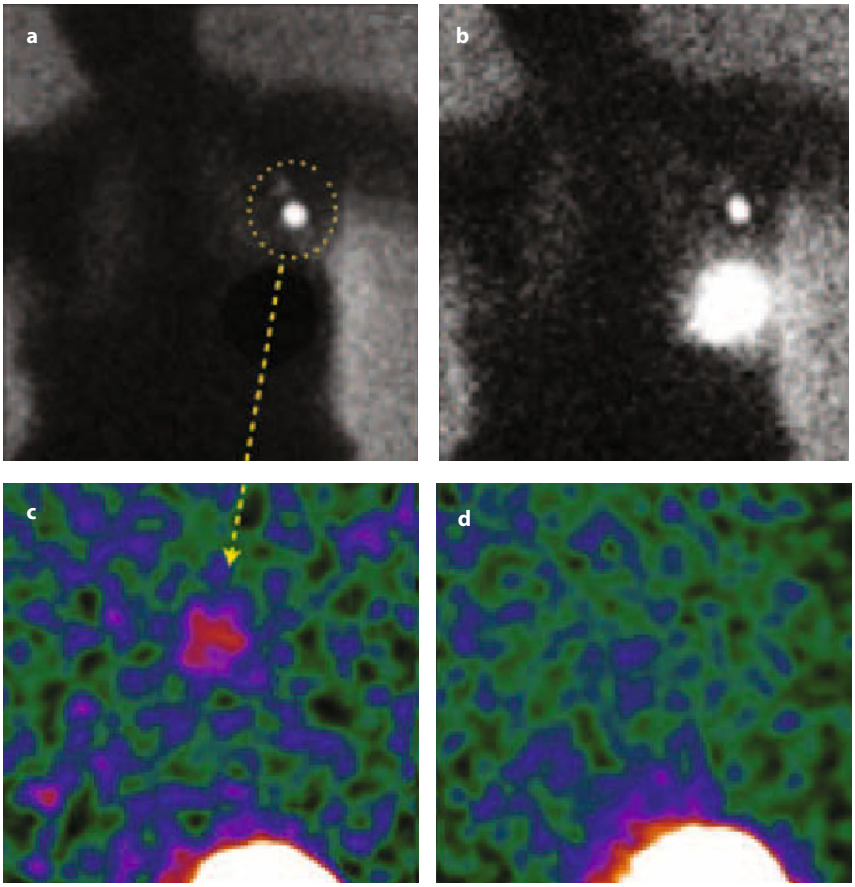

Fig. 7.12 A 57-year-old patient with breast cancer in her left upper outer quadrant. **a** Lymphoscintigraphic image acquired with a conventional, large-field-of-view gamma camera 2 hours after intratumoral injection of 111 MBq of ^{99m}Tc-nanocolloid; at least one axillary SLN is clearly depicted (*yellow circle*). **b** The same image without lead shielding of the injection site shows similar radiocolloid distribution. **c** Operating room image obtained with a portable gamma camera prior to starting the SLN procedure, confirming similar findings (*yellow arrow*). **d** Image obtained with the portable gamma camera after completing radioguided SLN excision, showing no residual activity except in the intratumoral injection site. The use of the portable gamma camera, in addition to the hand-held, nonimaging gamma probe, was especially useful to confirm the completeness of SLN removal

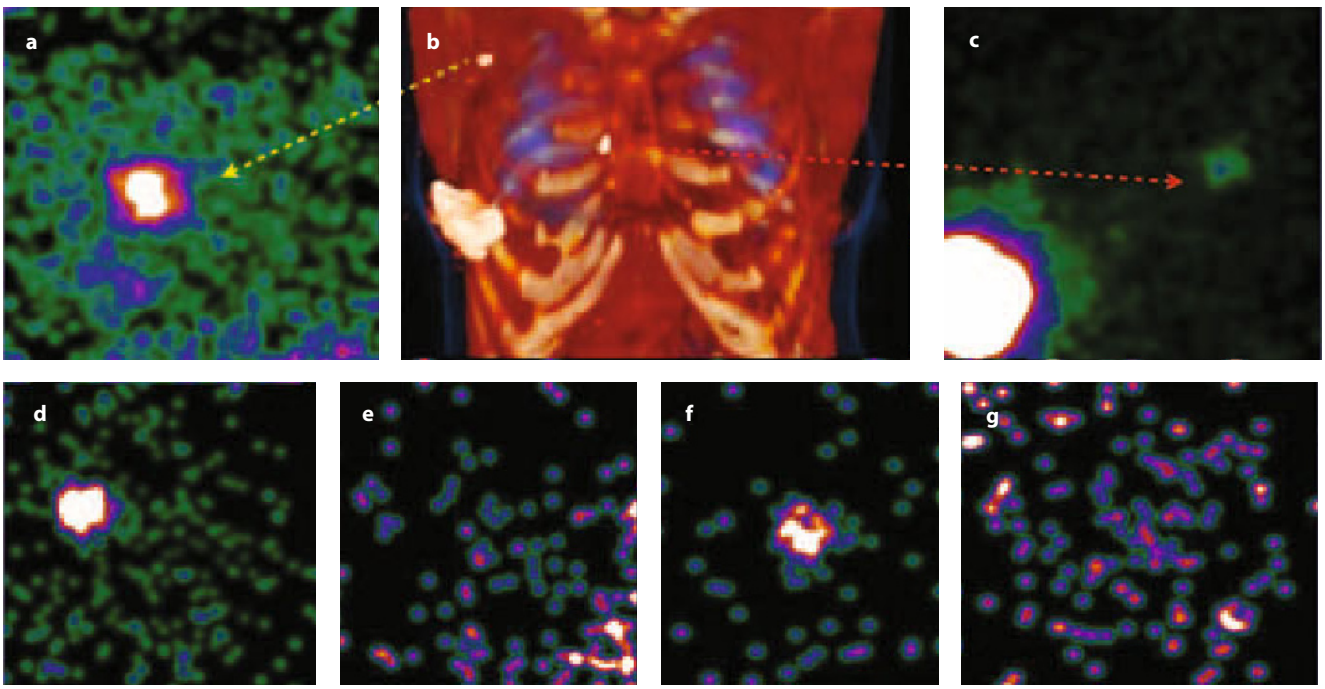

Fig. 7.13 Utility of the portable gamma camera during surgery for the certainty of SLN resection. **a** Radiotracer uptake displayed on gamma camera, corresponding to the node depicted in the axillary area (*yellow arrow*) on the 3D volume rendering reconstruction of a breast cancer patient with lymphatic drainage to the axilla and inner mammary chain (**b**). **c** A parasternal sentinel node (*red arrow*) is also depicted with the gamma camera. **d** Preoperative image of the axilla showing a highly active sentinel node. **e** Image after axillary node retrieval informs about the absence of other significant tracer uptake. **f**, **g** A similar approach in the internal mammary chain sentinel node

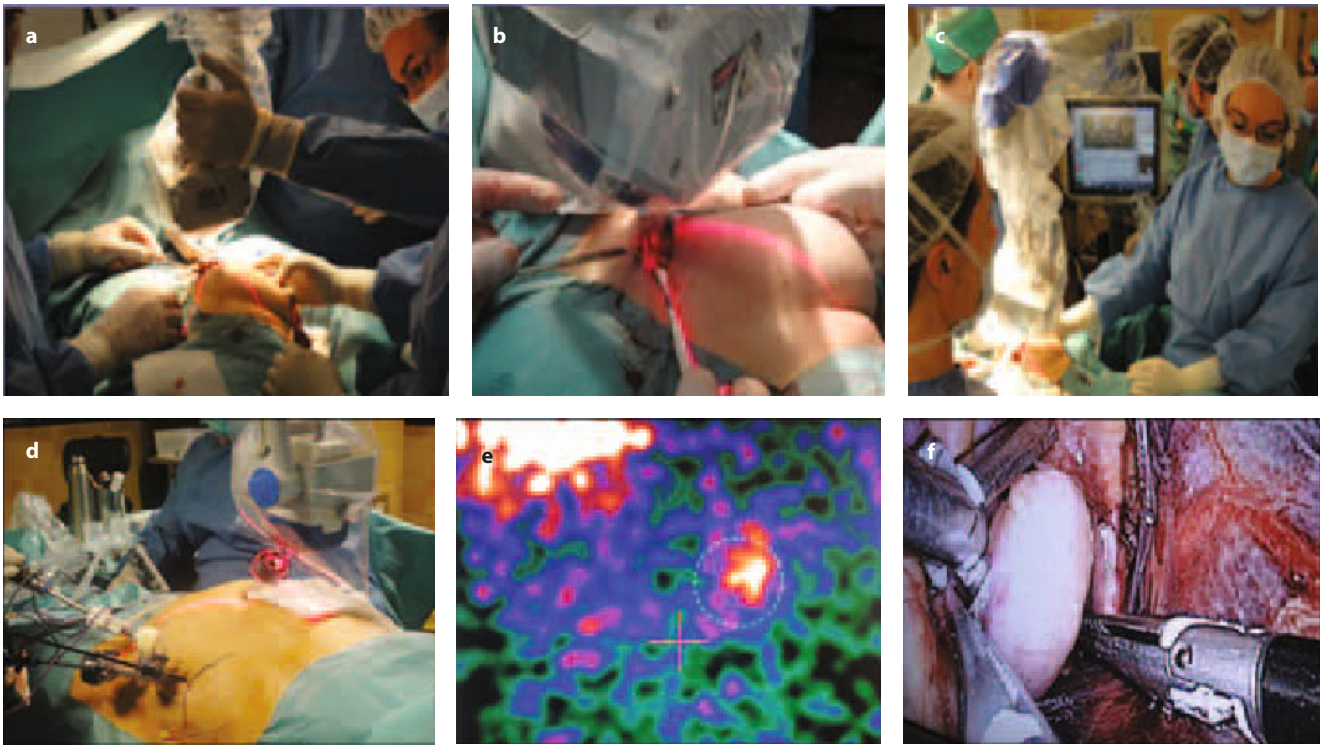

Fig 7.14 Portable gamma camera intraoperative approach. **a** The device is placed over the area of interest in the most convenient way. **b** A red cross shows the central position of image on the gamma camera's screen. **c** This feature allows a better understanding and awareness of the potential sentinel nodes on the surgical field. **d–f** Laparoscopic approach. **d** The portable gamma camera is positioned over abdominal wall to continuously assess the tracer uptake. **e** Usual uptake in a sentinel node close to the common iliac vein (*green circle*). **f** This node was clearly located in that area and subsequently removed

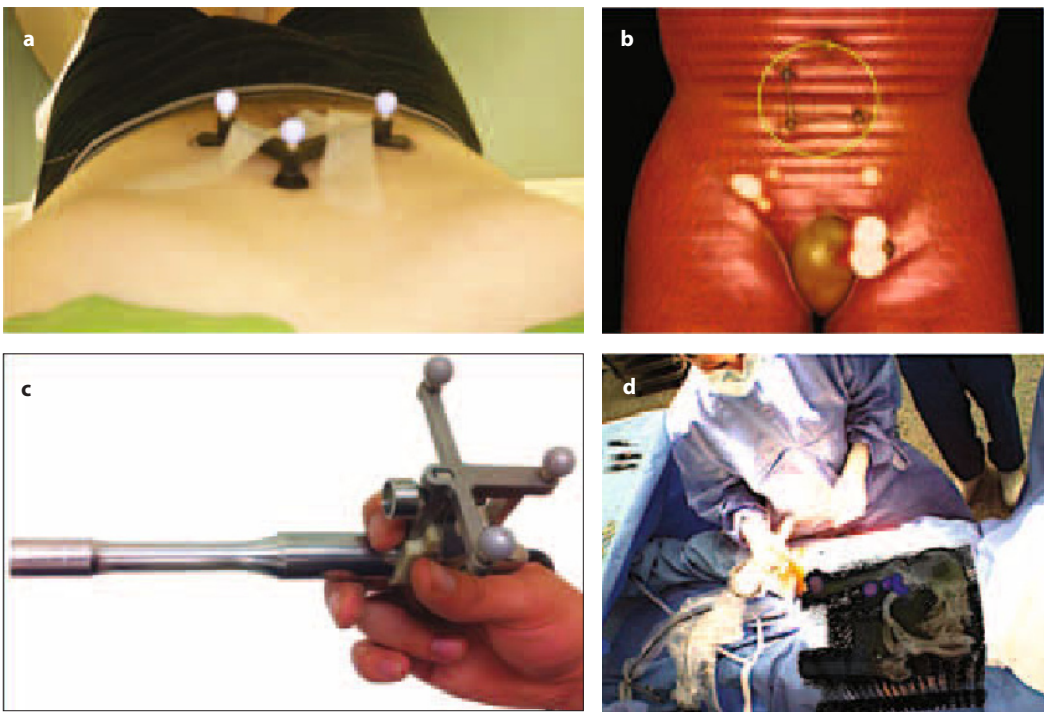

Fig. 7.15 Patient with penile cancer (same patient as in Fig. 7.8). **a** Positioning of the tracking device on the patient's body for radioguided SLNB. **b** 3D volume rendering SPECT/CT, showing the pattern of lymphatic drainage (the approximate position of the tracking device on the patient's body is also indicated in the *yellow circle*). **c** Tracking device attached to a gamma probe in order to generate freehand SPECT data. **d** By integrating preoperative SPECT/CT data, it is possible to overlay the generated 3D image to the patient's body, with simultaneous display of the SLNs on the right side of the pelvis

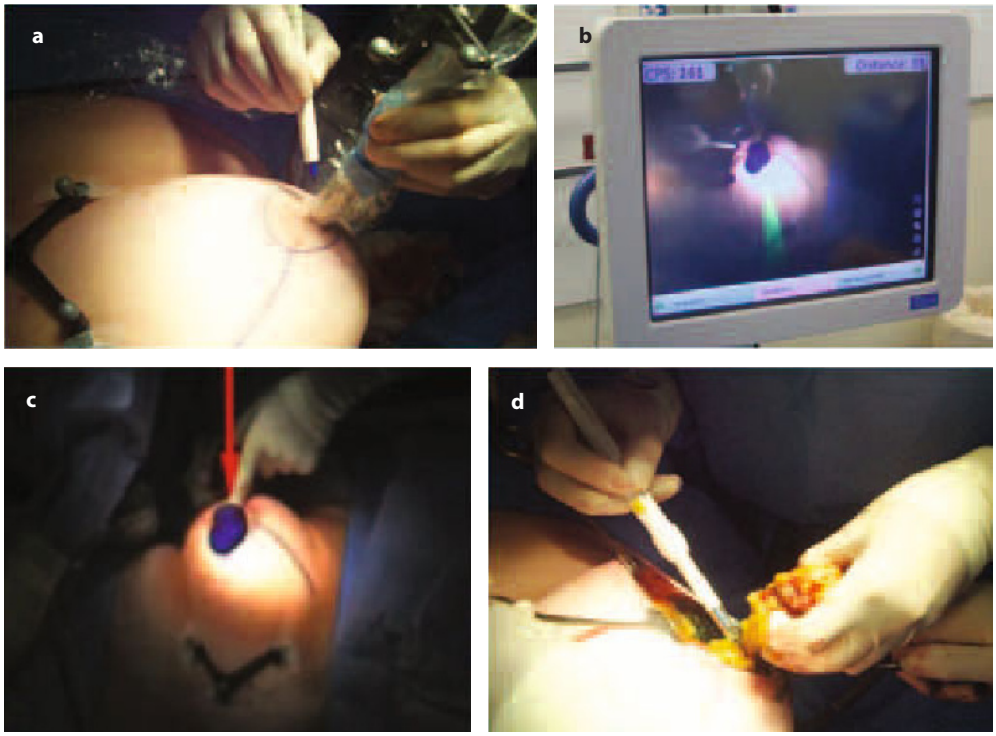

Fig. 7.16 Freehand SPECT-based device system used for radioguided occult lesion localization (ROLL) in a patient with nonpalpable breast cancer. **a** Surgical approach for ROLL; the tracking device positioned on the patient's body is visible on the left. **b**, **c** Overlay of freehand SPECT 3D images on the video displays, with the red arrow in **c** indicating the site of the tumor. **d** Completion of lumpectomy guided by the freehand SPECT-based system

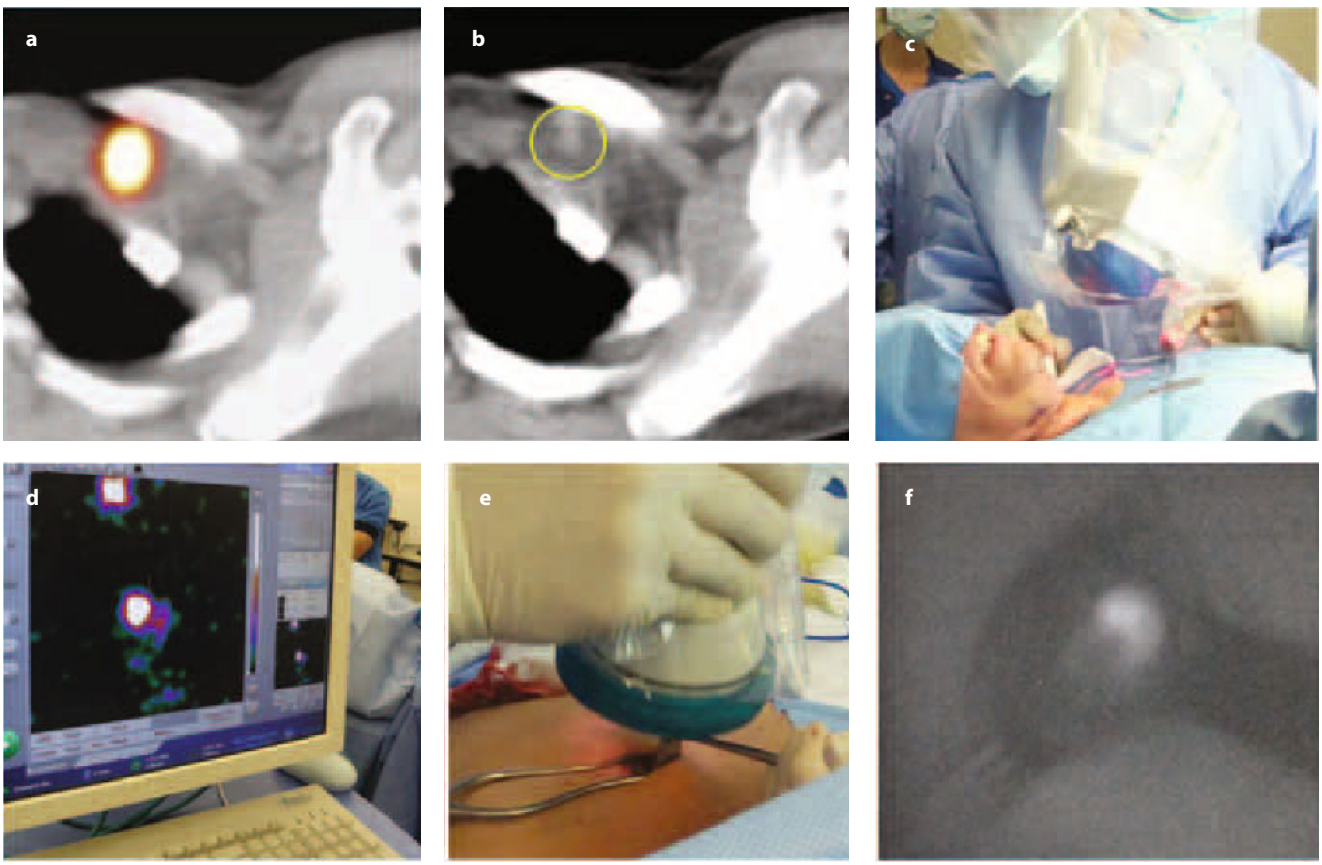

Fig. 7.17 Patient with breast cancer. **a** Fused axial SPECT/CT section showing a radioactive SLN in the left cervical area. **b** This focus of radioactive accumulation corresponds to a solitary lymph node seen in the CT section (*circle*). **c** The use of a portable gamma camera permits the surgeon to select the site for incision, and **d** also to monitor the procedure with intraoperative imaging guidance. The recent introduction of bimodal tracers for simultaneous radioguided (**e**) and fluorescent (**f**) detection is leading to the additional use of a fluorescence camera to better distinguish the SLN in anatomically complex areas

new 3D visualization of the traditional acoustic signal of the gamma probe. This feature, together with the real-time information on depth that the system may provide, expands the application of radioguided sentinel node biopsy in oncology, particularly for malignancies with deep lymphatic drainage [48, 49].

In this regard, the most recent interesting development in radioguided surgery is the system of so-called "freehand SPECT," in which a continuous positioning system installed in the operating room is based on a fixed pointing device, on the patient's body and, correspondingly, on the hand-held gamma counting probe, thus permitting a virtual reconstruction in a 3D environment. The position of the gamma probe relative to the fixed device is tracked by infrared positioning technology, and the output of the intraoperative gamma probe is spatially coregistered in the surgical field (depicted by a video camera) and displayed on a monitor in which the surgeon can easily check the location and depth of the foci of radioactivity accumulation to be resected. This 3D information may be further used for precise localization and targeting of the radioactive SLN(s) and of tumor tissue, thus implementing a radioguided navigation system. The device can ensure permanent assistance and transparent documentation of soft tissue removal during the intervention (Figs. 7.15 and 7.16).

On the other hand, the possibility of combining the current radiopharmaceuticals with other agents opens new fields to explore. In this regard, a radiolabeled nanocolloid agent has been combined with indocyanine green (ICG), a fluorescent agent, for sentinel node detection in robot-assisted lymphadenectomy [50].

In contrast to the use of a single fluorescent agent [51, 52], this bimodal tracer may allow the surgeons to integrate the standard approach based on radioguided detection with a portable gamma camera with a new optical modality based on fluorescent signal detection. This approach is being successfully applied in various malignancies (Fig. 7.17).

For all these new intraoperatives modalities, the preoperative anatomical SPECT/CT acquisition remains essential and is the starting point for surgical planning.

References

1. Kell MR, Burke JP, Barry M, Morrow M (2010) Outcome of axillary staging in early breast cancer: a meta-analysis. Breast Cancer Res Treat 120:441–447
2. Valsecchi ME, Silbermins D, de Rosa N et al (2011) Lymphatic mapping and sentinel lymph node biopsy in patients with melanoma: A meta-analysis. J Clin Oncol 29:1479–1487
3. Giuliano AE, Hunt KK, Ballman KV et al (2011)Axillary dissection vs no axillary dissection in women with invasive breast cancer and sentinel node metastasis: a randomized clinical trial. JAMA 305:569–575
4. Orsini F, Rubello D, Giuliano AE et al (2012) Radioguided surgery. In: Strauss HW, Mariani G, Volterrani D, Larson SM (eds) Nuclear oncology: pathophysiology and clinical applications. Springer, New York (in press)
5. Breast. In: Edge SB, Byrd DR, Compton CC et al (eds) (2010) AJCC Cancer staging manual, 7th ed. Springer, New York, pp 347–376
6. Giuliano AE, Han SH (2011) Local and regional control in breast cancer: role of sentinel node biopsy. Adv Surg 45:101–116
7. Obenaus E, Erba PA, Chinol M et al (2008) Radiopharmaceuticals for radioguided surgery. In: Mariani G, Giuliano AE, Strauss HW (eds) Radioguided surgery – a comprehensive team approach. Springer, New York, pp 3–11
8. Goyal A, Newcombe RG, Mansel RE et al (2005) ALMANAC Trialists Group. Role of routine preoperative lymphoscintigraphy in sentinel node biopsy for breast cancer. Eur J Cancer 41:238–243
9. Even-Sapir E, Lerman H, Lievshitz G et al (2003) Lymphoscintigraphy for sentinel node mapping using a hybrid SPECT/CT system. J Nucl Med 44:1413–1420
10. Lerman H, Metser U, Lievshitz G et al (2006) Lymphoscintigraphic sentinel node identification in patients with breast cancer: the role of SPECTCT. Eur J Nucl Med Mol Imaging 33:329–337
11. Lerman H, Lievshitz G, Zak O et al (2007) Improved sentinel node identification by SPECT/CT in overweight patients with breast cancer. J Nucl Med 48:201–206
12. Zanzonico P, Heller S (2000) The intraoperative gamma probe: basic principles and choices available. Semin Nucl Med 1:33–48
13. Classe JM, Fiche M, Rousseau C et al (2005) Prospective comparison of 3 gamma-probes for sentinel lymph node detection in 200 breast cancer patients. J Nucl Med 46:395–399
14. Mariani G, Vaiano A, Nibale O, Rubello D (2005). Is the "ideal" gamma-probe for intraoperative radioguided surgery conceivable? J Nucl Med 46:388–390
15. Mathelin CE, Guyonnet JL (2006). Scintillation crystal or semiconductor gamma-probes: an open debate. J Nucl Med 47:373
16. Meller B, Sommer K, Gerl J et al (2006) High energy probe for detecting lymph node metastases with 18F-FDG in patients with head and neck cancer. Nuklearmedizin 45:153–159
17. Curtet C, Carlier T, Mirallié E et al (2007) Prospective comparison of two gamma probes for intraoperative detection of 18F-FDG: in vitro assessment and clinical evaluation in differentiated thyroid cancer patients with iodine-negative recurrence. Eur J Nucl Med Mol Imaging 34:1556–1562
18. Schneebaum S, Essner R, Even-Sapir E (2008) Positron-sensitive probes. In: Mariani G, Giuliano AE, Strauss HW (eds) Radioguided surgery – a comprehensive team approach. Springer, New York, pp 23–28
19. Huh SS, Rogers WL, Clinthorne NH (2007) An investigation of an intra-operative PET imaging probe. Nuclear Science Symposium Conference Record. NSS '07 IEEE pp 552–555
20. Manca G, Biggi E, Lorenzoni A et al (2011) Simultaneous detection of breast tumor resection margins and radioguided sentinel node biopsy using an intraoperative electronically collimated probe with variable energy window – a case report. Clin Nucl Med 36:e196–e198
21. Mariani G, Bruselli L, Kuwert T et al (2010). A review on the clinical uses of SPECT/CT. Eur J Nucl Med Mol Imaging 37:1959–1985
22. Vermeeren L, van der Ploeg IM, Valdés Olmos RA et al (2010) SPECT/CT for preoperative sentinel node localization. J Surg Oncol 101:184–190
23. Kobayashi K, Ramirez PT, Kim EE et al (2009) Sentinel node mapping in vulvovaginal melanoma using SPECT/CT lymphoscintigraphy. Clin Nucl Med 34:859–861
24. Leijte JA, van der Ploeg IM, Valdés Olmos RA et al (2009) Visualization of tumor blockage and rerouting of lymphatic drainage in penile cancer patients by use of SPECT/CT. J Nucl Med 50:364–367

25. van der Ploeg IM, Valdés Olmos RA, Kroon BB et al (2009) The yield of SPECT/CT for anatomical lymphatic mapping in patients with melanoma. Ann Surg Oncol 16:1537–1542
26. Vermeeren L, Valdés Olmos RA, Meinhardt W et al (2009) Value of SPECT/CT for detection and anatomic localization of sentinel lymph nodes before laparoscopic sentinel node lymphadenectomy in prostate carcinoma. J Nucl Med 50:865–870
27. Pandit-Taskar N, Gemignani ML, Lyall A et al (2010) Single photon emission computed tomography SPECT-CT improves sentinel node detection and localization in cervical and uterine malignancy. Gynecol Oncol 117:59–64
28. Vermeeren L, Meinhardt W, Valdes Olmos RA (2010) Prostatic lymphatic drainage with sentinel nodes at the ventral abdominal wall visualized with SPECT/CT: a case series. Clin Nucl Med 35:71–73
29. Vermeeren L, Valdés Olmos RA, Klop WM et al (2011) SPECT/CT for sentinel lymph node mapping in head and neck melanoma. Head Neck 33:1–6
30. Buscombe J, Paganelli G, Burak ZE et al; European Association of Nuclear Medicine Oncology Committee and Dosimetry Committee (2007) Sentinel node in breast cancer procedural guidelines. Eur J Nucl Med Mol Imaging 34:2154–2159
31. Cox CE, Cox JM, Mariani G et al (2008) Sentinel lymph node biopsy in patients with breast cancer. In: Mariani G, Giuliano AE, Strauss HW (eds) Radioguided surgery – a comprehensive team approach. Springer, New York, pp 87–97
32. Estourgie SH, Nieweg OE, Valdés Olmos RA et al (2003) Eight fals negative sentinel lymph node procedures in breast cancer: what went wrong? Eur J Surg Oncol 29:336–340
33. Leijte J, van der Ploeg IM, Valdés Olmos RA et al (2009) Visualization of tumor blockage and rerouting of lymphatic drainage in penile cancer patients by use of SPECT/CT. J Nucl Med 50:364–367
34. Varghese P, Abdel-Rahman AT, Akberali S et al (2008) Methylene blue dye – a safe and effective alternative for sentinel lymph node localization. Breast J 14:61–67
35. Rodier JF, Velten M, Wilt M et al (2007) Prospective multicentric randomized study comparing periareolar and peritumoral injection of radiotracer and blue dye for the detection of sentinel lymph node in breast sparing procedures: FRANSENODE trial. J Clin Oncol 25:3664–3669
36. Valdés Olmos RA, Vidal-Sicart S, Nieweg OE (2009) SPECT-CT and real-time intraoperative imaging: new tools for sentinel node localization and radioguided surgery? Eur J Nucl Med Mol Imaging 36:1–5
37. Vermeeren L, Valdés Olmos RA, Meinhardt W et al (2009) Intraoperative radioguidance with a portable gamma camera: a novel technique for laparoscopic sentinel node localisation in urological malignancies. Eur J Nucl Med Mol Imaging 36:1029–1036
38. Hoffman EJ, Tornai MP, Janecek M et al (1999) Intra-operative probes and imaging probes. Eur J Nucl Med 26:913–935
39. Scopinaro F, Tofani A, di Santo G et al (2008) High-resolution, hand-held camera for sentinel-node detection. Cancer Biother Radiopharm 23:43–52
40. Mathelin C, Salvador S, Huss D, Guyonnet JL (2007) Precise localization of sentinel lymph nodes and estimation of their depth using a prototype intraoperative mini gamma-camera in patients with breast cancer. J Nucl Med 48:623–629
41. Zaknun JJ, Giammarile F, Valeds-Olmos RA et al (2012) Changing paradigms in radioguided surgery and intraoperative imaging: the GOSTT concept. Eur J Nucl Med Mol Imaging 39:1
42. Vermeeren L, Klop WM, van den Brekel MW et al (2009) Sentinel node detection in head and neck malignancies: innovations in radioguided surgery. J Oncol 2009:681746
43. Duch J (2011) Portable gamma cameras: the real value of an additional view in the operating theatre. Eur J Nucl Med Mol Imaging 38:633–635
44. Vidal-Sicart S, Paredes P, Zanón G et al (2010) Added value of intraoperative real-time imaging in searches for difficult-to-locate sentinel nodes. J Nucl Med 51:1219–1225
45. Cardona-Arboniés J, Mucientes-Rasilla J, Moreno Elola-Olaso A et al (2012) Contribution of the portable gamma camera to detect the sentinel node in breast cancer during surgery. Rev Esp Med Nucl 31:130–134
46. Vidal-Sicart S, Brouwer OR, Valdés-Olmos RA (2011) Evaluation of the sentinel lymph node combining SPECT/CT with the planar image and its importance for the surgical act. Rev Esp Med Nucl 30:331–337
47. Vidal-Sicart S, Vermeeren L, Solà O, Valdés-Olmos RA (2011) The use of a portable gamma camera for preoperative lymphatic mapping: a comparison with a conventional gamma camera. Eur J Nucl Med Mol Imaging 38:636–641
48. Wendler T, Herrmann K, Schnelzer A et al (2010). First demonsriegertration of 3-D lymphatic mapping in breast cancer using freehand SPECT. Eur J Nucl Med Mol Imaging 37:1452–1461
49. Rieger A, Saeckl J, Belloni B et al (2011) First experiences with navigated radio-guided surgery using freehand SPECT. Case Rep Oncol 4:420–425
50. van der Poel HG, Buckle T, Brouwer OR et al (2011) Intraoperative laparoscopic fluorescence guidance to the sentinel lymph node in prostate cancer patients: clinical proof of concept of an integrated functional imaging approach using a multimodal tracer. Eur Urol 60:826–833
51. Keereweer S, Kerrebijn JD, van Driel PB et al (2011) Optical image-guided surgery – where do we stand? Mol Imaging Biol 13:199–207
52. Polom K, Murawa D, Rho YS et al (2011) Current trends and emerging future of indocyanine green usage in surgery and oncology: a literature review. Cancer 117:4812–4822

SPECT/CT Image Generation and Criteria for Sentinel Node Mapping

8

Renato A. Valdés Olmos and Sergi Vidal-Sicart

8.1 Introduction

Since the introduction of the sentinel lymph node (SLN) procedure, lymphoscintigraphy has been an essential component for preoperative sentinel node identification in patients with melanoma or breast cancer.

With the new generation of large-field-of-view gamma cameras, single photon emission computed tomography/computed tomography (SPECT/CT) has been incorporated in the SLN procedure. The functional information from SPECT can be combined with the morphological information from CT by applying both techniques in one session. The resulting SPECT/CT fused images depict sentinel nodes in their precise anatomical setting, thus providing a helpful roadmap for surgeons. In recent years, SPECT/CT has been used in melanoma and breast cancer patients with unusual or complex drainage. This is the case in melanomas of the neck or the upper part of the trunk, and in breast cancer with drainage outside the axilla. SPECT/CT can also visualize SLNs in the axilla when lymph nodes are not depicted on planar images. Furthermore, SPECT/CT is becoming essential to localize SLNs in areas such as the pelvis, retroperitoneum, and upper abdomen in gastrointestinal, gynecological, and urological malignancies.

Due to the increasing role of SPECT/CT, evaluation of this modality in relation to planar lymphoscintigraphy for SLN detection and localization is necessary. On the other hand, the preoperative anatomical information obtained by SPECT/CT is becoming an essential roadmap for surgeons in the operating room, leading at the same time to more effective use of portable devices for sentinel localization.

8.2 The Clinical Problem

The SLN procedure is based on the hypothesis of the existence of an orderly and predictable pattern of lymphatic drainage to a regional lymph node basin, and on the functioning of lymph nodes on a direct drainage pathway as effective filters for tumor cells [1]. This hypothesis means that all lymph nodes with direct drainage from the primary tumor are considered as sentinel nodes. The SLN is not necessarily the hottest or the nearest node, although that is often the case.

Another important notion is that the SLN procedure is a multidisciplinary modality based on the combination of preoperative imaging, intraoperative detection, and refined histopathological analysis. For preoperative imaging, colloid particles labelled with technetium-99m (^{99m}Tc) are currently used. Radioactive colloid particles are incorporated into the macrophages by phagocytosis, thus enabling prolonged lymph node retention. This leads to an adequate detection window, enabling not only delayed planar images and SPECT/CT, but also intraoperative sentinel node localization using portable devices based on gamma-ray detection.

Furthermore, the SLN procedure is oriented to the detection of lymph node metastases in patients without clinical evidence of regional metastasis [2]. An adequate preoperative selection is, today, capable of detecting patients with palpable lymph nodes at clinical examination, suspected lymph nodes at ultrasound or CT, or tumor-positive lymph nodes at cytological aspiration. In clinical practice, this means the SLN biopsy is considered as a procedure that is principally oriented to the detection of subclinical metastasis. This category mainly includes small macrometastases (≥2 mm and <5 mm), micrometastases (≥0.2 mm and <2 mm), and submicrometastases (<0.2 mm).

R. A. Valdés Olmos (✉)
Nuclear Medicine, Division of Diagnostic Oncology
Netherlands Cancer Institute – Antoni van Leeuwenhoek Hospital
Amsterdam, the Netherlands
e-mail: r.valdes@nki.nl

G. Mariani et al. (eds.), *Atlas of Lymphoscintigraphy and Sentinel Node Mapping*,
DOI 10.1007/978-88-470-2766-4_8

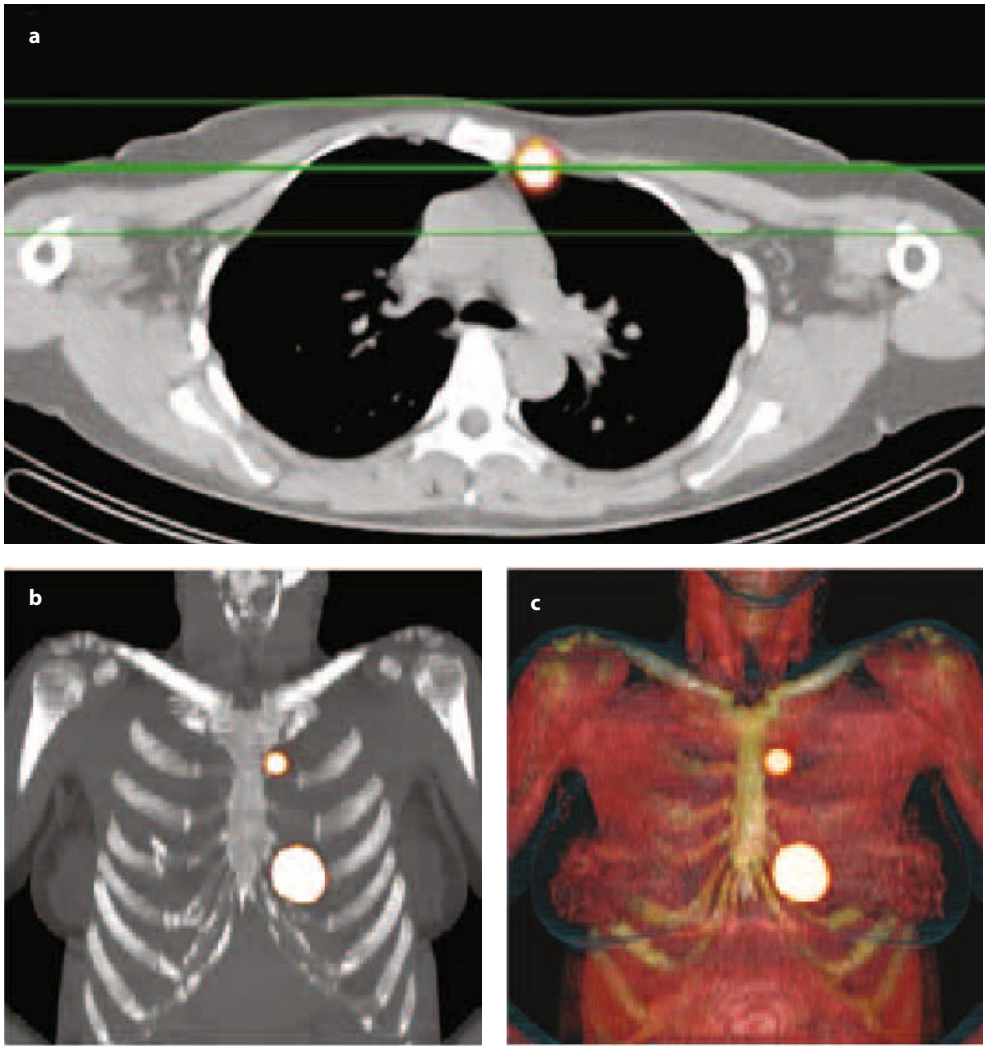

Fig. 8.1 A 51-year-old woman with a nonpalpable T1 carcinoma in the medial lower quadrant of the left breast. SPECT/CT performed 3 hours after ultrasound-guided intratumoral injection of 121 MBq ^{99m}Tc-nanocolloid. The use of maximum intensity projection (MIP) generated for the area between the green lines (**a**) enables a better anatomical recognition of an internal mammary SLN at the level of the first intercostal space (**b**). Volume rendering (**c**) allows a 3D display of the SLN and the tumor site in relation to the anatomical structures

8.3 Image Generation with SPECT/CT

SPECT/CT is principally oriented to the anatomical localization of SLNs. This is the principal reason why SPECT/CT is acquired using low-dose CT. The use of a diagnostic high-dose CT, with or without intravenous contrast, is not necessary because the SLN procedure primarily aims to detect subclinical metastasis in nonenlarged lymph nodes.

However, for SLN localization, the CT component of SPECT/CT must be able to provide optimal anatomical information. This is possible in the second generation of SPECT/CT gamma cameras and enables evaluation of the lymph nodes corresponding to the radioactive nodes on fused SPECT/CT images with low-dose CT (40 mA). For superficial areas such as the groin and the axilla, 5 mm slices are recommended. For more complex anatomical areas (head/neck, pelvis, abdomen), 2 mm slices may be necessary. With this approach, SPECT/CT can accurately localize SLNs in relation to the vascular structures in deep anatomical areas.

CT is also used to correct the SPECT signal for tissue attenuation and scattering. After these corrections, SPECT is fused with CT [3]. A gray scale is used to display the morphology in the background image (CT), whereas a color scale is used to display the SLN in the foreground image (SPECT).

The display of SPECT/CT is similar to that of conventional tomography. Multiplanar reconstruction (MPR) enables two-dimensional (2D) display of fusion images in relation to CT and SPECT. The use of cross-reference lines allows navigation between axial, coronal, and sagittal views. At the same time, this tool allows correlation of the radioactive SLNs seen on fused SPECT/CT with the lymph nodes seen on CT. This information may be helpful for the intraoperative procedure and post-excision control using portable gamma cameras or probes.

Fused SPECT/CT images may also be displayed using maximum intensity projection (MIP). MIP is a specific type of rendering in which the brightest voxels are projected into a three-dimensional (3D) image, thus allowing improved anatomical SLN localization and recognition by the sur-

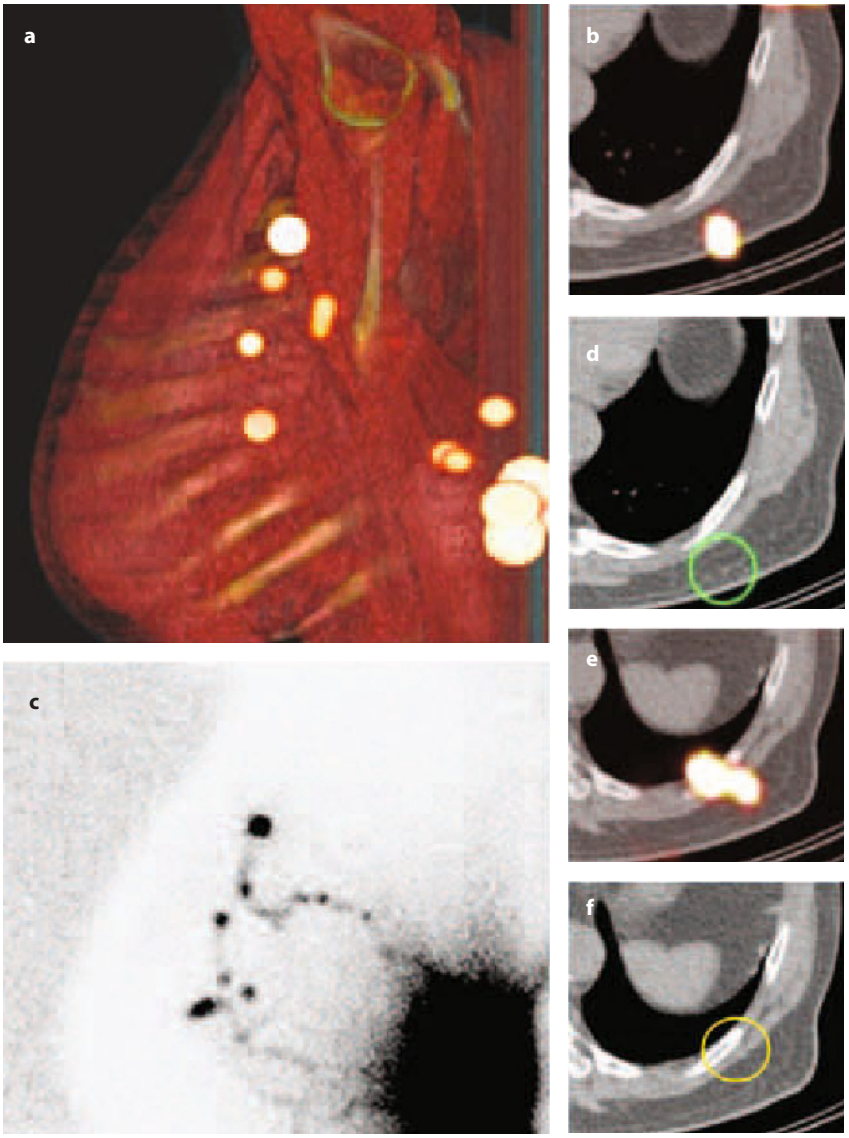

Fig. 8.2 A 79-year-old man with a 1.6 Breslow melanoma on the left in the back. The lateral planar image (**c**), performed after injection of 80 MBq ^{99m}Tc-nanocolloid, shows drainage to the left axilla, with visualization of various lymphatic ducts and nodes. Volume rendering (**a**) also depicts additional lymph nodes in the vicinity of the injection site. These additional sentinel nodes are lymph nodes (*green circles*) localized in subcutaneous fat and in the muscle, as seen on axial SPECT/CT and CT (**b**, **d**, **e**, **f**)

geon. One limitation of MIP is that the presence of other high-attenuation voxels on CT may obscure recognition of the vasculature and of other anatomical structures. Another limitation is that the MIP display is a 2D representation that cannot accurately depict the actual relationships of the vessels and other structures [4].

When using volume rendering for 3D display, different colors are assigned to anatomical structures such as vessels, muscle, bone, and skin. This allows better anatomical reference points to be obtained, and incorporates an additional dimension in the recognition of SLNs. By incorporating a color display, volume rendering improves the visualization of complex anatomy and of 3D relationships (see example in Fig. 8.1).

8.4 General Indications and Contraindications for SPECT/CT

Indications for SPECT/CT in the SLN procedure depend on the type of malignancy and the complexity of lymphatic drainage. They will also depend on the criteria adopted by the surgeons and nuclear medicine physicians in different hospitals.

In general, indications for SPECT/CT in the SLN procedure are as follows:

- detection of SLNs in cases without visualization or with poor visualization at planar imaging [5] (Fig. 8.2). Due to the correction for tissue attenuation, SPECT/CT is usu-

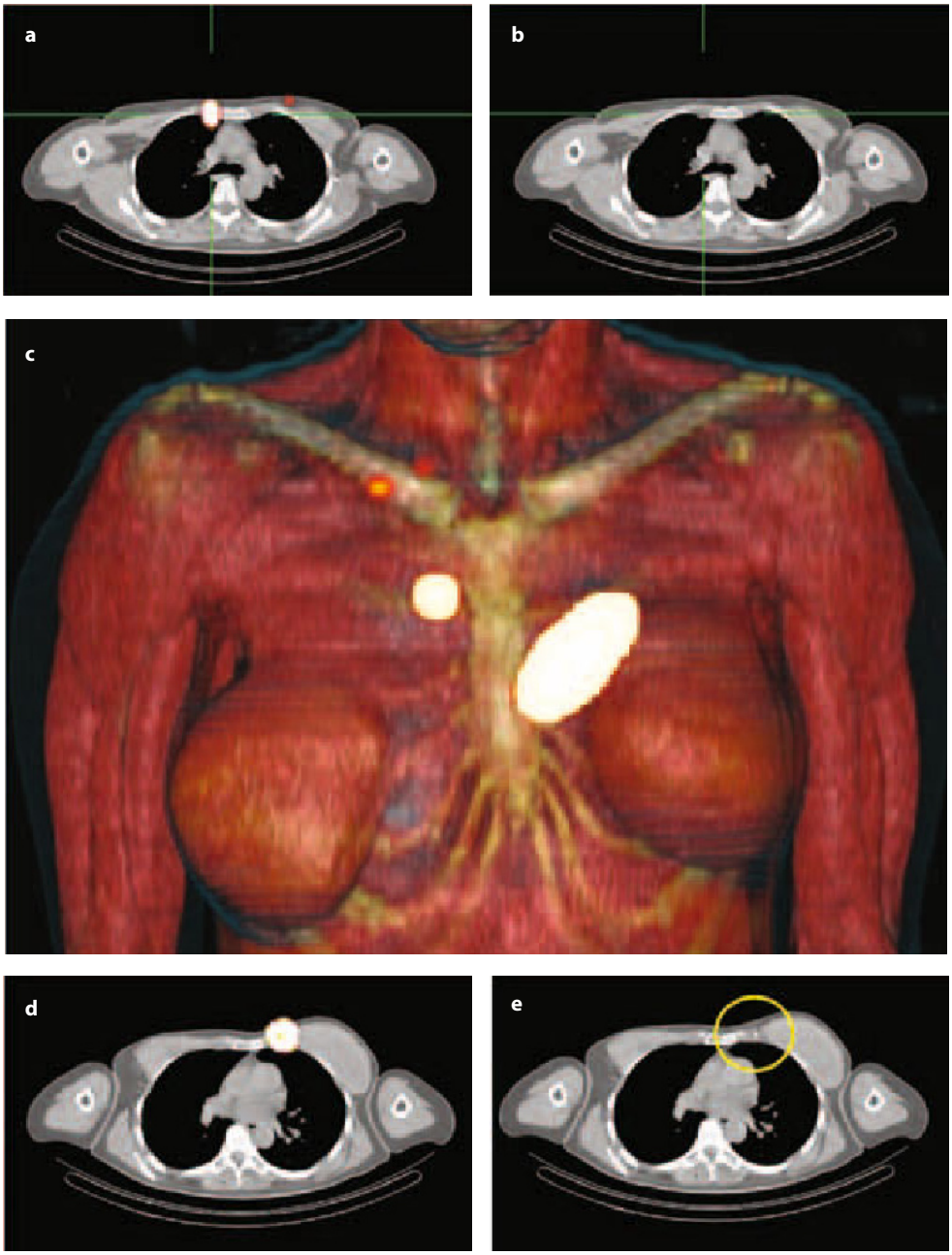

Fig. 8.3 A 42-year-old woman with recurring breast cancer in the upper inner quadrant of the left breast. Eight years earlier the patient had been treated with mastectomy and left axillary dissection due to a T1N1 breast carcinoma. SPECT/CT was performed 3 hours after intratumoral injection of 114 MBq ^{99m}Tc-nanocolloid. Orthogonal multiplanar reconstruction (MPR) and the use of cross-reference lines, as shown on SPECT/CT and CT axial images, facilitates the localization of an internal mammary sentinel node on the right (**a**, **b**). Volume rendering (**c**) allows a 3D display of the contralateral drainage, with the SLN at the level of the first intercostal space on the right. Radiocollloid accumulation seen on axial SPECT/CT (**d**) corresponds on CT (**e**) with the site of the tumor recurrence (*yellow circle*)

ally more sensitive than planar imaging, and may be particularly useful in obese patients

- localization of SLNs in areas with complex anatomy and a high number of lymph nodes, such as the head and neck, or in cases with unexpected lymphatic drainage (e.g., between the pectoral muscles, internal mammary chain, level II or III of the axilla, or in the vicinity of the scapula) at planar imaging. Examples of unexpected patterns of lymphatic drainage in patients with various cancers are shown in Figs. 8.3–8.5
- anatomical localization and detection of additional SLNs in areas of deep lymphatic drainage such as the pelvis (see example in Fig. 8.6), abdomen, or mediastinum [6].

8.5 Comprehensive Interpretation of Preoperative Imaging of Sentinel Lymph Nodes

SPECT/CT does not replace planar lymphoscintigraphy, but should rather be considered as a complementary modality. In fact, SPECT/CT aims to anatomically localize SLNs already visualized on planar images, although in some cases SPECT/CT can detect additional sentinel nodes. In order to understand the combined use of lymphoscintigraphy and SPECT/CT, it is necessary to elucidate some issues [7]. First, by acquiring early and delayed planar images, lymphoscintigra-

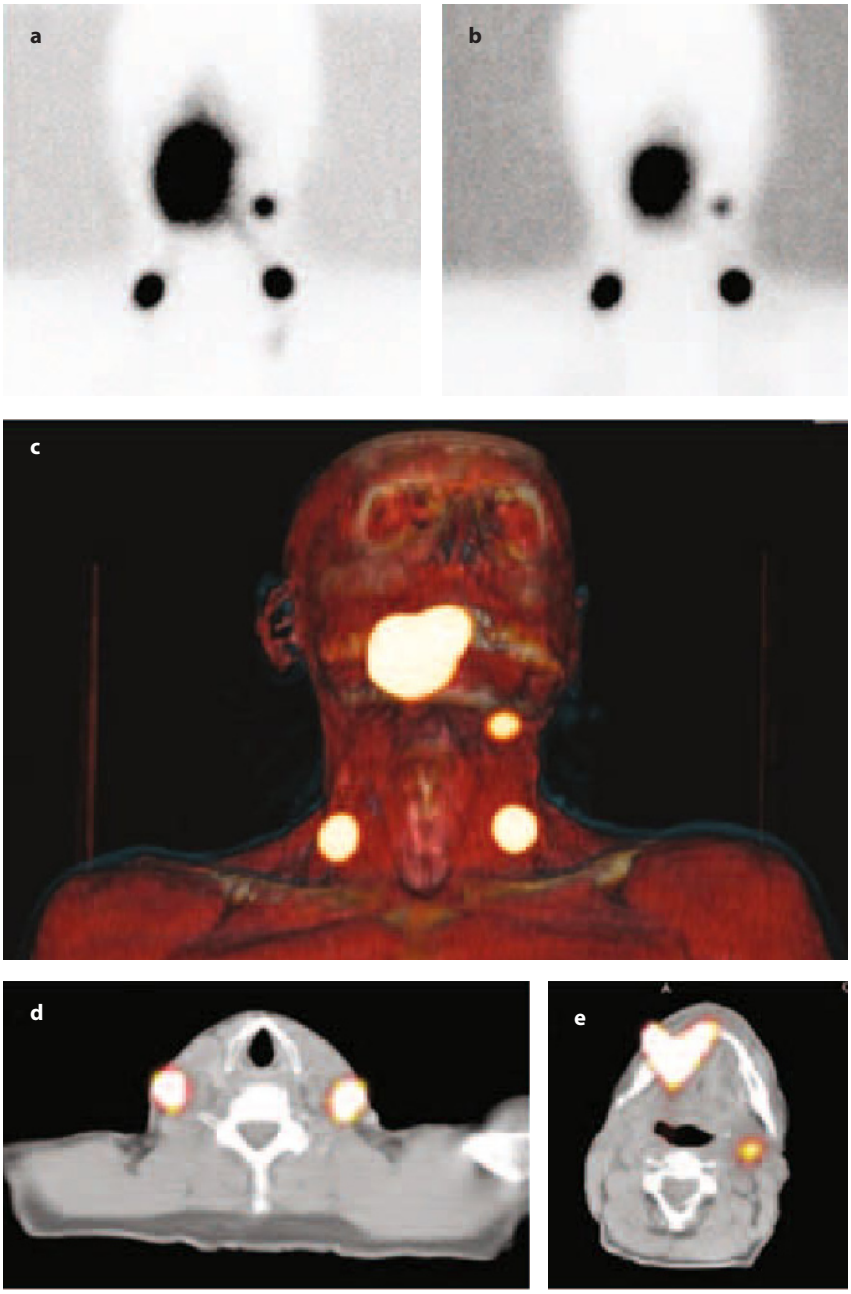

Fig. 8.4 A 60-year-old man with a T1 carcinoma of the right border of the tongue. Lymphoscintigraphy and SPECT/CT performed after injection of 84 MBq ^{99m}Tc-nanocolloid divided into four aliquots injected around the tumor. **a** Early planar anterior imaging shows bilateral drainage to both sides of the neck, with visualization of two lymph nodes with an own lymphatic duct. These two nodes are considered as definite SLNs. A third lymph node seen in the vicinity of the injection on the left is also considered as a sentinel node, due to its location in a different basin. **b** Delayed planar imaging shows no other additional nodes. On volume rendering (**c**) and axial SPECT/CT fusion images (**d**, **e**), these SLNs, free of tumor at histopathology, are localized in level II and III on the left and level III on the right

phy can identify SLNs in most cases. In current protocols, SPECT/CT is performed following delayed planar imaging (mostly 2–4 hours after radiocolloid administration). This sequential acquisition helps to clarify the role of both modalities. However, it is necessary to specify the criteria for SLN identification on preoperative images. Major criteria for identification of lymph nodes as sentinel nodes are the visualization of lymphatic ducts, the time of appearance, the lymph node basin, and the intensity of lymph node uptake [8]. Following these criteria, visualized radioactive lymph nodes may be classified as:

1. *definite sentinel lymph nodes*: this category includes all lymph nodes draining from the site of the primary tumor through an afferent lymphatic vessel, or a single radioactive lymph node in a lymph node basin [9]
2. *highly probable sentinel lymph nodes*: this category includes lymph nodes appearing between the injection site and a first draining node, or nodes with increasing uptake appearing in other lymph node stations
3. *less probable sentinel lymph nodes*: all higher-echelon nodes (in trunk and extremities) or lower-echelon nodes (head and neck) may be included in this category.

An example of lymph nodes visualized at lymphoscintigraphy, with different degrees of probability of being sentinel nodes is shown in Figure 8.7.

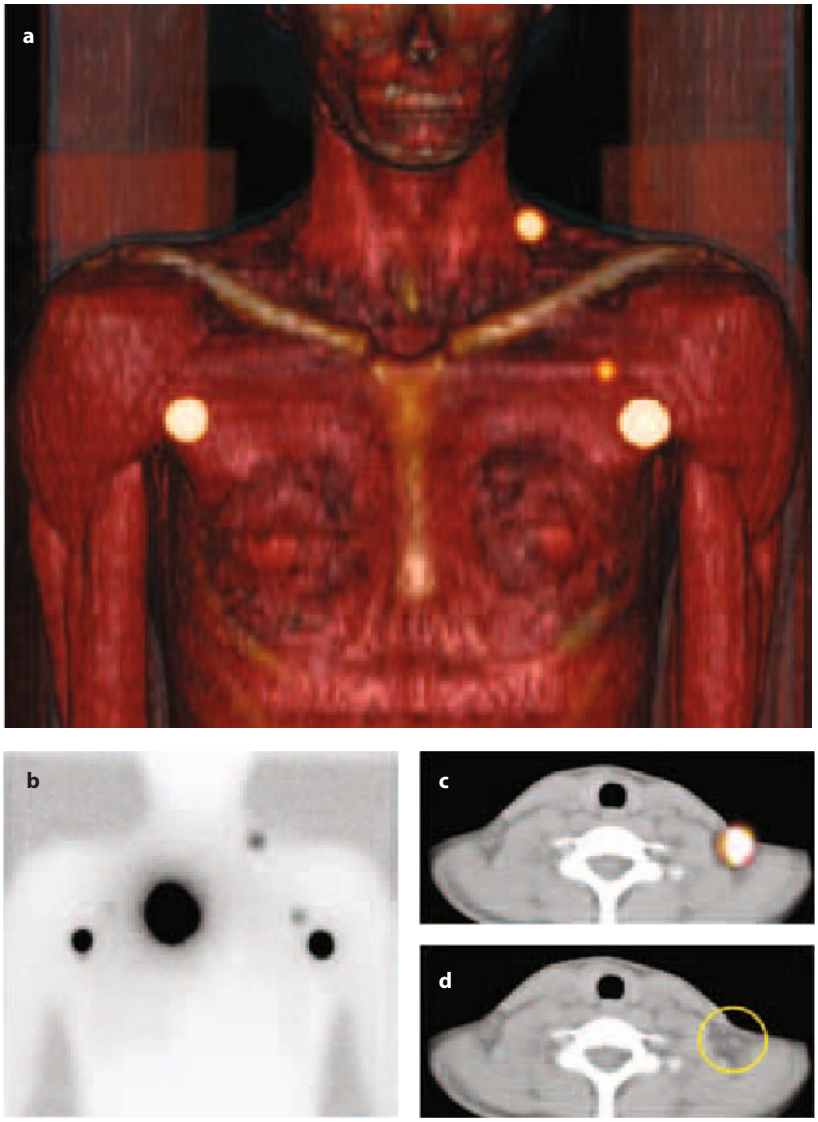

Fig. 8.5 A 15-year-old woman with a 1.9 Breslow melanoma in the periscapular area of the back on the right. A total activity of 67 MBq ^{99m}Tc-nanocolloid was administered. Volume rendering (**a**) and planar anterior images depict drainage to both axillas and to the left supraclavicular area. The supraclavicular sentinel node is also seen on axial SPECT/CT (**c**), and is indicated with a *green circle* on CT (**d**)

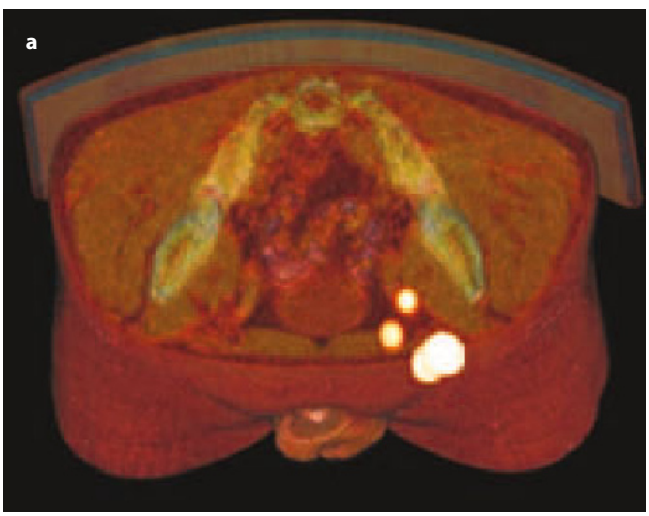

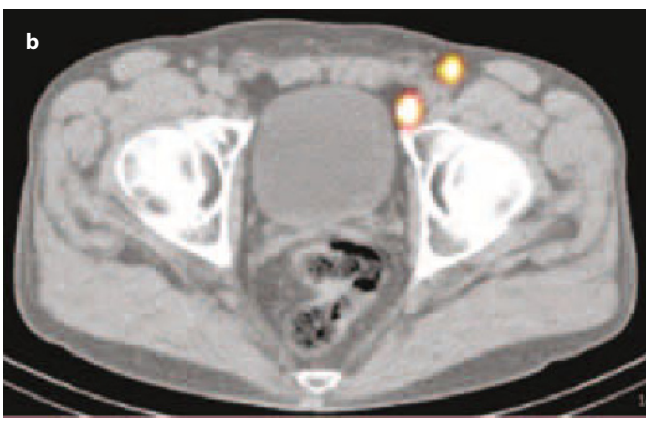

Fig. 8.6 A 59-year-old man with a 1.4 mm Breslow melanoma in the left lower area of the back. SPECT/CT performed 2 hours after injection of 79 MBq ^{99m}Tc-nanocolloid. **a** Volume rendering displayed with cranial tilt is able to differentiate inguinal sentinel nodes from iliac second-echelon lymph nodes in a 3D context. **b** On the axial SPECT/CT fusion image, two of the lymph nodes are also displayed. SLNs of the groin were tumor free at histopathology

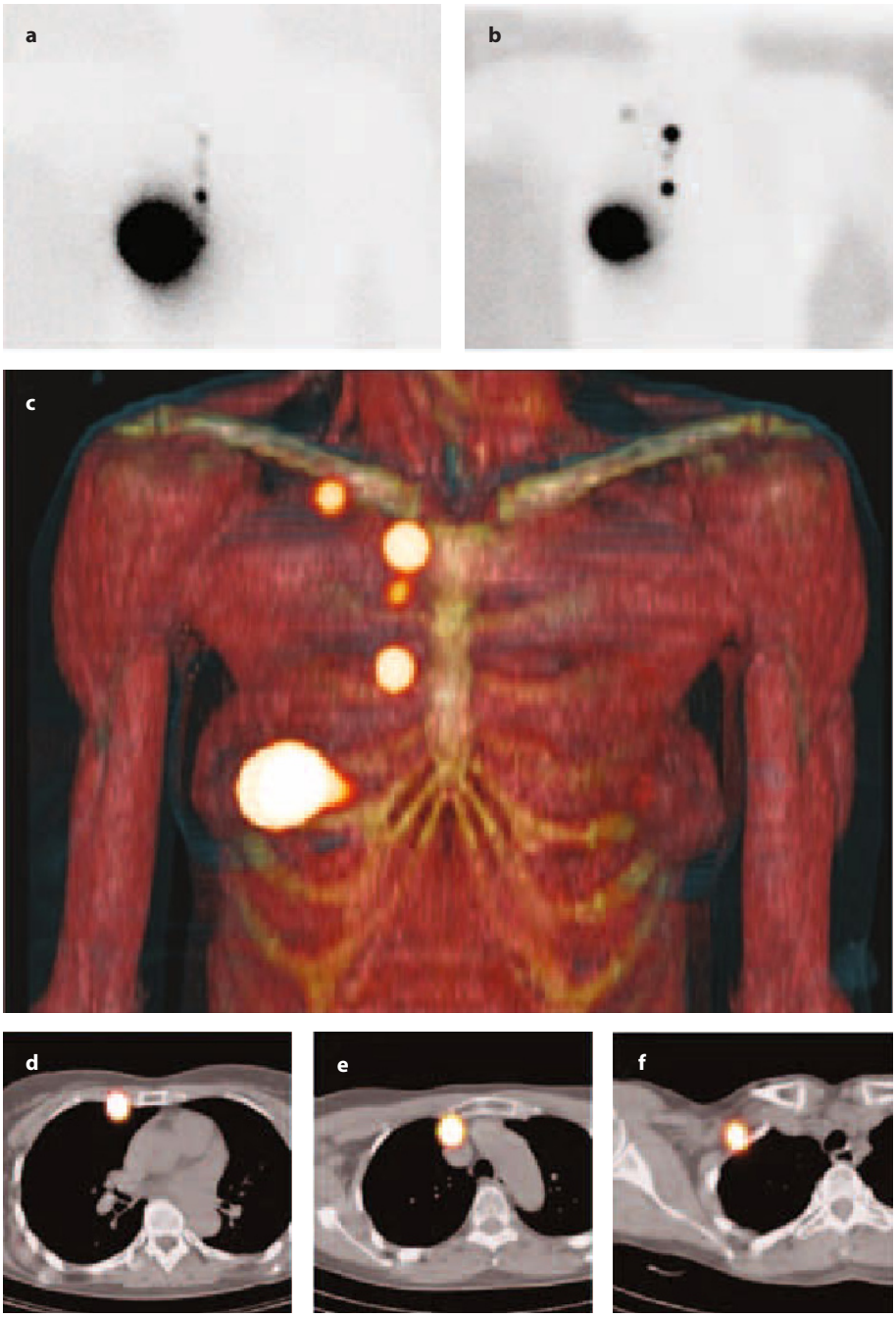

Fig. 8.7 A 64-year-old patient with a T2 carcinoma in the central area of the right breast. After intratumoral injection of 120 MBq ^{99m}Tc-nanocolloid, early drainage to the internal mammary chain is observed on planar imaging (**a**); the most caudal lymph node is considered as a definite sentinel node. However, on delayed planar imaging (**b**) another lymph node in the internal mammary chain shows increasing uptake; this lymph node is considered as highly probable sentinel node. On volume rendering (**c**) and axial SPECT/CT fusion images (**d**–**f**) the most cranial node of the internal mammary chain is identified as a mediastinal lymph node (**e**). This leads to consideration of the lymph node of the infraclavicular basin, seen on delayed planar image and SPECT/CT, also as a sentinel node

Early planar images are essential to identify the first draining lymph nodes as sentinel nodes by visualization of lymphatic ducts. These nodes (category 1) can be distinguished from secondary lymph nodes (category 3), mostly appearing on delayed planar images.

In other cases, a single lymph node is seen on early and/or delayed images. This lymph node is also considered a definite sentinel node (category 1). However, in some cases SPECT/CT can detect additional lymph nodes in other basins. These nodes can be considered as definite (category 1) or highly probable SLNs (category 2). Less frequently, a radioactive lymph node may appear between the injection site and a first draining node; its increasing uptake can confirm this node as a highly probable sentinel node (category 2) and helps to differentiate this node from prolonged valve activity in a lymphatic duct.

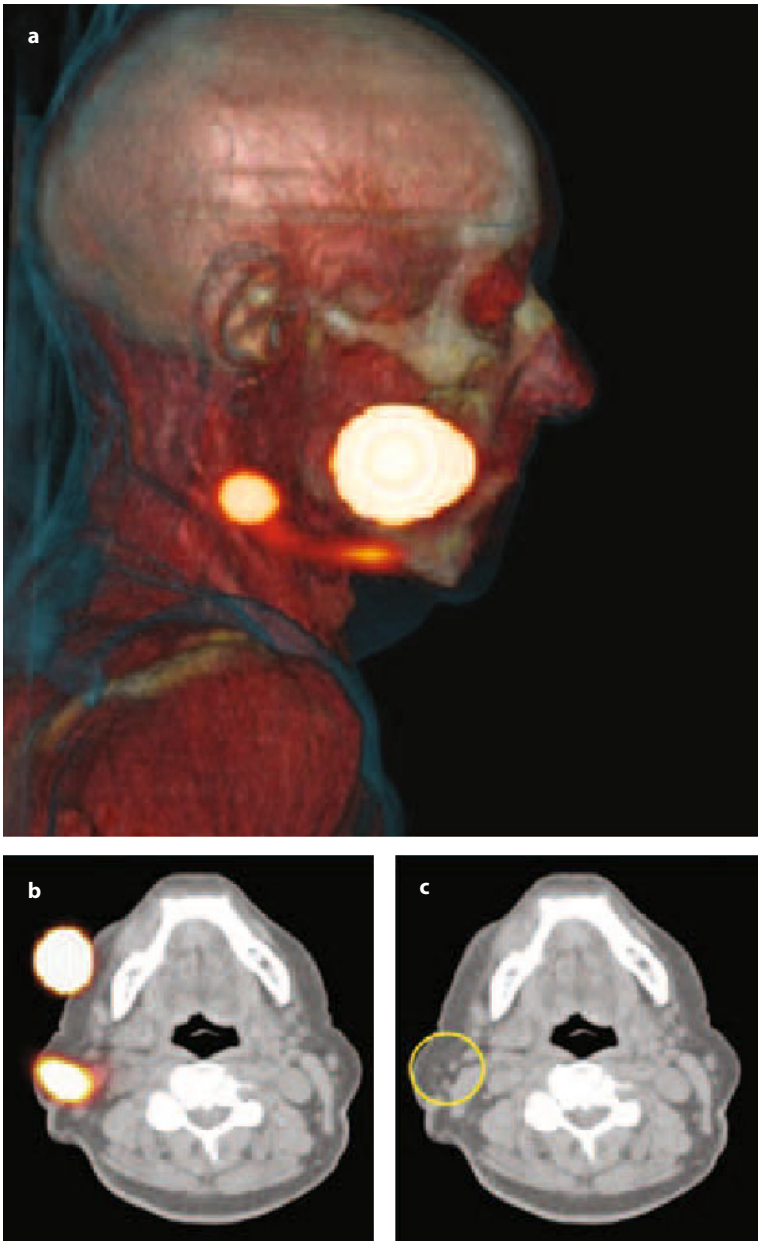

Fig. 8.8 An 84-year-old man with a 3 mm Breslow melanoma of the right cheek. SPECT/CT performed 2 hours after injection 77 MBq ^{99m}Tc-nanocolloid. **a** Volume rendering shows a radioactive node in level II of the neck, with drainage from the injection site through an afferent lymphatic vessel. On axial SPECT/CT fusion image (**b**), the radioactive node corresponds to a cluster of small lymph nodes (*green circle*) on CT (**c**)

8.6 SPECT/CT as a Roadmap for Intraoperative Detection of Sentinel Lymph Nodes

Use of the scintigraphic categories defined above to characterize radioactive lymph nodes also contributes to surgical decision-making. Lymph nodes of the first two categories (definite sentinel node or highly probable sentinel node) are the nodes recognized by the nuclear medicine physician and those that must be removed in the operating room by the surgeon. Less probable sentinel nodes may sometimes be removed, depending on the degree of remaining radioactivity measured by the gamma probe or the portable gamma camera during control of the excision fossa [10].

Another important issue is the need to correlate the findings of fused SPECT/CT with those of CT. In many cases, radioactive sentinel nodes correspond to single lymph nodes. However, in some cases, radioactivity on SPECT/CT corresponds to a cluster of lymph nodes on CT (see example in Fig. 8.8). This preoperative information may lead to a strong post-excision control after removal of the first radioactive node by the surgeon, particularly for areas such as the pelvis and head/neck [10].

Continuous display of SPECT/CT images on screen in the operating room can help the surgeons in their intraop-

erative search, by identifying anatomical structures adjacent to the SLN. In the future, the incorporation of coregistered SPEC/CT to 3D navigation devices will probably improve these features even further.

When using volume rendering for 3D display, different colors are assigned to different anatomical structures such as muscle, bone, and skin. This configuration offers a 3D roadmap to the surgeon and facilitates the interpretation of SPECT/CT.

References

1. Morton DL, Wen DR, Wong JH et al (1992) Technical details of intraoperative lymphatic mapping for early stage melanoma. Arch Surg 127 392–399
2. Sobin LH (2003) TNM, sixth edition: new developments in general concepts and rules. Semin Surg Oncol 21**:**19–22
3. Delbeke D, Coleman RE, Guiberteau et al (2006) Procedure guidelines for SPECT/CT imaging. J Nucl Med 47:1227–1234
4. Fishman EK, Ney DR, Heath DG et al (2006) Volume rendering versus maximum intensity projection in CT angiography: what works best, when, and why. RadioGraphics 26:905–922
5. Van der Ploeg IM, Valdés Olmos RA, Nieweg OE et al (2007) The additional value of SPECT/CT in lymphatic mapping in breast cancer and melanoma. J Nucl Med 48:1756–1760
6. Vermeeren L, van der Ploeg IM, Valdés Olmos RA et al (2010) SPECT/CT for preoperative sentinel node localization. J Surg Oncol 101:184–190
7. Vidal-Sicart S, Valdés Olmos RA (2011) Evaluation of the sentinel lymph node combining SPECT/CT with the planar images and its importance for the surgical act. Rev Esp Med Nuc 30:331–337
8. Nieweg OE, Estourgie S, Valdés Olmos RA (2004) Lymphatic mapping and sentinel node biopsy. In: Ell PJ, Gambhir SS (eds) Nuclear medicine in clinical diagnosis and treatment, 3rd edn, Churchill Livingstone, Edinburgh, pp 229–260
9. Alazraki N, Glass EC, Castronovo F et al (2002) Procedure guideline for lymphoscintigraphy and the use of intraoperative gamma probe for sentinel lymph node localization in melanoma of intermediate thickness 1.0. J Nucl Med 43: 1414–1418
10. Vermeeren L, Valdés Olmos RA, Klop WM et al (2010) A portable gamma-camera for intraoperative detection of sentinel nodes in the head and neck region. J Nucl Med 51: 700–703

9 Preoperative and Intraoperative Lymphatic Mapping for Radioguided Sentinel Node Biopsy in Breast Cancer

Gianpiero Manca, Manuel Tredici, Valerio Duce, Sara Mazzarri, Federica Orsini, Serena Chiacchio, Armando E. Giuliano, and Giuliano Mariani

9.1 Introduction

Axillary lymph node status still is a major prognostic factor in early-stage breast cancer, providing information that is important for tailoring post-surgical treatment [1, 2].

Since imaging techniques have limited sensitivity for detecting metastasis in axillary lymph nodes, the axilla must be explored surgically. Histology of all resected nodes at the time of axillary lymph node dissection (ALND) has traditionally been thought to be the most accurate method for assessing metastatic spread of disease to the locoregional lymph nodes. However, the anatomic disruption caused by ALND may result in lymphedema, nerve injury, shoulder dysfunction, and other short-term and long-term complications that may compromise functionality and quality of life. Sentinel lymph node biopsy (SLNB) is a less invasive method of assessing nodal involvement [3]. The concept of the sentinel lymph node (SLN) is intimately embedded in the notion that, as a consequence of the orderly pattern of lymph flow, metastatic spread of solid tumors through the lymphatic route follows a predictable pattern [4] (Fig. 9.1).

Based on this assumption, histologic evaluation of the SLN (the first node encountered in the direct lymphatic pathway draining from the primary tumor) increases the likelihood of detecting metastasizing tumor cells. According to this concept, the tumor status of the SLN accurately predicts the tumor status of the entire regional lymphatic basin draining the tumor; in particular, a SLN free from tumor metastasis excludes tumor spread to the at-risk regional lymphatic basin. Although it is possible that a SLN does not bear metastasis, while a second-tier node does, this occurrence is very rare, especially when the primary tumor is in an early stage of growth. Therefore, in most patients, the SLN concept remains valid [6].

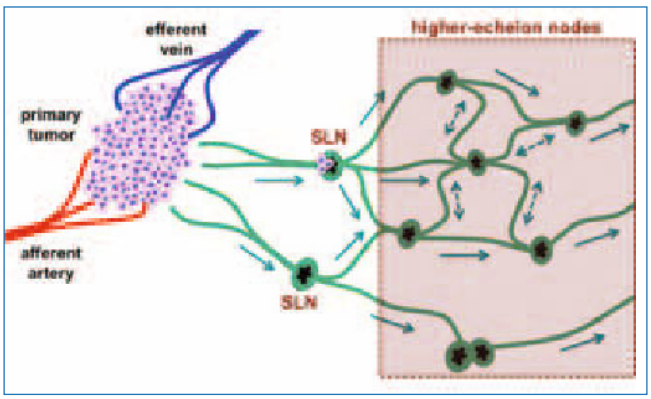

Fig. 9.1 Schematic representation of the "sentinel limph node" (SLN) concept, as the lymphatic station first encountered by tumor cells entering the lymphatic circulation. Direction of lymph flow in higher-echelon nodes can vary according to a variety of pathophysiologic conditions; reproduced with permission from [5]

According to this concept, early systematic studies in patients with breast cancer [7, 8] have suggested that SLNB can be reliably performed in selected patients with early-stage breast cancer, by a carefully trained multidisciplinary team (surgeon, pathologist, nuclear physician), thus reducing the need for ALND and avoiding the associated morbidity [7].

The SLNB procedure uses a radiotracer, a blue dye, or both [9]. Radiopharmaceuticals for SLNB are colloids labeled with technetium-99 (^{99m}Tc) [6, 10]. They enter the lymphatic system and are engulfed by histiomonocytic cells of the sentinel node, thus allowing SLN visualization with a gamma camera before surgery, as well as intraoperative detection with a hand-held gamma probe. Dyes bind weakly to interstitial proteins, mostly albumin, and cause the blue coloring as they pass slowly through the sentinel node. Despite the risk of allergic reactions to vital dyes, most teams favor the dual-mapping procedure [9, 11].

G. Manca (✉)
Regional Center of Nuclear Medicine, University of Pisa Medical School
Pisa, Italy
e-mail: g.manca@med.unipi.it

G. Mariani et al. (eds.), *Atlas of Lymphoscintigraphy and Sentinel Node Mapping*,
DOI 10.1007/978-88-470-2766-4_9 © Springer-Verlag Italia 2013

Identifying women who can be offered SLNB is a highly debated issue (see further below). Some centers adopt SLNB only in patients with a unifocal tumor smaller than 2–3 cm, whereas others have extended the application to patients with large T2 or T3 (5 cm) tumors, or with multiple ipsilateral carcinomas (multifocal/multicentric), or even to patients who have received neoadjuvant chemotherapy [12].

As techniques and histologic analysis for SLNs have evolved, most of the emphasis has not been simply on enhanced detection of metastatic disease and consequent lowering of the false-negative rate. Rather, the primary focus of attention has been on operators' experience and on the clinical relevance of micrometastatic nodal disease. There is a definite learning curve for performing SLNB, and an experienced team reduces the rate of failure to identify a sentinel node and lowers the rate of false-negative results.

In 2001, Mariani et al. summarized the state of the art in radioguided SLNB for breast cancer [6]. More recent guidelines and reviews have updated the field, which encompasses an ever growing body of literature dealing with several aspects of the procedure, from technical modalities to immediate and long-term clinical implications [13, 14].

9.2 The Clinical Problem

ALND has been an integral part of the management of breast cancer since Halsted described the radical mastectomy in the 1890s [15]. This operation was designed to achieve locoregional control in women with large locally advanced tumors that had metastatized to the axillary lymph nodes. Since then, breast cancer has been detected earlier, with smaller tumors and less nodal involvement [16]. Since Halsted's work, operations on the breast itself have become less radical. The radical mastectomy was replaced by the modified radical mastectomy, which has largely been replaced by the lumpectomy for patients with early breast cancer.

Despite the revolution in surgery on the breast itself, ALND continued largely unchanged until the 1990s, when SLN dissection was first introduced [17].

Knowledge of the axillary status has been essential in the management of early breast cancer. Axillary nodal status is the most important predictor of overall survival, and control of the axilla remains essential to patient wellbeing. Axillary dissection, however, is associated with a number of significant morbidities and complications such as seroma, infection, decreased range of motion, axillary web syndrome, shoulder pain, paresthesias, and lymphedema [18].

The SLNB procedure was introduced as a means of accurately identifying axillary metastases by removing only one or two lymph nodes and avoiding the complications and morbidity of ALND. Numerous prospective single-institutional and multicenter randomized controlled studies have shown the accuracy and safety of SLNB in early breast cancer [7, 19, 20].

While there are minor disagreements on the precise indications, the majority of surgeons perform SLNB for patients whose axillae are clinically free of metastases and have either T1 or T2 tumors. The American Society of Clinical Oncology (ASCO) has published guidelines on the use of sentinel node biopsy alone without ALND (Table 9.1) [9]. Patients who undergo SLNB and are found to have a tumor-free SLN may avoid axillary dissections. Prospective non-randomized and randomized studies from Veronesi's group, ALMANAC (Axillary Lymphatic Mapping Against Nodal Axillary Clearance), and NSABP (National Surgical Adjuvant Breast and Bowel Project) have shown the safety and efficacy of SLNB, with no diminution in survival for patients with a tumor-free sentinel node who undergo SLNB alone [21].

There are relatively few contraindications for SLNB. Pregnancy is considered a contraindication for the use of blue dye, since blue dye is a pregnancy category C substance whose teratogenic effects are unknown. However, lymphoscintigraphy may be safely performed in the pregnant patient. Inflammatory breast cancer and large matted nodes are considered the most significant contraindications.

Large randomized studies have shown that SLNB may result in morbidity and complications similar to axillary dissection. However, the rate of complications and severity of complications are markedly less. In the American College Of Surgeons Oncology Group (ACOSOG) Z0011 trial, lymphedema was reported by only 2% of patients and sensory loss was noted in 12% of patients 6 months after SLNB, compared to 13% and 44%, respectively, 6 months after ALND [22]. This large multicenter randomized trial also demonstrated fewer adverse effects on range of motion, quality of life, and resumption of normal activities of daily life after SLNB. The NSABP B-32 study also noted less morbidity in patients randomized to SLNB alone compared to those randomized to SLNB plus completion ALND [21]. All studies comparing SLNB to ALND show fewer complications and less morbidity with SLNB alone. SLNB alone is clearly preferable to ALND for management of node-negative women.

More controversial, however, is the management of patients with sentinel node metastases. Intense examination of the sentinel node has resulted in many patients with micrometastases or isolated tumor cells (ITC) detected in the sentinel node. The American Joint Committee on Cancer (AJCC) staging system has been modified to reflect these findings and has defined isolated tumor cells as "small clusters of cells not greater than 0.2 mm, or single tumor cells, or a cluster of fewer than 200 cells in a single histologic cross-section," and micrometastases as "tumor deposits greater than 0.2 mm but not greater than 2.0 mm in largest dimension" [23].

Nonrandomized retrospective studies have shown vari-

ous different outcomes for patients with occult metastases or micrometastases. Some studies such as the MIRROR (Micrometastases and Isolated tumor cells: Relevant and Robust Or Rubbish?) trial from the Netherlands have identified an adverse outcome for patients with micrometastases [24]. Other retrospective studies have shown no effect of micrometastases on survival [25].

Two large prospective studies from the United States examined patient outcomes for patients with occult micrometastases. ACOSOG Z0010 included over 5,000 women who underwent SLNB and, if node negative, were treated on the basis of hematoxylin and eosin (H&E) examination of the sentinel node, which was sent then to a central laboratory where multiple sections were examined by immunohistochemical analysis (IHC) with antibodies to cytokeratin. The results of the central laboratory findings were blinded to the clinicians and patients in this study. The detection of metastases with IHC revealed no adverse impact on survival. Patients with H&E metastases were treated with SLNB followed by ALND and had a significantly worse survival than patients with occult IHC-detected metastases. However, survival at 5 years was the same for patients with IHC-detected metastases and for those with no IHC-detected metastases [26].

NSABP B-32 was a randomized trial comparing SLNB alone with SLNB plus ALND. Sentinel nodes were similarly examined in a central laboratory with IHC. In this study, 2,804 patients were treated with SLNB alone, and 2,807 were treated with SLNB followed by completion ALND. A central laboratory performed a slightly more intense examination of sentinel nodes than was done in ACOSOG Z0010. NSABP B-32 revealed 15.9% of 3,887 H&E node-negative women with occult metastases detected by multiple sections and IHC; 11.1% had ITC, and 4.4% had micrometastases. In this study, occult metastases slightly decreased overall survival and distant disease-free survival. Patients with occult metastases had a 5-year survival rate of 94.6% compared to 95.8% with no IHC-detected metastases. This study concluded that, while there was a small difference in overall survival, this difference was not clinically relevant [27].

These two prospective studies lend considerable support to the concept of not performing IHC on sentinel nodes and not completing ALND if occult metastases are detected with more intense scrutiny than standard H&E staining. The detection of micrometastases or ITC should not alter clinical management.

SLNB has radically altered the management of the axilla for patients with early breast cancer. After more than a century, axillary management has finally changed to a less morbid and less radical approach. Patients have far fewer complications after SLNB alone than they do after ALND, and quality of life and time missed from the activities of daily living are markedly improved with the less radical operation.

9.3 Lymphatic Drainage of the Breast

Examination of lymphatics of the breast began in the late 18th century, using mercury injection on cadavers to identify drainage from the breast [28, 29]. These studies identified drainage directly to the axillary lymph nodes from the nipple and lateral part of the breast, and drainage to the internal mammary lymph nodes from the posterior and medial aspects of the breast. A small number of lymphatics were seen to drain directly under the clavicle to the central axilla.

A century later, Sappey, also using mercury injections, identified two groups of lymphatic vessels with extensive interconnections: one group was from the superficial aspect of the breast, primarily the skin and subcutaneous tissue, while a deep group drained the gland itself [30]. Sappey believed that the deep lymphatics of the breast parenchyma drained to a subareolar plexus, which then drained primarily to the axilla. Subsequent and more contemporary studies of breast lymphatics involve not only post-mortem injection, but routes of metastases of breast cancer and, more recently, lymphangiography and lymphoscintigraphy. However, these have not resulted in significant changes to our knowledge of the lymphatic anatomy of the breast.

The breast drains to lymph nodes at different sites. Most of the breast lymph drains to the axilla. The lymphatics within the breast parallel the milk ducts. There is clearly a large subareolar plexus, which drains a large portion of the breast directly to the axilla. This plexus has become the site of injection for a number of investigators seeking to perform axillary SLNB. However, injection of the subareolar plexus will not identify sites of metastases other than the axilla. In fact, subareolar plexus injection rarely identifies internal mammary, parasternal, or intramammary metastases. Posterior to the breast parenchyma itself is a second plexus in the retromammary space, which drains not only to the axilla but also to the internal mammary chain, as well as to the intercostal and diaphragmatic lymph nodes. There is overlap of drainage area and extensive anastomosis of the lymphatics of the breast [31, 32].

The axillary lymph nodes are not only the predominant drainage basin of the breast, but are the most important nodal basin for the management of breast cancer. There are three groups of axillary nodes, arbitrarily defined by their anatomic relationship to the pectoralis major and minor muscles. These nodes are caudal to the axillary vein. Level I nodes extend from the lateral edge of the pectoralis major muscle to the lateral edge of the pectoralis minor muscle. Level II nodes are those directly posterior to the pectoralis minor muscle, and level III nodes are medial to the medial border of the pectoralis minor muscle and extending to the Halsted's ligament at the chest wall. There are very few nodes in level III.

Within level I, there are a number of nodal groups. The

external mammary node group runs parallel and along the lateral thoracic artery, draining primarily the lateral breast. The lateral axillary vein group is posterior along the anterior border of the latissimus dorsi and contains the largest amount of nodal tissue. The subscapular nodal group runs parallel to the scapular vessels and drains the lower posterior neck, posterior trunk, and posterior shoulder, as well as the breast. The axillary vein group medial and posterior to the axillary vein receives drainage primarily from the upper extremity and not the breast. Axillary dissections for breast cancer should not routinely remove tissue posterior or superior to the axillary vein.

Level II nodes may receive lymphatic drainage directly from the breast, but also drainage from afferent vessels of level I nodes. Level III lymph nodes are the most medial nodal group in the axilla, which not only drain the other axillary nodal groups but merge with lymphatic vessels from the subclavicular group and form the subclavian trunk. Rotter's nodes are located between the pectoralis major and minor muscles. Some lymphatics from the retromammary plexus penetrate the pectoralis major muscle and travel along the thoraco-acromial vessel, terminating directly in level III. Superior and medial aspects of the breast may also drain directly to level III. However, isolated nodal metastases are rarely seen in level III nodes without extensive involvement of level I and level II nodes. For this reason, most surgeons perform a level I and level II axillary dissection without removing level III, unless palpable lymph nodes are encountered or there is extensive nodal disease in the first two levels. Sentinel nodes are encountered primarily in level I, less so in level II, and rarely in level III [17]. Good exposure of level III lymph nodes often requires partial or full transection of the pectoralis minor muscle.

Internal mammary nodes primarily drain posterocentral and posteromedial aspects of the breast. Usually, nodal metastases are seen in the internal mammary chain only when there are concomitant axillary metastases. Only about 3–5% of the patients have nodal metastases identified in the internal mammary sentinel node without axillary involvement. For this reason, many surgeons do not perform internal mammary SLNB. Indeed, nodal metastases to the internal mammary chain have been largely ignored since abandonment of the extended radical mastectomy.

The ipsilateral supraclavicular nodal metastases are no longer considered stage IV disease in the AJCC staging system, because of the direct drainage of the upper inner portion of the breast to the supraclavicular nodes. Metastases in these nodes result in classification of these patients as AJCC nodal stage N3. Internal mammary node metastases result in classification as N1, N2, or N3 [23].

Curiously, surgeons eagerly perform ALND, removing axillary metastases and expecting improvement in both regional control and survival. Yet, these same surgeons routinely ignore internal mammary node metastases. A large study examining the relevance of internal mammary node metastases showed that patients with internal mammary node metastases and no axillary metastases have the same diminution in survival as patients with axillary node metastases and no internal mammary node metastases. However, patients with both axillary and internal mammary node metastases have a markedly decreased overall survival. There is no survival advantage to removal of internal mammary nodal metastases [33].

Variations in lymphatic drainage of the breast have important implications for the performance of lymphoscintigraphy. Injections in the skin or subareolar plexus will result in identification of only axillary nodal drainage. Circumferential injection at the level of the tumor in the breast, or more posteriorly, can identify internal mammary, supraclavicular, or even intramammary SLNs. The nuclear medicine physician and surgeon must have precise knowledge of the site of injection, as they use this information to identify nodal drainage for SLNB.

9.4 Lymphoscintigraphy

Hundreds of studies have been published on lymphoscintigraphy for radioguided SLNB in breast cancer, and the data reported have often been discordant. The main areas of controversy concern the radiopharmaceuticals to be used, the site and mode of radiocolloid injection, the optimal activity, and the appropriate volume of the radiocolloid.

9.4.1 Radiopharmaceuticals

Three types of radiocolloid preparations are commonly used for lymphoscintigraphy, combined with intraoperative identification of the SLN with a hand-held gamma probe. ^{99m}Tc–sulfur colloid is the most commonly used agent in the United States, either unfiltered (particle size about 15–5,000 nm) or filtered (particle size depending on the filter employed). In this regard, different pore sizes (100 or 220 nm) have been proposed, with the goal of obtaining particles in the range of about 50–100 nm or 50–200 nm. Although some authors still claim the superiority of the unfiltered versus the filtered preparation [34, 35], the prevailing trend now favors the routine use of filtered ^{99m}Tc–sulfur colloid for SLN studies. Most European investigators use a ^{99m}Tc-nanocolloid preparation of human serum albumin with particles ranging in size between 4 nm and about 100 nm (95% of the particles being <80 nm). At present, this radiopharmaceutical offers the best range of particle size, approaching the ideal range, and offers the additional benefits of instant labeling at room temperature and stability both in vitro and in vivo. ^{99m}Tc–antimony

trisulfide (3–30 nm) is commercially available in Australia and Canada, where it is widely used for SLN procedures. Finally, although the average particle size of ^{99m}Tc–rhenium sulfide is reported by the manufacturer to be about 100 nm, this agent actually has a trimodal distribution in particle size: about 40 nm (8% of the particles), 440 nm (61%), and between 650 nm and 2,200 nm (31%) [36].

It is generally considered that a radiocolloid with most of the particles ranging in size between 100 nm and 200 nm represents the best compromise between fast and efficient lymphatic drainage from the site of interstitial injection and satisfactory retention in the SLN.

9.4.2 Modalities of Radiocolloid Injection

At least three main parameters define the optimal techniques for administering the radiocolloid for lymphatic mapping and SLNB in breast cancer surgery: the site of injection, the volume of the injectate, and the activity injected. An additional parameter is the timing of injection relative to surgery, though with lesser importance in the overall procedure. Criteria for defining the optimal combination of these parameters partly overlap with each other; the site of injection is the most crucial parameter, which heavily affects the final choice of the other two main parameters – volume and activity (Fig. 9.2).

Direct intratumoral injection has originally represented a natural extension of the technique developed earlier with vital blue dye: it is generally characterized by a relatively large volume of radiocolloid (at least 4 mL) and a relatively large amount of injected activity (37–370 MBq) [37].

For intraparenchymal (i.e., peritumoral) administration, the radiocolloid is injected into a site immediately adjacent to the tumor, in the space with a supposedly normal lymphatic system that is the only possible drainage pathway for fluids, particles, and cells leaving the tumor through the extravascular route. In this approach, the radiocolloid is given in 4–6 deposits around the tumor circumference. Each aliquot is about 0.5–1 mL and contains 7–18 MBq ^{99m}Tc-labeled colloid. Although in most centers such peritumoral injections are directed simply by palpation, it is advisable to inject the tracer under sonographic guidance (or stereotactic devices) within about 2 mm from the tumor periphery.

Irrespective of the quadrant where the primary tumor is located, the peritumoral, intraparenchymal route of radiocolloid injection results in a high rate of visualization of SLNs in the internal mammary chain, an occurrence reported in an average 20% of the patients, with a maximum of about 30% [38]. Although the long-term clinical impact of identifying pathways of lymphatic drainage to the internal mammary chain in patients with early breast cancer is still unclear (see further below), this finding is a definite advantage of the peritumoral administration route when one compares its merits with those of the subdermal–intradermal injection technique.

The likelihood of visualizing a lymphatic duct and a draining lymph node increases when the radiocolloid is injected into the skin overlying the mammary gland (subdermal–intradermal injection) [39]. Therefore, axillary SLNs can be efficiently visualized as early as 20–30 minutes after intradermal injection of radiocolloid (versus 30–40 minutes for the peritumoral and 40–60 minutes for the intratumoral routes of administration), thus making the entire lymphoscintigraphic procedure highly practicable. Clearly, a radiocolloid injected intradermally or subdermally is less likely to drain toward the deep fascial lymphatic collectors to visualize the internal mammary chain. Using this administration approach, a small volume of tracer (0.15–0.3 mL containing 10–20 MBq ^{99m}Tc-colloid) is injected as a single aliquot in the skin directly overlying the tumor. Advantages of the intradermal–subdermal injection technique are represented by its high practicability with minimum training, small volume administered as a single injection, fast visualization of lymphatic drainage pathways, and low activity administered. Based on how deep the injection is performed, radiocolloid administration is defined as intradermal when the needle is almost tangential to the skin surface and a classic urticarial pomphus develops. Instead, when the injection is a little deeper (this occurrence is signaled by reduced resistance to penetration of the needle), the pomphus is less obvious and administration is defined as subdermal.

Finally, peri-areolar/subareolar radiocolloid injection [40] is based on the presence of a lymphatic plexus around each lobule of the mammary gland that follows the path of the galactophore ducts, converging to the areola to form the Sappey subareolar plexus, which is part of the general subcutaneous plexus. It is in fact reasonable to assume that these various techniques are complementary [6].

Some studies have compared the lymphoscintigraphic pattern and performance of SLN identification by adopting, in the same patients, the intradermal approach, the peritumoral/intraparenchymal approach, and the peri-areolar/subareolar approach [38, 41, 42]. Although the three techniques are reported to yield virtually equivalent results in the vast majority of patients [42–44], some authors report a sizable proportion of discordant results concerning SLNs either in the axilla or in the internal mammary chain (or both) [38, 44].

Perfect equivalence between the three approaches requires further comparative studies and better understanding of the role of tumor status of the internal mammary chain lymph nodes in therapy planning and in the long-term outcome of patients. It is reasonable to assume that the three injection techniques (intradermal, peritumoral, and peri-areolar/subareolar) are complementary [38]. Another reasonable approach might be to inject the radiocolloid intradermally

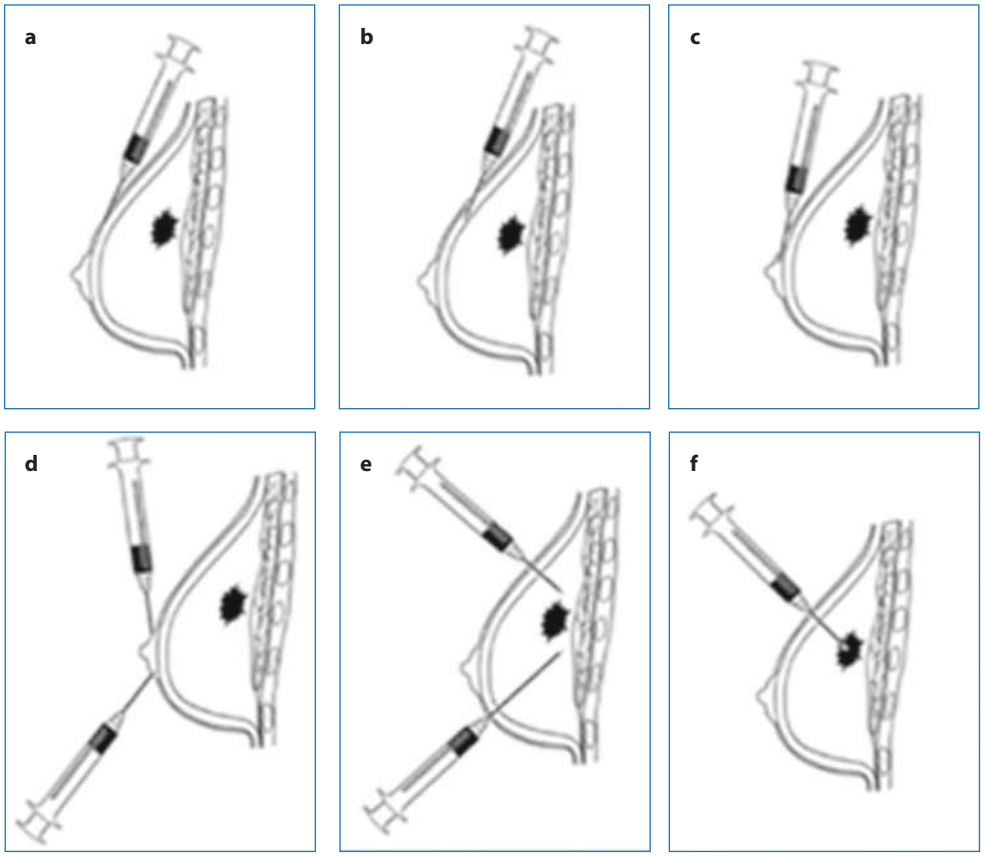

Fig. 9.2 Modalities of radiotracer injection for SLN mapping in breast cancer. Superficial injections (**a**–**d**) and deep injections (**e**, **f**). **a** Intradermal, **b** subcutaneous, **c** subareolar, **d** peri-areolar, **e** peritumoral, **f** intratumoral; images supplied by courtesy of Renato A. Valdés Olmos and Sergi Vidal-Sicart

or peri-areolarly/subareolarly when a T1a–b tumor (=1 cm in diameter) is located rather superficially in the breast, and peritumorally in the case of larger tumors or tumors located deep within the mammary gland.

9.4.3 Preoperative Imaging

Whichever technical approach is followed in the choice of the radiocolloid and modality of injection, there is more general consensus on how to perform lymphoscintigraphic acquisitions for SLN identification. The energy setting of the gamma camera should be centered on the 140 keV emission peak of ^{99m}Tc, with a ±10% window. The use of a high-resolution collimator and an acquisition matrix of 256×256 pixels is highly recommended. Large-field-of-view gamma cameras are useful to depict the lymphoscintigraphic pattern of the entire lymphatic basin in a single image. However, in some cases, small-field-of-view gamma cameras are especially helpful for accurate topographic localization, because they can be placed closer to the axilla. Nevertheless, it should be noted that the increasing use of single photon emission computed tomography/computed tomography (SPECT/CT) acquisitions improves considerably the topographic localization properties of lymphoscintigraphy. An anterior scintigraphic view is frequently used initially, but it is usually changed to oblique anterior views, with some craniocaudal tilting, during visualization of radiocolloid drainage (Figs. 9.3-9.5).

The angles are modified as needed to distinguish between the injection site and focal accumulations corresponding to the draining lymph nodes. A final, integral phase of lymphoscintigraphy is to mark the exact position of the SLN(s) using indelible ink, either with the aid of a radioactive point source or preferably using the probe (or both) for counting the axilla externally, focusing on the spot(s) visualized by lymphoscintigraphy. In this topographic localization phase, the arm should be abducted at about 90°, approximately in the same position as on the operating table during surgery, to identify accurate topographic coordinates that the surgeon can use during the surgical procedure. Marking the skin projection of the sentinel node and having the images available may assist the surgeon in reducing the operating time to locate the sentinel node, thus keeping the surgical incision to a minimum [6].

By providing the surgeon with a map of SLNs, scintigraphy has the potential of both improving accuracy and reducing morbidity relative to gamma probing alone [6, 44–46].

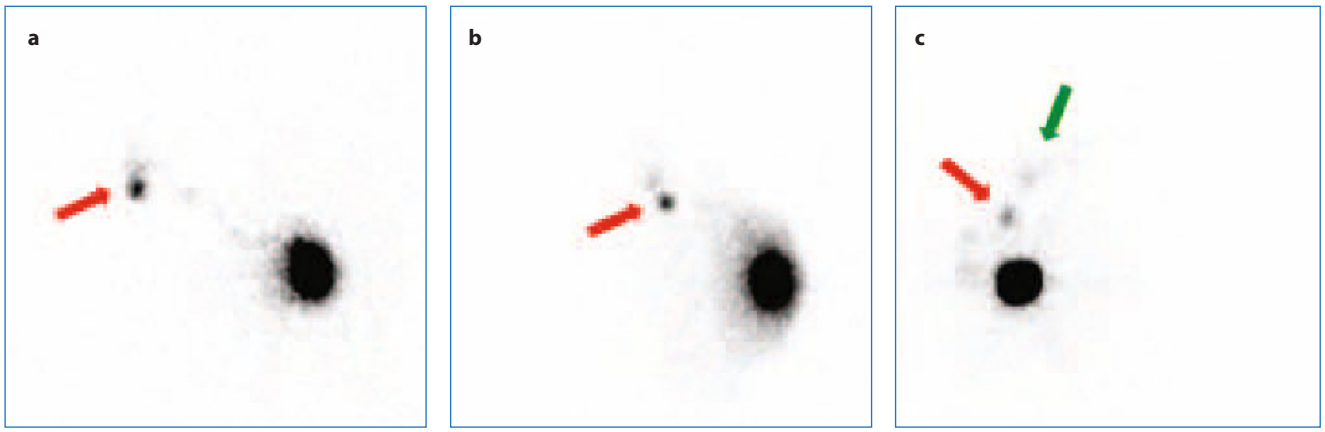

Fig. 9.3 Planar lymphoscintigraphy of a patient with cancer in the upper external quadrant of her right breast. After injecting 37 MBq of ^{99m}Tc-nanocolloid intradermally, the right anterior oblique view (**a**) and the lateral view (**b**) show a single lymphatic vessel leading to a single axillary SLN (*red arrow*). The anterior view (**c**, acquired at a later time) confirms the presence of a single SLN (*red arrow*), with subsequent visualization of higher-tier nodes (*green arrow*)

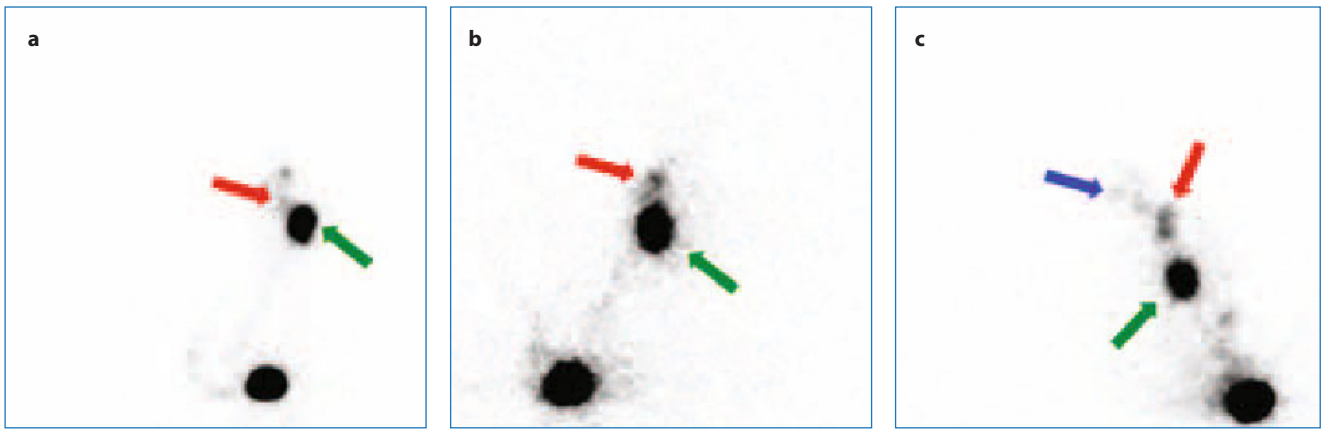

Fig. 9.4 Lymphoscintigraphy of a patient with cancer in the upper external quadrant of her left breast. After injecting 37 MBq of ^{99m}Tc-nanocolloid intradermally, the left anterior oblique view (**a**) and the left lateral view (**b**) show two separate lymphatic channels leading to two separate axillary SLNs (*green arrow* and *red arrow*, respectively, the latter more deeply located). The anterior view (**c**, acquired at a later time point) shows subsequent visualization of higher-tier node (*blue arrow*)

In order to identify all SLNs and to avoid confusion with radiocolloid stasis in a lymphatic vessel, images are acquired with an adequate delay after injection. This delay may vary according to the radiopharmaceutical used, injection site, and patient's characteristics (lymphatic drainage can be slower in elderly or overweight patients). With planar scintigraphy, combining two views may help to prevent some SLNs from being missed.

Lymphoscintigraphy frequently identifies atypical/unexpected patterns of lymphatic drainage. Drainage to the internal mammary basin occurs in 20% of patients after intratumoral or peritumoral radiocolloid injection [9]. Other unusually located SLNs are also seen in a non-negligible fraction of patients: intramammary (prepectoral) in 6%, interpectoral in 2%, and infraclavicular (axilla level III) in 3% [47].

The advent of SPECT/CT reinforces the potential of preoperative scintigraphy [48, 49]. Low-dose CT is sufficient to

Fig. 9.5 Lymphoscintigraphy of a patient with cancer in the upper inner quadrant of her right breast. After injecting 37 MBq of ^{99m}Tc-nanocolloid intradermally, the anterior view shows two separate lymphatics leading respectively to an axillary SLN (*green arrow*) and to an internal mammary SLN in the right parasternal space (*red arrow*). Migration to higher-tier lymph nodes is also visualized (*blue arrow*)

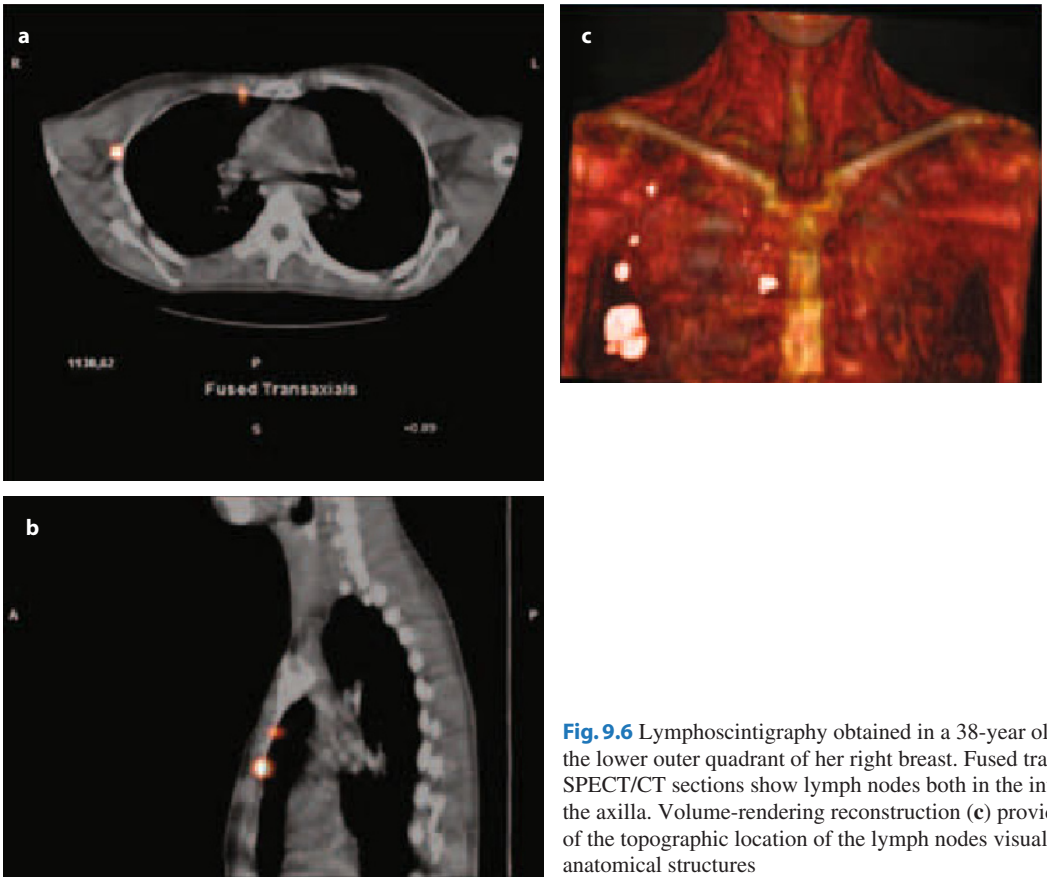

Fig. 9.6 Lymphoscintigraphy obtained in a 38-year old woman with cancer in the lower outer quadrant of her right breast. Fused transaxial (**a**) and sagittal (**b**) SPECT/CT sections show lymph nodes both in the internal mammary chain and in the axilla. Volume-rendering reconstruction (**c**) provides a more accurate overview of the topographic location of the lymph nodes visualized with respect to other anatomical structures

pinpoint atypically located sentinel nodes. SPECT/CT can also detect hot lymph nodes possibly missed by planar imaging because of the shine-through effect from the injection site, or in overweight patients [48, 50].

Thus, SPECT/CT can be useful when planar imaging is negative or ambiguous, or shows unexpected drainage patterns (Figs. 9.6-9.10).

9.5 Contribution of SPECT/CT

With the new generation of large-field-of-view gamma cameras, hybrid SPECT/CT has been incorporated in the sentinel node procedure. The functional information provided by SPECT can be combined with the morphological information provided by CT, by employing such hybrid imaging in a single session. The fused SPECT/CT images depict the SLNs (visualized by lymphoscintigraphy) in an anatomical landscape, thus providing additional helpful roadmaps for surgeons. In recent years, SPECT/CT has been used in patients with breast cancer with unusual or complex drainage, such as lymphatic drainage outside the axilla [51]. SPECT/CT may also visualize SLNs within the axilla when no nodes are visualized by planar imaging.

SPECT/CT is principally oriented to the anatomical localization of SLNs, by acquiring a low-dose CT. In fact, the use of a diagnostic high-dose CT, with or without intravenous contrast, is in principle not necessary because the SLN procedure primarily aims at detecting subclinical metastasis in normal-sized lymph nodes. Nevertheless, for sentinel node localization, the CT component of SPECT/CT must provide optimal anatomical information. For superficial areas such as the axilla, 5 mm slices are recommended. The CT component is also used to correct the SPECT signal for tissue attenuation and scattering. After these corrections, SPECT is fused with CT [51]. A gray scale is used to display the anatomic information in the background image (CT), whereas a color scale is used to depict lymphoscintigraphic mapping in the foreground image (SPECT).

The display of SPECT/CT is similar to that of conventional tomography. Multiplanar reconstruction (MPR) enables two-dimensional (2D) display of fusion images in relation to CT and SPECT. The use of cross-reference lines allows navigation between axial, coronal, and sagittal views.

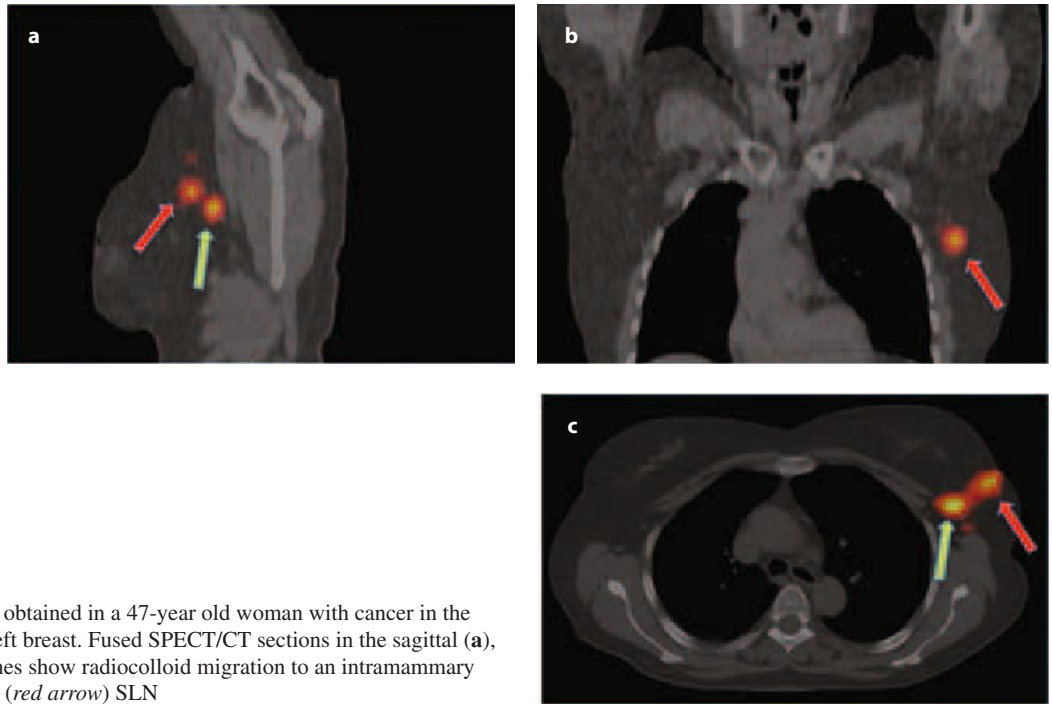

Fig. 9.7 Lymphoscintigraphy obtained in a 47-year old woman with cancer in the lower inner quadrant of her left breast. Fused SPECT/CT sections in the sagittal (**a**), coronal (**b**), and axial (**c**) planes show radiocolloid migration to an intramammary (*green arrow*) and an axillary (*red arrow*) SLN

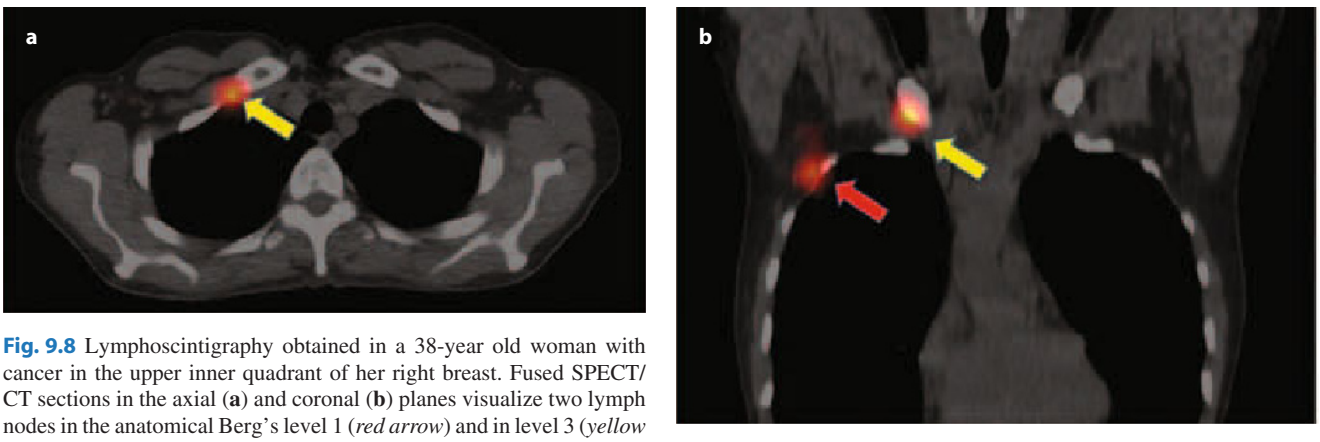

Fig. 9.8 Lymphoscintigraphy obtained in a 38-year old woman with cancer in the upper inner quadrant of her right breast. Fused SPECT/CT sections in the axial (**a**) and coronal (**b**) planes visualize two lymph nodes in the anatomical Berg's level 1 (*red arrow*) and in level 3 (*yellow arrow*), respectively

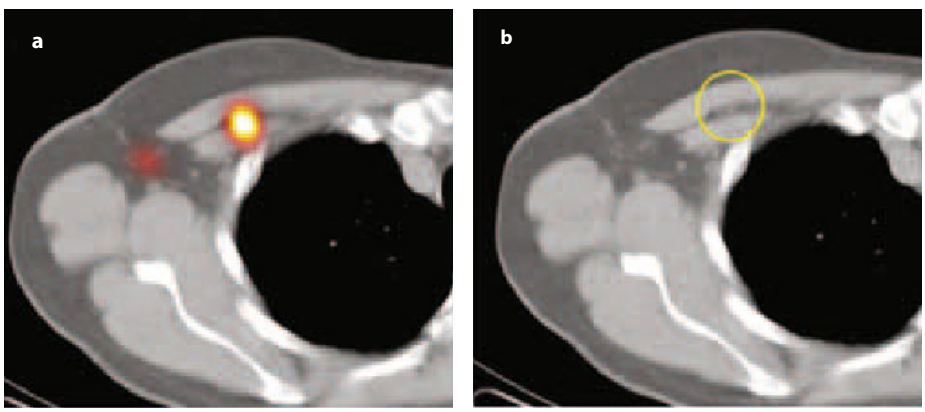

Fig. 9.9 Lymphoscintigraphy obtained in a 52-year-old woman with cancer in the upper inner quadrant of her right breast. **a** Axial fused SPECT/CT section showing a SLN between the pectoral muscles. **b** This sentinel node can be identified as the single lymph node visible in the corresponding CT section (*yellow circle*); images supplied by courtesy of Renato A. Valdés Olmos and Sergi Vidal-Sicart

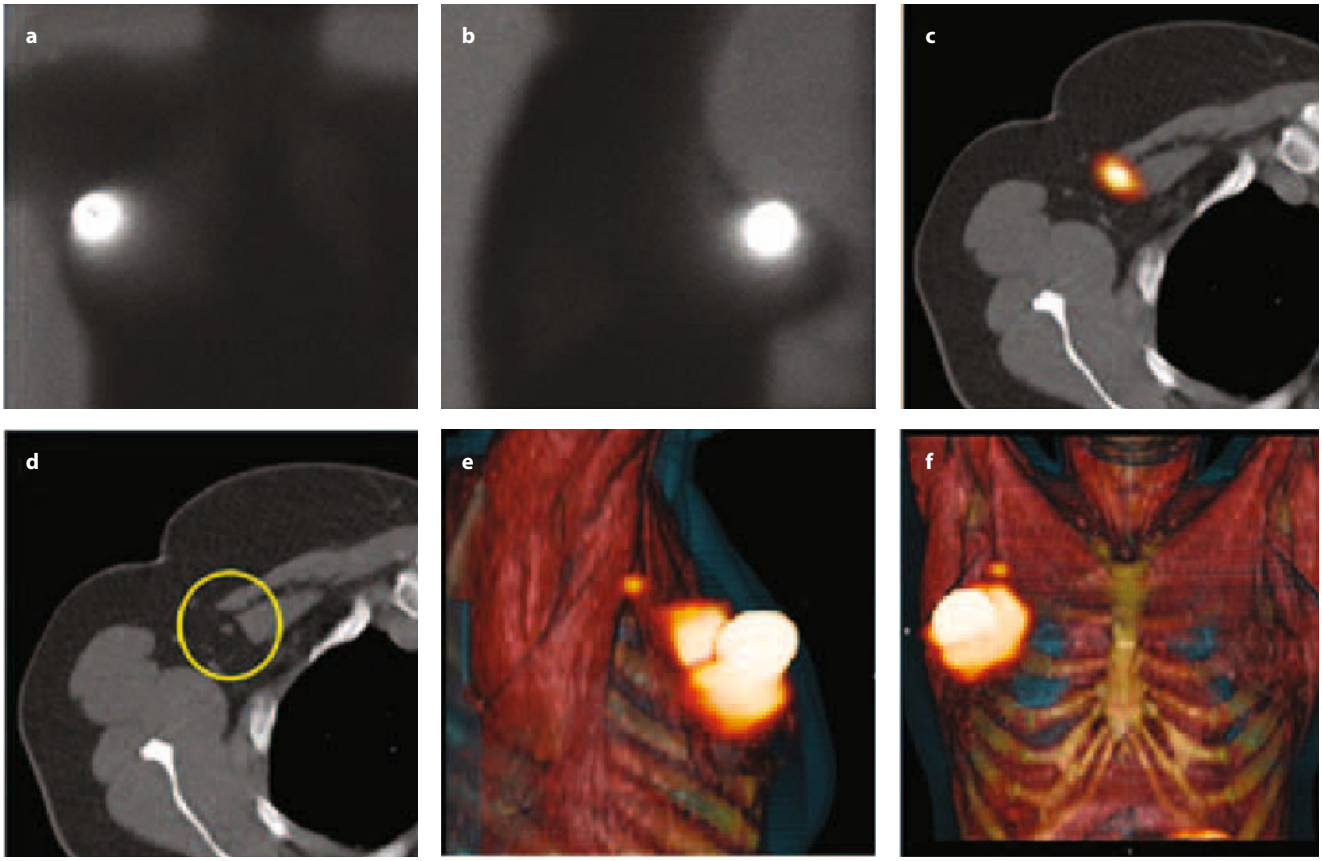

Fig. 9.10 Anterior (**a**) and lateral (**b**) planar lymphoscintigraphic images showing no drainage from the site of ^{99m}Tc-nanocolloid injection. By contrast, in the axial fused SPECT/CT section (**c**) a SLN, corresponding to the lymph node visibile in the CT section (*yellow circle* in **d**), is clearly detected at the border of the pectoral muscle. This SLN is displayed using 3D volume rendering for better anatomical recognition (**e**, **f**); images supplied by courtesy of Renato A. Valdés Olmos and Sergi Vidal-Sicart

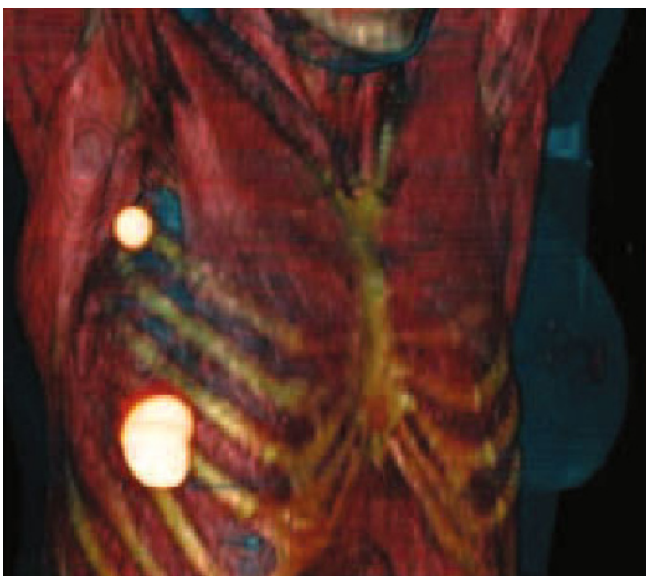

Fig. 9.11 SPECT/CT with volume rendering for 3D display, showing a SLN in the right axilla; image supplied by courtesy of Renato A. Valdés Olmos and Sergi Vidal-Sicart

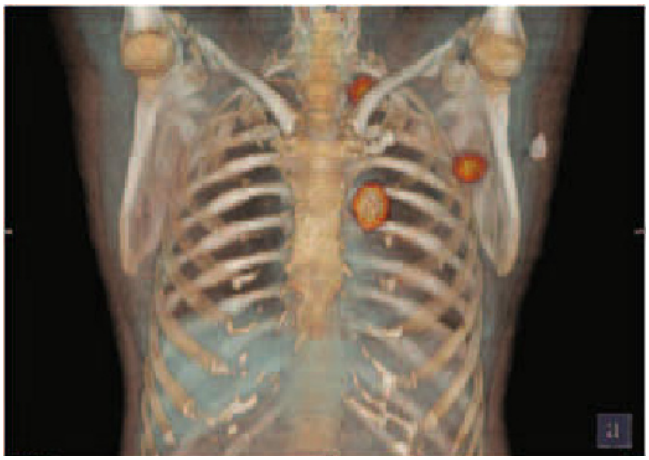

Fig. 9.12 SPECT/CT with volume rendering for 3D display showing an axillary SLN (level I) in the left axilla, an internal mammary SLN in the second left intercostal space, and an ipsilateral infraclavicular lymph node (level III)

At the same time, this procedure enables correlation of radioactive sentinel nodes seen on fused SPECT/CT images with lymph nodes seen on the CT portion. This information may be helpful for the intraoperative procedure, as well as for post-excision control using portable gamma cameras or probes.

Fused SPECT/CT images may also be displayed using maximum intensity projection (MIP). This tool enables three-dimensional (3D) display by adding various slices, thus improving anatomical localization of SLNs, and, in turn, their intraoperative identification by the surgeon.

When using volume rendering for 3D display, different colors are assigned to anatomical structures such as muscle, bone, and skin. This leads to better identification of anatomical reference points and incorporation of an additional dimension in the recognition of sentinel nodes (Figs. 9.11-9.12).

In general, indications for SPECT/CT evaluation in breast SLN procedures include: (a) cases without SLN visualization in the planar images [51], since the possibility of correcting for tissue attenuation provided by SPECT/CT enhances sensitivity with respect to planar imaging (and may therefore be particularly useful in obese patients); (b) localization of SLNs in areas with complex anatomy; or (c) in cases with unexpected lymphatic drainage (e.g., between the pectoral muscles, internal mammary chain, level II or III of the axilla) at planar imaging.

Nevertheless, SPECT/CT imaging must be considered as complementary and not alternative to planar lymphoscintigraphy. In fact, SPECT/CT is most frequently employed to anatomically localize SLNs already visualized on planar imaging, although in some cases it may detect additional SLNs.

9.6 Intraoperative Detection

After positioning the patient on the operating table before starting the surgical procedure, location of the SLN(s) should be confirmed further by external counting with the gamma probe. Minor variations in the sequence of operating procedures exist: some surgeons remove the primary tumor first and then proceed to perform SLNB, whereas other surgeons perform SLNB first and then proceed to remove the tumor while waiting for the results of intraoperative frozen section histopathology.

In most recent reports, the overall success rate of lymphoscintigraphy in SLN identification is very high, at around 97%. The vital blue dye technique has a much lower success rate when used alone (mostly around 75–80%), while it marginally improves radioguided identification of the SLN. Nevertheless, the vital blue dye technique can usefully complement the radioguided procedure to reach a combined success rate of 98–99%, especially when the SLN is diffusely metastatic (therefore, its capacity to retain the radiocolloid is impaired). Many surgeons combine the two techniques, using the blue dye in the lymphatics as a roadmap helping to find the radioactive sentinel node, especially when a noninvolved lymph node is only few millimeters in diameter and very soft to palpation. A gamma-probe-guided search of the SLN is based on detecting a focal spot of radioactivity accumulation in the area of interest (open surgical field). The probe is now in direct contact with the hot spot and is adequately shielded from radiation scattered from the injection site.

Thus, counting rates change almost instantly from tens or hundreds of counts per second to nearly zero (as the patient's background virtually corresponds to room background) when moving the detector – for instance, simply changing the angle – from the hot spot (lymph node) to nearby tissues. Therefore, the concept of target-to-background ratio as commonly used for nuclear medicine procedures in vivo takes on a new meaning; typically, the ratio of counts in the hot spot relative to background is in the range of 10–100, though with wide variations depending on the activity injected, type of radiocolloid injected, time elapsed between radiocolloid injection and surgery, and type of gamma probe used.

Re-examination of the operative site should then be performed, to ensure that the area of focal radioactivity accumulation has been removed and that a second node is not also active; if this is the case, this lymph node should also be removed and the axilla re-examined until no further areas of focal radioactivity accumulation are found. Complete removal of the sentinel node(s) is confirmed by reduction of the count rate in the axilla to background levels. Intraoperative frozen section histopathology is performed on the lymph node with the highest count rate, as well as on any additional lymph nodes with count rates at least 10% or 20% of the count rate in the hottest node [6, 52, 53].

9.6.1 Combining Existing Technologies with New Modalities

As mentioned earlier, the recent SPECT/CT technology has been fully integrated in the preoperative approach for a better anatomical baseline and more accurate SLN or lesion depiction, and for decision-making during surgery. Intraoperative surgical guidance, even when taking into account the information provided by SPECT/CT, is achieved by conventional hand-held gamma probes, and, more recently, with portable gamma cameras. This interaction between technologies permits refinement of the methodology and further improvement of the results of radioguided surgery

Nowadays, there are new possibilities to explore for possible integration in this procedure. One of them is the free-hand SPECT-based device that integrates a positioning system attached to the conventional gamma probe and permits a virtual reconstruction in a 3D environment [54]. This 3D information may be further used for precise localization and targeting of radioactive SLNs, thus implementing a radioguided navigation system. The device can ensure permanent assistance and transparent documentation of soft tissue removal during the intervention.

On the other hand, the possibility of combining the current radiotracers with other agents opens new avenues for further developments. In this regard, a nanocolloidal radiopharmaceutical has been combined with indocyanine green (ICG), a fluorescent agent for SLN detection in robot-assisted lymphadenectomy [55]. In contrast to single-fluorescent agents [56], this bimodal tracer procedure may allow surgeons to integrate the standard approach based on radioguided detection with a portable gamma camera with a new optical modality based on fluorescent signal detection. This approach is being successfully applied in various malignancies. For all these new modalities of intraoperative imaging, preoperative SPECT/CT imaging remains essential and is the starting point for surgical planning.

9.7 Internal Mammary Chain

Although, like the axilla, the internal mammary lymph nodes (IMNs) are a first-echelon nodal drainage site, the importance of their treatment in breast cancer has long been debated. "Seminal" randomized trials have failed to demonstrate a survival benefit from surgical IMN treatment, and several retrospective studies have shown that IMNs are rarely the first site of recurrence [57–60].

However, the recent widespread diffusion of SLNB has stimulated a critical reappraisal of such early results, also considering the higher proportion of screening-detected cancers, improved imaging (i.e., lymphoscintigraphy for radioguided SLNB, which makes it possible to visualize lymphatic drainage to the IMNs), and the virtually systematic application of adjuvant systemic therapy. Recently, the positive results of the Danish and British Columbia trials of post-mastectomy radiation therapy [61–63], as well as the results of the Early Breast Cancer Trialists' Collaborative Group (EBCTCG) meta-analysis [64], established the importance of locoregional control for long-term survival. These demonstrations have led to renewed interest in IMN treatment in the current management of breast cancer. The controversy lies in the facts that: (a) there are no published results from clinical trials formally testing the value of IMN irradiation; (b) there have been several negative trials testing the value of IMN surgery; and (c) there are concerns about the potential added cardiac toxicity from IMN irradiation.

Other recent studies have also led to renewed interest in IMN staging, particularly regarding its implications for systemic therapy. Several studies have consistently found that medial breast cancers carry a worse prognosis compared with lateral cancers, even after adjusting for other known prognostic factors [65, 66]. Since there is no plausible evidence that medial tumors are more biologically aggressive, it is likely that the worse outcome is the result of understaging, possibly resulting undertreatment of patients with IMN metastasis, which is more common in medial cancers [65–70]. Therefore, the development of SLNB aided by lymphoscintigraphy, providing a less invasive method of assessing the IMN lymph nodes than surgical dissection, may affect decisions regarding not only locoregional treatment, but also systemic therapy.

9.7.1 Lymphatic Drainage to the Internal Mammary Chain

At present, lymphoscintigraphy is almost invariably used to visualize the pattern of lymphatic drainage before SLNB, but studies using different techniques have shown different results. It is clear that superficial injection of the radiocolloid into the subareolar area or dermis over the tumor have a very low chance of showing lymphatic drainage to the internal mammary chain [44, 71–78].

In this regard, a recent anatomic study [30] shows that the deep lymphatic system of the breast drains to the axilla and also interacts with the "perforating system," which drains exclusively to the IMNs. The authors reported that the superficial system drains to the axilla, usually to a lymph node just behind the pectoralis minor muscle. In this regard, classical anatomic notions maintain that the deep system drains to the axilla and also interacts with the perforating system, which drains to the IMNs. Nevertheless, Suami et al. found that the perforating system does not interact with the superficial system [30]. Thus, the frequency of IMN drainage tends to reflect the method of lymphoscintigraphy, where peritumoral

(deep lymphatic system) injections have a much higher frequency of IMN drainage than subareolar or subdermal (superficial lymphatic system) injections. When the primary tumor lesions are medially and inferiorly located in the breast, the highest rate of sentinel IMN visualization will occur after peritumoral injections of the radiocolloid [79–83]. Approximately 15% of lateral tumors also drain to internal mammary lymph nodes [74, 77–85]. Up to 8% of patients had sentinel internal mammary lymph nodes but not axillary sentinel nodes on lymphoscintigraphy, whereas one in five patients with sentinel nodes in the axilla also had drainage to the IMN chain [77]. One additional factor that favours IMN visualization is the breast size. Krynyckyi et al. noted the relevant effect that breast size has on the rate of IMN visualization (besides depth of radiocolloid injection) [86]. In patients with small breasts, the IMN visualization rate was 46.2%; in those with medium-size breasts, 21.1%; and in those with large breasts, 0%. This could be explained by a proximity effect to the internal mammary chain nodes. The average lesion in the center of a large breast, and the injected perilesional (subtumoral) radioactivity, would be much farther from the chest wall and from the deeper lymphatic channels that drain to the parasternal sentinel IMNs than the average lesion in the center of a small breast, which would be much closer to these channels. The closer the injected activity to these channels, the higher the probability that injected radioactivity would reach the IMN connected to them [87].

Leppänen et al. have shown that there is a greater chance of detecting IMNs in patients who are younger and thinner (lower body mass index), as well in those with primary lesions lower in the breast, and when the lesion is nonpalpable [87]. Additional speculations have been put forward regarding factors that affect axillary lymph node visualization, such as increasing age; in particular, in postmenopausal patients, replacement of macrophage-type tissue by fat and/or decreased tissue turgor resulting in collapsed lymphatic vessels has been suggested as the mechanism of decreased visualization of axillary sentinel nodes [88].

9.7.2 Internal Mammary Node Positivity Rates

In studies where biopsy was performed for hot sentinel IMNs on lymphoscintigraphy, tumor cells have been detected at histopathology in 8–27% of patients, with about 7% having metastasis to the IMNS and not to the axillary nodes [76–82].

Several studies have documented the change in clinical management caused by the additional information provided by IMN biopsy [78–83, 89]. According to the latest version of the AJCC staging, positive IMN biopsies change the tumor stage. In some studies, a positive IMN biopsy led to the addition of chemotherapy for those patients with negative axillary lymph nodes, to omission of axillary dissection for those with an otherwise "failed" lymphoscintigraphy (no axillary sentinel node visualization), and to modification of radiation fields to encompass the IMN chain. These findings demonstrate that visualization of IMN drainage on lymphoscintigraphy, and biopsy of internal mammary sentinel nodes can potentially impact surgical, chemotherapeutic, and radiation treatment decisions.

9.8 Accuracy of Radioguided Sentinel Lymph Node Biopsy

In a single-institution randomized trial from Milan published in 2003 by Veronesi et al. [7], the authors investigated the predictive power of the SLN status, estimated as the fraction of patients with axillary metastatic involvement detected by SLNB compared to the fraction found by routine ALND. A total of 516 patients with breast tumors <2 cm were randomly assigned to undergo either SLNB and simultaneous ALND, or SLNB followed by ALND only in the event of a positive SLNB. SLN positivity was found in 32.3% of the patients in the ALND group and in 35.5% of the SLN group. In the ALND group, the overall accuracy, sensitivity, and specificity of SLNB were 96.9%, 91.2%, and 100%, respectively. The false-negative rate was 8.8% and the negative predictive value 95.4%. After a median follow up of 46 months, disease-free and overall survival rates were not significantly different between the two groups [7]. In a subsequent publication based on the same cohort of patients after a 95-month follow up [89], the axillary recurrence rate among patients with a negative sentinel node in the SLNB group was as low as 1.2% (2/167). Interestingly, a 4.6% rate would, in principle, have been expected based on the findings for the group with SLNB + routine ALND [90].

In a follow-up study by Veronesi et al. [91], 953 patients with negative SLNs, therefore not submitted to ALND, were followed up until 7 years post surgery (median follow up 38 months). A total of 55 unfavourable events were recorded, 37 of which (3.9% of the total population) related to the primary breast carcinoma. Only three cases of overt axillary metastases occurred, that is, in 0.31% of the total population; these patients received total axillary dissection and were alive and well at the time of last follow up. The 5-year overall survival rate of the whole series was 98%. It is noteworthy that, at long-term follow up, patients with negative SLNB not submitted to axillary dissection had a lower than expected rate of overt axillary metastasis.

In 2006, a meta-analysis based on 69 trials [14] evaluated a total of 8,059 patients with breast cancer submitted to SLNB with routine axillary dissection; 7,765 of these patients had successful SLN mapping (96% identification rate). This systematic review revealed a wide variation in test

performance: the proportion of patients who had successfully mapped SLNs ranged from 41% to 100%, with more than 50% of the studies reporting a rate below 90%. Lymph node involvement was found in 3,132 patients (42%), ranging from 17% to 74% across studies. The false-negative rate ranged from 0% to 29%, averaging 7.3% overall. Eleven trials (15.9%) reported a 0% false-negative rate, whereas 26 trials (37.7%) reported a false-negative rate above 10%. Significant inverse correlations were observed between the false-negative rate and both the number of patients studied ($r = –0.42$; $p < 0.01$) and the proportion of patients who had successfully mapped SLNs nodes ($r = –0.32$; $p = 0.009$).

The "Sentinella/GIVOM" trial (Gruppo Interdisciplinare Veneto di Oncologia Mammaria) included 749 women with a palpable tumor <3 cm. After a median follow up of 55.6 months, locoregional recurrence occurred in 16 patients of the SLNB group versus 3 in the ALND group. The 5-year relapse-free survival rate was actually slightly, although not significantly, lower in the SLNB group (87.6% versus 89.9%) [92].

The NSABP B-32 trial randomized 5,611 women to SLNB versus SLNB + ALND. The primary endpoint was overall survival, compared in patients with a negative SLN in both arms [21]. After a mean follow up of 95.6 months, 169 out of the 2,011 SLN-negative patients in the SLNB group and 140 out of 1,975 in the SLNB + ALND group had died. The 8-year overall survival rate was 90.3% in the SLNB arm versus 91.8% in the ALND arm [21].

The aim of a meta-analysis published in 2010 was to systematically appraise the outcome of SLNB when compared to ALND. Primary outcomes were nodal positivity and surgery-related morbidity. A total of 9,608 patients were identified from trials comparing ALND and SLNB. The overall rate of axillary lymph node positivity for those with no clinically palpable nodes was 28.8% for ALND and 27.6% for SLNB, though there was a trend for greater detection of metastatic disease with SLNB compared to ALND alone. Patients who underwent SLNB were significantly less likely to suffer from postoperative morbidity relative to ALND (risk of infection, seroma, arm swelling, and numbness). The conclusion of this meta-analysis was that SLNB is the optimum approach in terms of morbidity for the assessment of axillary metastasis in clinically node-negative breast cancer [93].

The false-negative rate is the safety parameter of SLNB. The strongest predictor of the false-negative rate (the proportion of ALND-positive cases with a negative SLN) across trials appears to be the proportion of patients for whom lymphatic mapping is successful (identification rate) [14]. The American Society of Breast Surgeons recommends a minimum rate of of SLN identification of 85%, with a false-negative rate of 5% or less in order to definitely adopt SLNB in place of ALND. These recommendations also maintain that performing a minimum of 20 SLNB procedures in combination with ALND or with mentoring is necessary to minimize the risk of false-negative results [94].

However, recent results from large multi-institutional trials [21, 92, 94] showed that all have achieved excellent identification rates, ranging from 93.5% to 97.2%, but that none achieved a false-negative rate lower than 5%. The false-negative rate was 9.8% in the NSABP B-32 trial [21] and dramatically higher (16.7%, with a weighted average of 9.2%) in the "Sentinella/GIVOM" trial [93]. The identification rate may thus provide false reassurance about the overall quality of the SLNB procedure. The lowest false-negative rates were obtained in the two studies [95, 96] in which preoperative lymphoscintigraphy and combined blue dye mapping during surgery were required. Direct comparison of protocols between different studies is not possible, however, since they refer to different surgeons and different settings.

Some false-negative cases may result from massive metastatic involvement of the first relay node, an event that interferes with the uptake of both the radiocolloid and dye and diverts lymph flow to a lymph node other than the true sentinel node [97].

False-negative SLNB results might impair patients' outcomes for several reasons: missed metastatic lymph nodes might lead to axillary recurrence that is difficult to treat, metastatic lymph nodes left in the axilla are a potential source of distant metastases, and understaging affects decisions about systemic therapy and specific radiation therapy to the chest wall and nodal basins [2, 63].

Differentiating a true SLN from a second-echelon lymph node can be difficult. Furthermore, lymphatic channels from a certain tumor site can drain simultaneously to more than one SLN. Both the NSABP B-32 trial and the ALMANAC validation study showed the influence of the number of resected lymph nodes on the false-negative rate [21, 96]. In NSABP B-32, the false-negative rate was 17.7% if only one lymph node was resected, 10% if two were rescted, 6.9% if three were resected, 5.5% if four were resected, and 1% if five or more SLNs were resected [21].

Failure to visualize a SLN at lymphoscintigraphy predicts difficult intervention [98]. Negative lymphoscintigraphy also heralds a higher risk of axillary involvement [46, 49]. In one study, lymph node metastasis was found in 28.5% of patients with a visualized SLN versus 63.3% in cases of negative lymphoscintigraphy [46]. In cases of nonvisualization after peritumoral injection, some authors reinject the radiocolloid superficially. However, SLNs that appeared on imaging following such rescue injection were associated with a high false-negative rate (24%) [99]. Thus, when lymphoscintigraphy is negative even on delayed imaging, one should check for the presence of macrometastases by ultrasound before surgery. When no SLN is identified at surgery, ALND should be performed [2, 9].

9.9 Long-term Outcome of Sentinel Lymph Node Biopsy

A number of small retrospective studies have reported excellent results of SLNB alone, with long-term follow up. A study by Wernicke et al. of 265 patients with tumor-free sentinel node, treated with breast-conserving surgery, revealed a 10-year progression-free survival of 88.2% in those patients treated with SLNB alone, with a 0% axillary recurrence in these sentinel-node-tumor-free patients [100]. In the very first study of SLNB alone, Giuliano reported no axillary recurrence at 33 months' median follow up [17]. To date, over 15 years later, none have still been seen.

Another large study was recently reported, of patients from the same institution treated from 1995 to 2002 with SLNB alone, who had H&E tumor-free sentinel nodes [101]. A total of 811 patients with a median follow up of 103 months showed only 2 (0.2%) isolated axillary recurrences; 4.9% of patients had in-breast recurrences; and 0.5% of patients had local and regional recurrences. The median time to recurrence in this study was 57 months, with 5- and 10-year disease-free survival of 95% and 90% respectively. As expected, patients were more likely to have disease recurrence with high-grade tumors and were more likely to die if they were older and had large tumor size.

A 10-year study from Milan of histopathologically node-negative patients treated with SLNB alone compared to those treated with SLNB plus ALND showed similar results [90]. A total of 516 patients were studied. In the ALND arm, eight patients were found to have false-negative sentinel nodes and subsequent tumor-involved nodes at axillary dissection. However, at 8 years, only two cases in the SLNB-alone arm revealed overt axillary metastases. Overall survival was slightly greater in the SLNB-alone arm. The research group concluded that preservation of healthy lymph nodes may have beneficial consequences, and axillary dissection should not be performed in patients with tumor-free sentinel nodes.

The ACOSOG recently reported long-term results of Z0010 [102]. This study of patients with T1 and T2 clinically node-negative breast cancer planned for lumpectomy and whole-breast irradiation included 3,904 patients with H&E-negative sentinel nodes who had no axillary treatment. At a median follow up of 8.4 years, there were only 0.5% regional recurrences, 3.3% local recurrences, and 3.4% distant recurrences [103]. Factors associated with locoregional recurrence were estrogen-receptor negativity and younger age. Locoregional recurrence was less often seen in patients with hormone receptor-positive tumors and those who received chemotherapy.

While long-term studies are few, a large number of patients have now been followed over 10 years, and the long-term survival and recurrence results of SLNB alone for women who are node negative appear excellent. Very few axillary recurrences have been noted, and survival is as good as with ALND. Long-term complications have not been reported from many studies. Wernicke et al. reported chronic lymphedema rates of 4.6% among patients treated with SLNB alone compared to 34.8% of those treated with ALND [100].

Z0011, a recent study of the ACOSOG group, was a prospective randomized trial of patients with H&E-detectable metastases in the sentinel node, who were treated with either no further axillary surgery or complete axillary dissection. In this study, there were 446 women in the SLNB-alone group and 445 women in the complete ALND group. No third-field radiotherapy was permitted. At a median follow up of 6.3 years, 5-year overall survival in the group receiving SLNB alone was 92.5%, while in the group receiving SLNB plus ALND it was 91.8% [102]. This randomized prospective study has altered the management of breast cancer at major centers throughout the United States and Europe. Patients with early metastatic breast cancer and sentinel node metastases who have limited axillary disease found at operation may be spared the morbidity of ALND, further increasing the role of SLNB in the management of early breast cancer.

Of biologic interest, 27% of the patients in the ALND group had residual non-SLN metastases removed with ALND. Since this was a prospective randomized study, approximately 27% of the patients in the SLNB-alone group had non-SLN metastases left in place. Presumably, this was treated either by the adjuvant systemic therapy (which was given to nearly all patients in the study) or by whole-breast irradiation therapy (which would irradiate the lower axilla). More interestingly, perhaps the biology of breast cancer is such that axillary metastases do not always become clinically relevant. This observation confirms the findings of NSABP B-04, a study performed in the 1970s, in which patients with clinically negative nodes were randomized to radical mastectomy, total mastectomy with chest wall and nodal irradiation, or total mastectomy alone with no axillary treatment [104]. In this group, the axillary recurrence rate in the group that had total mastectomy alone (with no axillary treatment) was approximately half of the expected rate from the prevalence of metastases in the group that had radical mastectomy, in whom axillary contents were removed and examined. This study was performed without the use of adjuvant systemic therapy, suggesting that there are biologic factors that may determine the clinical growth of axillary metastases. Long-term results of SLNB for patients with limited axillary metastases show a very low rate of regional failure, excellent survival, and less morbidity than for ALND. In addition, patients with early sentinel node metastases should be given the option of omitting ALND and third-field irradiation from their management.

Acceptable	Not recommended
T1 or T2 tumors	T3 or T4 tumors
Multicentric tumors	Inflammatory breast cancer
Ductal carcinoma in situ with mastectomy	Ductal carcinoma in situ without mastectomy (not recommended except for large tumors [>5 cm] on core biopsy, or with suspected or proven microinvasion)
Older age	Suspicious, palpable axillary lymph nodes
Obesity	Pregnancy
Male breast cancer	Prior axillary surgery
Evaluation of internal mammary lymph nodes	Prior nononcologic breast surgery (reduction or augmentation mammoplasty, breast reconstruction, etc.)
Prior diagnostic or excisional breast biopsy	After preoperative systemic therapy
Before preoperative systemic therapy	

Table 9.1 American Society of Clinical Oncology guidelines for sentinel lymph node biopsy in breast cancer; adapted from [9]

9.10 Indications and Contraindications for Sentinel Lymph Node Biopsy

Lymphoscintigraphic SLN localization should be considered in women who have a biopsy-proven carcinoma of the breast in whom definitive surgery and axillary node clearance is planned, and in whom there are no palpable axillary lymph nodes [10].

The recommendations of the expert panel of the ASCO in 2005 [9] (Table 9.1) are followed in the treatment of early breast cancer. Consensus meetings, both national and international, have confirmed these indications and contraindications, although the emergence of molecular biology and new techniques in imaging and histopathology pose new challenges in SLNB [23, 105].

Several meta-analyses and guidelines have been presented on the use of SLNB after neoadjuvant therapy and in the case of micrometastases. In 2010, an international expert consensus on the current recommendations of locoregional treatment in breast cancer issued several recommendations regarding the assessment of axillary lymph nodes [106].

Based on available literature, the ASCO guidelines also concluded that SLNB is not recommended for large or locally advanced invasive breast cancers (T3 and T4), for inflammatory breast cancer, for ductal carcinoma in situ, when breast-conserving surgery is planned, after preoperative systemic therapy during pregnancy, in the setting of prior nononcologic breast surgery or axillary surgery, and in the presence of suspicious palpable axillary lymph nodes. SLNB is instead recommended for smaller tumors (T1 and T2), multicentric tumors, ductal carcinoma in situ when mastectomy or immediate reconstruction is planned, for older or obese patients, in male patients with breast cancer, and also in patients who have already submitted to prior excisional or diagnostic biopsy (Table 9.1).

9.11 Controversial Indications

Some authors consider that previous plastic surgery does not contraindicate SLNB. In this regard, although plastic surgery with breast augmentation or reduction involves major tissue disruptions, the SLN is identified irrespective of the technique used [107]. Current data indicate that SLNB should be considered as standard in patients who have undergone previous breast surgery, with accuracy comparable to the results obtained in the general population of patients with breast cancer [107]. Indeed, lymphatic drainage is changed in patients who have undergone prior procedures, as nonaxillary drainage has been identified more often in reoperative SLNB than in primary SLNB. In 73% of patients, radiocolloid migration to the regional draining lymphatic basins has been noted in the ipsilateral axillary, supraclavicular, internal mammary, interpectoral, and contralateral axillary lymph nodes [108].

Multifocal breast cancer is defined as separate foci of ductal carcinoma more than 2 cm apart within the same quadrant, while multicentric breast cancer indicates the presence of separate independent foci of carcinoma in different quadrants [109]. Until recently, SLNB was contraindicated in patients with multicentric and multifocal breast cancer, because it was believed that it would be difficult to localize the true SLN; therefore, a negative SLNB would not exclude the possibility of metastasis in lymph nodes draining from other regions of the breast. However, some investigators consider that most of the breast can be considered as a single unit with lymph drainage to only a few designated lymph nodes in the axilla [110, 111].

Many studies have demonstrated an accuracy of SLNB in patients with multicentric/multifocal cancer equal to that in patients with unicentric breast cancer. The presence of lymph node metastasis is significantly higher in SLNs as well as in

non-SLNs in patients with multicentric breast cancer; however, the sensitivity, false-negative rate, and overall accuracy of SLNB are similar in both situations, although there are discordant results among groups [112, 113].

Debate is ongoing as to whether SLNB is accurate enough after neoadjuvant chemotherapy in patients with locally advanced breast cancer, or whether it should be performed before starting chemotherapy. To perform SLNB before or after primary systemic treatment has advantages and disadvantages in either circumstance. Before neoadjuvant chemotherapy (accepted in the ASCO guidelines), SLNB provides a more precise axillary staging, with more information about the nodal spread. However, performing the procedure can delay the beginning of treatment, and two operations may be needed. On the other hand, SLNB performed after neoadjuvant chemotherapy can assess the response at lymphatic level, but may lead to underestimation of the initial stage [114].

After neoadjuvant chemotherapy, the SLN detection rate decreases and the false-negative rate increases, while the long-term local recurrence rate in patients in whom lymphadenectomy has not been performed has yet to be determined. This group of patients was previously regarded as ineligible for SLNB, considering that the preoperative lymph-drainage pattern visualized after neoadjuvant chemotherapy might not represent the pattern in the tumor basin before chemotherapy, therefore possibly leading to false-negative results. In this regard, available data show that there are no significant differences in the success rate of SLNB according to clinical tumor size or clinical nodal status, and that the false-negative rate is not affected by the tumor response to chemotherapy. Recently, a systematic review was undertaken of 24 clinical SLNB trials in patients with breast carcinoma, after neoadjuvant chemotherapy. Metastatic SLN involvement was found in 37% of the patients, with a global SLN identification rate of 89.6% and an overall false-negative rate of 8.4% [115, 116]; these performance parameters are similar to those observed in patients with early breast cancer, not submitted to neoadjuvant chemotherapy.

Until a few years ago, pregnancy was considered a contraindication to perform SLNB; however, the dose of radiation involved in the procedure is very low, and the benefit should be considered in those patients presenting with early lesions. The possibility of performing a one-day procedure with a low radioactivity should be considered for pregnant patients with early lesions and clinically/ultrasound-negative axillae. Available data indicate that SLNB can be applied safely and successfully in pregnant women with breast cancer, with minimal risk to the fetus [117, 118]. The radiation exposure of the fetus deriving from radiocolloid interstitial administration is very low and does not increase the risk of prenatal death, congenital malformation, or mental impairment. On the other hand, blue dyes should not be used in patients who are pregnant [10].

Finally, some conditions that were previously considered as formal contraindications to SLNB have changed to possible applications for some expert panels, based on a patient-to-patient evaluation [23, 106]. These include: large or locally advanced invasive breast cancers (T3), in situ ductal carcinoma, prior nononcologic breast surgery or axillary surgery, and the presence of suspicious palpable axillary lymph nodes.

9.12 Certification for Sentinel Lymph Node Biopsy in Patients with Breast Cancer

In 2005, guidelines from ASCO stressed that appropriate training in the procedure of radioguided SLNB and issues of quality control are very important [9]. In this regard, the SLNB procedure is very much a team effort, with active skilled involvement of multiple disciplines including surgery, nuclear medicine, medical physics, pathology, radiology, nursing, and pharmacy, among others. In addition to the individual training and experience required for all team members, achieving optimal results with SLNB requires the integrated and highly coordinated effort that derives from experience and frequent application of the procedure [9].

Clinical Cases

Case 9.1
Sentinel Node Mapping in Breast Cancer: Drainage to Axillary Nodes After Periareolar Injection (Planar Imaging)

Giuseppe Rubini and Maria Antonia Renna

Background Clinical Case

A 40-year-old woman with a focal mass detected by ultrasound and localized in the lower internal quadrant of the right breast underwent mammography spot compression, which confirmed the presence of an oval circumscribed mass in the same quadrant. The patient was submitted to lymphoscintigraphy for biopsy of the sentinel lymph node after core biopsy had demonstrated invasive ductal carcinoma.

Lymphoscintigraphy

The day before surgery, lymphoscintigraphy was performed following intradermal periareolar injection of 0.4 mL of 42 MBq ^{99m}Tc-albumin nanocolloid (divided into four aliquots) in the right breast. A dual-detector SPECT gamma camera (Infinia Hawkeye GE Healthcare, Milwaukee, WI) equipped with low-energy high-resolution (LEHR) collimators was used to obtain right axillary and thoracic planar images 40 min after radiopharmaceutical injection. Planar images were acquired in anteroposterior and lateral projection, with a 128×128 matrix and zoom factor 1.00.

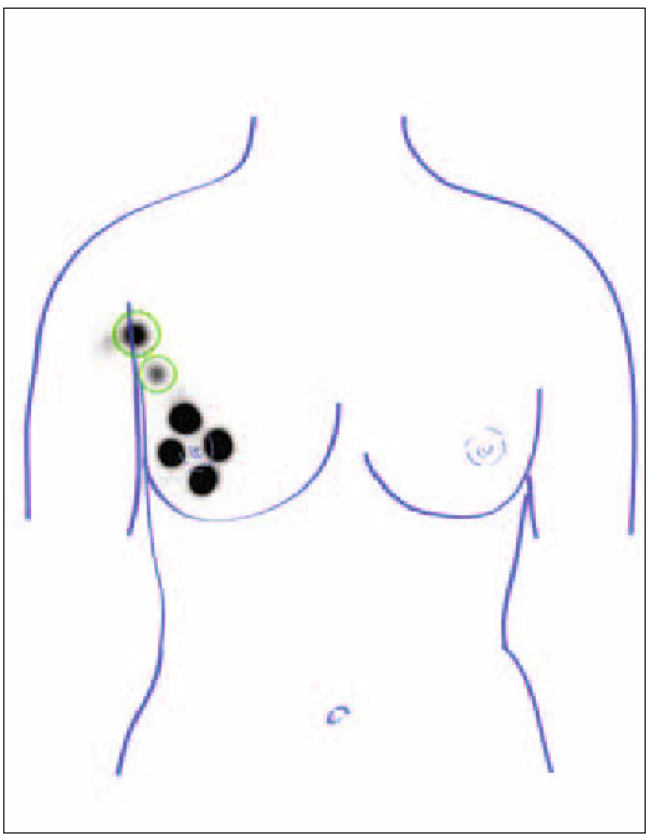

Fig. 1 Anterior view shows a single lymphatic vessel leading to a sentinel lymph node (*lower green circle*) with serial visualization of a subsequent-tier node (*upper green circle*)

Case 9.2
Sentinel Node Mapping in Breast Cancer: Drainage to Multiple Axillary Nodes After Intradermal Injection (Planar Imaging)

Lucio Mango and Guido Ventroni

Background Clinical Case

A 60-year-old woman with of 1.5-cm palpable mass located in the upper central quadrant of the left breast, positive for carcinoma (C5) by FNAB, underwent lymphoscintigraphy for sentinel node biopsy, after biopsy had demonstrated ductal invasive carcinoma.

Lymphoscintigraphy

Lymphoscintigraphy was performed following intradermal injection of 0.2 mL of 50 MBq ^{99m}Tc-nanocolloid on the cutaneous projection of the tumor in the left breast. A dual-detector SPECT/CT gamma camera (Infinia Hawkeye 4, GE Healthcare, Milwaukee, WI) equipped with low-energy general purpose (LEGP) collimators was used to obtain left axillary and thoracic planar images. Planar images were acquired 15 min after injection of the tracer in anteroposterior, left anterior oblique and lateral projection (acquisition time 5 minutes, matrix 128×128 and zoom factor 1.33).

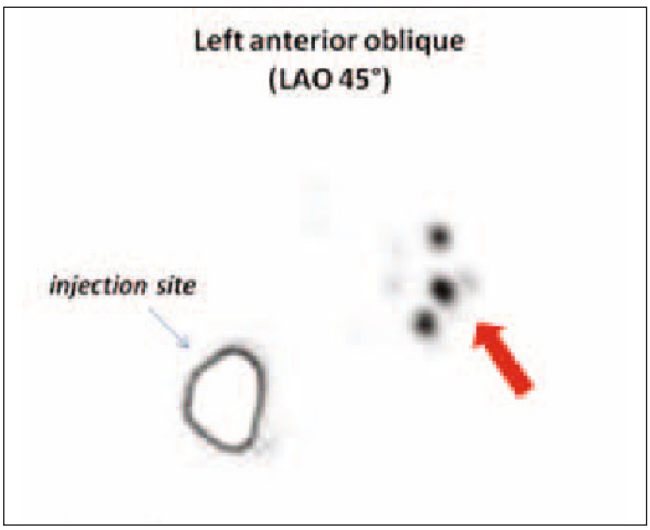

Fig. 1 Planar images in left anterior oblique projection show multiple axillary sentinel lymph nodes (*red arrow*). The injection site was covered with a lead shield to improve sentinel node visualization. During surgery, six nodes were correctly identified and removed. Histopathologic analysis of these lymph nodes using the one-step nucleic acid amplification (OSNA) technique revealed no metastases

Case 9.3
Sentinel Node Mapping in Breast Cancer: Drainage to Single Axillary Node After Intra-Peritumoral Injection (Planar Imaging)

Luciano Feggi, Chiara Peterle, Corrado Cittanti, Valentina de Cristofaro, Stefano Panareo, Ilaria Rambaldi, Virginia Rossetti, Ivan Santi, and Paolo Carcoforo

Background Clinical Case

A 54-year-old woman with a lesion in the upper outer quadrant of the right breast detected by mammography was referred for lymphoscintigraphy after needle core biopsy had demonstrated invasive lobular carcinoma.

Lymphoscintigraphy

In the afternoon before surgery, lymphoscintigraphy was performed following administration of 0.2 mL of 74 MBq ^{99m}Tc-nanocolloid, half intratumoral and half just a little outside the lesion. A dual-detector SPECT gamma camera (E-cam Siemens Medical Solutions, Hoffman Estates, IL) equipped with low-energy high-resolution (LEHR) collimators was used to obtain right axillary and thoracic planar images. Planar images were acquired 3 h after injection in anterior and right lateral projection (256×256 matrix, zoom factor 1.00, acquisition time 200 s for each view).

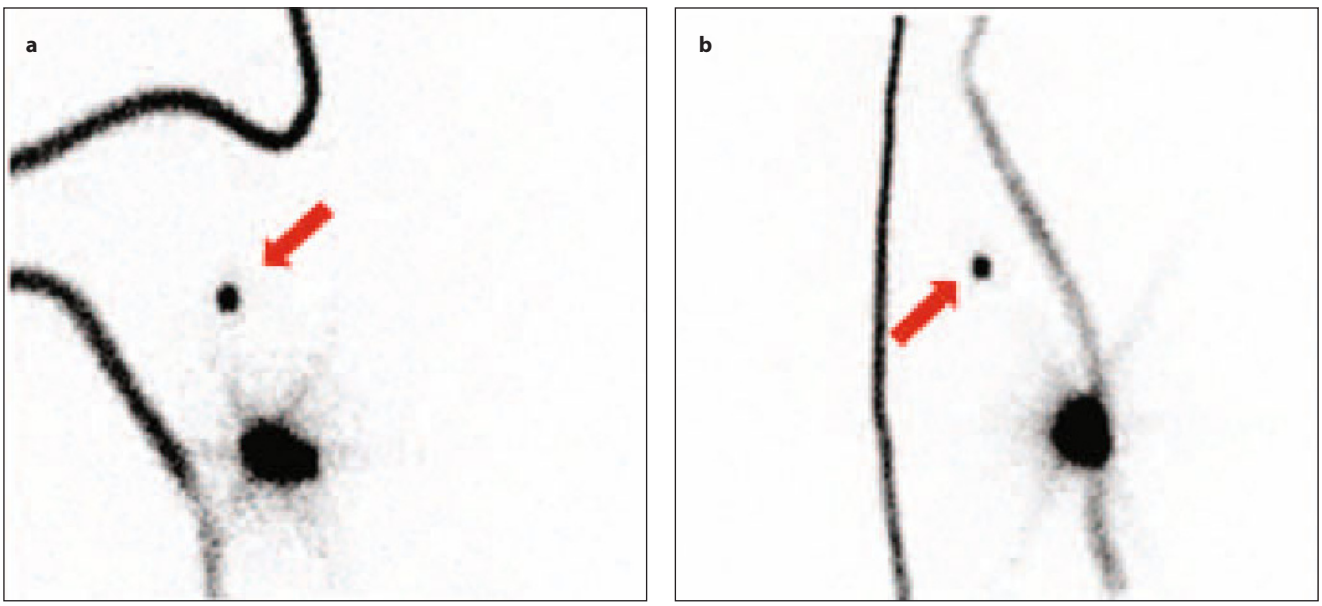

Fig. 1 Anterior (**a**) and lateral (**b**) views show a single right axillary sentinel lymph node (*red arrow*). The silhouette of the patient was drawn using two cobalt wires as landmarkers

Case 9.4
Sentinel Node Mapping in Breast Cancer: Drainage to Axillary Nodes After Intradermal Injection (Planar and SPECT/CT Imaging)

Gianpiero Manca, Manuel Tredici, Valerio Duce, Sara Mazzarri, and Giuliano Mariani

Background Clinical Case

A 64-year-old woman with a mass in the upper outer quadrant of the right breast detected at mammography was referred for radioguided biopsy of the sentinel lymph node after needle core biopsy had demonstrated an invasive breast cancer (T1N0 ductal carcinoma).

Lymphoscintigraphy

In the afternoon before surgery, lymphoscintigraphy was performed following intradermal injection of 0.3 mL of 37 MBq ^{99m}Tc-nanocolloid in the cutaneous projection of the tumor. A dual-detector SPECT/CT gamma camera (Discovery NM/CT 670 GE Healthcare, Milwaukee, WI) equipped with low-energy high-resolution (LEHR) collimators and multislice spiral CT was used to obtain right axillary and thoracic planar images as well as SPECT/CT acquisition. Planar images were acquired with a 128×128 matrix and zoom factor 1.33 (anterior, right lateral and 45° right anterior oblique views), while SPECT was acquired over 360° in the step-and-shoot mode (20 s/step, 128×128 matrix, zoom factor 1.00). CT was performed immediately after SPECT acquisition. The parameters included a current of 40 mA, a voltage of 120 kV, and a slice thickness of 3.75 mm.

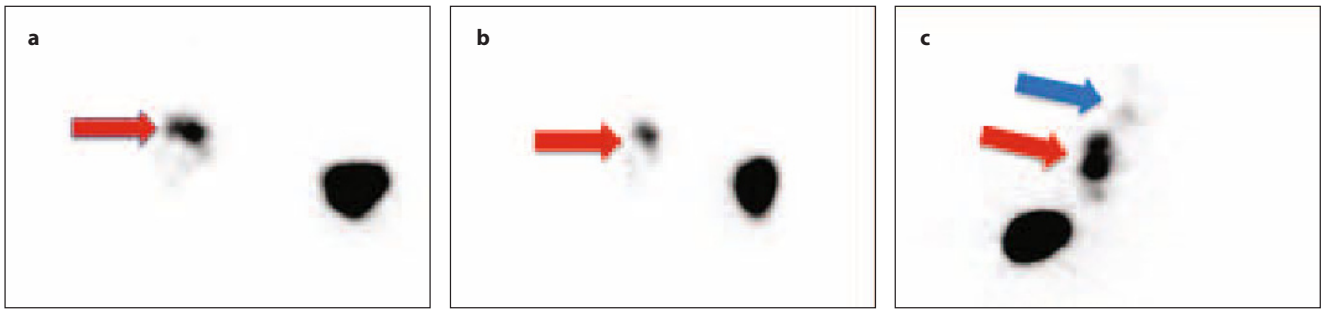

Fig. 1 The right anterior oblique view (**a**) and lateral view (**b**) show a single lymphatic vessel leading to a single axillary sentinel lymph node (*red arrow*). The anterior view (**c**) confirms the presence of a single sentinel lymph node (*red arrow*), with serial visualization of subsequent-tier nodes

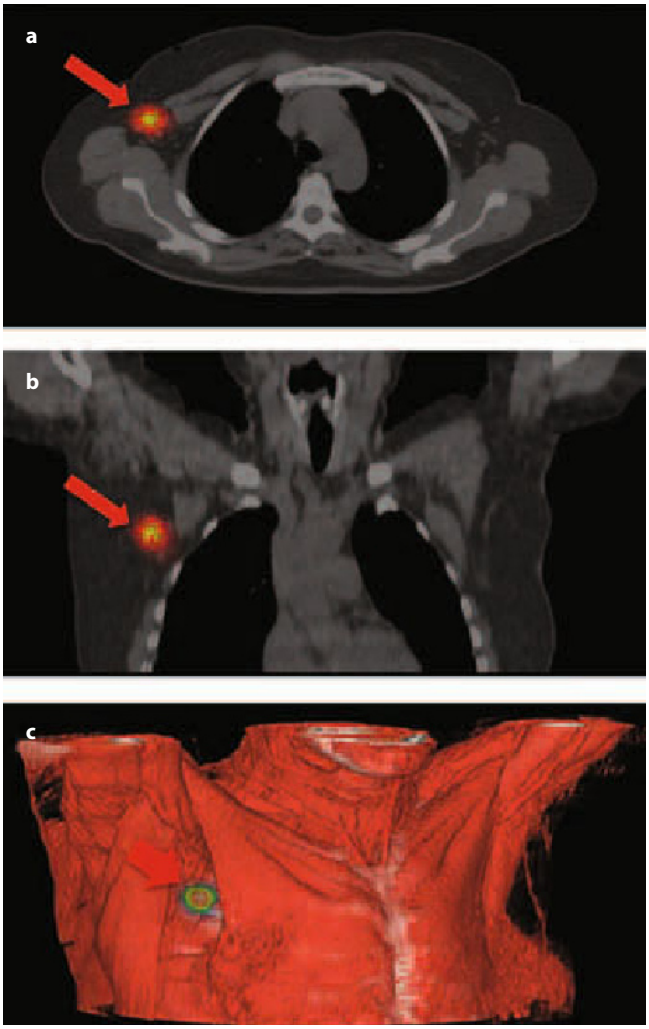

Fig. 2 The axillary sentinel lymph node on axial (**a**) and coronal (**b**) fused SPECT/CT is seen at the border of the pectoral muscle (*red arrow*). This sentinel node is displayed using 3D volume rendering (**c**) for better anatomical identification

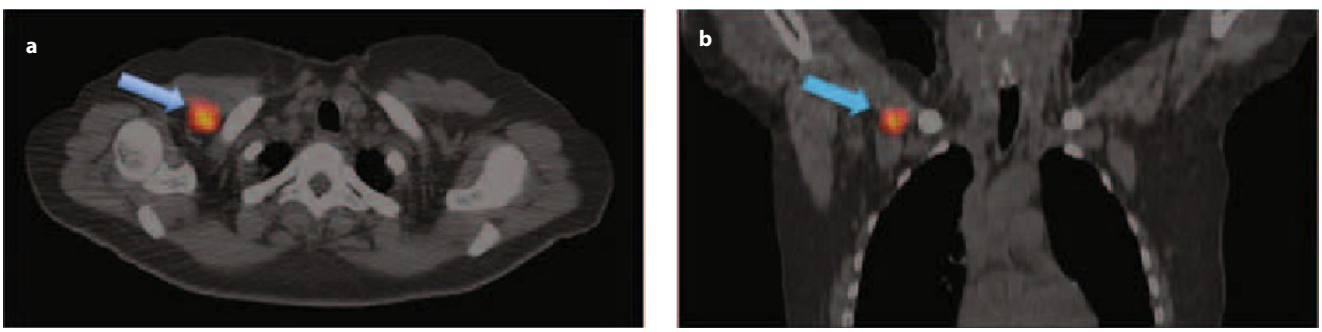

Fig. 3 SPECT/CT fused images on the axial (**a**) and coronal axis (**b**) locate another lymph node at Berg's anatomical level 3 (*blue arrow*)

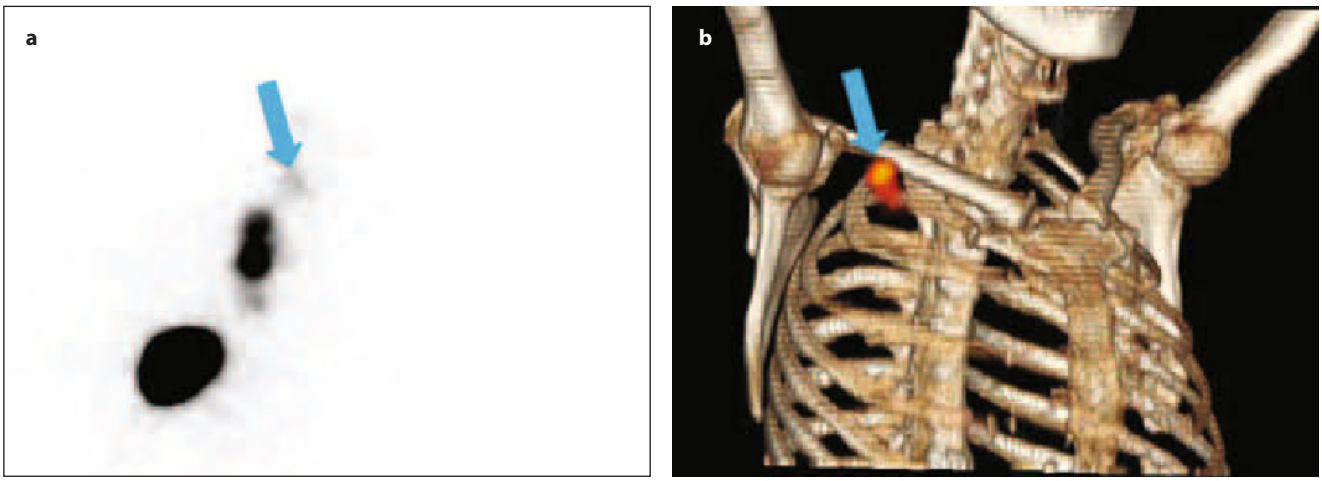

Fig. 4 The same lymph node as in the previous figure is displayed using 3D volume rendering (**b**) for better anatomical identification (*red, blue arrow*). **a** The planar image (anterior view) on the right shows the same node without specifying its topographic location

Case 9.5
Sentinel Node Mapping in Breast Cancer: Drainage to Axillary Nodes After Subareolar Injection (Planar and SPECT/CT Imaging)

Gianpiero Manca, Valerio Duce, Manuel Tredici, Sara Mazzarri, and Giuliano Mariani

Background Clinical Case

A 65-year-old woman with non-palpable infiltrating breast cancer identified by ultrasonography in the upper inner quadrant of the left breast was referred for radioguided sentinel node biopsy after needle core biopsy had demonstrated an invasive breast cancer (T1N0 lobular carcinoma).

Lymphoscintigraphy

In the afternoon before surgery, lymphoscintigraphy was performed following subareolar injection of 0.3 mL of 25 MBq ^{99m}Tc-nanocolloid in the left breast and intradermal injection of 0.3 mL of 12 MBq on the cutaneous projection of the tumor (localized in the upper inner quadrant). A dual-detector SPECT/CT gamma camera (Discovery NM/CT 670 GE Healthcare, Milwaukee, WI) equipped with low-energy high-resolution (LEHR) collimators and multislice spiral CT was used to obtain left axillary and thoracic planar images (128×128 matrix and zoom factor 1.33) and SPECT/CT acquisition (using a step-and-shoot protocol of 25 s/3° for a total of 60 views per camera head, 128×128 matrix, zoom factor 1.00). CT parameters included a current of 40 mA, a voltage of 120 kV, and a slice thickness of 3.75 mm.

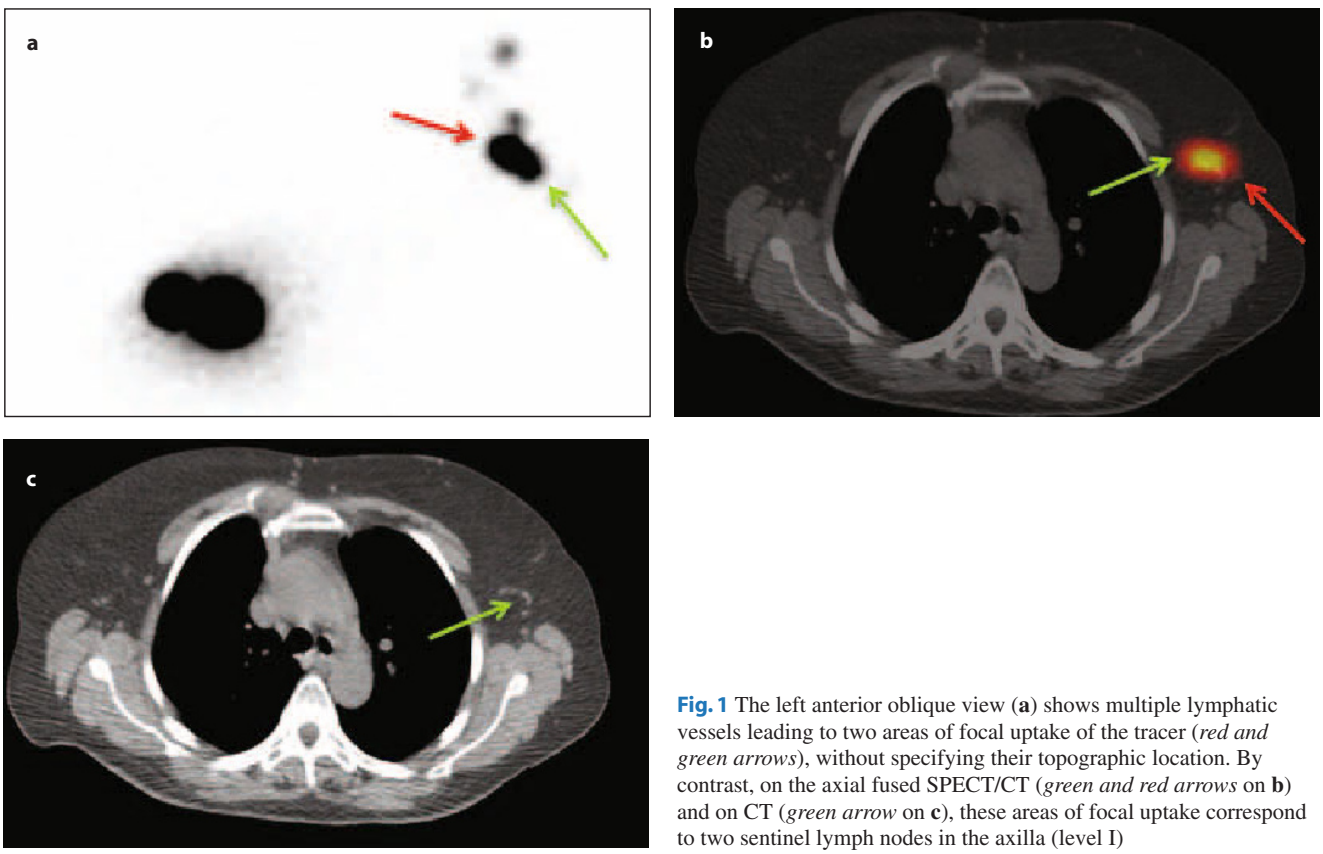

Fig. 1 The left anterior oblique view (**a**) shows multiple lymphatic vessels leading to two areas of focal uptake of the tracer (*red and green arrows*), without specifying their topographic location. By contrast, on the axial fused SPECT/CT (*green and red arrows* on **b**) and on CT (*green arrow* on **c**), these areas of focal uptake correspond to two sentinel lymph nodes in the axilla (level I)

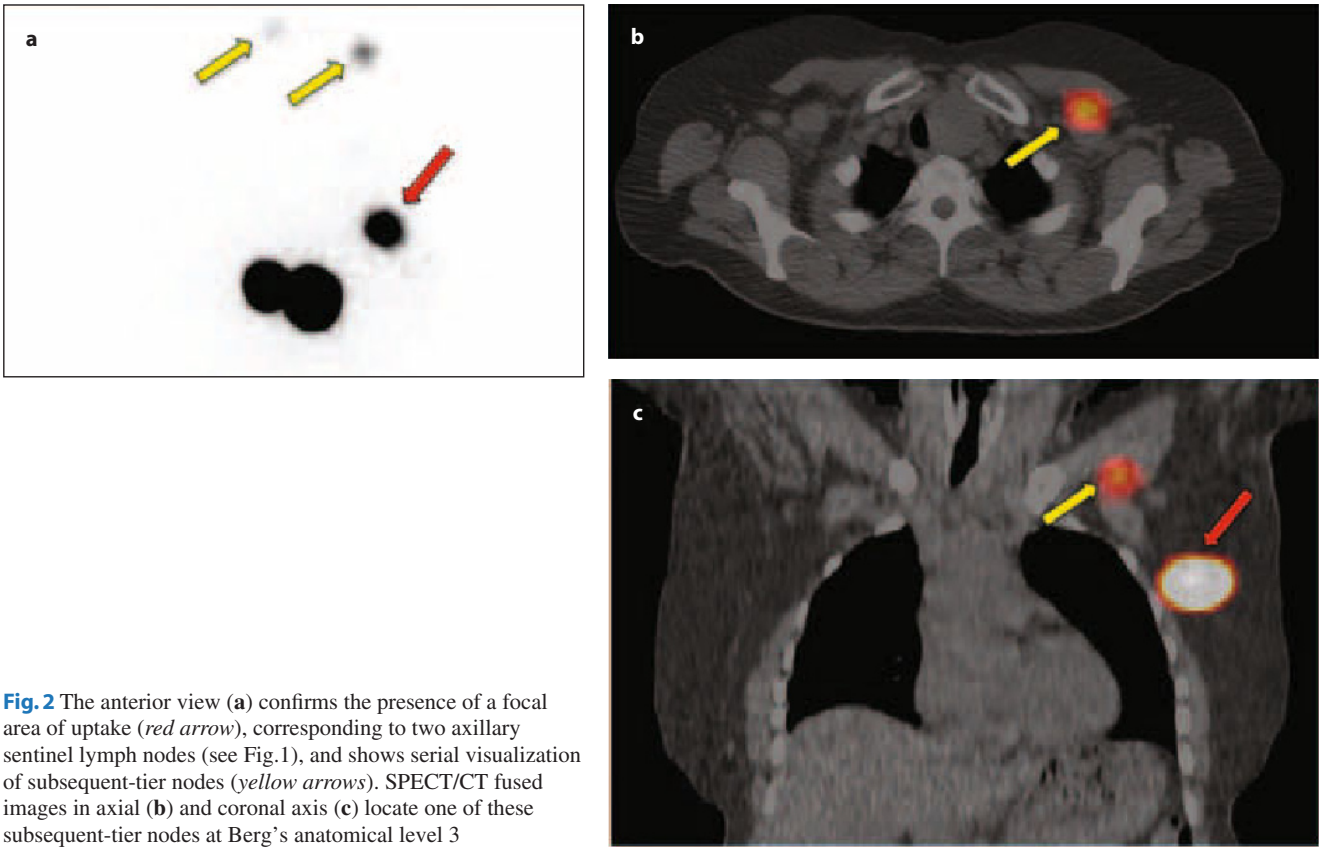

Fig. 2 The anterior view (**a**) confirms the presence of a focal area of uptake (*red arrow*), corresponding to two axillary sentinel lymph nodes (see Fig.1), and shows serial visualization of subsequent-tier nodes (*yellow arrows*). SPECT/CT fused images in axial (**b**) and coronal axis (**c**) locate one of these subsequent-tier nodes at Berg's anatomical level 3

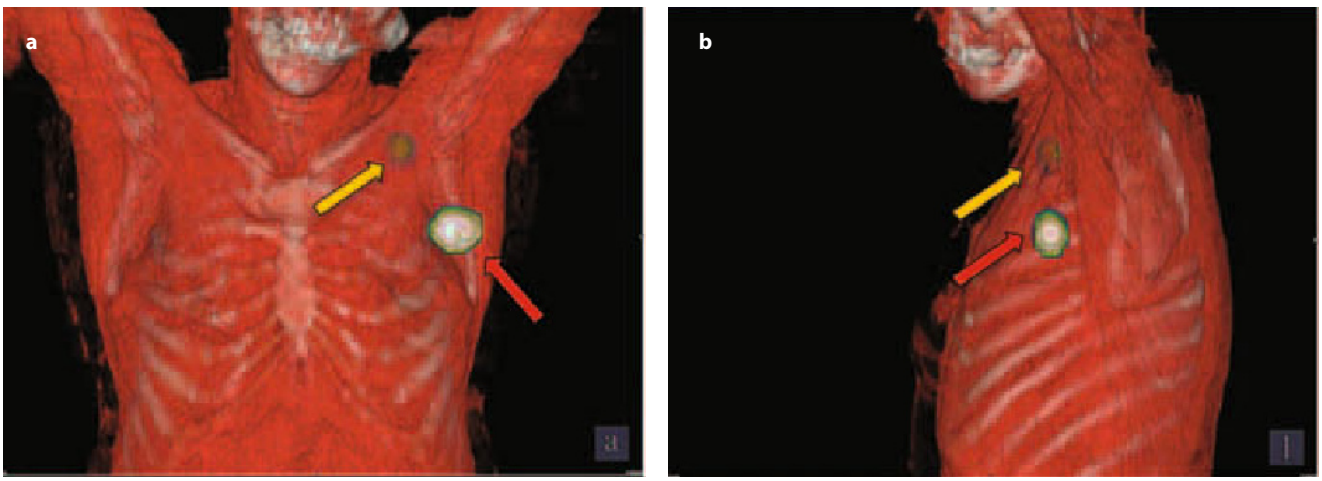

Fig. 3 The axillary sentinel lymph node (*red arrow*) and an ipsilateral infraclavicular (*yellow arrow*) are displayed using 3D volume rendering (**a**, **b**) for improved anatomical identification

Case 9.6
Sentinel Node Mapping in Breast Cancer: Failure of Lymphatic Drainage (Due to Metastatic Axillary Nodes) After Intratumoral and Subdermal Injection (Planar and SPECT/CT Imaging)

Luciano Feggi, Chiara Peterle, Corrado Cittanti, Valentina de Cristofaro, Stefano Panareo, Ilaria Rambaldi, Virginia Rossetti, Ivan Santi, and Paolo Carcoforo

Background Clinical Case

A 58-year-old woman with infiltrating lobular carcinoma in the upper outer quadrant of the left breast underwent lymphoscintigraphy for radioguided sentinel node biopsy. The patient did not present any clinically palpable left axillary lymph nodes.

Lymphoscintigraphy

In the afternoon before surgery lymphoscintigraphy was performed following administration of 0.2 mL of 74 MBq ^{99m}Tc-nanocolloid, split into two doses (one injected inside the tumor and one just a little outside from it, subdermally). A dual-detector SPECT/CT gamma camera (Symbia-T2 Siemens Medical Solutions, Hoffman Estates, IL) equipped with low-energy high-resolution (LEHR) collimators was used to obtain left axillary and thoracic planar images. These were acquired 3 h after injection of the tracer in anterior and left lateral views (256×256 matrix, zoom factor 1.00, acquisition time 500 s for each view), as well as SPECT/CT acquisition (using a step-and-shoot protocol of 25 s/3° for a total of 60 views per camera head, 256×256 matrix, zoom factor 1.00). CT parameters included a tube current of 40 mA, a tube voltage of 120 kV, and a slice thickness of 1 mm.

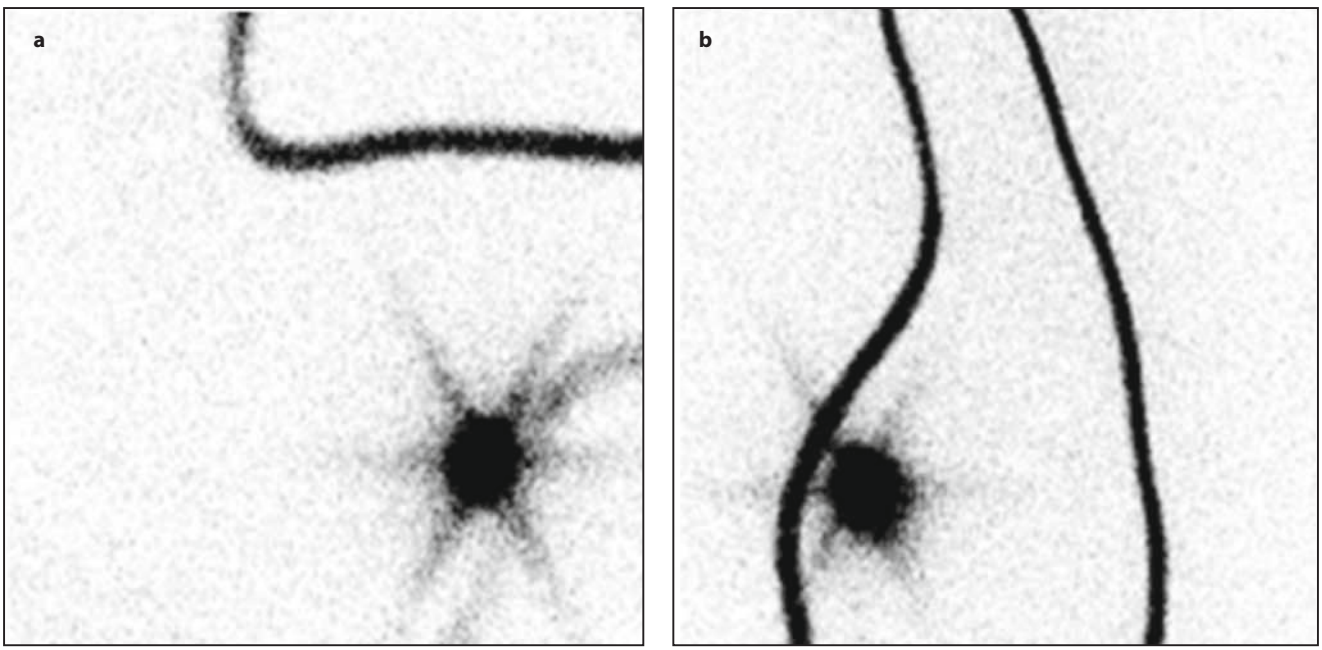

Fig. 1 Planar lymphoscintigraphy in anterior (**a**) and left lateral (**b**) views: there is no visualization of radioactive lymph nodes in the left axilla and inner mammary chain

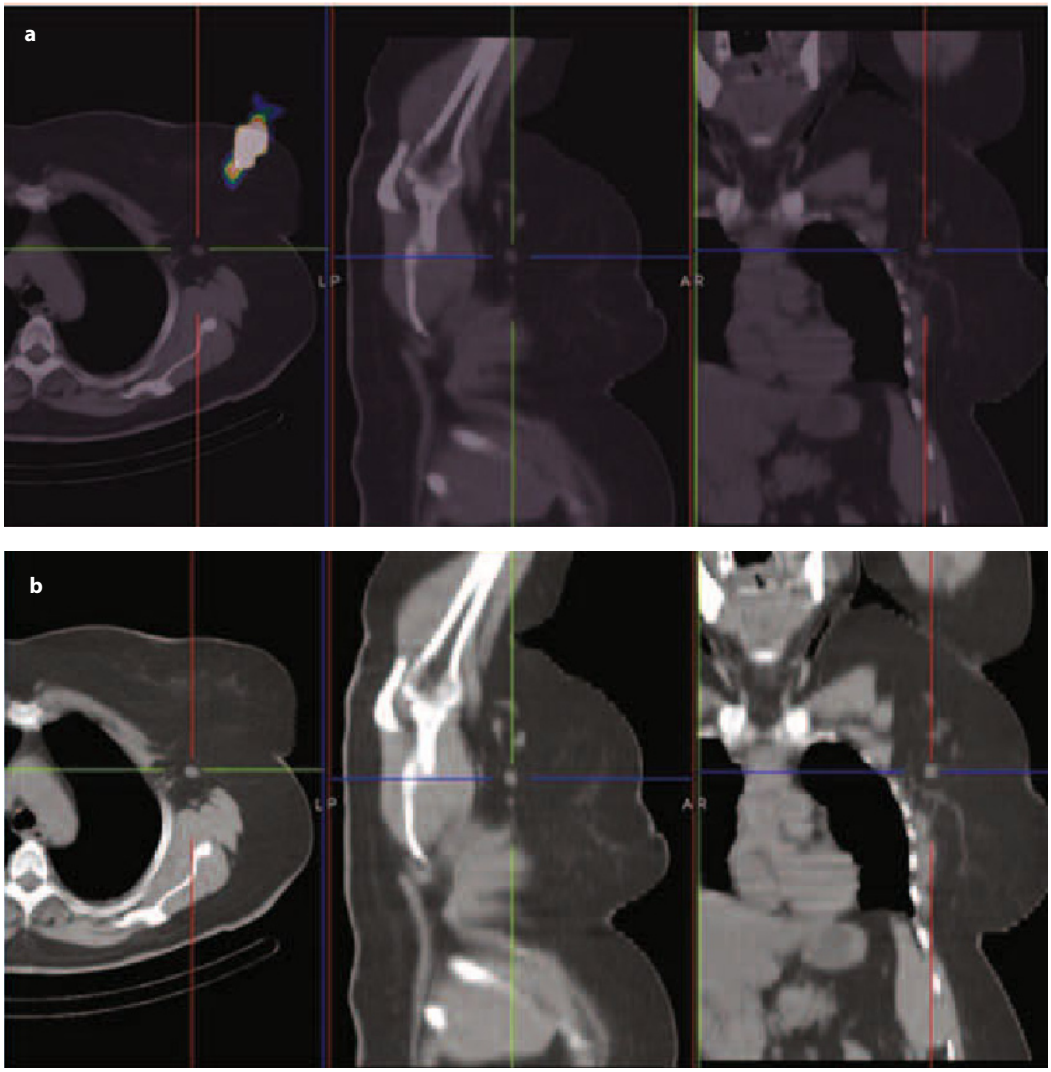

Fig. 2 Multiplanar reconstruction fused SPECT/CT images (**a**) confirm there is no uptake of the tracer in axillary lymph nodes detected on the low-dosage CT images (**b**). After surgery, histopathology showed metastatic involvement of several axillary lymph nodes responsible for the absence of lymphatic uptake

Case 9.7
Sentinel Node Mapping in Breast Cancer: Failure of Lymphatic Drainage After Intratumoral and Subdermal Injection; Subsequent Visualization of Axillary Nodes After Periareolar Injection (Planar Imaging)

Luciano Feggi, Chiara Peterle, Corrado Cittanti, Valentina de Cristofaro, Stefano Panareo, Ilaria Rambaldi, Virginia Rossetti, Ivan Santi, and Paolo Carcoforo

Background Clinical Case

A 69-year-old woman with a mass in the upper outer quadrant of the left breast detected by mammography was referred for lymphoscintigraphy and radioguided sentinel lymph node biopsy after needle core biopsy had demonstrated invasive breast cancer.

Lymphoscintigraphy

In the afternoon before surgery, lymphoscintigraphy was performed following administration of 0.2 mL of 74 MBq ^{99m}Tc-nanocolloid, divided into two doses (one injected outside the tumor and one just a little outside from it, subdermally). A dual-detector SPECT gamma camera (E-cam Siemens Medical Solutions, Hoffman Estates, IL) equipped with low-energy high-resolution (LEHR) collimators was used to obtain left axillary and thoracic planar images. Planar images were acquired 3 h after views in anterior and left lateral views (256×256 matrix, zoom factor 1.00, acquisition time 600 s for each view).

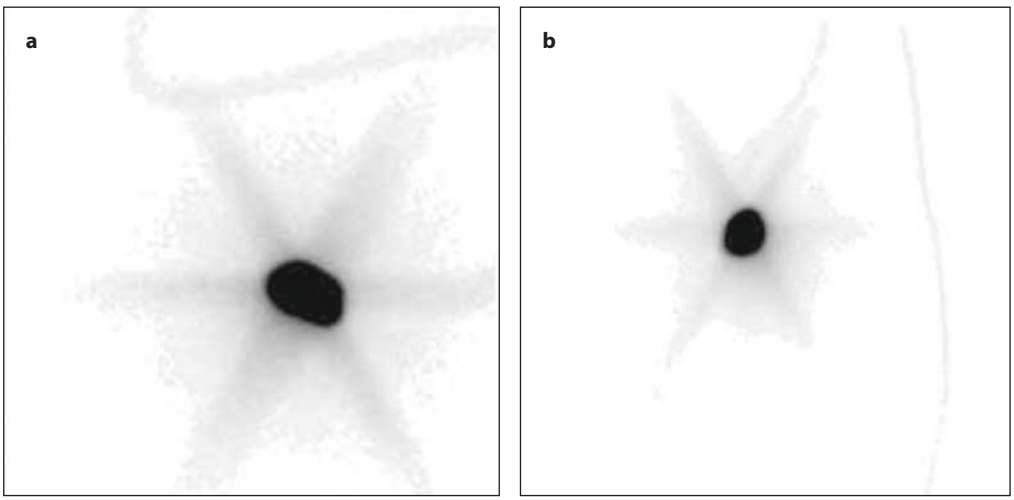

Fig. 1 Planar lymphoscintigraphy in anterior (**a**) and left lateral (**b**) views: there is no visualization of radioactive lymph nodes in the left axilla and inner mammary chain

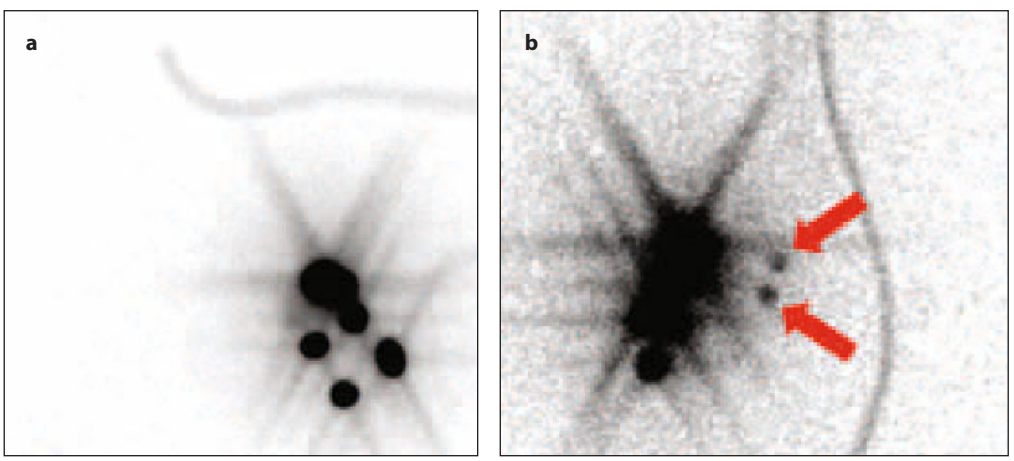

Fig. 2 After peri-areolar reinjection of 0.4 mL of 30 MBq ^{99m}Tc-albumin nanocolloid (divided into four aliquots), two radioactive lymph nodes were visualized only in lateral view (*red arrows* in **b**). **a** Planar lymphoscintigraphy in anterior view (radioactive lymph nodes are not visualized because in this view they are hidden by previous tracer injection)

Case 9.8
Sentinel Node Mapping in Breast Cancer: Prior Axillary Lymph Node Dissection with Controlateral Axillary Migration After Subdermal Injection (Planar Imaging)

Girolamo Tartaglione, Pierluigi Bonatti, Dalila Serafini, and Marco Pagan

Background Clinical Case

A 61-year-old woman with a history of left breast cancer (pT2N1M0), axillary surgery, and treatment with radiotherapy in 2004. In June 2010, a second ipsilateral carcinoma (cT1N0) was found and she underwent sentinel lymph node biopsy and surgery.

Lymphoscintigraphy

In the afternoon before surgery, lymphoscintigraphy was performed following intradermal injection of 0.3 mL of 50 MBq ^{99m}Tc-nanocolloid on the cutaneous projection of the tumor in the left breast. A dual-detector SPECT/CT gamma camera (Infinia Hawkeye GE Healthcare, Milwaukee, WI) equipped with low-energy general purpose (LEGP) collimators was used to obtain thoracic planar images. These were acquired in anteroposterior and lateral projection (acquisition time 5 min), with 128×128 matrix and zoom factor 1.33.

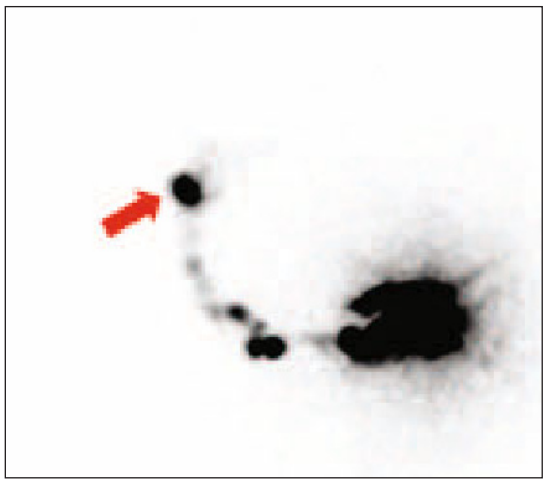

Fig. 1 Lymphoscintigraphy showed one sentinel lymph node in the right axilla (*red arrow*). In this previously treated breast cancer patient, lymphoscintigraphy demonstrated aberrant lymph drainage pathways across the midline of the thorax and evidenced a contralateral axillary sentinel node with respect to the location of the primary breast cancer. Serial hematoxylin and eosin and immunohistochemistry examination of sentinel node histological sections from the right axilla was negative for tumor (pN0)

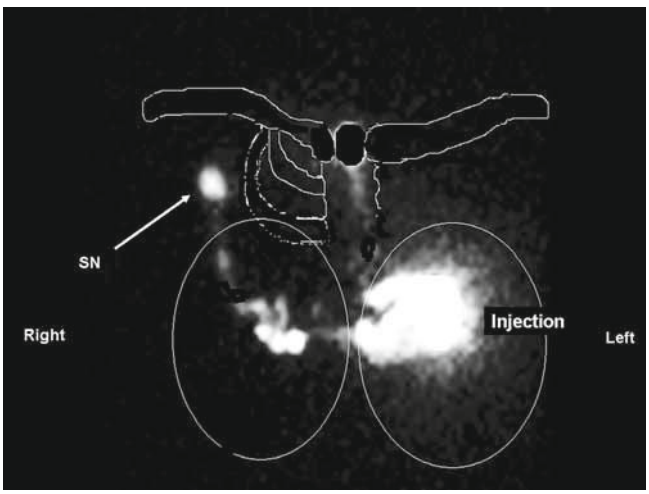

Fig. 2 Schematic anatomical representation of the lymphoscintigraphic anterior projection; *SN* sentinel node

Case 9.9
Sentinel Node Mapping in Breast Cancer: Drainage to a Single Node of the Inner Mammary Chain After Peritumoral Injection (Planar Imaging)

Giuseppe Rubini and Maria Antonia Renna

Background Clinical Case

A 39-year-old woman with a 6 mm nodule detected by mammography and located in the upper external quadrant of the right breast underwent FNAC which resulted positive for isolated neoplastic cells (C5). The patient was therefore submitted to lymphoscintigraphy for radioguided biopsy of the sentinel lymph node.

Lymphoscintigraphy

In the afternoon before surgery, lymphoscintigraphy was performed following periareolar injection of 0.4 mL of 55 MBq ^{99m}Tc-albumin nanocolloid (divided into four aliquots) in the right breast. A dual-detector SPECT gamma camera (Infinia Hawkeye GE Healthcare, Milwaukee, WI) equipped with low-energy high-resolution (LEHR) collimators was used to obtain right axillary and thoracic planar images 30 min after radiopharmaceutical injection. Planar images were acquired in anteroposterior and lateral projection, with a 128×128 matrix and zoom factor 1.00.

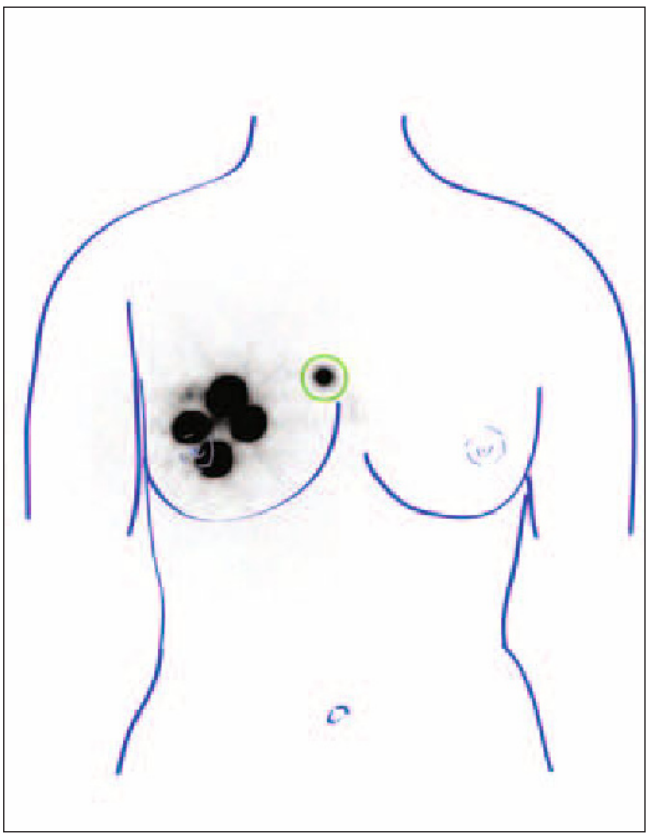

Fig. 1 Schematic representation of anterior static acquisition of the thoracic region 30 min after peri-areolar radiopharmaceutical injections. The image shows a sentinel lymph node of the right inner mammary chain (*green circle*). No axillary radiopharmaceutical migration was shown

Case 9.10
Sentinel Node Mapping in Breast Cancer: Drainage to Multiple Axillary and Inner Mammary Chain Nodes After Subareolar Injection (Planar and SPECT/CT Imaging)

Gianpiero Manca, Valerio Duce, Manuel Tredici, Sara Mazzarri, and Giuliano Mariani

Background Clinical Case

A 48-year-old woman with breast cancer (T2N0 ductal carcinoma) in the upper inner quadrant of the right breast was submitted to lymphoscintigraphy for biopsy of the sentinel lymph node. The patient had already undergone breast lumpectomy in the same quadrant 3 years earlier.

Lymphoscintigraphy

In the afternoon before surgery, lymphoscintigraphy was performed following subareolar injection of 0.3 mL of 37 MBq ^{99m}Tc-nanocolloid in the left breast. A dual-detector SPECT/CT gamma camera (Discovery NM/CT 670 GE Healthcare, Milwaukee, WI) equipped withlow-energy high-resolution (LEHR) collimators and multislice spiral CT was used to obtain right axillary and thoracic planar images as well as SPECT/CT acquisition. Planar images were acquired with a 128×128 matrix and zoom factor 1.33 (anterior, left lateral and 45° left anterior oblique views), while SPECT was acquired over 360° in step-and-shoot mode (20 s/step, 128×128 matrix, zoom factor). CT was performed immediately after SPECT acquisition. The parameters included a current of 40 mA, a voltage of 120 kV, and a slice thickness of 3.75 mm.

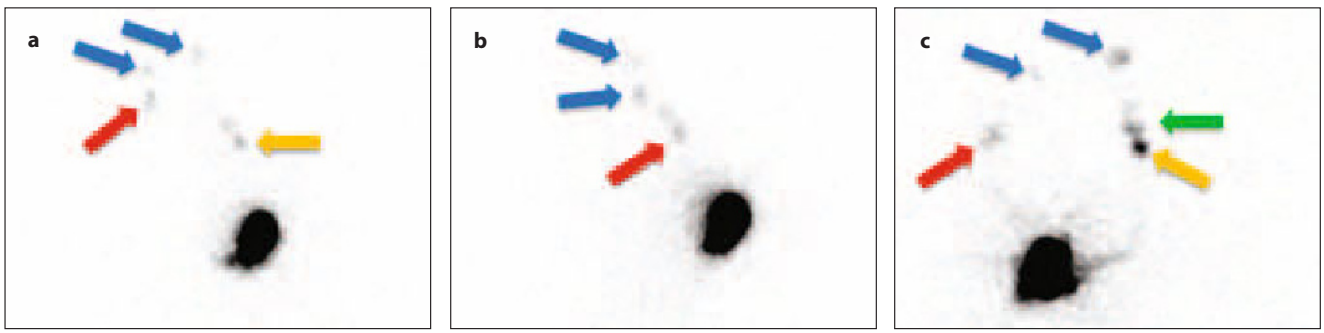

Fig. 1 The right anterior oblique (**a**), lateral (**b**), and anterior views (**c**) show two separate lymphatic vessels leading respectively to an axillary sentinel lymph node (*red arrow*) and to an internal mammary sentinel node on the right (*yellow arrow*). There is serial visualization of subsequent-tier nodes on the axilla (*blue arrows*) and parasternal region (*green arrow*)

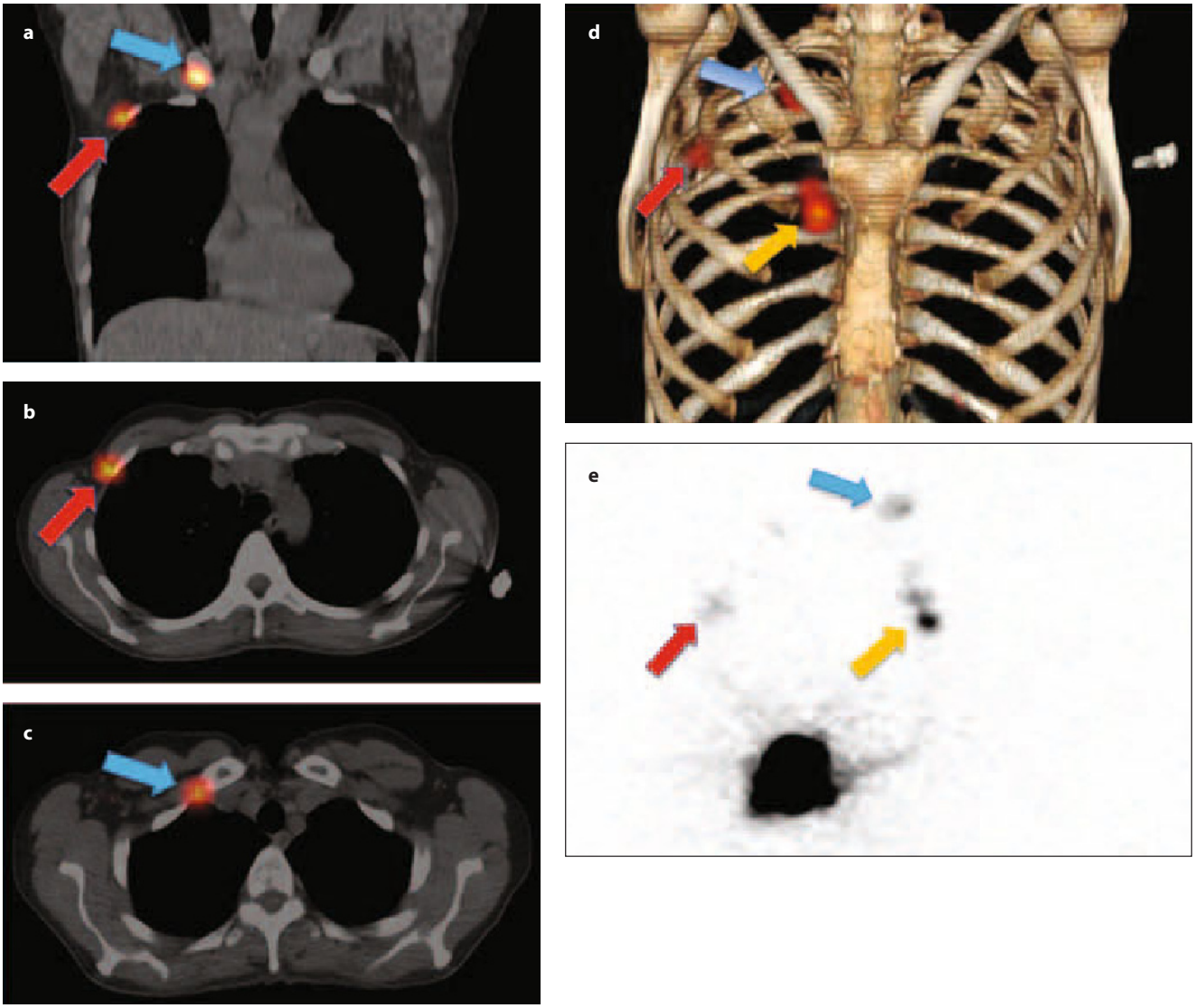

Fig. 2 The axillary sentinel lymph node (*red arrow*, at the border of the pectoral muscle) and the infraclavicular lymph node (*blue arrow*) are seen on axial and coronal fused SPECT/CT (**a**, **b**, **c**). These two nodes (with internal mammary sentinel node, *yellow arrow*) are displayed using 3D volume rendering for better anatomical identification (**d**). **e** Planar scintigraphy in the anterior projection

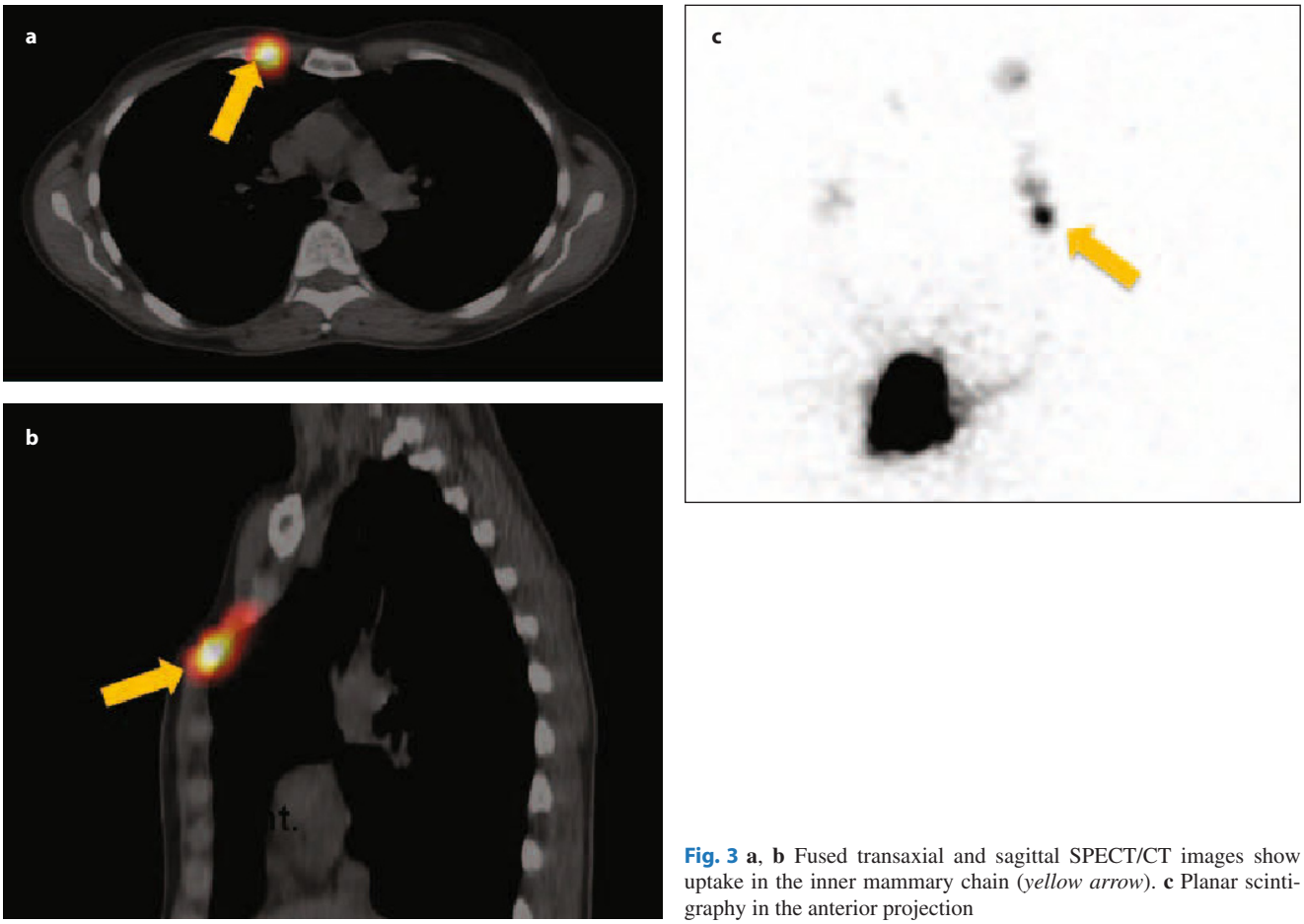

Fig. 3 **a**, **b** Fused transaxial and sagittal SPECT/CT images show uptake in the inner mammary chain (*yellow arrow*). **c** Planar scintigraphy in the anterior projection

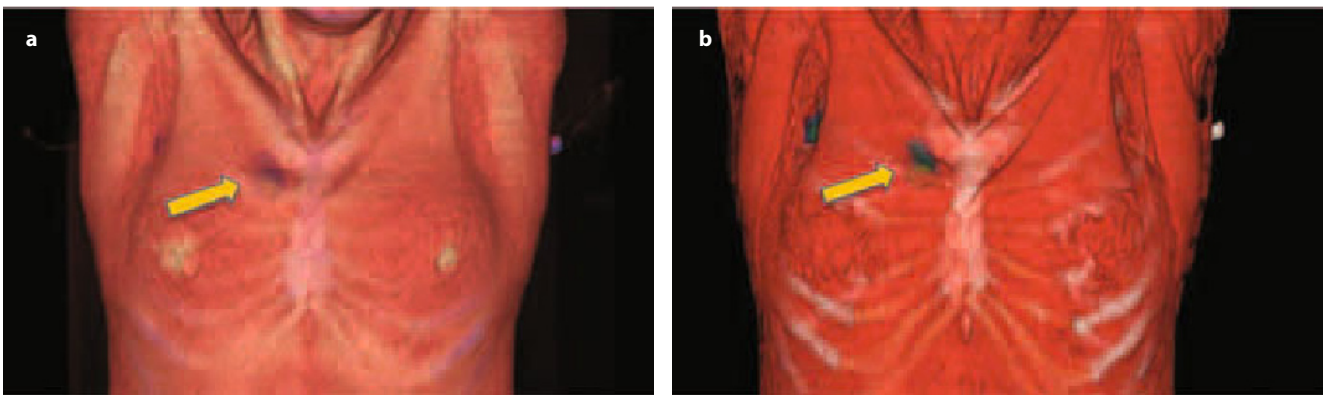

Fig. 4 **a, b** The internal mammary sentinel node (*yellow arrow*) shown by 3D volume rendering

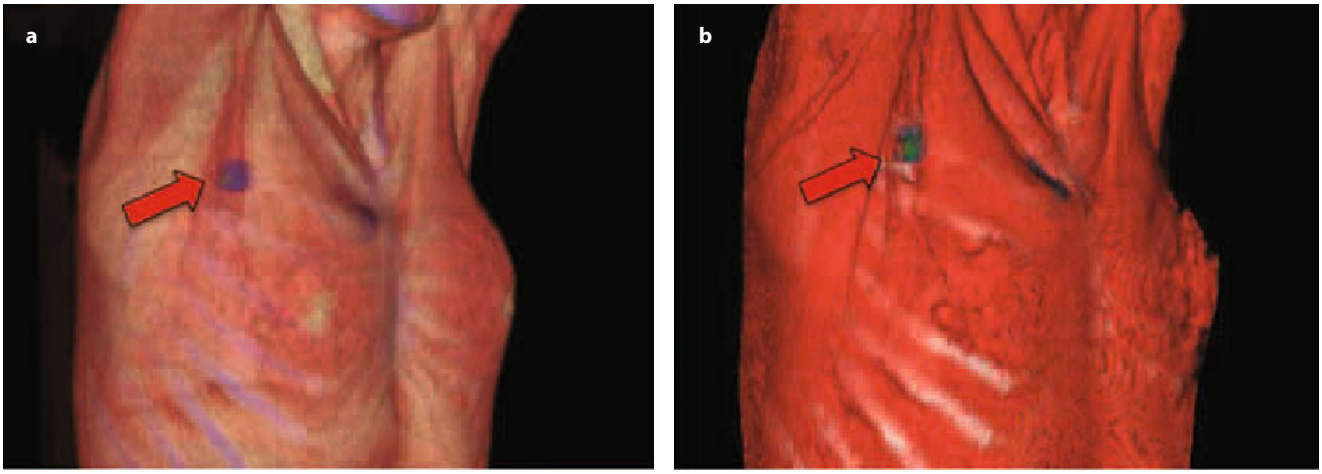

Fig. 5 **a, b** The internal mammary sentinel node (*red arrow*) shown by 3D volume rendering

Case 9.11
Sentinel Node Mapping in Breast Cancer: Drainage to Multiple Axillary and Inner Mammary Chain Nodes After Subareolar Injection (Planar and SPECT/CT Imaging)

Gianpiero Manca, Valerio Duce, Manuel Tredici, Sara Mazzarri, and Giuliano Mariani

Background Clinical Case

A 50-year-old woman with a mass located in the upper outer quadrant of the left breast detected at mammography. The patient was submitted to lymphoscintigraphy for biopsy of the sentinel lymph node, following needle core biopsy which demonstrated an infiltrating breast cancer (T1N0 ductal carcinoma).

Lymphoscintigraphy

In the afternoon before surgery, lymphoscintigraphy was performed following subareolar injection of 0.3 mL of 37 MBq ^{99m}Tc-nanocolloid in the left breast. A dual-detector SPECT/CT gamma camera (Discovery NM/CT 670 GE Healthcare, Milwaukee, WI) equipped with low-energy high-resolution (LEHR) collimators and multislice spiral CT was used to obtain right axillary and thoracic planar images as well as SPECT/CT acquisition. Planar images were acquired with a 128×128 matrix and zoom factor 1.33 (anterior, left lateral and 45° left anterior oblique views), while SPECT was acquired over 360° in step-and-shoot mode (20 s/step, 128×128 matrix, zoom factor 1.00). CT was performed immediately after SPECT acquisition. The parameters included a current of 40 mA, a voltage of 120 kV, and a slice thickness of 3.75 mm.

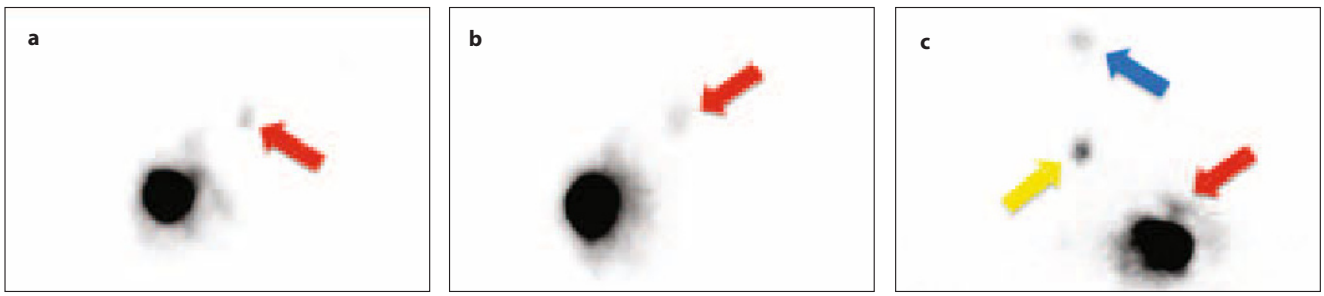

Fig. 1 The left anterior oblique (**a**), lateral (**b**), and anterior views (**c**) show two separate lymphatic vessels leading respectively to an axillary sentinel lymph node (*red arrow*) and to an internal mammary sentinel node on the right (*yellow arrow*). Serial visualization of subsequent-tier nodes on the right axilla is also shown (*blue arrow*)

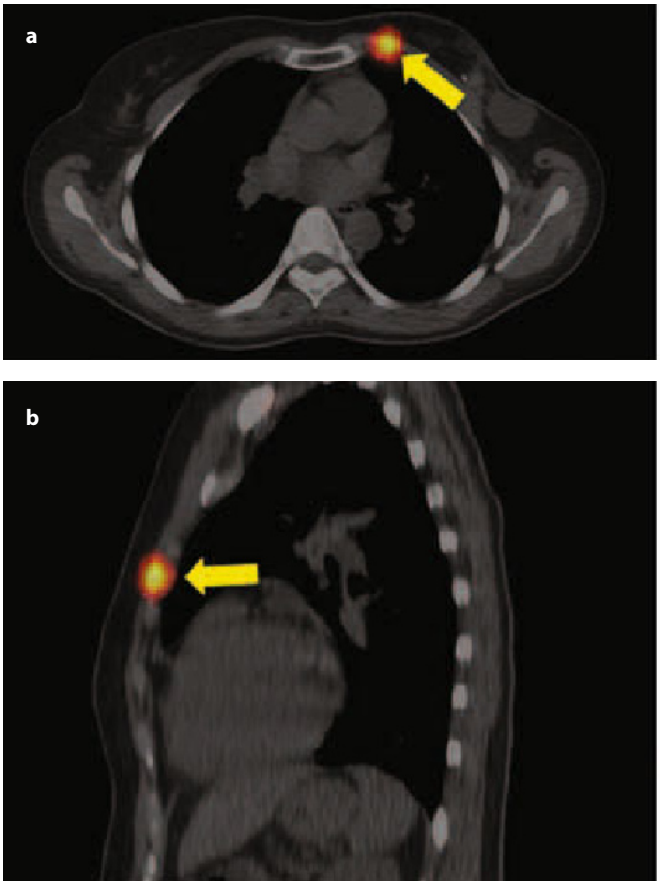

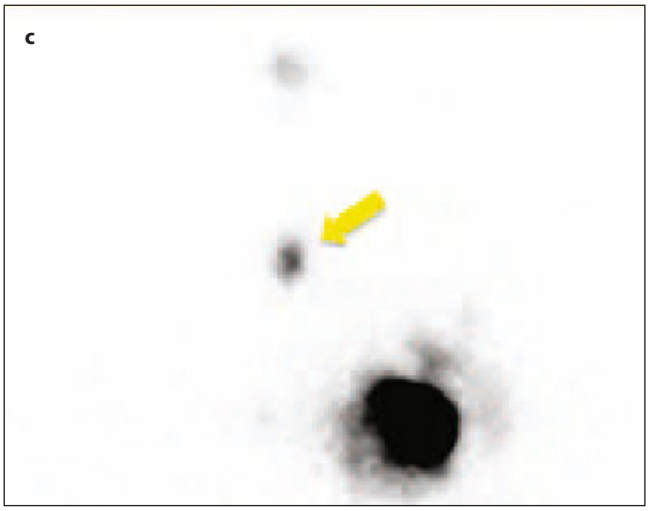

Fig. 2 Fused transaxial and sagittal SPECT/CT images (**a**, **b**) show uptake in the inner mammary chain on the left (*yellow arrow*). **c** Planar scintigraphy in the anterior projection

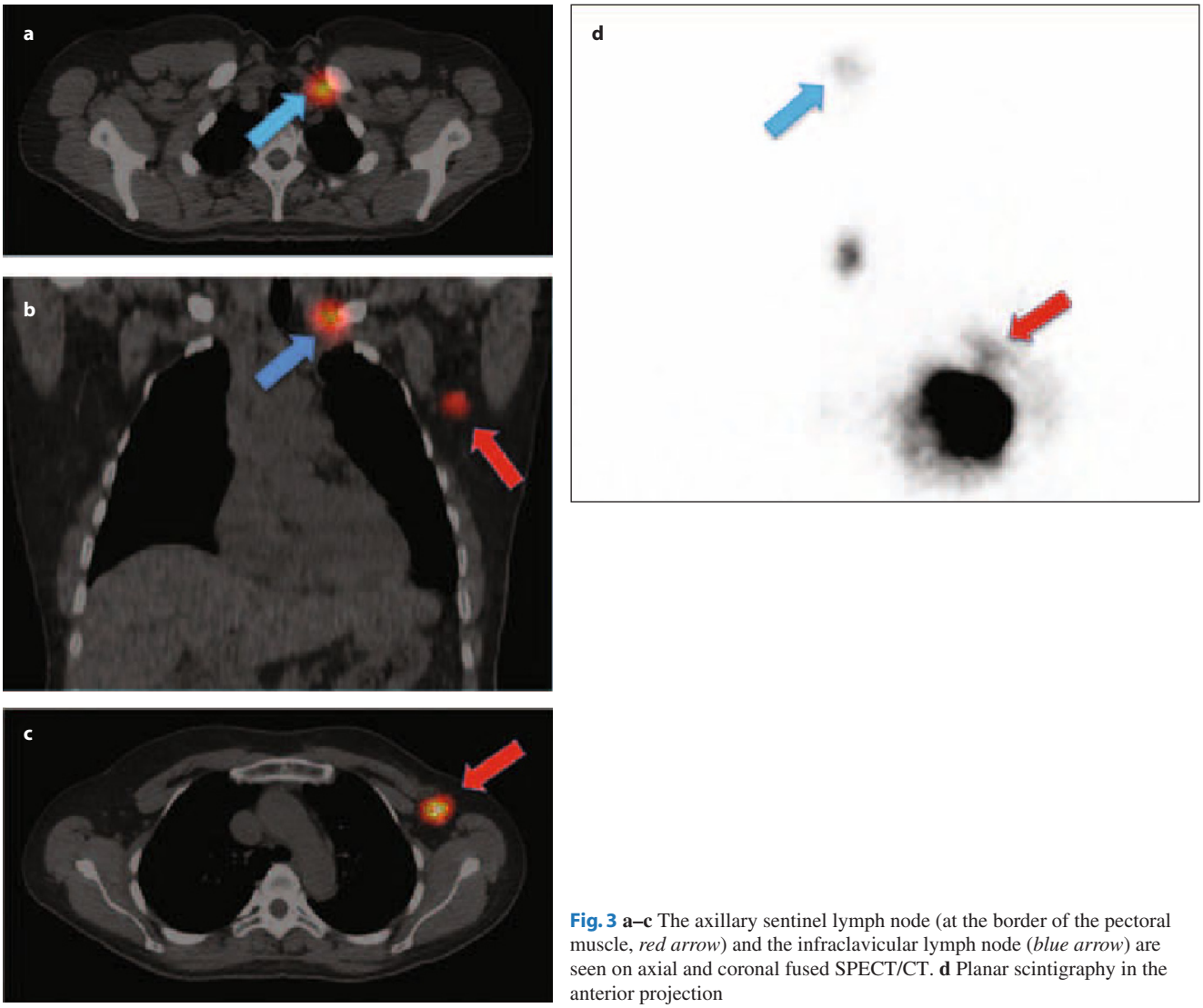

Fig. 3 **a–c** The axillary sentinel lymph node (at the border of the pectoral muscle, *red arrow*) and the infraclavicular lymph node (*blue arrow*) are seen on axial and coronal fused SPECT/CT. **d** Planar scintigraphy in the anterior projection

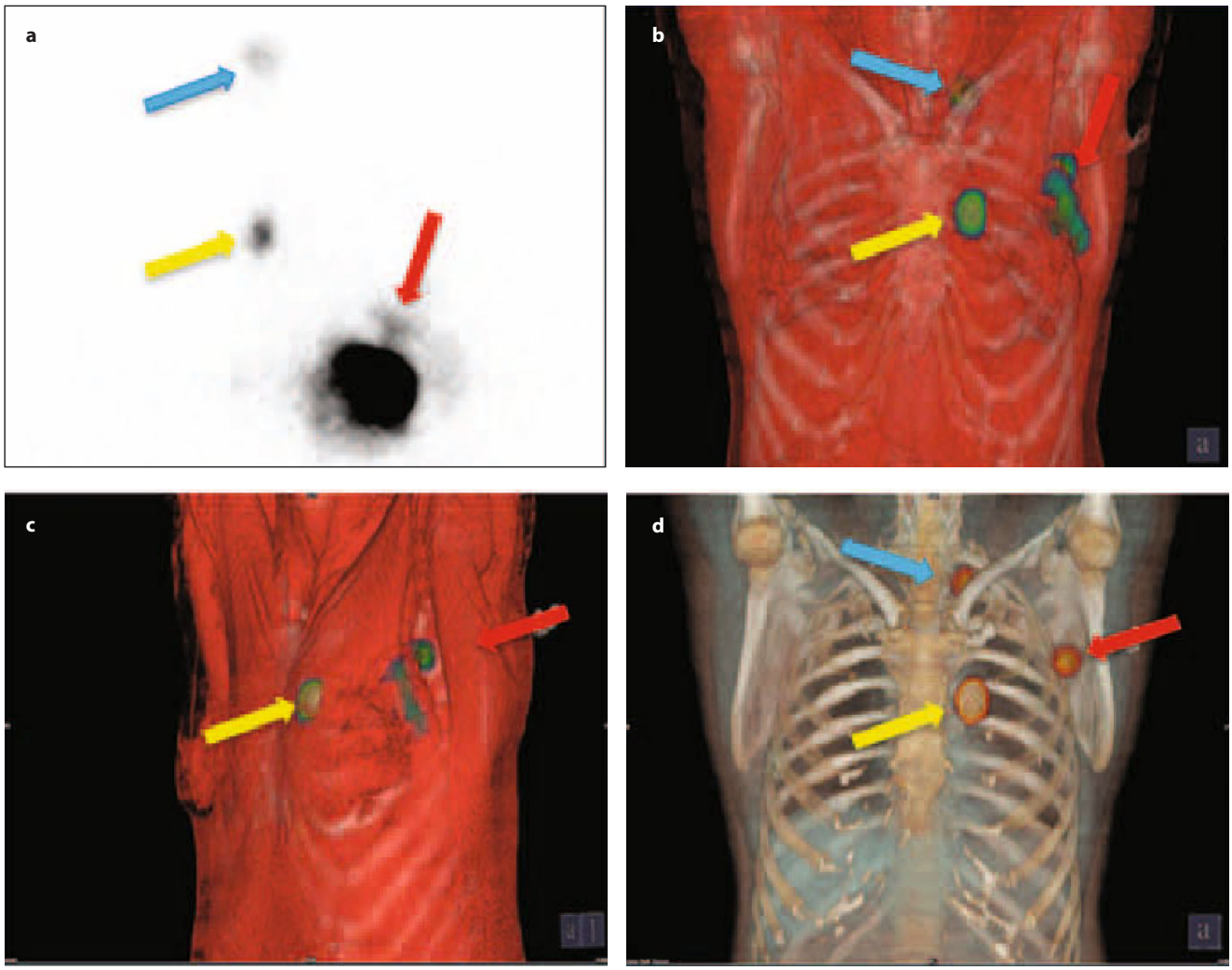

Fig. 4 **a** Planar scintigraphy in the anterior projection. **b–d** The axillary sentinel lymph node (*red arrow*), the infraclavicular lymph node (*blue arrow*), and the internal mammary sentinel node (*yellow arrow*) are visualized using 3D volume rendering

Case 9.12
Sentinel Node Mapping in Breast Cancer: Drainage to Multiple Intramammary and Axillary Nodes After Subareolar and Intradermal Injection (Planar and SPECT/CT Imaging)

Gianpiero Manca, Valerio Duce, Manuel Tredici, Sara Mazzarri, and Giuliano Mariani

Background Clinical Case

A 65-year-old woman with a lesion detected in the upper outer quadrant of the left at mammography underwent needle core biopsy that demonstrated a ductal carcinoma. The patient was submitted to lymphatic mapping with radiocolloids for radioguided sentinel lymph node biopsy; surgery confirmed a T2N0 cancer.

Lymphoscintigraphy

In the afternoon before surgery, lymphoscintigraphy was performed following subareolar injection of 0.3 mL of 30 MBq ^{99m}Tc-nanocolloid in the left breast and intradermal injection of 0.3 mL of 20 MBq on the cutaneous projection of the tumor (localized in the upper outer quadrant). A dual-detector SPECT/CT gamma camera (Discovery NM/CT 670 GE Healthcare, Milwaukee, WI) equipped with low-energy high-resolution (LEHR) collimators and multislice spiral CT was used to obtain left axillary and thoracic planar images (128×128 matrix and zoom factor 1.33) as well as SPECT/CT acquisition (using a step-and-shoot protocol of 25 s/3° for a total of 60 views per camera head, 128×128 matrix, zoom factor 1). CT parameters included a current of 40 mA, a voltage of 120 kV, and a slice thickness of 3.75 mm.

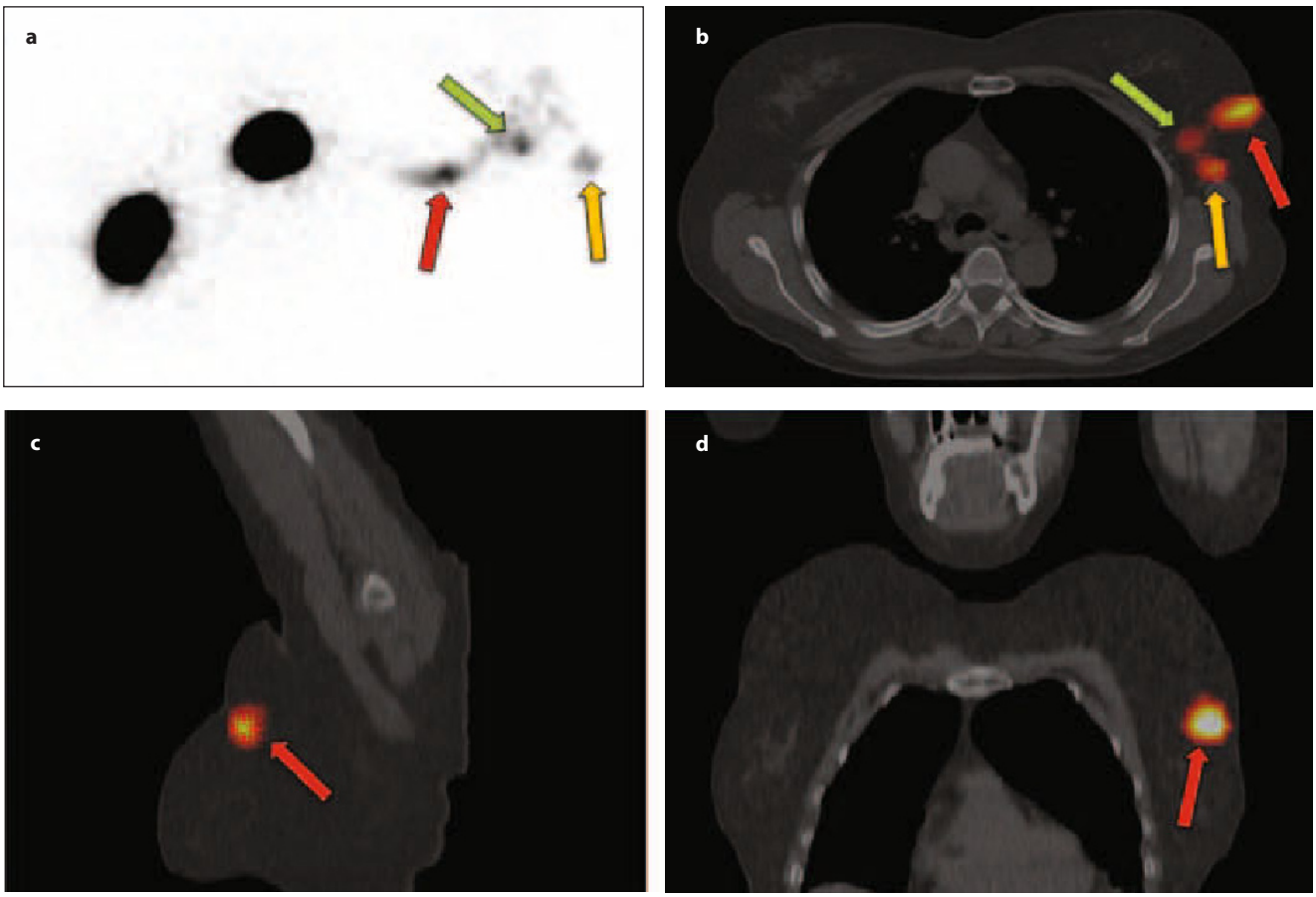

Fig. 1 **a** The left anterior oblique view shows three areas of focal uptake of the tracer (*red, green and yellow arrows*) corresponding to three lymph nodes without specifying their topographic location. SPECT/CT fused images in axial (**b**), sagittal (**c**), and coronal axis (**d**) show that these three areas of focal uptake correspond to an intramammary (prepectoral) sentinel lymph node (*red arrow*) and two axillary lymph nodes respectively (*green and yellow arrows*)

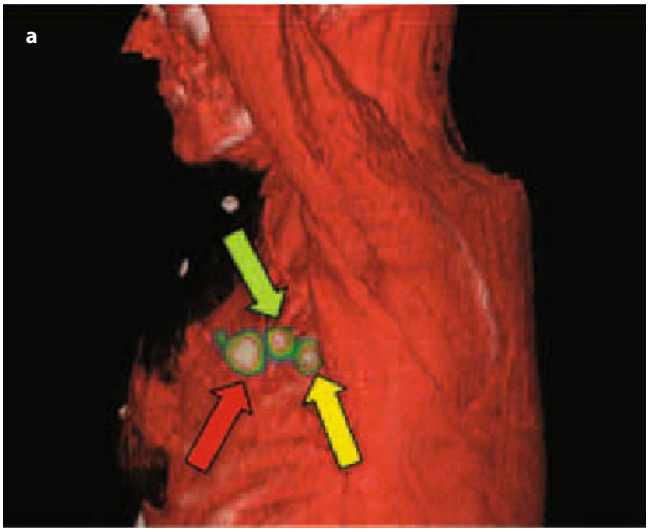

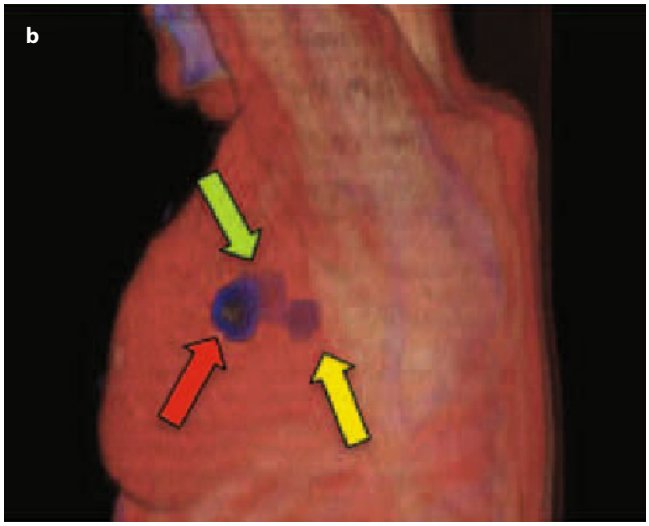

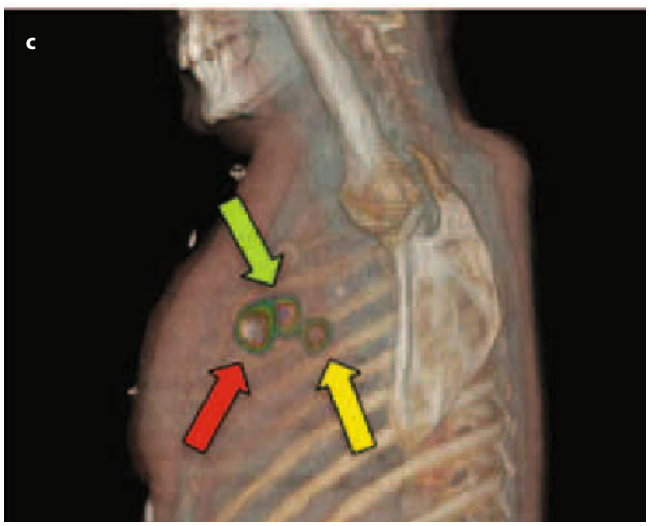

Fig. 2 **a–c** Intramammary (prepectoral) sentinel lymph node (*red arrow*) and the axillary lymph nodes (*green and yellow arrows*) are displayed using 3D volume rendering (**a**, **b**, **c**, with different levels of soft tissue visualization) for enhanced anatomical identification

Case 9.13
Sentinel Node Mapping in Breast Cancer: Drainage to Multiple Intramammary and Axillary Nodes After Subareolar and Intradermal Injection (Planar and SPECT/CT Imaging)

Gianpiero Manca, Valerio Duce, Manuel Tredici, Sara Mazzarri, and Giuliano Mariani

Background Clinical Case

A 65-year-old woman with a lesion identified by ultrasonography in the inferior inner quadrant of the left breast underwent needle core biopsy that demonstrated invasive breast cancer (T1N0 lobular carcinoma at surgery). The patient was submitted to lymphatic mapping with radiocolloids for radioguided sentinel node biopsy.

Lymphoscintigraphy

In the afternoon before surgery, lymphoscintigraphy was performed following subareolar injection of 0.3 mL containing 30 MBq ^{99m}Tc-nanocolloid in the left breast and intradermal injection of 0.3 mL containing 20 MBq in the cutaneous projection of the tumor (localized in the inferior inner quadrant). A dual-detector SPECT/CT gamma camera (Discovery NM/CT 670 GE Healthcare, Milwaukee, WI) equipped with low-energy high-resolution (LEHR) collimators and multislice spiral CT was used to obtain left axillary and thoracic planar images (128×128 matrix and zoom factor 1.33) as well as SPECT/CT acquisition (using a step-and-shoot protocol of 25 s/3° for a total of 60 views per camera head, 128×128 matrix, zoom factor 1.00). CT parameters included a current of 40 mA, a voltage of 120 kV, and a slice thickness of 3.75 mm.

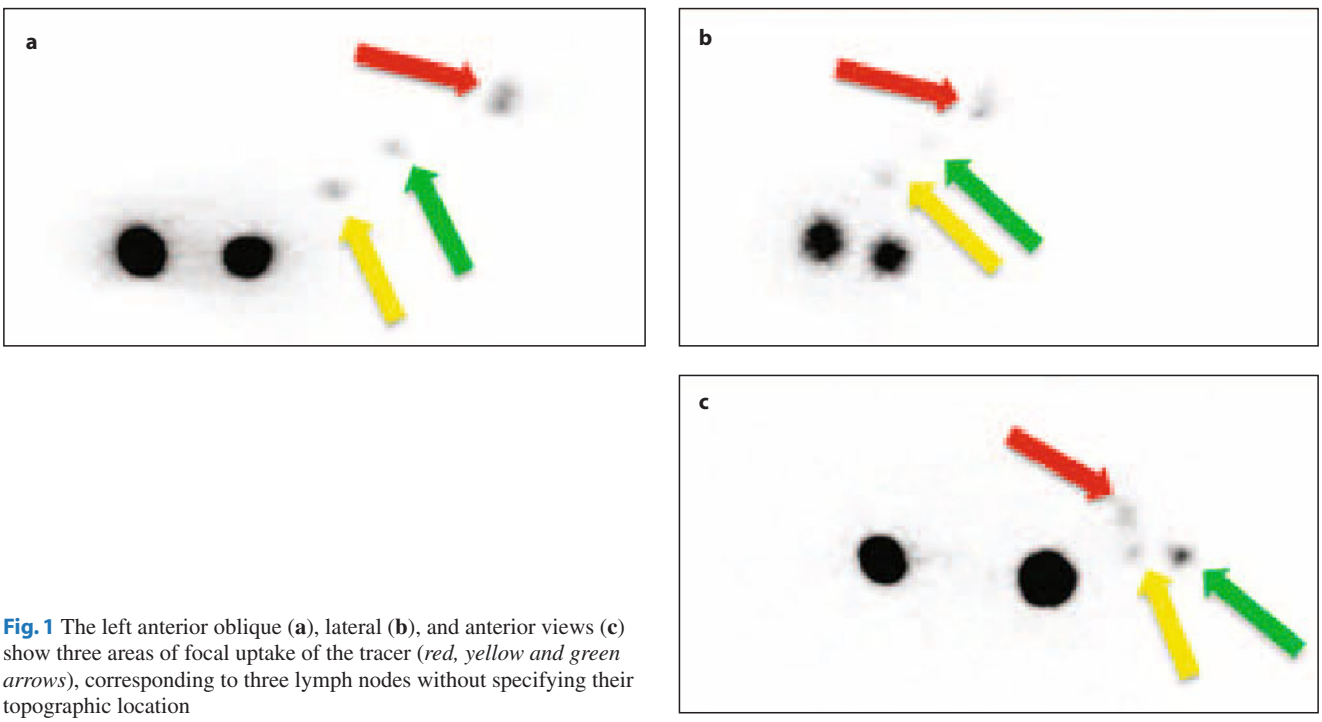

Fig. 1 The left anterior oblique (**a**), lateral (**b**), and anterior views (**c**) show three areas of focal uptake of the tracer (*red, yellow and green arrows*), corresponding to three lymph nodes without specifying their topographic location

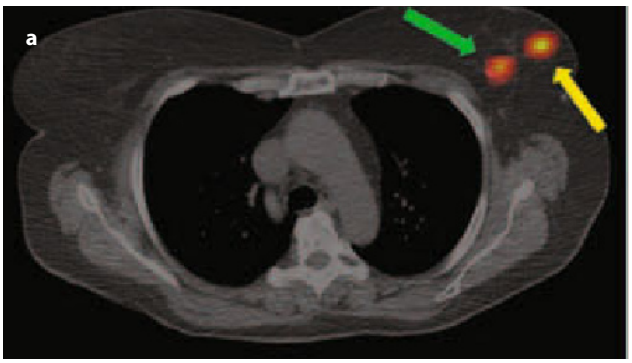

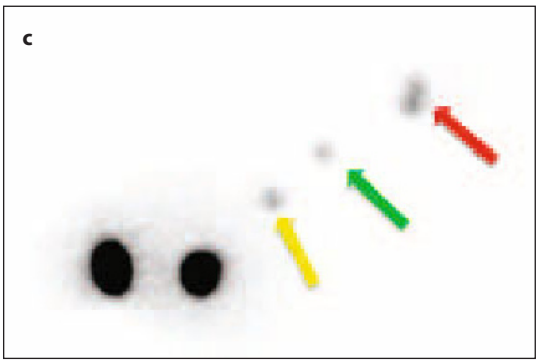

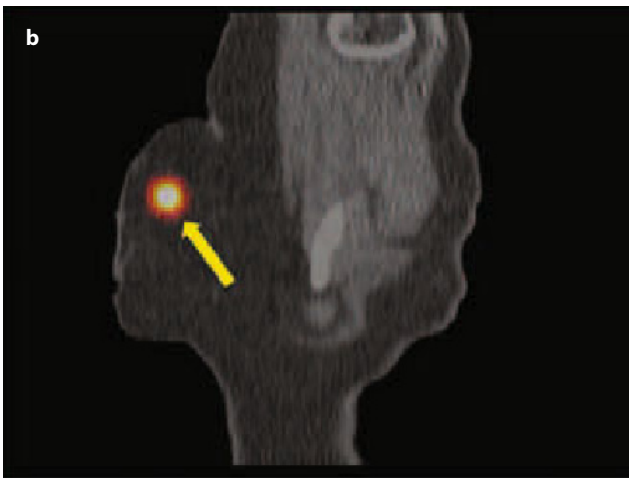

Fig. 2 SPECT/CT fused images in axial (**a**) and sagittal (**b**) sections show that two out of three areas of focal uptake correspond to two intramammary (prepectoral) lymph nodes (*yellow and green arrows*). **c** Planar lymphoscintigraphy in left anterior oblique view

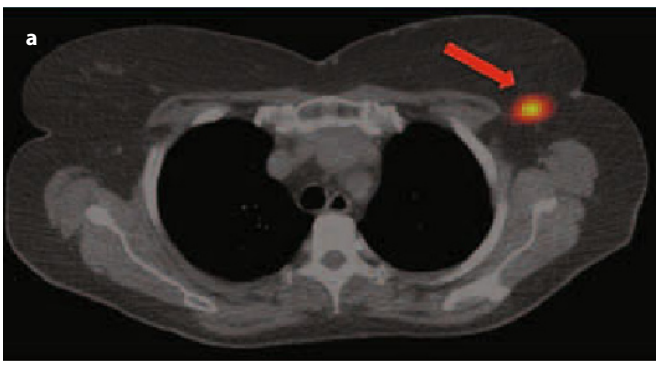

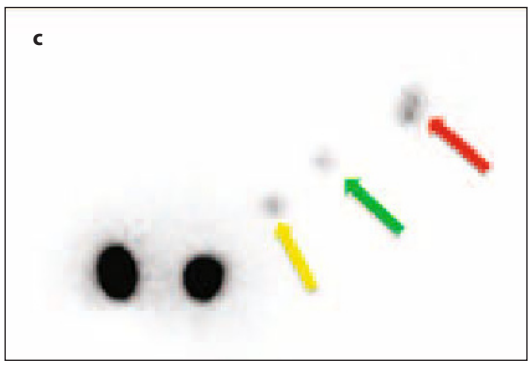

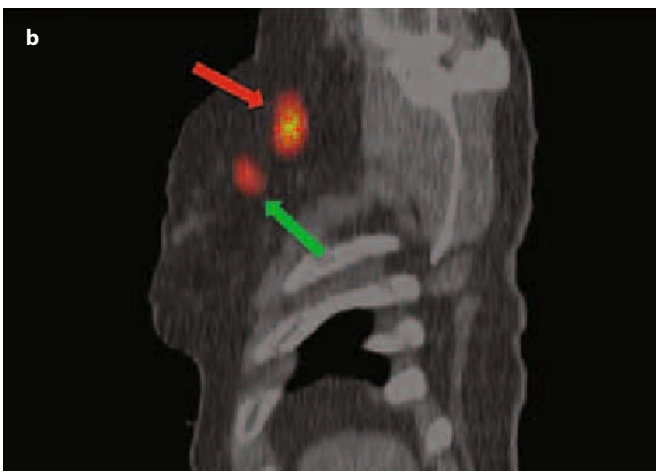

Fig. 3 SPECT/CT fused images in axial (**a**) and sagittal (**b**) sections show that one out of three areas of focal uptake shown on the planar imaging (see **Fig 1**) corresponds to axillary lymph nodes (*red arrow*). SPECT/CT fused image in sagittal section (**b**) also shows one of the two intramammary lymph nodes (*green arrow*). **c** Planar scintigraphy in left anterior oblique view

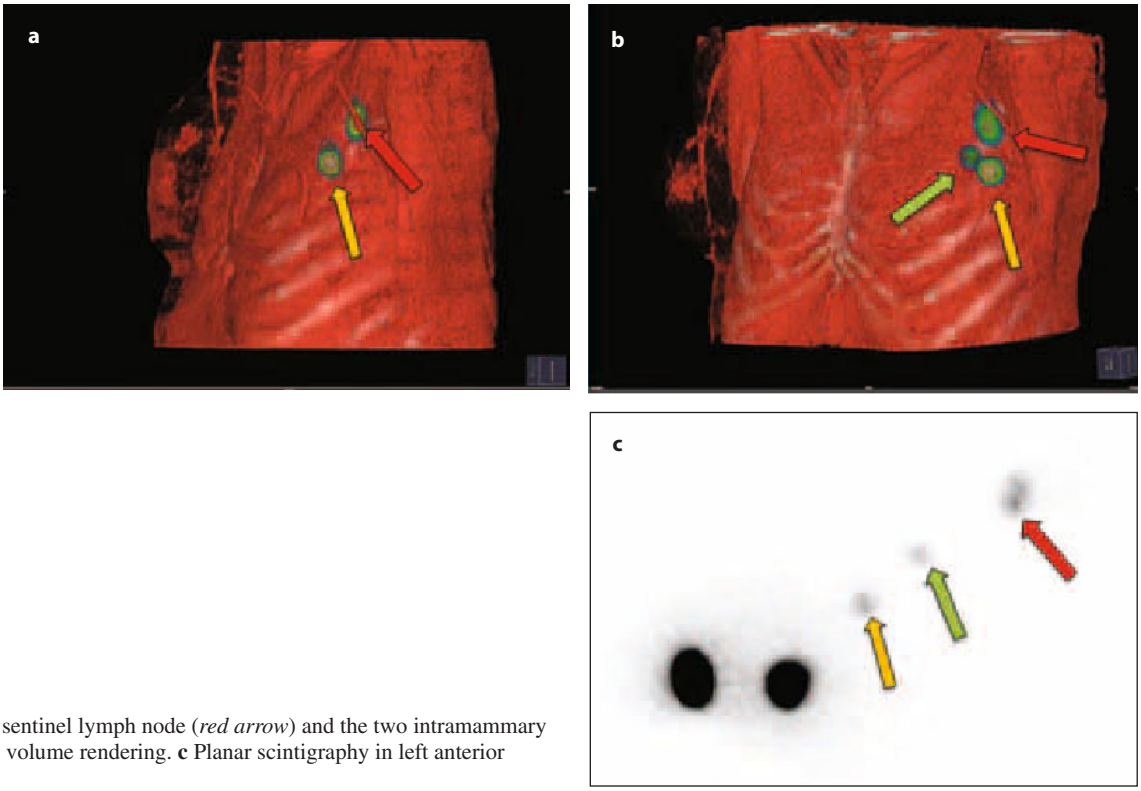

Fig. 4 **a**, **b** Axillary sentinel lymph node (*red arrow*) and the two intramammary lymph nodes by 3D volume rendering. **c** Planar scintigraphy in left anterior oblique view

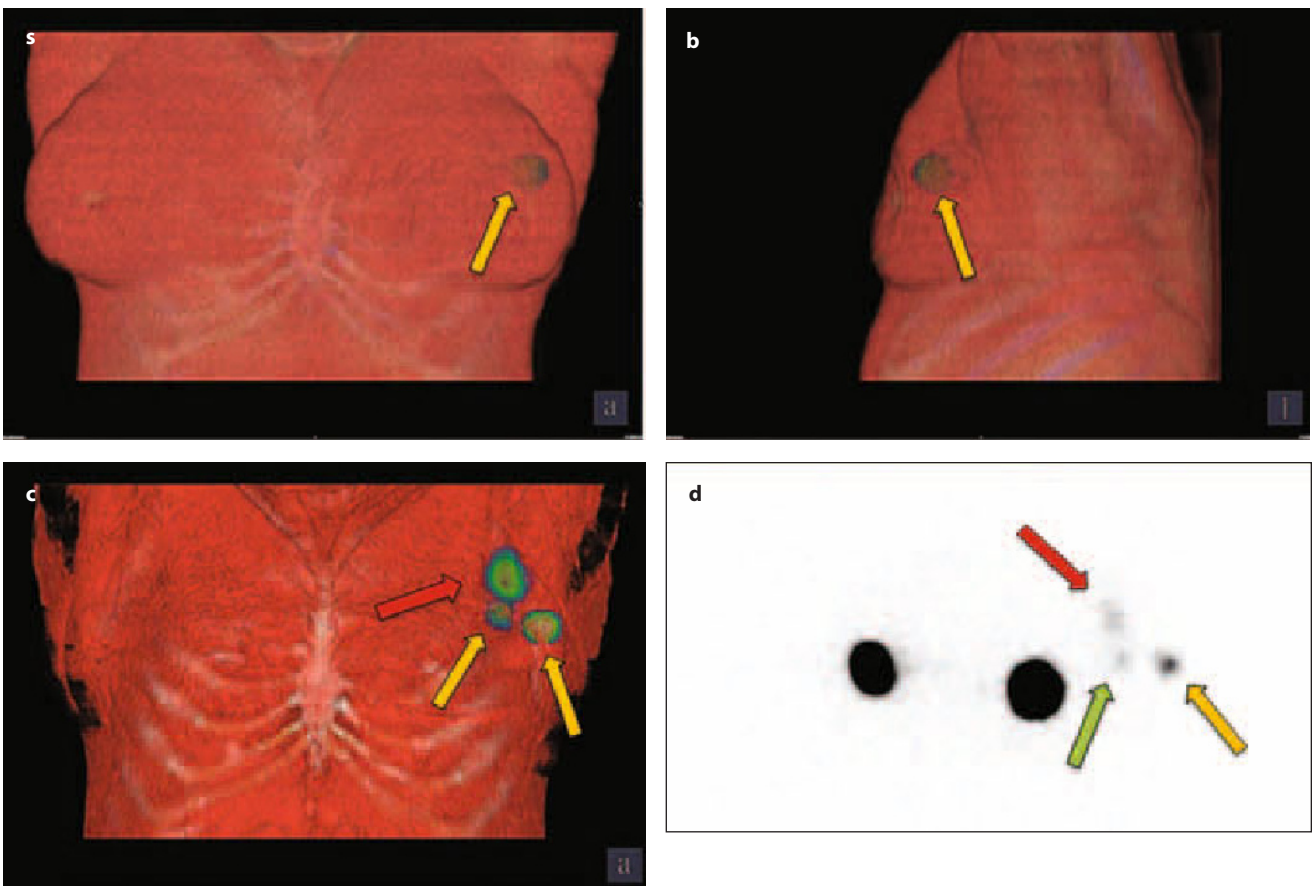

Fig. 5 **a–c** Axillary sentinel lymph node (*red arrow*) and the two intramammary lymph nodes (*green and yellow arrows*) by 3D volume rendering. **d** Planar scintigraphy in anterior view

References

1. Carter CL, Allen C, Henson DE (1989) Relation of tumor size, lymph node status, and survival in 24,740 breast cancer cases. Cancer 63:181–187
2. Carlson RW, Allred DC, Anderson BO et al (2009) Breast cancer: clinical practice guidelines in oncology. J Natl Compr Canc Netw 7:122–192
3. Krag DN, Weaver DL, Alex JC, Fairbank JT (1993) Surgical resection and radiolocalization of the sentinel lymph node in breast cancer using a gamma probe. Surg Oncol 2:335–339
4. Reintgen DS, Cruse CW, Wells K et al (1994) The orderly progression of melanoma and nodal metastases. Ann Surg 22:759 –767
5. Orsini F, Rubello D, Giuliano AE, Mariani G (2012) Radioguided surgery. In: Strauss HW, Mariani G, Volterrani D, Larson SM (eds). Nuclear oncology: pathophysiology and clinical applications. Springer, New York, (in press)
6. Mariani G, Moresco L, Viale G et al (2001) Radioguided sentinel lymph node biopsy in breast cancer surgery. J Nucl Med 42:1198–215
7. Veronesi U, Paganelli G, Viale G et al (2003) A randomized comparison of sentinel-node biopsy with routine axillary dissection in breast cancer. N Engl J Med 349:546–553
8. Morton DL, Thompson JF, Essner R et al (1999) Validation of the accuracy of intraoperative lymphatic mapping and sentinel lymphadenectomy for early-stage melanoma: a multicenter trial – Multicenter Selective Lymphadenectomy Trial Group. Ann Surg 230:453–465
9. Lyman GH, Giuliano AE, Somerfield MR et al (2005) American Society of Clinical Oncology guideline recommendations for sentinel lymph node biopsy in early stage breast cancer. J Clin Oncol 23:7703–7720
10. Buscombe J, Paganelli G, Burak ZE et al (2007) Sentinel node in breast cancer procedural. Eur J Nucl Med Mol Imaging 34:2154–2159
11. Hindié E, Groeux D, Espie M et al (2009) Sentinel node biopsy in breast cancer. Bull Cancer 96:713–725
12. Tan VK, Goh BK, Fook-Chong S et al (2011) The feasibility and accuracy of sentinel lymph node biopsy in clinically node-negative patients after neoadjuvant chemotherapy for breast cancer – a systematic review and meta-analysis. J Surg Oncol 104:97–103
13. Chagpar AB, McMasters KM (2004) Sentinel lymph node biopsy for breast cancer: from investigational procedure to standard practice. Expert Rev Anticancer Ther 4:903–912
14. Kim T, Giuliano AE, Lyman GH (2006) Lymphatic mapping and sentinel lymph node biopsy in early stage breast carcinoma: a metaanalysis. Cancer 106:4–16
15. Halsted WS (1907) The results of operations for the cure of carcinoma of the breast. Ann Surg 46:1–19
16. Cady B, Michaelson JS, Chung MA (2011) The “tipping point” for breast cancer mortality decline has resulted from size reductions due to mammographic screening. Ann Surg Oncol 18:903–906
17. Giuliano AE, Kirgan DM, Guenther JM, Morton DL (1994) Lymphatic mapping and sentinel lymphadenectomy for breast cancer. Ann Surg 220:391–398
18. Yeoh EK, Denham JW, Davies SA, Spittle MF (1986) Primary breast cancer: complications of axillary management. Acta Radiol Oncol 25:105–108
19. Ivens D, Hoe AL, Podd TJ et al (1992) Assessment of morbidity from complete axillary dissection. Br J Cancer 66:136–138
20. Mansel, R.E., Fallowfield L, Kissin M et al (2006) Randomized multicenter trial of sentinel node biopsy versus standard axillary treatment in operable breast cancer: the ALMANAC Trial. J Natl Cancer Inst 98:599–609
21. Krag DN, Anderson SJ, Julian TB et al (2010) Sentinel-lymph-node resection compared with conventional axillary-lymph-node dissection in clinically node-negative patients with breast cancer: overall survival findings from the NSABP B-32 randomized phase 3 trial. Lancet Oncol 11:927–933
22. Lucci A, McCall LM, Beitsch PD et al (2007) Surgical Complications associated with sentinel lymph node dissection (SLND) plus axillary lymph node dissection compared with SLND alone in the American College of Surgeons Oncology Group Trial Z0011. J Clin Oncol 5:3657–3663
23. Edge SB, Byrd DR, Compton CC et al (2010) AJCC cancer staging manual, 7th edn. Springer, New York
24. Tjan-Heijnen VC, de Boer M (2009) Minimal lymph node involvement and outcome of breast cancer. The results of the Dutch MIRROR study. Discov Med 8:137–139
25. Fisher ER, Swamidoss S, Lee CH et al (1978) Detection and significance of occult axillary node metastases in patients with invasive breast cancer. Cancer 42:2025–2031
26. Giuliano AE, Hawes D, Ballman KV et al (2011) Association of occult metastases in sentinel lymph nodes and bone marrow with survival among women with early-stage invasive breast cancer. JAMA 306:385–393
27. Weaver DL, Ashikaga T, Krag DN et al (2011) Effect of occult metastases on survival in node-negative breast cancer. N Engl J Med 364:412–421
28. Suami H, aylor GI, Pan WR (2005) A new radiographic cadaver injection technique for investigating the lymphatic system. Plast Reconstr Surg 115:2007–2013
29. Cruikshank WC (1786) The anatomy of the absorbing vessels of the human body. Nicol, London
30. Suami H, Pan WR, Mann GB, Taylor GI (2008) The lymphatic anatomy of the breast and its implications for sentinel lymph node biopsy: a human cadaver study. Ann Surg Oncol 15:863–871
31. Ellis H, Colborn GL, Skandalakis JE (1993) Surgical embryology and anatomy of the breast and its related anatomic structures. Surg Clin North Am 73:611–632
32. Tanis PJ, Nieweg OE, Valdés Olmos RA, Kroon BB (2001) Anatomy and physiology of lymphatic drainage of the breast from the perspective of sentinel node biopsy. J Am Coll Surg 192:399–409
33. Veronesi U, Marubini E, Mariani L (1999) The dissection of internal mammary nodes does not improve survival of breast cancer patients: 30-year results of a randomized trial. Eur J Cancer 35:1320–1325
34. Linehan DC, Hill AD, Tran KN et al (1999) Sentinel lymph node biopsy in breast cancer: unfiltered radioisotope is superior to filtered. J Am Coll Surg 188:377–381
35. Cody HS 3rd, Borgen PI (1999) State-of-the-art approaches to sentinel node biopsy for breast cancer: study design, patient selection, technique, and quality control at Memorial Sloan-Kettering Cancer Center. Surg Oncol 8:85–91
36. Tsopelas C (2001) Particles size analysis of ^{99m}Tc-labeled and unlabeled antimony trisulfide and rhenium sulfide colloids intended for lymphoscintigraphic application. J Nucl Med 42:460–466
37. Tanis Valdés Olmos RA, Muller SH, Nieweg OE (2003) Lymphatic mapping in patients with breast carcinoma: reproducibility of lymphoscintigraphic results. Radiology 228:546–551
38. Alazraki NP, Styblo T, Grant SF, Cohen C et al (2000) Sentinel node staging of early breast cancer using lymphoscintigraphy and the intraoperative gamma-detecting probe. Semin Nucl Med 30:56–64
39. Borgstein PJ, Pijpers R, Comans EF et al (1998) Sentinel lymph node biopsy in breast cancer: guidelines and pitfalls of lymphoscintigraphy and gamma probe detection. J Am Coll Surg 186:275–283
40. Smith LF, Cross MJ, Klimberg VS (2000) Subareolar injection is a better technique for sentinel lymph node biopsy. Am J Surg 180:434–437; discussion 437–438

41. Borgstein PJ, Meijer S, Pijpers R (1997) Intradermal blue dye to identify sentinel lymph node in breast cancer. Lancet 349:1668–1669
42. Pelosi E, Bellò M, Giors M et al (2004) Sentinel lymph node detection in patients with early-stage breast cancer: comparison of periareolar and subdermal/peritumoral injection techniques: J Nucl Med 45:220–225
43. Borgstein PJ, Meijer S, Pijpers RJ, van Diest PJ (2000) Functional lymphatic anatomy in breast cancer: echoes from the past and the periareolar blue method. Ann Surg 232:81– 89
44. Roumen RM, Geuskens LM, Valkenburg JG (1999) In search of the true sentinel node by different injection techniques in breast cancer patients. Eur J Surg Oncol 25:347–351
45. Kim SC, Kim DW, Moadel RM et al (2005) Using the intraoperative hand held probe without lymphoscintigraphy or using only dye correlates with higher sensory morbidity following sentinel lymph node biopsy in breast cancer: a review of the literature. World J Surg Oncol 3:64
46. Brenot-Rossi I, Houvenaeghel G, Jacquemier J et al (2003) Non-visualization of axillary sentinel node during lymphoscintigraphy: is there a pathologic significance in breast cancer? J Nucl Med 44:1232–1237
47. Van Rijk MC, Tanis PJ, Nieweg OE et al (2006) Clinical implications of sentinel nodes outside the axilla and internal mammary chain in patients with breast cancer. J Surg Oncol 94:281–286
48. Lerman H, Lievshitz G, Zak O et al (2007) Improved sentinel node identification by SPECT/CT in overweight patients with breast cancer. J Nucl Med 48:201–206
49. Ibusuki M, Yamamoto Y, Kawasoe T et al (2010) Potential advantage of preoperative three-dimensional mapping of sentinel nodes in breast cancer by a hybrid single photon emission CT (SPECT)/CT system. Surg Oncol 19:88–94
50. Van der Ploeg IM, Nieweg OE, Kroon BB et al (2009) The yield of SPECT/CT for anatomical lymphatic mapping in patients with breast cancer. Eur J Nucl Med Mol Imaging 36:903–909
51. Vermeeren L, van der Ploeg IM, Olmos RA et al (2010) SPECT/CT for preoperative sentinel node localization. J Surg Oncol 101:184–1190
52. Martin RC 2nd Edwards MJ, Wong SL et al (2000) Practical guidelines for optimal gamma probe detection of sentinel lymph nodes in breast cancer: results of a multi-institutional study. For the University of Louisville Breast Cancer Study Group. Surgery 128:139–144
53. Manca G, Romanini A, Pellegrino D et al (2008) Optimal detection of sentinel lymph node metastases by intraoperative radioactive threshold and molecular analysis in patients with melanoma. J Nucl Med 49:1769–1775
54. Wendler T, Herrmann K, Schnelzer A et al (2010) First demonstration of 3-D lymphatic mapping in breast cancer using freehand SPECT. Eur J Nucl Med Mol Imaging 37:1452–1461
55. Van der Poel HG Buckle T, Brouwer OR et al (2011) Intraoperative laparoscopic fluorescence guidance to the sentinel lymph node in prostate cancer patients: clinical proof of concept of an integrated functional imaging approach using a multimodal tracer. Eur Urol 60:826–833
56. Keereweer S. Kerrebijn JD, van Driel PB et al (2011) Optical image-guided surgery--where do we stand? Mol Imaging Biol 13:199–207
57. Stefanik D, Goldberg R, Byrne P et al (1985) Local-regional failure in patients treated with adjuvant chemotherapy for breast cancer J Clin Oncol 3:660–665
58. Buzdar AU McNeese MD, Hortobagyi GN et al (1990) Is chemotherapy effective in reducing the local failure rate in patients with operable breast cancer? Cancer 65:394–399
59. Galper S, Recht A, Silver B et al (1999) Factors associated with regional nodal failure in patients with early stage breast cancer with 0–3 positive axillary nodes following tangential irradiation alone. Int J Radiat Oncol Biol Phys 45:1157–1166
60. Recht A, Gray R, Davidson NE et al (1999) Locoregional failure 10 years after mastectomy and adjuvant chemotherapy with or without tamoxifen without irradiation: experience of the Eastern Cooperative Oncology Group. J Clin Oncol 17:1689–1700
61. Overgaard M, Hansen PS, Overgaard J et al (1997) postoperative radiotherapy in high-risk premenopausal women with breast cancer who receive adjuvant chemotherapy. Danish Breast Cancer Cooperative Group 82b Trial. N Engl J Med 337:949–955
62. Højris I, Overgaard M, Christensen JJ, Overgaard J (1999) Morbidity and mortality of ischaemic heart disease in high-risk breast-cancer patients after adjuvant postmastectomy systemic treatment with or without radiotherapy: analysis of DBCG 82b and 82c randomised trials. Radiotherapy Committee of the Danish Breast Cancer Cooperative Group. Lancet 354:1425–1430
63. Ragaz J, Olivotto IA, Spinelli JJ et al (2005) Locoregional radiation therapy in patients with high-risk breast cancer receiving adjuvant chemotherapy: 20-year results of the British Columbia randomized trial. J Natl Cancer Inst 97:116–126
64. Clarke M, Collins R, Darby S et al (2005) Effects of radiotherapy and of differences in the extent of surgery for early breast cancer on local recurrence and 15-year survival: an overview of the randomised trials. Early Breast Cancer Trialists' Collaborative Group (EBCTCG). Lancet 366:2087–2106
65. Kroman N, Wohlfahrt J, Mouridsen HT et al (2003) Influence of tumor location on breast cancer prognosis. Int J Cancer 105:542–545
66. Lohrisch C, Jackson J, Jones A et al (2000) Relationship between tumor location and relapse in 6,781 women with early invasive breast cancer. J Clin Oncol 18:2828–2835
67. Zucali R, Mariani L, Marubini E et al (1998) Early breast cancer: evaluation of the prognostic role of the site of the primary tumor. J Clin Oncol 16:1363–1366
68. Gaffney DK, Lee CM, Leavitt DD et al (2003) Electron arc irradiation of the postmastectomy chest wall in locally recurrent and metastatic breast cancer. J Clin Oncol 26:241–246
69. Colleoni M, Rotmensz N, Peruzzotti G et al (2005) Size of breast cancer metastases in axillary lymph nodes: clinical relevance of minimal lymph node involvement. J Clin Oncol 23:1379–1389
70. Sarp S, Fioretta G, Verkooijen HM et al (2007) Tumor location of the lower-inner quadrant is associated with an impaired survival for women with early-stage breast cancer. Ann Surg Oncol 14:1031–1039
71. Tuttle TM, Zogakis TG, Dunst CM et al (2002) A review of technical aspects of sentinel lymph node identification for breast cancer. J Am Coll Surg 195:261–268
72. Klauber-DeMore N, Bevilacqua JL, Van Zee KJ et al (2001) Comprehensive review of the management of internal mammary lymph node metastases in breast cancer. J Am Coll Surg 193:547–555
73. Paredes P, Vidal-Sicart S, Zanón G et al (2005) Clinical relevance of sentinel lymph nodes in the internal mammary chain in breast cancer patients. Eur J Nucl Med Mol Imaging 32:1283–1287
74. Park C, Seid P, Morita E (2005) Internal mammary sentinel lymph node mapping for invasive breast cancer: implications for staging and treatment. Breast J 11:29–33
75. Benda RK, Cendan JC, Copeland EM et al (2004) Should decisions on internal mammary lymph node irradiation be based on current lymphoscintigraphy techniques for sentinel lymph node identification? Cancer 100:518–523
76. Shimazu K. Tamaki Y, Taguchi T et al (2003) Lymphoscintigraphic visualization of internal mammary nodes with subtumoral injection of radiocolloid in patients with breast cancer. Ann Surg 237:390–398
77. Paganelli G, Galimberti V, Trifirò G et al (2002) Internal mammary node lymphoscintigraphy and biopsy in breast cancer. Q J Nucl Med 46:138–144

78. Farrús B, Vidal-Sicart S, Velasco M et al (2004) Incidence of internal mammary node metastases after a sentinel lymph node technique in breast cancer and its implication in the radiotherapy plan. Int J Radiat Oncol Biol Phys 60:715–721
79. Madsen E, Gobardhan P, Bongers V et al (2007) The impact on post-surgical treatment of sentinel lymph node biopsy of internal mammary lymph nodes in patients with breast cancer. Ann Surg Oncol 14:1486–1492
80. Estourgie SH, Tanis PJ, Nieweg OE et al (2003) Should the hunt for internal mammary chain sentinel nodes begin? An evaluation of 150 breast cancer patients. Ann Surg Oncol 10:935–941
81. Carcoforo P, Sortini D, Feggi L et al (2006) Clinical and therapeutic importance of sentinel node biopsy of the internal mammary chain in patients with breast cancer: a single-center study with long-term follow-up. Ann Surg Oncol 13:1338–1343
82. Lamonica D, Edge SB, Hurd T et al (2003) Mammographic and clinical predictors of drainage patterns in breast lymphoscintigrams obtained during sentinel node procedures. Clin Nucl Med 28:558–564
83. Van der Ent FW, Kengen RA, van der Pol HA et al (2001) Halsted revisited: internal mammary sentinel lymph node biopsy in breast cancer. Ann Surg 234:79–84
84. Byrd DR, Dunnwald LK, Mankoff DA et al (2001) Internal mammary lymph node drainage patterns in patients with breast cancer documented by breast lymphoscintigraphy. Ann Surg Oncol 8:234–240
85. Shahar KH, Buchholz TA, Delpassand E et al (2005) Lower and central tumor location correlates with lymphoscintigraphy drainage to the internal mammary lymph nodes in breast carcinoma. Cancer 103:1323–1329
86. Krynyckyi BR, Chun H, Kim HH et al (2003) Factors affecting visualization rates of internal mammary sentinel nodes during lymphoscintigraphy. J Nucl Med 44:1387–1393
87. Leppänen E, Leidenius M, Krogerus L, von Smitten K (2002) The effect of patient and tumour characteristics on visualization of sentinel nodes after a single intratumoural injection of Tc 99m labelled human albumin colloid in breast cancer. Eur J Surg Oncol 28:821–826
88. Tanis PJ, Nieweg OE, Valdés Olmos RA et al (2002) Impact of non-axillary sentinel node biopsy on staging and treatment of breast cancer patients. Br J Cancer 87:705–710
89. Dupont E, Cox CE, Nguyen K et al (2001) Utility of internal mammary lymph node removal when noted by intraoperative gamma probe detection. Ann Surg Oncol 8:833–836
90. Veronesi U, Viale G, Paganelli G et al (2010) Sentinel lymph node biopsy in breast cancer: ten-year results of a randomized controlled study. Ann Surg 251:595–600
91. Veronesi U, Galimberti V, Mariani L et al (2005) Sentinel node biopsy in breast cancer: early results in 953 patients with negative sentinel node biopsy and no axillary dissection. Eur J Cancer 41:231–237
92. Zavagno G, De Salvo GL, Scalco G et al (2008) A randomized clinical trial on sentinel lymph node biopsy versus axillary lymph node dissection in breast cancer: results of the Sentinella/GIVOM trial. Ann Surg 247:207–213
93. Kell MR, Burke JP, Barry M et al (2010) Outcome of axillary staging in early breast cancer: a meta-analysis. Breast Cancer Res Treat 120:441–447
94. McMasters KM, Tuttle TM, Carlson DJ et al (2000) Sentinel lymph node biopsy for breast cancer: a suitable alternative to routine axillary dissection in multi-institutional practice when optimal technique is used. J Clin Oncol 18:2560–2566
95. Gill G, SNAC Trial Group of the Royal Australasian College of Surgeons (RACS) and NHMRC Clinical Trials Centre (2009) Sentinel-lymph-node-based management or routine axillary clearance? One-year outcomes of sentinel node biopsy versus axillary clearance (SNAC): a randomized controlled surgical trial. Ann Surg Oncol 16:266–275
96. Goyal A, Newcombe RG, Chhabra A, ALMANAC Trialists Group et al (2006) Factors affecting failed localisation and false-negative rates of sentinel node biopsy in breast cancer: results of the ALMANAC validation phase. Breast Cancer Res Treat 99:203–208
97. Bleiweiss IJ (2006) Sentinel lymph nodes in breast cancer after 10 years: rethinking basic principles. Lancet Oncol 7:686–692
98. Johnson MT, Guidroz JA, Smith BJ et al (2009) A single institutional experience of factors affecting successful identification of sentinel lymph node in breast cancer patients. Surgery 146:671–676
99. Bourgeois P, Nogaret JM, Veys I et al (2008) Isotope labelling and axillary node harvesting strategies for breast cancer. Eur J Surg Oncol 34:615–619
100. Wernicke AG, Goodman RL, Turner BC et al (2011) A 10-year F/U of treatment outcomes in patients with early stage breast cancer and clinically negative axillary nodes treated with tangential breast irradiation following sentinel lymph node dissection or axillary clearance. Breast Cancer Res Treat 125:893–902
101. Kapoor NS, Sim MS, Lin J et al (2012) Long-term outcome of patients managed with sentinel lymph node biopsy alone for node-negative invasive breast cancer. Arch Surg (in press)
102. Hunt KK, Ballman KV, McCall LM et al (2012) Factors associated with local-regional recurrence following a negative sentinel node dissection: results of the ACOSOG Z0010 trial. Ann Surg (in press)
103. Giuliano AE, Jones RC, Brennan M et al (2011) Axillary dissection vs. no axillary dissection in women with invasive breast cancer and sentinel node metastasis – a randomized clinical trial. JAMA 305:569–575, comment 606–607
104. Fisher B, Redmond C, Fisher ER et al (1985) Ten-year results of a randomized clinical trial comparing radical mastectomy and total mastectomy with or without radiation. N Engl J Med 312:674–681
105. Goldhirsch A. Ingle JN, Gelber RD et al (2009) Thresholds for therapies: highlights of the St Gallen International expert consensus on the primary therapy of early breast cancer 2009. Ann Oncol 20:1219–1229
106. Kaufmann M, Morrow M, von Minckwitz G et al (2010) Locoregional treatment of primary breast cancer. Cancer 116:1184–1191
107. Rodriguez-Fernandez J, Martella S, Trifirò G et al (2009) Sentinel node biopsy in patients with previous breast aesthetic surgery. Ann Surg Oncol 16:989–992
108. Taback B, Nguyen P, Hansen N et al (2006) Sentinel lymph node biopsy for local recurrence of breast cancer after breast-conserving therapy. Ann Surg Oncol 13:1099–1104
109. Kumar R, Jana S, Heiba SI et al (2003) Retrospective analysis of sentinel node localization in multifocal, multicentric, palpable, or nonpalpable breast cancer. J Nucl Med 44:7–10
110. Klimberg VS, Rubio IT, Henry R et al (1999) Subareolar versus peritumoral injection for location of the sentinel lymph node. Ann Surg 229:860–864
111. Nieweg OE, Estourgie SH, van Rijk MC et al (2004) Rationale for superficial injection techniques in lymphatic mapping in breast cancer patients. J Surg Oncol 87:153–156
112. Knauer M, Konstantiniuk P, Haid A et al (2006) Multicentric breast cancer: a new indication for sentinel node biopsy – a multi-institutional validation study. J Clin Oncol 24 :3374–3380
113. Giard S, Chauvet MP, Penel N et al (2010) Feasibility of sentinel lymph node biopsy in multiple unilateral synchronous breast cancer: results of a French prospective multi-institutional study (IGASSU 0502). Ann Oncol 21:1630–1635
114. Veronesi U, Gentilini O, Fernandez JR et al (2009) Breast conservation and sentinel lymph node after neoadjuvant systemic therapy. Breast 18:590–592

115. Mamounas EP, Brown A, Anderson S et al (2005) Sentinel node biopsy after neoadjuvant chemotherapy in breast cancer: results from National Surgical Adjuvant Breast and Bowel Project Protocol B-27. J Clin Oncol 23:2694–2702
116. Piñiero A, Giménez J, Vidal-Sicart S et al (2010) Selective sentinel lymph node biopsy and primary systemic therapy in breast cancer. Tumori 96:17–23
117. Gentilini O, Cremonesi M, Toesca A et al (2010) Sentinel lymph node biopsy in pregnant patients with breast cancer. Eur J Nucl Med Mol Imaging 37:78–83
118. Khera SY, Kiluk JV, Hasson DM et al (2008) Pregnancy-associated breast cancer patients can safely undergo lymphatic mapping. Breast J 14:250–254

Preoperative and Intraoperative Lymphatic Mapping for Radioguided Sentinel Node Biopsy in Cutaneous Melanoma

10

Sergi Vidal-Sicart and Renato A. Valdés Olmos

10.1 Introduction

The first descriptions of the lymphatic drainage of the skin were based on the work of Sappey, a 19th century anatomist who injected mercury into the lymphatic system of corpses to visualize the lymphatic channels [1]. He reported drainage to the axilla and groin from the skin of the trunk and showed a vertical midline zone anteriorly and posteriorly where drainage to lymphatic basins in both sides of the body tended to overlap. A similar zone was identified horizontally around the waist, from the umbilicus to the region of the second lumbar vertebra. In these zones, called "Sappey's lines" by others, drainage was said to be possible to either side in the case of the vertical zone, or to either the groin or the axilla in the case of the horizontal zone. On the other hand, outside these zones lymphatic drainage always occurred to the ipsilateral groin or axilla, depending on whether the skin site of interest was above or below the horizontal band around the waist [2].

Sappey's concept of the predictability of lymphatic drainage of the trunk was accepted as correct for 130 years, until somewhat modified by Haagensen et al. [3], who enlarged the ambiguous zone to a 5 cm band down the midline and around the waist. Sugarbaker and McBride [4] confirmed that drainage was ambiguous from these areas, but the perception persisted that lymph drainage from the skin of the trunk outside these ambiguous zones would be highly predictable to the axilla or groin [5].

It was only with the introduction of lymphoscintigraphy that it became possible to identify the variability of lymphatic drainage on an individual basis, not only for the different areas of the trunk, but also for areas with minor (e.g., extremities) or major (e.g., head and neck, scapular, etc.) unpredictability of drainage.

10.2 The Clinical Problem

The therapeutic value of immediate lymphadenectomy in the clinically node-negative patient has been one of the longest standing and most controversial issues in the clinical management of cutaneous melanoma. Several studies expanded the zone of uncertainty around Sappey's lines, and also demonstrated that drainage in the head and neck was quite unpredictable as well. The results of lymphoscintigraphy began to be used as a guide to determine which lymph node basins should be subjected to elective lymphadenectomy. It also became increasingly apparent that lymphatic drainage could sometimes be identified with lymphatic basins that would not be considered potential metastatic sites on clinical grounds [6, 7].

The zones of ambiguity on the trunk and elsewhere were continually expanded, as more and more exceptions to the expected patterns of lymphatic drainage were demonstrated. Thus, cutaneous lymphoscintigraphy was used to identify which lymph node fields received lymphatic drainage from the primary melanoma site on the skin and, therefore, which node fields were potential sites of occult metastases. Lymphoscintigraphy should be performed before wide local excision or lymphadenectomy, as it has been shown that these procedures disrupt the normal lymphatic drainage pathways [8].

Sentinel lymph node biopsy (SLNB) in patients with melanoma was first introduced in 1992 by Morton et al. [9], who used intradermal injection of vital blue dye. In 1993, intraoperative use of the hand-held gamma detection probe for radioguided SLNB in melanoma was reported by Alex et al. [10], using intradermally injected technetium-99 (^{99m}Tc)-sulfur colloid. Since then the use of radioguided SLNB has

S. Vidal-Sicart (✉)
Nuclear Medicine, Hospital Clínic Barcelona
Barcelona, Spain
e-mail: svidal@clinic.ub.es

G. Mariani et al. (eds.), *Atlas of Lymphoscintigraphy and Sentinel Node Mapping*,
DOI 10.1007/978-88-470-2766-4_10

Location	Areas of drainage
Dorsum of the foot	Femoral, inguinal, external iliac, para-aortic
Dorsum of the hand	Epitrochlear, arm, axillary, supraclavicular
Mammary	Axillary, supraclavicular, upper parasternal
Thorax	Subcutaneous, axillary, supraclavicular, upper parasternal, diaphragmatic, parasternal, internal mammary ± mediastinal
Facial	Pre- and post-auricular, cervical
Neck	Cervical, supraclavicular, axillary

Table 10.1 Predictable lymphatic drainage depending on the location of the primary melanoma

surpassed the use of vital blue dye alone for the surgical evaluation of at-risk nodal basins in patients with cutaneous malignant melanoma.

The SLN concept is that tumor cells from a primary tumor in a particular location spread first to a lymph node of a well-defined regional lymph node basin. A radioactive colloidal substance injected into the dermis at the primary tumor site provides a roadmap leading to the SLNs. This lymphatic mapping may today be obtained for every patient, using a gamma camera. In addition, careful examination of the SLNs indicates the status of the entire lymph node basin, a notion that has now been validated by several large-scale studies. The technique of SLNB with selective lymph node dissection has been widely adopted by surgical oncologists as an alternative to elective lymphadenectomy, or to observation for patients with clinically negative regional lymph nodes, but who are at high risk for nodal metastasis [11].

Another goal of SLNB is to identify the 20–25% of patients who present with clinically occult lymphatic regional disease at diagnosis. It can also minimize the morbidity associated with elective lymphadenectomy for melanoma patients, by identifying those most likely to benefit from lymphadenectomy after a minor procedure, with a greatly diminished risk of lymphedema or other complications with respect to elective lymphadenectomy. The technique also increases the identification rate of occult lymph node metastases, by guiding the pathologist to the lymph node (or nodes) most likely to contain metastatic disease; however, there is a non-negligible false-negative rate [12].

10.3 Lymphatic Drainage of the Skin and Nodal Groups

In experienced hands, lymphoscintigraphy can identify the sentinel node in almost all patients with cutaneous melanoma. Lymphatic drainage is highly variable, thus making lymphoscintigraphy mandatory. The predictability of lymphatic drainage in cutaneous melanoma depends on the location of the primary lesions, being approximately 98% in the lower limbs, 88% in the upper extremities, 56% in the anterior thorax, and 39% for the posterior trunk. Lymphatic drainage is almost completely unpredictable in the head and neck region [13].

With increasing experience, interpretation of lymphoscintigrams becomes more and more reliable (for instance in identifying more abnormal drainage patterns). This means that fewer SLNs will go unnoticed by the nuclear medicine physician and by the surgeon. Since the spatial resolution of gamma cameras is not likely to improve dramatically in the near future, advances in lymphoscintigraphy will have to derive from the use of better radiopharmaceuticals, or from their combination with nonradioactive compounds [14–16]. Nevertheless, learning the physiologic and "lymphoscintigraphic" drainage patterns is useful, at least as a preliminary estimation of the most likely draining territories, depending on the location of the primary tumor (Table 10.1).

10.4 Indications and Contraindications for Sentinel Lymph Node Biopsy

10.4.1 Clinical Indications for Sentinel Lymph Node Biopsy in Melanoma

1. Intermediate-stage primary melanoma (1–4 mm Breslow)
2. No clinical evidence of lymph node involvement
3. No clinical evidence of distant tumor spread
4. Patients with high-risk lesions of 0.75–0.99 mm in thickness should be considered for SLNB if their melanoma is Clark level IV or V, ulcerated, shows a vertical growth phase, or has lymphatic invasion or a high mitotic rate
5. Patients with tumors thicker than 4 mm may potentially benefit from SLNB.

10.4.2 Clinical Contraindications for Sentinel Lymph Node Biopsy in Melanoma

1. Extensive previous surgery in the region of the primary tumor site or targeted lymph node circulation

2. Patients with known metastases
3. SLNB is not indicated for those patients with tumors thinner than 0.75 mm, because less than 2% of the SLNs harbour metastasis in these patients
4. SLNB is contraindicated in situations such as a poor general health status or severe concurrent disease [13].

10.5 Radiocolloid Injection

Luer-lock tuberculin syringes are recommended. Approximately 0.4–0.5 mL containing 15–74 MBq of the radiocolloid of choice is administered, depending on the operating room schedule, as 4–8 intradermal 0.1 mL injections (fewer than four may be applied if appropriate) within 1 cm from the melanoma or the excisional biopsy site at which the melanoma is located.

The intradermal injection should be performed using a 25- or 27-gauge needle. The needle is inserted in a direction that is as tangential as possible to the skin surface, at a few millimeters inside the skin; this technique injects small volumes of radiotracer, just enough to produce a bleb in the skin. Injections should surround the lesion or biopsy site to best provide lymphatic drainage in all directions. In patients with melanomas located in the head, neck, and trunk, radiocolloid injections must be given roughly equatorially around the lesion (at 3, 6, 9, 12 o'clock), because lymphatic drainage may occur both cranially and caudally, as well as across the midline of the body. In the case of large excision scars, more injection depots must be given. In the extremities, two to three injections will usually be enough in this situation, given cranially, medially, and laterally to the tumor/scar.

Cutaneous lymphoscintigraphy is highly reproducible when the distance of the injection from the border of tumor/scar does not exceed 10 mm. On the other hand, increasing this distance may result in injection of the radiocolloid across a lymphatic watershed, thus visualizing other lymph nodes that are not relevant to the primary melanoma. A larger distance from the primary lesion is only recommended in patients with hypertrophic scars or inflammation after biopsy, or in patients without lymph node visualization after the first set of injections.

Care must be taken to avoid skin contamination that may be confused with lymph node "uptake." The injection site should be covered with a bandaid or cotton ball, to prevent leakage of radioactivity through the needle puncture site.

In patients who have previously undergone wide excision, the injection can be administered at four sites around the wide excision. However, it should be noted that some groups regard wide excision of a large primary melanoma as an exclusion criterion, since the altered lymphatic drainage following wide excision increases the failure rate of SLN detection [17, 18].

The injection technique can vary, depending on the anatomical region involved, as follows:

- *toes and fingers*: generally, two to four sites are injected at the base of the nail. Local injections with lidocaine or xylocaine, surrounding the nail, are enough to provide anesthesia in patients with subungueal melanoma. After anesthesia is obtained, the radiocolloid can be injected
- *sole of the foot*: this is an extremely difficult area to inject. Anesthesia involves local block of the sole of the foot, but generally a lidocaine injection suffices (although it is painful). The area is quite bloody when the needle is inserted. Injecting radiocolloid into a callus or hyperkeratosis will show no migration
- *scalp*: it is useful to shave the area to be injected. The skin of the scalp is difficult to inject; therefore, the needle tends to penetrate slightly deeper than is optimal, but should be kept in the intradermal site. Contamination of the injection area is a real problem and good coverage by a sheet around the injection site is required. Care must be taken to avoid any leakage from the injection, since it can be a source of significant contamination
- *ear*: the site of previous biopsy on the ear may be difficult to recognize. When patients are not able to precisely indicate the site of the excision scar, it is recommended to ask the surgeon or dermatologist to define the exact site of the biopsy. The injection is carried out at four poles surrounding the tumor, or the biopsy scar. The skin is quite loose, thus the amount of anesthesia and radiocolloid used are generally increased in volume. Special care must be taken in the helix area, and preventing contamination of the injection site is of utmost importance
- *trunk*: midline melanomas can be problematic, because the radiocolloid can drain to almost any lymphatic basin: axillary, groin, or even the supraclavicular, paravertebral, or intra-abdominal nodes. In-transit lymph nodes can also be found (parascapular area, paracostal nodes, submammary). Imaging in the posterior view is especially important in this area
- *other areas*: injecting in areas of induration, inflammation, or infection should be avoided, and these special circumstances should be discussed with the surgeon. Before injecting near the eye, it is convenient to place a gauze over the eye and to take adequate precautions against possible contamination (Fig. 10.1) [19].

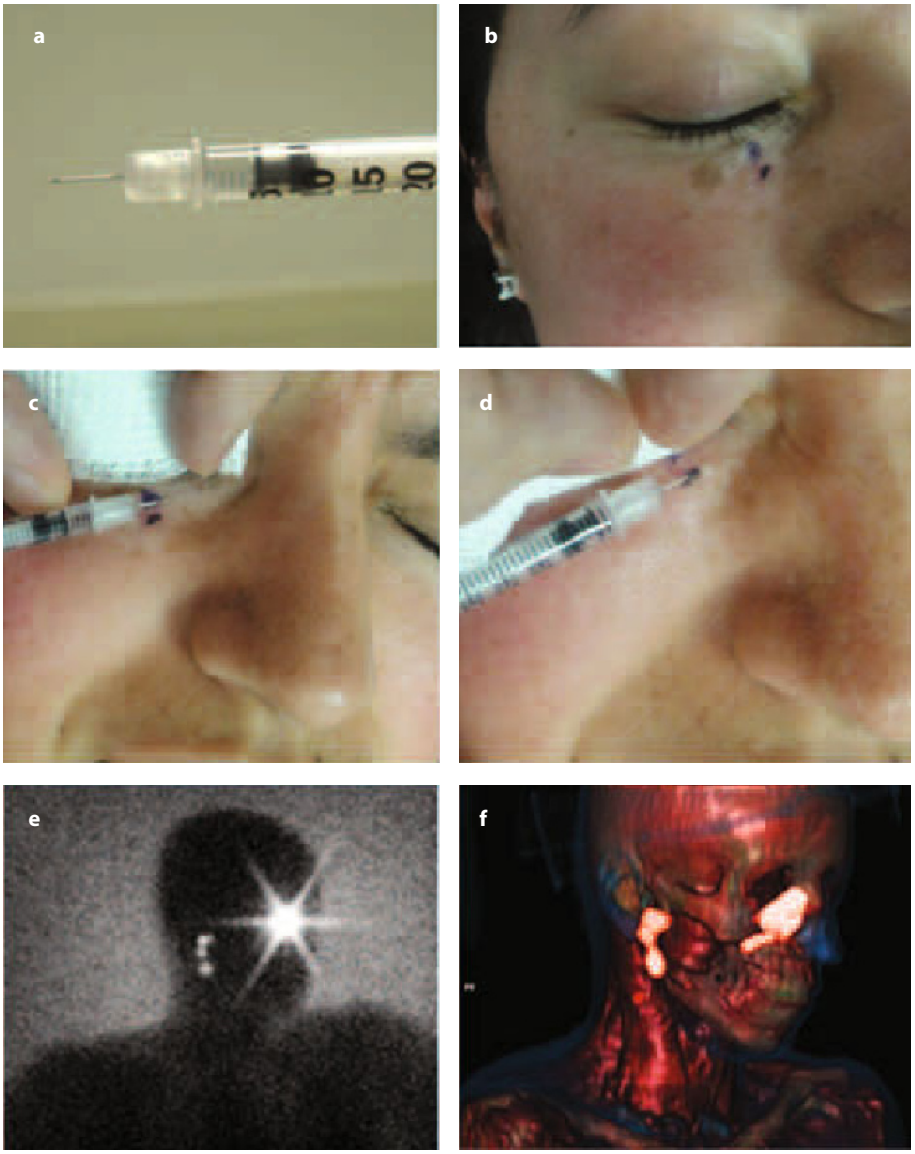

Fig. 10.1 The use of tuberculin syringes with a small volume of radiocolloid is recommended (**a**). In periorbital areas (**b**), it is advisable to cover the eye with a bandaid or cotton ball, to prevent leakage of tracer through the needle puncture site (**c**). The intradermal injection should be performed as tangentially as possible to the skin surface, raising a wheal in the cutis (**d**). In the majority of patients, lymph from this area drains to preauricular and cervical lymph nodes (level II). Three-dimensional reconstruction helps the surgeon to better select the most appropriate surgical incision, and provides a correct overview of the lymphatic mapping shown in planar images (**e** and **f**)

10.6 Preoperative Imaging of Sentinel Lymph Nodes

Preoperative lymphoscintigraphy is the first step in the lymphatic mapping procedure and is considered as a "roadmap" to guide the surgeon, especially useful for localizing unpredictable lymphatic drainage patterns.

Following injection, lymphatic imaging is performed to assess appropriate radiocolloid drainage and uptake. A large-field-of-view gamma camera is preferable, and dual-head cameras will save time. The use of flood sources (cobalt-57 [^{57}Co] or technetium-99m [^{99m}Tc]) placed beneath the patient's body in order to highlight the body contours is helpful to provide some anatomical information for the surgeon. If flood sources are not available, the use of a pointer to draw the silhouette of the patient's body may give some anatomical reference.

Dynamic acquisition is started immediately after radiocolloid injection, to define the lymphatic collectors as they head towards and reach the SLNs. Lead shielding covering the injection site may be helpful during static image acquisition, in order to detect lymph nodes close to the injection site. However, the lead shield itself carries a risk of masking draining lymph nodes. A 10–20-minute dynamic acquisition at the rate of 1 frame/minute in a 128×128 matrix is suggested, to determine where the lymphatic collectors are headed.

For delayed imaging, 5 minutes of static acquisitions in a 256×256 matrix size should be recorded over the potential lymph node field, in order to identify the collectors as they reach the actual SLNs. This procedure is important, since sometimes, especially in the groin for leg melanomas, some

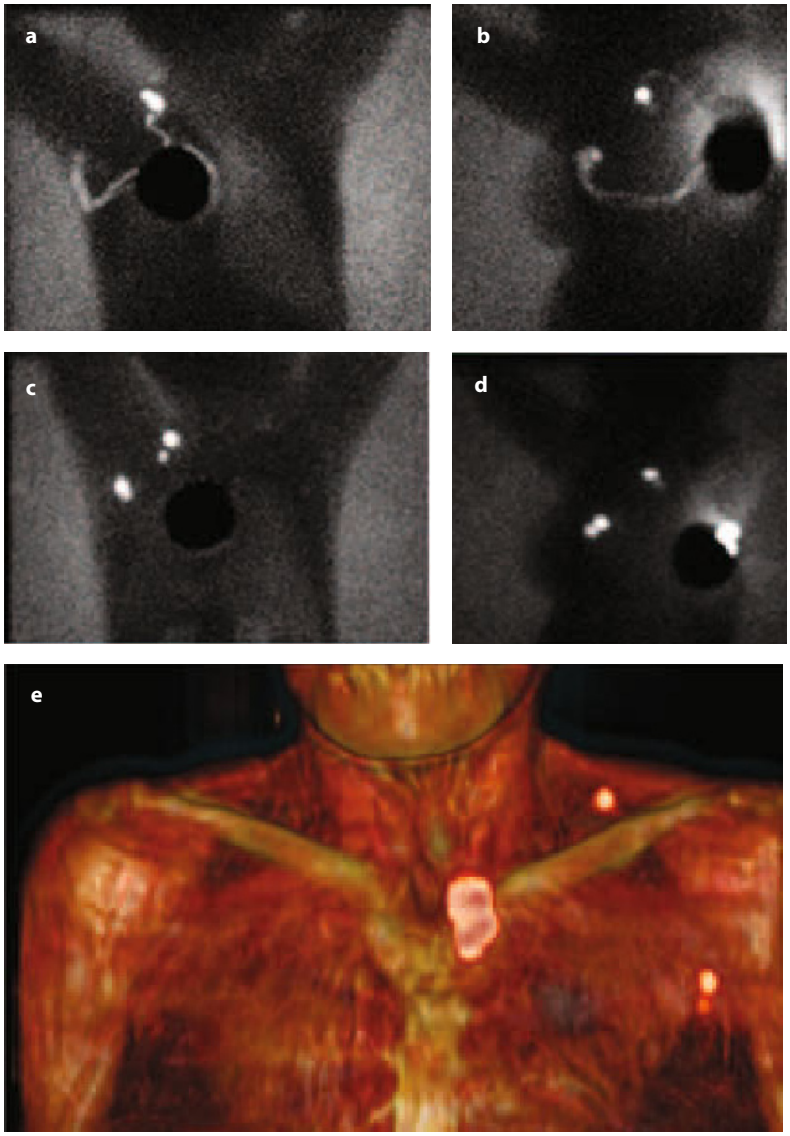

Fig. 10.2 A 37-year-old man with a 3.5 mm cutaneous melanoma located on the right upper back area. Early planar images in oblique (**a**) and right lateral (**b**) views demonstrate clearly depicted lymphatic channels going to the right axilla and right supraclavicular area. Delayed images (**c**, **d**) confirm this drainage pattern, and depict two supraclavicular SLNs and two additional SLNs in the right axilla. **e** The volume rendering image demonstrates the topographic relationship of the lymph nodes relative to other anatomical structures. All nodes were resected and micrometastasis was demonstrated in one of the supraclavicular SLNs

tracer will be seen passing through the SLN on to a second-tier node. Usually, SLN(s) are identified within 30 minutes after radiocolloid injection, but it is advisable to record 2-hour images as well, due to the possibility of delayed or slow drainage to other areas/basins.

If, during dynamic imaging, no drainage of the radiocolloid is observed from the injection site, massage with a gloved hand for 5 minutes may help. If lymph nodes are not seen or are weakly depicted, more delayed imaging may be considered, up to 24 hours after injection. If no visualization persists, reinjection of the radiocolloid is necessary. The site of each hot SLN is marked on the patient's skin, for easier identification in the operating room [17, 20].

10.7 Contribution of SPECT/CT

In melanoma patients, single photon emission computed tomography/computed tomography (SPECT/CT) is especially helpful for localizing the lymph nodes draining from primary tumors high on the trunk and in the head and neck area. This anatomic–functional technique enables more accurate nodal staging and has the potential to reduce morbidity from primary melanomas of the trunk and the head and neck.

SLNB in the head and neck region is technically demanding, because the lymph nodes are often small and located close to the injection site, where the bulk of the injected radioactivity resides. The high variability of lymphatic drainage pathways is the reason why, in many cases, elective neck dis-

sections and/or parotid gland excision do not detect the SLN. Knowing whether the node is located deep or superficially, and whether it is within or just outside the parotid gland, has important implications. The added value of SPECT/CT is clear for patients with nonvisualization on conventional scans and for patients with SLNs close to the tumor injection site. The benefit is also significant for patients with melanoma on the trunk, while it is minor in patients with melanoma of the extremities.

According to the surgeon's experience, SLNs are more accurately localized by SPECT/CT imaging, which can identify other "unseen locations" in more than of one-third of procedures. The surgical approach can be better planned on the basis of the SPECT/CT images, and in the majority of cases the incision is placed differently or the intraoperative search is facilitated. One of the major advantages is the significant reduction of operating time due to the exact anatomical and three-dimensional (3D) localization of the SLN determined by the SPECT/CT.

Another significant improvement added by the introduction of SPECT/CT in the clinical setting is the possibility of generating 3D images based on volume rendering software, to localize SLNs in relation to anatomic structures. The possibility of using different colors for different anatomical structures provides the surgeon with an excellent overview of SLNs, especially in areas such as the neck and upper part of the trunk. These images can be available on a separate screen in the operating room and thus facilitate a better roadmap for the surgeon. These images are very useful in patients with melanoma, especially in cases where the primary location is close to the site of radiocolloid injection, and for depicting in-transit SLNs, or when different lymphatic basins are explored (Fig. 10.2) [21, 22].

10.8 Intraoperative Imaging

Blue dye can be injected around the primary tumor or scar (in a similar way as the radiocolloid has been injected) 10–20 minutes before to the operation, in a volume of 0.5–1 mL. The injection should be performed after the patient is anesthetized (with either local or general anesthesia), to avoid a painful injection. Massaging the injection site for 5 minutes enhances movement of the dye through the lymphatics to the SLNs. Washout is evident after approximately 45 minutes. Blue dye is cointraindicated in pregnancy and when earlier allergic reaction to the dye has occurred [17].

Using the scintigraphic images and skin markings for initial guidance, the hand-held gamma probe (placed usually over the regions of highest counts) can be used to select the optimum location for incision. The surgeon uses the probe to guide dissection to the hot node(s) and places the probe in the surgical bed after node excision, to confirm removal of the hot node(s). A background tissue count is also recorded with the probe pointing away from the injection site, nodal activity, or other physiologic accumulations (i.e., bladder, liver).

Although a hand-held, nonimaging gamma probe is helpful in the majority of radioguided SLNBs, an intraoperative imaging technique that provides a clear perspective of the location of the sentinel node in its anatomical surroundings can facilitate the operation. As mentioned earlier, hybrid SPECT/CT has the ability to provide such information, offering a better roadmap compared to conventional images. However, there is still room for improvement during the intraoperative approach, because those images are "static" and, although the classical tracer + blue dye combination enables detection of the SLNs in most cases, in some circumstances SLN retrieval is complicated or even impossible [21].

The combination of "hot" and "blue" in the operating room has been successful in localizing the SLN in the expected lymph drainage basin. Blue dye is less effective in areas of aberrant drainage, which may be indicated preoperatively by lymphoscintigraphy. It also has a limited value in deep nodal basins. However, for cutaneous melanoma it is well known that the SLN identification rate in the head and neck is about 85%, which is considerably less than the almost 100% success rate commonly experienced for other locations. The head and neck as the site of a primary cutaneous melanoma has been found to be a predictive factor for a false-negative SLNB, as the false-negative procedures in this region have been reported to vary between 12% and 44%.

Portable gamma cameras have recently been introduced for intraoperative use. These portable devices can be oriented to the surgical targets in the operating room, based on the anatomical landmarks previously established by the SPECT/CT fused images. In both open surgery and laparoscopy, these small devices may be used in combination with a conventional, hand-held gamma probe. Some portable small-field-of-view gamma cameras can make a significant contribution, by indicating the location of the SLN in the skin, by means of laser or external radioactive pointers. This is especially valuable when the melanoma is located in the head or neck, and for SLNs located in close relationship with the injection site, which are difficult to locate by the gamma probe on its own. The portable gamma camera is also helpful to exclude a remaining hot spot after the hottest lymph node has been harvested. These devices can also help with retrieval of in-transit SLNs, which, under some circumstances, appear in rare locations [23].

The use of tomographic and fused images in the preoperative setting provides the surgeon with valuable information for planning the most suitable surgical approach. The introduction of a portable gamma camera for intraoperative guidance and real-time imaging is the next step to refine the SLN procedure in various cancer types [23, 24]. The acquisition of additional real-time scintigraphic images implies

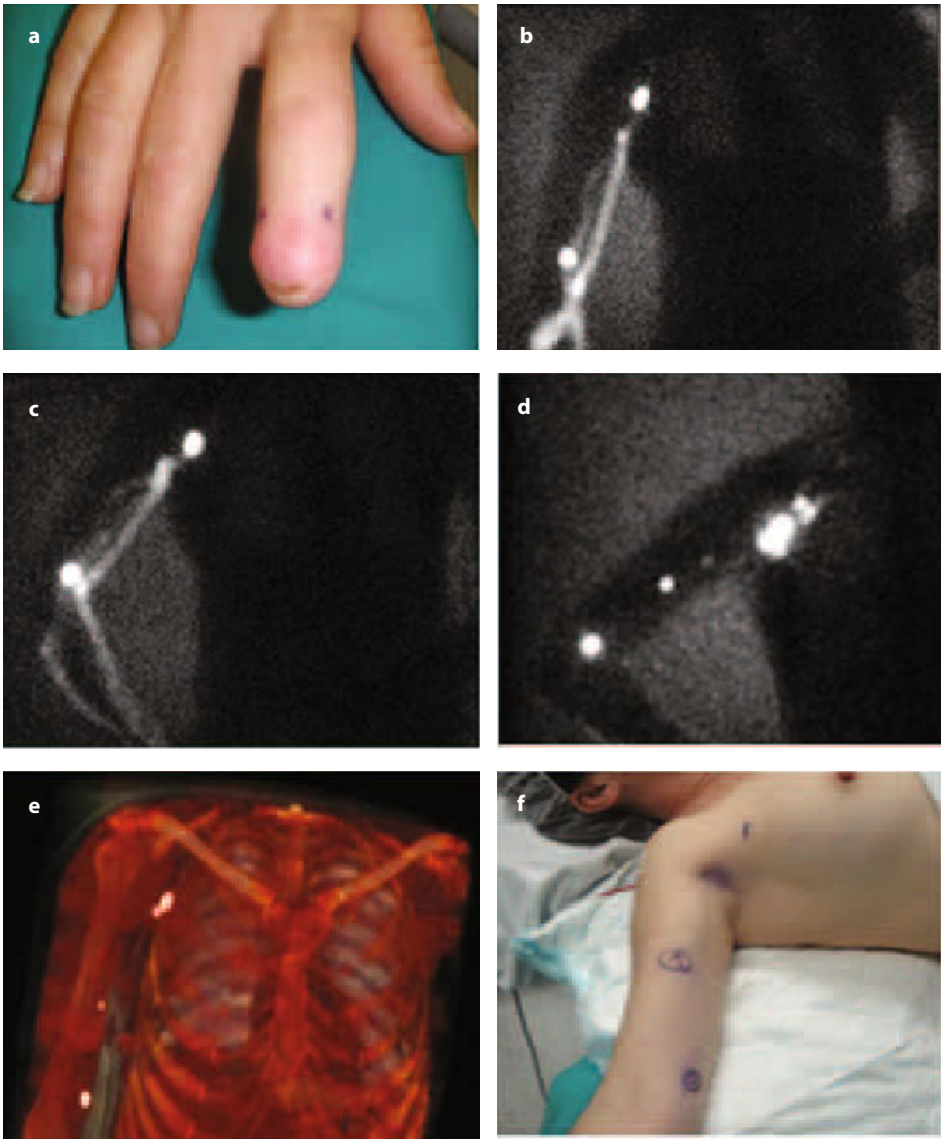

Fig. 10.3 A 35-year-old woman with a previously excised 2.3 mm Breslow subungueal melanoma. The radiocolloid was administered surrounding the base of the amputation (**a**). Early images (**b**, **c**) showed clearly different lymphatic vessels going to the elbow, arm, and axilla. Delayed planar (**d**) and SPECT/CT volume rendering (**e**) images demonstrated several foci of radiocolloid uptake at those levels, which were marked on the skin (**f**) for better identification by the surgeon during the surgical procedure. Four SLNs were harvested, and all of them were metastasis free

that surgical time may increase, depending on the level of team coordination. On the other hand, if a portable camera is not available, the surgeon may need to spend a significant amount of extra time seeking additional nodes or confirming that no more SLNs are likely to be found. Nevertheless, even if additional time is needed, this extra time could be worthwhile in the context of SLN procedures that are likely to be difficult, as the use of the gamma camera might reduce the possibility of missing a malignant SLN [24].

10.9 Common and Rare Variants

Clinicians should be aware that the majority of SLNs are found in the major nodal basins (axilla, inguinal, and cervical); in particular, predictable lymphatic drainage to the inguinal or axillary basins is observed in the majority of patients with cutaneous melanoma located in an extremity. In the groin, the drainage usually occurs to two or three superficial SLNs below the inguinal ligament. Sometimes lymph flow goes directly to Cloquet's node or to the obturator or iliac nodes, bypassing the aforementioned superficial nodes. In the axilla there are frequently one or two nodes located in Berg's level I.

However, a SLN can also be found in aberrant areas of drainage, such as the epitrochlear/epicondyleal nodal basin in the upper extremities and the popliteal nodal basin in the lower extremities (Fig. 10.3).

In the thoracic-abdominal region, lymphoscintigraphy has fundamentally modified Sappey's concept of lymphatic watersheds and ambiguous drainage along the midline of the trunk for drainage to the right or left, and along the line between a point 2 cm above the umbilicus and the level of the second lumbar vertebra on the back for cranial or cau-

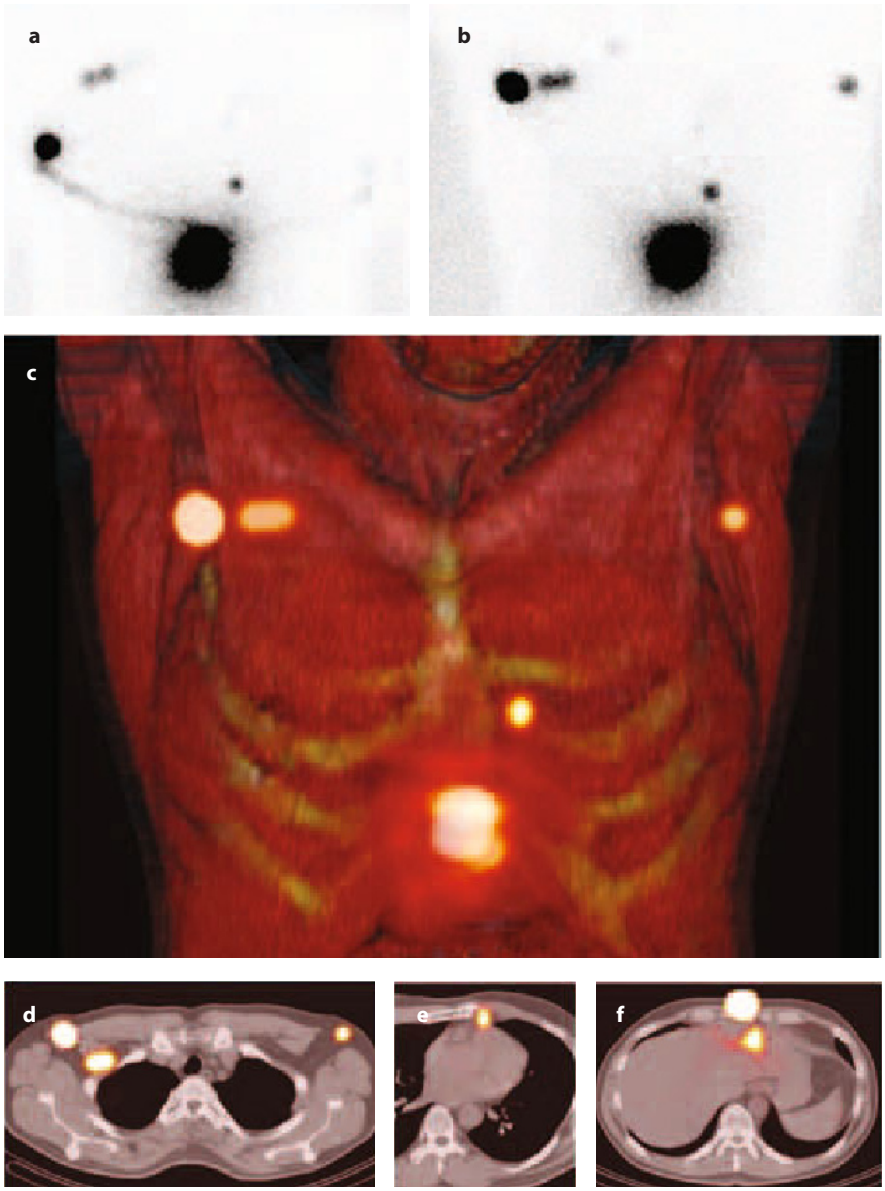

Fig. 10.4 A 42-year-old man with a 1.25 mm Breslow melanoma in the abdominal skin at the level of the xiphoid process. Planar lymphoscintigraphy and SPECT/CT performed after administration of 74 MBq ^{99m}Tc-nanocolloid in four intradermal injections around the excision scar. **a** Anterior planar image shows drainage to both axillas, with visualization of the lymphatic ducts. In the right axilla there is initial uptake in a first draining lymph node and in two second-echelon nodes. **b** In the left axilla SLN uptake is only visualized on delayed planar imaging. **c** At the level of the third intercostal space, there is a parasternal SLN, anatomically localized on the volume rendering image. **d** The axillary SLN on the right was found to contain metastasis at histopathology, whereas the SLNs of the internal mammary chain (**e**) and left axilla (**d**) were tumor free. Note the focal radioactivity in the liver region behind the injection site (**f**), which is probably related to drainage through the falciform ligament

dal drainage. Currently, the width of the area of ambiguous drainage has been extended to more than 20 cm instead of the original 5 cm, and the lymphatic drainage can reach multiple nodal basins.

When a cutaneous melanoma is located in the trunk region, preoperative lymphoscintigraphic localization to multiple nodal basins has been demonstrated in 17–32% of patients undergoing radioguided SLNB (Fig. 10.4). A melanoma in the flank may drain to the groin or the axilla, or to both. Melanomas located in the scapular region often drain to the axilla, but may also drain to a supraclavicular fossa or to an interval node located in the intermuscular space of the shoulder (Fig. 10.5). In patients with melanoma in the lower trunk or lumbar region, there is often one SLN located cranially with respect to the inguinal ligament.

Likewise, preoperative lymphoscintigraphic localization to in-transit (interval, aberrant) SLNs has been demonstrated in 3–10% of these patients. Metastatic disease is found in approximately 18% of these in-transit SLNs (a rate that is similar to the rate found in conventional lymph node basins), and the status of one basin does not predict the status of the other (Fig. 10.6). The highest incidence of in-transit SLNs occurs in the posterior trunk, followed by the anterior trunk, the head and neck, the upper limbs, and the lower limb areas. On the other hand, the use of preoperative lymphoscintigraphy has shown results that are discordant with clinical predictions of nodal drainage. In fact, the SLN is not always found in the closest nodal basin. Accurate lymphoscintigraphy helps to identify all the nodes receiving direct lymphatic drainage from a primary tumor site, regardless of the location.

Several studies have demonstrated that the lymphatic drainage of melanomas of the head, neck, and trunk cannot

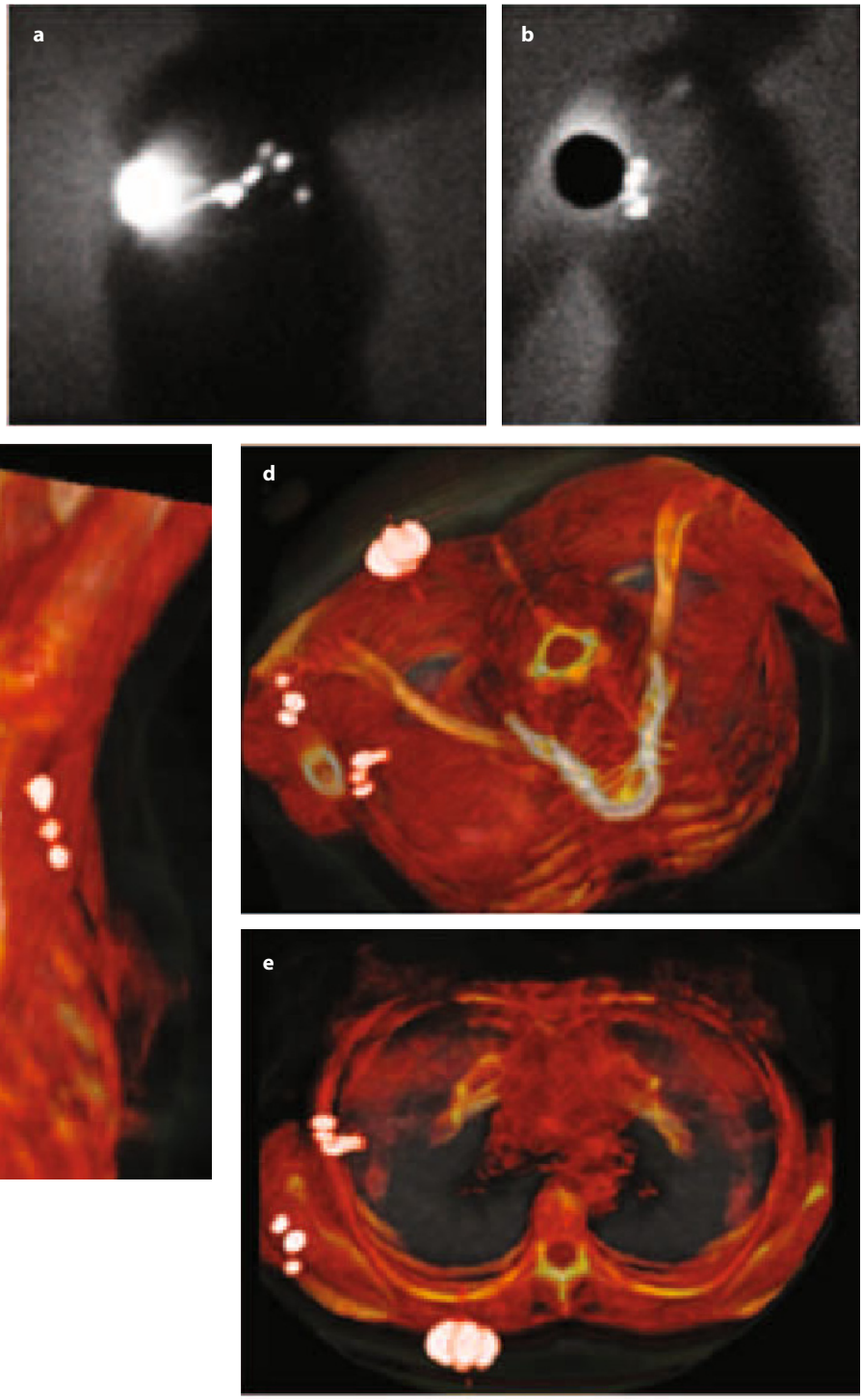

Fig. 10.5 A 29-year-old woman with a melanoma in the right upper back. After injection of 111 MBq ^{99m}Tc-nanocolloid in four intradermal depots around the excision scar, planar images were obtained (**a**, **b**). These images showed lymphatic drainage with multiple depots towards the right axilla. Fused SPECT/CT images and volume rendering reconstruction (**c**–**e**) clearly demonstrated the intermuscular and axillary location of these lymph nodes. In melanomas of the upper back region, obtaining several views or/and SPECT/CT is of utmost importance to rule out the possibility of interval or aberrant SLNs

be predicted reliably by the classic anatomic guidelines of Sappey, as lymphoscintigraphy demonstrates direct drainage from these sites to SLNs in aberrant locations. Multiple-basin drainage or interval lymph nodes may also be identified. This possibility highlights the importance of preoperative lymphoscintigraphy for these patients. Bilateral drainage can be seen in about 10–15% of patients, and visualization of multiple SLNs is frequent (Fig. 10.7). It is also important to note that the highly concentrated radioactivity remaining at the injection site can obscure a nearby SLN. Therefore, lateral and oblique views are mandatory (and SPECT/CT whenever available) [25]. A summary of potential lymphatic drainage from a certain skin area can be obtained from a 3D computer model of the skin and lymph nodes. This tool displays heat maps to visualize the likelihood of drainage of any skin region of the body to a specific node field [26].

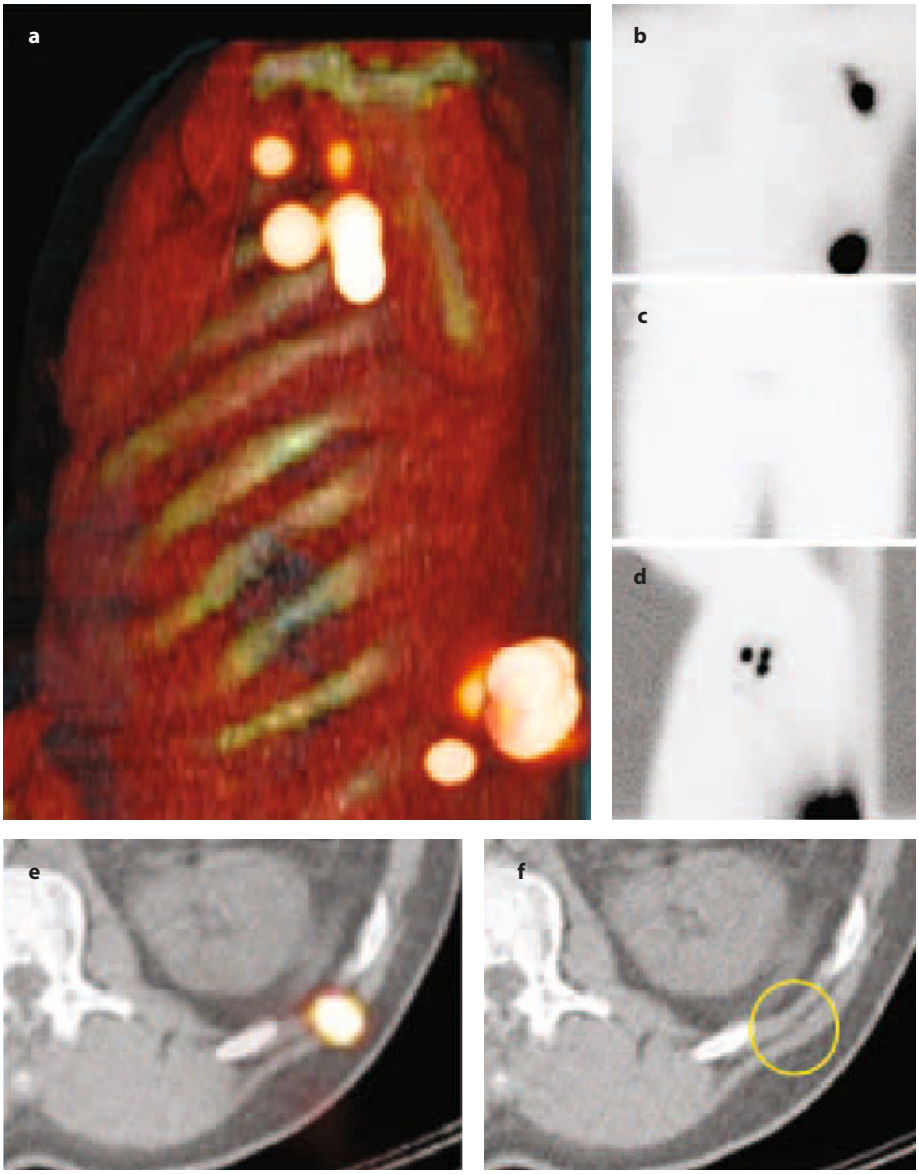

Fig. 10.6 A 36-year-old man with a 2.8 mm Breslow melanoma of the left side of the back. Planar lymphoscintigraphy and SPECT/CT performed after administration of 71 MBq ^{99m}Tc-nanocolloid in four intradermal injections around the excision scar. **a** On volume rendering image, not only axillary lymph nodes are seen, but also a lymph node close to the injection site. This SLN was not depicted on planar imaging (**b**–**d**) and was localized by axial SPECT/CT (**e**) and CT (**f**) between the muscles in the intercostal space (*yellow circle*). All SLNs were surgically removed and found to be tumor free at histopathology

10.10 Technical Pitfalls in Lymphatic Mapping

Improvements in the technique of lymphoscintigraphy lead to an extremely high SLN visualization in melanoma patients (virtually 100%).

However, there are some pitfalls when interpreting lymphoscintigraphic images. There is a need to confirm a true nodal versus non-nodal sites of uptake, such as skin folds, radiopharmaceutical contamination, and lymphangiomas, which are common causes of false-positive results on conventional planar imaging (Fig. 10.8). At present, the addition of SPECT/CT to the SLN mapping has contributed to solving many of these situations.

Contamination will occur if the needle is not tightly set, or the injection site leaks under pressure. Furthermore, leakage can result from high resistance to penetration of the injection fluid in the skin (typically, on the head and soles of the feet and hands). Injection of part of the radiocolloid into a blood vessel is another pitfall that is frequently observed.

On the other hand, no apparent radiocolloid migration and no hot spot is observed at all in some other patients; there are several possible explanations for this situation: unsatisfactory radiocolloid quality, small amount of radioactivity injected, the patient's age, lymphatic blockade by metastatic cells, tumor involvement of the SLN, interval between injection and lymphoscintigraphy, and when a skin graft has been applied to cover the skin resection. Delayed images (up

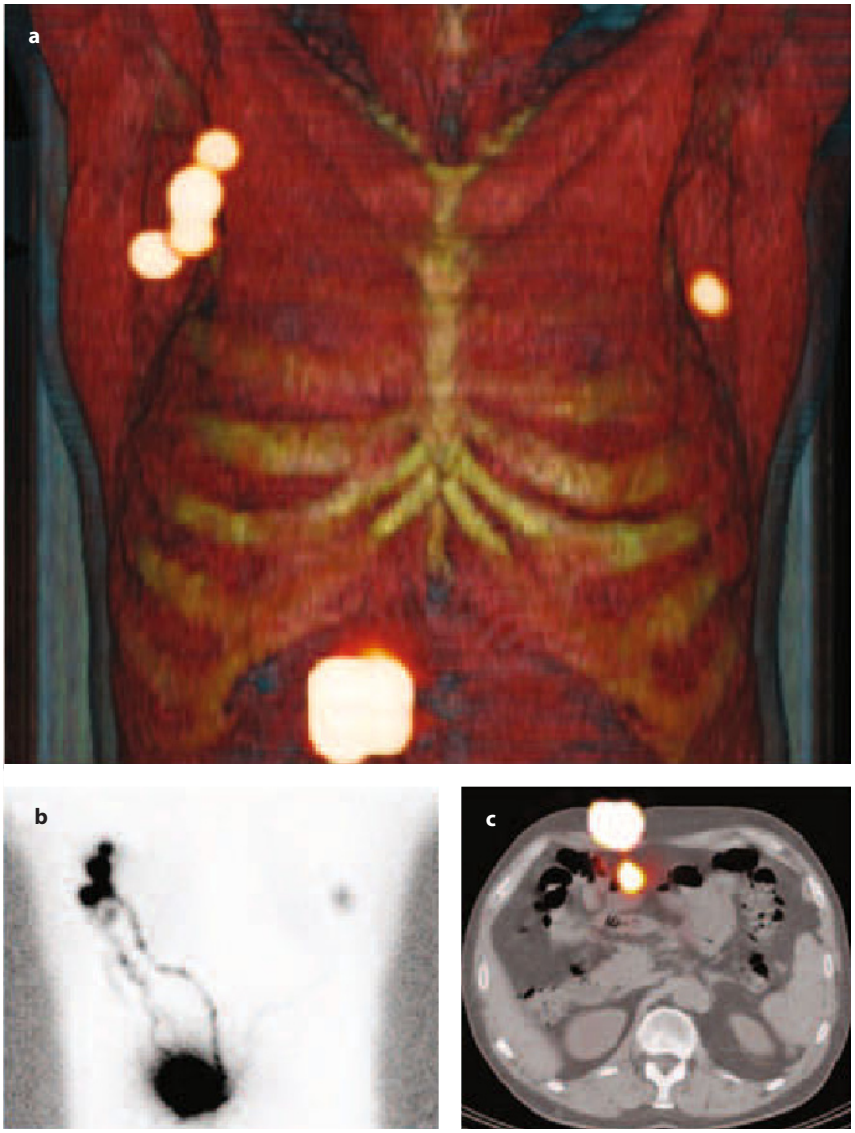

Fig. 10.7 A 66-year-old patient with a 2.1 mm Breslow melanoma of the abdominal skin. Planar lymphoscintigraphy and SPECT/CT performed after administration of 108 MBq ^{99m}Tc-nanocolloid in four intradermal injections around the excision scar. **a** Volume rendering image shows radioactive lymph nodes in both axillas. **b** Early anterior planar imaging shows three lymphatic ducts from the injection site to the lymph nodes of the right axilla, and one to the left axilla. Four SLNs in the right axilla and one in the left axilla were removed, and found to be free of metastases. **c** Note on the fused axial SPECT/CT image a radioactive accumulation behind the injection site, which is probably related to uptake in a mesenterial lymph node

to 20 hours after injection) can solve many of these cases, although a second set of radiocolloid administrations might be another option.

Images of all areas from the injection site to the primary lymphatic basin must be acquired, since in-transit nodes can be missed if the path of radiocolliod is not followed. In areas below the knee, evaluation of the popliteal area is important. For sites below the elbow, the epitrochlear and arm areas must be explored, since SLNs at these locations can occur in about 10% of patients. If a lead shield is placed over the injection site to reduce the shine-through effect, care must be taken not to mask a nearby SLN.

Dynamic and early static images are essential in identifying SLNs as the nodes that receive direct lymphatic drainage from the tumor site. SLNs are not necessarily the hottest nodes, although it may often be the case. In melanoma, lymph nodes with their own lymphatic duct, or single nodes in a basin, may frequently be visualized and identified as definite SLNs. Lymph nodes with increasing intensity or appearing between the injection site and the first draining nodes are considered highly probable SLNs. Nodes indicated as definite or highly probable SLNs on lymphoscintigraphy must be sampled by surgeons, regardless of the count rate (see Chapter 8).

Delayed images are helpful in detecting SLNs close to the primary tumor (the injection site), which may have been obscured on early imaging, and to detect lymphatic drainage to multiple nodal basins. After recording an anterior view, a lateral view in the groin is often helpful to identify collectors passing to deep iliac or obturator lymph nodes. In

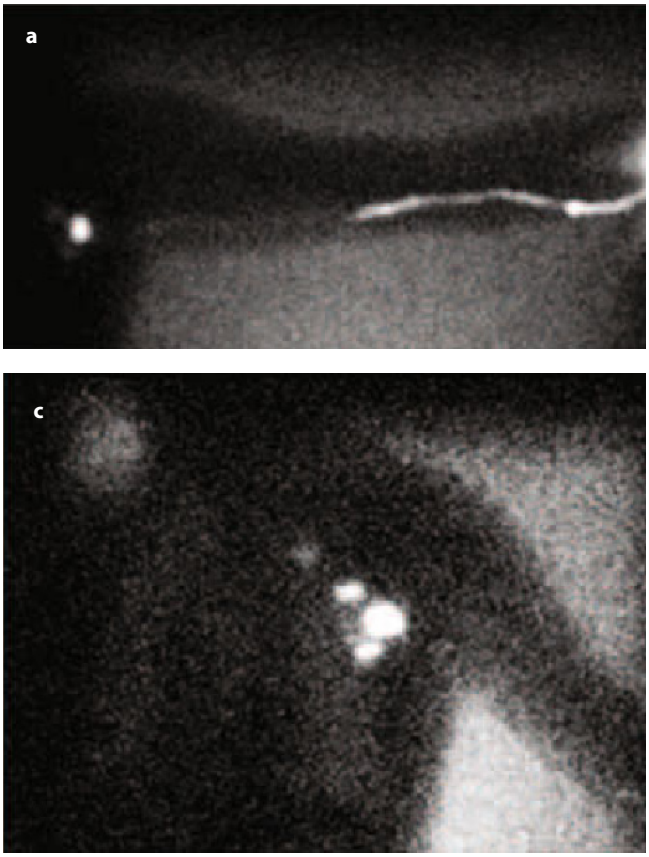

Fig. 10.8 A 37-year-old woman with a 2.10 mm Breslow melanoma on the left forehand. Planar lymphoscintigraphic images after administration of 111 MBq ^{99m}Tc-nanocolloid in four intradermal injections around the biopsy scar. **a** Anterior early planar imaging shows early visualization of a lymphatic channel through the medial part of the extremity and a SLN in the left axilla. **b**, **c** Delayed images show a higher uptake in the axillary nodes and confirm the presence of a hot spot near the injection site. This uptake can be mistaken for an in-transit SLN. In this case, it was a lymphangioma. The identification of such a hot spot near the injection site can be misleading. During surgery, portable gamma cameras can be of great utility to ascertain these focal areas of radiocolloid accumulation (colored square on **b**; image obtained with a portable gamma camera Sentinella S102)

the head/neck region, other views (such as oblique or vertex views) are often necessary after acquiring the conventional orthogonal views. Nevertheless, as summarized above, all these features are today more succesfully solved by using SPECT/CT.

Clinical Cases

Case 10.1
Sentinel Node Mapping in Melanoma of the Head and Neck: Drainage to "in Transit" Nodes in the Occipital Region (Planar Imaging)

Giuseppe Rubini and Maria Antonia Renna

Background Clinical Case

A 66-year-old man with black, ulcerated lesion of the scalp (10 mm in diameter and a black satellite macula) located in the median parieto-occipital region with dermatoscopic features compatible with nodular melanoma, underwent excisional biopsy. At histology, the melanoma was composed by spindle and epithelioid cells, round to oval nuclei, large nucleoli and heavy intracytoplasmic accumulation of melanin (3.3 mm Breslow thickness, IV Clark). Physical and preoperative examinations (ultrasonography) did not reveal lymphadenopathy.

Lymphoscintigraphy

Lymphoscintigraphy was performed 6 h before sentinel node biopsy, to define the draining lymphatic basin at risk for metastatic disease and to identify the corresponding sentinel lymph node. Aliquots of 0.4 mL containing 18 MBq of ^{99m}Tc-albumin nanocolloid (Nanocoll) were injected intradermally around the skin margins of the surgical scar, since the primary lesion had already been excised for biopsy. A dual-detector SPECT/CT gamma camera (Infinia Hawkeye GE Healthcare, Milwaukee, WI) equipped with low-energy general purpose (LEGP) collimators was used to obtain planar images of the abdominal region by early dynamic imaging (1 frame/min for 30 min, 256×256 matrix, zoom 1.00) and delayed static imaging in anterior, and lateral views (128×128 matrix, zoom 1.00).

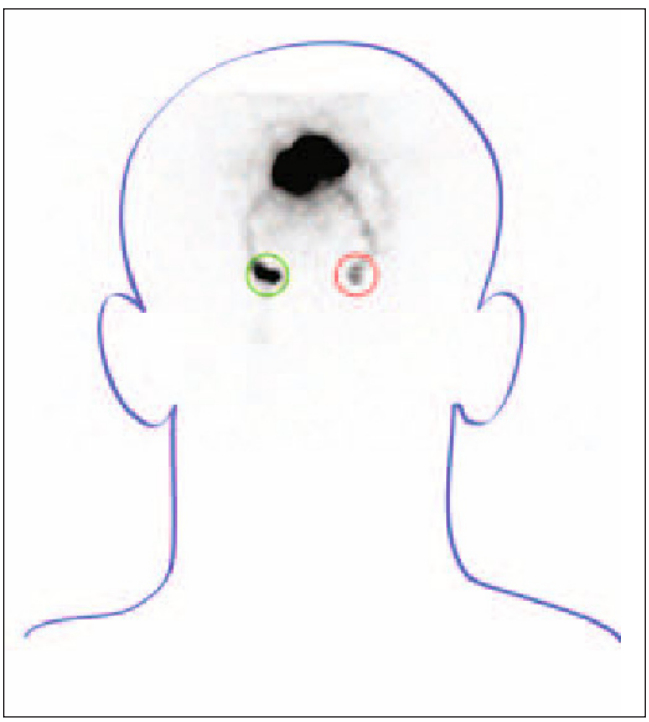

Fig. 1 Schematic representation of posterior static acquisition of the head 30 min after radiopharmaceutical injections showing two upper occipital focal areas of uptake (*green and red circles*), corresponding to two "in-transit" sentinel lymph nodes

Case 10.2
Sentinel Node Mapping in Melanoma of the Abdomen: Drainage to Axillary and Parasternal Nodes (Planar Imaging)

Giuseppe Rubini and Maria Antonia Renna

Background Clinical Case

A 51-year-old man with ulcerative nodular lesion of the right portion of the abdomen underwent excisional biopsy. Histology revealed a heavily pigmented dermal, asymmetric and poorly circumscribed neoplasm, involving the dermo-epidermal junction (Clark's level IV, Breslow 1.6 mm). Preoperative computed tomography (CT) of the head, neck, chest and abdomen was normal.

Lymphoscintigraphy

Lymphoscintigraphy was performed 3 h before sentinel node biopsy, to define the draining lymphatic basin at risk for metastatic disease and to identify the corresponding sentinel lymph node. Aliquots of 0.4 mL containing 14 MBq of ^{99m}Tc-albumin nanocolloid (Nanocoll) were injected intradermally around the skin margins of the surgical scar, since the primary lesion had already been excised for biopsy. A dual-detector SPECT gamma camera (Millennium MG GE Healthcare, Milwaukee, WI) equipped with low-energy high-resolution (LEHR) collimators was used to obtain planar images of the abdominal region by early dynamic imaging (1 frame/min for 30 min) and delayed static imaging (anterior and lateral views), with a 128×128 matrix and zoom factor 1.00.

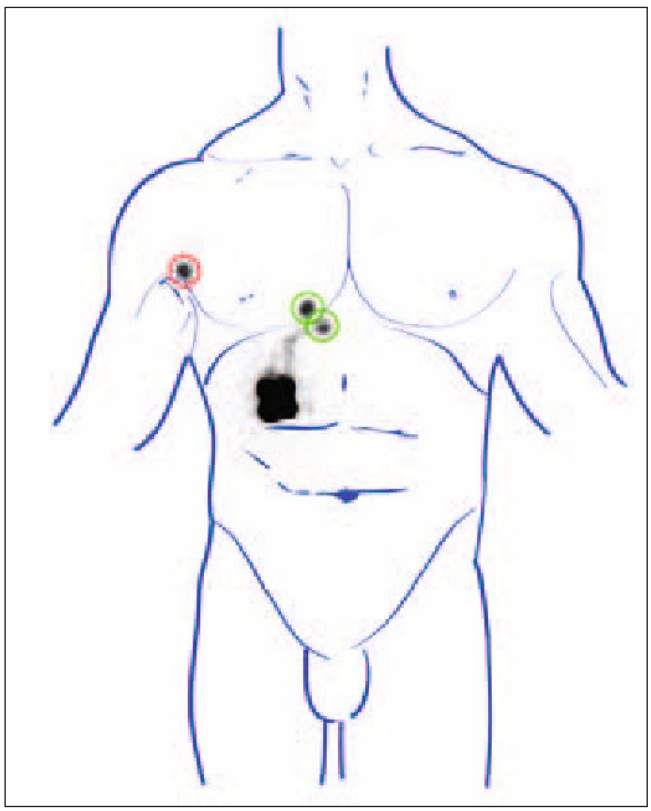

Fig. 1 Schematic representation of anterior static acquisition of the abdomen 30 min after radiopharmaceutical injections showing one right axillary sentinel lymph node (*red circle*), and two right parasternal sentinel lymph nodes (*green circles*)

Case 10.3
Sentinel Node Mapping in Melanoma of the Back: Drainage to "in Transit" Paravertebral Nodes (Planar Imaging)

Giuseppe Rubini and Maria Antonia Renna

Background Clinical Case

A 74-year-old man with a lesion of the left lumbar region underwent excisional biopsy. At histological examination the melanoma was in radial growth phase, with epithelioid cells, and extended to the reticular dermis (Breslow 0.75 mm; Clark's level III). No axillary or groin lymphadenopathy was detected at ultrasonography examination.

Lymphoscintigraphy

Lymphoscintigraphy was performed 2 h before sentinel node biopsy, to define the draining lymphatic basin at risk for metastatic disease and to identify the corresponding sentinel lymph node. Aliquots of 0.4 mL containing 5 MBq of ^{99m}Tc-albumin nanocolloid (Nanocoll) were injected intradermally around the skin margins of the surgical scar, since the primary lesion had already been excised for biopsy. A dual-detector SPECT gamma camera (Infinia Hawkeye GE Healthcare, Milwaukee, WI) equipped with low-energy general purpose (LEGP) collimators was used to obtain planar images of the back region by early dynamic imaging (1 frame/min for 30 min, 256×256 matrix) and delayed static imaging in anterior, oblique, and lateral views (128×128 matrix, zoom factor 1.00).

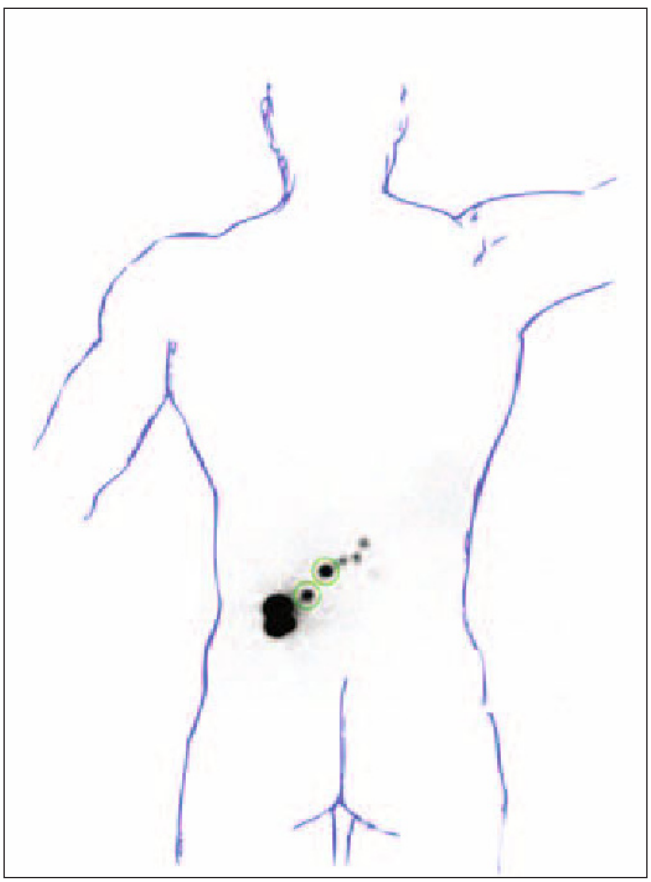

Fig. 1 Schematic representation of static posterior acquisition of the back 30 min after radiopharmaceutical injections showing several areas of focal uptake corresponding to left paravertebral "in-transit" sentinel lymph nodes (*green circles*)

Case 10.4
Sentinel Node Mapping in Melanoma of the Back: Bilateral Drainage to Left "in Transit" Subscapular and Left Axillary Nodes (Planar Imaging)

Giuseppe Rubini and Maria Antonia Renna

Background Clinical Case

A 68-year-old man with nodular melanoma of the back, already surgically removed for biopsy. At histological examination the melanoma was in radial growth stage, with spindle-like cells, and extended to the reticular dermis (Breslow 1.2 mm; Clark's level IV).

Lymphoscintigraphy

Lymphoscintigraphy was performed 3 h before sentinel node biopsy, to define the draining lymphatic basin at risk for metastatic disease and to identify the corresponding sentinel lymph node. Aliquots of 0.4 mL containing 5 MBq of ^{99m}Tc-albumin nanocolloid (Nanocoll) were injected intradermally around the skin margins of the surgical scar, since the primary lesion had already been excised for biopsy. A dual-detector SPECT gamma camera (Infinia Hawkeye GE Healthcare, Milwaukee, WI) equipped with low-energy general purpose (LEGP) collimators was used to obtain planar images of the back region by early dynamic imaging (1 frame 60s/30 fremes 256×256 matrix, zoom factor 1.00) and delayed static imaging in anterior, oblique, and lateral views (128×128 matrix, zoom factor 1.00).

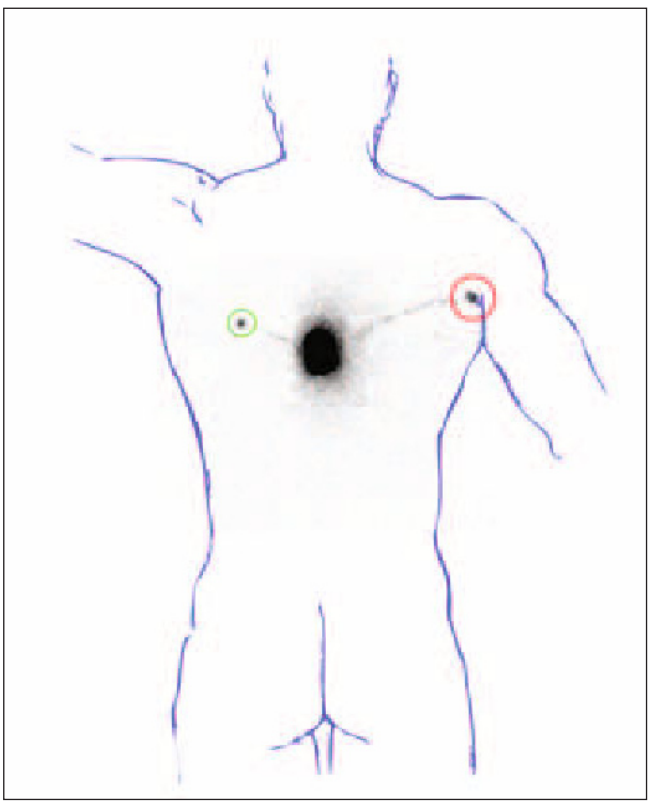

Fig. 1 Schematic representation of static posterior acquisition of the back 30 min after radiopharmaceutical injections showing one right axillary sentinel lymph node (*red circle*) and one left "in-transit" subscapular sentinel lymph node (*green circle*)

Case 10.5
Sentinel Node Mapping in Melanoma of the Head and Neck: Drainage to Ipsilateral Cervical Nodes (Planar and SPECT/CT Imaging)

Gianpiero Manca, Valerio Duce, Manuel Tredici, Sara Mazzarri, and Giuliano Mariani

Background Clinical Case

A 65-year-old man with melanoma (ulcerative nodular melanoma, 2.2 Breslow thickness, IV Clark, 3 mitoses per mm^2) in the left zygomatic region was submitted to lymphoscintigraphy for radioguided sentinel lymph node biopsy.

Lymphoscintigraphy

Lymphoscintigraphy was performed 18 h before sentinel node biopsy, to define the draining lymphatic basin at risk for metastatic disease and to identify the corresponding sentinel lymph node. Aliquots of 0.1–0.2 mL containing 4–8 MBq of ^{99m}Tc-albumin nanocolloid were injected intradermally around the skin margins of the surgical scar, since the primary lesion had already been excised for biopsy. A dual-detector SPECT/CT gamma camera (Discovery NM/CT 670 GE Healthcare, Milwaukee, WI) equipped with low-energy high-resolution (LEHR) collimators and multislice spiral CT was used to obtain head-neck planar images, by early dynamic imaging (1 frame/min for 30 min), delayed static imaging (anterior and lateral views), and SPECT/CT acquisition (using a step-and-shoot protocol of 25 s/3° for a total of 60 views per camera head, 128×128 matrix, zoom factor 1.00). CT parameters included a current of 40 mA, a voltage of 120 kV, and a slice thickness of 3.75 mm slice.

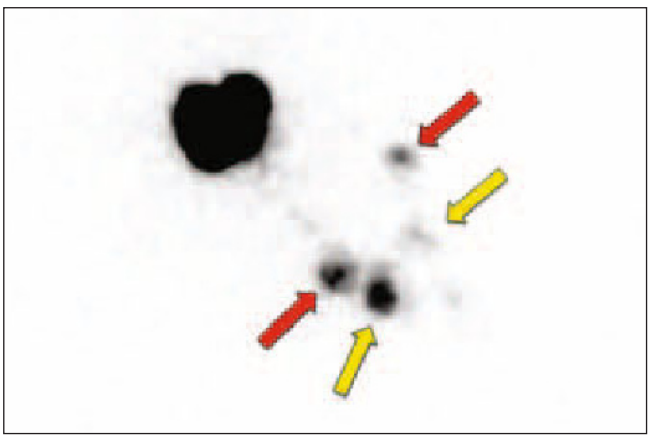

Fig. 1 Planar imaging (left lateral view) shows two separate lymphatic channels leading to two separate areas of focal uptake of the tracer corresponding to two left laterocervical sentinel lymph nodes (*red arrows*), without specifying their topographic location. Serial visualization of at least two subsequent-tier nodes (*yellow arrows*)

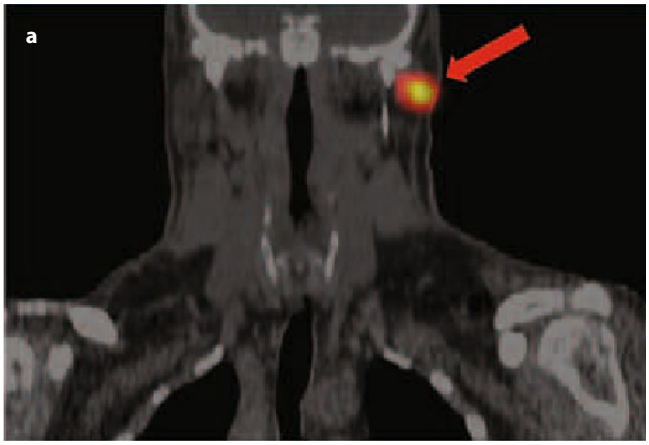

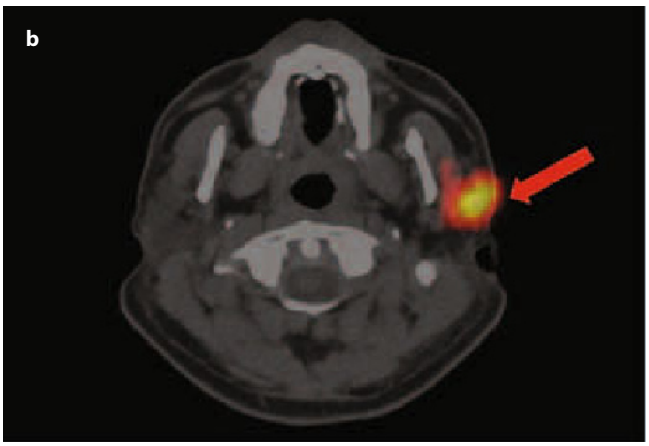

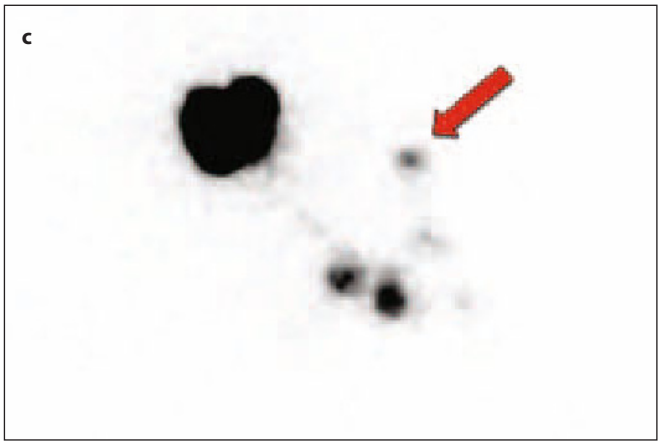

Fig. 2 SPECT/CT fused images in coronal (**a**) and axial (**b**) planes show that one out of two sentinel lymph nodes (*red arrow*) observed in left lateral view (**c**) is located at Robbins's anatomical level IIb

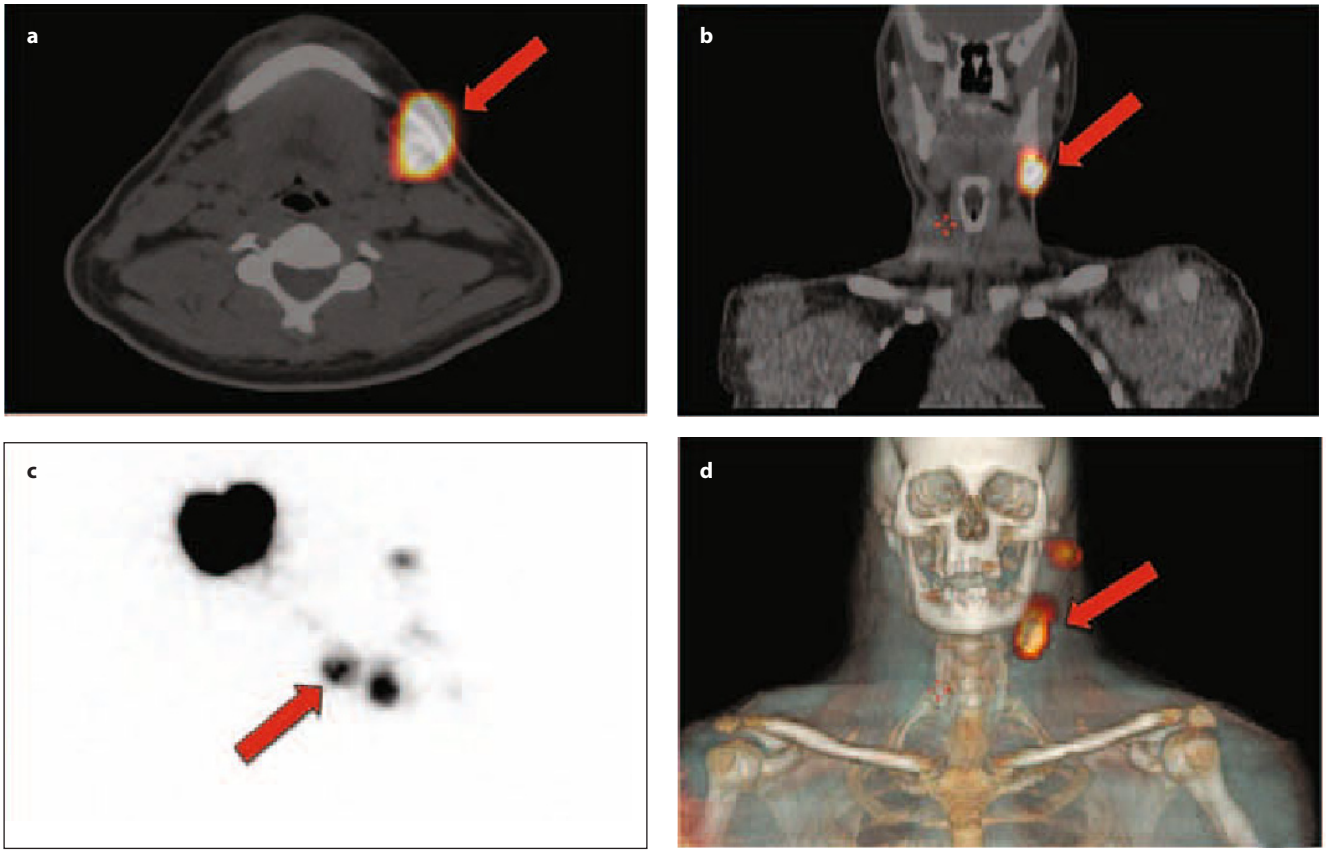

Fig. 3 SPECT/CT fused images in axial (**a**) and coronal (**b**) sections show that the other area of focal uptake (*red arrow*) demonstrated on the planar imaging (**c**) corresponds to a laterocervical sentinel lymph node located at Robbins's anatomical level IIa. This sentinel lymph node is displayed using 3D volume rendering (**d**) for better anatomical identification (*red arrow*)

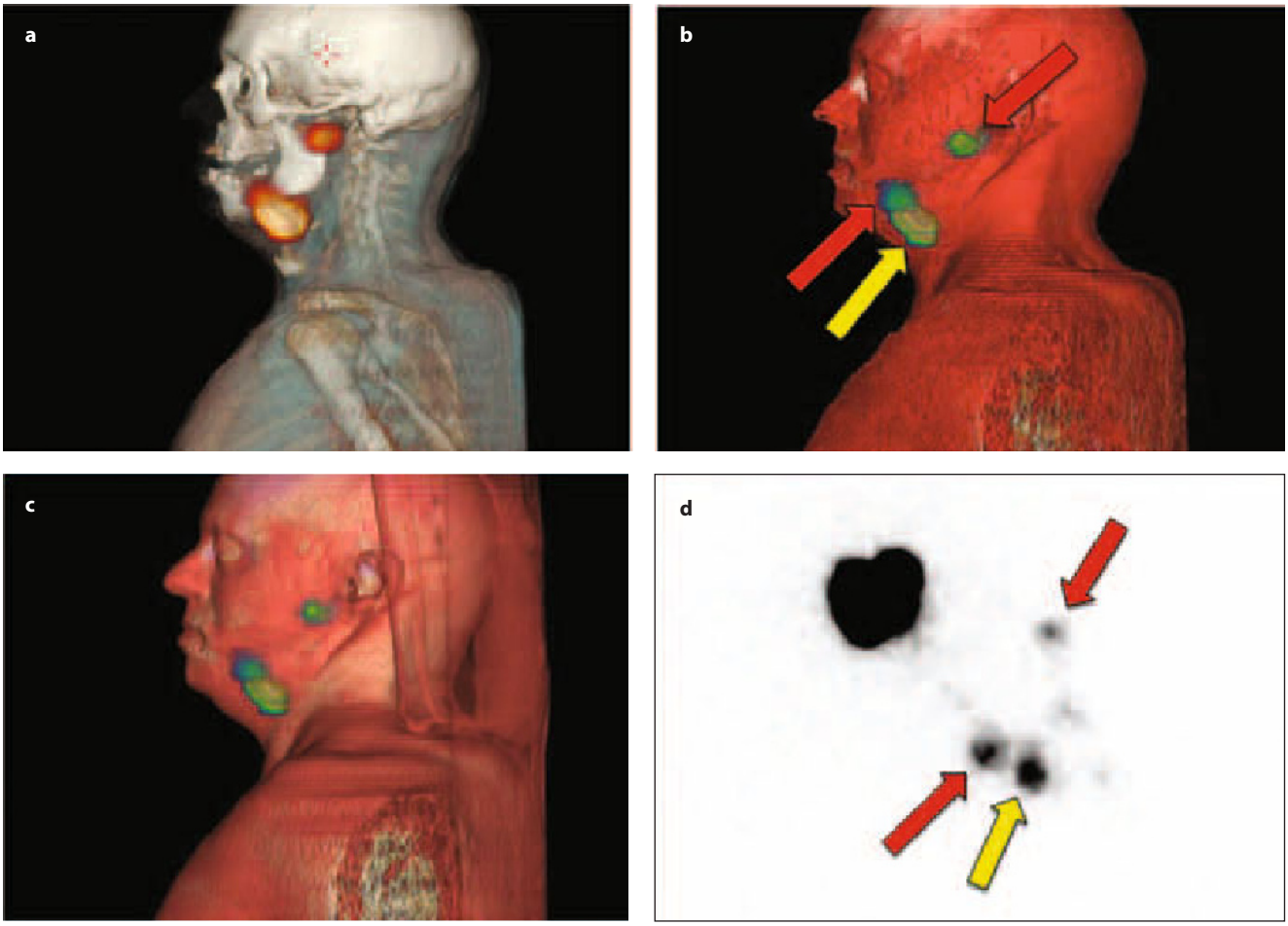

Fig. 4 **a–c** Laterocervical sentinel lymph nodes (*red arrows*) and a subsequent laterocervical-tier radioactive node (*yellow arrow*) by 3D volume rendering. **d** Planar scintigraphy in the left lateral view

Case 10.6
Sentinel Node Mapping in Melanoma of the Right Scapular Region: Drainage to Ipsilateral Cervical Nodes (Planar and SPECT/CT Imaging)

Gianpiero Manca, Valerio Duce, Manuel Tredici, Sara Mazzarri, and Giuliano Mariani

Background Clinical Case

A 56-year-old man with pigmental lesion of the skin in the right scapular region was submitted to lymphoscintigraphy for radioguided sentinel lymph node biopsy, after excisional biopsy had demonstrated a melanoma (1.6 Breslow thickness, IV Clark, 2 mitoses per mm^2).

Lymphoscintigraphy

Lymphoscintigraphy was performed 18 h before sentinel node biopsy, to define the draining lymphatic basin at risk for metastatic disease and to identify the corresponding sentinel lymph node. Aliquots of 0.1–0.2 mL containing 4–8 MBq ^{99m}Tc-albumin nanocolloid (Nanocoll) were injected intradermally around the skin margins of the surgical scar, since the primary lesion had already been excised for biopsy. A dual-detector SPECT/CT gamma camera (Discovery NM/CT 670 GE Healthcare, Milwaukee, WI) equipped with low-energy high-resolution (LEHR) collimators and multislice spiral CT was used to obtain planar images of the cervical thoracic region, by early dynamic imaging (1 frame/min for 30 min), delayed static imaging (anterior, oblique, and lateral views), and SPECT/CT acquisition (using a step-and-shoot protocol of 25 s/3° for a total of 60 views per camera head, 128×128 matrix, zoom factor 1). CT parameters included a current of 40 mA, a voltage of 120 kV, and a slice thickness of 3.75 mm.

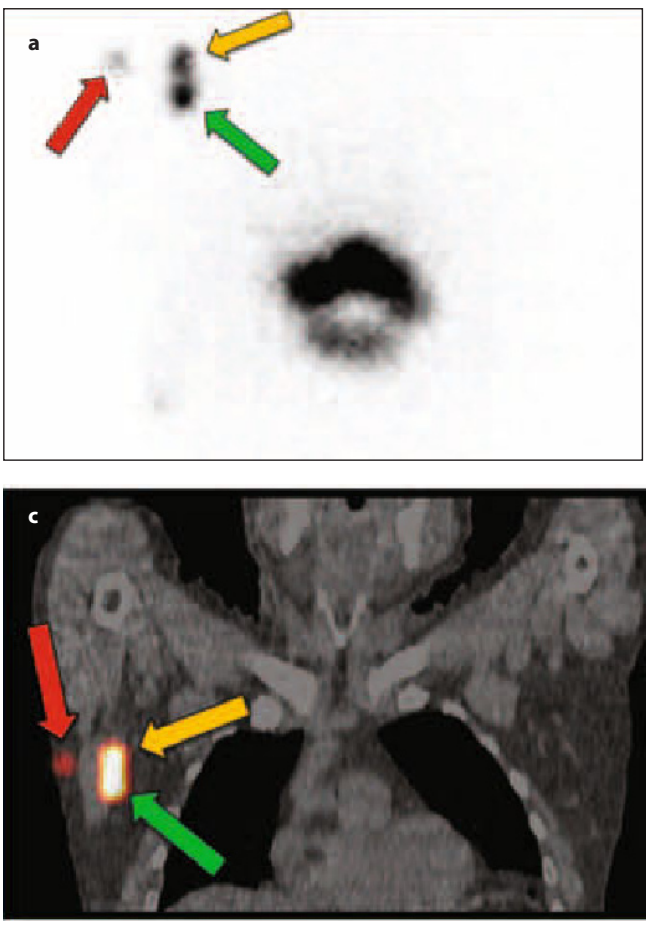

Fig. 1 **a** Planar lymphoscintigraphy (anterior view) shows three radioactive nodes in right axilla (*red, green, and yellow arrows*). SPECT/CT fused images in axial (**b**, **d**) and coronal (**c**) planes demonstrate that two out of three nodes are axillary sentinel lymph nodes (*green and yellow arrows*), while the other is a subcutaneous ("in-transit") sentinel lymph node (*red arrow*)

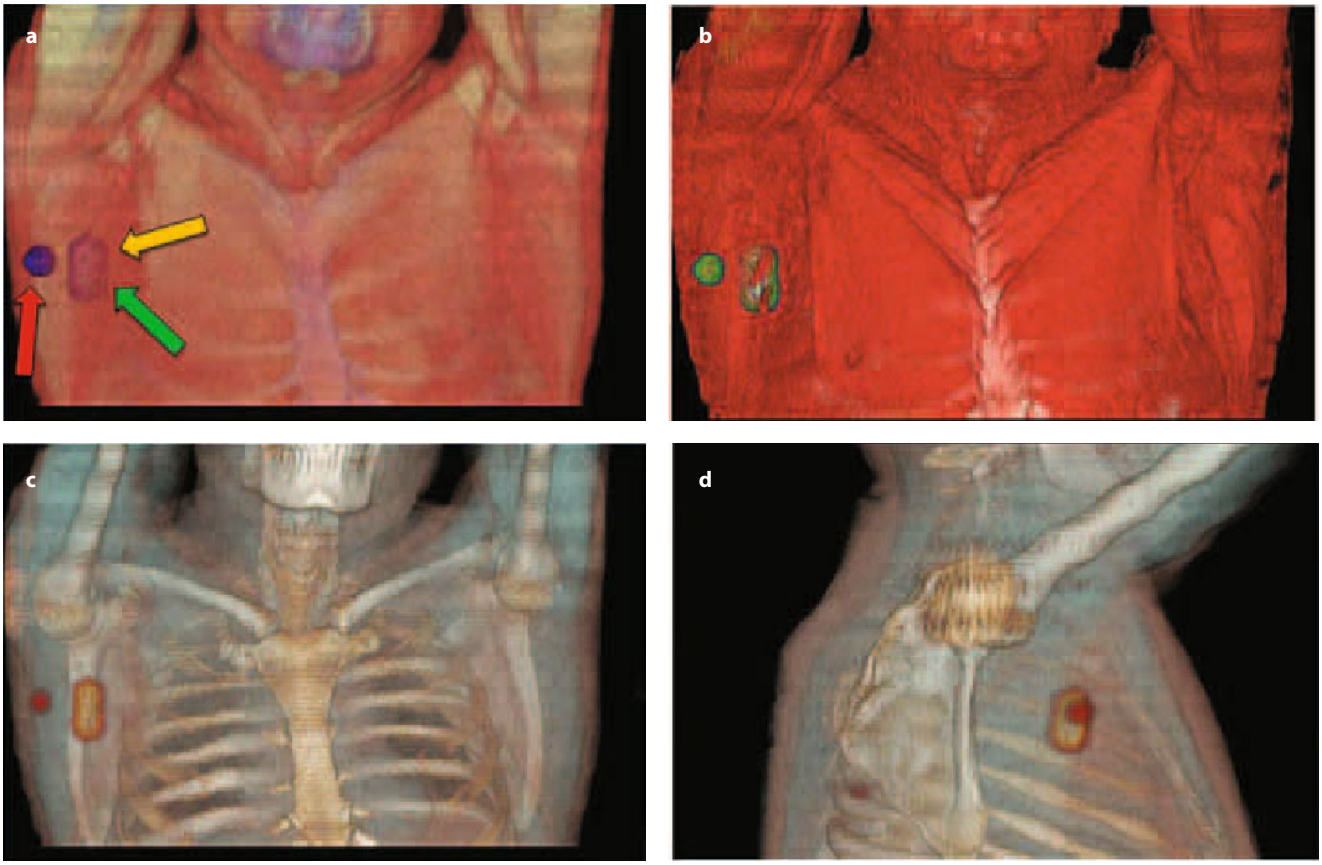

Fig. 2 a–d Axillary sentinel lymph nodes (*green and yellow arrows*) and subcutaneous ("in-transit") sentinel lymph node (*red arrow*) are displayed using 3D volume rendering for better anatomical identification

Case 10.7
Sentinel Node Mapping in Melanoma of the Back: Drainage to Bilateral Supraclavicular Nodes and Ipsilateral Cervical and Axillary Nodes (Planar and SPECT/CT Imaging)

Gianpiero Manca, Valerio Duce, Manuel Tredici, Sara Mazzarri, and Giuliano Mariani

Background Clinical Case

A 34-year-old man with melanoma (ulcerative nodular melanoma, 1.8 Breslow thickness, IV Clark, 2 mitoses per mm2) localized on the paramedian region of the upper back on the left was submitted to lymphoscintigraphy for radioguided sentinel lymph node biopsy.

Lymphoscintigraphy

Lymphoscintigraphy was performed 18 h before sentinel node biopsy, to define the draining lymphatic basin at risk for metastatic disease and to identify the corresponding sentinel lymph node. Aliquots of 0.1–0.2 mL ontaining 4–8 MBq ^{99m}Tc-albumin nanocolloid (Nanocoll) were injected intradermally around the skin margins of the surgical scar, since the primary lesion had already been excised for biopsy. A dual-detector SPECT/CT gamma camera (Discovery NM/CT 670 GE Healthcare, Milwaukee, WI) equipped with low-energy high-resolution (LEHR) collimators and multislice spiral CT was used to obtain planar images of the cervical thoracic region by early dynamic imaging (1 frame/min for 30 min), delayed static imaging (anterior, oblique and lateral views), and SPECT/CT acquisition (using a step-and-shoot protocol of 25 s/3° for a total of 60 views per camera head, 128×128 matrix, zoom factor 1.00). CT parameters included a current of 40 mA, a voltage of 120 kV, and a slice thickness of 3.75 mm.

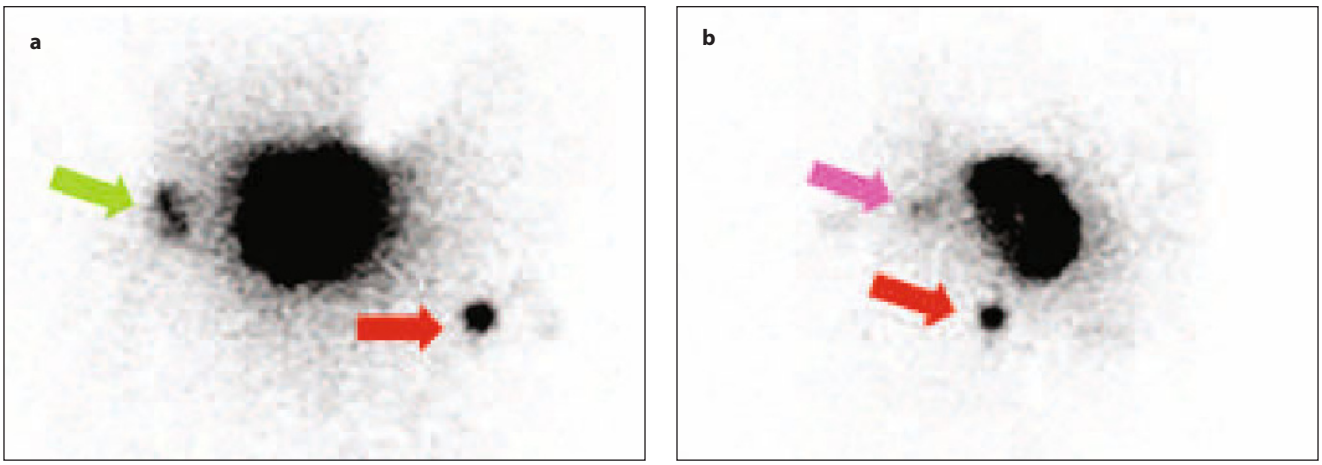

Fig. 1 **a** The anterior view shows two areas of focal uptake of the tracer, located in the left axillary region (*red arrow*) and in the right supraclavicular region (*green arrow*), corresponding to two sentinel lymph nodes. **b** The left lateral view confirms the presence of a left axillary sentinel lymph node (*red arrow*) and shows the presence of another sentinel lymph node in the lower third of the left laterocervical region (*pink arrow*)

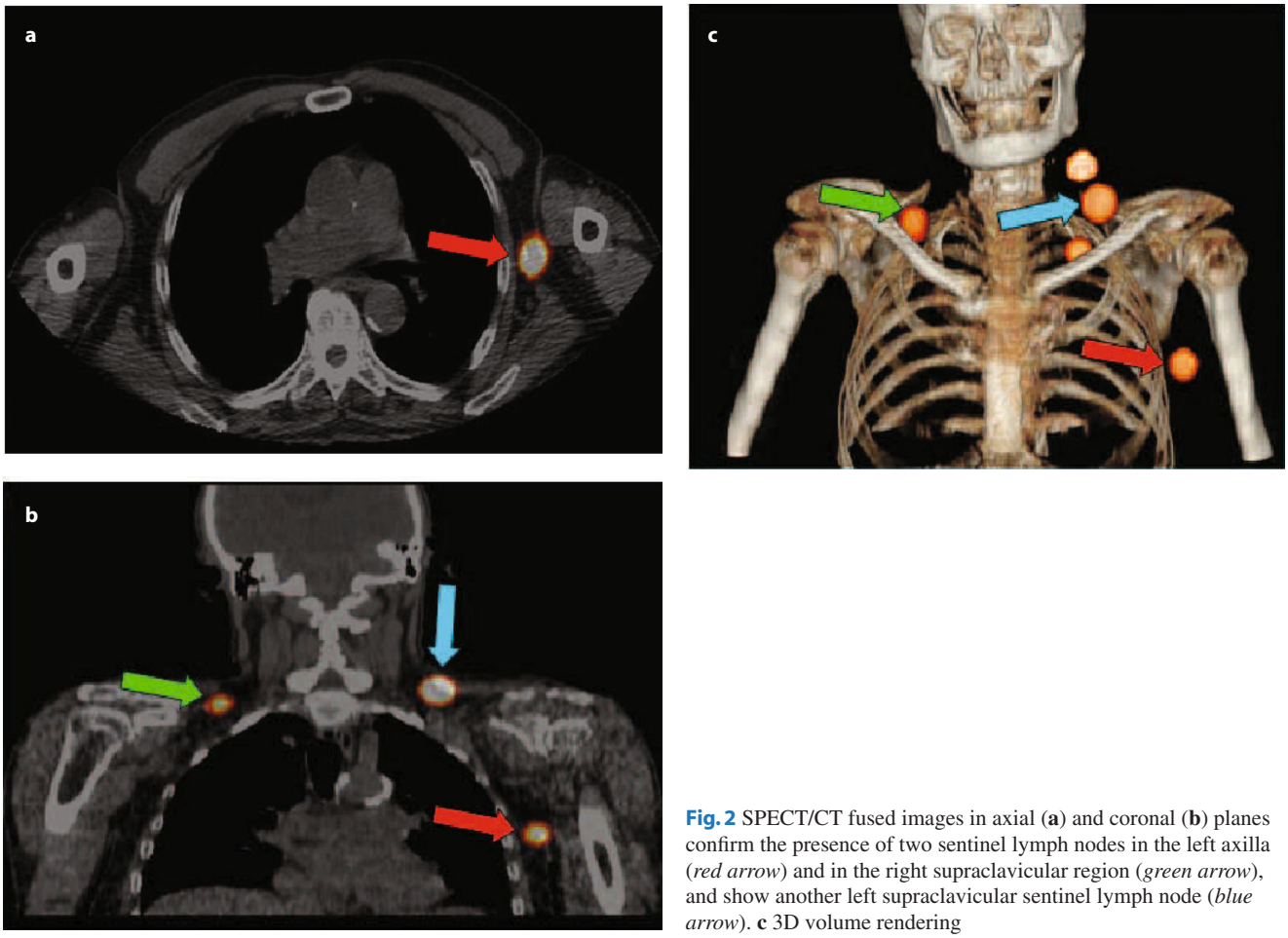

Fig. 2 SPECT/CT fused images in axial (**a**) and coronal (**b**) planes confirm the presence of two sentinel lymph nodes in the left axilla (*red arrow*) and in the right supraclavicular region (*green arrow*), and show another left supraclavicular sentinel lymph node (*blue arrow*). **c** 3D volume rendering

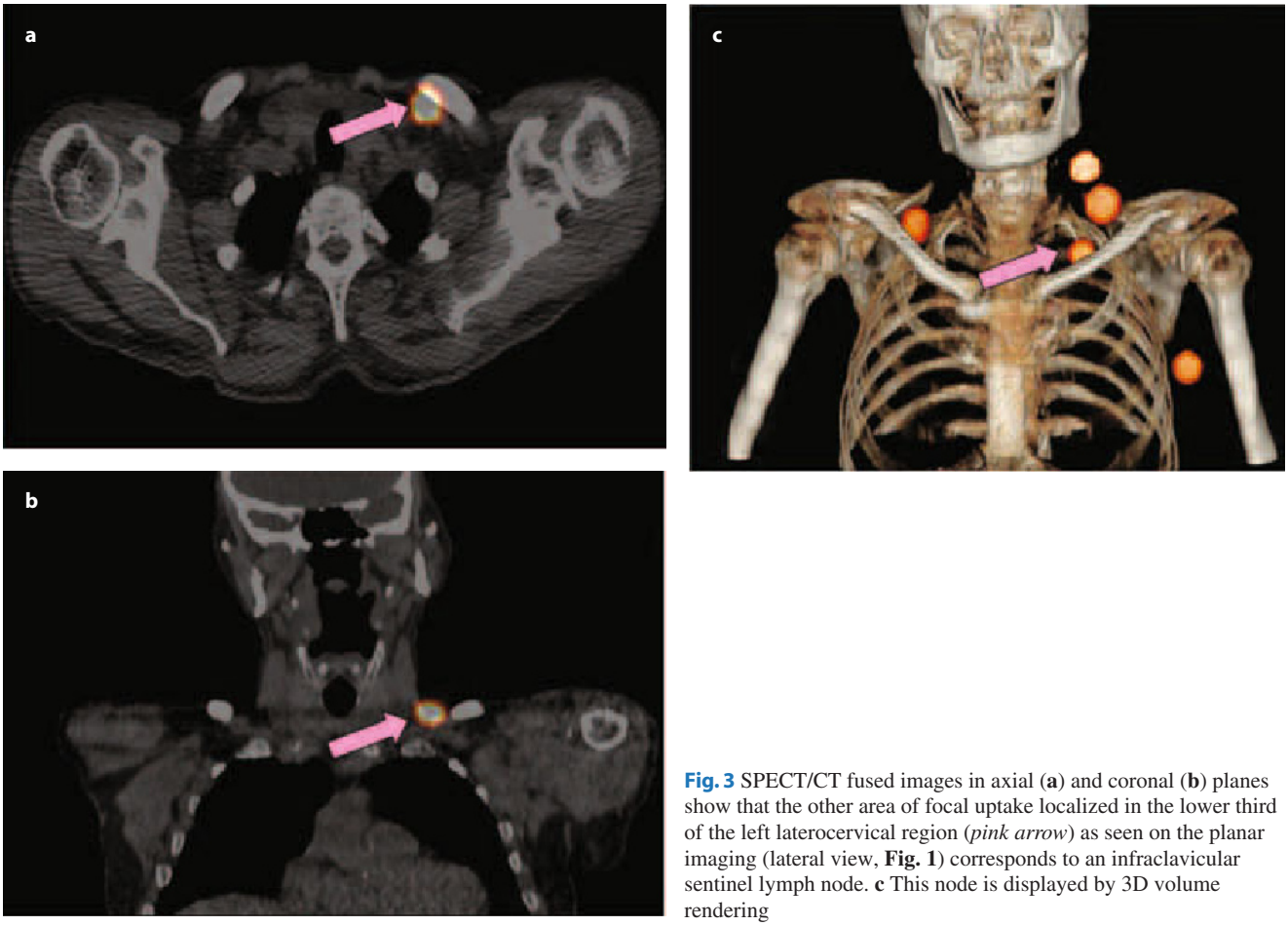

Fig. 3 SPECT/CT fused images in axial (**a**) and coronal (**b**) planes show that the other area of focal uptake localized in the lower third of the left laterocervical region (*pink arrow*) as seen on the planar imaging (lateral view, **Fig. 1**) corresponds to an infraclavicular sentinel lymph node. **c** This node is displayed by 3D volume rendering

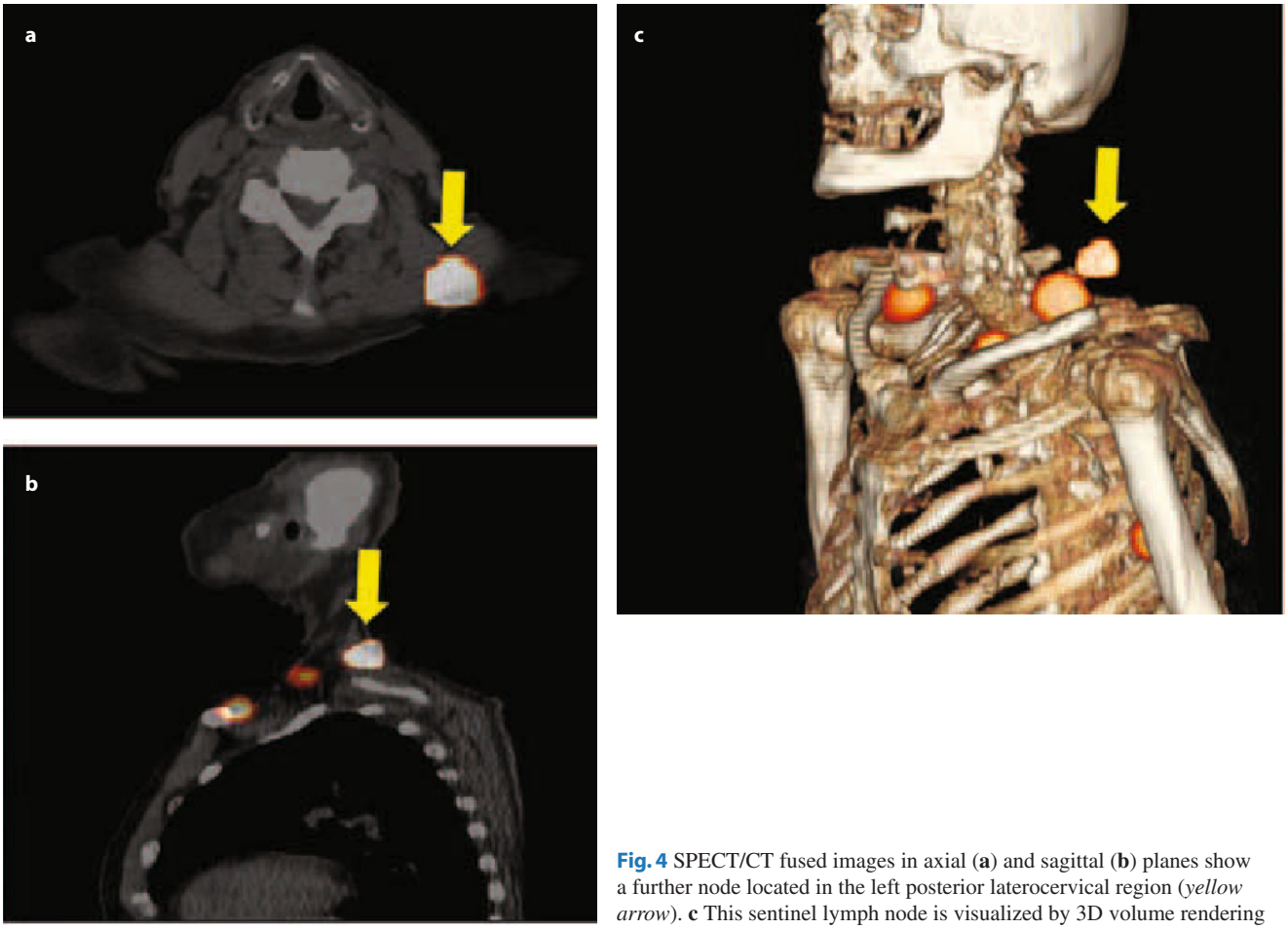

Fig. 4 SPECT/CT fused images in axial (**a**) and sagittal (**b**) planes show a further node located in the left posterior laterocervical region (*yellow arrow*). **c** This sentinel lymph node is visualized by 3D volume rendering

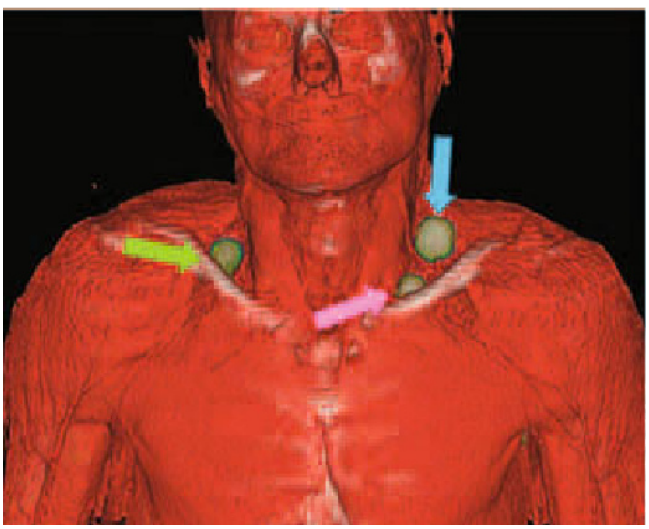

Fig. 5 The left infraclavicular sentinel lymph node (*pink arrow*), and right and left laterocervical sentinel lymph nodes (*green and blue arrows respectively*) are displayed using 3D volume rendering for better anatomical identification

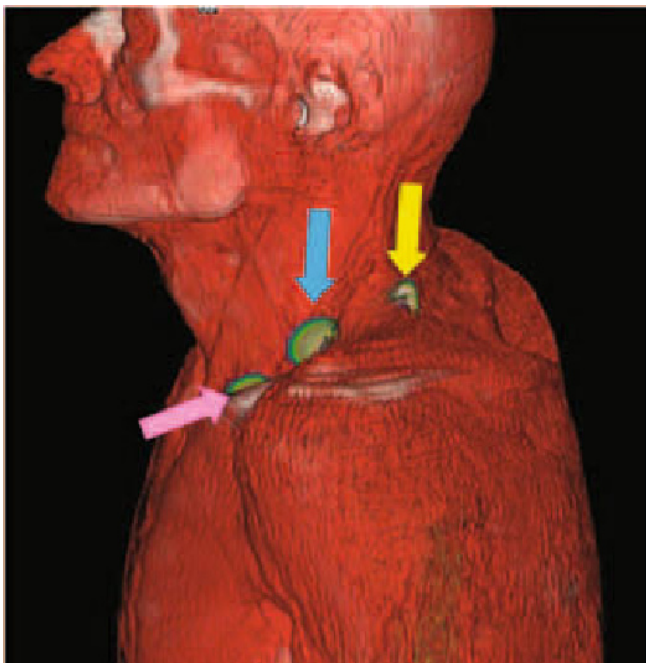

Fig. 6 Left infraclavicular sentinel node (*pink arrow*), laterocervical sentinel node (at Robbins's anatomical level V; *blue arrow*), and posterior laterocervical sentinel node (below border of the latissimus dorsi muscle, *yellow arrow*), using 3D volume rendering

Case 10.8
Sentinel Node Mapping in Melanoma of the Back: Drainage to Groin Nodes (Planar and SPECT/CT Imaging)

Gianpiero Manca, Valerio Duce, Manuel Tredici, Sara Mazzarri, and Giuliano Mariani

Background Clinical Case

A 41-year-old man with melanoma (1.2 Breslow thickness, IV Clark, 2 mitoses per mm2), already surgically removed for biopsy and located on the anterior surface of the left leg was submitted to lymphoscintigraphy for radioguided sentinel lymph node biopsy.

Lymphoscintigraphy

Lymphoscintigraphy was performed 18 h before sentinel node biopsy, to define the draining lymphatic basin at risk for metastatic disease and to identify the corresponding sentinel lymph node. Aliquots of 0.1–0.2 mL containing 4–8 MBq ^{99m}Tc-albumin nanocolloid (Nanocoll) were injected intradermally around the skin margins of the surgical scar, since the primary lesion had already been excised for biopsy. A dual-detector SPECT/CT gamma camera (Discovery NM/CT 670 GE Healthcare, Milwaukee, WI) equipped with low-energy high-resolution (LEHR) collimators and multislice spiral CT was used to obtain planar images of the groin and pelvic region by early dynamic imaging (1 frame/min for 30 min), delayed static imaging (anterior and lateral views), and SPECT/CT acquisition (using a step-and-shoot protocol of 25 s/3° for a total of 60 views per camera head, 128×128 matrix, zoom factor 1.00). CT parameters included a current of 40 mA, a voltage of 120 kV, and a slice thickness of 3.75mm.

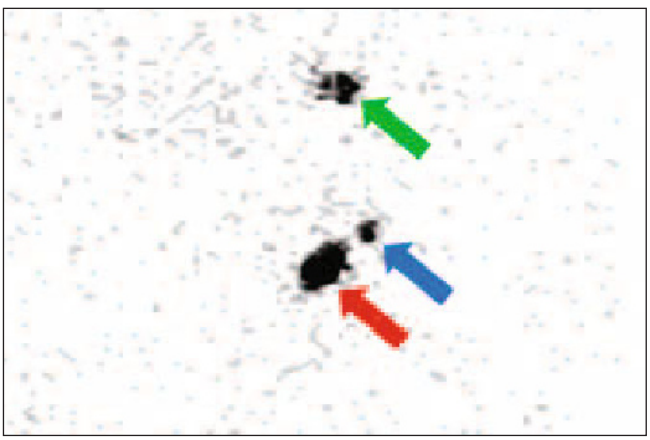

Fig. 1 The anterior view shows one focal uptake area of the tracer projecting in the proximal third of the left thigh (*red arrow*), which corresponds to a sentinel lymph node. The figure also shows the presence of two subsequent-tier nodes located, respectively, near the sentinel lymph node (*blue arrow*) and at the level of the ipsilateral inguinal region (*green arrow*)

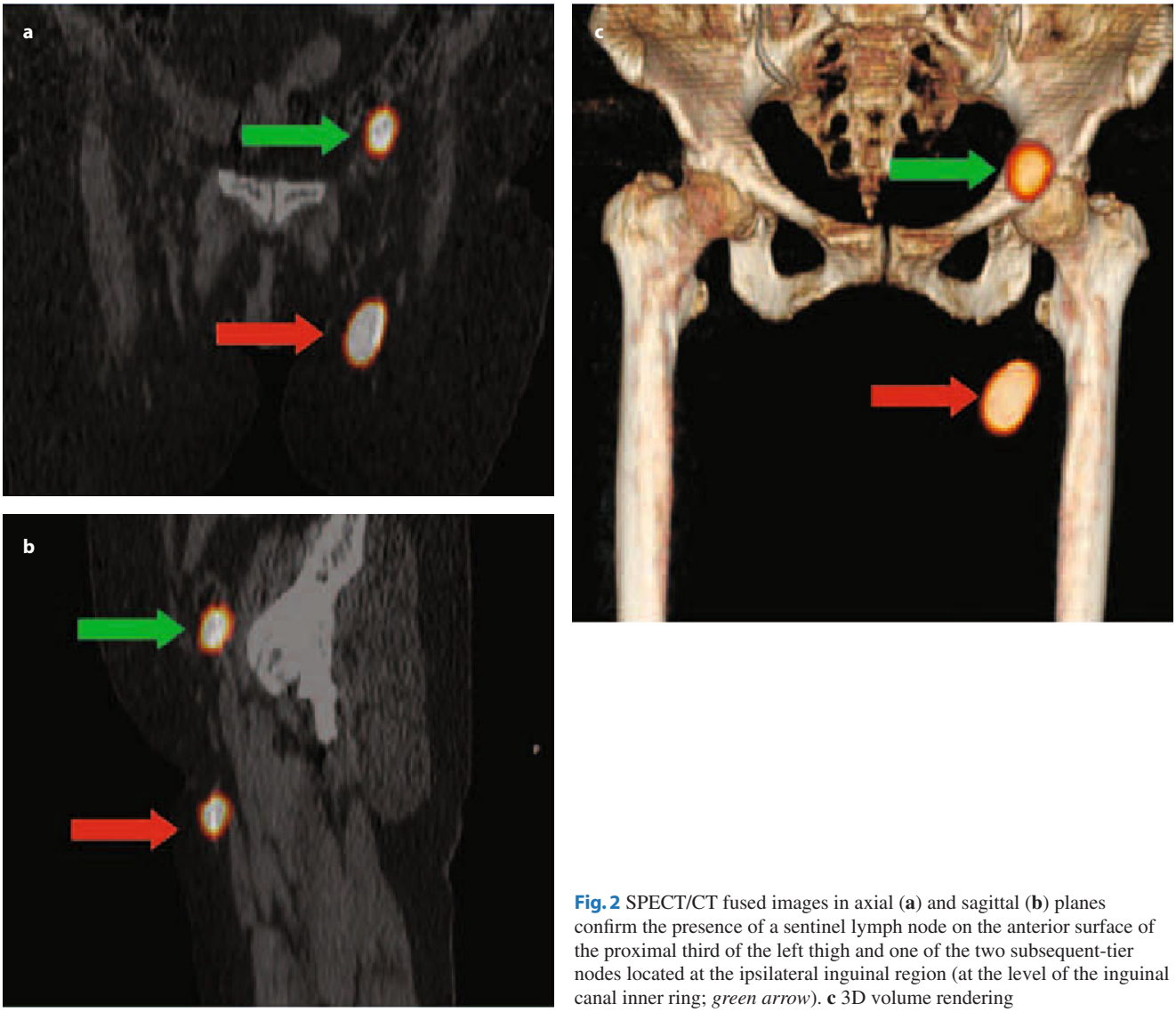

Fig. 2 SPECT/CT fused images in axial (**a**) and sagittal (**b**) planes confirm the presence of a sentinel lymph node on the anterior surface of the proximal third of the left thigh and one of the two subsequent-tier nodes located at the ipsilateral inguinal region (at the level of the inguinal canal inner ring; *green arrow*). **c** 3D volume rendering

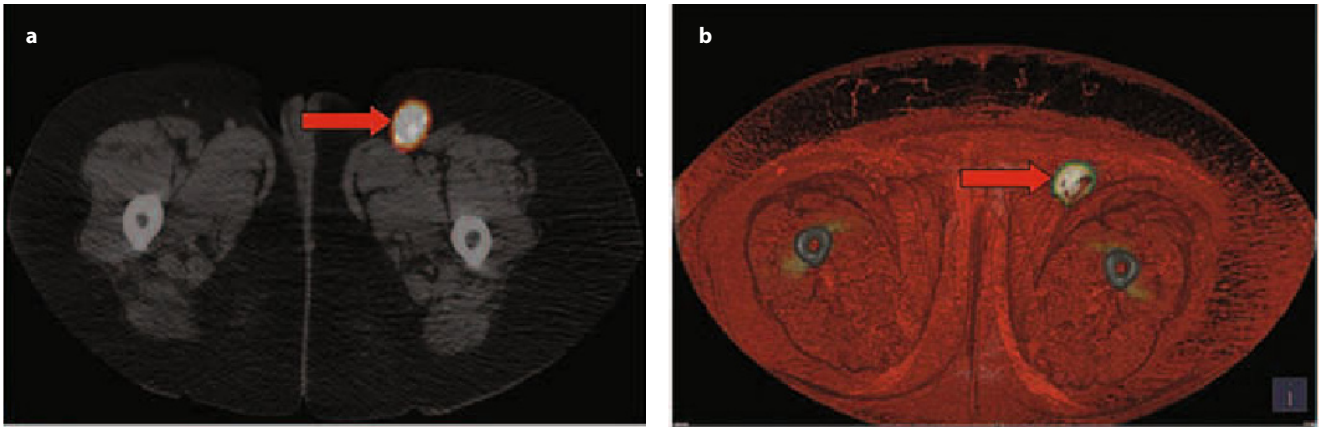

Fig. 3 **a**, **b** SPECT/CT fused images and 3D volume rendering in axial planes show that the sentinel lymph node (*red arrow*) is located at Scarpa's femoral triangle

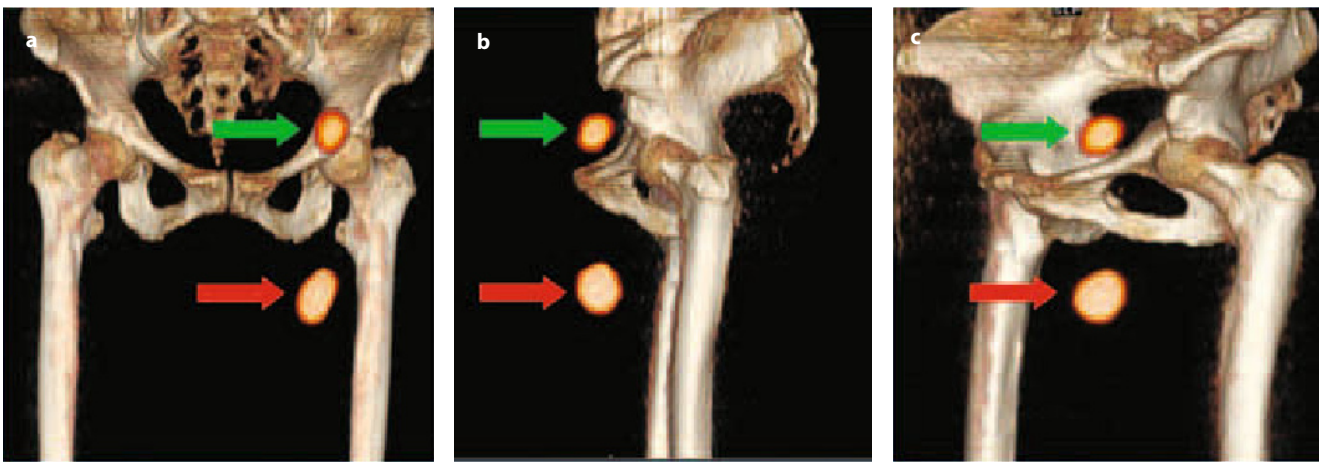

Fig. 4 **a–c** The sentinel lymph node (*red arrow*) and the subsequent-tier node (*green arrow*) located at the level of the ipsilateral inguinal region are displayed by 3D volume rendering (anterior, lateral, and oblique anterior views, **a**, **b**, **c**, respectively)

References

1. Sappey MPC (1874) Anatomie, physiologie, pathologie des vaisseaux lymphatiques considerez chez l'homme et les vertebres. In: DeLahaye A, Lecrosnier E (eds) Paris
2. Nieweg OE, Estourgie S, Valdes Olmos RA (2004) Lymphatic mapping and sentinel node biopsy. In: Ell PJ, Gambhir SS (eds) Nuclear medicine in clinical diagnosis and treatment, 3rd edn. Churchill Livingstone, Edinburgh, pp 229–260
3. Haagensen D, Feind CR, Herter FP et al (1972) Lymphatics of the trunk. In: Haagensen CD (ed) The lymphatics in cancer. Philadelphia, WB Saunders, pp 437-458
4. Sugarbaker EV, McBride CM (1976) Melanoma of the trunk: the results of surgical excision and anatomic guidelines for predicting nodal metastases. Surgery 80:22-30
5. Uren RF (2004) Lymphatic drainage of the skin. Ann Surg Oncol 11(Suppl):179S–185S
6. Uren RF, Howman-Giles RB, Shaw HM et al (1993) Lymphoscintigraphy in high-risk melanoma of the trunk: predicting draining node groups, defining lymphatic channels and locating the sentinel node. J Nucl Med 34:1435–1440
7. Uren RF, Thompson JF, Howman-Giles R (2000) Interval nodes, lymphatic lakes and accurate sentinel node identification. Clin Nucl Med 35:234–236
8. Kelley MC, Ollila DW, Morton DL (1998) Lymphatic mapping and sentinel lymphadenectomy for melanoma. Semin Surg Oncol 14:283–290
9. Morton DL, Wen DR, Wong JH et al (1992) Technical details of intraoperative lymphatic mapping for early stage melanoma. Arch Surg 127:392–399
10. Alex JC, Weaver DL, Fairbank JT et al (1993) Gamma probe guided lymph node localization in malignant melanoma. Surg Oncol 2:303-308
11. Gershenwald JE, Ross MI (2011) Sentinel lymph node biopsy for cutaneous melanoma. N Eng J Med 364:1738–1745
12. Valsecchi ME, Silbermins D, de Rosa N et al (2011) Lymphatic mapping and sentinel node biopsy in patients with melanoma: a meta-analysis. J Clin Oncol 29:1479–1487
13. Statius Muller MG, Hennipman FA, van Leeuwen PAM et al (2002) Unpredictability of lymphatic drainage patterns in melanoma patients. Eur J Nucl Med Mol Imaging 29:255–261
14. Amersi F, Morton DL (2007) The role of sentinel lymph node biopsy in the management of melanoma. Adv Surg 41:241–256
15. Leong SP, Morita ET, Südmeyer M et al (2005) Heterogeneous patterns of lymphatic drainage to sentinel lymph nodes by primary melanoma from different anatomic sites. Clin Nucl Med 30:150–158
16. Porter GA, Ross MI, Berman RS et al (2000) Significance of multiple nodal basin drainage in truncal melanoma patients undergoing sentinel lymph node biopsy. Ann Surg Oncol 7:256–261
17. Chakera A, Hesse B, Burak Z et al (2009) EANM-EORTC general recommendations for sentinel node diagnostics in melanoma. Eur J Nucl Med Mol Imaging 36:1713–1742
18. Alazraki N, Glass EC, Castronovo F et al (2002) Procedure guideline for lymphoscintigraphy and the use of intraoperative gamma probe for sentinel lymph node localization in melanoma of intermediate thickness 1.0. J Nucl Med 43:1414–1418
19. Morita ET (2002) Lymphoscintigraphy in the detection of sentinel lymph nodes. In: Leong SPL (ed) Atlas of selective sentinel lymphadenectomy for melanoma, breast cancer and colon cancer. Kluver Academic Publishers, New York, Boston, Dordrecht, London, Moscow, pp 9–37
20. Scarsbrook AF, Ganeshan A, Bradley KM (2007) Pearls and pitfalls of radionuclide imaging of the lymphatic system. Part 1: sentinel node lymphoscintigraphy in malignant melanoma. Br J Radiol 80:132–139
21. Van der Ploeg IM, Valdes Olmos RA, Kroon BBR et al (2009) The yield of SPECT/CT for anatomical lymphatic mapping in patients with melanoma. Ann Surg Oncol 16**:**1537–1542
22. Vermeeren L, Valdes Olmos RA, Klop WMC et al (2011) SPECT/CT for sentinel lymph node mapping in head and neck melanoma. Head Neck 33:1–6
23. Valdes Olmos R, Vidal-Sicart S, Nieweg OE (2009) SPECT-CT and real-time intraoperative imaging: new tools for sentinel node localization and radioguided surgery? Eur J Nucl Med Mol Imaging 36:1–5
24. Vidal-Sicart S, Paredes P, Zanón G et al (2010) Added value of intraoperative real-time imaging in searches for difficult-to-locate sentinel nodes. J Nucl Med 51:1219–1225
25. de Rosa N, Lyman GH, Silbermins D et al (2011) Sentinel node biopsy for head and neck melanoma: a systematic review. Otolaryngol Head Neck Surg 145:375–382
26. Reynolds H, Dunbar R, Uren R et al (2007) Mapping melanoma. Lymphoscintigraphy onto a 3D anatomically based model. Ann Biomed Engin 35:1444–1457

Preoperative and Intraoperative Lymphatic Mapping for Radioguided Sentinel Node Biopsy in Head and Neck Cancers

11

Renato A. Valdés Olmos, W. Martin C. Klop, and Oscar R. Brouwer

11.1 Introduction

The two most important applications of the sentinel lymph node (SLN) procedure in the head and neck region are melanoma and cancer of the oral cavity. The SLN status provides relevant prognostic information in patients with melanoma, and a positive sentinel node is also an unfavorable prognostic factor in oral cancer. Due to the poor sensitivity of modalities such as ultrasound-guided fine needle aspiration cytology (FNAC) and the increased morbidity of elective lymph node dissection, the SLN procedure is emerging as the most promising modality to stage the clinical and radiological N0 neck.

11.2 The Clinical Problem

SLNB in the head and neck region may be complex, due to difficult anatomic relations and unpredictable lymphatic drainage. This is probably one of the reasons for the relatively high false-negative rates in head and neck melanoma. Generally, drainage of melanomas located in the occipital region is expected in the dorsal areas of the neck, and melanomas of the temporal region are expected to drain to the pre-auricular lymph node stations. However, in many cases unexpected drainage is observed in multiple basins, including lower areas of the neck [1]. In cancer of the oral cavity, lymphatic drainage is also highly unpredictable, and contralateral drainage is often seen, even in well-lateralized malignancies of the tongue or floor of the mouth (Fig. 11.1) [2].

R. A. Valdés Olmos (✉)
Nuclear Medicine, Division of Diagnostic Oncology
Netherlands Cancer Institute – Antoni van Leeuwenhoek Hospital
Amsterdam, the Netherlands
e-mail: r.valdes@nki.nl

11.3 Indications and Contraindications for Sentinel Lymph Node Biopsy

In melanoma, patients with clinically and radiologically negative lymph node assessment (stage N0) are considered for the procedure. SLN mapping is generally considered in patients with a Breslow thickness between 1 mm and 4 mm. Due to the low risk of finding lymph nodal metastasis in melanoma lesions smaller than 1 mm, SLN staging can be omitted in these patients; on the other hand, in lesions that are larger than 4 mm, the high risk of synchronous distant metastases may outweigh the possible therapeutic and prognostic benefits of lymphadenectomy or of SLN mapping [3, 4]. However, patients with high-risk lesions of 0.75–0.99 mm thickness should be considered for SLNB if their melanoma is Clark IV or V, ulcerated, shows a vertical growth phase, or has lymphatic invasion or a high mitotic rate.

The role of SLNB in oral cancer is not as well established, and some controversy still persists regarding the appropriate indication. The procedure has been used to stage T1 or T2 lesions [5, 6], although several authors find selective neck dissection more appropriate in view of the high risk of nodal metastasis [7]. In general, patients with transoral resectable T1–T2 tumors and with negative lymph node assessment on clinical and radiological examination (including FNAC) are considered for SLNB.

11.4 Radiocolloid and Modalities of Injection

Although a number of different radiopharmaceuticals are suitable for lymphoscintigraphy worldwide, in Europe the most frequently used radiocolloid is technetium-99 (^{99m}Tc)-nanocolloid. For both melanoma and cancer of the oral cavity, an activity of 60–80 MBq in a total volume of 0.4 mL is sufficient for adequate visualization of the lymphatic vessels and lymph nodes. The activity can be increased to 100 MBq

G. Mariani et al. (eds.), *Atlas of Lymphoscintigraphy and Sentinel Node Mapping*,
DOI 10.1007/978-88-470-2766-4_11

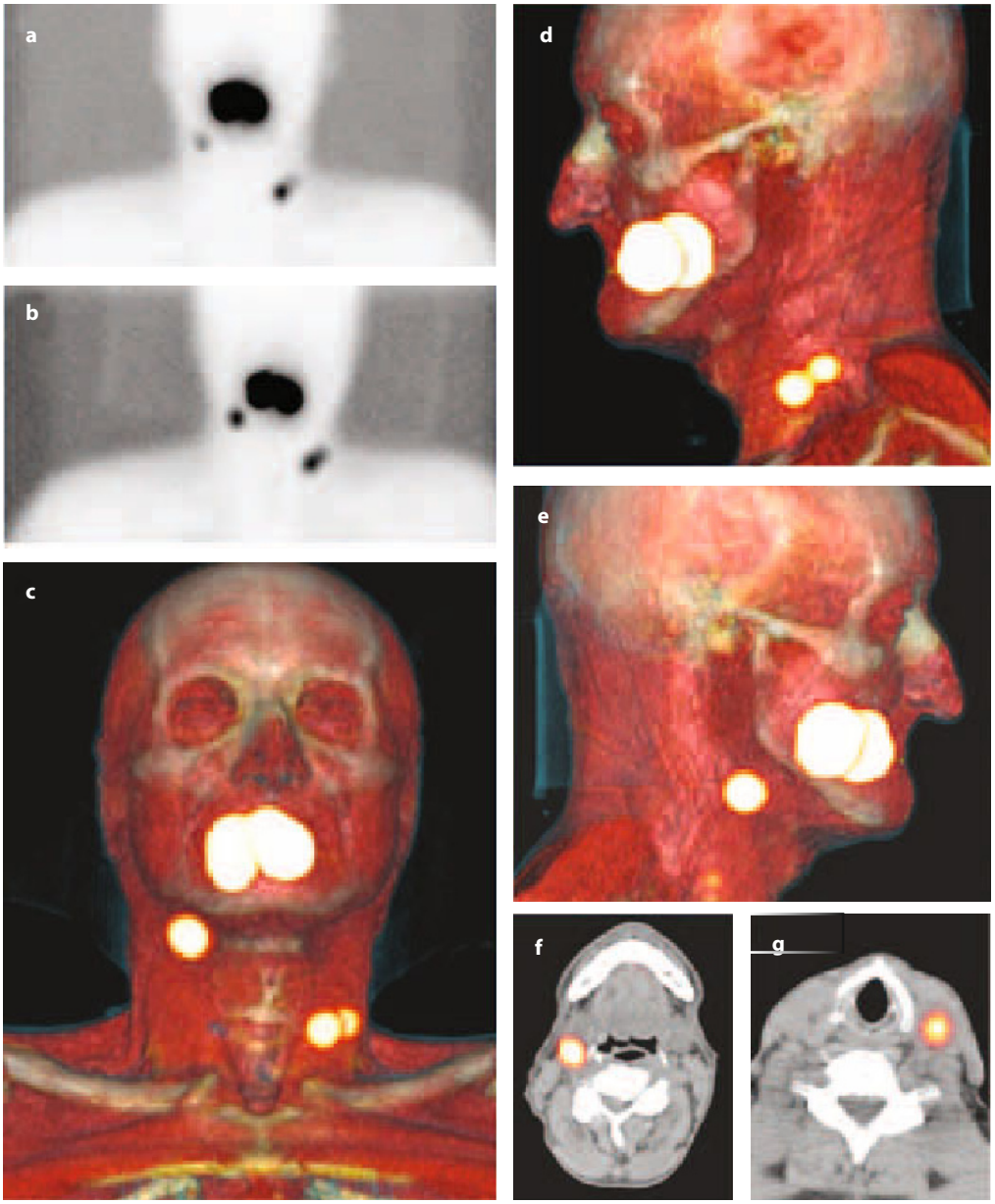

Fig. 11.1 An 81-year-old man with a T1 carcinoma on the right side of the lingual apex. After administration of 82 MBq ^{99m}Tc-nanocolloid in four injections into the mucosa around the tumor, early drainage to both sides of the neck is seen on anterior planar imaging (**a**), with subsequent increasing lymph node uptake on delayed images (**b**). Volume rendering (**c–e**) and axial SPECT/CT fusion images (**f**, **g**) show the SLNs in level II on the right and in level III on the left. All SLNs were tumor-free at histopathology

when the operation takes place on the following day. Four intradermal injections are used for melanoma, whereas in oral cavity malignancies the radiocolloid is administered into the mucosa in three to four sites around the primary lesion. The use of a local anesthetic for topical application (10% xylocaine spray), a few minutes before radiocolloid injection, is recommended for tumors of the oral cavity. In patients with melanoma, generally no local anaesthesia is given. However, in areas such as the scalp or ear, injections are painful, and local topical anesthesia is recommended. In the case of melanoma, radiocolloid administration must be applied intradermally, raising a bleb after each injection. Subcutaneous injection is easier to accomplish, but may not delineate the route of lymphatic drainage from an overlaying cutaneous site. The radiocolloid must be administered in close proximity to the lesion or excision site, no further than 1 cm from the borders [8]. This factor may be critical in melanomas of the ear, in which small excision scars are difficult to recognize; in the scalp, it is sometimes necessary to shave the area to facilitate adequate radiocolloid injections. For cancer of the oral cavity, injection into the intact mucosa close to the tumor is recommended.

11.5 Preoperative Imaging of Sentinel Lymph Nodes

The combination of lymphoscintigraphy and single photon emission computed tomography/computed tomography (SPECT/CT) is essential for lymphatic mapping and SLN localization in head and neck malignancies.

Lymphoscintigraphy is based on sequential images depicting subsequent phases of lymph drainage. Due to the short distance between the injection site and the first draining lymph nodes in the head and neck region, dynamic images must be obtained as soon as possible after radiocolloid administration. This approach frequently leads to visualization of the lymphatic vessels, whereas static planar images recorded after 15 minutes usually depict the first draining lymph nodes. Delayed images (2–3 hours after injection) enable discrimination of SLNs and second-tier nodes. Static images are based on both anterior and lateral views. For lateral views, the patients are asked to turn their head, in order to enable positioning of the gamma camera as close as possible to the area of interest.

Planar images provide a 2-dimensional overview, and SLNs can be localized and marked on the patient's skin with the use of an external radioactive marker, such as a cobalt-57 (^{57}Co)-source pen. Anterior images must be complemented by oblique or lateral images, in order to define the location of the lymph nodes relative to the neck levels. The sentinel nodes identified in this way are marked on the skin of the neck on the basis of lateral views, in order to reproduce the patient's position during surgery.

Interpretation of planar images can be difficult, because no anatomical information is provided and the three-dimensional (3D) surface of the structures of the head is not visualized. Moreover, the injection site on planar imaging may mask SLNs located in the proximity of, or underneath the injection area. To avoid masking of a SLN, injections inferior to the lesion might be omitted. Transmission images can be used to improve anatomical orientation; to obtain these images, a ^{57}Co flood source is placed so that the patient's head is between the camera and the source during static imaging.

SPECT/CT is mostly performed after recording the delayed planar images. A SPECT/CT system consisting of a dual-head variable-angle gamma camera equipped with low-energy high-resolution collimators and a multislice spiral CT optimized for rapid rotation is generally used. SPECT acquisition is based on a 128×128 matrix and 25 seconds per view, using steps of 4–6 degrees. CT is based on 2-mm slices, and settings are aimed at obtaining a low-dose CT (e.g., 130 KV, 30 mAs, B30s kernel), which is appropriate for both attenuation correction and anatomic mapping. The patient's head rests on a head-holder and is taped in order to avoid motion during acquisition and possible misalignment between SPECT and CT. After reconstruction, SPECT images are corrected for attenuation and scatter. Axial SPECT and CT slices are fused and are displayed in axial, sagittal, and coronal orientations. A 3D image may also be generated using volume rendering.

11.6 Lymphatic Drainage and Lymph Node Groups of the Neck

The lymphatic system of the head and neck includes approximately 250–350 lymph nodes, divided into various nodal groups: the occipital lymph nodes, the retroauricular or mastoid lymph nodes, the pre-auricular nodes and deep parotid nodes, the jugular chain nodes, the superficial and deep cervical nodes, the buccinator lymph nodes, and the submental and submandibular nodes. Lymph nodes of the spinal accessory chain are also included in the lymphatic network of the neck [9].

There are marked variations in the lymphatic drainage of the head and neck. For instance, for the scalp, drainage from the frontal zone is expected into the pre-auricular parotid lymph nodes, whereas the parietal zone drains to the retroauricular nodes, and the occipital skin to the internal jugular or spinal accessory nodes. The face above the commissure of the lip and anterior to the pinna of the ear drains to the parotid lymph nodes, whereas the face inferior to the commissure of the lip drains to the cervical nodal basin. For the forehead, drainage is expected to the superficial parotid lymph nodes, whereas the lower lip, external nose, cheeks, upper lip, and mucous membranes of the lips drain to the submandibular lymph nodes. For the central part of the lower lip, floor of the mouth, and lingual apex, lymphatic drainage to the submental nodes is expected [10].

According to the American Joint Committee on Cancer (AJCC)–Union for International Cancer Control (UICC) TNM (tumor, node, metastastases) staging system [11], the lymph nodes in the neck may be subdivided into specific anatomic subsites and grouped into seven levels in each side of the neck (Fig. 11.2). Level I includes the submental (sublevel IA) and submandibular (sublevel IB) lymph nodes. Level II contains the upper jugular lymph nodes that extend from the inferior border of the hyoid bone to the base of the skull; in relation to the vertical plane defined by the spinal accessory nerve, the lymph nodes located anteriorly (medial) constitute sublevel IIA, and the nodes located posteriorly (lateral) correspond to sublevel IIB. Level III includes the middle jugular nodes, and level IV the lower jugular nodes. The posterior border of regions II, III, and IV is the posterior border of the sternocleidomastoid muscle, which is the anterior border of level V. This latter group is composed of

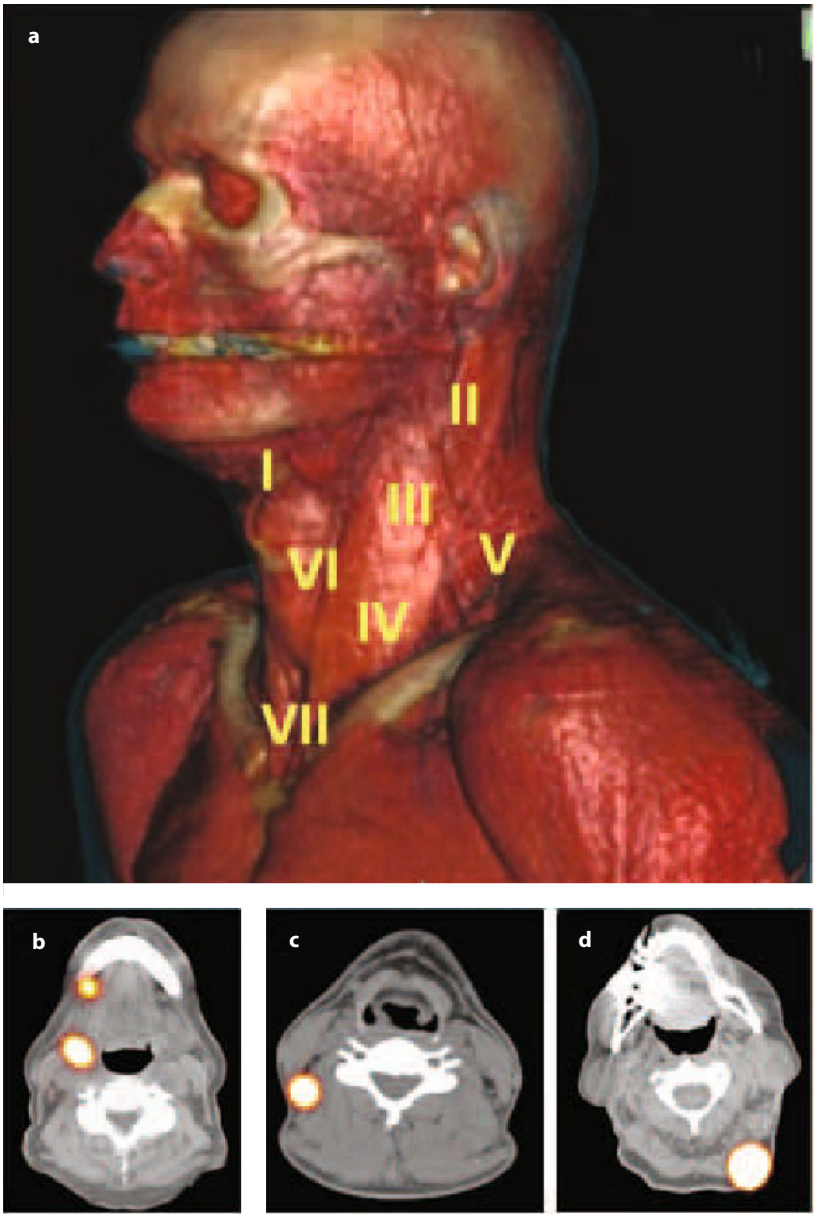

Fig. 11.2 Lymph node levels of the neck. **a** Volume rendering of the head and neck showing the anatomical levels of the neck. **b–d** Fused axial SPECT/CT images showing examples of SLNs located in right levels I and II (**b**), right level III (**c**), and level V of the left side of the neck (**d**)

the sublevels VA (which includes the spinal accessory nodes) and VB (which includes lymph nodes along the transverse cervical vessels) and the supraclavicular lymph nodes (with the exception of the Virchow node which is located in level IV). Level VI contains the pretracheal and paratracheal nodes, the precricoid Delphian node, and the perithyroidal nodes, including the lymph nodes along the recurrent laryngeal nerves. Finally, level VII includes the superior mediastinal lymph nodes.

11.7 Intraoperative Detection of Sentinel Lymph Nodes

A gamma-ray detection hand-held probe is routinely used for intraoperative detection of the SLNs in the head and neck region, while patent blue is commonly added as an additional indicator of lymphatic flow. However, SLNs in the head and neck region are frequently not stained blue, due to the fast

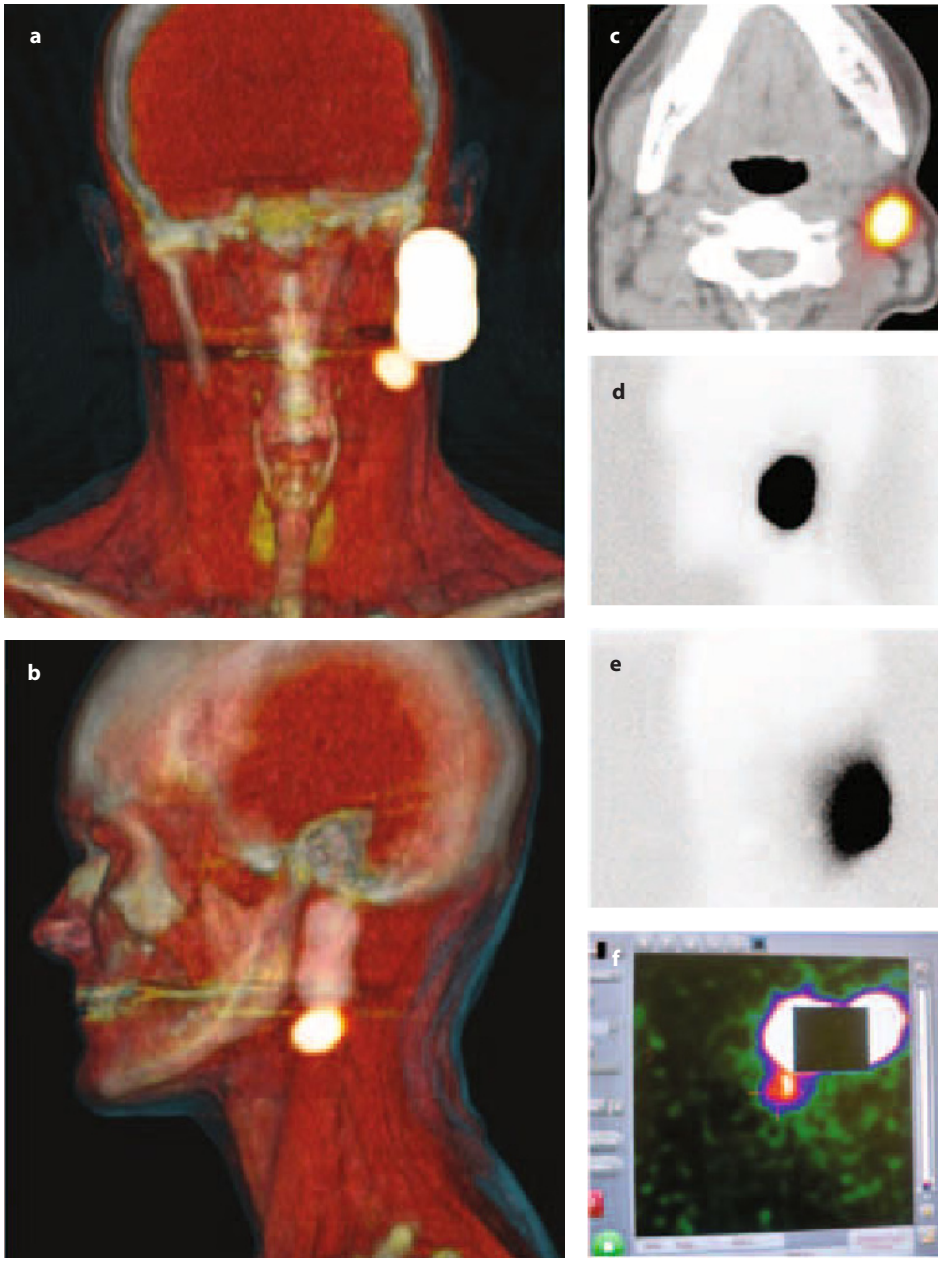

Fig. 11.3 A 46-year-old woman with an infrauricular melanoma (5 mm Breslow thickness) on the left. Planar lymphoscintigraphy and SPECT/CT performed after intradermal administration of 70 MBq ^{99m}Tc-nanocolloid divided in four injections around the excision scar. Volume rendering (**a**, **b**) and fused axial SPECT/CT (**c**) show a SLN in level II, very close to the inferior part of the injection site. This lymph node was not seen in the planar lateral (**d**) and anterior (**e**) images. The SLN localized during surgery with a portable gamma camera (**f**) was tumor free at histopathology

lymphatic migration of vital blue dyes. This limitation has led to combination of radioguided detection with real-time near-infrared fluorescence imaging using hybrid tracers [12].

The gamma-ray detection probe provides an acoustic signal when pointed straight towards the radioactive lymph node. Deeply located SLNs can be difficult to detect because of tissue attenuation, while the relatively large amount of radioactivity at the injection site may cause SLNs located nearby to be missed (Fig. 11.3). Checking the position of the sentinel node with the gamma probe is necessary prior to skin incision. This is particularly important in sites such as the submandibular region, where the skin marking guided by the gamma camera is less accurate and may be masked by the injection site. Also, after removing sentinel nodes, the activity of the injection site can complicate measurement of the residual activity in the excision fossa.

11.8 Contribution of SPECT/CT

SPECT/CT can optimize SLN visualization and localization in the head and neck region. SPECT/CT has visualized one or more additional SLNs in more than half of published studies [13]. These additional SLNs found on SPECT/CT imaging might be tumor positive. Lymph nodes adjacent to the injection site in particular are more frequently detected by SPECT/CT, while they are frequently missed on planar imaging. Furthermore, non-nodal radioactivity accumulation (radiocolloid leakage or contamination) can be more easily identified on the basis of SPECT/CT images [14].

SPECT/CT appears to be very useful for exact anatomic localization of the SLNs. In the head and neck area, it is very important to identify the relation of SLNs to several vital vascular and neural structures, in order to be able to safely remove these lymph nodes. SPECT/CT can localize these sentinel nodes in relation to anatomical structures such as the mandible, parotid gland, jugular vein, and sternocleidomastoid muscle. SPECT/CT also shows whether the nodes are located superficially underneath the skin or hidden below other structures. SPECT/CT thus gives anatomical reference points for planning the surgical approach. The superior location information provided by SPECT/CT frequently leads to adaptation of the surgical approach, with significant shortening of operation times.

In melanoma of the head or neck, SPECT/CT not only provides the anatomical information, but can also visualize additional SLNs in comparison with conventional planar images. In approximately 30% of cases, SLNs can be more accurately localized by SPECT/CT, and in more than 50% of cases, the surgical approach can be adapted on the basis of the SPECT/CT images, resulting in modification of the incision site or a more efficient intraoperative search procedure.

Location of a melanoma in the head and neck has been found to be a predictive factor for a false-negative SLNB, and the number of false-negative sentinel node biopsies reported for this region is higher than in other areas [15]. This relatively high rate might be reduced by optimal preoperative localization with SPECT/CT.

Another important issue is the need to correlate the findings of fused SPECT/CT with those of CT. With the improvement of the CT component in the new generation of SPECT/CT devices, it is possible to obtain more accurate morphological information in the head and neck. In many cases, radioactive SLNs correspond to single nodes. However, in some cases, the radioactive signal on SPECT/CT may correspond to a cluster of lymph nodes on CT. This preoperative information may lead to more careful post-excision control after removal of the first radioactive lymph node by the surgeon.

11.9 Intraoperative Imaging

In recent years, a number of portable and hand-held mini gamma cameras have been developed to provide intraoperative visualization. The entire lymph node excision procedure in the head and neck area can be monitored with a portable gamma camera, as these images provide an overview of all radioactive hot spots in the surgical field. SLNs located close to the injection site are easily overlooked using the counting probe, but can be visualized with a gamma camera. If there is difficulty in localizing a preoperatively identified SLN, the intraoperative gamma camera may be able to show the surgeon where the node is located.

By determining residual radioactivity after excision of the SLNs, the gamma camera can help to assess the completeness of the procedure. Imaging after excision can also reveal additional SLNs in more than 20% of cases [16]. In some cases, intense radioactive uptake at the site of the SLN on preoperative imaging corresponds to a cluster of sentinel nodes. Imaging after excision of the first hot node can reveal the remaining sentinel node. Acquiring intraoperative images only takes a few minutes, but if more lymph nodes are found and excised because of intraoperative imaging, the procedure is likely to be prolonged.

Although not yet constituting routine clinical practice, intraoperative visualization of SLNs with a portable gamma camera is feasible and may improve intraoperative detection of sentinel nodes in the head and neck region. Recently, the use of intraoperative gamma cameras has been combined with fluorescence cameras for synchronous sentinel node signal detection using hybrid tracers such as ^{99m}Tc-nanocolloid combined with indocyanine green (ICG) [12]. The high resolution of the fluorescent signal complements the radioguided localization in cases where the SLNs are close to the injection site, for instance in patients with malignancies of the floor of the mouth and submental sentinel nodes, or in periauricular melanomas and sentinel nodes in the parotid region (Figs. 11.4 and 11.5).

11.10 Common and Rare Variants

On lymphoscintigraphy, the pre-auricular lymph node basin usually receives drainage from melanomas of the face, anterior and coronal midline scalp, and coronal neck. In contrast, the ipsilateral level II lymph node field can receive drainage from any region in the head and neck area [17]. More specifically, the expected drainage of melanomas of the coronal and posterior scalp is to lymph nodes of neck level V and the suboccipital nodes; drainage to neck level II, the parotid area, and retroauricular areas is less frequent. Anterior scalp melanomas are expected to drain to levels I–III or IV but drainage to level V has been observed on lymphoscintigrams. In

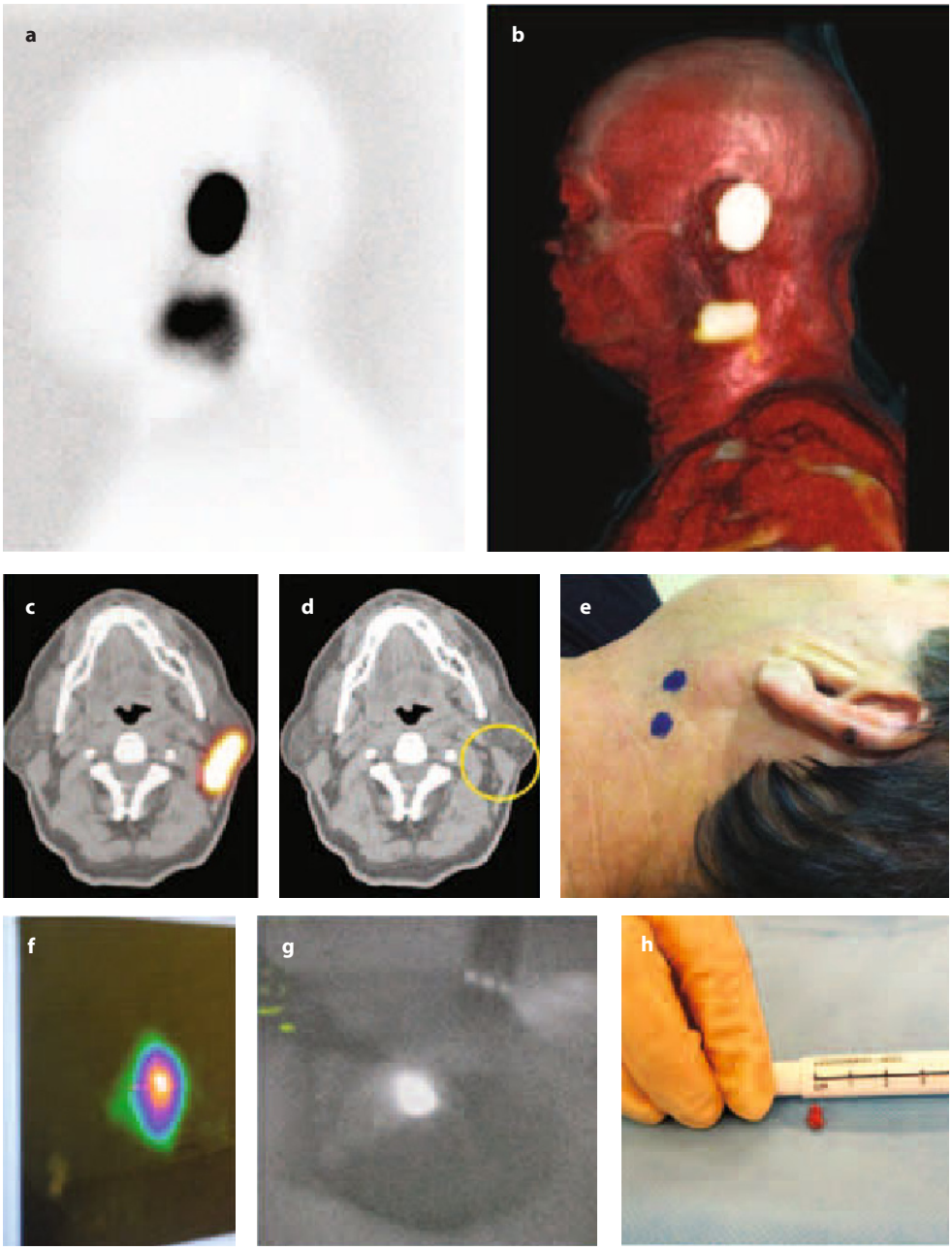

Fig. 11.4 A 59-year-old man with a 2 mm Breslow melanoma of the left ear. A total of 88 MBq of the hybrid imaging agent ^{99m}Tc/ICG-nanocolloid was injected in four sites around the lesion in the border of the ear. **a** Planar lateral image shows drainage to the left side of the neck. Volume rendering (**b**) and axial SPECT/CT (**c**, **d**), show the radioactive lymph nodes in level II and behind the parotid gland. After incision at the site marked on the skin (**e**), two sentinel nodes in level II and nodes 2 in the parotid area were found using the radioactive (**f**) and fluorescent (**g**) signals. The sentinel nodes were smaller than 3 mm (**h**) and were tumor free

lateralized scalp melanomas, unexpected contralateral drainage is also seen. Drainage from posterior scalp melanomas to high occipital scalp SLNs can also be observed. Pre-auricular melanomas usually drain to level I–III or IV and to the parotid basin, while SLNs are rarely found in level V. For melanomas on the ear, drainage is expected to levels II–V, but can also occur toward occipital and parotid nodes.

Melanomas of the upper face, nose, and lower face can drain to nodes of levels I–III or IV, or to the parotid region, while drainage to sentinel nodes in level V has been observed more rarely.

Melanomas located in the neck may frequently drain to levels I to IV and, depending on the location (anterior or dorsal, lower, or upper), to level V or to the parotid area. More rarely, occipital sentinel nodes have been seen in melanomas of the posterior upper neck [1] (Fig. 11.6).

Malignancies of the oral cavity located in the lateral tongue and posterior floor of the mouth generally drain to ipsilateral neck level II nodes [18]. However, drainage to levels I and III is also possible, as well as drainage to contralateral lymph nodes (Fig. 11.7). From the anterior floor of the mouth and lingual apex, drainage to level I is expected; however, not infrequently, bilateral drainage to level II/III can be observed.

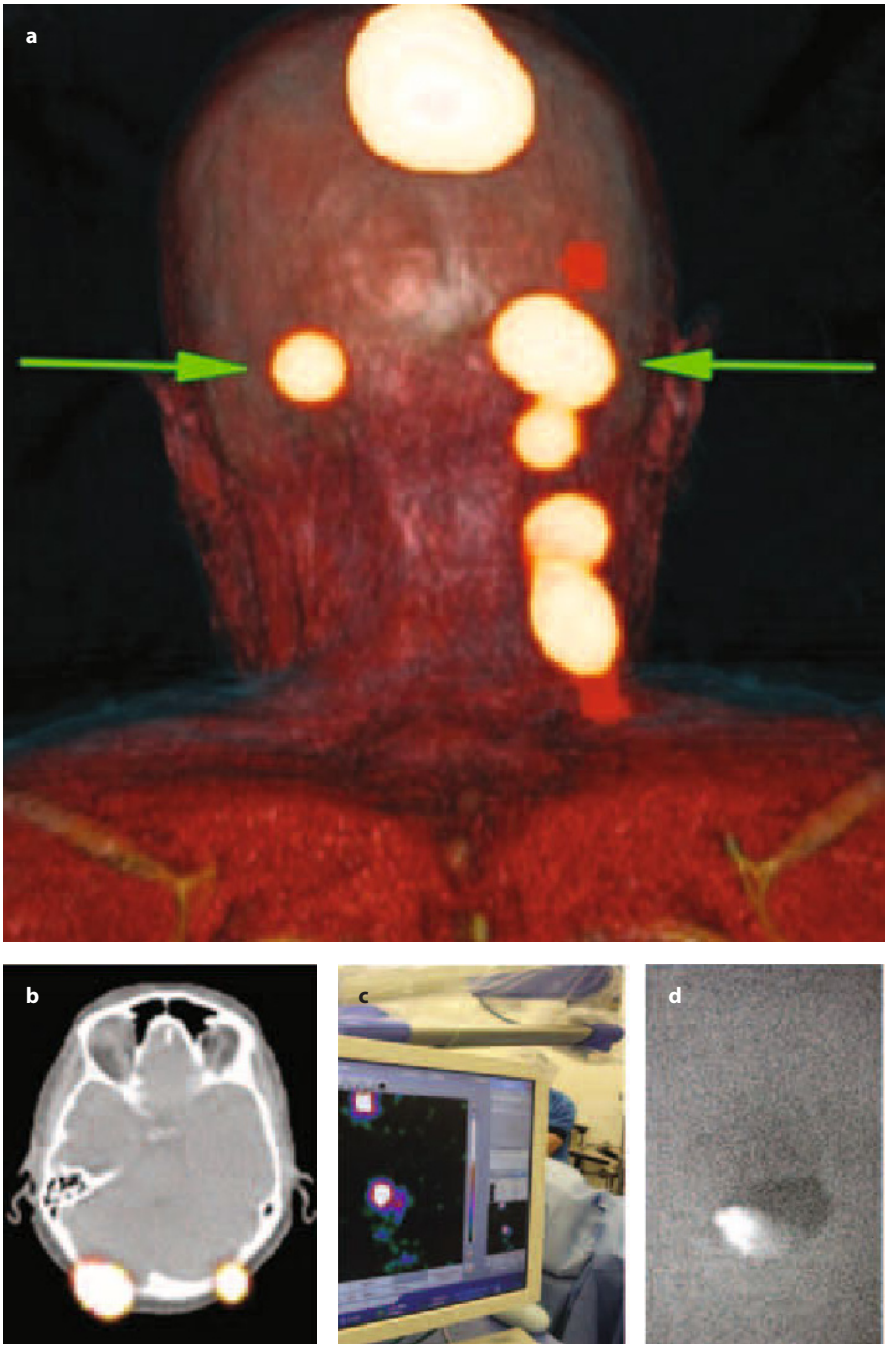

Fig. 11.5 A 64-year-old woman with a 5 mm Breslow melanoma in the posterior area of the scalp. Volume rendering (**a**) and fused axial SPECT/CT (**b**) show bilateral drainage to two SLNs in the occipital region (*arrows* in **a**). These lymph nodes, localized by detecting the radioactive (**c**) and fluorescent (**d**) signals, were free of metastasis

11.11 Technical Pitfalls

The most frequent pitfall is skin contamination. The high pressure of the intradermal bleb can result in leakage during injection or after removal of the needle. This may occur more frequently on the skin of the scalp, ear, and nose. The use of lights to adequately visualize the site of injection, and a fenestrated drape to cover the area, may help to avoid contamination. Also in tumors of the oral cavity, some contamination may be observed after peritumoral injections. The hot spots due to contamination may be confused with SLNs in the vicinity of the tumor, thus leading to unnecessary intraoperative pursuit. In these cases, skin decontamination is mandatory. Complementary SPECT/CT may also be helpful in detecting these artifacts, as mentioned above.

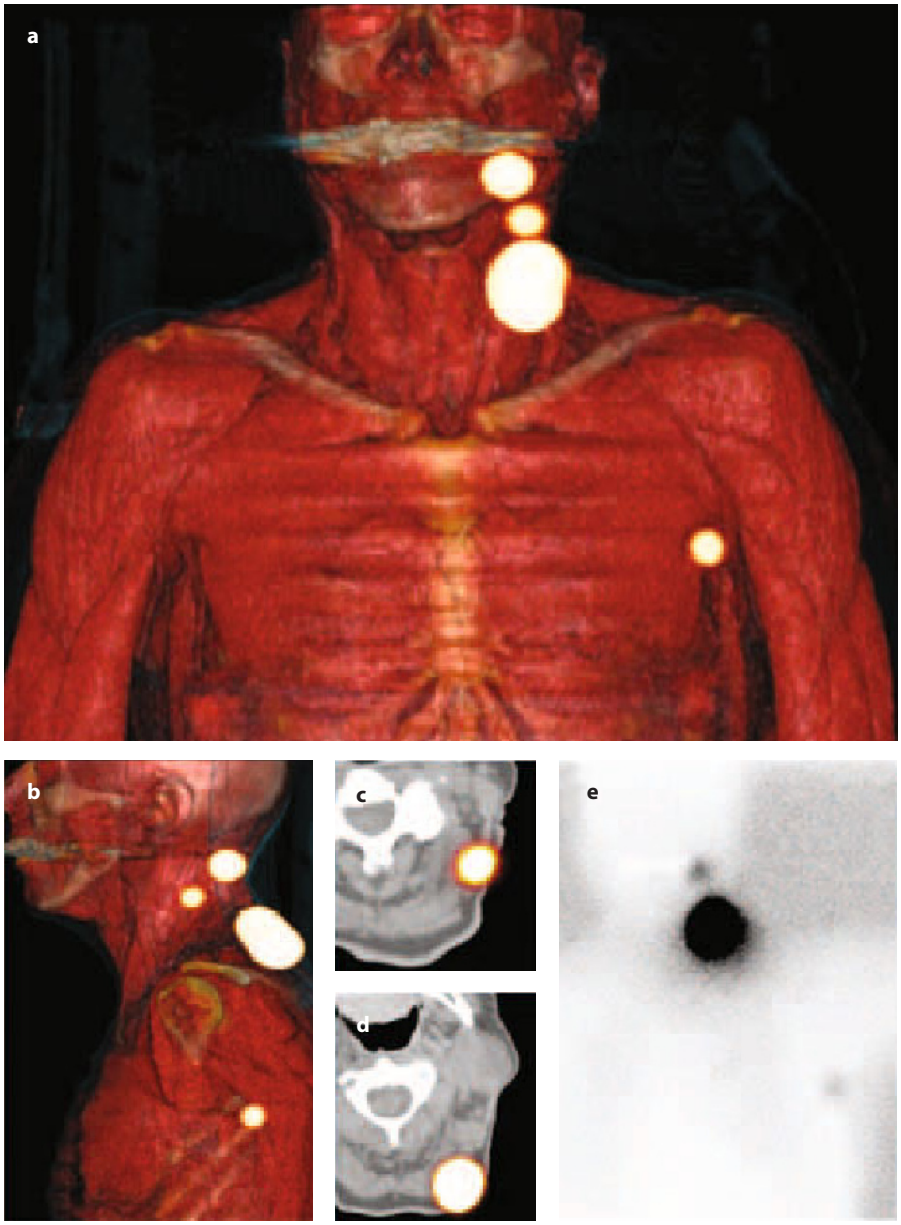

Fig. 11.6 A 64-year-old woman with a 3 mm Breslow melanoma of the posterior part of the neck. Volume rendering (**a**, **b**) and fused SPECT/CT axial images (**c**, **d**) show drainage to upper part of the left neck (with SLNs in the occipital region and in level II) as well as to the left axilla. Note that on planar imaging (**e**), one of the neck lymph nodes is masked by the injection site. The occipital SLN was tumor positive. The SLNs in level II and in the axilla were tumor free

Another pitfall may be caused by differences in patient position between the time when projection of the SLN is marked on the overlying skin in the nuclear medicine department, and the time of surgery. Verifying the site of incision in the operation room, using a gamma probe or the portable gamma camera, may solve this problem. A pitfall related to SPECT/CT may be caused by misalignment between SPECT and CT, which can cause spurious results in the anatomical localization of SLNs. Immobilization of the head and, if necessary, the use of manual image alignment may help to correct this artifact.

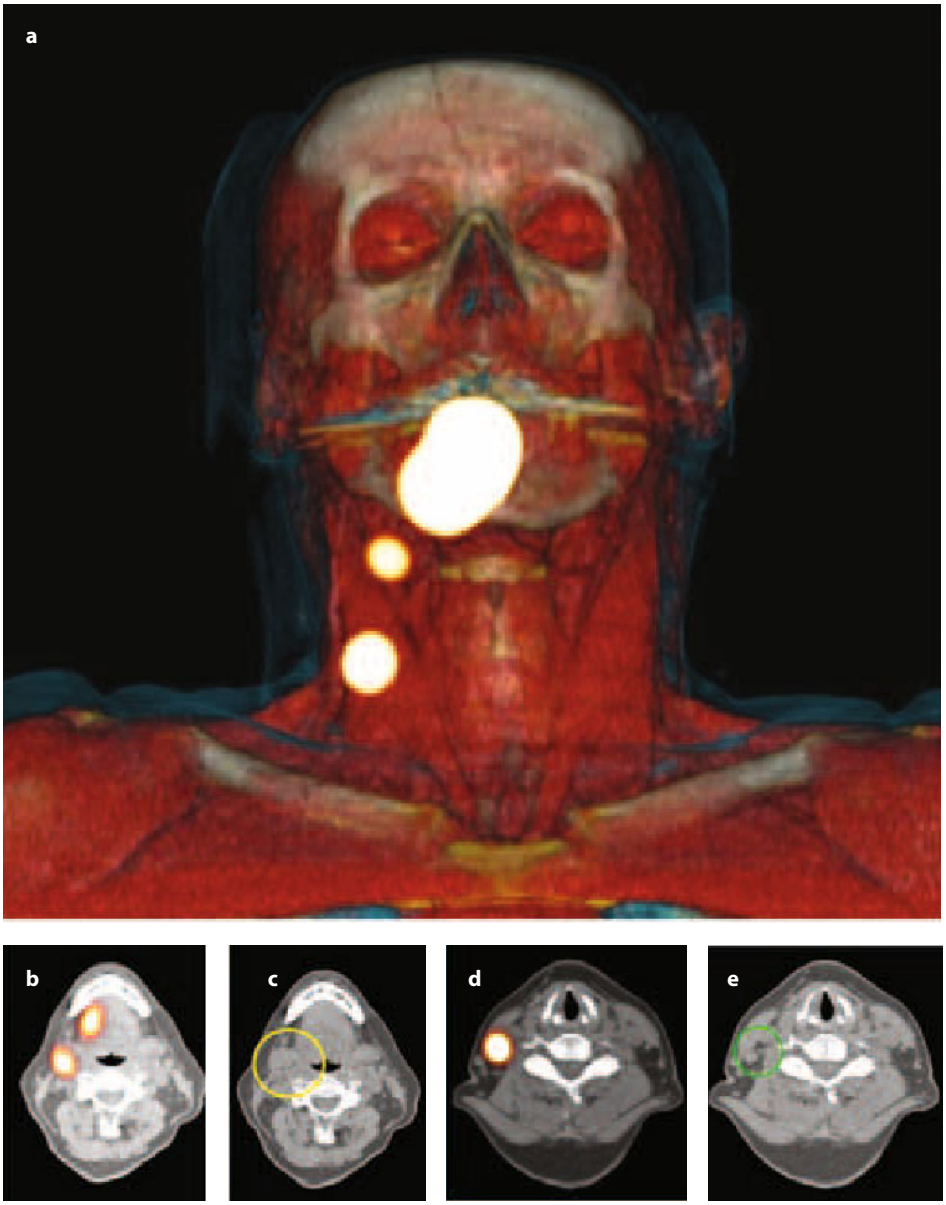

Fig. 11.7 A 60-year-old woman with a T1 carcinoma of the right border of the tongue. SPECT/CT performed 2 hours after peritumoral administration of 80 MBq ^{99m}Tc-nanocolloid. Early imaging had depicted two early-draining lymph nodes on the right side of the neck. Volume rendering (**a**) and axial SPECT/CT (**b**, **d**) localized these sentinel nodes in levels II and III of the neck. On CT (**c**, **e**) the corresponding lymph nodes are indicated with *green circles*

11.12 Accuracy of Radioguided Sentinel Lymph Node Biopsy

In head and neck melanoma, false-negative rates appear to be higher (more than 10% in various series) than the value of 2–3% commonly reported for other sites [19]. However, when performed by head and neck surgeons, the SLN procedure may achieve negative-predictive values close to 98%, similar to those for other cutaneous malignancies [20].

With respect to oral cavity malignancies, a multi-institutional trial including 140 patients with T1–T2 oral squamous cell carcinomas (95 tongue, 26 floor of the mouth, and 19 other cancers) was conducted, in which both the SLN procedure and a completion selective neck dissection were performed. The SLNB was shown to accurately stage the regional lymph nodes, with a negative-predictive value of 96% [21].

Clinical Cases

Case 11.1
Sentinel Node Mapping in Carcinoma of the Hard Palate: Drainage to Bilateral Submandibolar Nodes After Submucosal Peritumoral Injection (Planar Imaging)

Giuseppe Rubini and Maria Antonia Renna

Background Clinical Case

Patient presenting with pain and difficulty in swallowing; physical examination revealed an ulcerated lesion of the hard palate (1 cm × 0.7 cm) surrounded by areas of leucoplachya. Histopathologic findings: tumor cells were large and showed a polygonal epitelioid shape. An abnormally high nucleus/cytoplasm ratio was present. The patient was referred for radioguided sentinel lymph node biopsy.

Lymphoscintigraphy

In the afternoon before surgery, lymphoscintigraphy was performed following submucosal injections of 0.8 mL of a of 74 MBq ^{99m}Tc-albumin nanocolloid (divided into four aliquots) around the tumor. A dual-detector SPECT gamma camera (Millennium MG, GE Healthcare, Milwaukee, WI) equipped with low-energy high-resolution (LEHR) collimators was used to obtain cervical dynamic images immediately after radiopharmaceutical injection and planar static images at 30 and 60 min after radiopharmaceutical injection. The dynamic image was acquired in anteroposterior projection with a 256×256 matrix and zoom factor 1.00, while planar images were acquired in right lateral and left lateral projections with a 128×128 matrix and zoom factor 1.00.

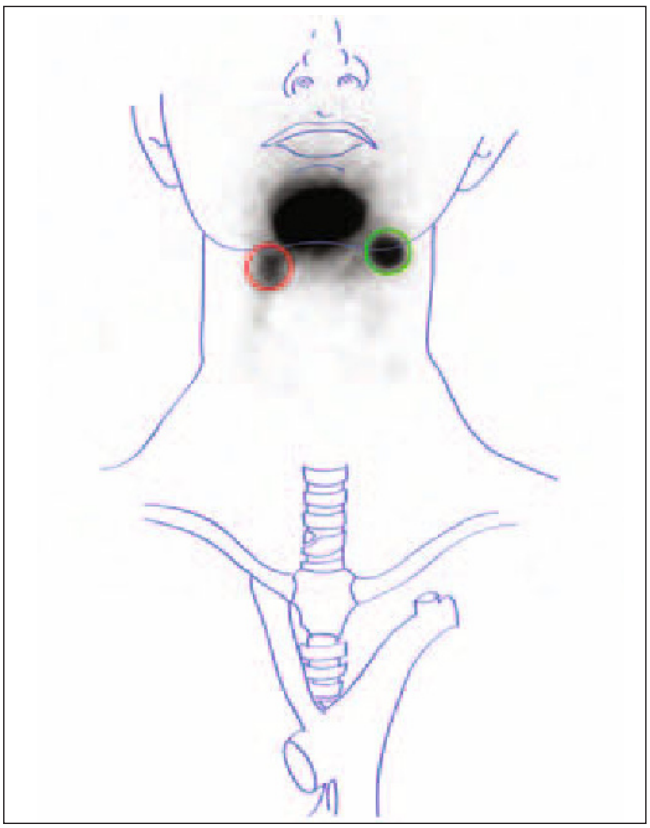

Fig. 1 Schematic representation of anterior static image of the cervical region 30 min after submucosal radiopharmaceutical injection shows two separate lymphatic vessels leading respectively to a left submandibular lymph node (*green circle*) and to a right sudmandibular lymph node (*red circle*)

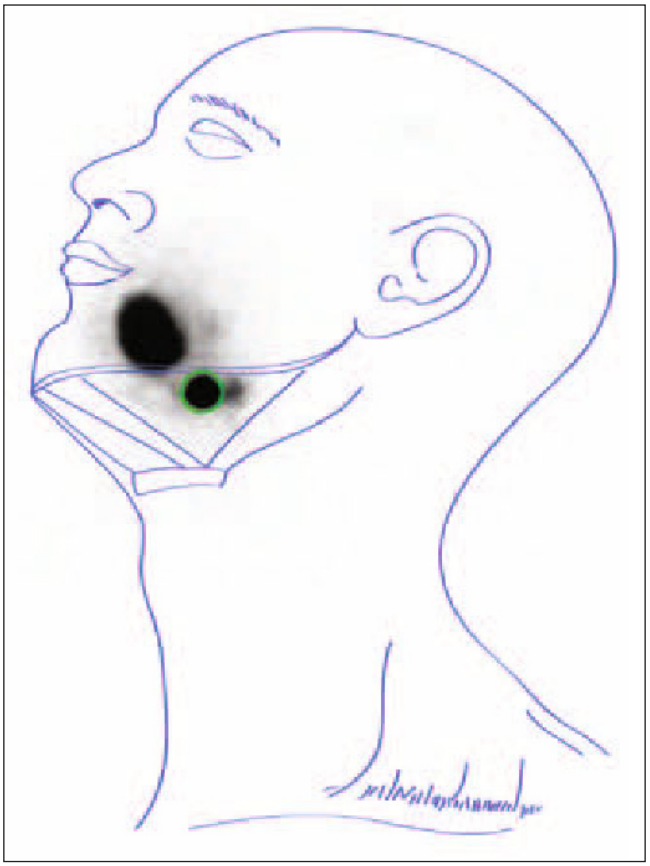

Fig. 2 Schematic representation of left lateral static image of the cervical region 35 min after intradermal radiopharmaceutical injections (*green circle* = left submandibular lymph node)

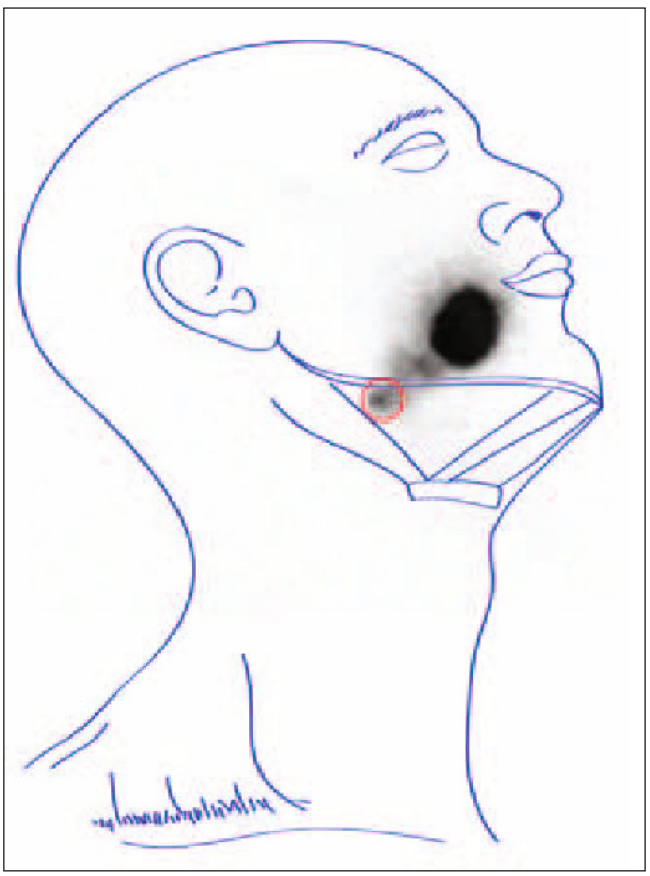

Fig. 3 Schematic representation of right lateral static image of the cervical region 60 min after intradermal radiopharmaceutical injections (*red circle* = right sudmandibular lymph node)

Case 11.2
Sentinel Node Mapping in Oral Cavity Carcinoma: Drainage to Ipsilateral Submandibolar Nodes After Submucosal Peritumoral Injection (Planar Imaging)

Giuseppe Rubini and Maria Antonia Renna

Background Clinical Case

A 62-year-old tobacco smoker with poorly fitting dentures and pain presented with a carcinoma of the oral cavity located in the right cheek. His tongue had scattered plaques with inflamed cheeks. Biopsy showed high mitotic activity and obvious cytologic atypias as well as architectural complexity of papillary squamous cell carcinomas.

Lymphoscintigraphy

In the afternoon before surgery, lymphoscintigraphy was performed following submucosal peritumoral injection of 0.4 mL of 18 MBq ^{99m}Tc-albumin nanocolloid in the right cheek. A dual-detector SPECT gamma camera (Millennium MG GE Healthcare, Milwaukee, WI) equipped with low-energy high-resolution (LEHR) collimators was used to obtain cervical dynamic images immediately after injection and cervical static images 30 min after radiopharmaceutical injection in anterior and right lateral projection. Dynamic images were acquired in anteroposterior projection with a 128×128 matrix and zoom factor 1.00, while static planar images were acquired in right lateral projection with a 128×128 matrix and zoom factor 1.00.

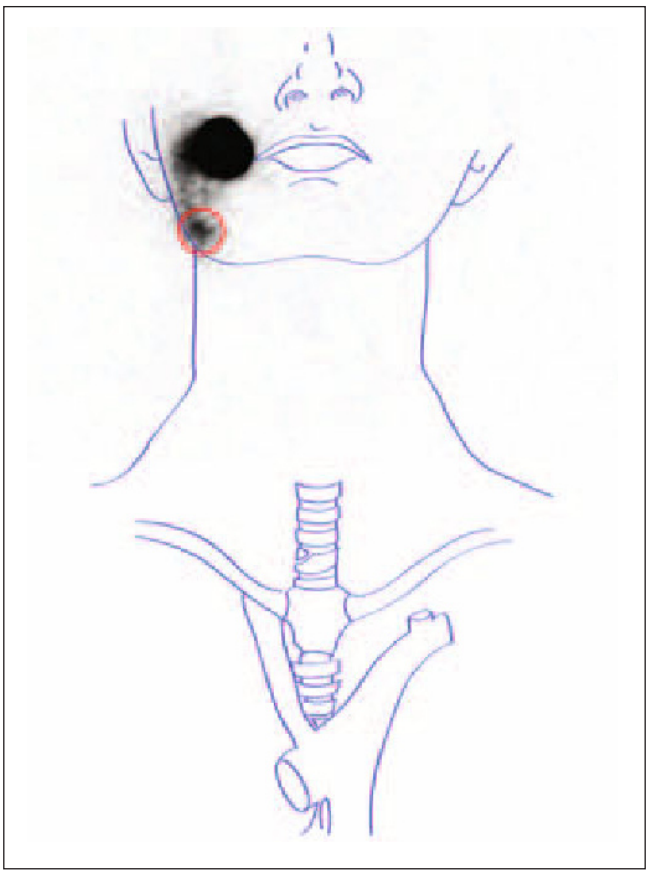

Fig. 1 Static scan in anteroposterior projection shows a focal area in the right submandibular region, corresponding to the sentinel lymph node (*red circle*) of the lesion

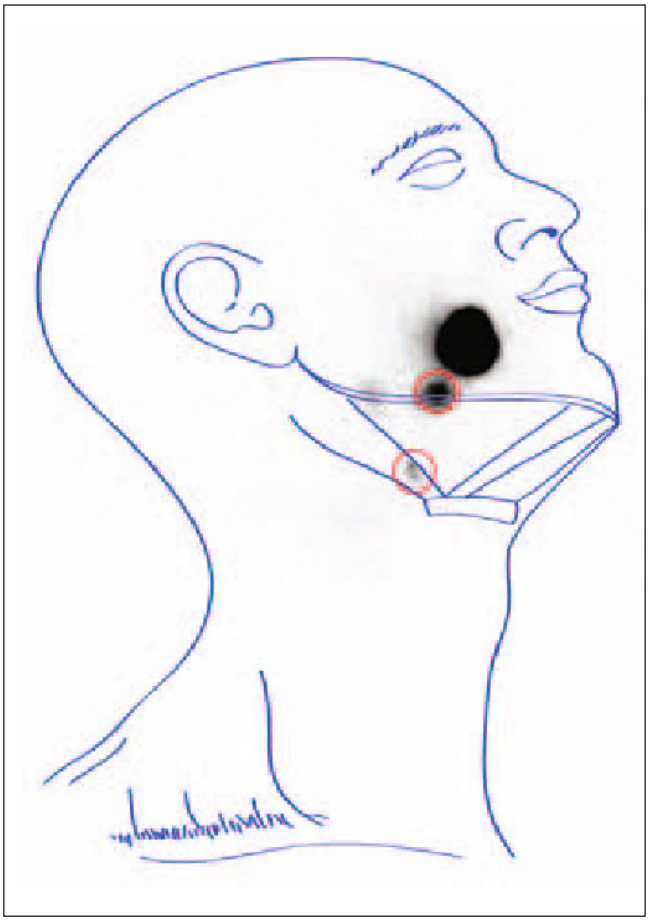

Fig. 2 Static scan in lateral right projection (patient with head in lateral decubitus during acquisition) confirms the presence of a laterocervical sentinel lymph node (*red circle*) with serial visualization of a subsequent-tier node (*green circle*)

Case 11.3
Sentinel Node Mapping in Carcinoma of the Tongue: Drainage to Bilateral Cervical Nodes After Submucosal Peritumoral Injection (Planar Imaging)

Giuseppe Rubini and Maria Antonia Renna

Background Clinical Case

A 52-year-old alcohol drinker with painless white patch on the left side of the tongue and lining of the mouth. Following biopsy demonstrating invasive and proliferative squamous epithelium with keratin pearls, he was referred for lymphoscintigraphy and radioguided sentinel lymph node biopsy.

Lymphoscintigraphy

In the afternoon before surgery, lymphoscintigraphy was performed following submucosal perilesional injections of 0.4 mL of 18 MBq ^{99m}Tc-albumin nanocolloid. A dual-detector SPECT gamma camera (Millennium MG, GE Healthcare, Milwaukee, WI) equipped with low-energy high-resolution (LEHR) collimators was used to obtain cervical dynamic images immediately after radiopharmaceutical injection and planar static images at 30 and 60 min after radiopharmaceutical injection. Dynamic images were acquired in anteroposterior projection with a 128×128 matrix and zoom factor 1.00, while planar images were acquired in anterior right lateral and left lateral projection, with a 128×128 matrix and zoom factor 1.00.

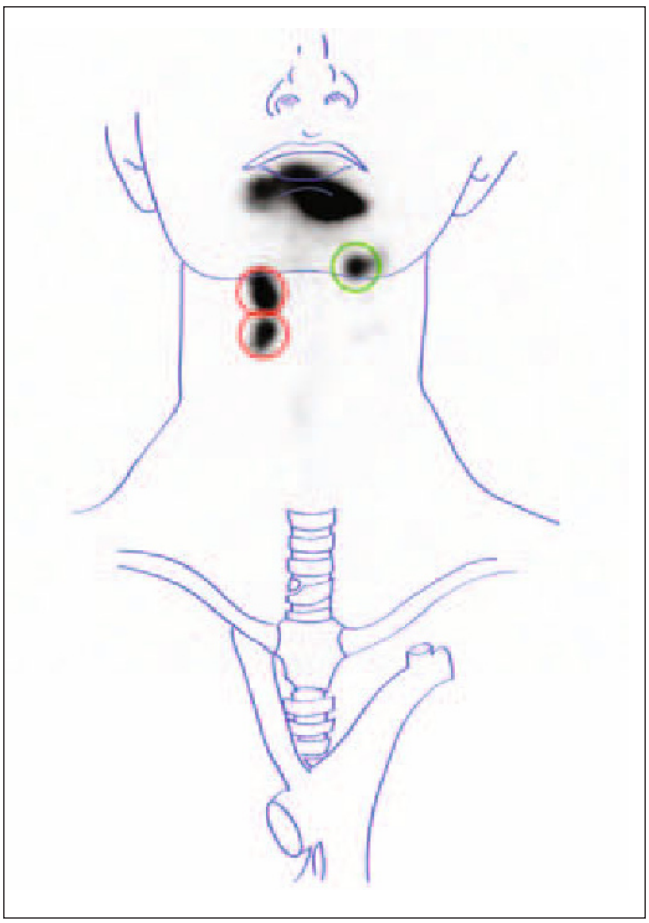

Fig. 1 Schematic representation of lymphoscintigraphy in anteroposterior projection, showing two focal areas of uptake respectively in the right laterocervical region (*upper red circle*) and in the left laterocervical region (*green circle*), corresponding to the sentinel lymph nodes. There was serial visualization of a subsequent right laterocervical-tier node (*lower red circle*)

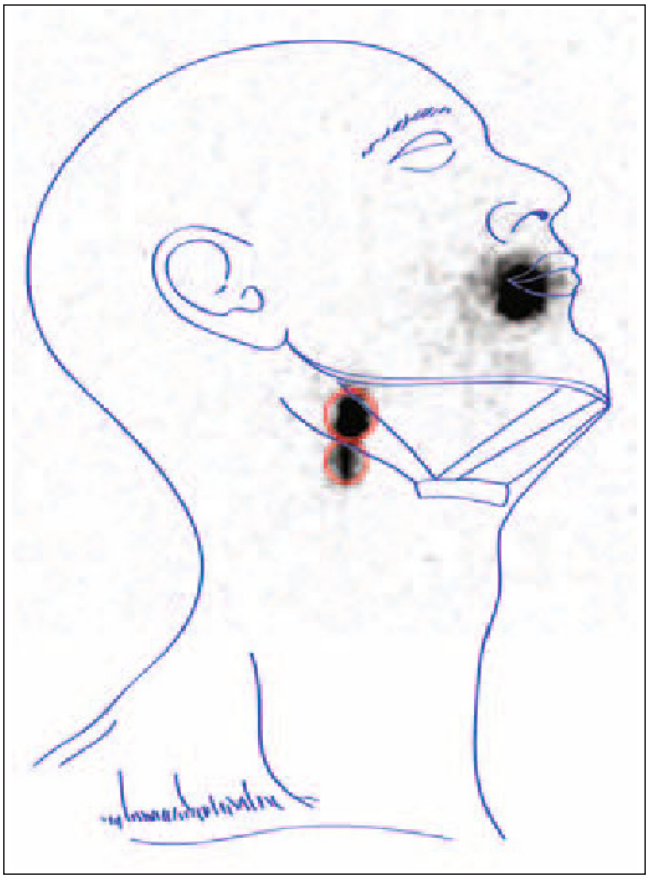

Fig. 2 Static scans in right lateral projection (patient with head in lateral decubitus during acquisition). Right laterocervical sentinel lymph node (*upper red circle*) and subsequent right laterocervical-tier node (*lower red circle*) are seen

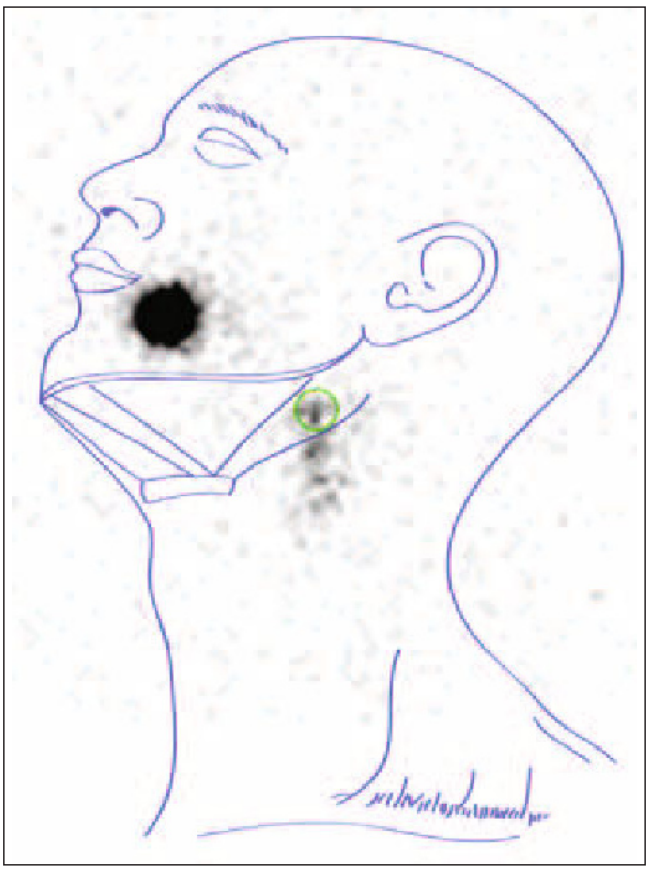

Fig. 3 Static scans in left lateral projection (patient with head in lateral decubitus during acquisition). A left laterocervical sentinel lymph node (*green circle*) is seen

Case 11.4
Sentinel Node Mapping in Carcinoma of the Tongue: Drainage to Ipsilateral Cervical Nodes After Submucosal Peritumoral Injection (Planar Imaging)

Girolamo Tartaglione, Maurizio Giovanni Vigili, Siavash Rahimi, and Marco Pagan

Background Clinical Case

A 78-year-old woman with a squamous cell carcinoma (clinical stage T1N0M0) of the right margin of the tongue was submitted to transoral lateral glossectomy and radioguided sentinel lymph node biopsy.

Lymphoscintigraphy

Three hours before surgery, after a local anesthesia with lidocaine spray (10%), lymphoscintigraphy was performed following injection of 0.3 mL of 100 MBq of ^{99m}Tc-nanocolloid, divided into four aliquots around the tumor. A dual-detector SPECT/CT gamma camera (Infinia Hawkeye GE Healthcare, Milwaukee, WI) equipped with low-energy general purpose (LEGP) collimators was used to obtain planar images of the cervical region immediately after injection. A planar image was acquired in right lateral projection (acquisition time of 5 min), with 128×128 matrix and zoom factor of 1.00-1.50.

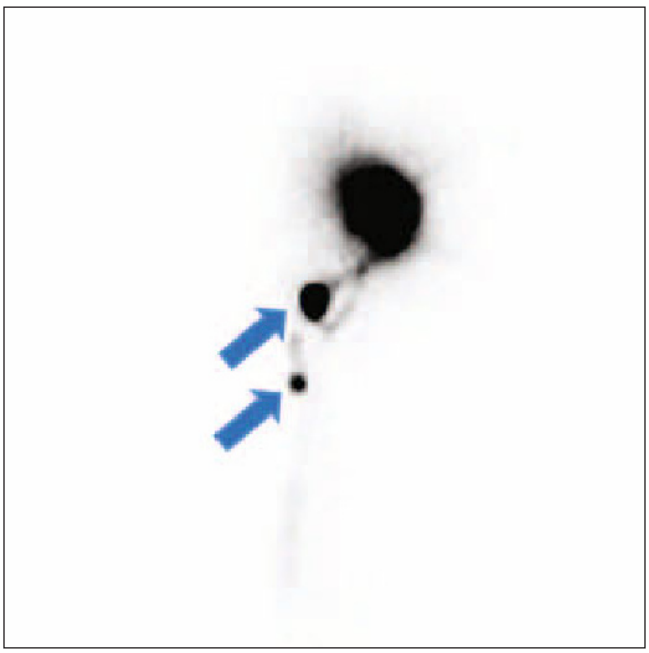

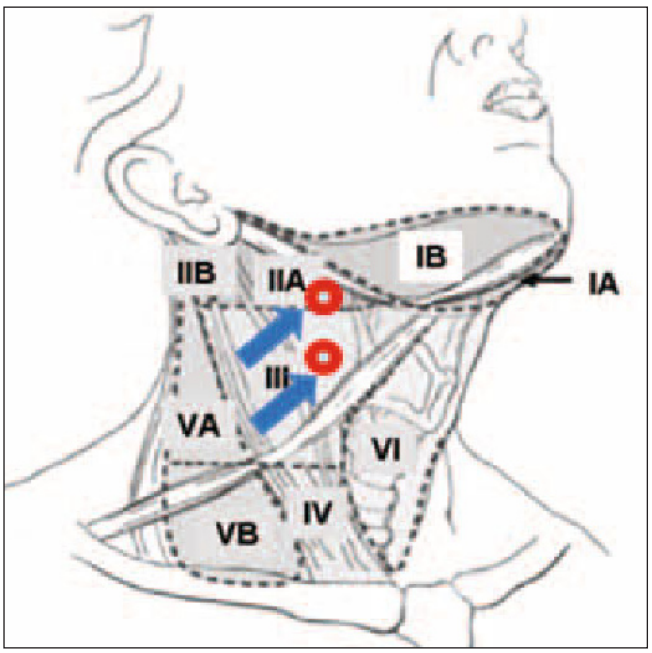

Fig. 1 The planar image in right lateral projection (**a**) of lymphoscintigraphy showed two lymphatic vessels leading to two right cervical sentinel lymph nodes at Robbins' anatomical levels IIA and III respectively (**b**). Serial hematoxylin and eosin staining and immunohistochemistry examination of histological sections of sentinel lymph nodes were negative for tumor (pN0)

Case 11.5
Sentinel Node Mapping in Thyroid Carcinoma: Drainage to Ipsilateral Cervical Node After Intratumoral Injection (Planar and SPECT/CT Imaging)

Luciano Feggi, Chiara Peterle, Corrado Cittanti, Valentina de Cristofaro, Stefano Panareo, Ilaria Rambaldi, Virginia Rossetti, Ivan Santi, and Paolo Carcoforo

Background Clinical Case

A 46-year-old woman presented with a nodule in the right thyroid lobe detected by ultrasonography. A fine needle aspiration biopsy (FNAB) was performed, which demonstrated a papillary thyroid carcinoma. The patient underwent radioguided sentinel lymph node biopsy.

Lymphoscintigraphy

In the afternoon before surgery, lymphoscintigraphy was performed following intratumoral injection of 0.2 mL of 74 MBq ^{99m}Tc-nanocolloid. About 3 h after injection, a dual-detector SPECT/CT gamma camera (Symbia-T2 Siemens Medical Solutions, Hoffman Estates, IL) equipped with low-energy high-resolution (LEHR) collimators and dual spiral CT was used to obtain cervical and thoracic planar images in anterior view with a 128×128 matrix and zoom factor 1, as well as SPECT/CT acquisition (using a step-and-shoot protocol of 25 s/3° for a total of 60 views per camera head, 256×256 matrix, zoom factor 1). CT parameters included a tube current of 40 mA, a tube voltage of 120 kV, and slice thickness of 1 mm.

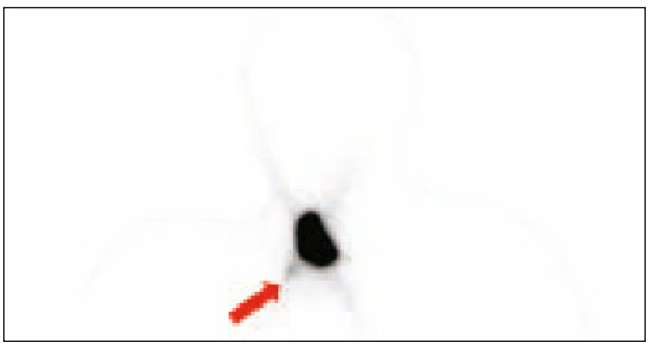

Fig. 1 Lymphoscintigraphy of the neck in anterior view shows an area of faint uptake below and on the right of the injection site, which is difficult to diagnose (*red arrow*)

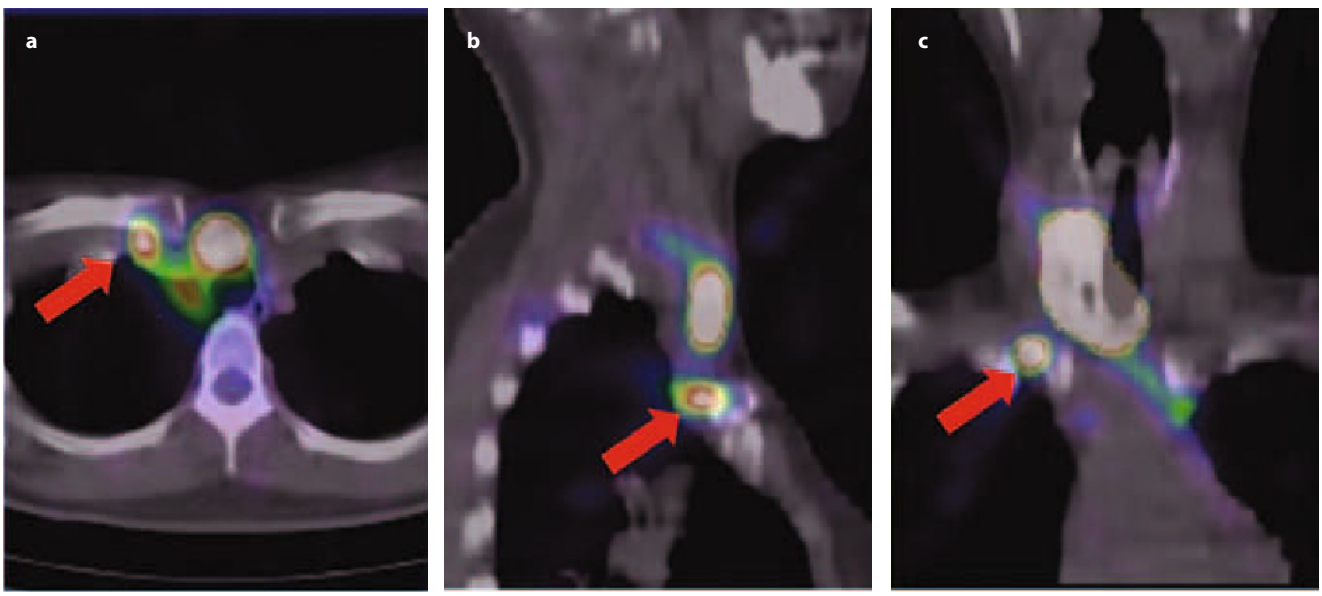

Fig. 2 Fused SPECT/CT images in axial, sagittal and coronal planes (**a**, **b**, **c**, respectively) show one right laterocervical sentinel lymph node (*red arrows*). The day after scintigraphy, during total thyroidectomy, only right laterocervical basin was removed (because of unilateral drainage of the lesion), thus decreasing surgical risck, surgery duration and post-operative complications

Case 11.6
Sentinel Node Mapping in Thyroid Carcinoma: Drainage to Bilateral Cervical Nodes After Intratumoral Injection (SPECT/CT Imaging)

Luciano Feggi, Chiara Peterle, Corrado Cittanti, Valentina de Cristofaro, Stefano Panareo, Ilaria Rambaldi, Virginia Rossetti, Ivan Santi, and Paolo Carcoforo

Background Clinical Case

A 30-year-old woman with no history of thyroid disease underwent ultrasonography of the neck during a routine check-up, which demonstrated a nodular lesion in the right thyroid lobe. A fine needle aspiration biopsy (FNAB) was performed, demonstrating a papillary carcinoma. The patient was submitted to radioguided sentinel lymph node biopsy.

Lymphoscintigraphy

In the afternoon before surgery, lymphoscintigraphy was performed following intratumoral injection of 0.2 mL of 74 MBq ^{99m}Tc-nanocolloid. About 3 h after injection, a dual-detector SPECT/CT gamma camera (Symbia-T2 Siemens Medical Solutions, Hoffman Estates, IL) equipped with low-energy high-resolution (LEHR) collimators and dual spiral CT was used to obtain cervical, and thoracic planar images in anterior view with a 128×128 matrix and zoom factor 1, as well as SPECT/CT acquisition (using a step-and-shoot protocol of 25 s/3° for a total of 60 views per camera head, 256×256 matrix, zoom factor 1). CT parameters included a tube current of 40 mA, a tube voltage of 120 kV, and a slice thickness of 1 mm.

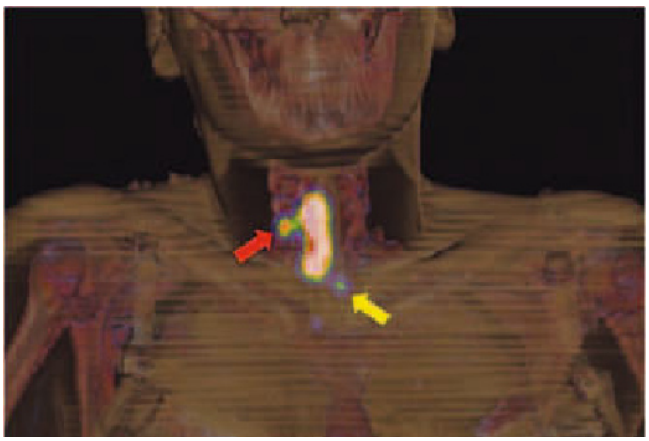

Fig. 1 3D volume rendering of a SPECT/CT image shows the injection site and two faint areas of tracer uptake localized both in VI level, one just a little on the right of the injection site (*red arrow*) and the 2nd below and on the left of it (*yellow arrow*)

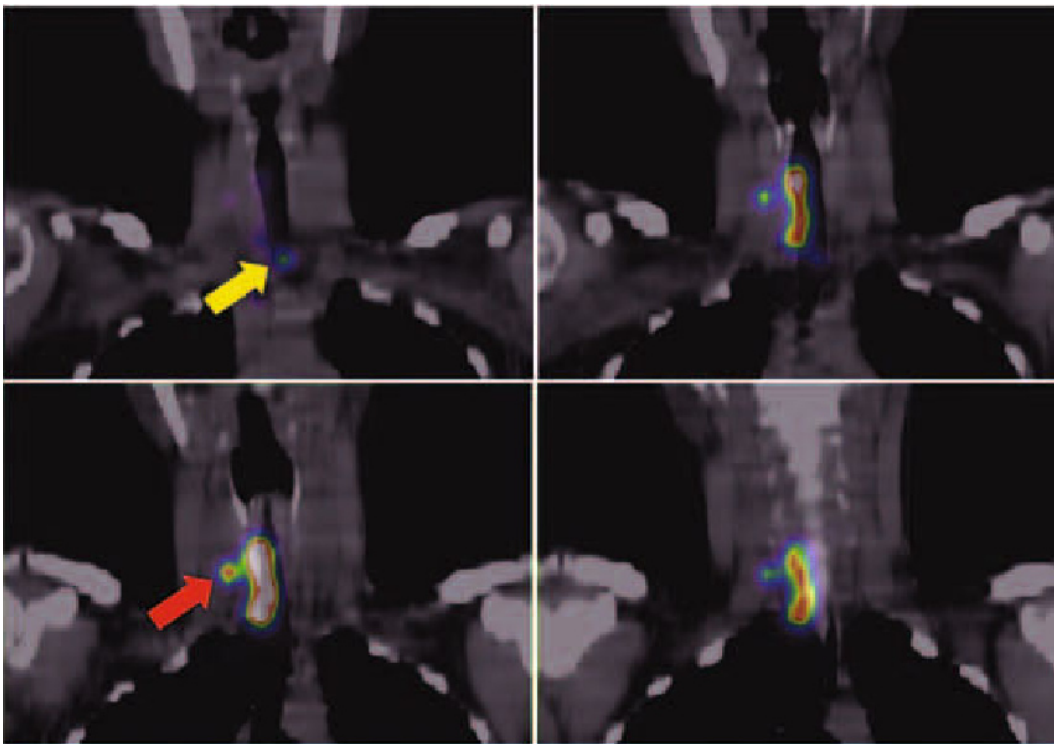

Fig. 2 Fused SPECT/CT images in coronal plane show radiotracer uptake into two cervical lymph nodes localized both at level VI (*red arrow and yellow arrow*)

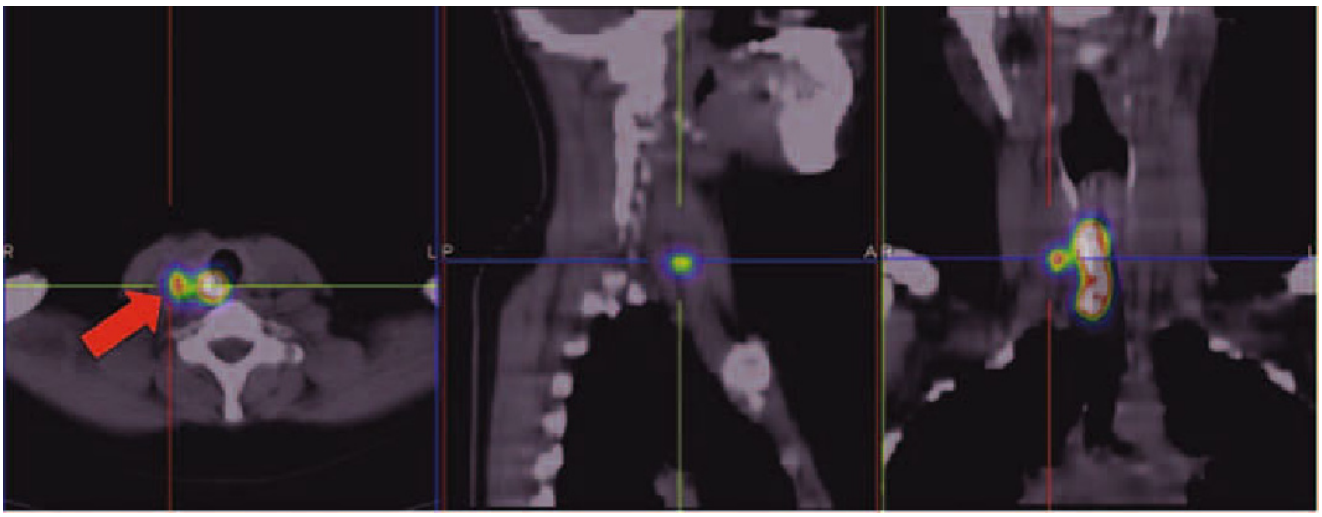

Fig. 3 Fused SPECT/CT images in axial, sagittal, and coronal planes showing the cervical lymph node at level VI (*red arrow*) which has the most intense uptake and the nearest to the injection site (sentinel lymph node, SLN)

Case 11.7
Sentinel Node Mapping in Thyroid Carcinoma: Drainage to Multiple Ipsilateral Cervical Nodes After Intratumoral Injection (Planar and SPECT/CT Imaging)

Luciano Feggi, Chiara Peterle, Corrado Cittanti, Valentina de Cristofaro, Stefano Panareo, Ilaria Rambaldi, Virginia Rossetti, Ivan Santi, and Paolo Carcoforo

Background Clinical Case

A 39-year-old woman with histological diagnosis of thyroid follicular carcinoma (BRAF-negative) in the left lobe. The patient underwent radioguided sentinel lymph node biopsy. After surgery, pTNM staging was pT1N0Mx.

Lymphoscintigraphy

In the afternoon before surgery, lymphoscintigraphy was performed following intratumoral injection of 0.2 mL of 74 MBq ^{99m}Tc-nanocolloid. About 3 h after injection, a dual-detector SPECT/CT gamma camera (Symbia-T2 Siemens Medical Solutions, Hoffman Estates, IL) equipped with low-energy high-resolution (LEHR) collimators and dual spiral CT was used to obtain cervical and thoracic planar images in anterior view with a 128×128 matrix and zoom factor 1, as well as SPECT/CT acquisition (using a step-and-shoot protocol of 25 s/3° for a total of 60 views per camera head, 256×256 matrix, zoom factor 1). CT parameters included a tube current of 40 mA, a tube voltage of 120 kV, and a slice thickness of 1 mm.

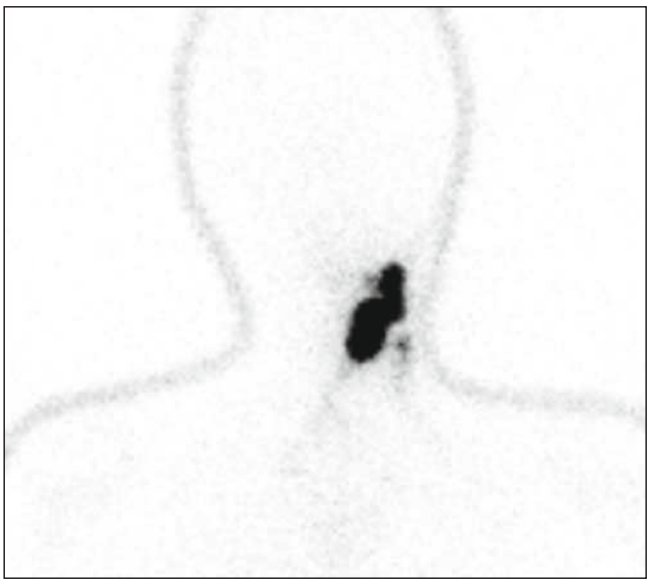

Fig. 1 Lymphoscintigraphy of the neck in anterior view shows two areas of intense uptake in the left cervical region and one area of faint uptake below the previous ones, corresponding to three sentinel lymph nodes

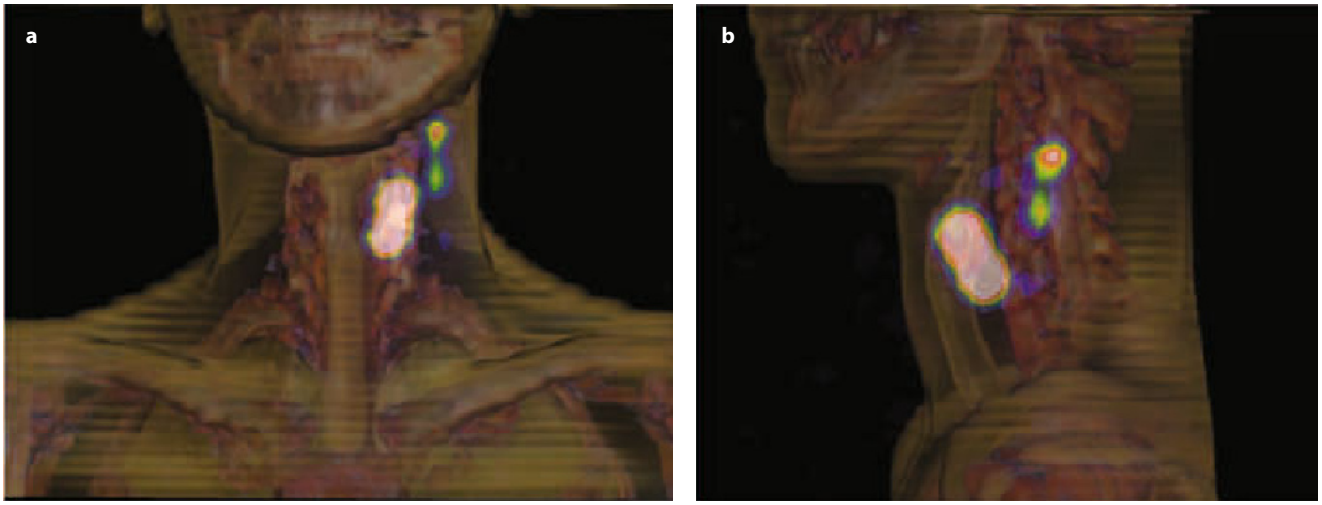

Fig. 2 The 3D volume rendering SPECT/CT reconstruction in anterior (**a**) and left lateral (**b**) views showing three left cervical lymph nodes

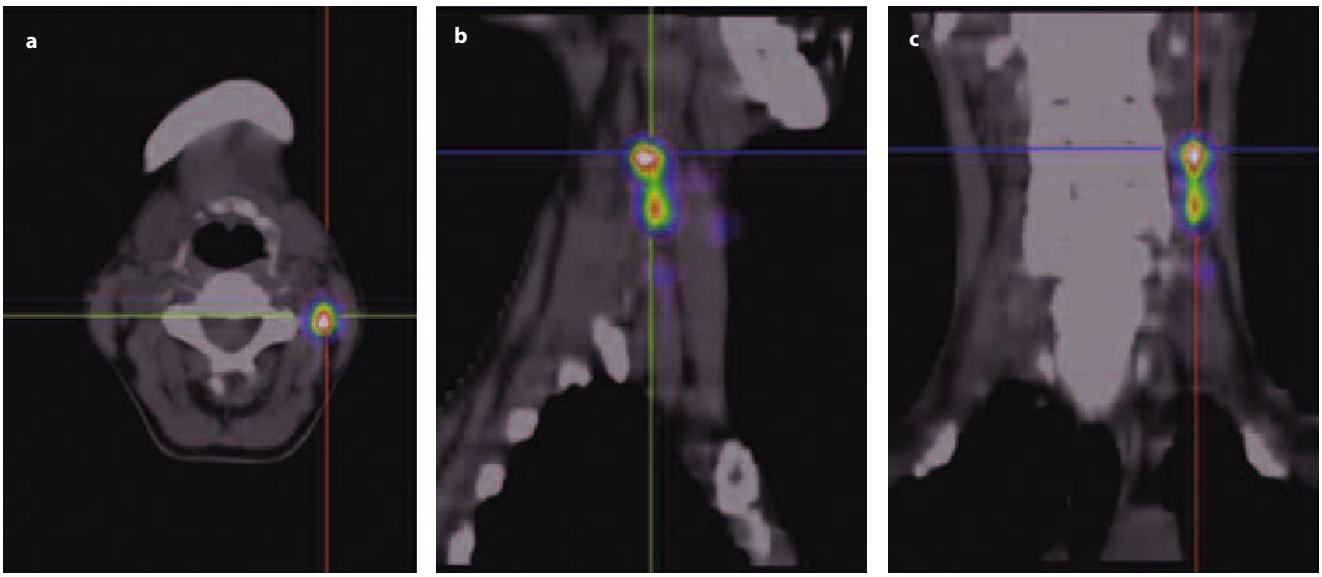

Fig. 3 Fused SPECT/CT images in axial, sagittal, and coronal planes (**a**, **b**, **c**, respectively) show two left cervical lymph nodes with the most intense tracer uptake, both in level III. The identification of unilateral lymphatic drainage of the lesion allowed surgeon to perform a total thyroidectomy with a unilateral dissection of the left laterocervical lymphatic basin thus decreasing surgical risk, surgery duration and post-operative complications

Case 11.8
Sentinel Node Mapping in Carcinoma of the Tongue: Drainage to Ipsilateral Cervical Nodes After Intratumoral Injection (Planar and SPECT/CT Imaging)

Luciano Feggi, Chiara Peterle, Corrado Cittanti, Valentina de Cristofaro, Stefano Panareo, Ilaria Rambaldi, Virginia Rossetti, and Ivan Santi

Background Clinical Case

A 79-year-old man with squamous cell carcinoma of the right edge of the tongue underwent preoperative lymphoscintigraphy to investigate whether lymphatic drainage from the lesion was unilateral or bilateral; radioguided sentinel lymph node biopsy was performed concomitantly with surgical resection of the primary tumor.

Lymphoscintigraphy

In the afternoon before surgery, lymphoscintigraphy was performed following intratumoral injection of 0.2 mL of 74 MBq ^{99m}Tc-nanocolloid. About 3 h after injection, a dual-detector SPECT/CT gamma camera (Symbia-T2 Siemens Medical Solutions, Hoffman Estates, IL) equipped with low-energy high-resolution (LEHR) collimators and dual spiral CT was used to obtain cervical and thoracic planar images in anterior view with a 128×128 matrix and zoom factor 1, as well as SPECT/CT acquisition (using a step-and-shoot protocol of 25 s/3° for a total of 60 views per camera head, 256×256 matrix, zoom factor 1). CT parameters included a tube current of 40 mA, a tube voltage of 120 kV, and a slice thickness of 1 mm.

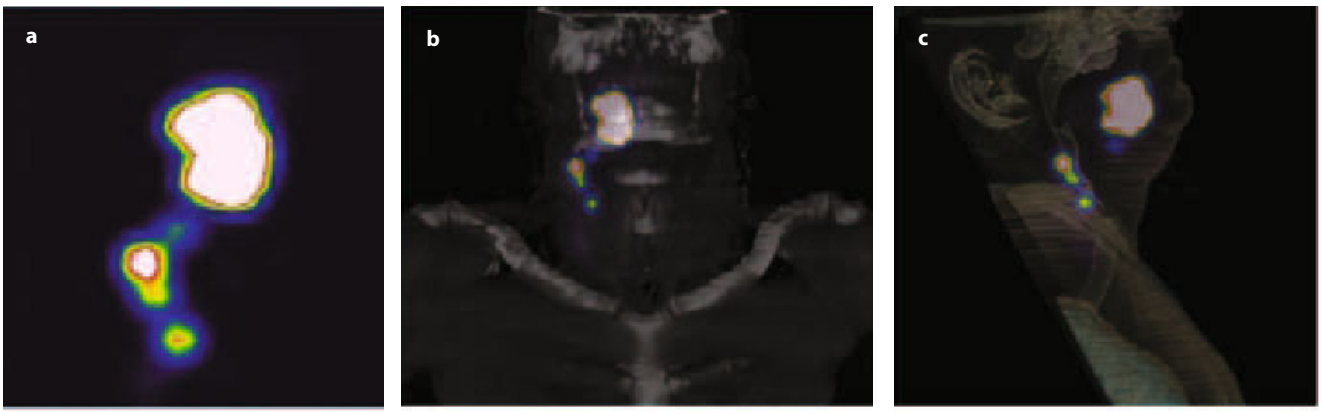

Fig. 1 SPECT (**a**) and 3D volume rendering SPECT/CT reconstructions (**b**, **c**, anterior and lateral view respectively) showing the three right cervical lymph nodes all in right laterocervical lymphatic basin

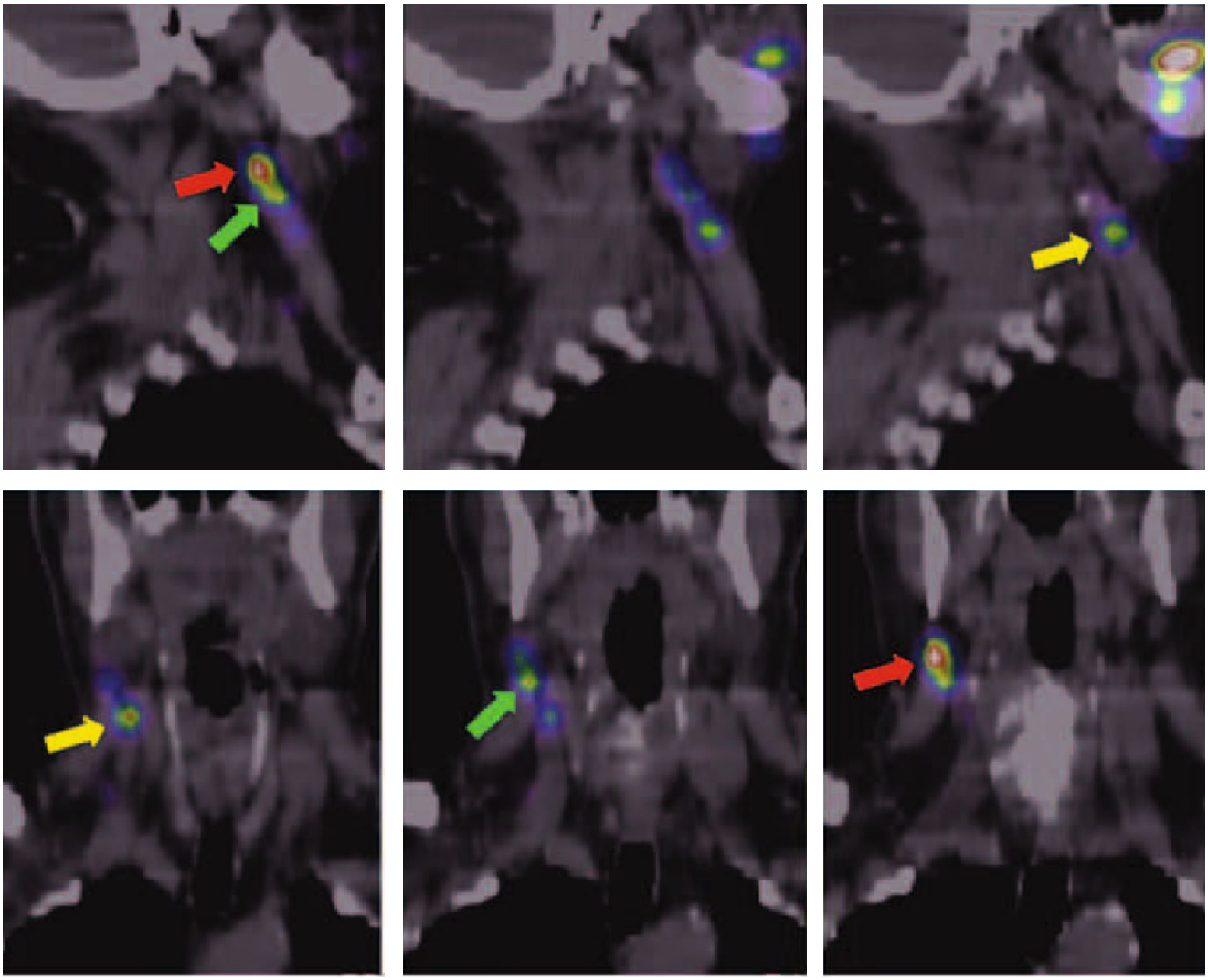

Fig. 2 Fused SPECT/CT images in sagittal (*upper panel*) and coronal (*lower panel*) planes, showing one right cervical lymph node at level II (*red arrow*) and two right cervical lymph nodes at level III (*yellow and green arrows*)

References

1. Klop MC, Veenstra HJ, Vermeeren L et al (2011) Assessment of lymphatic drainage patterns and implications for the extent of neck dissection in head and neck melanoma patients. J Surg Oncol 103:7566–7760
2. Shoaib T, Soutar DS, MacDonald DG et al (2005) The nodal neck level of sentinel lymph nodes in mucosal head and neck cancer. Br J Plast Surg 58:790–794
3. Thompson JF, Shaw HM (2006) Is sentinel lymph node biopsy appropriate in patients with thin melanomas: too early to tell? Ann Surg Oncol 13:279–281
4. Essner R, Chung MH, Bleicher R (2002) Prognostic implications of thick (>or=4-mm) melanoma in the era of intra-operative lymphatic mapping and sentinel lymphadenectomy. Ann Surg Oncol 9:754–761
5. Civantos F, Zitsch R, Bared A et al (2008) Sentinel node biopsy for squamous cell carcinoma of the head and neck. J Surg Oncol 97:683–690
6. Paleri V, Rees G, Arullendran P et al (2005) Sentinel node biopsy in squamous cell cancer of the oral cavity and oral pharynx: a diagnostic meta-analysis. Head Neck 27:739–747
7. Ferlito A, Silver CE, Rinaldo A (2009) Elective management of the neck in oral cavity squamous carcinoma: current concepts supported by prospective studies. Br J Oral Maxillofac Surg 47:5–9
8. Alazraki N, Glass EC, Castronovo D et al (2002) Procedure guideline for lymphoscintigraphy and the use of intraoperative gamma probe for sentinel lymph node localization in melanoma of intermediate thickness 1.0. J Nucl Med 43:1414–1418
9. Schauer AJ, Becker W, Reiser M, Possinger K (2005) The sentinel lymph node concept. Springer, Berlin
10. Ananthakrishnan P, Mariani G, Moresco L, Giuliano AE (2008) The anatomy and physiology of lymphatic circulation. In: Mariani G, Giuliano AE, Strauss WH (eds) Radioguided surgery: a comprehensive team approach. Springer Science, New York, pp 57–71
11. American Joint Committee on Cancer (2010) Cancer staging handbook, 7th ed. Springer, New York
12. Brouwer OR, Klop WM, Buckle T et al (2012) Feasibility of sentinel node biopsy in head and neck melanoma using a hybrid radioactive and fluorescent tracer. Ann Surg Oncol 19:1988–1994
13. Khafif A, Schneebaum S, Fliss DM et al (2006) Lymphoscintigraphy for sentinel node mapping using a hybrid single photon emission CT (SPECT)/CT system in oral cavity squamous cell carcinoma. Head Neck 28:874–879.
14. Vermeeren L, Valdés Olmos RA, Klop WM et al (2011) SPECT/CT for sentinel lymph node mapping in head and neck melanoma. Head Neck 33:1–6
15. De Wilt JH, Thompson JF, Uren RF et al (2004) Correlation between preoperative lymphoscintigraphy and metastatic nodal disease sites in 362 patients with cutaneous melanomas of the head and neck. Ann Surg 239:544–552
16. Vermeeren L, Valdés Olmos RA, Klop WM et al (2010) A portable gamma camera for intraoperative detection of sentinel nodes in the head and neck region. J Nucl Med 51:700–703
17. Reynolds HM, Smith NP, Uren RF et al (2009) Three-dimensional visualization of skin lymphatic drainage patterns of the head and neck. Head Neck 31:1316–1325
18. Calabrese L, Soutar D, Werner J et al (2008) Sentinel lymph node biopsy in cancer of the head and neck. In: Mariani G, Giuliano AE, Strauss WH (eds) Radioguided surgery: a comprehensive team approach. Springer Science, New York, pp 120–129
19. Alkureishi L, Ross GL (2011) Sentinel node biopsy for head and neck cancer. In: Bernier J (ed) Head and neck cancer: multimodality management. Springer-Science, New York, pp 241–253
20. Civantos FJ, Zitsch R, Bared A (2007) Sentinel node biopsy in oral squamous cell carcinoma. J Surg Oncol 94:330–336
21. Civantos FJ, Zitsch RP, Schuller DE et al (2010) Sentinel lymph node biopsy accurately stages the regional lymph nodes for T1–T2 oral squamous cell carcinomas: results of a prospective multi-institutional trial. J Clin Oncol 28:1395–1400

12 Preoperative and Intraoperative Lymphatic Mapping for Radioguided Sentinel Node Biopsy in Non-Small-Cell Lung Cancer

Giuseppe Boni, Franca M. A. Melfi, Gianpiero Manca, Federico Davini, and Giuliano Mariani

12.1 Introduction

Non-small-cell lung cancer (NSCLC) is the most common malignancy worldwide and a major cause of cancer-related death [1]. It represents 85% of all lung cancers and usually grows and spreads more slowly than small-cell lung cancer. Despite advances in surgery, chemotherapy, and radiation therapy over the last decades, the death rate from NSCLC has remained largely unchanged. Such poor long-term survival probably results from the fact that early-stage disease is asymptomatic and the onset of symptoms marks the presence of advanced, incurable disease.

The presence or absence of mediastinal lymph node metastasis is a key prognostic factor in NSCLC, and lymph node dissection is an effective therapeutic procedure when carried out in patients with nodal metastasis [2, 3].

The sentinel lymph node (SLN) mapping procedure has been developed in recent years and validated in a variety of solid epithelial tumors, mainly breast cancer and melanoma, as a way to avoid the complications associated with systematic lymph node dissection; this procedure has recently also been tested in patients with NSCLC [4–7].

12.2 The Clinical Problem

Mediastinal lymph node staging is one of the most important prognostic factors for patients with operable lung cancers. In fact, the presence of lymph node involvement decreases the 5-year survival rate by nearly 50% as compared to similar patients without nodal metastasis [8].

G. Boni (✉)
Regional Center of Nuclear Medicine, University of Pisa Medical School
Pisa, Italy
e-mail: g.boni@med.unipi.it

Furthermore, many investigators have clearly demostrated that more careful histopathologic evaluation of previously reported negative lymph nodes in resected lung cancer patients reveals that over 20% of patients classified as having negative lymph nodes (N0) were actually upstaged by immunohistochemistry (IHC), a procedure that is capable of identifying previously undetected micrometastatic disease [9, 10].

Preoperative staging modalities include imaging techniques (standard chest X-ray, high-resolution contrast computed tomography (HRCT), fluorine-18 fludeoxyglucose positron emission tomography ([^{18}F]FDG PET)/CT, magnetic resonance imaging [MRI], bone scan). If these tests do not reveal the presence of metastatic disease or unresectable local disease, then further invasive staging procedures (including bronchoscopy, mediastinoscopy, and video-assisted thoracoscopic surgery [VATS]) may be necessary. Moreover, invasive N-staging modalities, such as complete thoracic lymphadenectomy or nodal sampling, may help to further stratify patients into appropriate therapeutic and prognostic categories.

The choice between systematic mediastinal lymph node dissection and selective lymph node sampling for the staging and treatment of NSCLC is the subject of ongoing debate. Advocates of complete lymphadenectomy believe that residual cancer may remain if complete resection of nodal tissue is not performed, leading to poorer prognosis due to locoregional recurrence and to understaging of disease [11, 12]. Conversely, proponents of lymph node sampling argue that sampling does not impair the local immune response, which may reduce the potential for local recurrence; moreover, the more limited sampling procedure is not associated with the important morbidity associated with systematic mediastinal lymph node dissection such as increased perioperative blood loss, recurrent nerve injury, chylothorax, or bronchopleural fistula [13]. To date, neither survival advantage nor signficant differences in morbidity or mortality rates have been clearly demonstrated using either surgical procedures [14].

G. Mariani et al. (eds.), *Atlas of Lymphoscintigraphy and Sentinel Node Mapping*,
DOI 10.1007/978-88-470-2766-4_12

If the prognosis of NSCLC is not affected by complete mediastinal lymph node dissection, then it can be argued that the morbidity of selective mediastinal lymph node sampling can be further reduced and histopathologic staging of lung cancer can be improved by SLN mapping [15]. This procedure allows detection of occult micrometastasic disease in SLNs by sensitive IHC and/or molecular biology analysis based on the reverse transcription polymerase chain reaction (RT-PCR), thus avoiding extensive serial sectioning and IHC of all dissected lymph nodes [16, 17].

12.3 Indications for Sentinel Lymph Node Biopsy

Patients with cT1N0M0 NSCLC are the best candidates for sentinel lymph node biopsy (SLNB). The recent widespread diffusion of HRCT has resulted in more frequent detection of this subset of NSCLC patients, in whom limited mediastinal lymph node dissection and/or segmentectomy could be as curative as lobectomy with mediastinal lymph node dissection.

12.4 Sentinel Lymph Node Biopsy Techniques in Non-Small-Cell Lung Cancer

12.4.1 Nonradionuclide Methods

Several techniques using nonradionuclide tracers for SLN mapping in patients with NSCLC have been proposed and developed [18–20]. The first SLN mapping procedure in patients with NSCLC was performed using intratumoral injection of isosulfan blue [18]. Unfortunately, since it was difficult to detect the blue dye in the anthracotic lymph nodes in the thoracic cavity, the identification rate of the SLN was too low to be clinically useful. Similar problems were encountered with other dyes, such as indocyanine green (ICG) [19].

Japanese authors from a single institution have developed a novel method for SLN mapping, based on the use of magnetic particles [20, 21]. In particular, colloidal ferumoxides (a superparamagnetic iron) were injected during thoracotomy at the periphery of the tumor. A highly sensitive, hand-held magnetometer was then used to detect, ex vivo, the presence of the ferumoxides within sentinel lymph nods. The in-vivo SLN detection rate was 80%, and more recent results indicate the feasibility and efficacy of this technique, which has 97.6% accuracy, 75% sensitivity, and 2.4% false-negative rate for SLN mapping in patients with NSCLC. Furthermore, Minamiya et al. have proposed to combine subpleural tracer injection with injection in the peritumoral quadrants, in order to improve the identification rate and diagnostic accuracy for mediastinal SLNs [22]. More recently, fluorescent-labeled agents, such as indocyanine (ICG), have been used for SLN mapping in patients with NSCLC [23]. After peritumoral ICG injection during surgery, fluorescence imaging was employed using an infrared-light charge coupled device (CCD) system, and SLNs were identified and dissected in over 80% of cases [23].

12.4.2 Radiocolloids and Modalities of Injection

Since the pioneering work by Liptay and colleagues [7], several articles have been published on the feasibility, technical aspects, and efficacy of radioguided SLNB in the surgical management of patients with NSCLC [6, 7, 24–40]. Radiolabelled colloids (technetium-99 [^{99m}Tc]–tin colloid, ^{99m}Tc–sulfur colloid, or ^{99m}Tc-nanocolloidal human albumin) have been used for radioguided SLNB in NSCLC patients. The total activity administered varies from 9.25 MBq to 296 MBq, which is injected in a total volume of 0.5–2 mL of normal saline.

Three different modalities of injection of the radiocolloids have been described. Liptay et al. have advocated intraoperative radiocolloid injection into or around the primary tumor after direct visualization of the lesion, injecting the radiocolloid in a four-quadrant peritumoral fashion at the time of thoracotomy [7]. An average period of 30–60 minutes from the injection is necessary for radiocolloid migration into the lymphatic vessels and to the SLN basin. During this time, the operation proceeds normally, taking care to avoid the peribronchial lymphatic vessels until the last phase of the resection. Some disadvantages of this modality of injection are the long intraoperative time required while waiting for radiocolloid migration, possible contamination of the pleural cavity after the injection, and accumulation of the radiocolloid in the trachea, due to the absence of coughing in the anesthetized patient. Scintigraphic imaging of lymphatic drainage is virtually impossible when the procedure is based on such intraoperative radiocolloid administration.

A second modality is preoperative injection of radiocolloid into or around the primary tumor under CT guidance on the day of surgery, or the day before [6, 25]. Lymphoscintigraphy can be performed preoperatively, and the main advantage of the preoperative injection technique is that it enables intraoperative measurement of count rates in the upper mediastinal lymph node, because coughing by the patient rapidly removes radiocolloid accumulated in the trachea.

A useful alternative to CT-guided injection of the radiocolloid seems to be preoperative endobronchial injection of the radiocolloid into the directly visualized endobronchial tumor, or transbronchially at the most distal pulmonary subsegment that can be reached endobronchially within proximity of the primary tumor [26].

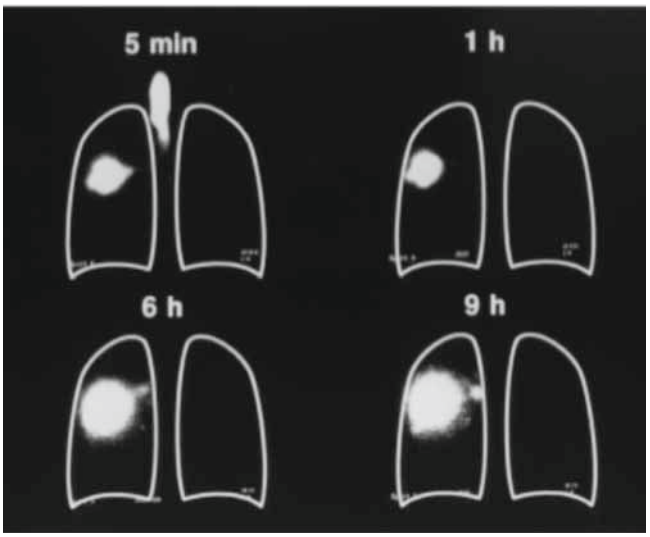

Fig. 12.1 Planar lymphoscintigraphic images acquired sequentially after injection of ^{99m}Tc–tin colloid for SLN mapping in a patient with NSCLC. The early image shows important accumulation of radioactivity at the injection site and in the trachea; the latter is already cleared at the 1-hour imaging point. Migration of the radiocolloid is barely detectable at 1 hour post-injection, becoming, however, more clear at the later imaging time points (6 hours and 9 hours post-injection) (reproduced with permission from [6])

12.5 Preoperative Imaging of Sentinel Lymph Nodes

The feasibiliy of preoperative imaging of the SLN in NSCLC has been tested by Nomori et al. [6]. On the same day, or on the the day before surgery, 111–296 MBq of ^{99m}Tc–tin colloid in a volume of 1–1.5 mL is injected with a single shot through a transthoracic 23-gauge needle inserted into the peritumoral region. In order to determine the optimal timing for radiocolloid injection before surgery, in a subset of patients the authors acquired planar scintigraphic images at 5 minutes, then at 1, 6, 9, and 24 hours after the injection. Based on this preliminary protocol, the authors then performed routine lymphoscintigraphy by acquiring planar images of the chest 5 minutes after the injection, then immediately before surgery.

The early planar images usually visualize radioactivity accumulation at the site of injection and in the tracheobronchial lumen, due to physiological leakage. After about 1 hour, washout of the radiocolloid from the tracheobronchial tree is observed, but migration to the mediastinal lymph nodes is not yet visualized. More than 6 hours after the injection, sufficient radiocolloid has been taken up by the lymph nodes, with a virtually unchanged pattern until 24 hours post-administration (Fig. 12.1).

12.6 Intraoperative Detection of Sentinel Lymph Nodes

Intraoperative SLN detection is guided by a hand-held gamma-detecting probe. During the operation (open thoracotomy or thoracoscopy), the radioactivity in the lymph nodes is counted before (in vivo) and after (ex vivo) dissection.

For in-vivo counting, SLNs are usually identified as any lymph node with a count rate 3- to 10-fold higher than a preset intrathoracic background value. For ex-vivo counting, the SLNs are usually defined in a similar fashion, as any lymph node with a count rate 3–10-fold that of the resected lung tissue with the lowest count. The ex-vivo "hot" lymph node(s) are considered to be the true SLNs because, in this condition, the radioactivity measurements are not influenced by the "shine-through" effect of radioactivity retained at the site of injection [29, 31].

In the case of mediastinal dissection, after lobectomy and SLN excision, the mediastinal stations are also explored with the gamma probe before performing a complete lymph node dissection. Upon completion of the procedure, exploration with the gamma probe is repeated, checking for any residual activity. If indicated by high count rates, resection of the nodal stations is completed.

12.7 Accuracy and Perspectives of Radioguided Sentinel Lymph Node Biopsy

In all series reporting more than 200 patients undergoing radioguided SLNB for NSCLC [29, 31, 34, 40], a SLN was identified in 70% to 100% of the patients, with false-negative rates generally reported as 10% or lower. However, a recently completed multicenter phase 2 trial investigating the use ^{99m}Tc–tin colloid for SLN biopsy reported an identification rate as low as 51% [41].

A promising, relatively simple and reliable method for SLN mapping in NSCLC is the new intraoperative instrumentation that uses the invisible near-infrared (NIR) fluorescent light of ICG for imaging in vivo the lymphatic drainage and the SLNs (Fig. 12.2). This technique has been validated in human trials carried out in breast and gastric cancer, and preliminary data in NSCLC patients suggest that intraoperative NIR SLN mapping is feasible, with a satisfactory detection rate and a very low false-negative rate [23].

Concerning the detection of micrometastatic involvement of mediastinal lymph nodes by RT-PCR or IHC, similar results have been obtained by biopsy of the SLN with different techniques versus analysis of all metastasis-positive lymph nodes [15–17]. These reports also suggest that micrometastasis is limited to SLNs in early NSCLC, but tends to spread

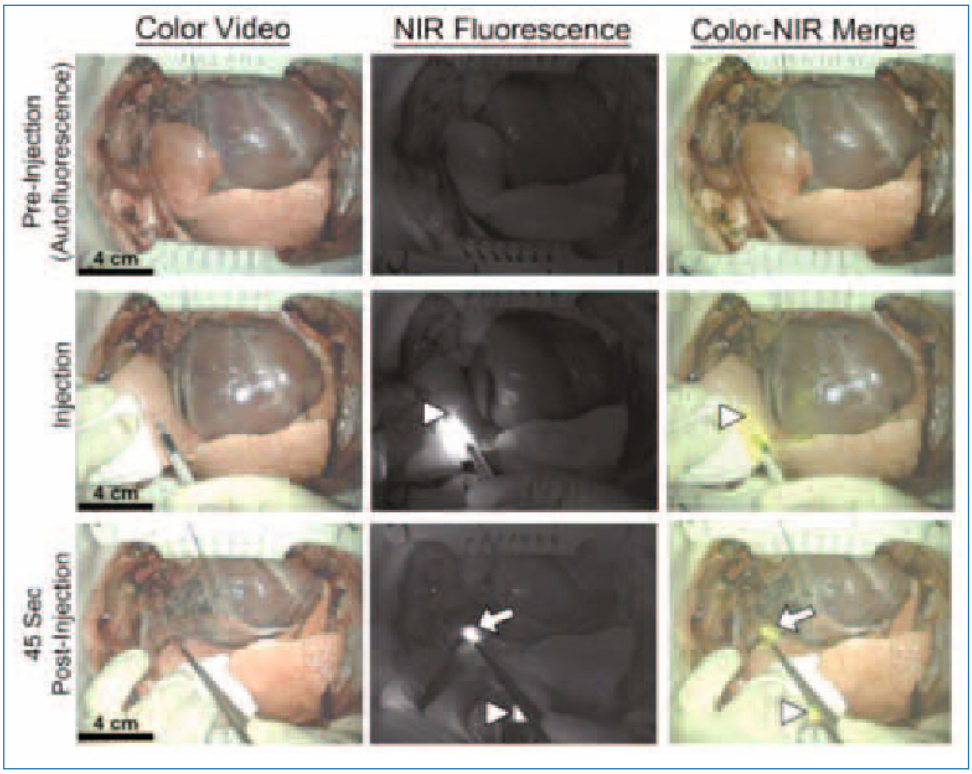

Fig. 12.2 SLN mapping of the lung with near-infrared (NIR) quantum dots (QD) in an animal model (adult Yorkshire pigs). Color video (left), NIR fluorescence (middle), and color–NIR merge (right) are presented. The SLN (*arrow*) was identified 45 seconds after QD injection into the right upper lobe of the lung (*arrowhead*) (reproduced with permission from [42])

to lymph nodes other than the SLNs, with the progression of metastasis.

In conclusion, SLN biopsy is an effective tool that may allow reduction of the number of lymph nodes to be examined for micrometastasis, and selection of patients with micrometastatic mediastinal lymph node involvment who could benefit from postoperative adjunctive therapy. Since most of the studies published so far have adopted direct intratumoral or peritumoral injection of the radiocolloid in the operating theatre at the time of thoracotomy, this procedure basically precludes the possibility of imaging with large-field-of-view gamma cameras. New perspectives in this regard can perhaps be opened up by the use of dedicated small-field-of-view cameras to be used also in the intraoperative setting.

References

1. Siegel R, Naishadham D, Jemal A (2012) Cancer statistics, 2012. CA Cancer J Clin 62:10–29
2. Keller SM, Adak S, Wagner H, Johnson DH (2000) Mediastinal lymph node dissection improves survival in patients with stages II and IIIa non-small cell lung cancer. Eastern Cooperative Oncology Group. Ann Thorac Surg 70:358–365
3. Naruke T, Goya T, Tsuchiya R, Suemasu K (1988) The importance of surgery to non-small cell carcinoma of lung with mediastinal lymph node metastasis. Ann Thorac Surg 46:603–610
4. Shen J, Wallace AM, Bouvet M (2002) The role of sentinel lymph node biopsy for melanoma. Semin Oncol 29:341–352
5. Petrek JA, Senie RT, Peters M, Rosen PP (2001) Lymphedema in a cohort of breast carcinoma survivors 20 years after diagnosis. Cancer 92:1368–1377
6. Nomori H, Horio H, Naruke T et al (2002) Use of technetium-99m tin colloid for sentinel lymph node identification in non-small cell lung cancer. J Thorac Cardiovasc Surg 124:486–492
7. Liptay MJ, Grondin SC, Fry WA et al (2002) Intraoperative sentinel lymph node mapping in non-small-cell lung cancer improves detection of micrometastases. J Clin Oncol 20:1984–1988
8. Mountain CF, Dresler CM (1997) Regional lymph node classification for lung cancer staging. Chest 111:1718–1723
9. Kubuschock B, Passlick B, Izbicki JR et al (1999) Disseminated tumor cells in lymph nodes as a determinant for survival in surgically resected non-small cell lung cancer. J Clin Oncol 17:19–24
10. Riquet M, Manac'h D, Pimpec-Barthes F et al (1999) Prognostic significance of surgical-pathologic N1 disease in non-small cell carcinoma of the lung. Ann Thorac Surg 67:1572–1576
11. Passlick B, Kubuschock B, Sienel W et al (2002) Mediastinal lymphadenectomy in non-small cell lung cancer: effectiveness in patients with or without nodal micrometastases – results of a preliminary study. Eur J Cardiothorac Surg 21:520–526
12. Naruke T, Tsuchiya R, Kondo H et al (1999) Lymph node sampling in lung cancer: how should it be done? Euro Eur J Cardiothorac Surg 16:17–24
13. Izbicki JR, Thetter O, Habekost M et al (1994) Radical systematic mediastinal lymphadenectomy in non-small cell lung cancer: a randomized controlled trial. Br J Surg 81:229–235
14. Allen MS, Darling G, Pechet T et al (2006) Morbidity and mortality of major pulmonary resection in patients with early stage lung cancer initial results of the randomized, prospective ACOSOG Z0030 Trial. Ann Thorac Surg 81:1013–1019
15. Li SH, Wang Z, Liu XY, Liu FY (2008) Gene diagnosis and prognostic significance of lymph node micrometastasis after complete resection of histologically node-negative non-small cell lung cancer. World J Surg 32:1651–1656

16. Tezel C, Ersev AA, Kiral H et al (2006) The impact of immunohistochemical detection of positive lymph nodes in early stage lung cancer. Thorac Cardiovasc Surg 54:124–128
17. Nosotti M, Falleni M, Palleschi A et al (2005) Quantitative real-time polymerase chain reaction detection of lymph node lung cancer micrometastasis using carcinoembryonic antigen marker. Chest 128:1539–1544
18. Little AG, DeHoyos A, Kirgan DM et al (1999) Intraoperative lymphatic mapping for non-small cell lung cancer: the sentinel node technique. J Thorac Cardiovasc Surg 117:220–234
19. Sugi K, Fukuda M, Nakamura H, Kaneda Y (2003) Comparison of three tracers for detecting sentinel lymph nodes in patients with clinical N0 lung cancer. Lung Cancer 39:37–40
20. Nakagawa T, Minamiya Y, Katayose Y et al (2003) A novel method for sentinel lymph node mapping using magnetite in patients with non-small cell lung cancer. J Thorac Cardiovasc Surg 126:563–567
21. Sugi K, Kobayashi S, Yagi R, Matsuoka T (2008) Sentinel node mapping and micrometastasis in patients with clinical stage IA non-small cell lung cancer. Interact Cardiovasc Thorac Surg 7:913–915
22. Minamiya Y, Ito M, Hosono Y et al (2007) Subpleural injection of tracer improves detection of mediastinal sentinel lymph nodes in non-small cell lung cancer. Eur J Cardiothorac Surg 32:770–775
23. Khullar O, Frangioni JV, Colson Y (2009) Image-guided sentinel lymph node mapping and nanotechnology-based nodal treatment in lung cancer using invisible near-infrared fluorescent light. Semin Thorac Cardiovasc Surg 21:309–315
24. Schmidt FE, Woltering EA, Webb WR et al (2002) Sentinel nodal assessment in patients with carcinoma of the lung. Ann Thorac Surg 74:870–874
25. Melfi FM, Chella A, Menconi GF et al (2003) Intraoperative radioguided sentinel lymph node biopsy in non-small cell lung cancer. Eur J Cardiothorac Surg 23:214–220
26. Lardinois D, Brack T, Gaspert A et al (2003) Bronchoscopic radioisotope injection for sentinel lymph-node mapping in potentially resectable non-small-cell lung cancer. Eur J Cardiothorac Surg 23:824–827
27. Sugi K, Kaneda Y, Sudoh M et al (2003) Effect of radioisotope sentinel node mapping in patients with cT1 N0 M0 lung cancer. J Thorac Cardiovasc Surg 126:568–573
28. Sugi K, Kitada K, Murakami T et al (2004) Sentinel node biopsy for staging of small peripheral lung cancer. Kyobu Geka 57:14–17
29. Liptay MJ (2004) Sentinel node mapping in lung cancer. Ann Surg Oncol 11:271S–274S
30. Ueda K, Suga K, Kaneda Y et al (2004) Radioisotope lymph node mapping in nonsmall cell lung cancer: can it be applicable for sentinel node biopsy? Ann Thorac Surg 77:426–430
31. Nomori H, Watanabe K, Ohtsuka T et al (2004) In vivo identification of sentinel lymph nodes for clinical stage I non- small cell lung cancer for abbreviation of mediastinal lymph node dissection. Lung Cancer 46:49–55
32. Tiffet O, Nicholson AG, Khaddage A et al (2005) Feasibility of the detection of the sentinel lymph node in peripheral non-small cell lung cancer with radioisotopic and blue dye techniques. Chest 127:443–448
33. Atinkaya C, Ozlem Küçük N, Koparal H et al (2005) Mediastinal intraoperative radioisotope sentinel lymph node mapping in non-small-cell lung cancer. Nucl Med Commun 26:717–720
34. Rzyman W, Hagen OM, Dziadziuszko R et al (2006) Intraoperative, radio-guided sentinel lymph node mapping in 110 nonsmall cell lung cancer patients. Ann Thorac Surg 82:237–242
35. Nomori H, Ikeda K, Mori T et al (2007) Sentinel node navigation segmentectomy for clinical stage IA non-small cell lung cancer. J Thorac Cardiovasc Surg 133:780–785
36. Nomori H, Ikeda K, Mori T et al (2007) Sentinel node identification in clinical stage Ia non-small cell lung cancer by a combined single photon emission computed tomography/computed tomography system. J Thorac Cardiovasc Surg 134:182–187
37. Meyer A, Cheng C, Antonescu C et al (2007) Successful migration of three tracers without identification of sentinel nodes during intraoperative lymphatic mapping for non-small cell lung cancer. Interact Cardiovasc Thorac Surg 6:214–218
38. Di Lieto E, Gallo G, Scarpati VD et al (2007) Lymph node sentinel detection in lung resection for non small cell lung cancer: our experience. Recenti Prog Med 98:327–328
39. Melfi FM, Lucchi M, Davini F et al (2008) Intraoperative sentinel lymph node mapping in stage I non-small cell lung cancer: detection of micrometastases by polymerase chain reaction. Eur J Cardiothorac Surg 34:181–186
40. Sugi K, Kobayashi S, Yagi R, Matsuoka T (2008) Usefulness of sentinel lymph node biopsy for the detection of lymph node micrometastasis in early lung cancer. Interact Cardiovasc Thorac Surg 7:913–915
41. Liptay MJ, D'amico TA, Nwogu C et al (2009) Intraoperative sentinel node mapping with technetium-99m in lung cancer: results of CALGB 140203 Multicenter Phase II Trial. J Thorac Oncol 4:198–202
42. Soltesz EG, Kim S, Laurence RG et al (2005) Intraoperative sentinel lymph node mapping of the lung using near-infrared fluorescent quantum dots. Ann Thorac Surg 79:269–277

13 Preoperative and Intraoperative Lymphatic Mapping for Radioguided Sentinel Node Biopsy in Cancers of the Gastrointestinal Tract

Carmen Balagué and José Luis Pallarés

13.1 Introduction

Accurate evaluation of lymph node status is one of the most important factors for predicting the clinical outcome of gastrointestinal tumors. SLN mapping has clearly become highly feasible and accurate in staging gastrointestinal cancers [1]. In this regard, the technical feasibility of radioguided SLN identification while performing a laparotomy in patients with esophageal, gastric, or colorectal cancer has been demonstrated [2]. This method can also identify and characterize cases with aberrant/unexpected lymphatic drainage from the primary lesion.

The progressively increasing application of laparoscopic surgical procedures has significantly influenced gastrointestinal surgery. Preliminary results indicate that SLN detection is a valid technique to identify micrometastasis in lymph nodes, also during laparoscopic surgery, and can thus become an important component of minimally invasive treatment of early gastrointestinal tumors. Furthermore, the combination of radiotracer and vital-blue staining optimizes SLN identification. Single photon emission computed tomography/computed tomography (SPECT/CT), as well as intraoperative imaging with dedicated gamma cameras, allows better SLN detection than conventional planar imaging with conventional gamma cameras.

C. Balagué (✉)
General and Digestive Surgery
Hospital de la Santa Creu I Sant Pau
Barcelona, Spain
e-mail: cbalague@santpau.cat

13.2 Sentinel Lymph Node Mapping in Esophagogastric Cancer

The term "orderly progression" is hardly applicable to describing the pattern of lymphatic spread of esophageal and gastric cancer. Sano et al. [3] reported that the perigastric nodal area, close to the primary tumor, is the first lymphatic station in only 62% of patients with gastric cancer, based on a retrospective analysis of patients with solitary metastasis. Based on these clinical observations, the standard procedure is radical resection with D2 lymphadenectomy in patients with gastric cancer, and three-field lymph node dissection in esophageal cancer, even in patients with negative lymph nodes [4, 5]. However, implementation of these surgical procedures implies a significant increase in morbidity and mortality [6, 7].

SLN detection can play an important role for individual patients' tailored treatment, and can therefore lead to modification of the surgical procedure and/or other treatments [8]. Several studies support the validity of the SLN concept in esophageal and gastric cancer [9–13]. Among visceral tumors, gastric cancer is currently one of the suitable targets for SLN navigation surgery. Despite the multidirectional and complicated lymphatic flow from the gastric mucosa, the anatomical situation of the stomach is relatively suitable for SLN mapping in comparison with organs embedded in closed spaces, such as would be the case for rectal cancers [14].

13.2.1 Sentinel Lymph Node Mapping in Gastric Cancer

SLN mapping in gastric cancer must be considered for the early stages of this tumor, since no benefit for the patient would derive from this procedure in advanced gastric cancer. Rabin et al. [15] compared SLN mapping in patients with different T (tumor) stages. They concluded that SLN

G. Mariani et al. (eds.), *Atlas of Lymphoscintigraphy and Sentinel Node Mapping*,
DOI 10.1007/978-88-470-2766-4_13

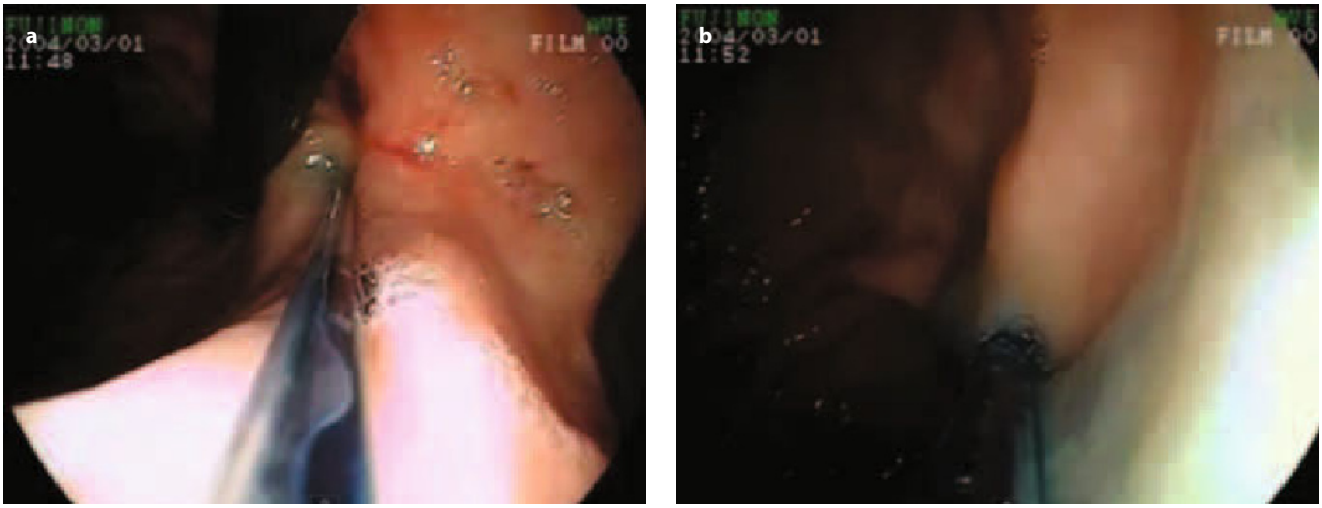

Fig. 13.1 Intraoperative endoscopic staining. **a**, **b** Intraoperative submucosal blue dye injection during endoscopy (images from Hideki Hayashi in SAGES videos, www.sages.org/video/details.php?id=101101, with permission)

mapping in T1 and T2 tumors may be of assistance in the decision-making process regarding the extent of lymphadenectomy (100% sensitivity, 90–100% negative-predictive value), while it will be misleading in one-third of patients with T3 tumors, and should therefore not be adopted [15].

There are currently two methods for SLN mapping:

- method based on radionuclide imaging
- method based on vital dye staining.

Several types of radiocolloids can be used for lymphoscintigraphy. Technetium-99m (^{99m}Tc)–tin colloid and ^{99m}Tc–phytate are the most commonly used in Japan. In initial pilot studies, Kitagawa et al. [2] used the ^{99m}Tc–tin colloid; the particles of this colloid are relatively large and migrate to lymph nodes within the first 2 hours post-administration, remaining there for more than 20 hours through phagocytosis by macrophages. This feature allows lymphoscintigraphic imaging with radiolabeled particles of this size to be less dependent on detection time. The particles of ^{99m}Tc–phytate are smaller in size, and can migrate to secondary lymph nodes beyond the SLN. At present, we recommend the use of ^{99m}Tc–tin colloid as an optimal radiopharmaceutical for SLN mapping in gastric cancer.

The most frequently used agent in the staining method is blue dye (patent blue).

13.2.1.1 Preoperative Mapping with Radiocolloid

A total of 148 MBq (in 2 mL) ^{99m}Tc–tin colloid suspension is endoscopically injected into the gastric submucosa at four sites (0.5 mL each) around the primary tumor, using a disposable 23-gauge needle [16]. Inoculation is performed the day before the operation (or at least 3 hours before surgery). Lymphoscintigraphic imaging is recommended and can be performed 2 hours after endoscopic inoculation [16].

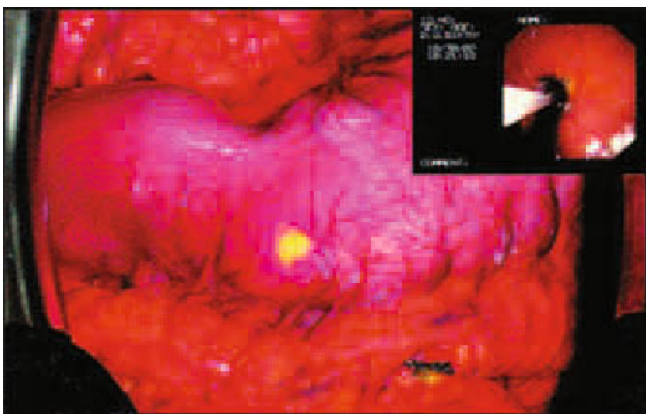

Fig. 13.2 Endoscopic submucosal injection during laparoscopic approach in gastric cancer (from [18], with permission)

13.2.1.2 Intraoperative Sentinel Lymph Node Mapping by a Combination of Radiocolloid and Staining

Intraoperative SLN detection is performed using a hand-held gamma probe. It is crucial that the probe is not oriented towards the primary tumor (the site of radiocolloid injection).

Evaluation of lymphatic drainage with the blue staining is useful to support/complement the radiocolloid-based procedure. The staining method involves endoscopic injection of 2 mL of 2% patent blue into the submucosal layer, at four points around the site of the primary tumor [13] (Fig. 13.1).

The submucosal and subserosal injection approaches are proven to be equivalent in their detection rates [17]. However, it is difficult to identify a T1 lesion in the case of the subserosal route of administration. Intraoperative subserosal inoculation is also difficult during laparoscopy, so submucosal injection is preferable in the laparoscopic approach (Fig. 13.2). It is important that mobilization of the stomach

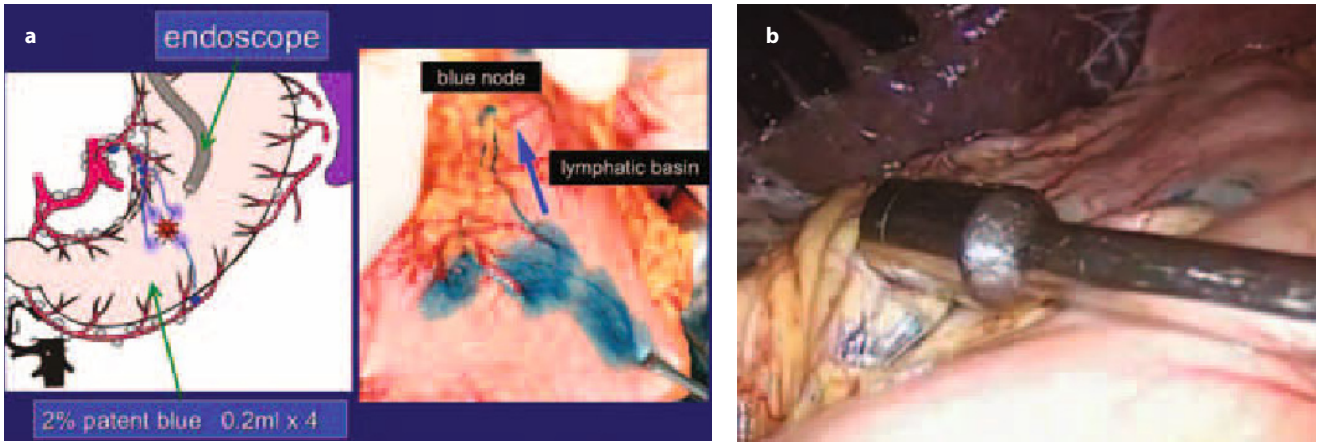

Fig. 13.3 Sentinel lymph node detection system. **a** Blue-stained lymph nodes within 5–10 minutes after the dye injection (from Gastroenterologic Surgery, Kanazawa University). **b** Gamma-probe counting of the SLN containing 10 times more radioactivity than the surrounding tissue (image from Hideki Hayashi in SAGES videos, www.sages.org/video/details.php?id=101101, with permission)

Table 13.1 Methods of sentinel lymph node detection in gastric cancer

First author and year	Tracer	Cases (n)	Detection (%)	Sensitivity (%)
Hiratsuka, 2001 [9]	ICG	74	99	90
Ichikura, 2002 [20]	ICG	62	100	85
Miwa, 2003 [13]	PB	211	96	89
Kim, 2004 [21]	RI	46	94	85
Kitagawa, 2004 [22]	RI	270	97	92
Uenosono, 2006 [23]	RI	180	95	–
Arigami, 2006 [16]	RI	61	100	–

ICG, indocyanine green; *PB*, patent blue; *RI*, radioisotope.

before the injection is carried out without destroying the lymphatic drainage.

SLNs are defined as nodes that are stained blue within 5–10 minutes after injection of the dye and/or those containing 10 times more radioactivity than the surrounding tissue (background) during intraoperative counting with a gamma probe [19] (Fig. 13.3). Once SLNs are detected, tissue excision is performed. Normally, all resected nodes are examined postoperatively by routine hematoxylin and eosin (H&E) staining, and those negative at H&E staining are examined further by immunohistochemistry using anti-cytokeratin antibody [19].

Based on single-institution results, SLN mapping for early gastric cancer is increasingly being considered acceptable (Table 13.1). Satisfactory SLN detection rates, as well as sensitivity in detecting micrometastasis based on SLN status, have been reported using the dye-guided method, as well as the radioguided method.

Use of the two mapping approaches combined (radiocolloid and blue dye) reduces the technical errors that can occur with the use of a single SLN mapping technique.

The radioguided method enables confirmation of the complete identification and removal of SLNs with multipath distribution, while the dye-based system allows direct, real-time visualization of the SLNs.

A multicenter prospective trial of SLN mapping in gastric cancer, based on the dual tracer approach, with blue dye and radiocolloid, has recently been completed by The Japan Society of Sentinel Lymph Node Navigation Surgery study group [19]. They reported a 7% false-negative rate, while the sensitivity of metastasis detection based on SLN status was 93% [25]. Based on these results, we recommend a combination of both techniques to carry out a proper and systematic mapping of SLNs in gastric cancer.

The results of clinical trials should provide useful perspectives on the future direction of SLN navigation surgery for gastric cancer [24]. In particular, cT1N0 gastric cancer seems to constitute a condition in which the results of SLN mapping might modify the therapeutic approach. From the data reported in the literature, micrometastases tend to be limited within the sentinel basins in cT1N0 gastric cancer. Sentinel basins are, therefore, good targets for selective lymphadenectomy in patients with cT1N0 gastric cancer with the potential risk of micrometastasis. Furthermore, laparoscopic local resection is, in principle, feasible for curative treatment of sentinel-lymph-node-negative early gastric can-

cer. For laparoscopic SLN mapping of gastric cancer, a radioguided method is essential in patients with gastric cancer, since it has great potential to provide a new paradigm shift for surgical management of early gastric cancer [14].

13.2.2 Sentinel Lymph Node Mapping in Esophageal Cancer

For a number of reasons, SLN mapping is more complex in the case of esophageal cancer. First, use of the blue dye is not possible in this tumor localization, because lymph nodes in the region of the thoracic esophagus are frequently pigmented by anthracosis, which complicates the identification of blue-stained lymph nodes. Moreover, in localizations such as the esophagus and rectum, prior mobilization of the primary lesion must be performed in order to achieve a proper real-time visualization of the lymphatic drainage routes by blue staining. However, such mobilization involves destruction or disruption of the lymphatic drainage patterns.

Therefore, the optimal method for use is based on radiocolloid lymphoscintigraphy [12, 26]. In western countries, the number of early-stage newly diagnosed esophageal cancers is very limited, so that it is difficult to conduct clinical studies to investigate SLN mapping in these patients. In esophageal cancer, there are several SLNs, widely distributed from the cervical to the abdominal area. In over 80% of cases, at least one SLN is located on the second or third compartment of regional lymph nodes [24]. This anatomic distribution of the SLNs is attributed to the multidirectional lymphatic drainage from the primary tumor.

The goal of SLN mapping in esophageal cancer is to reduce the need for extensive lymphadenectomy. Kitagawa proposed a new strategy using SLN biopsy for esophageal cancer patients with clinically early-stage disease [2]. Uenosono et al. [27] performed SLN mapping in 134 patients with newly diagnosed esophageal cancer. They concluded that SLN mapping can be applied to patients with cT1 and cN0 esophageal cancer and that the SLN concept might allow less-invasive surgery to be performed and the number of unnecessary lymphadenectomies to be reduced. Nevertheless, multicenter validation studies on SLN mapping in esophageal cancer are still lacking.

13.2.2.1 Harvesting the Sentinel Lymph Node

As indicated above, the technique of choice to be used is based on radiocolloid mapping. ^{99m}Tc–tin colloid is endoscopically injected into the esophageal wall around the tumor on the day before surgery [27].

Following lymphoscintigraphy, SLNs located in the cervical area can be percutaneously identified with external gamma-probe counting, and resection can be performed using less-invasive procedures. Moreover, the detection and harvesting of intra-abdominal SLNs can be carried out laparoscopically following the same procedure as in gastric cancer. However, removing the mediastinal SLNs is relatively complicated and invasive, because it requires mobilization of the thoracic esophagus. Moreover, the presence of the primary lesion (with the high activity retained at the peritumoral injection site) is an obstacle for localizing the SLNs by gamma-probe counting at this level.

Preoperative lymphoscintigraphy (usually performed 3 hours after endoscopic inoculation of the radiocolloid) is very useful for SLN detection in unexpected sites that are distant from the primary esophageal lesion.

13.3 Sentinel Lymph Node Mapping in Colon Cancer

Standard treatment of colon cancer patients is based on surgical resection with or without adjuvant treatment. Tumor staging at diagnosis is the most important prognostic factor for predicting survival. The survival rate increases with the number of tested lymph nodes that are negative for metastasis and, at present, no adjuvant treatment is recommended in patients without metastatic lymph nodes (in the absence of unfavorable characteristics of the primary tumor). Thus, lymph node involvement heavily influences patients' prognosis and the decision to perform adjuvant chemotherapy [28, 29].

However, 10–25% of the patients with localized colon cancer (American Joint Committee on Cancer [AJCC] stage I and II) will develop disease progression and distant metastases within 5 years after completion of surgery with curative intent. Therefore, some inaccuracy must be considered regarding the staging methods, possibly leading to understaging. Such understaging is considered to be around 10–20% [30], underlining the need to search for methods that can help to achieve a correct staging of the patient [31]. For histological examination of lymph nodes, these methods include serial sectioning [32], immunohistochemistry (IHC) for cytokeratin [33], and, more recently, analysis by reverse transcription polymerase chain reaction (RT-PCR) techniques. However, their implementation may be impractical for routine histology study due to the large number of lymph nodes retrieved in the surgical specimen.

In this regard, SLN mapping may allow identification of a smaller number of lymph nodes representing the tumor status of the entire nodal basin [34]. An exhaustive analysis of SLNs in order to achieve a more accurate staging of patients can influence the decision for adjuvant treatment.

Saha emphasized that SLN mapping for colorectal cancer is highly successful and accurate for predicting the presence or absence of nodal disease, with a relatively low incidence of skip metastases [30] . Such a technique provides

the "right nodes" to the pathologists for detailed analysis for appropriate staging and treatment with adjuvant chemotherapy [1].

13.3.1 Methods for Sentinel Lymph Node Mapping in Colorectal Cancer

The marker that is most frequently used for visual SLN mapping is isosulfan blue 1%, injected in a volume of 1–2 mL. In this regard, there have been reports of anaphylactic reactions [35–37] and possible interference with pulse oximetry monitoring [38, 39]. Moreover, in some countries isosulfan blue is not readily available or is prohibitively expensive.

In a prospective study, Soni et al. compared 1% lymphazurin (L) versus 1% methylene blue (M) as a dye for SLN mapping in gastrointestinal tumors (the majority were colon cancer) [40]. They concluded that the success rate, nodal positivity, average SLNs per patient, and overall accuracy were similar between L and M. Absence of anaphylaxis and lower cost make M more desirable than L for SLN mapping in gastrointestinal tumors.

Fluorescein 10% is more widely available, much cheaper, and, moreover, is not associated with known allergic reactions. Its application is comparable to that described for isosulfan blue in terms of both administration and the amount administered. Saha et al. [30] used fluorescein SLN mapping in 120 patients, with results that were comparable to those obtained with isosulfan blue. The agent migrates quickly to the SLNs, which therefore become fluorescent and can be identified with a Wood's lamp as bright yellow nodes.

The use of ^{99m}Tc–tin colloid has also been described for SLN mapping in colorectal cancer, with similar results [12].

There are therefore two methods for SLN mapping:

- staining method
- radioguided method.

13.3.1.1 Staining Method

SLN mapping can be performed in vivo and ex vivo:

In-vivo studies

One of the advantages observed in studies in vivo is the detection of aberrant lymph nodes, outside the expected drainage basins, thus allowing excision of the more appropriate lymphatic territories.

The staining method involves intraoperative injection of 2 mL of 1% blue dye into the subserosal layer at four points around the site of the primary tumor [30] (Fig. 13.4). Endoscopic submucosal inoculation is also possible, whenever adequate. The submucosal and subserosal injection routes are equivalent in terms of detection rate. However, in the case of the subserosal approach, it is difficult to identify the T1 lesions. Intraoperative subserosal inoculation is also difficult during laparoscopy, even though that technical approach has been described (Fig. 13.5).

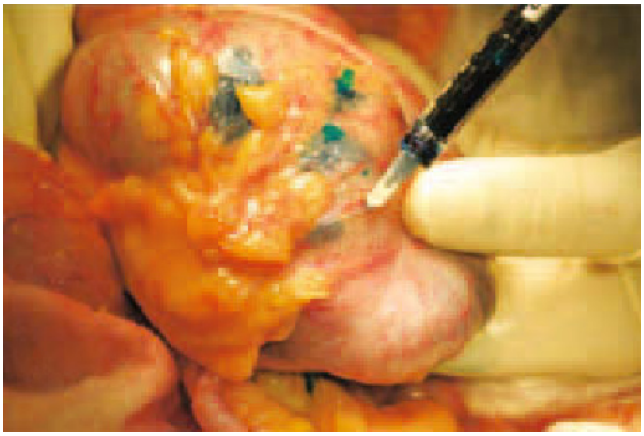

Fig. 13.4 Intraoperative injection of blue dye into the subserosal layer at four points around the site of the primary tumor (from [30], with permission)

Approximately 5–10 minutes after inoculation, the first lymph node begins to stain, and the first four stained nodes are marked for detailed histologic analysis (Fig. 13.6). Adopting this method, Saha reported a 100% detection rate, 89% sensitivity, 100% specificity, and 93.5% negative-predictive value. Using the same technical approach, Waters et al. [42] obtained a 100% detection rate, with 5% upstaging (SLN as the only one with metastasis). The same technical approach is feasible in cases of rectal cancer with intraperitoneal location, above the peritoneal reflection. In patients with medium or low rectal cancer, a total mesorectal excision is necessary. In-vivo submucosal inoculation during proctoscopy is feasible [30], and submucosal ex-vivo inoculation of 1–2 mL blue dye is also possible. Adopting this approach in patients with rectal cancer, Saha [30] achieved a 90.6% detection rate, with 100% negative-predictive value.

Ex-vivo studies

This staining method involves ex-vivo injection of 2 mL of 1% blue dye into the subserosa or submucosal layer at four points around the site of the primary tumor (Fig. 13.7). Previous longitudinal section of the specimen through the antimesenteric border is necessary to perform submucosal injection, which is followed by massage of the inoculated area for 5 minutes. Blue-stained nodes are designated as SLNs and resected (Fig. 13.8). Comparable results have been obtained between the ex-vivo and in-vivo staining methods (Table 13.2). Wong et al. [43] obtained a 92.3% detection rate, with a mean number of three SLNs obtained per patient, while Fitzgerald et al. [44] identified the SLN in 88% of their patients. Similar detection rates (94–100%) have been obtained by other authors using the same ex-vivo method [45, 46].

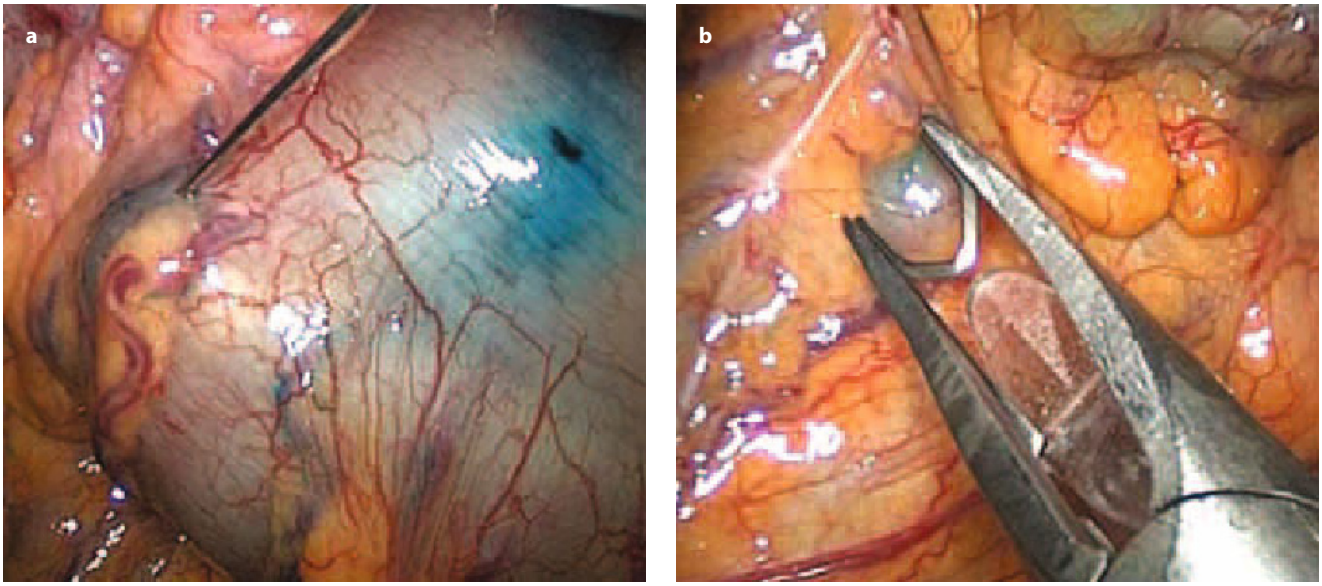

Fig. 13.5 SLN detection in color cancer. **a** Intraoperative injection of blue dye into the subserosa layer during laparoscopy. **b** Blue-stained lymph nodes within 5–10 minutes after dye injection during laparoscopy (from [41], with permission)

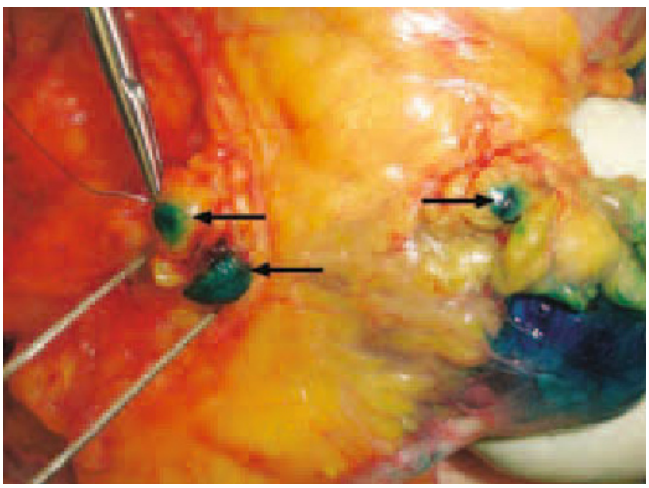

Fig. 13.6 The blue-stained lymph nodes are marked in order to be identified for separate extensive analysis by the pathologist (from [30], with permission)

13.3.1.2 Radioguided Method

In case of SLN mapping by radiocolloid lymphoscintigraphy, the study is performed following the same criteria as in gastric cancer: ^{99m}Tc–tin colloid is endoscopically injected into the colonic submucosa at four sites (0.5 mL each) around the primary tumor, using a disposable 23-gauge needle (Fig. 13.9). Radiocolloid administration is generally performed the day before the operation (or at least 3 hours before surgery). Lymphoscintigraphy is recommended, and can be performed 2 hours after endoscopic inoculation. SPECT/CT is useful for accurate preoperative evaluation, and can be helpful to establish the most adequate surgical strategy (Fig. 13.10).

As the best technique for SLN mapping in patients with colorectal cancer, Bilchik [1] recommended a combination of radiocolloid and blue dye, emphasizing that this technique will become increasingly popular for improving the accuracy of lymph node staging. In particular, this novel procedure offers the potential for significant upstaging of gastrointestinal cancer. It should also be noted that, because of the introduction of fast-track programs, no anterograde colon preparation before surgery is performed for colonic surgery. This precludes the possibility of endoscopic submucosal injection of the radiocolloid.

SLN mapping in colon cancer has also been described with the use of laparoscopic techniques. Wood et al. [49] reported a 100% SLN detection rate, with 100% accuracy in a small series of nine patients submitted to laparoscopy (mean of two SLN identified per patient).

In that case, the marker can be inoculated either ex vivo or in vivo, using either the blue dye or the radioicolloid. The blue dye can be injected in vivo at the submucosal level during endoscopy, or subserosally during laparoscopy, as described by Bianchi et al. [41] (Fig. 13.5), although the surgical approach makes it difficult to label the lesion.

Kitagawa et al. [12] have described correct SLN localization with the use of a laparoscopic gamma probe. Bianchi et al. [41], during minimally invasive surgery, have identified the SLN with good specificity using the blue dye, but still with low sensitivity (78%). According to these authors, these results have limited more widespread diffusion of the method, although it is possible to improve such performance

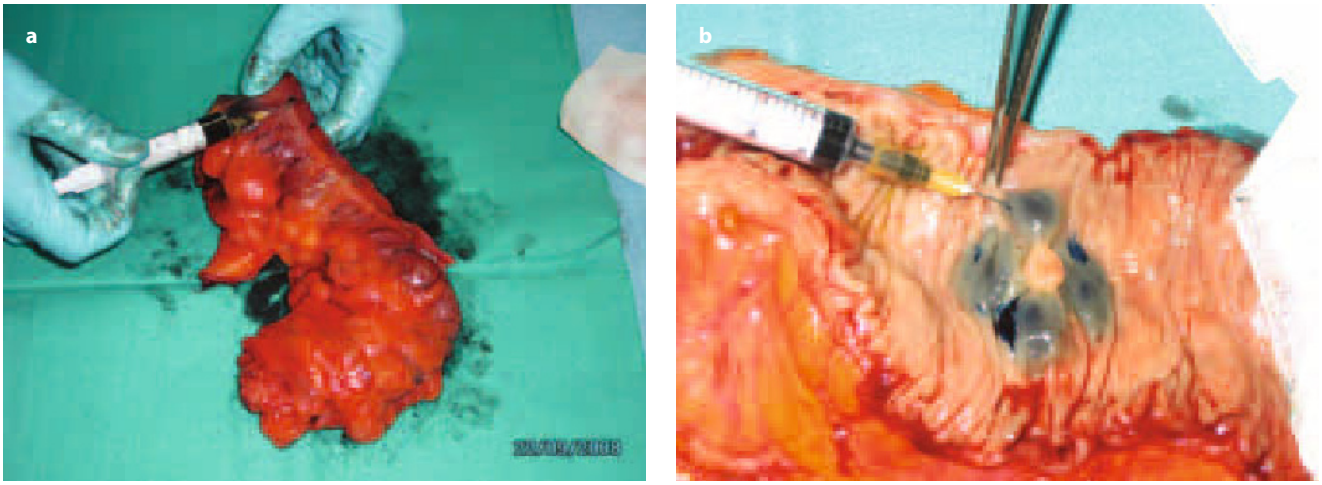

Fig. 13.7 Ex-vivo SLN detection. **a** Ex-vivo injection of 2 mL of 1% blue dye (methylene blue) into the subserosal layer. **b** Ex-vivo injection of 2 mL of 1% blue dye (methylene blue) into the submucosal layer

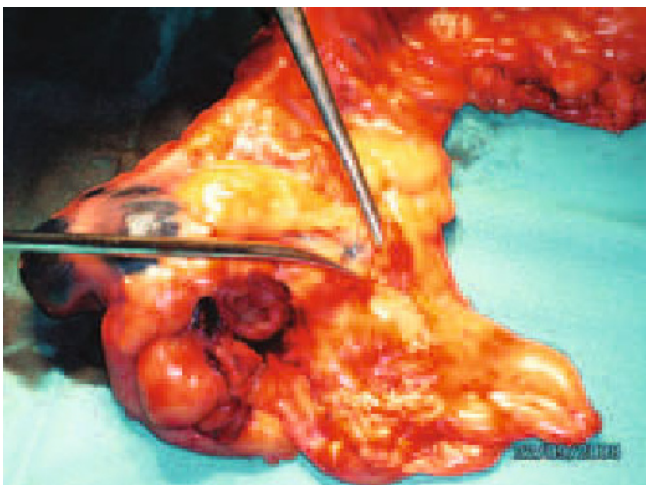

Fig. 13.8 The SLNs, stained blue after ex-vivo subserosal injection, are resected

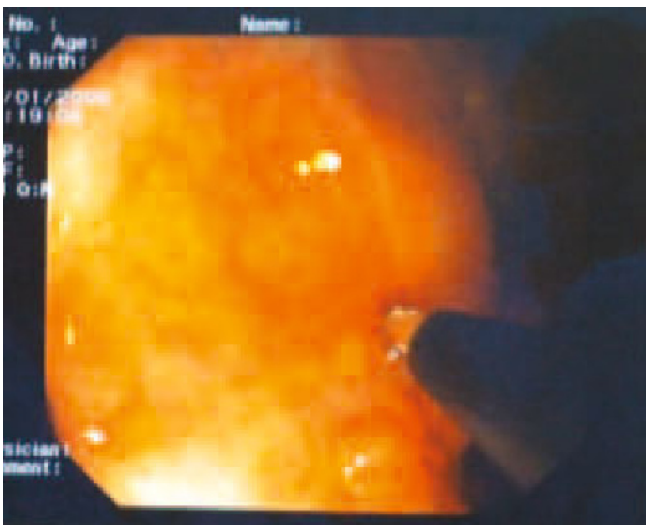

Fig. 13.9 Endoscopic injection of ^{99m}Tc–tin colloid into the colonic submucosa

Table 13.2 Results of ex-vivo and in-vivo staining methods in colon cancer

Author and year	In vivo	Ex vivo	Detection rate (%)	Negative predictive value (%)
Saha, 2005 [30]	X		100	93
Wong, 2001 [43]		X	92	–
Fitzgerald, 2002 [44]		X	88	–
Waters, 2000 [42]	X		100	100
Bianchi, 2011 [41]	X		100	94
Quadros, 2008 [47]	X		91	67
Bembenek, 2005 [48]	X		85	80
Balagué, [2012, in press]		X	91	87

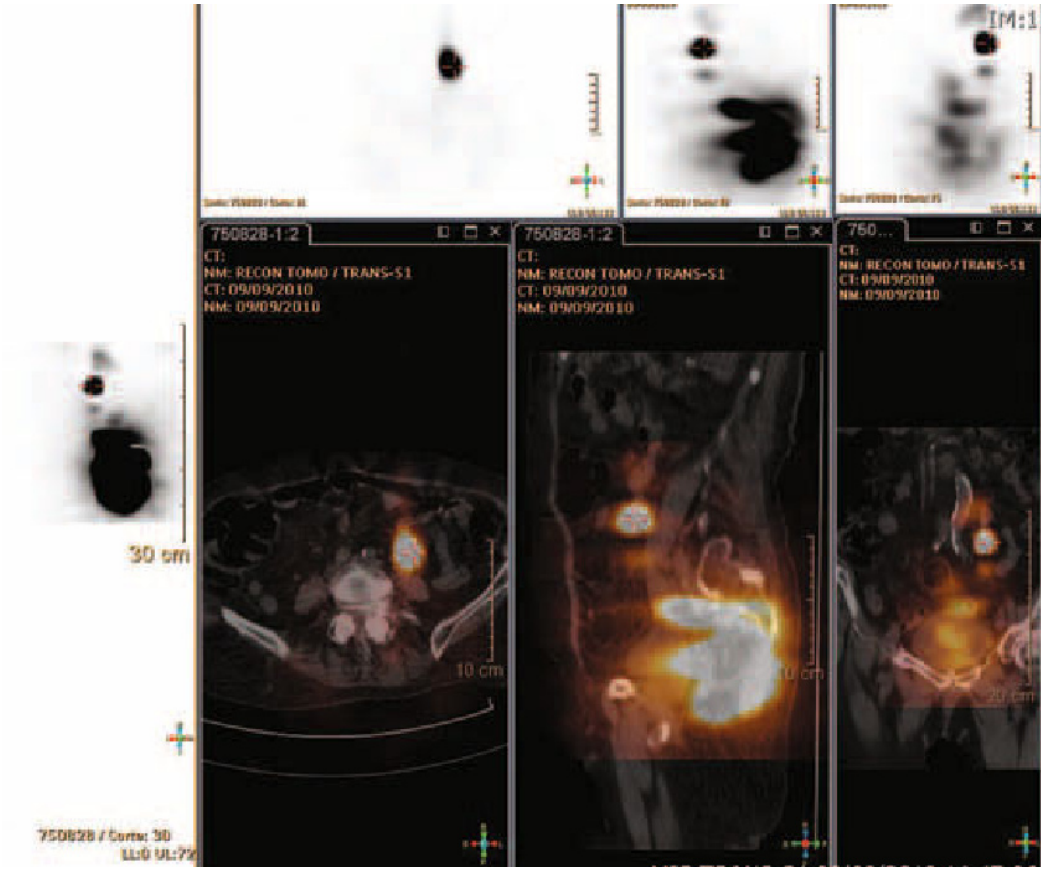

Fig. 13.10 SPECT/CT images acquired after submucosal injection of the radiocolloid can be helpful to optimize the surgical strategy

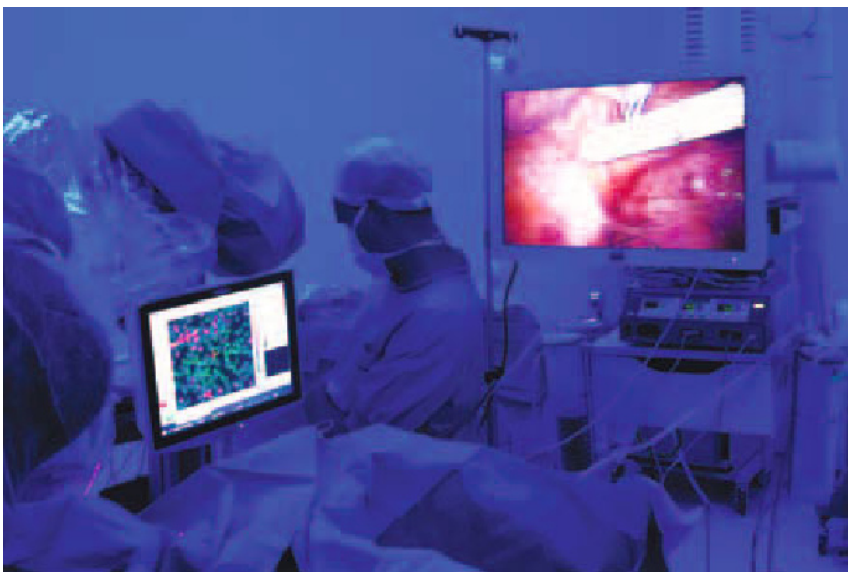

Fig. 13.11 A laparoscopic gamma probe assisted by portable gamma camera is used to identify possible drainage to the iliac lymphatic basin in rectal cancer

using an intraoperative gamma camera. The preliminary results of intraoperative lymphoscintigraphy obtained in a well-selected small group of patients are promising, with high sensitivity and specificity, although further prospective studies are necessary.

The intraoperative use of a portable gamma camera for SLN mapping in colorectal cancer is still under investigation. In our center, we use it in patients diagnosed with rectal cancer who are candidates for surgery without neoadjuvant radiotherapy, in order to evaluate the territory of the iliac vessels. In rectal cancer, anterograde colon preparation before surgery is still the established surgical approach. The day be-

fore surgery, ^{99m}Tc–tin colloid is endoscopically injected into the rectal submucosa, as already described for colon cancer (Fig. 13.9). Two hours later, SPECT/CT is performed (Fig. 13.10). Tumor resection is performed laparoscopically; once the tumor is resected with total mesorectal excision, possible drainage to iliac lymph nodes is identified by the combined use of a laparoscopic gamma probe and a portable gamma camera (Fig. 13.11).

Clinical Cases

Case 13.1
Sentinel Node Mapping in Rectal Cancer: Drainage to Hemorrhoidal Nodes After Submucosal Peritumoral Injection (Planar Imaging)

Giuseppe Rubini and Filippo Antonica

Background Clinical Case

An 87-year-old woman presented with a 5 cm ulcerated rectal cancer, 3 cm from the anal margin. Three months earlier routine blood chemistry had revealed anemia (Hb 10.4 g/dL). Colonoscopy showed ulcerated rectal and perirectal lesions with multiple polypoid formations. CT confirmed rectal and perirectal lesions with maximum size of 5 cm. The patient was referred for radioguided sentinel lymph node biopsy.

Lymphoscintigraphy

The day before surgery, lymphoscintigraphy was performed following submucosal injection of 0.6 mL of 18 MBq ^{99m}Tc-albumin nanocolloid (divided into four aliquots) around the tumor under endoscopic guidance. A dual-detector SPECT gamma camera (Millennium MG, GE Healthcare, Milwaukee, WI) equipped with low-energy high-resolution (LEHR) collimators was used to obtain abdominal-pelvic dynamic images (1 frame 60 s/30 frames) immediately after radiopharmaceutical injection, and planar static images at 30 min after radiopharmaceutical injection. Dynamic images were acquired in anterior and posterior projection with a 256×256 matrix and zoom factor 1.00, while static images were acquired in anterior and posterior projection with a 128×128 matrix and zoom factor 1.00.

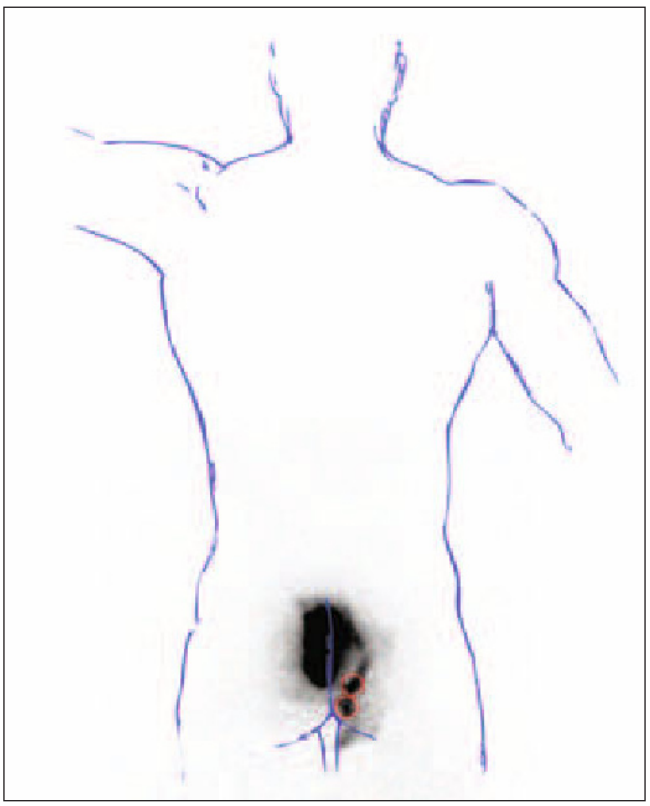

Fig. 1 Schematic representation of a posterior static planar image of the abdominal-pelvic region 30 min after peritumoral radiopharmaceutical injections showing two sentinel lymph nodes of the inferior hemorroidal chain (*red circles*)

Case 13.2
Sentinel Node Mapping in Cancer of Ascending Colon: Drainage to Lumbo-Aortic Nodes After Submucosal Peritumoral Injection (SPECT/CT Imaging)

Courtesy from Joan Duch

Background Clinical Case

A woman (age lost in follow up) with ascending colon cancer underwent lymphoscintigraphy for radioguided sentinel node.

Lymphoscintigraphy

The afternoon before surgery, lymphoscintigraphy was performed following submucosal injections of 0.5 mL of 74 MBq ^{99m}Tc-albumin nanocolloid (divided into two aliquots) around the tumor under endoscopic guidance. A dual-detector SPECT gamma camera (Millennium MG, GE Healthcare, Milwaukee, WI) equipped with low-energy high-resolution (LEHR) collimators was used to obtain early abdominal dynamic images and subsequent planar acquisitions in anterior and posterior projection at 30 min and 60 min after radiopharmaceutical injection. Dynamic images (1 frame 60 s/30 frames) were acquired in anterior and posterior projection with a 256×256 matrix and zoom factor 1.00, while static images were acquired in anterior and posterior projection with a 128×128 matrix and zoom factor 1.00.

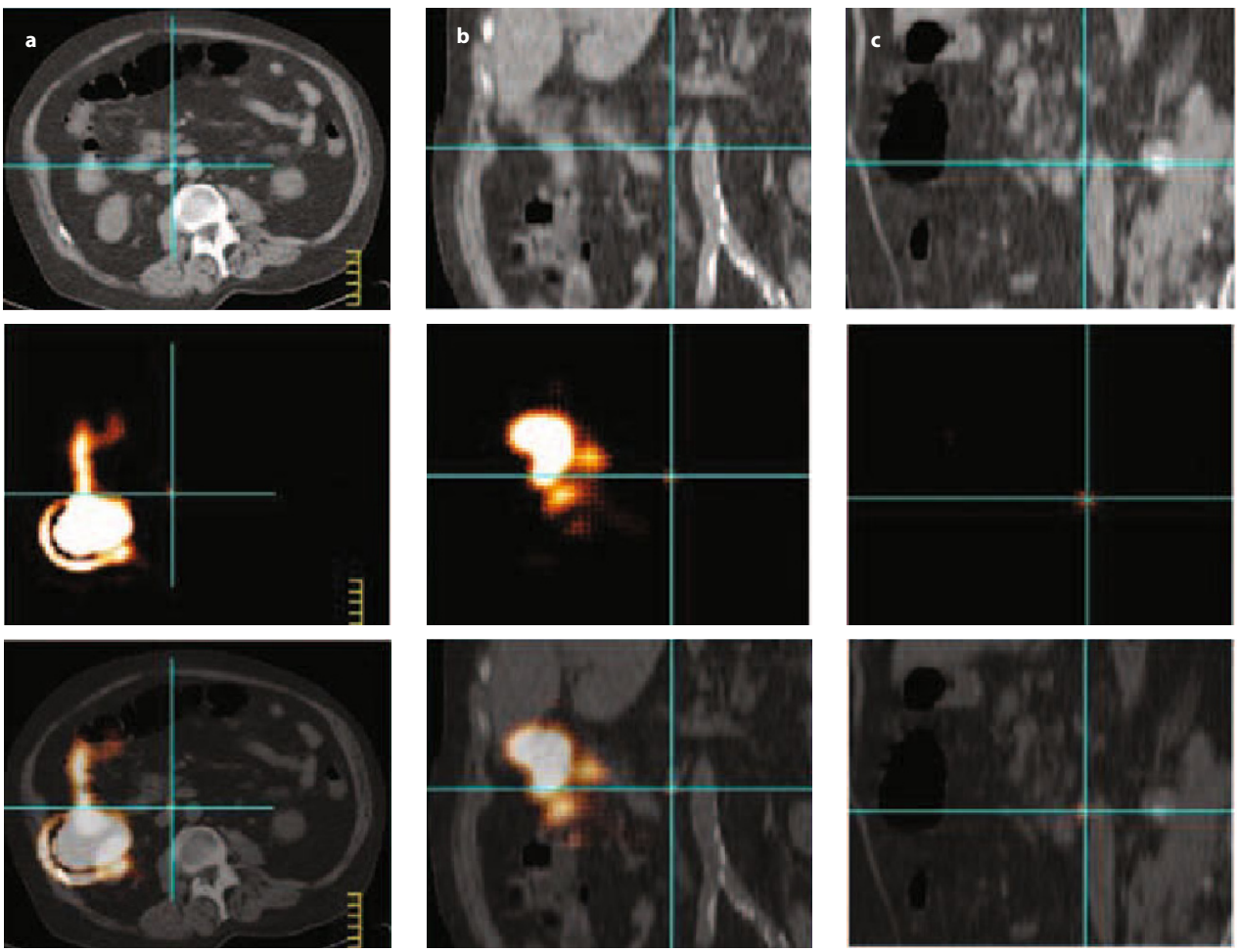

Fig. 1 Transverse (**a**), coronal (**b**), and sagittal (**c**) CT, SPECT, and fused SPECT/CT images show drainage to the interaortocaval region

Case 13.3
Sentinel Node Mapping in Rectal Cancer: Drainage to Lumbo-Aortic Nodes After Submucosal Peritumoral Injection (Planar, SPECT/CT and Intraoperative Imaging)

Carmen Balagué and José Luis Pallarés

Background Clinical Case

An 85-year-old woman with rectal bleeding underwent colonoscopy, which revealed a rectal lesion 8 cm from the anal verge. Histopathology: adenocarcinoma. Local evaluation with MR: T2N0. Further evaluation with CT scan for distant metastasis: M0. Neoadjuvant chemio-radiotherapy was not accepted by the patient. Before surgery (low anterior rectal resection) the patient was submitted to sentinel lymph node biopsy.

Anatomical location of primary malignancy: large bowel, rectum, 8 cm from anal verge.

Technical Background Acquisition

Sentinel Lymph node detected by in vivo study, using radiocolloid.
Staining method:
Endoscopic inoculation of 37 MBq of ^{99m}Tc-Albumin Nanocolloid at each of the quadrants around the site of the primary tumor the day before surgery. This was done in three quadrants given the difficulty to perform endoscopic inoculation behind the lesion. Two hours later, a planar lymphoscintigraphy was acquired using a Philips Brightview SPECT/CT, during 600 seconds and with an acquisition matrix of 256×256. SPECT/CT was also acquired in a Philips Brightview SPECT/CT, with an acquisition matrix of 64×64, with 64 projections (10 seconds/projection). CT was done with a Kv of 120 and a mA of 20. SPECT/CT lymphoscintigraphy demonstrated physiological uptake in left aortoiliac region, due to colonic uptake, and showed also a high mesorectal uptake, with no identification of sentinel lymph nodes. Low anterior resection (LAR) was performed. The pelvic study was completed by gamma probe assisted by portable gamma camera imaging (Sentinella), and no activity of nodal iliac territory was detected.
Histopathological results: pT2N0M0. Total lymph nodes detected: 22 (negative).

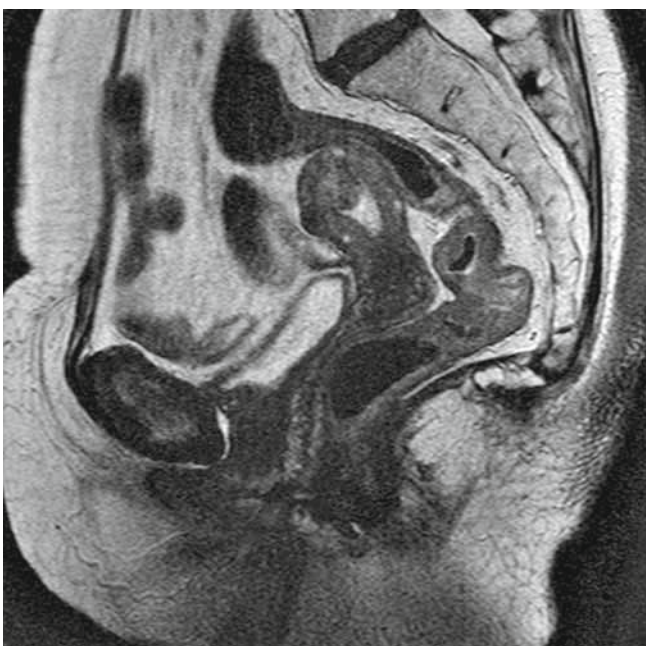

Fig. 1 MR for local evaluation of tumor. Rectal cancer 8 cm from anal verge

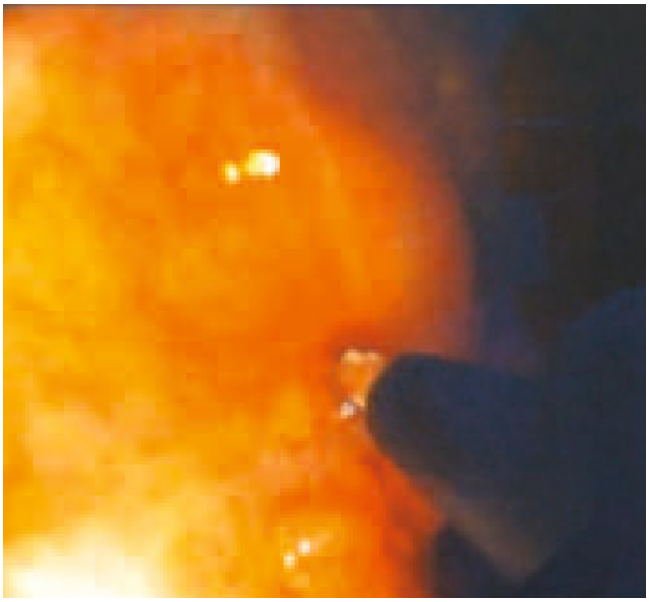

Fig. 2 Endoscopic submucosal inoculation of radiocolloid

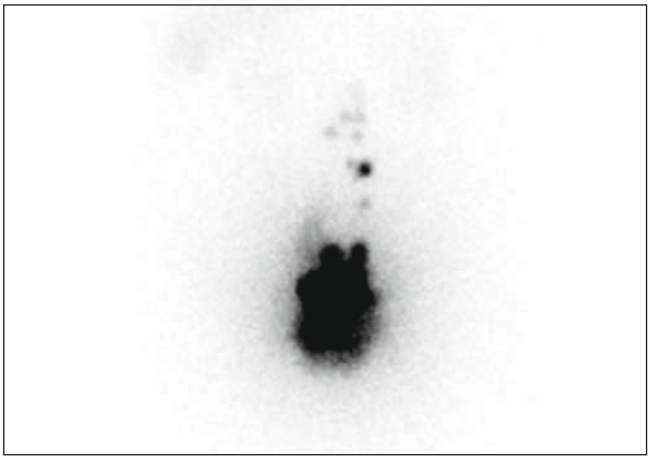

Fig. 3 Planar lymphoscintigraphy showed high uptake in the mesorectal region and in the left aortoiliac region

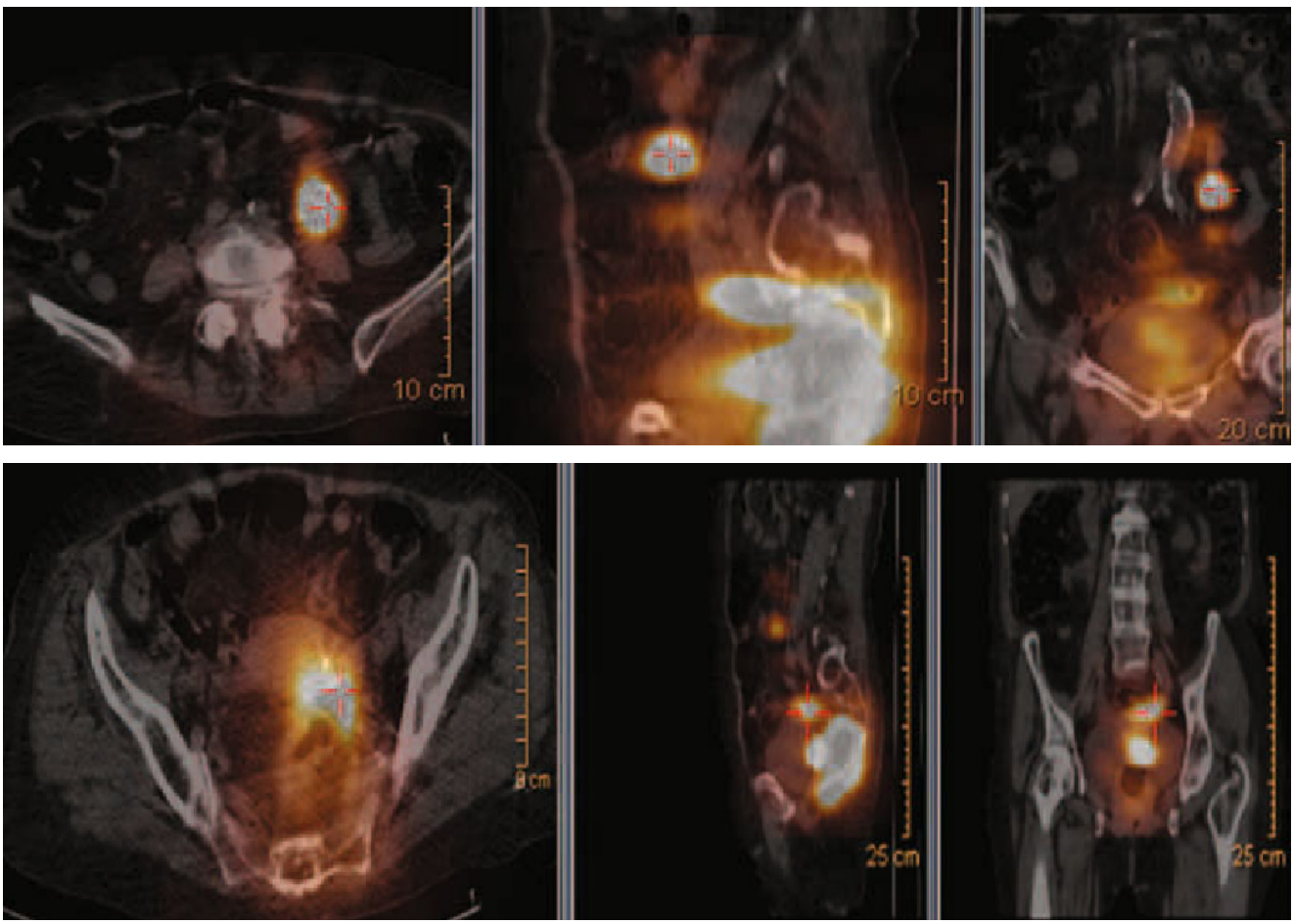

Fig. 4 SPECT/CT. *Upper panel*: SPECT/CT lymphoscintigraphy demonstrated that radioactivity apparently representing lymph node uptake in the left aortoiliac region was actually due to nonspecific colonic accumulation. *Lower panel*: SPECT/CT also showed a high mesorectal uptake, with no clear identification of sentinel lymph nodes

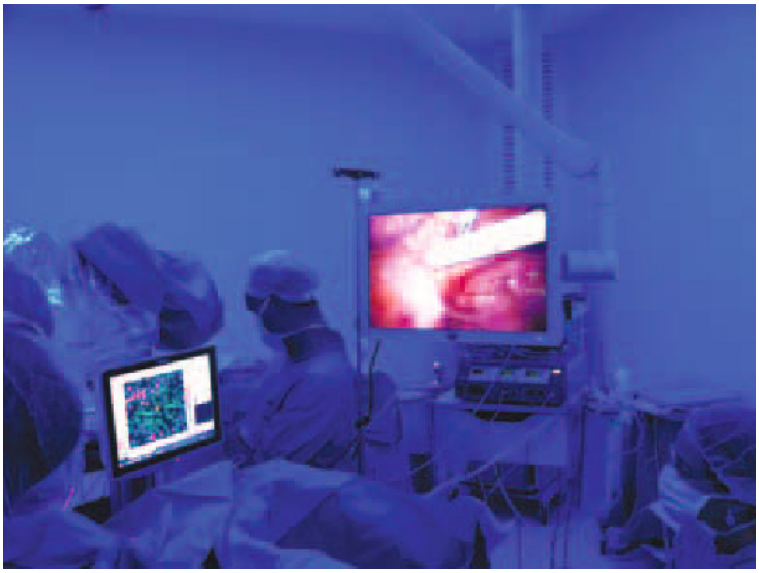

Fig. 5 Detection with gamma probe assisted by Sentinella gammacamera

Case 13.4
Sentinel Node Mapping in Cancer of Ascending Colon: "Ex Vivo" Technique with Peritumoral Blue Dye and Radiocolloid Injection

José Luis Pallarés, Joan Duch, and Carmen Balagué

Background Clinical Case

An 86-year-old woman with anemia. Colonoscopy showed a 5-6 cm ulcerated lesion in the right colon. Histopathologic examination revealed an adenocarcinoma. Staging with CT scan demonstrated no distant metastasis (T2-3N0M0). Before surgery (laparoscopic right hemicolectomy) the patient was submitted to radioguided sentinel lymph node biopsy.

Anatomical location of primary malignancy: large bowel, right colon.

Technical Background Acquisition

Sentinel lymph node detected by ex vivo study using blue dye and radiocolloid.
Staining method: ex vivo injection of 2 mL of 1% blue dye into the subserosa layer (0.5 mL at each of four points around the site of the primary tumor). The radiocolloid is inoculated in the same points (37 MBq of ^{99m}Tc-nanocolloid). Massage for five minutes of the inoculated area is necessary. After that, gamma probe (Gamma Finder II) is used in order to detect the SLNs. Two SLNs are detected through the blue dye, and three by the radiocolloid. Only one SLN has been detected combining the two methods.
Histopathological results: T2N0M0. Total lymph nodes detected: 19 (all negative). SLNs were all negative.

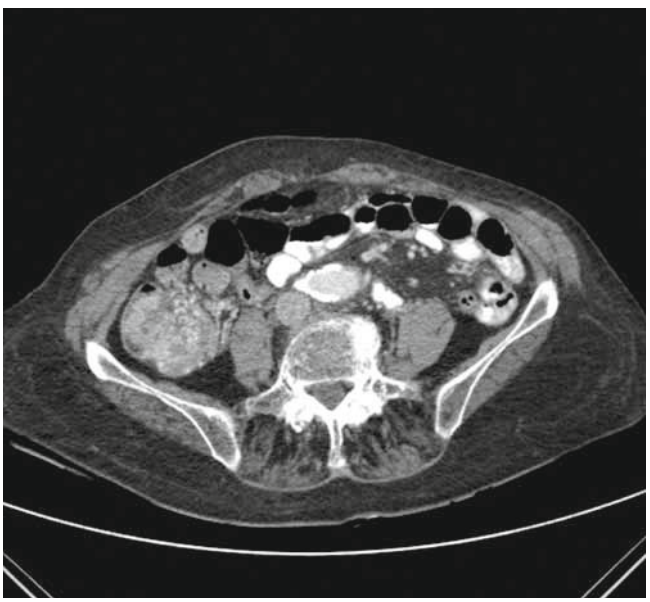

Fig. 1 Scanner: image of tumor. Large bowel: right colon

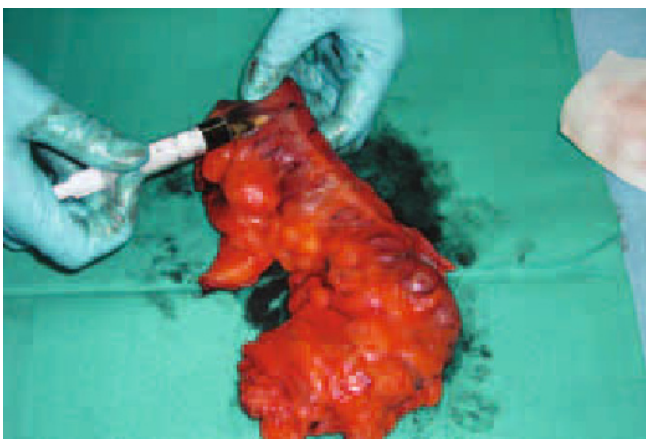

Fig. 2 Subserosal inoculation of blue dye and radiocolloid

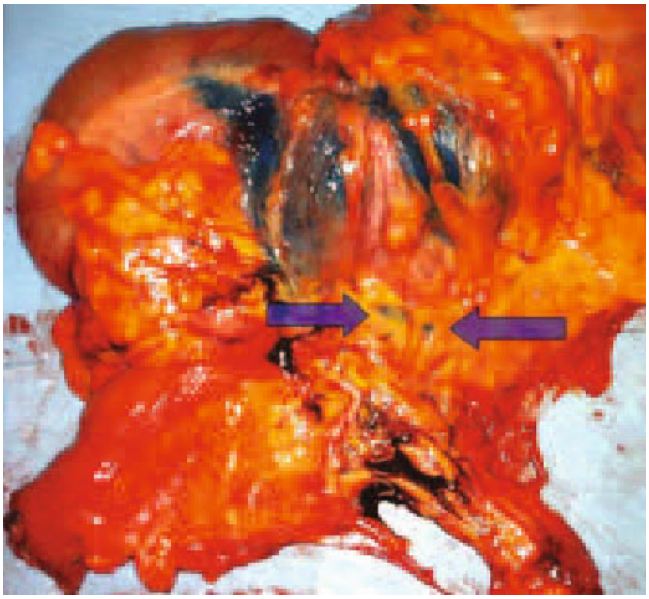

Fig. 3 Ex-vivo sentinel lymph node detection marked with blue dye

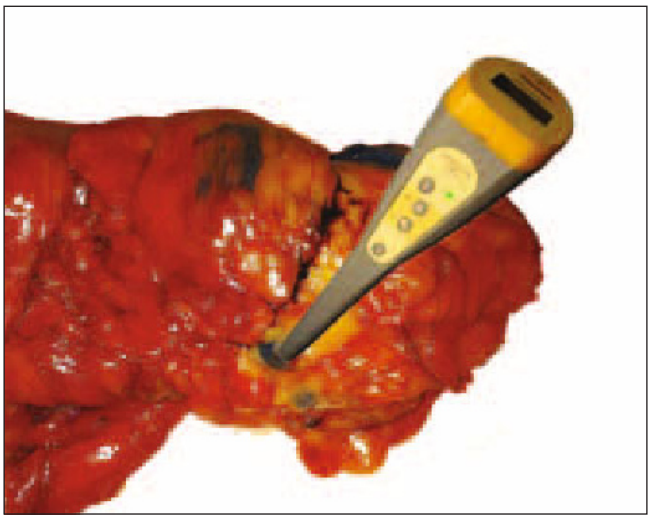

Fig. 4 Sentinel lymph node identification after radiopharmaceutical injection

References

1. Aikou T, Kitagawa Y, Kitajima M et al (2006) Sentinel lymph node mapping with GI cancer. Cancer Metastasis Rev 25:269–277
2. Kitagawa Y, Ohgami M, Fujii H et al (2001) Laparoscopic detection of sentinel lymph nodes in gastrointestinal cancer: a novel and minimally invasive approach. Ann Surg Oncol 8(Suppl 9):86S–89S
3. Sano T, Katai H, Sasako M et al (2000) Gastric lymphadenectomy and detection of sentinel nodes. Recent results. Cancer Res 157:253–258
4. Akiyama H, Tsurumaru M, Udagawa H et al (1994) Radical lymph node dissection for cancer of the thoracic oesophagus. Ann Surg 220:364–373
5. Maruyama K, Gunven P, Okabayashi K et al (1989) Lymph node metastases of gastric cancer. General pattern in 1931 patients. Ann Surg 210:596–602
6. Bonenkamp JJ, Hermans J, Sasako M et al (1999) Extended lymph-node dissection for gastric cancer. Dutch Gastric Cancer Group. N Engl J Med 340:908–914
7. Hulsher JBF, Van Sandick JW, de Boer AGEM et al (2002) Extended transthoracic resection compared with limited transhiatal resection for adenocarcinoma of the oesophagus. N Engl J Med 347:1662–1669
8. Thompson JF, Uren RF, Scolyer RA, Stretch JR (2005) Selective sentinel lymphadenectomy: progress to date and prospects for the future. Cancer Treat Res 127:269–287
9. Hiratsuka M, Miyashiro I, Ishikawa O et al (2001) Application of sentinel node biopsy to gastric cancer surgery. Surgery 129:335–340
10. Kitagawa Y, Fujii H, Mukai M et al (2002) Radio-guided sentinel node detection for gastric cancer. Br J Surg 89:604–608
11. Kitagawa Y, Fujii H, Mukai M et al (2002) Intraoperative lymphatic mapping and sentinel lymph node sampling in oesophageal and gastric cancer. Surg Oncol Clin North Am 11:293–304
12. Kitagawa Y, Fujii H, Mukai M et al (2000) The role of sentinel lymph node in gastrointestinal cancer. Surg Clin North Am 80;1799–1809
13. Miwa K, Kinami S, Taniguchi K et al (2003) Mapping sentinel nodes in patients with early-stage gastric carcinoma. Br J Surg 90:178–182
14. Kitagawa Y, Kitajima M (2006) Diagnostic validity of radio-guided sentinel node mapping for gastric cancer: a review of current status and future direction. Surg Technol Int 15:32–36
15. Rabin I, Chikman B et al (2010) The accuracy of sentinel node mapping according to T stage in patients with gastric cancer. Gastric Cancer 13:30–35
16. Arigami T, Natsugoe S, Uenosono Y et al (2006) Evaluation of sentinel node concept in gastric cancer based on lymph node micrometastasis determined by reverse transcription-polymerase chain reaction. Ann Surg 243:341–347
17. Toth D, Kathy S, Csoban T et al (2012) Prospective comparative study of sentinel lymph node mapping in gastric cancer – submucosal versus subserosal marking method. Magy Seb 65:3–8
18. Gretschel S, Bembenek A, Ulmer Ch et al (2005) Prediction of gastric cancer lymph node status by sentinel lymph node biopsy and the Maruyama computer model. Eur J Surg Oncol 31(4):393-400
19. Cheng LY, Chen XD, Zhang YX, Feng XD (2005) Clinical significance of sentinel lymph node detection by combining the dye-directed and radioguided methods in gastric cancer. Zhonghua Wai Ke Za Zhi 43:569–572
20. Ichikura T, Morita D, Uchida T et al (2002) Sentinel node concept in gastric carcinoma. World J Surg 26(3):318-22
21. Kim MC, Kim HH, Jung, GC et al (2004) Lymphatic mapping and sentinel node biopsy using 99mTc tin colloid in gastric cancer. Ann Surg 239:383–387
22. Kitagawa Y, Kitajima M (2004) Diagnostic validity of radioguided sentinel node mapping for gastric cancer. Surg Technol Int 15:32–36
23. Aikou T, Kitagawa Y, Kitajima M et al (2006) Sentinel lymph node mapping with GI cancer. Cancer Metastasis Rev 25(2):269-77. Review
24. Kitagawa Y, Kubota T, Kumai K (2005) Recent studies of sentinel lymph node. Multicenter prospective clinical trials of SN biopsy for gastric cancer. Gan To Kagaku Ryoho 32:695–698
25. Asakum M, Cahill RA, Lee SWB (2010) NOTES: The question for minimal resection and sentinel node in early gastric cancer. World J Gastrointest Surg 2:203–206
26. Yasuda S, Shimada H, Chino O et al (2003) Sentinel lymph node detection with Tc-99m tin colloids in patients with esophagogastric cancer. Jpn J Clin Oncol 33:68–72
27. Uenosono Y, Arigami T, Yanagita S (2011) Sentinel node navigation surgery is acceptable for clinical T1 and N0 esophageal cancer. Ann Surg Oncol 18:2003–2009
28. Cohen AM, Kelsen D, Saltz L et al (1998) Adjuvant therapy for colorectal cancer. Curr Probl Cancer 22:5–65
29. Wolmark N, Rockette H, Fisher B et al (1993) The benefit of leucovorin-modulated fluorouracil as postoperative adjuvant therapy for primary colon cancer: Results from National Surgical Adjuvant Breast and Bowel protocol C-03. J Clin Oncol 11:1879–1887
30. Saha S, Dan AG, Viehl CT et al (2005) Sentinel lymph node mapping in colon and rectal cancer: its impact on staging, limitations, and pitfalls. In: Leong SPL, Kitagawa Y, Kitajima M (eds) Selective sentinel lymphadenectomy for human solid cancer. Springer, New York pp 105–122
31. Mulsow J, Winter DC, O'Keane JC, O'Connell PR (2003) Sentinel lymph node mapping in colorectal cancer. Br J Surg 90:659–667
32. Pickreen JW (1961) Significance of occult metastases, a study of breast cancer. Cancer 14:1261–1271
33. Greenson JK, Isenhart CE, Rice R et al (1994) Identification of occult micrometastases in pericolic lymph nodes of Dukes B colorectal cancer patients using monoclonal antibodies against cytokeratin and CC49; correlation with long-term survival. Cancer 73:563–569
34. Thörn M (2000) Lymphatic mapping and sentinel node biopsy: is the method applicable to patients with colorectal and gastric cancer? Eur J Surg 166:755–758
35. Kuerer HM, Wayne JD, Ross MI (2001) Anaphylaxis during breast cancer lymphatic mapping. Surgery 129:119–120
36. Leong SP, Donegan E, Hefferson W et al (2000) Adverse reactions to isosulfan blue during selective sentinel lymph node dissection in melanoma. Ann Surg Oncol 7:361–366
37. Longnecker SM, Guzzardo MM, Van Voris LP (1985) Life-threatening anaphylaxis following subcutaneous administration of isosulfan blue 1%. Clin Pharmacol 4:219–221
38. Coleman RL, Whitten CW, O'Boyle J, Sidhu B (1999) Unexplained decrease in measured oxygen saturation by pulse oxymetry following injection of lymphazurin 1% (Isosulfan blue) during a lymphatic mapping procedure. J Surg Oncol 70:126–129
39. Larsen VH, Freudendal A, Fogh-Andersen N (1995) The influence of patent blue V on pulse oxymetry and haemoximetry. Acta Anaesthesiol Scand Suppl 107:53–55
40. Soni M, Saha S, Korant A et al (2009) A prospective trial comparing 1% lymphazurin vs 1% methylene blue in sentinel lymph node mapping of gastrointestinal tumors. Ann Surg Oncol 6:2224–2230
41. Bianchi PP, Petz W, Casali L (2011) Laparoscopic lymphatic roadmapping with blue dye and radioisotope in colon cancer. Colorectal Dis 13(Suppl 7):67–69
42. Waters GS, Geisenger KR, Garske DD et al (2000) Sentinel lymph node mapping for carcinoma of the colon: a pilot study. Am Surg 66:943–945
43. Wong JH, Steineman S, Calderia C et al (2001) Ex vivo sentinel

node mapping in carcinoma of the colon and rectum. Ann Surg 233:515–521
44. Fitzgerald TL, Khalifa MA, Al Zahrani M et al (2002) Ex vivo sentinel lymph node biopsy in colorectal cancer: a feasibility study. J Surg Oncol 80:27–32
45. Cox ED, Kellicut D, Adair C et al (2002) Sentinel lymph node evaluation is technically feasible and may improve staging in colorectal cancer. Curr Surg 59:301–306
46. Wood TF, Tsioulias GJ, Rangel D et al (2000) Focused examination of sentinel lymph nodes upstages early colorectal carcinoma. Am Surg 66:998–1003
47. Quadros CA, Lopes A, Araujo I et al (2008) Upstaging benefits and accuracy of sentinel lymph node mapping in colorectal adenocarcinoma nodal staging. J Surg Oncol 98(5):324-30
48. Bembenek A, Schneider U, Gretschel S et al (2005) Optimization of staging in colon cancer using sentinel lymph node biopsy. Chirurg 76(1):58-67
49. Wood T, Saha S, Morton D et al (2001) Validation of lymphatic mapping in colorectal cncer: in vivo, ex vivo, and laparoscopic techniques. Dis Colon Rectum 8:150–157

14 Preoperative and Intraoperative Lymphatic Mapping for Radioguided Sentinel Node Biopsy in Cancers of the Female Reproductive System

Pilar Paredes and Sergi Vidal-Sicart

14.1 Introduction

Sentinel lymph node biopsy (SLNB) has now become a routine procedure, employed as "standard of care" in patients with breast cancer or cutaneous melanoma. Radioguided SLNB following lymphoscintigraphy was first introduced in patients with melanoma in 1993, and quickly adopted and validated as an optimal method for lymphatic mapping, expanding in subsequent years to include breast, vulvar, and cervical cancer.

The aggressive impact of traditional surgery in vulvar cancer has spurred interest in more conservative surgical treatments. In 1979, DiSaia [1] considered superficial inguinal lymph nodes to be the first-echelon drainage station from vulvar tumors; therefore, he proposed limiting lymphadenectomy to this particular chain. Nevertheless, this approach was burdened by a high rate of local–regional recurrences. In a later study, Hacker observed that patients with negative inguinal lymph nodes did not have metastasis in the pelvic lymph nodes [2]. In 1983, Iversen observed bilateral lymphatic drainage in 67% of cases when performing lymphoscintigraphy using a radiocolloid [3]; furthermore, if the tumor was located in the clitoris, bilateral lymph node metastases were found in up to 40% of cases. Nevertheless, it was not until 1994 that sentinel lymph node (SLN) mapping was applied to vulvar malignancies, initially with blue dye tracers [4], then using the combined technique of blue dye and radiocolloid [5].

The use of both tracers simultaneously has more relevance for gynecological tumors than for other solid tumors explored previously. In fact, in the case of other tumors, use of the radiocolloid has relegated the use of blue dye to those specific clinical situations where lymphoscintigraphy cannot identify the SLN(s), or as an additional support for the surgical team. In gynecologic oncology, the most important application of the combined technique is in cervical cancer, where this approach has demonstrated a greater rate of SLN detection than with the blue dye or the radiocolloid employed alone.

Interstitial administration of the lymphatic mapping agent is relatively easy in the case of vulvar and cervical tumors, thus allowing a feasible implementation of SLNB without major technical demands. However, in endometrial cancer the optimal technique for radiocolloid injection still remains controversial, so in this cancer the technique is still considered to be in the initial phases of investigation.

On the other hand, SLN mapping has not yet been considered in patients with ovarian cancer, because the incidence of lymph node metastasis in early ovarian cancer is low (5–15%) and pelvic/para-aortic lymphadenectomy involves a more complex and time-consuming surgical approach, and can result in possible complications. To date, there are no published articles describing SLN mapping in patients with ovarian cancer, although Negishi et al. [6] have described lymphatic mapping of the tumor with the use of carbon particles; however, this study was conducted in patients without ascertained diagnosis of ovarian cancer.

14.2 The Clinical Problem

Gynecological tumors have a considerable incidence in the female population. Endometrial cancer is the most common tumor of the female tract, with more than 46,000 new cases reported annually in the USA alone.

Similarly as with other malignancies, lymph node status is the most important prognostic factor in gynecological tumors. In vulvar cancer, the 5-year survival rate decreases from 94.7% when the lymph nodes are negative to 62% when

P. Paredes (✉)
Nuclear Medicine, Hospital Clínic Barcelona,
Barcelona, Spain
e-mail: pparedes@clinic.ub.es

G. Mariani et al. (eds.), *Atlas of Lymphoscintigraphy and Sentinel Node Mapping*,
DOI 10.1007/978-88-470-2766-4_14 © Springer-Verlag Italia 2013

they are positive for metastasis [7]. Although inguino-femoral lymphadenectomy is considered to constitute an integral component of primary treatment for vulvar cancer, the long-term consequences of this treatment, especially lower-limb lymphedema, can result in a reduced quality of life for these patients. In this regard, it is important to obtain a map of lymphatic drainage from the tumor and to know in advance whether or not lymphatic drainage is bilateral; in fact, when a tumor is confined to one side of the vulva, more than 80% of nodal metastases are ipsilateral. If unilateral lymphatic drainage is seen in midline tumors, then metastatic blockage of the other side should be suspected. On the other hand, when bilateral lymphatic drainage is seen in patients with lateral tumors, the lymphatic basins of both sides should be explored.

In cervical and endometrial cancer, pelvic lymphadenectomy is only performed for diagnostic purposes. In some situations (such as high-risk endometrial cancer), para-aortic lymphadenectomy is additionally performed, due to the higher risk of nodal metastases in this field. The standard treatment in early-stage cervical cancer is hysterectomy and pelvic lymphadenectomy; nevertheless, up to 90% of pelvic lymph nodes are found to be free from metastasis in these patients. Moreover, where lymph node metastasis is found, the best therapeutic option is chemoradiotherapy; therefore, these patients do not benefit at all from surgery, and increased morbidity can derive as a result of either treatment – surgery or chemoradiotherapy. SLN mapping helps in the detection of lymphatic drainage patterns to basins not routinely explored in conventional surgery, such as the para-aortic chains. Furthermore, SLN mapping has an important role even in the validation phase of the technique, because when a metastatic lymph node is detected during surgery, surgical treatment is changed to chemoradiotherapy.

It has been shown that when pelvic lymph nodes are positive for tumor metastasis, the likelihood of finding tumor-positive para-aortic nodes increases to around 15–20%. This finding suggests that, when a positive pelvic lymph node is detected during surgery, a para-aortic lymphadenectomy should be performed for diagnostic purposes, even though it had not initially been planned [8].

The main problem in the application of SLN mapping in cervical cancer lies in the low number of tumor-positive lymph nodes detected. Thus, in order to achieve a sufficient number of false-negative cases, a very high number of patients must be recruited. This factor has prolonged the validation phase more than expected in several single-center studies. The experience of multicenter studies, such as SENTICOL (Ganglion Sentinelle dans le Cancer du Col) [9], should allow other centers to implement the phase of clinical application once their surgical team has achieved the learning curve.

Finally, in endometrial cancer, lymph node staging is performed by pelvic (and in high-risk cases, para-aortic) lymphadenectomy. However, patients who are found to be free of lymph node metastasis have not benefited at all from this lymphadenectomy, which involves prolonged surgical time and associated surgical and anesthetic morbidity. The excellent clinical outcome of patients included in SLNB programs for other neoplastic conditions (with subsequent upstaging) has recently led to a greater effort to expand this novel application to patients with endometrial cancer [10].

14.3 Lymphatic Drainage of Gynecological Tumors

14.3.1 Lymphatic Drainage from the Vulva

Lymph from the vulva drains first to the superficial inguinal nodes, then on to the deep group (crural and deep inguinal lymph), and finally to the pelvic lymph nodes. The confluence of bilateral lymphatic networks can lead to contralateral lymph node invasion. Midline structures, such as the clitoris, can drain directly to deep lymph nodes. The deepest lymph node, located under the inguinal ligament, is Cloquet's node, which drains to the external iliac chain. Although tumor cells from the clitoris can drain directly to pelvic lymph nodes, there is no evidence of nodal pelvic metastasis without inguino-femoral metastatic involvement [11].

14.3.2 Lymphatic Drainage from the Cervix Uteri

The first lymphatic drainage stations from the cervix uteri are the obturator (external iliac), hypogastric and presacral lymph nodes. Lymph nodes on common iliac (junctional node) and para-aortic groups become second-echelon nodes. Inguinal chain is considered a second-echelon group. In parametrial and paracervical cancer, nearby lymph nodes are involved by proximity. Nevertheless, lymph from these areas can drain directly to the para-aortic nodes.

14.3.3 Lymphatic Drainage from the Corpus Uteri

The lower segment of the uterus drains to the pelvic lymph nodes through the broad ligament, while the upper segment drains to the para-aortic nodes via the ovarian lymphatic vessels. Four nodal echelons can be distinguished: external iliac and obturator, hypogastric inframesenteric para-aortic, and supramesenteric infra-renal lymph nodes. The pelvic groups are interconnected and drain bilaterally to para-aortic groups, merging then into the supramesenteric infra-renal lymph nodes.

Table 14.1 Indications and contraindications for sentinel lymph node biopsy in gynecological tumors

Tumor	Indications	Contraindications
Vulvar cancer	• Squamous cell carcinoma • Ib to II (FIGO classification) • Tumors less than 4 cm	• Pregnancy • Previous surgery including lymphadenectomy in the area of tumor drainage[a] • Nodal or parametrial invasion detected by other imaging techniques
Vulvo-vaginal melanoma	• Breslow (depth invasion) 1–4 mm	
Cervical cancer	• Squamous cell carcinoma • Ia2 to Ib1 (FIGO classification) • Tumors <4 cm (better results if <2 cm)	
Endometrial cancer	• Potential group of candidates: low- and intermediate-risk endometrial cancer • Histological subtype: endometrioid • Histological grade I or II • Myometrial invasion <50%	

[a]Previous cone biopsy is not a contraindication for SLN biopsy in cervical cancer.
FIGO, International Federation of Gynecology and Obstetrics.

14.4 Indications and Contraindications for Sentinel Lymph Node Biopsy

Clinical indications for SLNB in gynecological tumors are described below. Indications and general contraindications are summarized in Table 14.1.

14.4.1 Clinical Indications

14.4.1.1 Vulvar Cancer

- Squamous cell carcinoma Ib-II (FIGO [International Federation of Gynecology and Obstetrics] classification) of less than 4 cm
- Vulvo-vaginal melanoma – although not yet fully validated, it is acceptable to perform SLNB with the same indications as for cutaneous melanoma.

14.4.1.2 Cervical Cancer

- Cervical tumors of less than 4 cm (with best results in tumors of less than 2 cm [12, 13]) and in early stage, Ia2 to Ib1.

14.4.1.3 Endometrial Cancer

Despite a recent surge in the interest for this application, SLN mapping is still in the preliminary stages of evaluation for endometrial cancer. Subgroups with potential clinical benefit are the low-risk or the intermediate-risk endometrial tumors, since SLN mapping can result in an upstage in up to 10% and 15% of cases, respectively [14].

14.4.2 General Contraindications

- Extensive prior surgery in this region (except cone biopsy) or prior pelvic lymphadenectomy
- Prior external beam radiation therapy of the pelvic area
- Lymph node metastases or parametrial invasion detected clinically or by other diagnostic imaging modalities
- Distant metastatic spread of the disease.

14.5 Modalities of Radiocolloid Injection

14.5.1 Vulvar Cancer

Injection should be performed after application of an anesthetic cream or spray, such as lidocaine or ethyl chloride. The injection modality is similar to that commonly adopted for cutaneous melanoma. Luer-lock tuberculin syringes or 25-gauge needles are recommended. The radiocolloid can be divided into 2–3 aliquots of 0.1 mL each, with a total activity of 37–111 MBq depending on the time between injection and surgery. It is important to properly surround the whole lesion, especially in the case of lesions close to mid-line (Fig. 14.1). The currently accepted method is a combined technique using blue dye and radiocolloid, although even the use of radiocolloid alone provides a high SLN detection rate, in the range of 95–100% [15].

14.5.2 Cervical Cancer

With the patient in gynecological position, the external cervical orifice must be presented with the help of a speculum. Injection should be divided into four aliquots, at the four quadrants of the cervix, using a 20- or 22-gauge spinal needle, peritumorally or periorificially (around the tumor or orifice). A Pozzi forceps can be useful to hold the cervix, whenever needed. In the case of prior cone biopsy, periorificial injection at the four quadrants is recommended. The best detection rate is achieved using the blue

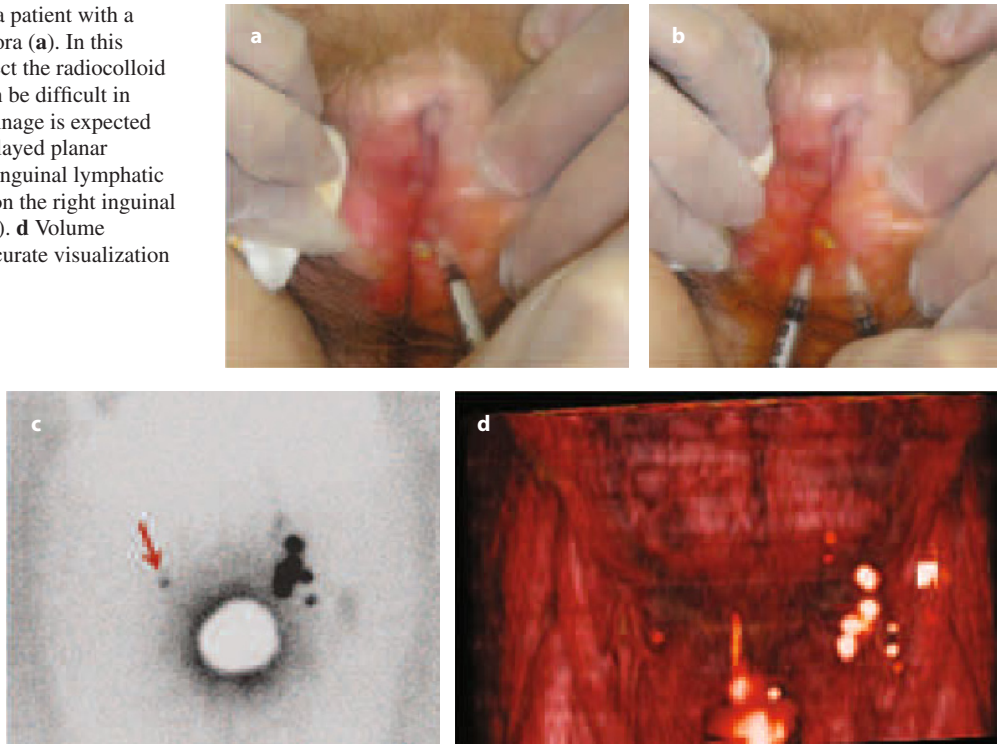

Fig. 14.1 Submucosal injection in a patient with a midline lesion in the left labia minora (**a**). In this situation it is very important to inject the radiocolloid around the tumor, although this can be difficult in the medial part (**b**), as bilateral drainage is expected in a high percentage of cases. **c** Delayed planar image shows a predominantly left inguinal lymphatic drainage. However, a faint uptake on the right inguinal side is observed as well (*red arrow*). **d** Volume rendering image depicts a more accurate visualization of lymph nodes

dye and radiocolloid combined, with a success rate of over 90% [13].

14.5.3 Endometrial Cancer

One of the most controversial aspects for SLN mapping is the modality of injection, since no single approach has been sufficiently validated. Three different modalities of injection are currently in use: preoperative cervical injection, myometrial peritumoral injection assisted by hysteroscopy, or myometrial/subserosal intraoperative injection. The advantages and drawbacks of each approach are set out below.

Cervical injection is the easiest modality. The radiocolloid can be injected the day prior to surgery, obtaining lymphatic mapping with planar and single photon emission computed tomography/computed tomography (SPECT/CT) images. The detection rate achieved using this method is the highest, ranging from 70% to 89% [14, 16], even higher than for hysteroscopic injection [17]. Some authors perform an additional subserosal [18] or fundal injection [19], but without achieving higher detection rates. It should be noted, however, that this modality of injection might not mirror lymphatic drainage from the organ, especially if the tumor is located in the upper third of the corpus uteri, and it detects very few para-aortic lymph nodes.

Myometrial/subserosal injection during hysteroscopy allows direct injection around the tumor. The procedure can be performed at the beginning of surgery, but then without the possibility of acquiring lymphoscintigraphic images (unless a portable gamma camera is available). Detection rates obtained with this modality of injection range from 40% to 65% [17, 20].

Although injection into the corpus uteri in a myometrial or subserosal location generally has a low detection rate (45–77%) [21], detection rates as high as 92% have been reported [22]. The tracer administered during surgery is usually blue dye, which requires nodal dissection to find the blue-stained lymph nodes. The number of injections seems to play an important role, with a minimum of three injections needed [23].

Promising but limited preliminary data for ultrasound-guided injection have also been reported at international meetings, although no full article has yet been published.

With either injection modality, the risk of radioactive contamination of the skin has to be considered, and adequate steps should be taken to avoid it. In the case of vulvar tumors, only standard precautions are needed, which include covering the injection site with lint or a dressing. For deeper injection sites, any fluid leakage through the vagina from the puncture site, in cervical cancer, or from the endometrial cavity, can contaminate not only the patient's skin but also the gamma camera. The use of an absorbent pad is recommended after injection, to be changed before acquisition.

Leakage between the syringe and needle, caused by the high resistance offered by cervical or endometrial tumors, can be avoided by wrapping the syringe in absorbent lint.

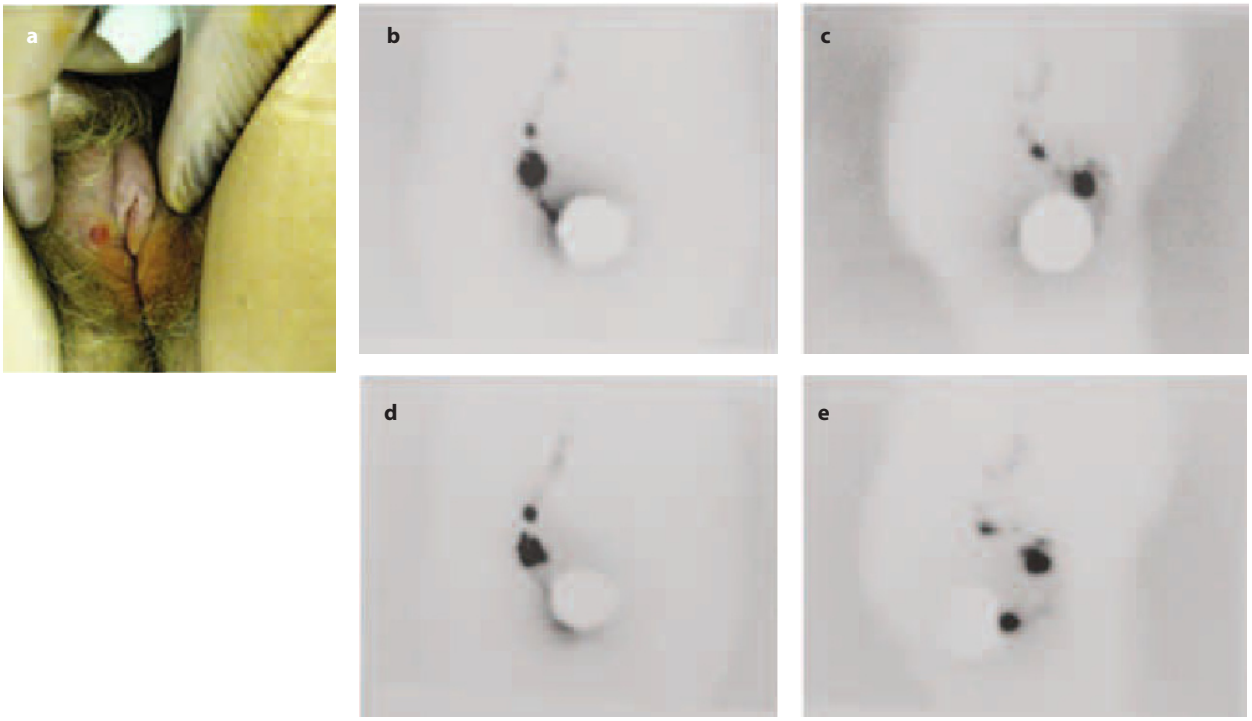

Fig. 14.2 Patient with a rounded ulcerated lesion on the middle part of the right labia majora of the vulva (**a**). Early planar anterior (**b**) and right lateral (**c**) images show lymphatic drainage from the injection site to the right side of the upper inguinal area. Two different SLNs are visualized, as there is one direct lymphatic channel to the iliac node below the most intense focal uptake in the inguinal area. In delayed images (**d**, **e**), the activity uptake remains in the same locations, although a cluster of lymph nodes is observed in the inguinal zone. In the iliac area, the uptake has increased and it is considered with high probability a SLN

14.6 Preoperative Sentinel Lymph Node Imaging

14.6.1 Dynamic Study

Evaluation of superficial lymphatic drainage from the tumor requires an early dynamic study, while this acquisition offers no benefit for those tumors that will drain into the pelvis. In vulvar tumors, the preoperative imaging study starts with a dynamic acquisition immediately after injection, since lymphatic drainage from this tumor is mainly superficial. The recommended protocol consists of a 10-minute acquisition time in a 128×128 matrix, at 1 frame/30 seconds.

14.6.2 Planar Study

Early planar images (3–5-minute acquisition time) in a 256×256 matrix can be acquired in anterior and lateral views immediately after the dynamic study (Fig. 14.2). In vulvar malignancies, it is advisable to mark on the skin the location of hot spots seen on early lymphoscintigraphy, in order to discriminate SLNs from second-echelon lymph nodes. In cervical or endometrial cancer, planar imaging can be delayed until 30 minutes after injection. Delayed images are useful for identifying other regions of lymphatic drainage, or in some selected clinical situations, such as unilateral drainage in vulvar cancer.

Lymphatic drainage can be slow in some patients, especially in endometrial cancer; later imaging, at 2 hours postinjection, is therefore highly recommended. Unlike other tumors, radiocolloid reinjection is not always feasible in gynecological malignancies; therefore, delayed images over time become a valuable tool for lymphatic mapping.

Particular attention must be paid to avoiding inadvertent radioactive contamination, which occurs with different modalities depending on the modality of radiocolloid injection. Lymphatic drainage from vulvar tumors occurs mostly to SLNs near the injection site; therefore, any radioactive contamination during injection can simulate a SLN. This type of contamination is much less common in cervical or endometrial tumors, whereas leakage of radiocolloid along the vagina is more frequent, possibly resulting in contamination of the gamma camera. For this reason, the use of an absorbent pad is recommended after injection, replacing it before scintigraphic acquisition in order to avoid possible misinterpretation of cutaneous hot spots.

Lead shielding over the injection site can help in the visualization of less active SLNs, although with this procedure there is a risk of masking some SLNs next to the injection site, such as the parametrial lymph nodes.

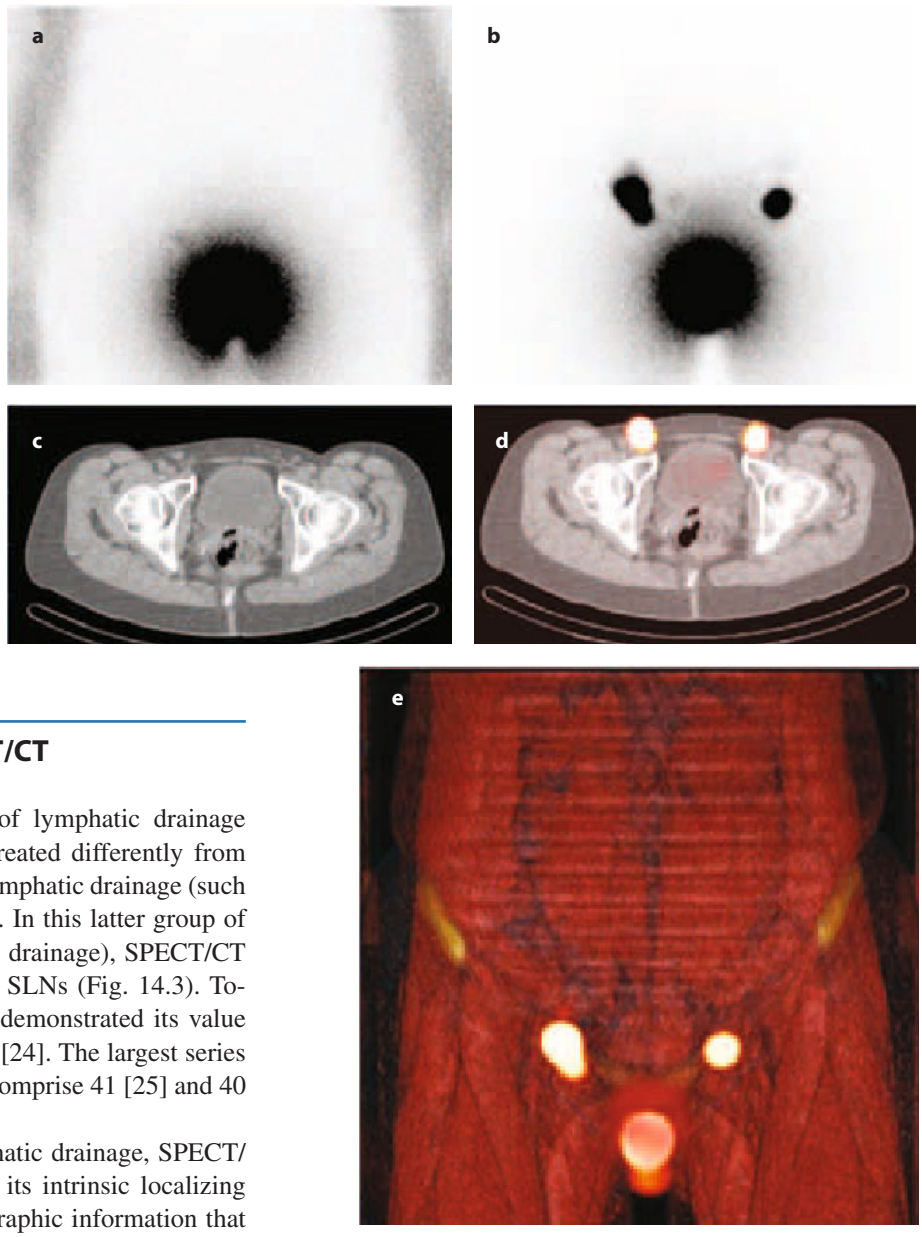

Fig. 14.3 Vulvar cancer. **a** Absence of lymphatic drainage in the early image. **b** Delayed imaging shows bilateral lymphatic drainage to both groins, with two hot spots in the right and a hot spot in the left groin. The radioactivity displayed in the fused images corresponds to several nodes depicted on the CT scan (**c**, **d**). 3D volume rendering image shows the symmetric disposition of nodes in the groin (**e**)

14.7 Contribution of SPECT/CT

Tumors with a superficial pattern of lymphatic drainage (such as vulvar cancer) should be treated differently from those with deeper, intra-abdominal lymphatic drainage (such as cervical and endometrial cancers). In this latter group of tumors (those with deeper lymphatic drainage), SPECT/CT will be of most benefit for mapping SLNs (Fig. 14.3). Tomographic SPECT/CT imaging has demonstrated its value in other tumors with pelvic drainage [24]. The largest series in cervical and endometrial cancers comprise 41 [25] and 40 [26] patients, respectively.

In case of deep abdominal lymphatic drainage, SPECT/CT improves SLN detection due to its intrinsic localizing properties and to the anatomo-topographic information that fusion imaging can provide. Smaller SLNs can thus be detected, including lymph nodes located outside the immediate area of standard lymphadenectomy.

Although acquiring SPECT/CT images increases the time required for preoperative imaging, its chief advantage in gynecological tumors is the ability to precisely localize SLNs for removal. Both the gynecologist and the nuclear medicine physician should be involved in the evaluation of fused images, as there is a certain learning curve involved in the correct interpretation of SPECT/CT images. Over time, Martinez et al. [25] were able to recognize an increasing proportion of patients with bilateral SLNs in cervical tumors (from 39% to 55%) (Fig. 14.4). Correct interpretation of preoperative images can actually reduce the surgical time spent searching all lymph node basins [26].

The most difficult area to evaluate for SLNs is the parametrial region, due to its close proximity to the primary tumor (radiocolloid injection site). In planar images, high activity from the injection site can hide a lymph node close to the uterus; on the other hand, the use of lead shielding is not an optimal solution, because it can hide the SLN. Nevertheless, in cervical and endometrial cancer, misinterpretation of parametrial lymph nodes is less important, since systematic hysterectomy includes parametrial resection, which minimizes the risk of underdetection in the first echelon of lymphatic drainage from the tumor. SPECT/CT has demonstrated better detection rates than planar imaging or even intraoperative gamma probe detection [25, 26] (Fig. 14.5).

A common pitfall in the interpretation of planar images is where lateralized radioactivity from the injection site leads

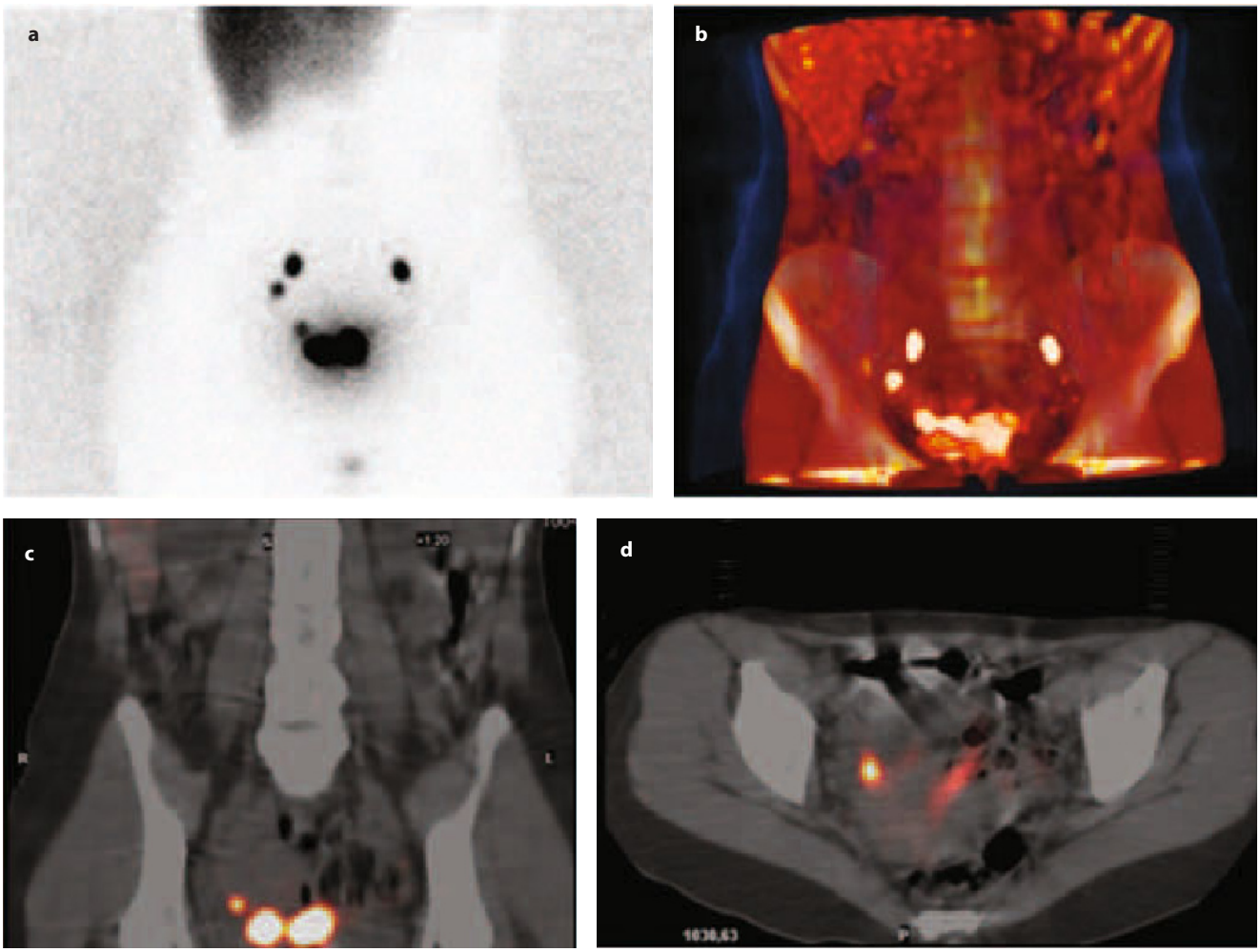

Fig. 14.4 Cervical cancer. **a** Delayed planar images show bilateral lymphatic drainage with two lymph nodes in the right pelvis and one in the left pelvis. Note a hot spot near the injection site, depicted on the right hand side. 3D volume rendering (**b**) and SPECT/CT slices (**c**, **d**) give a more precise location of this lymph node. Its position is in the parametrium, and this is considered an overt SLN

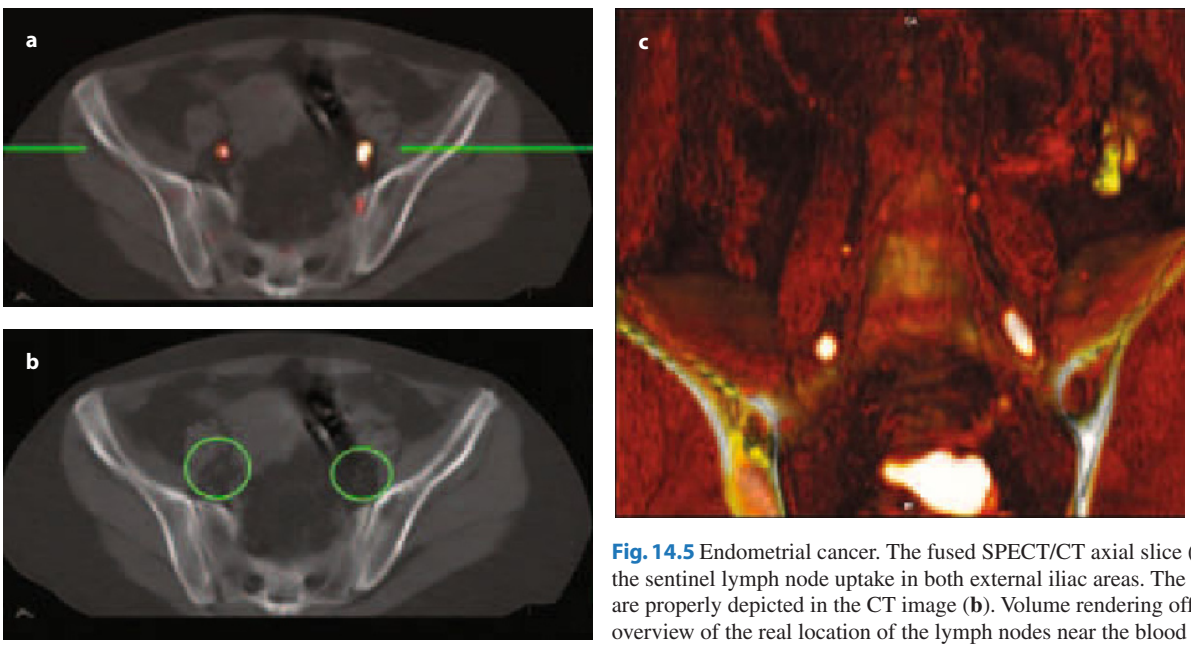

Fig. 14.5 Endometrial cancer. The fused SPECT/CT axial slice (**a**) shows the sentinel lymph node uptake in both external iliac areas. The lymph nodes are properly depicted in the CT image (**b**). Volume rendering offers a good overview of the real location of the lymph nodes near the blood vessels (**c**)

to false visualization of a pelvic lymph node. After reconstruction of SPECT acquisition, a careful examination of cross-sectional images (especially the fused SPECT/CT images) can provide all the clues needed to discriminate a very close pelvic lymph node from a small accumulation of radioactivity produced by injection of the tumor. This will reduce the rate of false-positive preoperative SLNs.

14.8 Intraoperative Detection of Sentinel Lymph Nodes

Although the combined technique (blue dye and radiocolloid) is used in vulvar cancer, its value is greater in cervical tumors. On the other hand, in endometrial cancer (where the majority of patients are obese), the fat located around the lymphatic vessels prevents sufficient visualization of blue nodes or pathways, thus making the combined technique of limited benefit.

Early studies in vulvar cancer were performed using the blue dye alone, with SLN detection rates as high as 86–88% [27]. Following the introduction of radiocolloid lymphoscintigraphy, the SLN detection rate has increased to 95–100% [15, 28]. Current standard practice includes the injection of both tracers – blue dye and radiocolloid. In cervical tumors, the highest detection rate is obtained using the combined technique [13].

The recommended volume of blue dye (50% dilution) is 0.5–1.0 mL for vulvar tumors and 4 mL (1 mL in each periorificial injection) for cervical tumors. The dye must be injected right at the start of surgery, because visual inspection will take place approximately 10–15 minutes into the surgical procedure.

During surgery, all hot and/or blue lymph nodes are usually considered as SLNs, together with those nodes with a count rate more than 10% of the count rate of any previously resected SLN. Lymphoscintigraphy is the best guide for planning an optimal surgical approach. In vulvar tumors, marks on the skin can indicate the best location for surgical incision. In lateral tumors, unilateral drainage is accepted to accurately depict lymphatic drainage from the tumor, whereas midline tumors require dissection of the inguino-femoral chain that does not show drainage, in order to identify a blue SLN and to perform a gamma-probe search. If a hot or blue node cannot be detected, lymphadenectomy must be performed anyway.

In cervical and endometrial tumors, laparoscopy is the most frequent surgical approach; therefore, cutaneous marks are less useful as a guide, due to overdistension of the abdominal wall. Under these conditions, tomographic SPECT/CT images can play a relevant role. In these tumors, it is important to consider SLN detection separately in both halves of the pelvis, rather than together in a per-patient analysis. The number of false-negative SLNs decreases if lymphadenectomy is performed on the side with no lymphatic drainage [29], even in more advanced FIGO stages (Ib2 to IIa) [30].

14.9 Intraoperative Imaging

The possibility of acquiring scintigraphic images during surgery has become a reality in the last 5 years, in several conditions involving the use of radioguided surgery, such as hyperfunctioning parathyroid gland resection or SLN detection in various tumors. For complex anatomic regions, such as the neck or internal mammary chain, such intraoperative imaging can provide valuable information, whereas its role is less important in other locations, such as the axilla. Although portable gamma cameras are usually employed in conjunction with gamma-probe counting, the camera can also be used alone, as has been described by Ortega [31]. The few groups that have reported their experience in gynecological tumor guidance [32] have focused on cervical and endometrial tumors, and successful detection rates of 92% have been quoted (Fig. 14.6). The main advantages reported are: (a) greater sensitivity in the localization of parametrial lymph nodes; (b) greater capacity to exclude interference from liver activity when resecting paraortic nodes; and (c) its potential to confirm the completeness of SLN excision.

Portable gamma cameras are equipped either as a handheld device or with a mobile arm for location over the surgical field and a control unit to display the images. For use within a surgical setting, a sterile cover is required. Some devices are equipped with a touch-sensitive screen that facilitates use by the surgical team. The acquisition time for intraoperative imaging is only 1 minute, so the whole procedure might take 5–10 minutes, which is not a significant increase in surgical time. Comparison of the images acquired before and after a SLNB provides crucial information about correct resection of the target, alerts to any remaining SLNs in the surgical bed, and confirms complete disappearance of hot spots. For increased precision in the localization of hot spots, a pointer tipped with an iodine-125 (^{125}I) seed can be used. This seed can be fixed to laparoscopic forceps or, when detection is combined with a gamma probe, attached to the distal end of the probe. In such cases, the surgical team will have simultaneous visual and acoustic information.

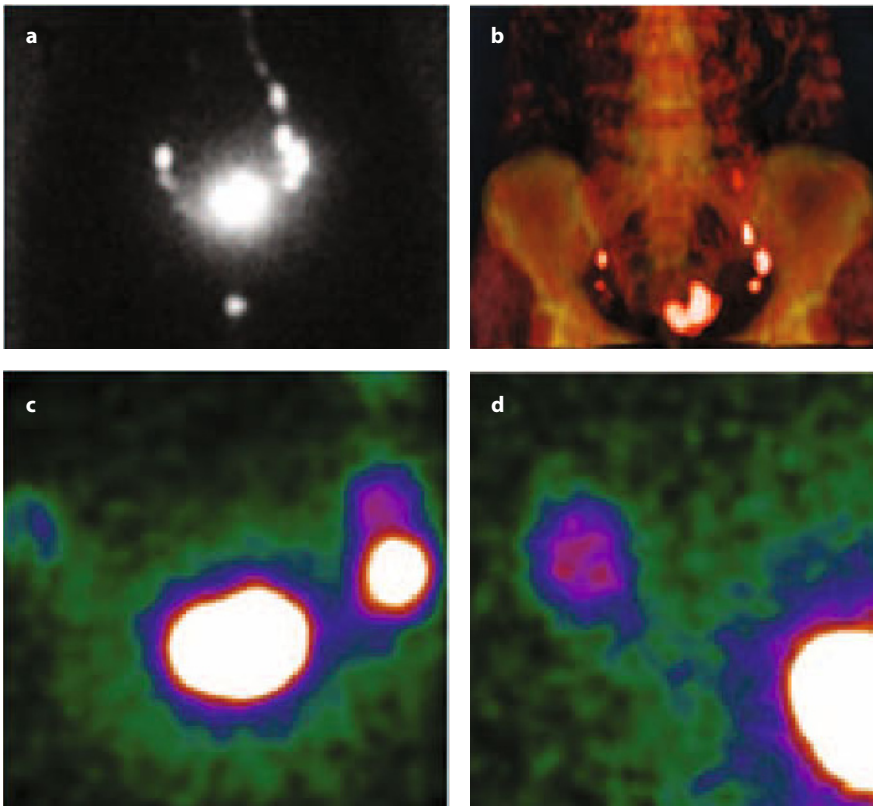

Fig. 14.6 Cervical cancer. **a** The anterior planar image (**a**) shows bilateral lymphatic drainage. **b** Volume rendering image displays more precise SLN location. **c, d** The portable gamma camera images show SLN uptake during the surgical procedure

14.10 Common and Rare Variants (with Possible Misinterpretation)

14.10.1 Vulvar Cancer

The majority of SLNs related to vulvar tumors are found in the superficial inguinal lymphatic group. In delayed images, secondary SLNs can be found under the fascia, belonging to the deep inguino-femoral group. Nevertheless, sometimes delayed images show a certain washout of radioactivity from the superficial hot spots, leaving only the deepest lymph node, which is then considered to be the true SLN.

The normal distribution pattern of lymphatic drainage and lymph nodes is ipsilateral in lesions more than 2 cm away from the midline. Thus, it is unusual to find contralateral drainage in lateralized vulvar tumors. Instead, bilateral drainage is the rule in the case of central lesions. If this is not the case, the clinical history should be carefully revised, in order to identify any prior surgical procedure in the region of interest that could explain this unexpected roadmap. If no justification is found, metastatic blockage should be assumed, and lymphadenectomy should be carried out (Fig. 14.7).

14.10.2 Cervical Cancer

The cervix of the uterus is a midline organ, so bilateral drainage is to be expected. The most frequent location of pelvic lymph nodal metastases is the obturator group, followed by the external iliac lymph nodes. It is common to find lymph nodes in a distal location, following radiocolloid progression to the common iliac artery and on to the aortic bifurcation (Fig. 14.8).

When a para-aortic lymph node is seen on lymphoscintigraphy as a sole hot spot, it is considered to be the SLN. The pelvic lymphatic basins must be carefully explored with both gamma-probe counting and visual inspection, in order to rule out possible metastatic blockade. On the other hand, if the para-aortic lymph node is associated with the presence of pelvic hot spots, it can be mistakenly considered as a part of the progression of lymphatic drainage rather than as a direct drainage path (especially when no direct lymphatic channel is visualized).

Unexpected drainage from cervical tumors has been described in retrouterine and presacral locations, as well as in the deep inguino-femoral chains.

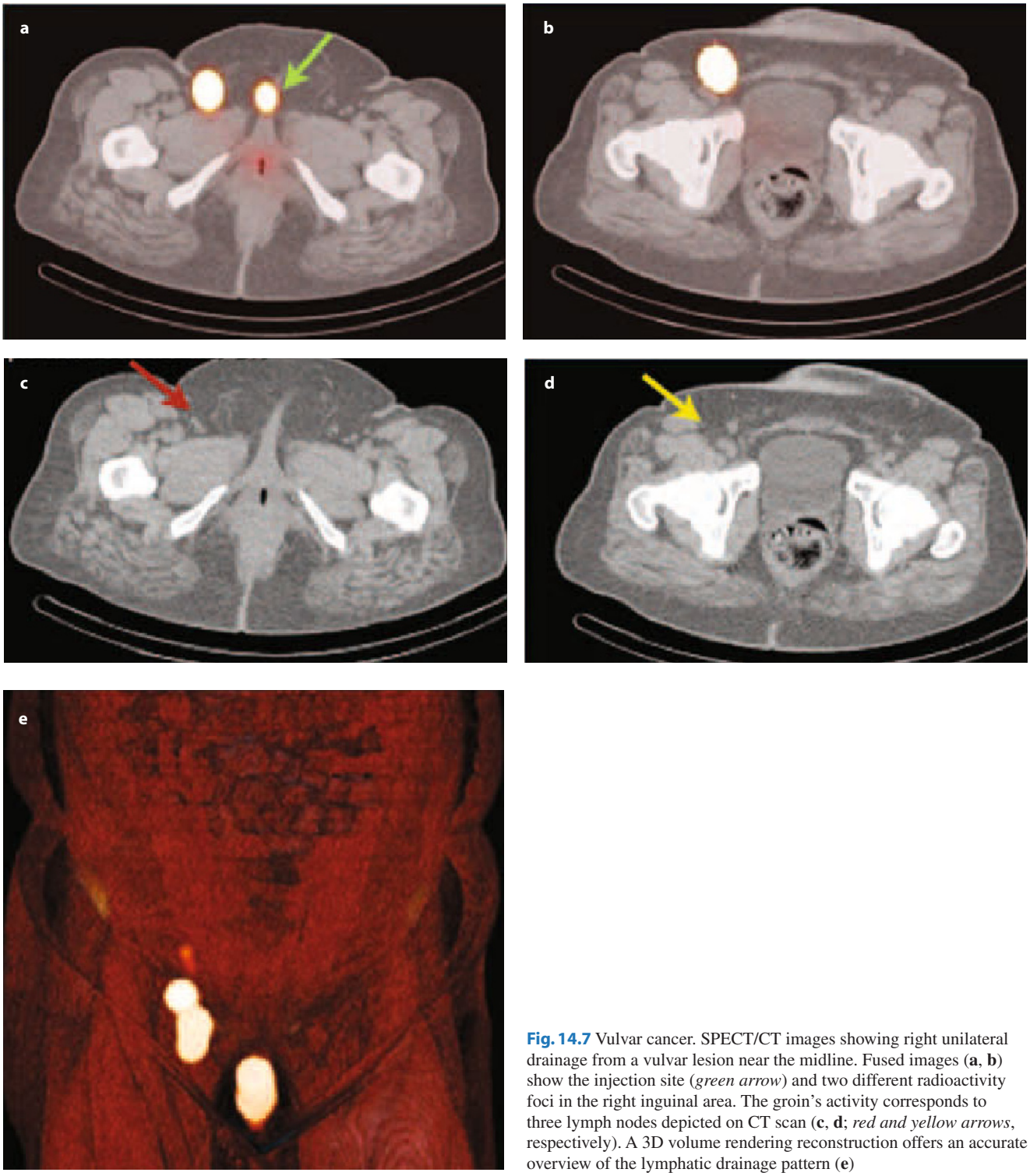

Fig. 14.7 Vulvar cancer. SPECT/CT images showing right unilateral drainage from a vulvar lesion near the midline. Fused images (**a**, **b**) show the injection site (*green arrow*) and two different radioactivity foci in the right inguinal area. The groin's activity corresponds to three lymph nodes depicted on CT scan (**c**, **d**; *red and yellow arrows*, respectively). A 3D volume rendering reconstruction offers an accurate overview of the lymphatic drainage pattern (**e**)

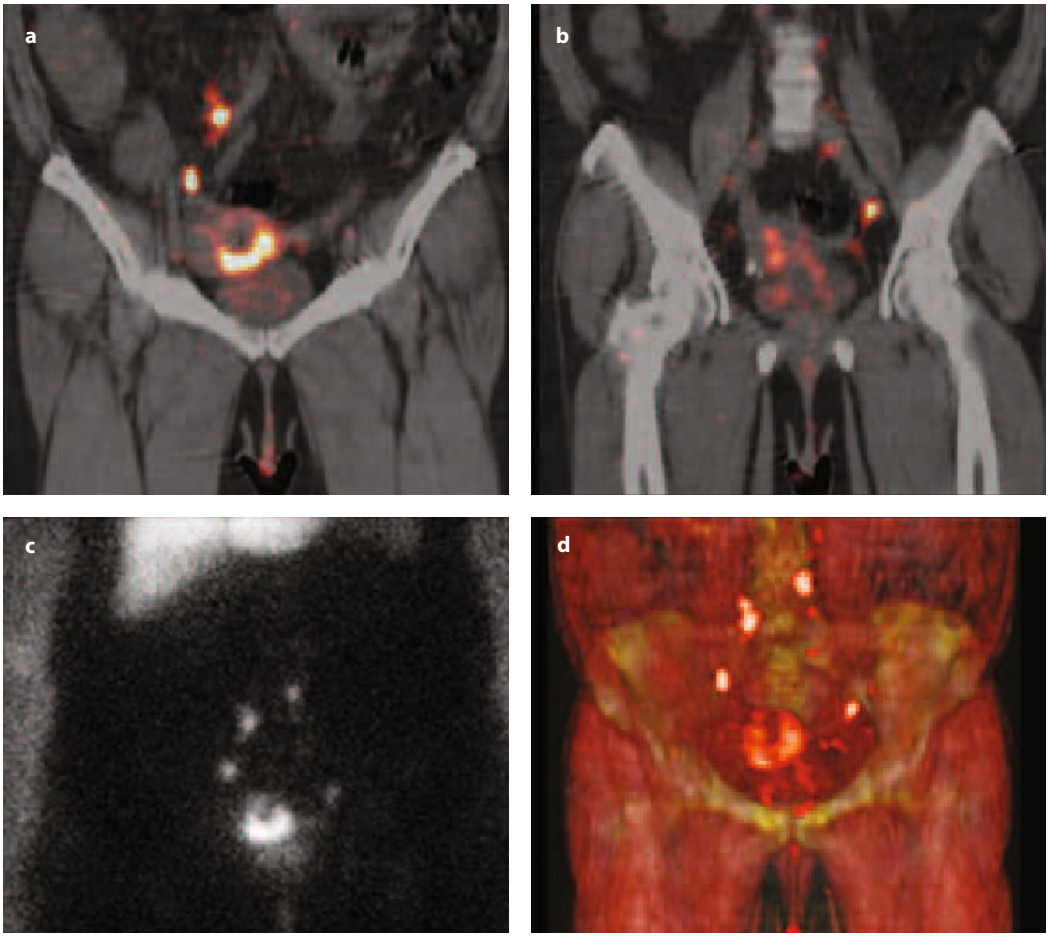

Fig. 14.8 Endometrial cancer. **a**, **b** SPECT/CT images depict the clear relationship between the SLNs and pelvic (iliac) structures. A good overview of lymphatic distribution is achieved by planar imaging (**c**). However, the 3D reconstruction offers a more concise setting and gives the surgeon the opportunity to navigate within the pelvis with more confidence (**d**)

14.10.3 Endometrial Cancer

In endometrial cancer, the normal pattern of lymphatic drainage includes pelvic and para-aortic lymph nodes (a pattern of drainage that is to be considered abnormal when performing cervical radiocolloid injection). Visualization of para-aortic lymph nodes is very low in the case of cervical injection – only up to 11% of cases (and without exclusive para-aortic SLNs) have been reported [14]. On the other hand, with myometrial, subserosal, or fundal injection, visualization of para-aortic lymphatic drainage increases up to 95%, with 16–25% of para-aortic-exclusive SLNs [23, 33].

14.11 Technical Pitfalls in Lymphatic Mapping

There are several technical pitfalls that can interfere with SLN mapping in all gynecological tumors. During radiocolloid injection, special attention must be paid to retrograde radioactivity leakage; in patients with cervical or endometrial cancer in particular, some of the radiocolloid will spill along the vagina to contaminate clothes, and also the gamma camera if the vaginal content leaks during acquisition. This situation can be avoided by using an absorbent pad following injection, which is then changed before lymphoscintigraphic acquisition. Otherwise, hot spots produced by contamination can be easily identified in the lateral view of planar images, or with SPECT/CT imaging. Contamination during injection of vulvar tumors is usually seen as radiocolloid drops on the skin. The use of an absorbent sheet under the patient and a lint wrap over the needle–syringe junction can prevent accidental spillage.

Although lead shielding is useful in the acquisition of lymphoscintigraphy to better visualize faint or less active SLNs, it can sometimes cover a hot spot close to the injection site, such as parametrial lymph nodes. To ensure that the true SLN is not overlooked, at least one non-lead-shielded image should be acquired.

During surgery, radioactivity from the injection site can interfere with the detection process. Should this be really disruptive, the tumor lesion can be removed at the start of the procedure; nevertheless, this is only an option in vulvar lesions, where vulvectomy is part of the planned treatment. In cervical tumors, hysterectomy will only be performed once

the SLNs have been examined and the possibility of nodal invasion excluded. In endometrial malignancies, the uterus is usually enlarged, thus possibly increasing the degree of interference. In laparoscopic procedures, hysterectomy will take place at the end of the intra-abdominal (retroperitoneal or transperitoneal) surgical procedure, with the preparation for vaginal resection.

Gamma-probe scanning along the intra-abdominal lymphatic pathways can be affected by physiological activity such as: (a) technetium-99 (^{99m}Tc) activity contained in the ureters (because of physiologic kidney excretion), or (b) liver activity due to radiocolloidal uptake in the reticulo-endothelial system (physiological uptake). Being aware of these possible interferences can avoid misinterpretations in the location and number of SLNs. Taking repeat measures while changing the direction of the probe (in order to blind the device to physiological activity) is not always possible in laparoscopic procedures, but is recommended whenever possible.

Clinical Cases

Case 14.1
Sentinel Node Mapping in Vulvar Carcinoma: Drainage to Bilateral Inguinal and Iliac Nodes After Intradermal Injection (Planar Imaging)

Giuseppe Rubini and Filippo Antonica

Background Clinical Case

A 73-year-old woman with squamous cell carcinoma of the vulva (T2 according to FIGO staging) and nonpalpable groin lymph nodes. Clinical examination revealed confluent blanching erythema on her right flank, lateral abdomen and thigh. The patient was afebrile and routine blood chemistry was normal. The patient was submitted to lymphoscintigraphy and radioguided sentinel lymph node biopsy.

Lymphoscintigraphy

About 12 hours before surgery, lymphoscintigraphy was performed following intradermic injection of 0.6 mL of a of 111 MBq ^{99m}Tc-albumin nanocolloid (divided into two aliquots) around the tumor under endoscopic guidance. A dual-detector SPECT gamma camera (Millennium MG, GE Healthcare, Milwaukee, WI) equipped with low-energy high-resolution (LEHR) collimators was used to obtain abdominal-pelvic dynamic images immediately after radiopharmaceutical injection and planar static images at 30 and 60 min after radiopharmaceutical injection. Dynamic images (1 frame 60 s/30 frames) were acquired in anterior and posterior projection with a 256×256 matrix and zoom factor 1.00, while static images were acquired in anterior and posterior projection with a 128×128 matrix and zoom factor 1.00.

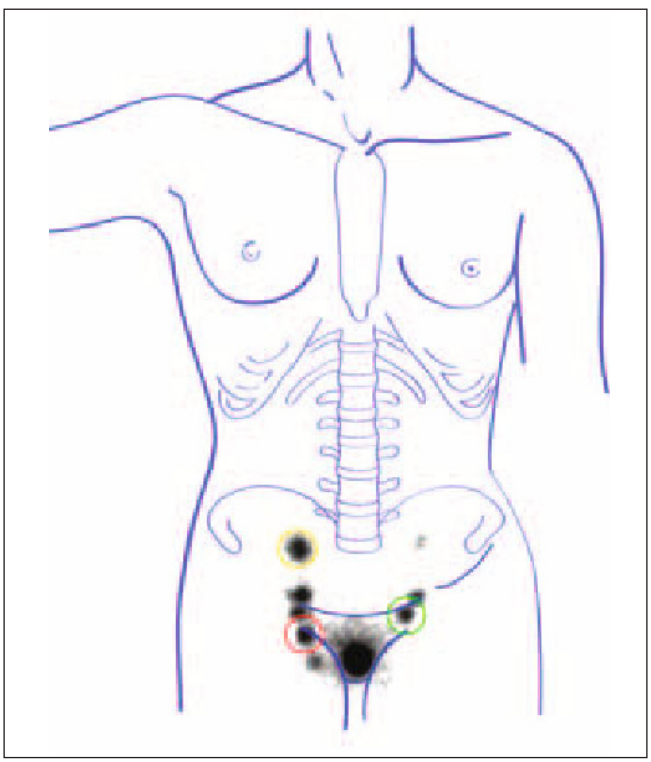

Fig. 1 Schematic representation of an anterior static planar image of the abdominal-pelvic region (30 min after intradermal radiopharmaceutical injections) shows a right inguinal sentinel lymph node (*red circle*) and a left inguinal sentinel lymph node (*green circle*). There is also serial visualization of subsequent bilateral inguinal-tier nodes and of one right iliac sentinel lymph node (*yellow circle*)

Case 14.2
Sentinel Node Mapping in Endometrial Carcinoma: Drainage to One-Sided Lumbo-Aortic Nodes After Submucosal Peritumoral Injection (Planar Imaging)

Giuseppe Rubini and Filippo Antonica

Background Clinical Case

A 58-year-old woman with a recent vaginal bleeding episode underwent hysteroscopic endometrial biopsy, which showed a grade 1 endometrial carcinoma. Routine blood chemistry was normal, except for mild anemia. The patient was submitted to radioguided sentinel lymph node biopsy.

Lymphoscintigraphy

The day before surgery, lymphoscintigraphy was performed following submucosal injections of 0.6 mL of a of 18 MBq ^{99m}Tc-albumin nanocolloid (divided into four aliquots) around the tumor under endoscopic guidance. A dual-detector SPECT gamma camera (Millennium MG, GE Healthcare, Milwaukee, WI) equipped with low-energy high-resolution (LEHR) collimators was used to obtain abdominal-pelvic dynamic images immediately after radiopharmaceutical injection and planar static images at 30 min and 12 h after radiopharmaceutical injection. Dynamic images (1frame 60 s/30 frames) were acquired in anterior and posterior projection with a 256×256 matrix and zoom factor 1.00, while static images were acquired in anterior and posterior projection with an acquisition time of 600 s, matrix 128×128 and zoom factor 1.00.

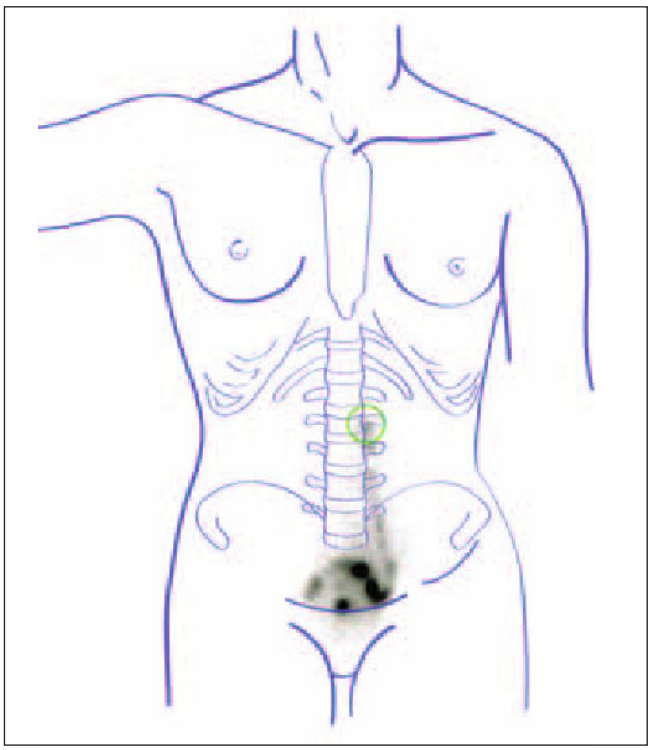

Fig. 1 Schematic representation of an anterior static planar image of the abdominal-pelvic region 30 min after four peritumoral radiopharmaceutical injections shows a left para-aortic sentinel lymph node (*green circle*)

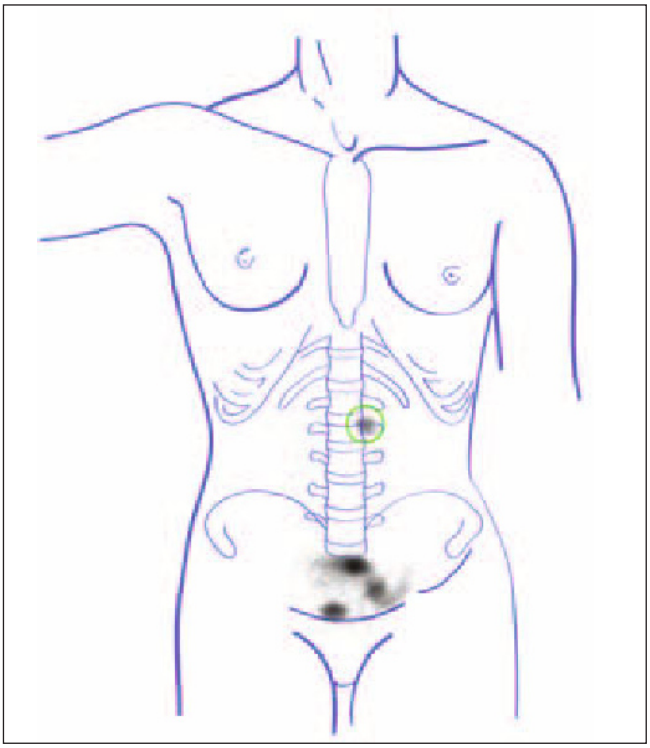

Fig. 2 Schematic representation of anterior static planar image of the abdominal-pelvic region 12 h following radiopharmaceutical injections. Uptake of the left para-aortic sentinel lymph node (*green circle*) has increased over time with respect to the previous image (**Fig. 1**)

Case 14.3
Sentinel Node Mapping in Endometrial Carcinoma: Drainage to One-Sided Lumbo-Aortic Nodes After Intratumoral Injection (Planar and SPECT/CT Imaging)

Sergi Vidal-Sicart

Background Clinical Case

A 63-year-old woman with a grade III endometrial carcinoma and a depth myometrial invasion higher than 50% was admitted in our hospital. The body mass index was 26.3 and she was scheduled for a laparoscopic assisted vaginal hysterectomy and a complete pelvic and paraaortic lymphadenectomy as well as radioguided biopsy of the sentinel lymph node.

Lymphoscintigraphy

In the afternoon before surgery, lymphoscintigraphy was performed following intratumoral injection of 8 mL containing 148 MBq ^{99m}Tc-nanocolloid with transvaginal ultrasound guidance. Planar images (256×256 matrix and 300 s each) were acquired in anterior views at 30 min and 2 h after radiotracer administration.

A dual-detector SPECT/CT gamma camera (Infinia Hawkeye 4, GE, Milwauke, WI) equipped with low-energy high-resolution (LEHR) collimators and multislice spiral CT was used to obtain abdominopelvic planar images as well as SPECT/CT acquisition. SPECT acquisition was performed using a step-and-shoot protocol of 20 s every 3 degrees.

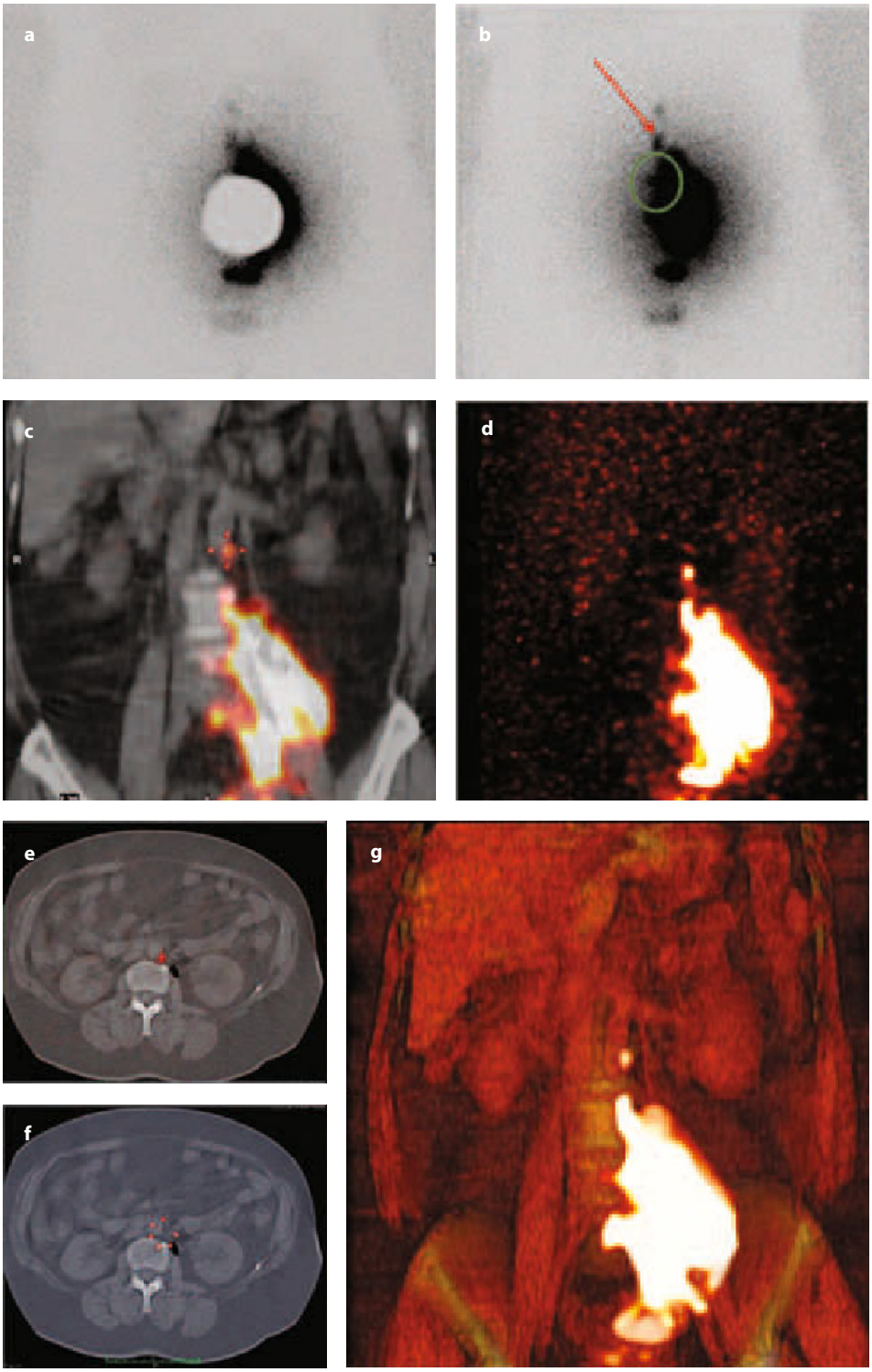

Fig. 1 **a** Early (30 min) planar image did not clearly show the potential sentinel nodes. Tracer spread was observed even with a lead shield covering the central injection points. **b** The image obtained at 2 h depicted a potential sentinel node in the central abdominal cavity (*red arrow*) and other potential nodes cranially and caudally (*green circle*). **c** Coronal fused SPECT-CT image depicted these potential nodes but only the most cranial was considered as a true sentinel node based on the maximum intensity projection and planar images (**d**). **e**, **f** Axial fused and CT slices showed a well-defined para-aortic node. **g** Volume rendering image nicely defined this paraaortic uptake. Tracer spread into the abdominal cavity is a major drawback in endometrial cancer if myometrial injection is performed. The use of SPECT-CT can solve some problems but not always

Case 14.4
Sentinel Node Mapping in Cervical Carcinoma: Drainage to Bilateral Iliac Nodes After Submucosal Peritumoral Injection (Planar and SPECT/CT Imaging)

Sergi Vidal-Sicart

Background Clinical Case

A 36-year-old lady with uterine cervical carcinoma (T1b-N0M0; stage Ib1) was referred for laparoscopic Celio-Scahuta procedure with radioguided biopsy of the sentinel lymph node. The body mass index was 19.3. Pelvic MRI showed that the tumor involved the cervical stroma up to 5 mm in depth.

Lymphoscintigraphy

In the afternoon before surgery, lymphoscintigraphy was performed following peritumoral injection of 4 aliquots of 0.5 mL each (total volume 2 mL) containing 111 MBq ^{99m}Tc-nanocolloid. Planar images (256×256 matrix and 300 s each) were acquired in anterior and right and left lateral views at 30 min and 2 h after radiotracer administration.

A dual-detector SPECT/CT gamma camera (Infinia Hawkeye 4, GE, Milwauke, WI) equipped with low-energy high-resolution (LEHR) collimators and multislice spiral CT was used to obtain abdominopelvic planar images as well as SPECT/CT acquisition. SPECT acquisition was performed using a step-and-shoot protocol of 20s every 3 degrees.

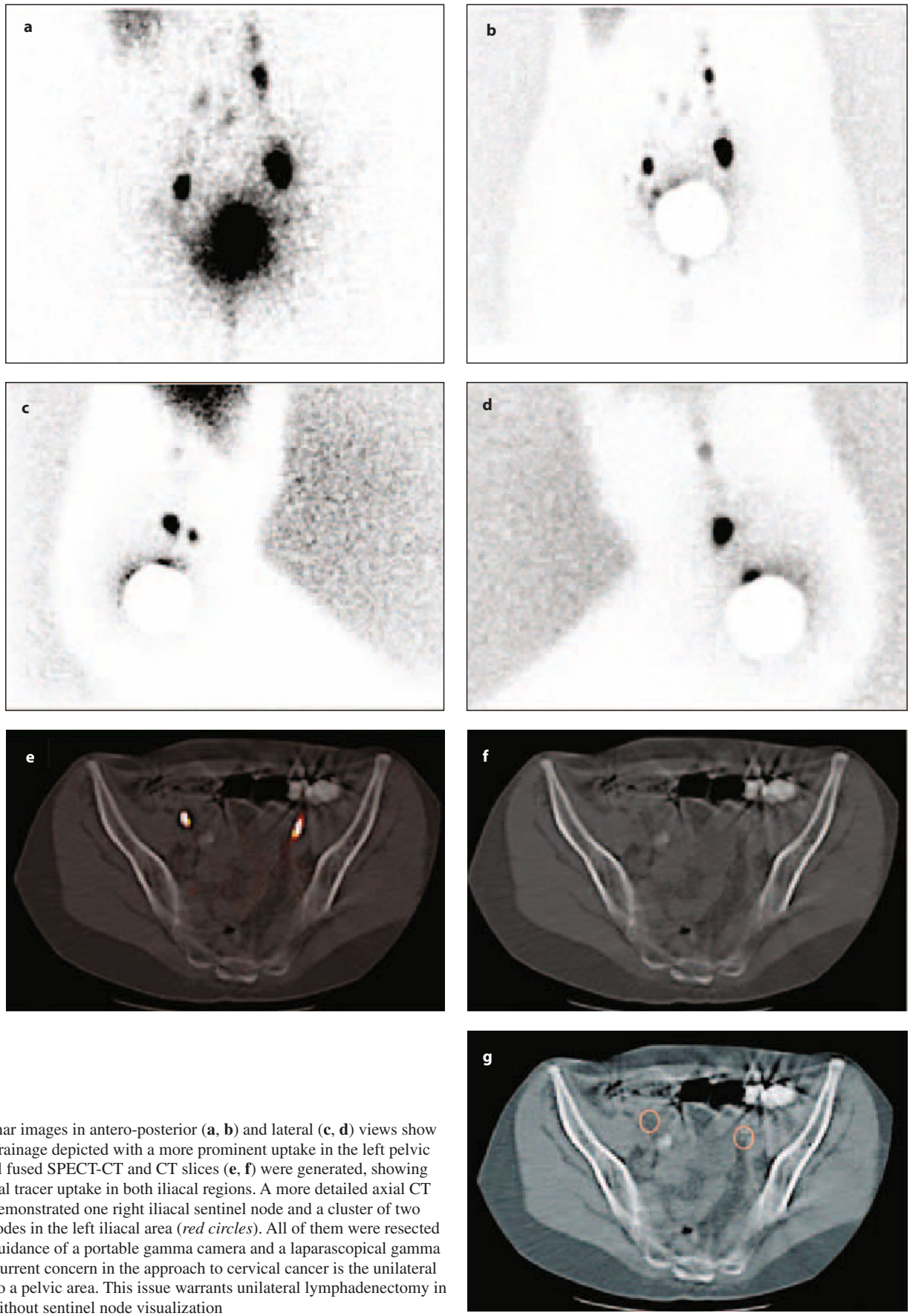

Fig. 1 Planar images in antero-posterior (**a**, **b**) and lateral (**c**, **d**) views show bilateral drainage depicted with a more prominent uptake in the left pelvic side. Axial fused SPECT-CT and CT slices (**e**, **f**) were generated, showing the bilateral tracer uptake in both iliacal regions. A more detailed axial CT slice (**g**) demonstrated one right iliacal sentinel node and a cluster of two sentinel nodes in the left iliacal area (*red circles*). All of them were resected with the guidance of a portable gamma camera and a laparascopical gamma probe. A current concern in the approach to cervical cancer is the unilateral drainage to a pelvic area. This issue warrants unilateral lymphadenectomy in the area without sentinel node visualization

References

1. DiSaia PJ, Creasman WT, Rich WM (1979) An alternate approach to early cancer of the vulva. Am J Obstet Gynecol 133:825–832
2. Hacker NF, Berek JS, Lagasse LD et al (1983) Management of regional lymph nodes and their prognostic influence in vulvar cancer. Obstet Gynecol 61:408-412
3. Iversen T, Aas M (1983) The lymph drainage of the vulva. Gynecol Oncol 16:179-189
4. O'Boyle JD, Coleman RL, Bernstein SG et al (2000) Intraoperative lymphatic mapping in cervix cancer patients undergoing radical hysterectomy: a pilot study. Gynecol Oncol 79:238–243
5. Verheijen RH, Pijpers RJ, Van Diest PJ et al (2000). Sentinel node detection in cervical cancer. Obstet Gynecol 96:135–138
6. Negishi H, Takeda M, Fujimoto T et al (2004) Lymphatic mapping and sentinel node identification as related to the primary sites of lymph node metastasis in early stage ovarian cancer. Gynecol Oncol 94:161–166
7. Burger MP, Hollema H, Emanuels AG et al (1995) The importance of the groin node status for the survival of T1 ad T2 vulval carcinoma patients. Gynecol Oncol 57:327–334
8. Hackett TE, Olt G, Sorosky JI et al (1995) Surgical predictors of para-aortic metastases in early-stage cervical carcinoma. Gynecol Oncol 59:15–19
9. Lécuru F, Mathevet P, Querleu D et al (2011) Bilateral negative sentinel nodes accurately predict absence of lymph node metastasis in early cervical cancer: results of the SENTICOL study. J Clin Oncol 29:1686–1691
10. Khoury-Collado F, Murray MP, Hensley ML et al (2011) Sentinel lymph node mapping for endometrial cancer improves the detection of metastatic disease to regional lymph nodes. Gynecol Oncol 122:251–254
11. van Der Zee AG, Oonk MH, de Hullu JA et al (2008) Sentinel node dissection is safe in the treatment of early-stage vulvar cancer. J Clin Oncol 26:884–889
12. Zarganis P, Jondi-Pafiti A, Arapantoni-Dadioti P et al (2009) The sentinel node in cervical cancer patients: role of tumor size and invasion of lymphatic vascular space. In Vivo 23:469–473
13. Altgassen C, Hertel H, Brandstädt A et al (2008) Multicenter validation study of the sentinel lymph node concept in cervical cancer: AGO Study Group. J Clin Oncol 26:2943–2951
14. Ballester M, Dubernard G, Lécuru F et al (2011) Detection rate and diagnostic accuracy of sentinel-node biopsy in early stage endometrial cancer: a prospective multicentre study (SENTI-ENDO). Lancet Oncol 12:469–476
15. Hampl M, Hantschmann P, Michels W et al (2008) Validation of the accuracy of the sentinel lymph node procedure in patients with vulvar cancer: results of a multicenter study in Germany. Gynecol Oncol 111:282–288
16. Bats AS, Clement D, Larousserie F et al (2008) Does sentinel node biopsy improve the management of endometrial cancer? Data from 43 patients. J Surg Oncol 97:141–145
17. Perrone AM, Casadio P, Formelli G et al (2008) Cervical and hysteroscopic injection for identification of sentinel lymph node in endometrial cancer. Gynecol Oncol 111:62–67
18. Holub Z, Jabor A, Kliment L (2002) Comparison of two procedures for sentinel lymph node detection in patients with endometrial cancer: a pilot study. Eur J Gynaecol Oncol 23:53–57
19. Abu-Rustum NR, Khoury-Collado F, Pandit-Taskar N et al (2009) Sentinel lymph node mapping for grade 1 endometrial cancer: is it the answer to the surgical staging dilemma? Gynecol Oncol 113:163–169
20. Clement D, Bats AS, Ghazzar-Pierquet N et al (2008) Sentinel lymph nodes in endometrial cancer: is hysteroscopic injection valid? Eur J Gynaecol Oncol 29:239–241
21. Lopes LA, Nicolau SM, Baracat FF et al (2007) Sentinel lymph node in endometrial cancer. Int J Gynecol Cancer 17:1113–1117
22. Altgassen C, Pagenstecher J, Jornung D et al (2007) A new approach to label sentinel nodes in endometrial cancer. Gynecol Oncol 105:457–461
23. Frumovitz M, Bodurka DC, Broaddus RR et al (2007) Lymphatic mapping and sentinel node biopsy in women with high-risk endometrial cancer. Gynecol Oncol 104:100–103
24. Vermeeren L, Valdés Olmos RA, Meinhardt W et al (2009) Value of SPECT/CT for detection and anatomic localization of sentinel lymph nodes before laparoscopic sentinel node lymphadenectomy in prostate carcinoma. J Nucl Med 50:865–870
25. Martínez A, Zerdoud S, Mery E et al (2010) Hybrid imaging by SPECT/CT for sentinel lymph node detection in patients with cancer of the uterine cervix. Gynecol Oncol 119:431–435
26. Pandit-Taskar N, Gemignani ML, Lyall A et al (2010) Single photon emission computed tomography SPECT-CT improves sentinel node detection and localization in cervical and uterine malignancy. Gynecol Oncol 117:59–64
27. Levenback C, Coleman RL, Burke TW et al (2001) Intraoperative lymphatic mapping and sentinel node identification with blue dye in patients with vulvar cancer. Gynecol Oncol 83:276–281
28. Vidal-Sicart S, Puig-Tintore LM, Lejarcegui JA et al (2007) Validation and application of the sentinel lymph node concept in malignant vulvar tumours. Eur J Nucl Med Mol Imaging 34:384–391
29. Hauspy J, Beiner M, Harley I et al (2007) Sentinel lymph nodes in early stage cervical cancer. Gynecol Oncol 105:285–290
30. Cibula D, Kuzel D, Sláma J et al (2009) Sentinel node (SLN) biopsy in the management of locally advanced cervical cancer. Gynecol Oncol 115:46–50
31. Ortega J, Ferrer-Rebolleda J, Cassinello N, Lledo S (2007) Potential role of a new handheld miniature gamma camera in performing minimally invasive parathyroidectomy. Eur J Nucl Med Mol Imaging 34:165-169
32. Vidal-Sicart S, Paredes P, Zanón G et al (2010) Added value of intraoperative real-time imaging in searches for difficult-to-locate sentinel nodes. J Nucl Med 51:1219–1225
33. Niikura H, Okamura C, Utsunomiya H et al (2004) Sentinel lymph node detection in patients with endometrial cancer. Gynecol Oncol 92:669–674

Preoperative and Intraoperative Lymphatic Mapping for Radioguided Sentinel Node Biopsy in Cancers of the Male Reproductive System

15

Oscar R. Brouwer, Willem Meinhardt, Simon Horenblas, and Renato A. Valdés Olmos

15.1 Introduction

This chapter describes the principles of lymphatic mapping and sentinel lymph node biopsy (SLNB) for cancers of the male reproductive system, which includes penile, prostate, and testicular cancer.

15.1.1 Penile Cancer

Penile cancer is a relatively rare disease in the western world, with an incidence of approximately 1 per 100,000 [1]. Nearly all penile tumors are squamous cell carcinomas. The presence of lymph node involvement is the single most important prognostic factor for cancer-specific death [2]. Since the introduction of the concept in penile carcinoma by Cabanas in 1977 [3], the sentinel lymph node (SLN) procedure has evolved into a reliable staging technique, with a low complication rate compared to (prophylactic) inguinal lymphadenectomy [4].

15.1.2 Prostate Cancer

In prostate cancer, lymph node staging may be important for both prognosis and therapeutic management. The presence of lymph node metastases may lead to avoidance of local therapy with curative intents, such as radiotherapy or radical (salvage) prostatectomy, and influences the duration of androgen-deprivation therapy [5]. To date, none of the available noninvasive diagnostic imaging modalities provide a reliable assessment of lymph node (micro)metastases. Therefore, surgical staging by extended pelvic lymphadenectomy (EPL) is still the current standard of care. However, SLNB is emerging as an alternative staging method, with a lower incidence of complications and with the potential to identify relevant lymph nodes outside the standard EPL field [6].

15.1.3 Testicular Cancer

Testicular cancer is the most frequent malignancy in young men, and the incidence has risen by almost 100% in the last 20 years. At the time of diagnosis, approximately two-thirds of patients have clinical stage I disease [7]. The optimal management of regional lymph nodes in stage I testicular cancer remains controversial. A surveillance policy requires intensive, frequent follow-up visits with costly examinations, and defers detection and treatment of lymph node metastases to a later stage. There is a need for diagnostic techniques that enable patients with lymph node metastasis to be treated at an early stage, while preventing unnecessary treatment for those patients without metastasis. In this respect, the SLN procedure is potentially highly valuable [8, 9].

15.2 The Clinical Problem

15.2.1 Penile Cancer

There is no consensus on the management of patients with clinically node-negative (cN0) penile carcinoma, in whom radical inguinal lymph node dissection (ILND) is routine [10]. However, only 20–25% of these patients harbor occult nodal metastasis. This means that, although prophylactic inguinal lymphadenectomy offers the best chance of cure, it is unnecessary in approximately 75–80% of patients [10]. In addition, this procedure is associated with substantial morbidity, such as lymphedema and infections. As currently

O. R. Brouwer (✉)
Nuclear Medicine, Division of Diagnostic Oncology
Netherlands Cancer Institute – Antoni van Leeuwenhoek Hospital
Amsterdam, the Netherlands
e-mail: oscarbrouwer@gmail.com

G. Mariani et al. (eds.), *Atlas of Lymphoscintigraphy and Sentinel Node Mapping*,
DOI 10.1007/978-88-470-2766-4_15

available noninvasive staging techniques lack sufficient accuracy, minimally invasive staging remains necessary for the time being. However, since its clinical introduction in 1994, there have been reservations about the use of radioguided SLNB for penile cancer, because of the supposedly long learning curve associated with the procedure and the possibility of false-negative cases (reported in up to 21% of the procedures) [11]. After analysis of false-negative cases, several modifications were made to the dynamic sentinel node biopsy (DSNB) procedure, to increase its sensitivity [12].

15.2.2 Prostate Cancer

Although extended pelvic lymphadenectomy (EPL) is the gold standard for the identification of lymph node metastasis in patients with prostate cancer, the incidence of postoperative complications increases with the number of excised lymph nodes, ranging from 10.5% for 1–5 lymph nodes to 24.3% when dissection includes more than 20 lymph nodes. The advantages of the sentinel node dissection are a lower incidence of complications and the possibility of identifying tumor-draining lymph nodes outside the field of an EPL [6]. However, accurate laparoscopic localization of sentinel nodes in the pelvis can be challenging, especially when SLNs are located near the prostatic injection site (because of the high radioactive background signal), or in the case of aberrantly located sentinel nodes (e.g., para-aortic) [13].

15.2.3 Testicular Cancer

To date, large-scale randomized clinical studies to validate and assess the added benefit of SLNB for testicular cancer are still lacking. This may be partially due to the fact that patients are usually referred to tertiary, specialized centers only after orchidectomy has already been performed, thus after removal of the potential injection site. Furthermore, although lymphatic drainage of the testis is mainly directed towards the areas along the aorta and vena cava, aberrant drainage has also been observed [9]. The identification of these SLNs in relation to the anatomical structures can be difficult using two-dimensional (2D) lymphoscintigraphy alone.

15.3 Indications and Contraindications for Sentinel Lymph Node Biopsy

15.3.1 Penile Cancer

Patients with >T1G2 tumors and cN0 groins defined by ultrasound-guided fine needle cytology are eligible for SLNB. Repeat SLNB after tumor recurrence is also a validated procedure [14]. If the sentinel node is tumor positive, completion ipsilateral lymphadenectomy is performed. Groins with tumor-free lymph nodes are managed with close surveillance, thereby avoiding the morbidity associated with lymphadenectomy.

15.3.2 Prostate Cancer

The chances of having lymph node metastasis from prostate cancer increase with the serum level of prostate-specific antigen (PSA), the biopsy grade (Gleason score), and clinical T stage. SLNB is generally reserved for patients in the intermediate-risk group (clinical stage >T2b/T3, PSA >10 ng/mL, or Gleason >6). Nevertheless, SLNB has been able to identify metastases in as many as 6.8% to 10.7% of patients with favorable risk factors [15]. In the intermediate-risk group, a tumor-bearing SLN may influence the boundaries of the radiotherapy field and duration of hormonal (androgen-deprivation) therapy. Another possible indication is to select patients who are eligible for salvage treatment of the prostate, as the usual parameters to stratify patients in risk groups do not apply to patients with intraprostatic recurrence [5]. Since salvage treatment of the prostate may result in serious complications, it should be considered when the prostate is actually the only tumor-bearing site.

15.3.3 Testicular Cancer

SLNB was introduced for patients with stage I disease. Clinical stage I seminoma and non-seminoma are defined by a negative computed tomography (CT) scan of the chest, abdomen, and pelvis, plus normal or normalized serum values of alpha-fetoprotein (AFP), human chorionic gonadotropin (HCG), and lactate dehydrogenase (LDH). In the case of mixed seminomatous/non-seminomatous tumors, treatment decisions are based on the factor with the highest malignant potential, which is the non-seminoma component. Generally, the absence of lymph nodes larger than 1 cm results in assignment of clinical stage I.

15.4 Radiocolloid and Modalities of Injection

15.4.1 Penile Cancer

The tracer (technetium-99 [^{99m}Tc]-nanocolloid in most European countries) is injected intradermally. In fact, subcutaneous administration is easier to accomplish, but may not accurately identify the route of drainage from an overlying cutaneous site. Furthermore, lymphatic drainage from the dermis is much faster than drainage from subcutaneous tissue.

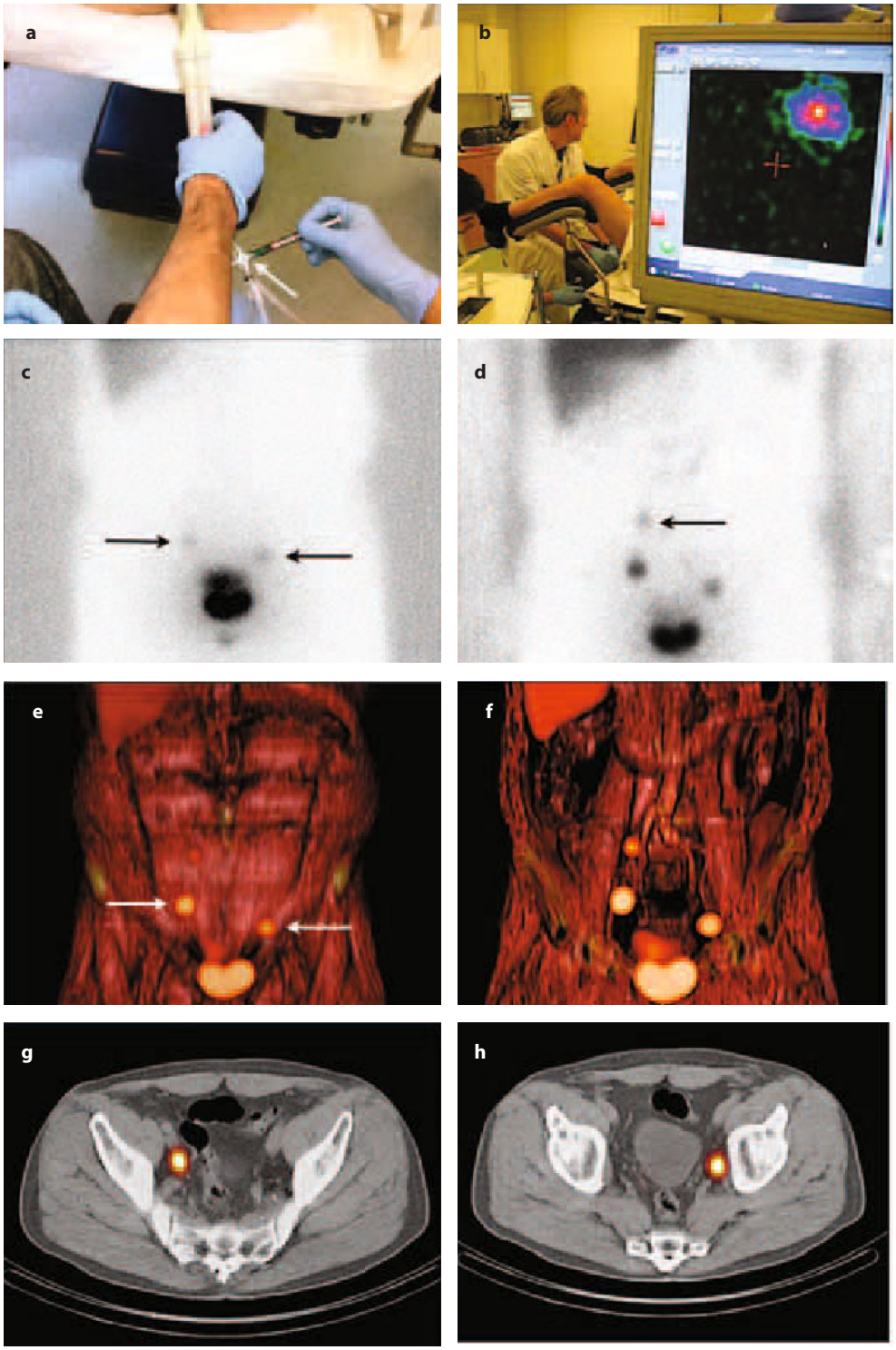

Fig. 15.1 Preoperative SLN mapping in a 65-year-old patient with intermediate-risk prostate cancer. **a** Tracer administration with transrectal ultrasound guidance using a long needle and a three-way system. **b** The radiocolloid is divided in 2–4 injections. The procedure is monitored using a portable gamma camera to verify adequate tracer retention within the prostate. **c** Early planar lymphoscintigram showing two sentinel nodes with direct drainage from the prostate (*arrows*). **d** The delayed lymphoscintigram enables differentiation of the sentinel nodes and a higher-echelon lymph node (*arrow*). **e**, **f** Three-dimensional (3D) volume-rendered SPECT/CT image displaying the location of the sentinel nodes in more detail (*arrows*). **g** Axial fused SPECT/CT image showing the sentinel node on the right side along the external iliac veins, and **h** the sentinel node on the left side in the obturator fossa

Application of a spray containing xylocaine 10%, 30 minutes before tracer administration, is recommended. As an alternative, a lidocaine/prilocaine-based crème can be used. This local anesthesia ensures that the radiocolloid injections are well tolerated and relatively easy to perform. A volume of 0.3 mL containing approximately 75 MBq divided into three depots (0.1 mL each) is subsequently administered intradermally around the tumor. Each depot is injected raising a bleb. The radiocolloid is injected proximally from the tumor. For large tumors not restricted to the glans, the radiocolloid can be injected in the prepuce. Injection margins within 1 cm from the primary tumor are recommended. A

reproducibility rate of 100% for penile lymphoscintigraphy has been reported with an injection distance of 5 mm [16]. In patients with a previous excision biopsy scar, injections may also be administered using similar margins.

15.4.2 Prostate Cancer

Most of the experience in the SLN procedure for prostate cancer has been acquired in European countries and the most frequently used radiopharmaceutical has been ^{99m}Tc-nanocolloid. Transrectal intraprostatic injection is guided by (transrectal) ultrasound, injecting the radiocolloid under continuous monitoring using a needle of 0.5×150 mm (Fig. 15.1). Prostate cancer may be multifocal; therefore injections are performed in both lobes. An activity of about 240 MBq in 0.4 mL is recommended. The lymph node visualization rate tends to be less optimal when lower activities are used. The particle concentration also appears to be important, and the use of a reduced labeling dilution volume (0.4 mL ^{99m}Tc per 0.2 mg nanocolloid) yields more visualized sentinel nodes with higher radioactivity count rates [17]. The radiocolloid is divided into 2–4 injections, depending on the prostate volume. A three-way system is recommended, and after each depot saline is used for flushing the residual radioactivity in the needle.

15.4.3 Testicular Cancer

The route of administration of ^{99m}Tc-nanocolloid was evaluated in a feasibility study in stage I testicular cancer [8]. While funicular administration showed only lymph node uptake in the inguinal region (which does not reflect the actual testicular tumor drainage pattern), intratesticular administration resulted in visualization of retroperitoneal sentinel node(s), in accordance with known drainage patterns. No side effects were observed using the latter method, which proved to be easy to perform and was well tolerated under local anesthesia (funicular block using lidocaine 2%, performed by the urologist in the outpatient clinic). Generally, a single aliquot of radioactivity (approximately 100 MBq) in a volume of 0.2 mL is injected into the testicular parenchyma with a fine needle.

15.5 Preoperative Imaging of Sentinel Lymph Nodes

15.5.1 Penile Cancer

Lymphoscintigraphy after radiocolloid injection consists of two phases: (a) dynamic scintigraphy, performed during the first 10 minutes after radiocolloid injection, preferably in both the anterior and lateral views. The dynamic study is helpful to identify lymphatic ducts and the first directly draining lymph nodes; (b) static planar imaging at 20–30 minutes and at 2 hours. The early planar images visualize the first draining lymph nodes in about 85% of cases. Additional images at 4 hours, or radiocolloid reinjection are recommended when no SLNs are visualized. Generally, the lymph nodes draining directly from the injection site are classified as sentinel nodes. In the case of multiple visible nodes without visible afferent vessels, the first node appearing in a basin is considered to be the SLN.

15.5.2 Prostate Cancer

In the pelvis, lymphatic ducts are seldom visualized and the relatively slower deep lymphatic drainage renders dynamic lymphoscintigraphy less useful. Early planar images of lymphoscintigraphy acquired 15 minutes after radiocolloid administration can visualize the first draining lymph nodes in almost 88% of cases [18]. Delayed imaging may be performed 2–4 hours after injection. On delayed imaging, the lymph node visualization rate increases to more than 95%. Comparing the early and delayed images enables differentiation of second-echelon lymph nodes from the first draining nodes. This discrimination is based on the anatomical lymph node basins of the pelvis. As a rule, late-appearing lymph nodes located higher in the same basin are considered as second-echelon lymph nodes. Late-appearing lymph nodes in distal or more ventral and dorsal basins suggest direct draining from the prostate. These lymph nodes may also be considered as sentinel nodes. If no single photon emission tomography/computed tomography (SPECT/CT) is available, lateral planar images can differentiate between dorsal and more ventrally located SLNs.

15.5.3 Testicular Cancer

The fast lymphatic drainage from the testicle requires dynamic gamma camera acquisition to facilitate differentiation between first- and second-echelon lymph nodes in the retroperitoneum. Immediately following radiocolloid injection, anterior and lateral dynamic images are obtained with a dual-head gamma camera over 10 minutes, and the lymphatic flow and early-draining lymph nodes are visualized in almost all cases. Static images are obtained 5 minutes after the dynamic study. Late static images are obtained 2–4 hours after injection and are required to differentiate first-echelon nodes from higher-echelon nodes (if there is no visualization of sentinel nodes on the early dy-

namic and static images), and to identify unexpected drainage patterns.

15.6 Lymphatic Drainage

15.6.1 Penile Cancer

The most frequently visualized lymphatic drainage pattern is bilateral drainage to both groins (80%). This pattern is, however, asynchronous in two-thirds of cases, and visualization of the contralateral lymph nodes is often only possible on delayed imaging [19]. Drainage from the injection site mostly occurs through one or two visualized afferent lymphatic ducts leading to one or two SLNs in each groin. In some cases, a cluster of inguinal lymph nodes is observed.

15.6.2 Prostate Cancer

The main lymph node basins where the prostate drains generally follow the iliac vessels [20]. The common iliac lymph nodes are located caudally of the aortic bifurcation and are subdivided into a lateral, medial, and middle group. This latter basin is located in the lumbosacral fossa and is demarcated by the promontorium, the psoas muscle, and the common iliac vessels. The external iliac lymph nodes are located caudally to the bifurcation of the common iliac vessels and cranially to the inguinal ligament; they are also subdivided into lateral, middle, and medial groups. The lateral (lateral of the artery) and middle (between the artery and the vein) lymph nodes are located more in the proximity of the anterior abdominal wall, while the medial nodes are located along the cranial segment of the external iliac artery. Although "subject of debate", the obturator lymph nodes are generally considered to be part of the medial subgroup. The internal iliac lymph nodes are located more posteriorly in the pelvis and include the lateral sacral nodes (adjacent to the paired lateral sacral arteries), the presacral nodes (anterior to the sacrum and posterior to the mesorectal fascia), and the anterior nodes (at the origin of the proximal branches of the anterior division of the internal iliac artery; this subgroup includes the hypogastric nodes).

15.6.3 Testicular Cancer

Lymphatics from the right testis drain primarily to regions lateral, anterior, and medial to the vena cava and anterior to the aorta (Fig. 15.2). Lymphatic drainage from the left testis is primarily directed towards areas lateral, anterior, and medial to the aorta. SLNs may therefore be preoperatively detected at interaortocaval, para-aortic, or pre-aortic locations.

15.7 Intraoperative Detection of Sentinel Lymph Nodes

15.7.1 Penile Cancer

As is customary for SLNB in melanoma and breast cancer, intraoperative sentinel node detection is guided by a gamma-ray detection probe and blue dye. After excision of all preoperatively defined SLNs, it is important to carefully search for any residual radioactivity using the probe, to ensure that no remaining/additional sentinel nodes are left behind. Furthermore, intraoperative palpation of the wound should take place, to identify suspicious lymph nodes that failed to pick up any radiocolloid [21].

15.7.2 Prostate Cancer

Initial validation of the SLNB in prostate cancer was based on open surgery and the use of a gamma-ray detection probe to guide detection of the radioactive sentinel nodes. More recently, laparoscopic SLNB has been validated, and the feasibility of robot-assisted SLNB has been demonstrated. In either approach, SLN localization is guided by a laparoscopic gamma probe [22]. Deeply located SLNs can be difficult to localize using a gamma-ray detection probe, because of tissue attenuation and because the large amount of radioactivity at the injection site may cause SLNs located nearby to be missed.

15.7.3 Testicular Cancer

SLNB in testicular cancer was introduced in a laparoscopic setting. As such, intraoperative SLN localization is also guided by the acoustic signals originated by a laparoscopic gamma-ray detection probe [9].

15.8 Contribution of SPECT/CT

15.8.1 Penile Cancer

SPECT/CT images are usually acquired after the 2-hour planar images, and contribute to better understanding of the location of the SLNs in penile carcinoma (Figs. 15.1 and 15.3). SPECT/CT enables anatomical localization of the sentinel nodes that were previously identified by lymphoscintigraphy. For instance, the modality can differentiate inguinal from iliac (most frequently second-echelon) lymph nodes. Moreover, SPECT/CT enables visualization of the SLNs in the so-called Daseler's superior and central inguinal zones, which are superior and directly overlying to the saphenofemoral junction, respectively. SPECT/CT has confirmed that

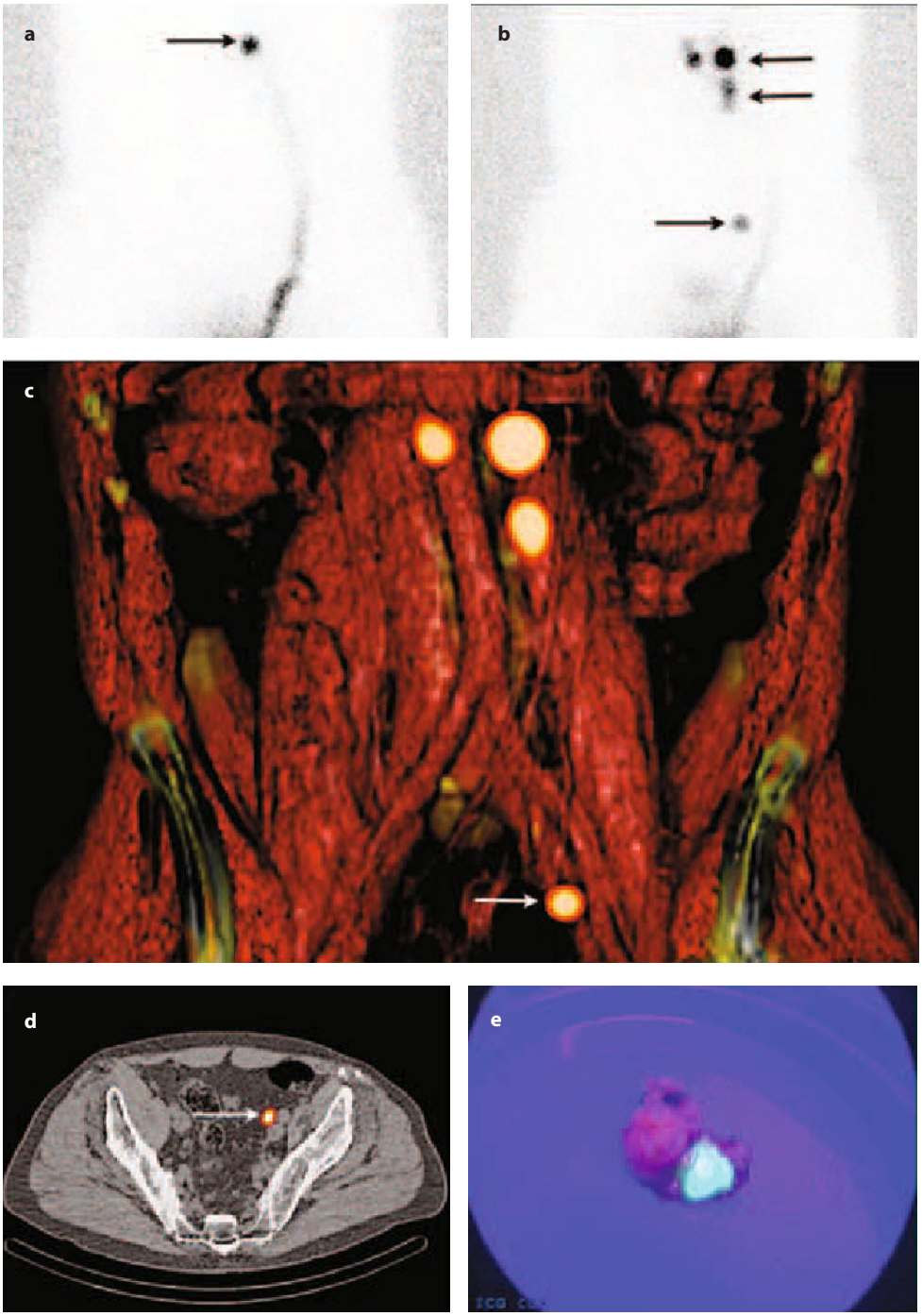

Fig. 15.2 Intratesticular injection of hybrid ICG–^{99m}Tc-nanocolloid (67.7 MBq) in a 52-year-old male patient with a seminoma in his left testicle, followed by lymphoscintigraphy and SPECT/CT. **a** Early planar anterior image showing drainage from the left testicle towards an abdominal sentinel node (*arrow*). **b** The delayed lymphoscintigram reveals an additional sentinel node just below the sentinel node that was visualized on the early image (*upper arrows*), a second-echelon node to the right, and an additional hotspot located more caudally (*lower arrow*), which was therefore also defined as a sentinel node. **c** Fused SPECT/CT image displayed with 3D volume rendering, showing the cranial two sentinel nodes alongside the aorta, the interaortocaval second-echelon node, and the more caudal sentinel node (*arrow*) next to the funiculus. **d** Axial fused SPECT/CT image depicting the caudal sentinel node along the external iliac vessels next to the funiculus. All sentinel nodes were excised during laparoscopy guided by a laparoscopic gamma probe and fluorescence endoscope. **e** Ex-vivo fluorescence image of a para-aortic sentinel node, revealing the location of the node within the excised tissue specimen

in the majority of patients, SLNs are found in the superior medial (73%), superior lateral (9%), and central quadrants (18%). Lymphatic drainage to the inferior quadrants is rare. Finally, SPECT/CT is able to identify contamination of the skin with the radiocolloid, an occurrence that can sometimes be erroneously interpreted on planar lymphoscintigrams as lymph nodes.

15.8.2 Prostate Cancer

Hybrid imaging with SPECT/CT enables anatomical localization of SLNs. A 98% sentinel node visualization rate has been reported for SPECT/CT (versus 91% for planar imaging). Moreover, in 96% of cases SLNs are localized inside the area of EPL; nevertheless, there is a considerable number

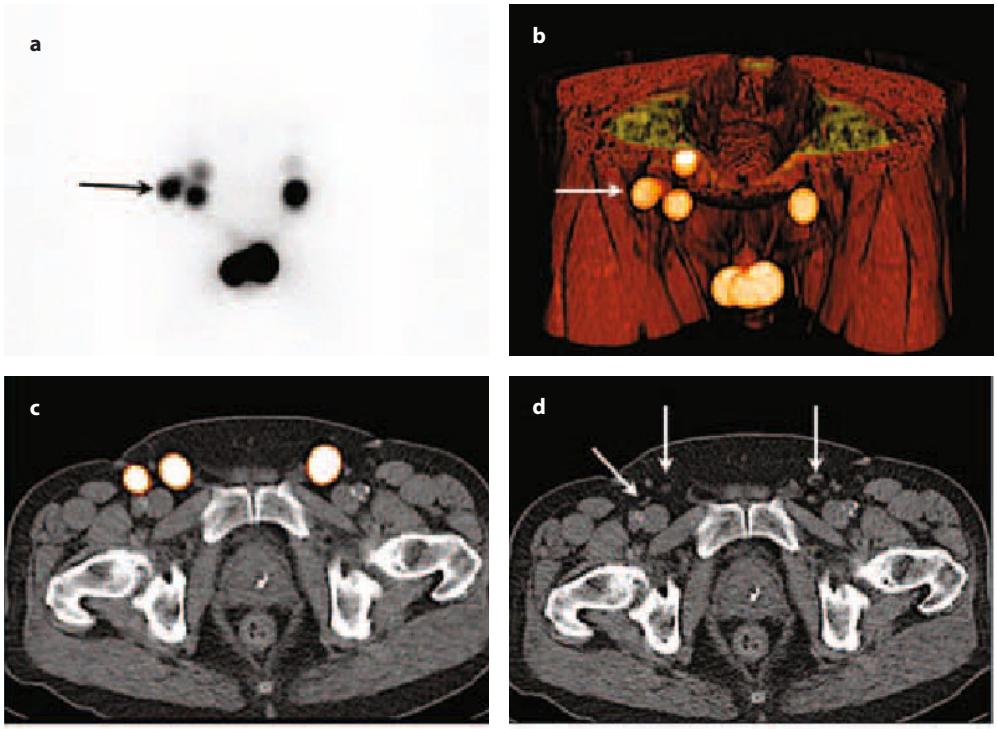

Fig. 15.3 **a** Intradermal injection of 82.92 MBq ^{99m}Tc-nanocolloid, resulting in visualization of a sentinel node in both groins, with a second more laterally localized sentinel node on the right side (*arrow*) on delayed planar lymphoscintigraphy. **b** 3D volume-rendered SPECT/CT images revealing a sentinel node in the superior medial quadrant on both sides, and a sentinel node in the superior lateral quadrant on the right side (*arrow*). The image also shows a second-echelon node in the right iliac area. **c**, **d** Axial fused SPECT/CT images depicting both radioactive sentinel nodes with the corresponding lymph nodes on CT (*arrows*). Histopathological examination revealed micrometastases in the left excised sentinel node

of SLNs in regions not routinely excised when performing an EPL [23]. SPECT/CT is mostly performed after the delayed planar imaging, and must be interpreted in combination with lymphoscintigraphy. Sequential planar images are able to identify the lymph nodes draining directly from the tumor site, but give only limited information about their anatomical location. With SPECT/CT, it is possible to better localize SLNs both inside and outside the pelvis. In many cases, early-appearing lymph nodes seen as a single hot spot on planar imaging are displayed as separate lymph nodes in different basins by SPECT/CT, and all of them must be considered as sentinel nodes. In other cases, intense lymph node uptake seen on fused images may correspond to a cluster of SLNs as depicted on the CT component of the SPECT/CT acquisition. As such, SPECT/CT provides valuable information for the urologist, which may lead to a significant shortening of the operation time, as less-extensive exploration might be required. Furthermore, SPECT/CT may also provide important information for planning radiotherapy, concerning especially treatment volume and optimization of irradiation fields in the pelvis.

15.8.3 Testicular Cancer

In the initial feasibility study, preoperative lymphatic mapping was performed using planar lymphoscintigraphy only [8]. However, this technique can only provide 2D information, and exact preoperative anatomical SLN localization is not possible. Not only does SPECT/CT provide useful anatomic information about the location of sentinel nodes, but its improved sensitivity and the added third dimension may also lead to the detection of additional SLNs (Fig. 15.2). Sequential planar imaging will remain important for the preoperative identification of early-appearing lymph nodes as sentinel nodes. To date, only one study evaluating the use of SPECT/CT for preoperative SLN localization in testicular cancer has been published [9]. SPECT/CT enabled accurate localization of the SLNs and provided anatomical reference points to plan their laparoscopic retrieval.

15.9 Intraoperative Imaging

15.9.2 Open Surgery: Penile Cancer

Accurate staging with SLNB can only be achieved if all nodes on a direct drainage pathway from the tumor are harvested. If SLNs are left behind, this constitutes one of the potential causes for false-negative results. The integration of a portable gamma camera in the intraoperative procedure may increase the detection sensitivity, as it provides an intraoperative overview image of the radioactive SLNs and enables post-excision confirmation of complete removal of the sentinel nodes in the operating room. For optical visualization of the SLN, vital blue dyes are traditionally used. However,

SLNs do not always stain blue. Recently, a hybrid tracer comprising the fluorescent dye indocyanine green (ICG) and ^{99m}Tc-nanocolloid has been developed [24]. Adding the fluorescent moieties does not alter the biological properties of the parental radiocolloid, and it enables near-infrared fluorescence imaging of all preoperatively identified radioactive SLNs [25]. These developments may help to further refine intraoperative retrieval of SLNs.

15.9.3 Laparoscopic Surgery: Prostate Cancer and Testicular Cancer

Since the (retroperitoneal) lymphatic drainage of the prostate and testes is directed to areas deep within the abdomen that can often be complex, preoperative anatomical information about the location of the SLNs is important for planning the surgical procedure. For this reason, the SPECT/CT images should be displayed in the operating room. Urological surgery has shifted from the open approach toward less-invasive laparoscopic and robot-assisted techniques. During laparoscopic surgery, the urologist localizes a SLN under guidance by the sound pitch originated by the laparoscopic gamma probe. However, intraoperative spatial orientation using this device can sometimes be difficult, as a laparoscopic probe does not provide visual information. The use of a portable gamma camera helps to intraoperatively guide laparoscopic SLN localization. Current portable gamma cameras are capable of detecting two different signals: the signal of ^{99m}Tc-nanocolloid for the visualization of SLNs, plus the signal of an iodine-125 (^{125}I) seed pointer placed on the tip of the laparoscopic gamma-ray detection probe [26]. The "hot" tip of the probe can be moved to the hot node, guided by the image of the portable camera. This approach helps navigate towards the location of the SLNs. After removal of all SLNs, the portable gamma camera can show whether there are any remaining sentinel nodes that have to be removed, or a second-echelon node that can confidently be left in place (Fig. 15.4). This approach provides certainty about the completeness of the surgical procedure and complements the laparoscopic probe. Currently, intraoperative navigation approaches that are based on the preoperative (SPECT/CT) images are being developed [27]. In prostate cancer, sentinel nodes may be located in close proximity to the primary injection site (the prostate), where the high radioactive background signal may hinder radioguidance with the gamma probe. By injecting the aforementioned hybrid radioactive and fluorescent tracer ICG–^{99m}Tc-nanocolloid, the high resolution of near-infrared fluorescence imaging (enabled by a fluorescence endoscope) may facilitate intraoperative visualization of the SLNs that were preoperatively identified by SPECT/CT [28] (Fig. 15.6).

15.10 Common and Rare Variants

15.10.1 Penile Cancer

One of the advantages of lymphatic mapping is its ability to identify SLNs outside the usual nodal basins. In penile cancer, direct drainage to prepubic SLNs has been described [29]. In particular, dynamic lymphoscintigraphy often shows one or two lymphatic vessels leading to the sentinel node(s). Such vessels have also been observed to directly lead to deep inguinal and even to iliac SLNs.

Blockage of the lymph flow by tumor metastasis in the lymph node may cause nonvisualization and lymph rerouting, and even retrograde flow of the ^{99m}Tc-nanocolloid containing lymphatic flow. This occurrence has been visualized by SPECT/CT imaging [21].

15.10.2 Prostate Cancer

In prostate cancer, lymphoscintigraphy and SPECT/CT may identify SLNs outside the extended dissection in 31% of cases [6]. These aberrantly located SLNs can be located proximal to the most distal part of the aorta, in the vicinity of the common iliac artery above the crossing of the ureter, around the inferior mesenteric vessels, in the perivesical area, and near the umbilical ligament [30, 31].

15.10.3 Testicular Cancer

Although drainage from the testes is usually directed to paracaval, interaortocaval, and para-aortic SLNs, in some patients sentinel nodes may also be seen along the testicular vessels [9].

15.11 Technical Pitfalls

15.11.1 Penile Cancer

The most frequent pitfall is skin contamination. The high pressure of the intradermal bleb can result in leakage during injection or after removal of the needle. The use of (surgical) lights to adequately visualize the site of injection, and of a fenestrated drape to cover the area, may help to avoid skin contamination. Furthermore, voiding of radioactive urine between the early and delayed scintigraphic imaging may also cause skin contamination. The hot spots due to contamination may be confused with SLNs, thus leading to an unnecessary intraoperative pursuit. In these cases, skin decontamination is mandatory. Complementary SPECT/CT may also be helpful in detecting these artefacts. Another possible pitfall

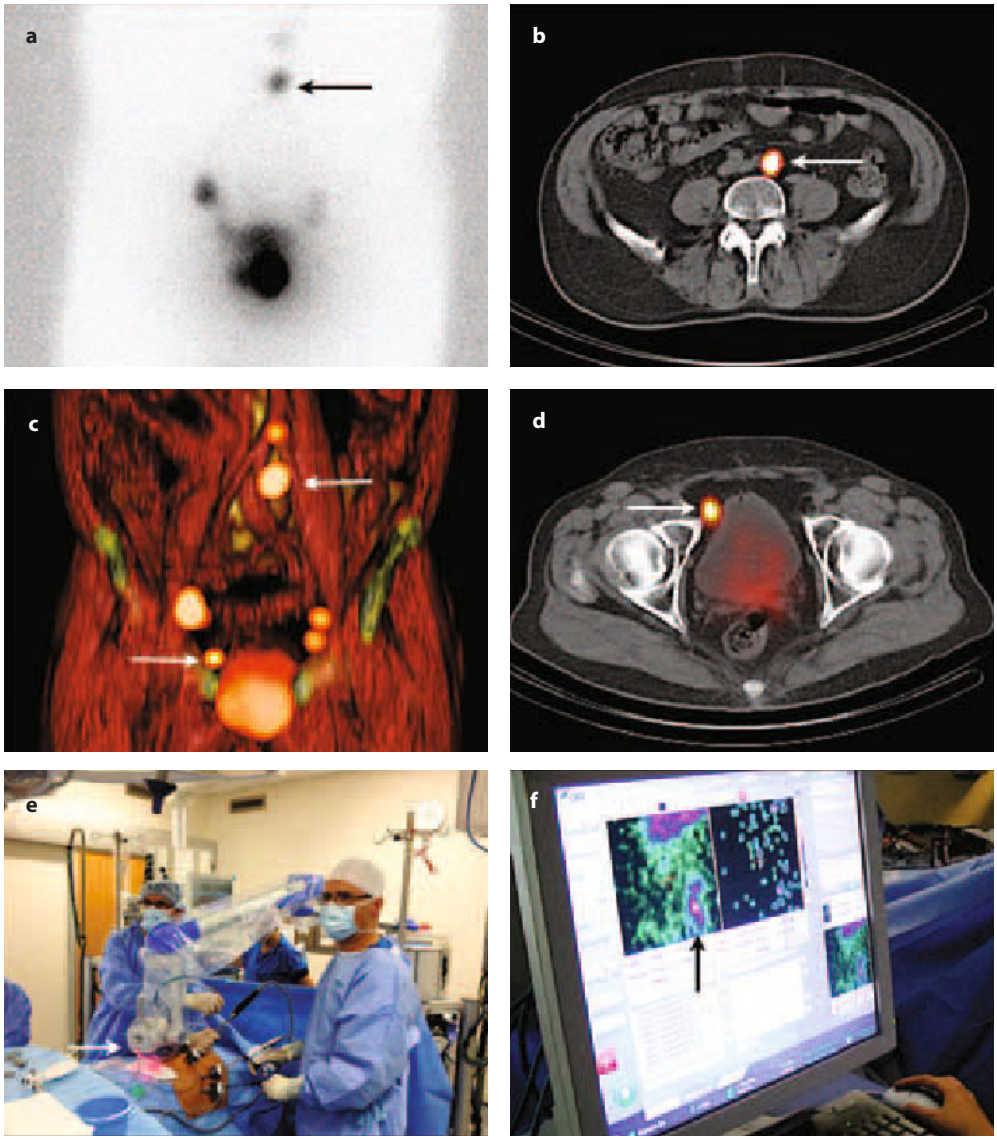

Fig. 15.4 **a** Early lymphoscintigraphy after transrectal intraprostatic tracer injection with visualization of bilateral lymphatic drainage with an early-appearing sentinel node along the great abdominal vessels (*arrow*). **b** Axial SPECT/CT image showing the exact location of this sentinel node next to the common iliac artery (*arrow*). **c** 3D volume-rendered SPECT/CT image providing an overview of all sentinel nodes: the upper sentinel node next to the common ilac artery (*upper arrow*), two along the external iliac vessels on the left side, one along the external iliac artery on the right side, but also an additional sentinel node located more mediocaudally (*lower arrow*). **d** The axial image shows that this sentinel node is located paravesically. **e** All sentinel nodes were harvested laparoscopically, aided by a portable gamma camera (*arrow*) and a laparoscopic gamma probe. **f** Intraoperative visualization of a sentinel node(s) (*arrow*) using a portable gamma camera, allowing post-excision confirmation that the sentinel node has been removed completely. After excision (right screen), no significant remaining activity is seen

is accidental injection into the corpus cavernosum, an occurrence that will cause no visualization of lymphatic flow. Furthermore, in some cases the injection site (penis) may obscure visualization of the more inferiorly located SLNs on anterior planar imaging.

15.11.2 Prostate Cancer

The relatively complicated radiocolloid injection procedure for prostate cancer is probably the most frequent cause of pitfalls. Care must be taken to avoid tracer leakage during injection, possibly resulting in subsequent contamination of the floor or of the ultrasound probe. It is therefore recommended to check for contamination of the room after injection, using a Geiger counter.

During injection, incorrect needle placement may result in passage of the radiocolloid directly to the bladder or bloodstream, which in turn may cause nonvisualization during scintigraphy. By monitoring the injection procedure with a portable gamma camera, it is possible to ensure adequate radiocolloid retention in the prostate. As the injection is performed transrectally, a possible pitfall is visualization of lymphatic drainage from the rectum, leading, for example, to visualization of inguinal lymph nodes on SPECT/CT imaging. Furthermore, accidental funicular administration can also occur, possibly leading to retrograde drainage towards the scrotum (Fig. 15.5).

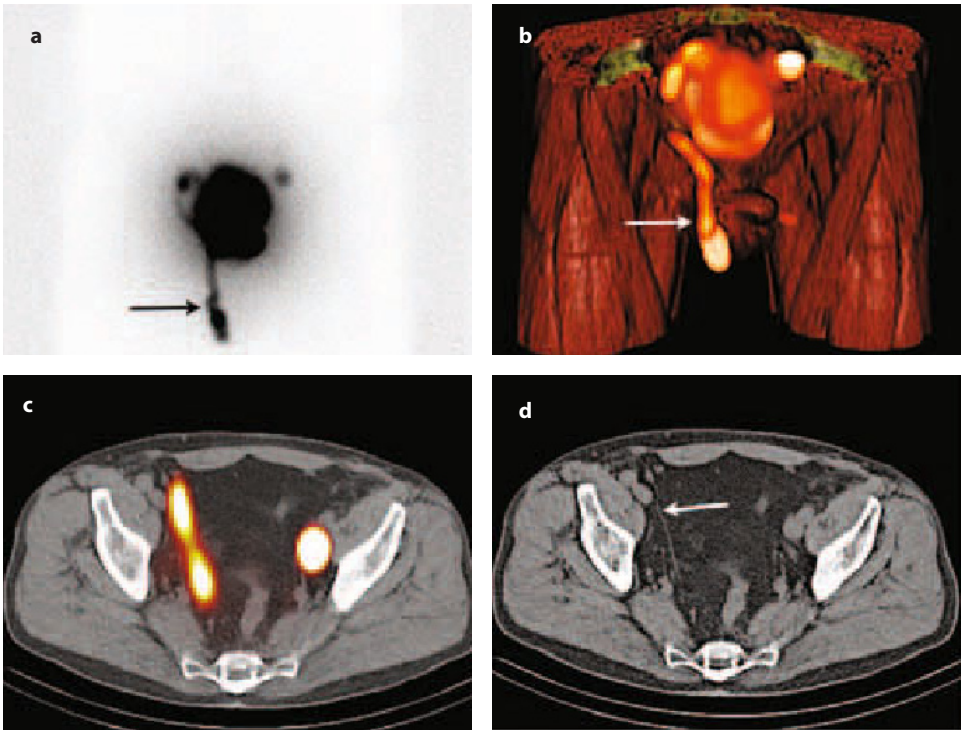

Fig. 15.5 Planar lymphoscintigraphy after intraprostatic injection of 180 MBq ^{99m}Tc-nanocolloid in a 60-year-old patient, showing bilateral drainage with a single hotspot on both sides, but also with drainage on the right side in a caudal direction (**a**, *arrow*). **b** 3D volume-rendered SPECT/CT image showing that the caudal drainage on the right side is directed towards the right testicle (*arrow*). **c**, **d** Axial images showing elongated drainage along the funiculus (*arrow*). The drainage towards the testicle thus reflects retrograde drainage after accidental funicular administration – one of the possible pitfalls of this procedure

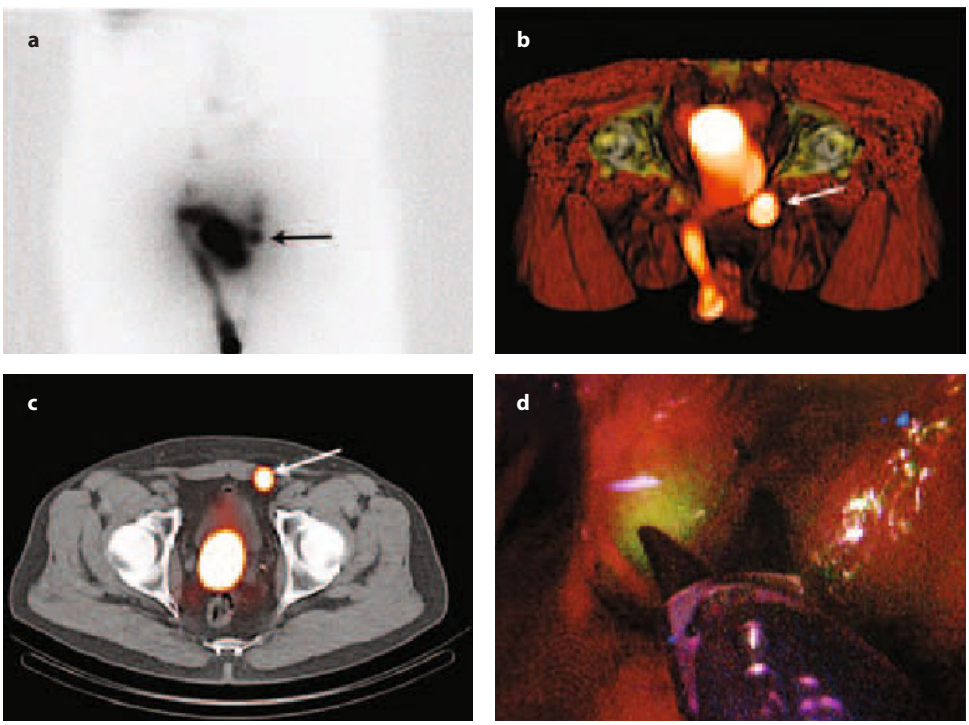

Fig. 15.6 A similar situation arose after transrectal intraprostatic injection (211 MBq) of hybrid radioactive and fluorescent ICG–^{99m}Tc-nanocolloid in a 59-year-old male patient with intermediate-risk prostate cancer. **a** Delayed planar lymphoscintigram showing retrograde drainage towards the scrotum on the right side, due to partial funicular tracer administration as well as drainage to sentinel nodes on both sides (obturator fossa); and a sentinel node located more caudally on the left side (*arrow*). **b**, **c** The 3D volume-rendered and axial SPECT/CT images reveal that the most caudal sentinel node on the left side reflects aberrant drainage ventrally against the abdominal wall (*arrow*). The sentinel nodes were harvested during robot-assisted laparoscopy guided by a laparoscopic gamma probe and fluorescence endoscope. **d** Fluorescence endoscope image showing the sentinel node against the abdominal wall along the umbilical ligament (*green*). This sentinel node (and an iliac sentinel node on the right side) contained metastases at histopathology

15.11.3 Testicular Cancer

The route of administration of ^{99m}Tc-nanocolloid may cause pitfalls. For instance, funicular administration may result in lymph node uptake in the inguinal region, which does not reflect testicular tumor drainage. Intratesticular administration in the parenchyma results in retroperitoneal sentinel node visualization, in accordance with known drainage patterns.

15.12 Accuracy of Radioguided Sentinel Lymph Node Biopsy

15.12.1 Penile Cancer

Initially, the most significant drawback of SLNB for penile cancer was found to be a relatively high false-negative rate (22%) [32]. After analysis of the false-negative cases, several modifications were made to the procedure to decrease the false-negative rate and thus increase sensitivity. Histopathologic analysis was expanded with serial sectioning of the harvested SLNs. Furthermore, preoperative ultrasonography of cN0 groins with fine needle aspiration cytology (FNAC) of suspicious lymph nodes was added, as well as exploration of the groin in the case of nonvisualization during scintigraphy, and intraoperative palpation of the wound to identify suspicious lymph nodes that failed to pick up any radiocolloid. Thanks to these modifications, the procedure has evolved into a reliable minimally invasive staging technique, with an associated sensitivity of 93–95% and low morbidity in experienced centers [33]. However, a recent multicenter meta-analysis reported pooled sensitivity rates of 88% [11]. One explanation for this lower sensitivity may be represented by differences in protocols (that is screening with ultrasound and FNAC to detect lymph node metastases that fail to pick up radioactivity), and/or by possibly different phases of the learning curve.

15.12.2 Prostate Cancer

Original validation of SLNB for prostate cancer was based on open surgery and on the use of a gamma probe to guide detection of the radioactive sentinel nodes. Out of more than 2,000 patients evaluated, only 11 false-negative cases (5.5%) were reported [34]. More recently, SLNB has been validated using a laparoscopic gamma probe during minimally invasive surgery [18]. A recent meta-analysis reported a pooled detection rate of 94% (89–96.6%) and a pooled sensitivity rate of 95% (92–97%) [35].

15.12.3 Testicular Cancer

To date, no studies have been published other than the aforementioned feasibility studies limited by small size of the study populations (<25 patients per study), which therefore lacked the statistical power and follow-up data to assess sensitivity/false-negative rates. Although refinement of the SLN procedure may enable better selection of patients who would benefit from adjuvant treatment after orchidectomy, further studies are required to substantiate the clinical value of the SLN procedure in this disease.

Clinical Cases

Case 15.1
Sentinel Node Mapping in Prostate Carcinoma: Drainage to Bilateral Iliac Nodes After Peritumoral Injection (Planar Image)

Giuseppe Rubini and Filippo Antonica

Background Clinical Case

An 80-year-man with moderately differentiated prostate carcinoma (Gleason score 4+3) of the left lobe, without infiltration of the prostate capsule and periprostatic adipose tissue. Blood chemistry revealed PSA 12 ng/mL. Histological examination after biopsy showed cell proliferation with moderate inversion of the nuclear/cytoplasmatic ratio inversion. The patient was submitted to radioguided sentinel lymph node biopsy.

Lymphoscintigraphy

About 12 hours before surgery, lymphoscintigraphy was performed following peritumoral injections of 0.8 mL of a of 128 MBq ^{99m}Tc-albumin nanocolloid (divided into two aliquots) around the tumor, under peri-rectal endoscopic guidance. A dual-detector SPECT gamma camera (Millennium MG, GE Healthcare, Milwaukee, WI) equipped with low-energy high-resolution (LEHR) collimators was used to obtain abdominal-pelvic dynamic images immediately after radiopharmaceutical injection and planar static images at 30 and 60 min after radiopharmaceutical injection. Dynamic images (1frame 60 s/30 frames) were acquired in anterior and posterior projection with a 256×256 matrix and zoom factor 1.00, while static images were acquired in anterior and posterior projection with a 128×128 matrix and zoom factor 1.00.

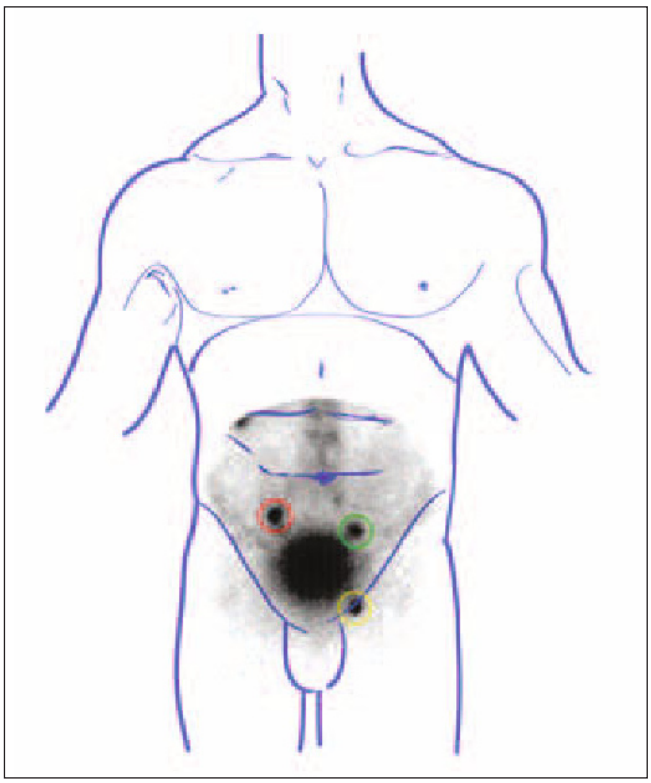

Fig. 1 Schematic representation of an anterior static planar image of the pelvic-abdominal region (30 min after peritumoral radiopharmaceutical injections) shows a right iliac sentinel node (*red circle*), a left iliac sentinel node (*green circle*), and a more caudally located left sentinel node (*yellow circle*)

Case 15.2
Sentinel Node Mapping in Penile Carcinoma: Drainage to Bilateral Groin Nodes After Peritumoral Injection (Planar Image)

Axel Bex, Oscar R. Brouwer, and Renato A. Valdés Olmos

Background Clinical Case

A 49-year-old patient was diagnosed with T1 penile squamous cell carcinoma.
Preoperative palpation and ultrasound guided fine needle aspiration cytology (FNAC) showed no evidence for lymph node metastases (cT1N0Mx).
The patient was scheduled for sentinel lymph node mapping followed by sentinel node biopsy and partial penectomy.

Lymphoscintigraphy

Lymphoscintigraphy was performed a few hours before sentinel node biopsy, to define the draining lymphatic basin at risk for metastatic disease and to identify the corresponding sentinel lymph node; 81 MBq of ^{99m}Tc-albumin nanocolloid were injected peritumorally. A dual-detector SPECT/CT gamma camera (Symbia T, Siemens, Erlangen, Germany) equipped with low-energy collimators and multislice spiral CT was used to obtain planar images of the abdominal region and SPECT/CT acquisition 2 h after radiopharmaceutical administration.

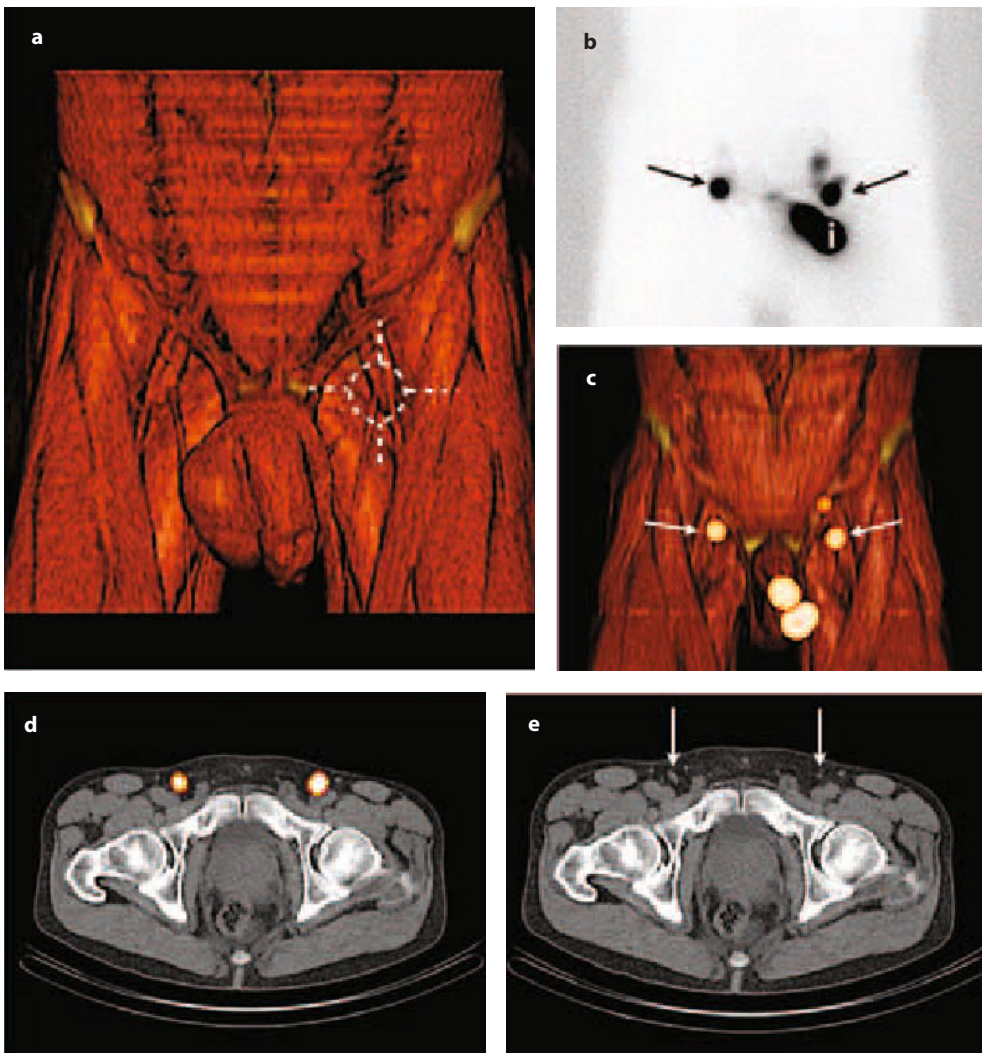

Fig. 1 **a** Lymphatic drainage in penile cancer and the five inguinal zones of Daseler: in the majority of patients, sentinel nodes are seen in the superior medial quadrant (73%), superior lateral (9%), and central (18%). Drainage to the inferior quadrants is rare. **b** Lymphoscintigraphy shows drainage to a sentinel node in both groins (*arrows*) and bilateral higher-echelon drainage. **c** 3D volume-rendered image revealing that both sentinel nodes are located in the central zone of Daseler. **d**, **e** Axial fused SPECT/CT images depicting both radioactive sentinel nodes, with the corresponding lymph nodes on CT (*arrows*)

Case 15.3
Sentinel Node Mapping in Testicle Cancer: Drainage to Lumbo-Aortic Nodes After Intratumoral Injection (Planar and SPECT/CT Imaging)

Axel Bex, Oscar R. Brouwer, and Renato A. Valdés Olmos

Background Clinical Case

A 42-year-old man presented with a painless palpable lesion on the right testicle.
Ultrasound showed a hypoechogenic mass in the right testicle (2.5×1.5 cm).
Abdominal CT showed no enlarged lymph nodes.
The patient was scheduled for lymphatic mapping followed by laparoscopic sentinel node biopsy and orchidectomy.

Lymphoscintigraphy

Lymphoscintigraphy was performed a few hours before sentinel node biopsy, to define the draining lymphatic basin at risk for metastatic disease and to identify the corresponding sentinel lymph node; 87 MBq of ^{99m}Tc-albumin nanocolloid was injected intratumorally under ultrasound guidance. A dual-detector SPECT/CT gamma camera (Symbia T, Siemens, Germany) equipped with low-energy collimators and multislice spiral CT was used to obtain planar images of the abdominal region and SPECT/CT acquisition 2 h after radiopharmaceutical administration.

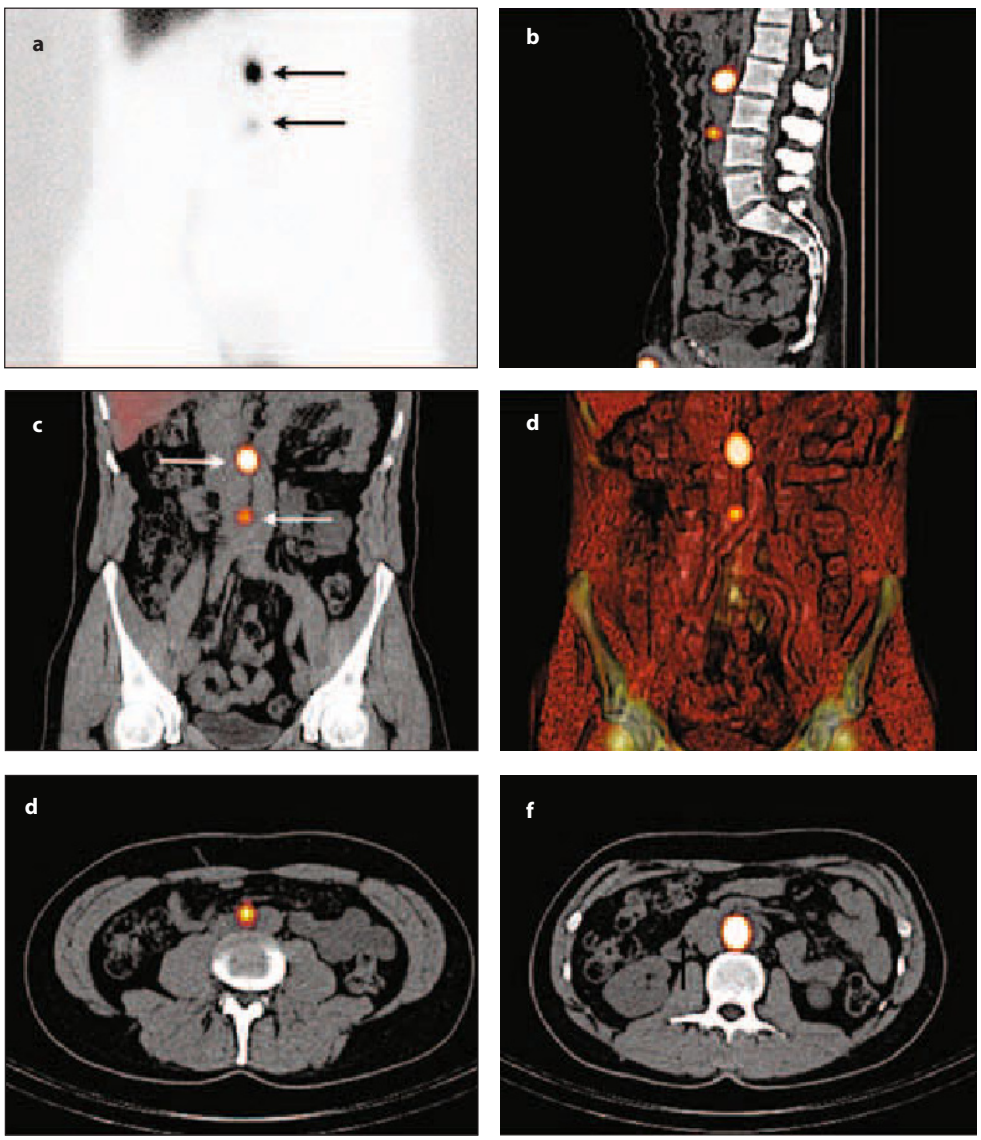

Fig. 1 **a** Early planar anterior image showing drainage to two abdominal sentinel lymph nodes (*arrows*) and radioactivity along the lymphatic channel, which decreased in time, indicating visualization of the lymphatic tract. **b** Saggital SPECT/CT image fusion showing the injection site and both sentinel nodes along the great abdominal vessels. **c**, **d** The coronal SPECT/ CT image fusion and 3D volume-rendered image reveal that both sentinel lymph nodes are located interaortocavally (*arrows*). **e**, **f** Axial SPECT/CT images providing additional anatomical information about the location of both sentinel nodes. Both sentinel nodes were harvested laparoscopically and were tumor free at histopathology

References

1. Hernandez BY, Barnholtz-Sloan J, German RR et al (2008) Burden of invasive squamous cell carcinoma of the penis in the United States, 1998–2003. Cancer 113:2883–2891
2. Horenblas S, van Tinteren H (1994) Squamous cell carcinoma of the penis. IV. Prognostic factors of survival: analysis of tumor, nodes and metastasis classification system. J Urol 151:1239–1243
3. Cabanas RM (1977) An approach for the treatment of penile carcinoma. Cancer 39:456-466
4. Leijte JAP, Hughes B, Graafland NM et al (2009) Two-center evaluation of dynamic sentinel node biopsy for squamous cell carcinoma of the penis. J Clin Oncol 27:3325–3329
5. Meinhardt W (2007) Sentinel node evaluation in prostate cancer. EAU-EBU Update Series 5:223–231
6. Meinhardt W, van der Poel H, Valdés Olmos RA et al (2012) Laparoscopic sentinel lymph node biopsy for prostate cancer: the relevance of locations outside the extended dissection area. Prostate Cancer 2012:751–753
7. Bray F, Richiardi L, Ekbom A et al (2006) Trends in testicular cancer incidence and mortality in 22 European countries: continuing increases in incidence and declines in mortality. Int J Cancer 118:3099–3111
8. Tanis PJ, Horenblas S, Valdés-Olmos RA et al (2002) Feasibility of sentinel node lymphoscintigraphy in stage I testicular cancer. Eur J Nucl Med Mol Imaging 29:670–673
9. Brouwer OR, Valdés-Olmos RA, Vermeeren L et al (2011) SPECT/CT and a portable gamma-camera for image-guided laparoscopic sentinel node biopsy in testicular cancer. J Nucl Med 52:551–554
10. Wespes E (2007) The management of regional lymph nodes in patients with penile carcinoma and reliability of sentinel node biopsy. Eur Urol 52: 5–6
11. Sadeghi R, Gholami H, Zakavi SR et al (2012) Accuracy of sentinel lymph node biopsy for inguinal lymph node staging of penile squamous cell carcinoma: systematic review and meta-analysis of the literature. J Urol 187:25–31
12. Kroon BK, Horenblas S, Estourgie SH et al (2004) How to avoid false-negative dynamic sentinel node procedures in penile carcinoma. J Urol 171:2191–2194
13. Vermeeren L, Valdés-Olmos RA, Meinhardt W et al (2011) Intraoperative imaging for sentinel node identification in prostate carcinoma: its use in combination with other techniques. J Nucl Med 52:741–744
14. Graafland NM, Leijte JAP, Valdés-Olmos RA et al (2009) Repeat dynamic sentinel node biopsy in locally recurrent penile carcinoma. BJU Int 105:1121–1124
15. Weckermann D, Wawroschek F, Harzmann R (2005) Is there a need for pelvic lymph node dissection in low risk prostate cancer patients prior to definitive local therapy? Eur Urol 47:45–50
15. Kroon BK, Valdés-Olmos RA, van Tinteren H et al (2005) Reproducibility of lymphoscintigraphy for lymphatic mapping in patients with penile carcinoma. J Urol 174:2214–2217
17. Vermeeren L, Muller SH, Meinhardt W et al (2010) Optimizing the colloid particle concentration for improved preoperative and intraoperative image-guided detection of sentinel nodes in prostate cancer. Eur J Nucl Med Mol Imaging 37:1328–1334
18. Meinhardt W, Valdés-Olmos RA, van der Poel HG et al (2008) Laparoscopic sentinel node dissection for prostate carcinoma: technical and anatomical observations. BJU Int 102:714–717
19. Valdés Olmos RA, Tanis PJ, Hoefnagel CA et al (2001) Penile lymphoscintigraphy for sentinel node identification. Eur J Nucl Med 28:581–585
20. McMahon CJ, Rofsky NM, Pedrosa I (2010) Lymphatic metastases from pelvic tumors: anatomic classification, characterization, and staging. Radiology 254:31–46
21. Leijte JAP, van der Ploeg IMC, Valdés-Olmos RA et al (2009) Visualization of tumor blockage and rerouting of lymphatic drainage in penile cancer patients by use of SPECT/CT. J Nucl Med 50:364–367
22. Jeschke S, Nambirajan T, Leeb K et al (2005) Detection of early lymph node metastases in prostate cancer by laparoscopic radioisotope guided sentinel lymph node dissection. J Urol 173:1943–1946
23. Vermeeren L, Valdés-Olmos RA, Meinhardt W et al (2009) Value of SPECT/CT for detection and anatomic localization of sentinel lymph nodes before laparoscopic sentinel node lymphadenectomy in prostate carcinoma. J Nucl Med 50:865–870
24. van Leeuwen AC, Buckle T, Bendle G et al (2011) Tracer-cocktail injections for combined pre- and intraoperative multimodal imaging of lymph nodes in a spontaneous mouse prostate tumor model. J Biomed Opt 16:016004
25. Brouwer OR, Buckle T, Vermeeren L et al (2012) Comparing the novel hybrid radioactive/fluorescent tracer ICG-^{99m}Tc-nanocolloid with ^{99m}Tc-nanocolloid for sentinel node identification: a validation study using lymphoscintigraphy and SPECT/CT. J Nucl Med 29 May, epub ahead of print
26. Vermeeren L, Valdés Olmos RA, Meinhardt W et al (2009) Intraoperative radioguidance with a portable gamma camera: a novel technique for laparoscopic sentinel node localisation in urological malignancies. Eur J Nucl Med Mol Imaging 36:1029–1036
27. Brouwer OR, Buckle T, Bunschoten A et al (2012) Image navigation as a means to expand the boundaries of fluorescence guided surgery. Phys Med Biol 57:3123–3136
28. van der Poel HG, Buckle T, Brouwer OR et al (2011) Intraoperative laparoscopic fluorescence guidance to the sentinel lymph node in prostate cancer patients: clinical proof of concept of an integrated functional imaging approach using a multimodal tracer. Eur Urol 60:826–833
29. Kroon BK, Vald s Olmos RA, van der Poel HG et al (2005) Prepubic sentinel node location in penile carcinoma. Clin Nucl Med 30:649–650
30. Vermeeren L, Meinhardt W, Valdés-Olmos RA (2010) Prostatic lymphatic drainage with sentinel nodes at the ventral abdominal wall visualized with SPECT/CT: a case series. Clin Nucl Med 35:71–73
31. Vermeeren L, Meinhardt W, Bex A et al (2010) Paraaortic sentinel lymph nodes: toward optimal detection and intraoperative localization using SPECT/CT and intraoperative real-time imaging. J Nucl Med 51:376–382
32. Tanis PJ, Lont AP, Meinhardt W et al (2002) Dynamic sentinel node biopsy for penile cancer: reliability of a staging technique. J Urol 168:76–80
33. Leijte JAP, Kroon BK, Valdés-Olmos RA et al (2007) Reliability and safety of current dynamic sentinel node biopsy for penile carcinoma. Eur Urol 52:170–177
34. Holl G, Dorn R, Wengenmair H, Weckermann D et al (2009) Validation of sentinel lymph node dissection in prostate cancer: experience in more than 2,000 patients. Eur J Nucl Med Mol Imaging 36:1377–1382
35. Sadeghi R, Tabasi KT, Bazaz SMM et al (2011) Sentinel node mapping in the prostate cancer. Nuklearmedizin 50:107–115

Preoperative and Intraoperative Lymphatic Mapping for Radioguided Sentinel Node Biopsy in Kidney and Bladder Cancers

16

Axel Bex, Oscar R. Brouwer, and Renato A. Valdés Olmos

16.1 Introduction

Renal cell cancer (RCC) is the tenth most common malignancy in Europe and the United States. In 2006, 63,000 new cases were diagnosed in the European Union and 26,000 people died from the disease [1]. However, RCC accounts for only 2–3% of cancers and is therefore relatively uncommon when compared to breast, bowel, and lung cancer [2]. Histologically, several subtypes can be identified, of which clear-cell carcinoma is predominant, representing up to 80% of the cases [3].

The management of early-stage RCC has traditionally been surgical, and nephrectomy and/or nephron-sparing strategies are often curative at this stage of the disease [4]. Even when patients present with metastases, nephrectomy and metastasectomy may be beneficial in selected cases [5, 6]. In this regard, the widespread use of ultrasound examination of the abdomen has led to more small renal tumors being diagnosed [7]. Stage shift may result in an increasing number of patients with early lymph node metastases only, who, in contrast to historical data, may benefit from removal of these lesions. In addition, the introduction of targeted agents has revived interest in adjuvant treatment concepts [8]. Accurate lymph node staging is warranted to determine the risk of recurrence or progression.

Bladder cancer is more common than RCC and is related to carcinogens [9]. The most prominent subtype is transitional cell carcinoma, representing about 90% of cases. In the United States, bladder cancer is the fourth most common type of cancer in men and the ninth most common cancer in women [10]. More than 50,000 men and 16,000 women are diagnosed with bladder cancer each year. Approximately 50% of bladder cancer in the United States is related to cigarette smoking. In addition, further occupational hazards play a role.

Lymph node metastases are common in patients with bladder cancer, and the risk of lymph node involvement is highly associated with the depth of invasion of the primary tumor [11]. The presence of lymph node metastases, their number, and the volume of involved nodes are strongly associated with survival [12]. Five-year survival rates up to 57% have been observed in patients with pathologically confirmed but occult N1 disease on imaging prior to surgery. The 5-year survival drops to 0–27% for patients with N2–N3 disease. In the majority of patients with muscle-invasive bladder cancer, local treatment fails, due to occult systemic disease, but extensive pelvic lymph node dissection (PLND) confers a survival benefit [11]. In addition to extensive PLND, survival can be increased by using systemic chemotherapy, in either the neoadjuvant or the adjuvant setting [13]. As for renal cancer, improving detection and successful removal of early lymph node metastasis may lead to a survival benefit.

16.2 The Clinical Problem

Generally, the clinical problem in renal and bladder cancer is a consequence of the fact that lymph node metastases may occur outside known and expected lymphatic basins.

Specifically for RCC, the role of lymph node dissection (LND) remains controversial despite a randomized study with a median follow up of 12.6 years [14]. This may be due to the unpredictability of lymphatic drainage of RCC, which undergoes a mainly hematogenous spread. A potential reason for the lack of evidence supporting locoregional retroperitoneal LND and the low detection of lymph node metastases in computed tomography (CT)-negative locoregional nodes may simply be the fact that, in a relevant proportion of

A. Bex (✉)
Urology, Division of Surgical Oncology
Netherlands Cancer Institute – Antoni van Leeuwenhoek Hospital
Amsterdam, the Netherlands
e-mail: a.bex@nki.nl

G. Mariani et al. (eds.), *Atlas of Lymphoscintigraphy and Sentinel Node Mapping*,
DOI 10.1007/978-88-470-2766-4_16

cases, lymphatic landing sites of RCC are located outside the expected LND templates. In addition, in the majority of patients with RCC, lymph node involvement is associated with hematogenous metastases [15], and is a significant indicator of systemic disease and adverse prognosis [16]. The likelihood of identifying lymph node metastasis seems to be low, given the high proportion of concurrent systemic disease.

However, there is evidence that patients with very early lymph node metastases and no distant disease can potentially be cured by LND [17]. The true incidence of lymph node involvement only is unknown, but seems to correlate with tumor size. In retrospective nephrectomy and autopsy studies, microscopic lymph node metastases were mainly observed in smaller tumors [18, 19]. On autopsy, patients with renal tumors smaller than 3 cm revealed lymph node metastases in 3.5%, which increased to 21% in tumors of 4–5 cm [20]. In nephrectomy series, this was 2.5% and 4 % for tumors of 4 cm and less [21, 22]. Therefore, the predominant clinical problem in early-stage RCC is the detection and subsequent removal of early metastatic disease.

In bladder cancer, the value of PLND is undisputed for muscle-invasive bladder cancer. Dhar et al. reported a rate of lymph node metastasis of 13% versus 26% for limited versus extended pelvic lymph node dissection [23]. These results, as well as anatomical and functional studies, underline the need for elective PLND at radical cystectomy to accurately stage these cases. The total number of resected lymph nodes is generally regarded as an indicator of surgical quality [24]. Other lymph node parameters have been introduced as prognostic factors, such as the total number of tumor-positive lymph nodes and lymph node density, that is, the number of positive lymph nodes divided by the total number of resected lymph nodes [25]. Although these parameters are widely accepted in clinical practice, they depend on evaluation by a pathologist. It was recently demonstrated that, despite equal anatomical clearance by the same experienced surgeons, there was a statistically significant difference between two pathology departments where the number of lymph nodes was evaluated after extended bilateral pelvic lymph node dissection for bladder cancer [26]. Without current standardized methods, the number of reported lymph nodes as an indicator of surgical quality, and lymph node density as a prognostic factor, are probably not reliable.

16.3 Lymphatic Drainage and Nodal Groups in Renal Cancer

The lymphatic drainage pattern has not been accurately ascertained in RCC. It may actually differ from the anatomical studies performed in nontumor-bearing kidneys, possibly because of multiple lymphatic tumor-draining vessels [27]. Lymphatic drainage from renal tumors may be outside the proposed retroperitoneal templates.

A general notion is that the draining lymph nodes are in the hilar region, branching off into the paracaval, inter-aortocaval, or para-aortic retroperitoneal lymph nodes, depending on the tumor side. The lymphatic drainage of renal tumors may, however, not always follow the known pattern, as has frequently been found for other tumor entities. As far back as 1935, Parker found extreme variations of lymphatic drainage between individuals by injecting blue dye at high pressure into normal cadaveric kidneys [28].

Lymphoscintigraphy of kidney tumors has been described in two pilot studies, and the exact direct lymphatic drainage patterns are still unknown [29, 30]. Drainage patterns were previously assessed by analyzing lymphatic metastasis within lymphadenectomy specimens, or at autopsy. In nephrectomy series, metastases are generally detected in "regional" lymphadenectomies, and the extent of LND is often ill-defined. The accuracy of detecting lymph node metastases increases with the number of sampled lymph nodes, irrespective of the extent of LND [31].

In an autopsy study involving 1,828 cases of RCC, a broad variation of the localization of lymph node metastases was seen [32]. Since most patients had multiple lymphatic metastases, it could not be concluded which node was involved first. Interestingly, ipsilateral renal hilar lymph node metastases were found in only 7% of cases, while pulmonary hilar lymph node metastases were found in 66.2%, retroperitoneal in 36%, para-aortic in 26.8%, and supraclavicular in 20.7% [32]. Single, isolated lymph node metastases have been described by Hulten et al., in a supraclavicular lymph node in one patient and in an iliac lymph node in two patients, without any further metastasis [33]. Furthermore, Johnsen et al. detected single lymph node metastases in ten patients, with a single mediastinal, supraclavicular, and axillary node in respectively 8, 1, and 1 patients [20]. Those single-node metastases may chronologically be the first site.

Interestingly, lymphatics from the kidney drain directly into the thoracic duct (TD), without any interposition of lymph nodes. This latter situation has been described by Assouad and coworkers, who injected normal kidneys of 16 cadavers with a blue modified Gerota mass and dissected lymph vessels until their termination [34]. Renal lymphatics reached distant lymph nodes (e.g., aortic bifurcation, celiac, mesenteric, and contralateral nodes). Furthermore, lymphatic vessels were always connecting to the origin of the TD, in several cases (38% on the right and 15% on the left) even directly without involving any lymph nodes (Fig. 16.1) [35]. Clinically, drainage through the TD may explain the isolated mediastinal lymph node, as well as pulmonary metastasis, which are frequently observed in RCC [18–21, 36–38].

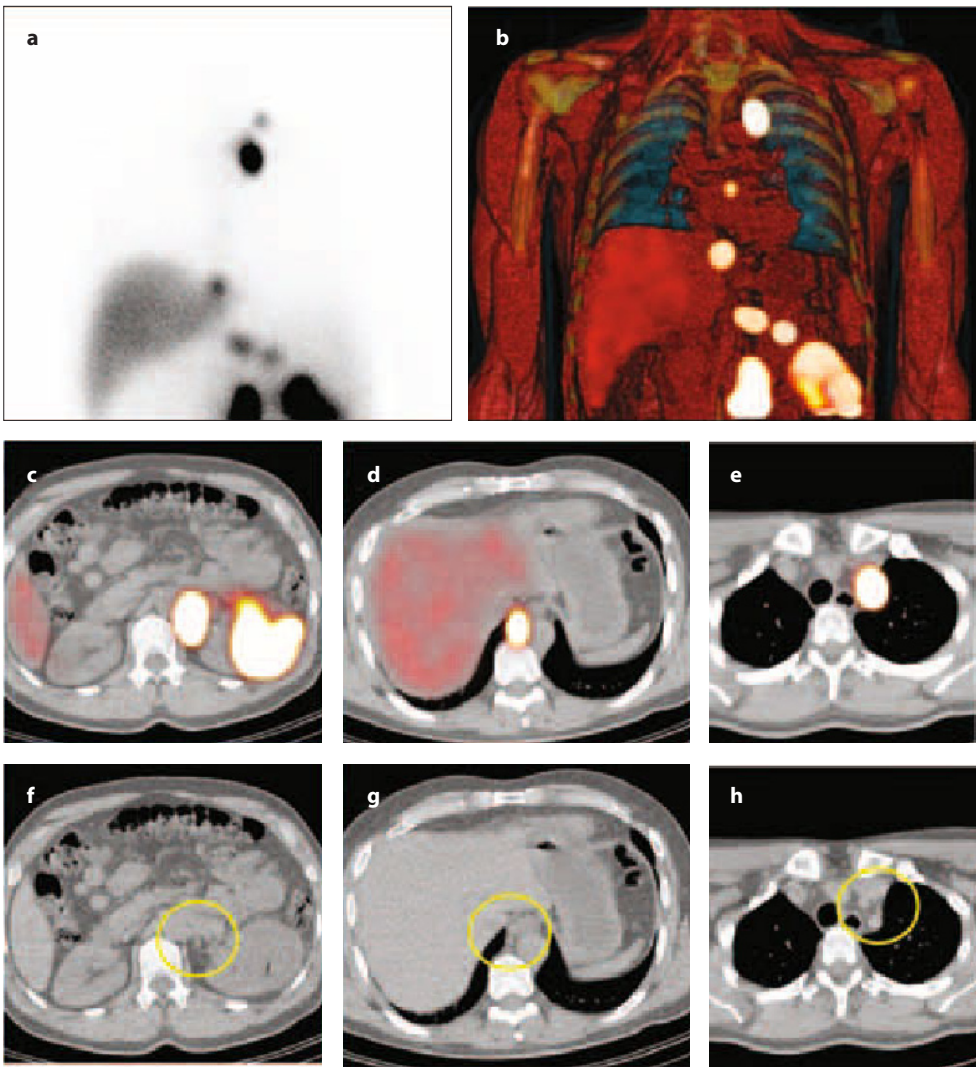

Fig. 16.1 A 39-year-old male patient with a T1 (5 cm) papillary renal cell carcinoma in the lateral part of the left kidney. Lymphoscintigraphy and SPECT/CT were performed after ultrasound-guided injection of 209 MBq ^{99m}Tc-nanocolloid into the tumor. The planar anterior image (**a**) and SPECT/CT volume rendering (**b**) show drainage to lymph nodes in the abdomen and in the thorax. Axial SPECT/CT images show para-aortic sentinel nodes (**c**), as well as retrocrural (**d**) and mediastinal lymph nodes (**e**). None of these nodes were enlarged on CT (**f**–**h**). At histopathology two para-aortic sentinel nodes were found to contain metastases. The *yellow circle* refers to the location of corresponding lymph nodes on conventional CT which may represent the sentinel node

16.4 Lymphatic Drainage and Nodal Groups in Bladder Cancer

In contrast to renal cancer, lymphatic drainage in bladder cancer is more predictable. However, autopsy and pathological postcystectomy studies have failed to accurately map the landing sites of lymphatic drainage from the urinary bladder. Contrary to renal cancer, the value of intraoperative sentinel lymph node (SLN) mapping and lymphoscintography has been evaluated and demonstrated in large series [39]. In well-lateralized bladder cancer, a 100% ipsilateral radiocolloid drainage rate has been observed, including drainage to the external iliac, obturator fossa, and common iliac stations [40]. In 40% of cases, additional lymphatic drainage to the contralateral side was seen.

16.5 Radiocolloid Administration in Renal and Bladder Cancer

In kidney cancer, technetium-99 (^{99m}Tc)-nanocolloid is injected percutaneously (0.4 mL, 225 MBq) into the primary renal lesion, under ultrasound or CT guidance, the day before surgery (Fig. 16.2). Using a spinal needle, primary tumors ≤4 cm are injected centrally with a single 0.4 mL aliquot. Tumors 4–10 cm in size receive a total of 2–3×0.4 mL, injected around the center into solid parts and avoiding areas of necrosis [29].

In bladder cancer, the radiocolloid is injected under cystoscopy guidance, using an endoscopic needle [39]. An amount of 240 MBq of the radiocolloid is administered into the detrusor muscle in four sites around the tumor following

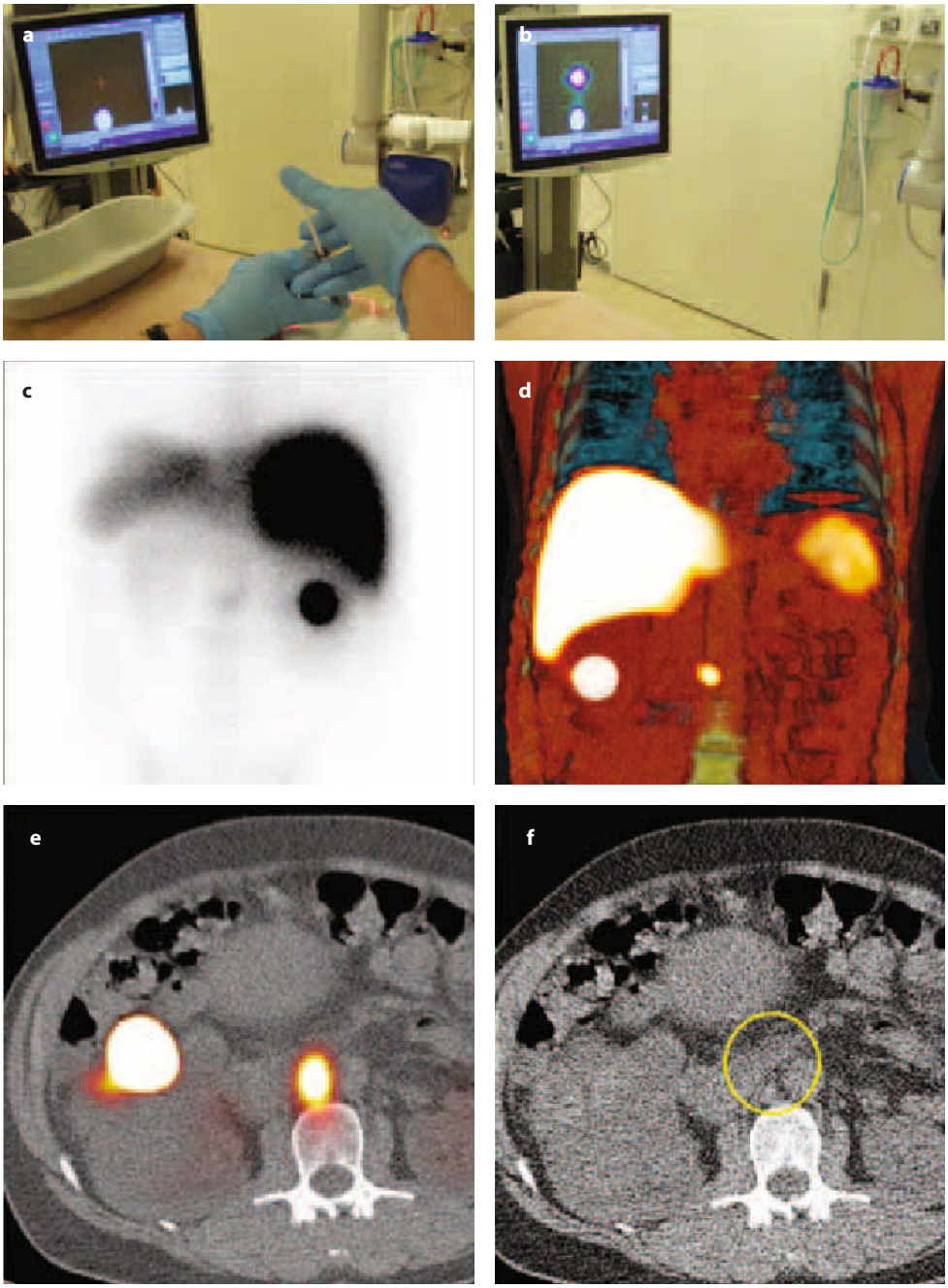

Fig. 16.2 A 47-year-old female patient with a T2 (8.8 cm) renal cell carcinoma in the lower pole of the right kidney. Following CT-guided needle placement into the tumor, 206 MBq ^{99m}Tc-nanocolloid was administered under continuous monitoring with a portable gamma camera (**a**), showing initial tumor retention of the tracer (**b**). Planar posterior image (**c**), SPECT/CT volume rendering (**d**), and axial SPECT/CT (**e**, **f**) show drainage to a sentinel node between the aorta and the vena cava. This node was tumor negative at histopathology. The *yellow circle* refers to the location of corresponding lymph nodes on conventional CT which may represent the sentinel node

a transurethral approach, with the patient in the lithotomy position.

16.6 Preoperative Imaging of Sentinel Lymph Nodes in Renal and Bladder Cancer

In renal cancer, lymphoscintigraphy is usually obtained 20 minutes and 2 hours postadministration, acquiring anterior and lateral planar images. Since radiocolloid admistration is performed at the department of radiology, dynamic scanning with a standard gamma camera is not possible. The use of a portable gamma camera may assist tracer injection and help to modify/repeat the injection procedure in case radioactivity is detected outside the tumor and the kidney. Single photon emission computed tomography/computed tomography (SPECT/CT) is usually acquired following delayed planar images. For this procedure, a low-dose CT is obtained, acquiring 2-mm slices for attenuation correction and for generation of SPECT/CT fusion images.

A similar procedure is performed for bladder cancer. Be-

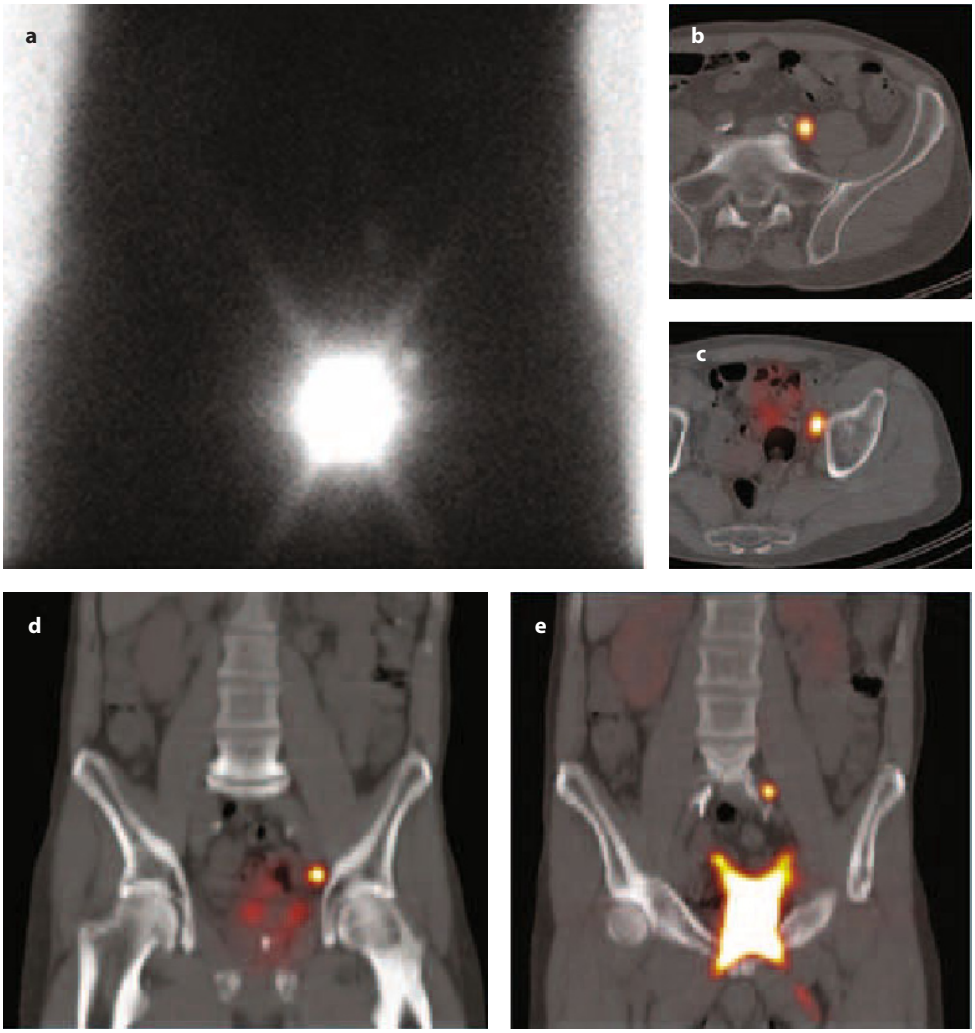

Fig. 16.3 A 50-year-old male patient with a carcinoma in the left dorsal wall of the bladder. On planar anterior image (**a**), drainage to the left iliac area is observed. On axial (**b**, **c**) and coronal (**d**, **e**) SPECT/CT fusion images, sentinel nodes are seen along the left external iliac artery and in the upper part of the left iliac common artery. Only the external iliac node was found to contain metastases at histopathology

fore lymphoscintigraphy, an indwelling catheter can be used to empty the bladder and wash out excess radiocolloid from the bladder cavity.

The lymph nodes appearing on early planar lymphoscintigraphy are considered to be SLNs (Fig. 16.3). Nodes appearing later in the same stations are considered to be second-echelon lymph nodes. Lymph nodes appearing late in other stations proximal to the injection site are also considered as highly probable sentinel nodes. In the pelvis, planar images are often not able to specifically distinguish the nodal groups, and in many cases SPECT/CT depicts radioactive lymph nodes in two different basins at the same level. These lymph nodes are also considered as sentinel nodes.

16.7 Intraoperative Detection of Sentinel Lymph Nodes in Renal and Bladder Cancer

The approach for renal surgery depends on the size and location of the tumor. As a result, intraoperative detection of SLNs in RCC has been performed during open, transabdominal nephrectomies, open retroperitoneal partial nephrectomies, and laparoscopic transperitoneal nephrectomies, as well as robotic-assisted laparoscopic nephron-sparing surgery. For both open and laparoscopic approaches, the same method is used.

For intraoperative SLN detection in open surgery, a standard gamma probe is used, whereas for laparoscopy a

special laparoscopic gamma probe is necessary. Patent blue is frequently not used, because of its limited contribution.

SLNs are separately excised, followed by LND (hilar, paracaval and inter-aortocaval on the right, or hilar, para-aortic, and inter-aortocaval on the left side). As these preliminary trials investigate feasibility and drainage patterns with a yet unproven clinical benefit, only SLNs that can be approached through the access for renal surgery are removed in study protocols.

Intraoperative SLN identification and sampling can be combined with the most common surgical approaches for renal tumors, with a mean extra time of 20 minutes. Most of the additional time is due to the locoregional LND, especially in laparoscopic nephrectomy. If future research proves that additional locoregional lymph node metastases are not missed in the case of pathologically negative SLNs, then LND may be abandoned.

In bladder cancer, intraoperative SLN identification is often performed in conjunction with open surgery and extended pelvic lymphadenectomy [39]. However, with the advent of laparoscopic cystectomy techniques, including robot-assisted laparoscopic cystectomies, laparoscopic gamma probes are used as described above.

16.8 Contribution of SPECT/CT

For both renal cell cancer and bladder cancer, the use of SPECT/CT is mandatory. SPECT/CT is able to identify SLNs in the vicinity of the iliac vessel or aorta, thus providing a useful road map to guide urologists during the operation. In bladder cancer, SPECT/CT is able to localize SLNs in the lymphatic basins of the pelvis. In many cases, early-appearing lymph nodes seen as a single hot spot on planar images are displayed by SPECT/CT as separate lymph nodes in different basins; in this case, all nodes are considered as SLNs. In other cases, intense lymph node uptake seen on fused images may correspond to a cluster of sentinel nodes as depicted on the CT component of the SPECT/CT.

16.9 Intraoperative Imaging

Intraoperative SLN search may be facilitated using the gamma probe in combination with a portable gamma camera [41]. It can both depict signals of ^{99m}Tc for SLN visualization and use an iodine-125 (^{125}I) seed placed on the tip of the laparoscopic probe to indicate its position in relation to the SLNs.

In addition, all SLNs removed can be examined ex situ with the portable camera. The use of a portable gamma camera also enables a better post-excision control and the identification of significant remaining radioactivity at the site of the SLN, as anatomically identified by SPECT/CT.

16.10 Accuracy of Radioguided Sentinel Lymph Node Biopsy in Renal Cancer

The absence of lymphatic drainage on imaging in 30% of patients is of concern, in relation to a potential clinical application of this technique. No SLN can be identified, although SPECT/CT has demonstrated technically correct intratumoral tracer deposition. This may be caused by lack of drainage of the radiocolloid through lymphatic vessels. Alternatively, the radiocolloid may have drained directly into the TD without any interposition of a lymph node, as has been described by Assouad [34]. Direct drainage into the TD may be rapid and difficult to detect in vivo, since the first planar images are taken after 20 minutes. We have not been able to visualize the presence of lymphatic vessels on lymphoscintigraphy in any patients with non-visualization. The radiocolloid was injected at the department of radiology and dynamic lymphoscintigraphy could not be performed. In four patients, radiocolloid injection was monitored with the portable camera, but drainage through lymphatic vessels was not detected. SLN identification and sampling after preoperative detection on SPECT/CT is surgically feasible and safe in patients with RCC. Preliminary data suggest that SLNs from the kidney are mainly located in the para-aortic, paracaval, and inter-aortocaval region, but aberrant lymph nodes might receive direct drainage through the TD, as was observed in 15% of our cases. Additional studies are required to demonstrate whether accurate mapping of lymphatic drainage and sampling of SLNs may lead to early detection of lymph node metastasis in clinically node-negative and nonmetastatic RCC. In addition, it will be of interest to ascertain whether or not LND can be abandoned in patients with pathologically negative SLNs.

Clinical Cases

Case 16.1
Sentinel Node Mapping in Renal Cancer: Drainage to Two Lumbo-Aortic Nodes After Intratumoral Injection (SPECT/CT Imaging)

Axel Bex, Oscar R. Brouwer, and Renato A. Valdés Olmos

Background Clinical Case

A 43-year-old woman presented with macroscopic hematuria. Ultrasound revealed a suspicious lesion in the lower pole of the left kidney. CT showed a tumor with a diameter of 5.4 cm and no enlarged lymph nodes (cT1N0Mx). The patient was scheduled for renal lymphoscintigraphy, followed by partial nephrectomy, radioguided sentinel node biopsy, and retroperitoneal lymph node dissection.

Lymphoscintigraphy

Lymphoscintigraphy was performed a few hours before sentinel node biopsy, to define the draining lymphatic basin at risk for metastatic disease and to identify the corresponding sentinel lymph node; 183 MBq of ^{99m}Tc-albumin nanocolloid was injected intratumorally under ultrasound guidance. A dual-detector SPECT/CT gamma camera equipped with low-energy collimators and multislice spiral CT was used to obtain planar images of the abdominal region, with SPECT/CT acquisition 2 h after radiopharmaceutical administration.

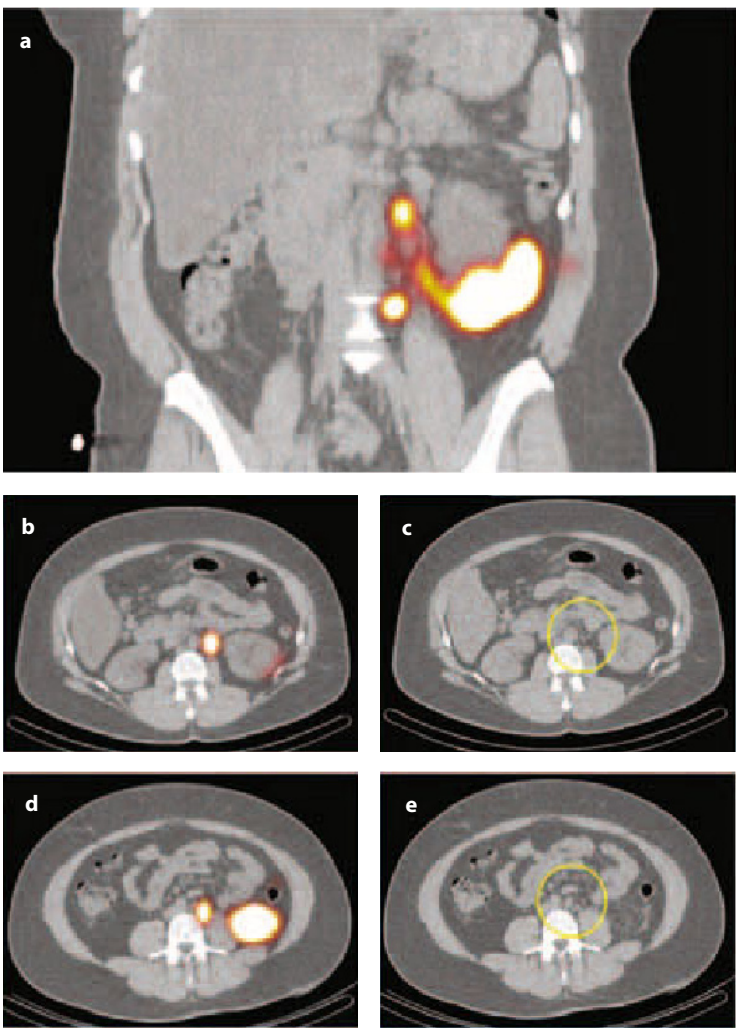

Fig. 1 Coronal (**a**) and axial (**b–e**) SPECT/CT show two sentinel nodes along the aorta (*yellow circles*). Both nodes were free of tumour at histopathology

Case 16.2
Sentinel Node Mapping in Bladder Cancer: Drainage to Iliac Node After Peritumoral Injection (Planar and SPECT/CT Imaging)

Axel Bex, Oscar R. Brouwer, and Renato A. Valdés Olmos

Background Clinical Case

A 46-year-old female patient presented with recurrent urinary tract infections.
Cystoscopy followed by cytology revealed an urachal carcinoma.
The patient was scheduled for sentinel lymph node mapping followed by laparoscopic sentinel node biopsy.

Lymphoscintigraphy

Lymphoscintigraphy was performed a few hours before sentinel node biopsy, to define the draining lymphatic basin at risk for metastatic disease and to identify the corresponding sentinel lymph node; 216 MBq ^{99m}Tc-nanocolloid was administered in four injections around the tumor, into the detrusor muscle under cystoscopy guidance using an endoscopic needle. A dual-detector SPECT/CT gamma camera equipped with low-energy collimators and multislice spiral CT was used to obtain planar images of the abdominal-pelvic region and SPECT/CT acquisition.

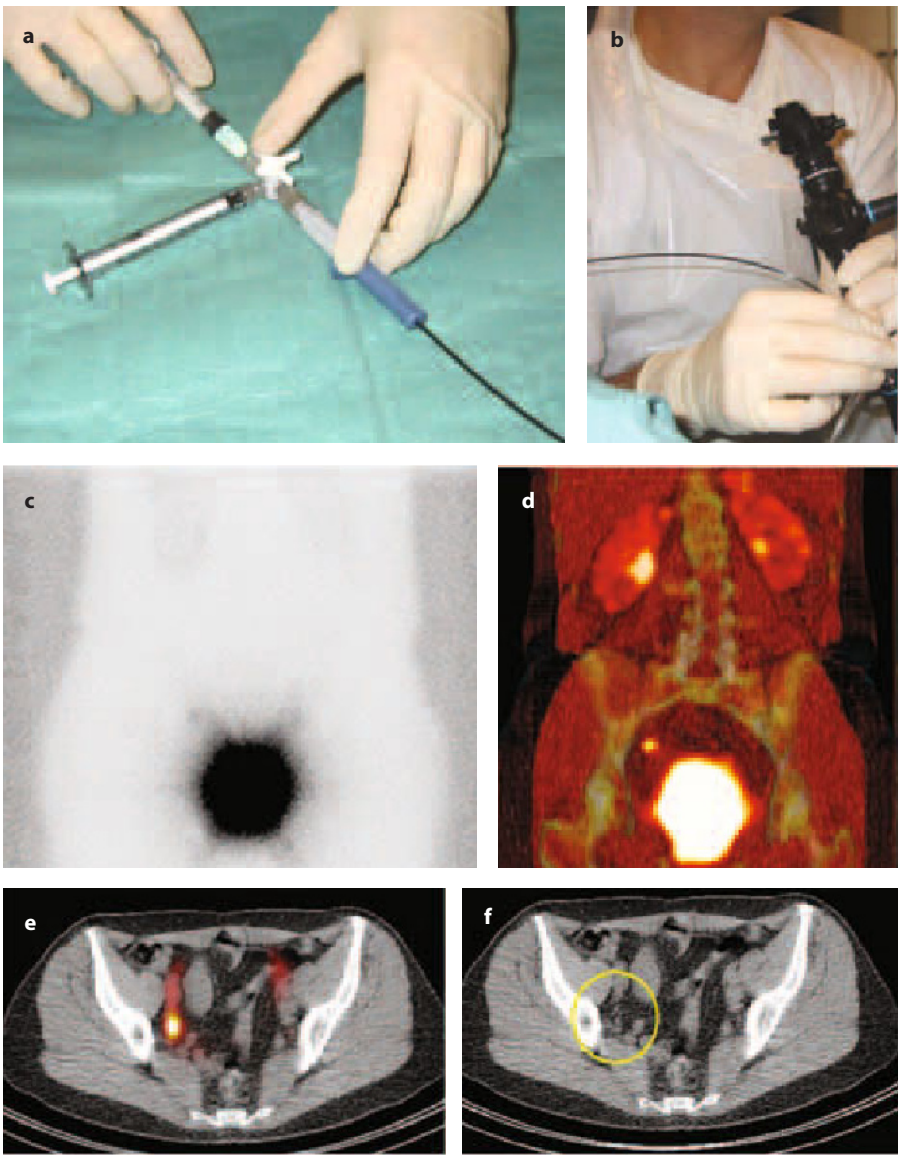

Fig. 1 **a**, **b** Radiopharmaceutical administration under cystoscopy guidance using an endoscopic needle. **c** On planar anterior image, a sentinel lymph node with faint uptake is seen above the bladder radioactivity on the right. This sentinel node, localized at the level of the bifurcation of the left common iliac artery, as seen on volume rendering (**d**) and axial SPECT/CT (*yellow circle*) (**e**, **f**), was free of tumour at histopathology

References

1. Ferlay J, Autier P, Boniol M et al (2007) Estimates of the cancer incidence and mortality in Europe in 2006. Ann Oncol 18:581–592
2. Jemal A, Siegel R, Ward E et al (2009) Cancer statistics, 2009. CA Cancer J Clin 59:225–249
3. Kovacs G, Akhtar M, Beckwith BJ et al (1997) The Heidelberg classification of renal cell tumours. J Pathol 183:131–133
4. Ljungberg B, Cowan NC, Hanbury DC et al (2010) EAU guidelines on renal cell carcinoma: the 2010 update. Eur Urol 58:398–406
5. Alt AL, Boorjian SA, Lohse CM et al (2011) Survival after complete surgical resection of multiple metastases from renal cell carcinoma. Cancer 117:2873–2882
6. Aben KK, Heskamp S, Janssen-Heijnen ML et al (2011) Better survival in patients with metastasised kidney cancer after nephrectomy: a population-based study in the Netherlands. Eur J Cancer 47:2023–2032
7. Volpe A, Mattar K, Finelli A et al (2008) Contemporary results of percutaneous biopsy of 100 small renal masses: a single center experience. J Urol 180:2333–2337
8. Bex A, Jonasch E, Kirkali Z et al (2010) Integrating surgery with targeted therapies for renal cell carcinoma: current evidence and ongoing trials. Eur Urol 58:819–828
9. David KA, Mallin K, Milowsky MI et al (2009) Surveillance of urothelial carcinoma: stage and grade migration, 1993–2005 and survival trends, 1993–2000. Cancer 115:1435–1447
10. Mallin K, David KA, Carroll PR et al (2011) Transitional cell carcinoma of the bladder: racial and gender disparities in survival (1993 to 2002), stage and grade (1993 to 2007). J Urol 185:1631–1636
11. Herr HW, Donat SM (2001) Outcome of patients with grossly node positive bladder cancer after pelvic lymph node dissection and radical cystectomy. J Urol 165:62–64
12. Stenzl A, Cowan NC, De Santis M et al (2012) Treatment of muscle-invasive and metastatic bladder cancer: update of the EAU guidelines. Actas Urol Esp 1 March, epub ahead of print
13. Wosnitzer MS, Hruby GW, Murphy AM et al (2012) A comparison of the outcomes of neoadjuvant and adjuvant chemotherapy for clinical T2-T4aN0-N2M0 bladder cancer. Cancer 118:358–364
14. Blom JH, Van Poppel H, Marechal JM et al (2009) Radical nephrectomy with and without lymph-node dissection: final results of European Organization for Research and Treatment of Cancer (EORTC) randomized phase 3 trial 30881. Eur Urol 55:28–34
15. Freedland SJ, deKernion JB (2003) Role of lymphadenectomy for patients undergoing radical nephrectomy for renal cell carcinoma. Rev Urol 5:191–195
16. Pantuck AJ, Zisman A, Dorey F et al (2003) Renal cell carcinoma with retroperitoneal lymph nodes. Impact on survival and benefits of immunotherapy. Cancer 97:2995–3002
17. Delacroix SE Jr, Chapin BF, Chen JJ et al (2011) Can a durable disease-free survival be achieved with surgical resection in patients with pathological node positive renal cell carcinoma? J Urol 186:1236–1241
18. Hellsten S, Berge T, Linell F (1983) Clinically unrecognised renal carcinoma: aspects of tumor morphology, lymphatic and haematogenous metastatic spread. Br J Urol 55:166–170
19. Pantuck AJ, Zisman A, Dorey F et al (2003) Renal cell carcinoma with retroperitoneal lymph nodes: role of lymph node dissection. J Urol 169:2076–2083
20. Johnsen JA, Hellsten S (1997) Lymphatogenous spread of renal cell carcinoma: an autopsy study. J Urol 157:450–453
21. Hashimoto K, Hisasue S, Yanase M et al (2005) Tumor size and regional lymph node metastasis in patients with M0 renal cell carcinoma: analysis in those having regional lymph node dissection. Hinyokika Kiyo 51:621–625
22. Matsuyama H, Hirata H, Korenaga Y et al (2005) Clinical significance of lymph node dissection in renal cell carcinoma. Scand J Urol Nephrol 39:30–35
23. Dhar NB, Campbell SC, Zippe CD et al (2006) Outcomes in patients with urothelial carcinoma of the bladder with limited pelvic lymph node dissection. BJU Int 98:1172–1175
24. Shariat SF, Ehdaie B, Rink M et al (2012) Clinical nodal staging scores for bladder cancer: a proposal for preoperative risk assessment. Eur Urol 61:237–242
25. Jensen JB, Ulhoi BP, Jensen KM (2012) Evaluation of different lymph node (LN) variables as prognostic markers in patients undergoing radical cystectomy and extended LN dissection to the level of the inferior mesenteric artery. BJU Int 109:388–393
26. Meijer RP, Nunnink CJ, Wassenaar AE et al (2012) Standard lymph node dissection for bladder cancer: significant variability in the number of reported lymph nodes. J Urol 187:446–450
27. Hadley DA, Stephenson RA, Samlowski WE, Dechet CB (2011) Patterns of enlarged lymph nodes in patients with metastatic renal cell carcinoma. Urol Oncol 29:751–755
28. Parker AE (1935) Studies on the main posterior lymph channels of the abdomen and their connections with the lymphatics of the genito-urinary system. Am J Anat 56:409
29. Bex A, Vermeeren L, de Windt G et al (2010) Feasibility of sentinel node detection in renal cell carcinoma: a pilot study. Eur J Nucl Med Mol Imaging 37:1117–1123
30. Sherif AM, Eriksson E, Thorn M et al (2011) Sentinel node detection in renal cell carcinoma. A feasibility study for detection of tumour-draining lymph nodes. BJU Int 109:1134–1139
31. Terrone C, Guercio S, de Luca S (2003) The number of lymph nodes examined and staging accuracy in renal cell carcinoma. BJU Int 91:37–40
32. Saitoh H, Nakayama M, Nakamura K, Satoh T (1982) Distant metastasis of renal adenocarcinoma in nephrectomized cases. J Urol 127:1092–1095
33. Hulten L, Rosencrantz M, Seeman T et al (1969) Occurrence and localization of lymph node metastases in renal carcinoma. Scand J Urol Nephrol 3:129–133
34. Assouad J, Riquet M, Foucault C et al (2006) Renal lymphatic drainage and thoracic duct connections: implications for cancer spread. Lymphology 39:26–32
35. Assouad J, Riquet M, Berna P, Danel C (2007) Intrapulmonary lymph node metastasis and renal cell carcinoma. Eur J Cardiothorac Surg 31:132–134
36. Mahon TG, Libshitz HI (1992) Mediastinal metastases of infradiaphragmatic malignancies. Eur J Radiol 15:130–134
37. Riquet M, Le Pimpec Barthes F, Souilamas R, Hidden G (2002) Thoracic duct tributaries from intrathoracic organs. Ann Thorac Surg 73:892–898
38. Wright FW (1977) Enlarged hilar and mediastinal nodes (and especially lower right hilar node enlargement) as a sign of metastasis of a renal tumour. Clin Radiol 28:431–436
39. Roth B, Wissmeyer MP, Zehnder P et al (2010) A new multimodality technique accurately maps the primary lymphatic landing sites of the bladder. Eur Urol 57:205–211
40. Roth B, Zehnder P, Birkhauser FD et al (2012) Is bilateral extended pelvic lymphadenectomy necessary for strictly unilateral invasive bladder cancer? J Urol 187:1577–1582
41. Vermeeren L, Valdes Olmos RA, Meinhardt W et al (2009) Intraoperative radioguidance with a portable gamma camera: a novel technique for laparoscopic sentinel node localisation in urological malignancies. Eur J Nucl Med Mol Imaging 36:1029–1036